Comprehensive Treatise of Electrochemistry

Volume 3: Electrochemical Energy Conversion and Storage

Edited by

J. O'M. Bockris
Texas A & M University
College Station, Texas

Brian E. Conway
University of Ottawa
Ottawa, Ontario, Canada

[illegible]nest Yeager
[illegible]se Western Reserve University
[illegible]veland, Ohio

Ralph E. White
Texas A & M University
College Station, Texas

PLENUM PRESS · NEW YORK AND LONDON

Library of Congress Cataloging in Publication Data

Main entry under title:

Electrochemical energy conversion and storage.

(Comprehensive treatise of electrochemistry; v. 3)
Includes bibliographical references and indexes.
1. Electric power production from chemical action. 2. Electrochemistry, Industrial. 3. Energy storage. I. Bockris, J. O'M. (John O'M.), 1923- . II. Series.
QD552.C64 vol. 3 [TK2901] 541.3'7s 81-2175
ISBN 0-306-40590-3 [621.31'242] AACR2

© 1981 Plenum Press, New York
A Division of Plenum Publishing Corporation
233 Spring Street, New York, N. Y. 10013

All rights reserved

No part of this book may be reproduced, stored in a retrieval system, or transmitted, in any form or by any means, electronic, mechanical, photocopying, microfilming, recording, or otherwise, without written permission from the Publisher

Printed in the United States of America

Contributors

M. Barak, Consulting Chemist and Engineer, 61 Folders Lane, Burgess Hill, Sussex RH15 0DY, England

D. Berndt, VARTA Batterie AG, Forschungs- und Entwicklungszentrum, D-6233 Kelkheim (Taunus), West Germany

George E. Blomgren, Battery Products Division, Union Carbide Corporation, Cleveland, Ohio 44101

J. O'M. Bockris, Department of Chemistry, Texas A & M University, College Station, Texas 77843

Elton J. Cairns, Head, Energy and Environment Division, Lawrence Berkeley Laboratory, University of California, Berkeley, California 94720

Earl H. Hietbrink, Electrochemistry Department, General Motors Research Laboratories, GM Technical Center, Warren, Michigan 48090

John H. Kennedy, Department of Chemistry, University of California, Santa Barbara, California 93106

Karl Kordesch, Institute for Inorganic Chemical Technology, Technical University of Graz, 8010 Graz, Austria

Akiya Kozawa, Battery Products Division, Union Carbide Corporation, Cleveland, Ohio 44101

Marvin L. Kronenberg, Battery Products Division, Union Carbide Corporation, Cleveland, Ohio 44101. Present address: CEN, Argonne National Laboratory, Argonne, Illinois 60439

63722

James McBreen, Department of Energy and Environment, Brookhaven National Laboratory, Upton, New York 11973

Samuel Ruben, Ruben Laboratories, New Rochelle, New York 10801

S. Srinivasan, Department of Energy and Environment, Brookhaven National Laboratory, Upton, New York 11973

B. V. Tilak, Hooker Chemical Corporation, Research Center, Grand Island, New York 14072

Ferdinand von Sturm, Sigri Elektrographit GmbH, D-8901 Meitingen, Federal Republic of Germany

R. S. Yeo, Department of Energy and Environment, Brookhaven National Laboratory, Upton, New York 11973

Preface to Comprehensive Treatise of Electrochemistry

Electrochemistry is one of the oldest defined areas in physical science, and there was a time, less than 50 years ago, when one saw "Institute of Electrochemistry and Physical Chemistry" in the chemistry buildings of European universities. But, after early brilliant developments in electrode processes at the beginning of the twentieth century and in solution chemistry during the 1930s, electrochemistry fell into a period of decline which lasted for several decades. Electrochemical systems were too complex for the theoretical concepts of the quantum theory. They were too little understood at a phenomenological level to allow their ubiquity in application in so many fields to be comprehended.

However, a new growth began faintly in the late 1940s, and clearly in the 1950s. This growth was exemplified by the formation in 1949 of what is now called The International Society for Electrochemistry. The usefulness of electrochemistry as a basis for understanding conservation was the focal point in the founding of this Society. Another very important event was the choice by NASA in 1958 of fuel cells to provide the auxiliary power for space vehicles.

With the new era of diminishing usefulness of the fossil fuels upon us, the role of electrochemical technology is widened (energy storage, conversion, enhanced attention to conservation, direct use of electricity from nuclear–solar plants, finding materials which interface well with hydrogen). This strong new interest is not only in the technological applications of electrochemistry. Quantum chemists have taken great interest in redox processes. Organic chemists are interested in situations where the energy of electrons is as easily controlled as it is at electrodes. Some biological processes are now seen in electrodic terms, with electron transfer to and from materials which would earlier have been considered to be insulators.

It is now time for a comprehensive treatise to look at the whole field of electrochemistry.

The present treatise was conceived in 1974, and the earliest invitations to authors for contributions were made in 1975. The completion of the early volumes has been delayed by various factors.

There has been no attempt to make each article emphasize the most recent situation at the expense of an overall statement of the modern view. This treatise is not a collection of articles from *Recent Advances in Electrochemistry* or *Modern Aspects of Electrochemistry*. It is an attempt at making a mature statement about the present position in the vast area of what is best looked at as a new interdisciplinary field.

Texas A & M University J. O'M. Bockris
University of Ottawa B. E. Conway
Case Western Reserve University Ernest Yeager
Texas A & M University Ralph E. White

Preface to Volume 3

Of events which have affected progress in the field of electrochemistry, the decision of NASA to use electrochemical auxiliary power in space vehicles was one of the more important. Another important decision was Ford's announcement of their sodium–sulfur cell for vehicular use in 1969.

In this volume, we begin by giving a perception of applications of the field of electrochemistry in the near future. Thereafter, the principles of electrochemical energy conversion and storage are discussed in some detail, followed by chapters which give a detailed account of important batteries and fuel cells. We include a chapter on electrochemical power for transportation, and, finally, we end with a presentation of the hydrogen economy.

Texas A & M University — J. O'M. Bockris
University of Ottawa — B. E. Conway
Case Western Reserve University — E. Yeager
Texas A & M University — Ralph E. White

Contents

1. Electrochemistry and the 21st Century
J. O'M. Bockris

1. Time Scale 1
2. Electrochemistry as "The Other Chemistry" 1
3. On the Nature of Electrochemistry 3
4. The Relationship of Electrochemistry to Other Sciences 5
5. The Currently Expanding World and the Steady State World of the 21st Century 5
6. On the Media of Energy 7
7. Present Electrochemical Industry 9
8. Difficulties of Our Present Society 9
9. A Latter-Day Coal Age 10
10. Near-Future Leads in the Electrochemical Industry 11
11. Biomedical Applications 15
12. The Electrodeposition of Materials from High-Temperature Melts 22
13. Mineral Processing 23
14. Electrocatalysis 25
15. Material Conservation 27
16. Electro-organic Chemistry 27
17. High-Temperature Electrolytes 28
18. Electrochemistry of Cleaner Environments 29
19. Electrochemistry for a Better World 30
20. Borderline Phenomena 34
21. Lack of Training in Electrochemistry 35

References 35

2. Electrochemical Energy Conversion—Principles
B. V. Tilak, R. S. Yeo, and S. Srinivasan

1. Introduction 39
   1.1. Historical Background of Fuel Cells 39

1.2. The Energy Conversion Methods: Advantages and Disadvantages of Fuel Cells Over Other Methods . . . 40
1.3. Types of Fuel Cells and the Most Promising Systems . . . 40
1.4. Role of Electrochemical Energy Conversion in Efficient Utilization of Primary Energy Sources . . . 42
1.5. The Relevant Electrochemical Principles in Electrochemical Energy Conversion . . . 43
2. Thermodynamic Aspects . . . 44
2.1. Reversible Potentials and Open-Circuit Potentials of Fuel Cells . . . 44
2.2. Temperature and Pressure Coefficients of Reversible Potentials . . . 45
2.3. Expressions for Efficiencies of Fuel Cells . . . 49
2.4. Heat Changes under Reversible Conditions . . . 50
3. Electrode Kinetic Aspects . . . 50
3.1. Dependence of Cell Potential and of Differential Cell Resistance on Current . . . 50
3.2. Dependence of Efficiency on Current Density . . . 51
3.3. Dependence of Power on Current Density . . . 52
3.4. Expressions for Maximum Power in Limiting Cases . . . 53
3.5. Heat Generation . . . 54
3.6. The Ideal Electrode Kinetic Parameters for Fuel Cells . . . 54
4. Electrocatalysis . . . 55
4.1. Major Role of Electrocatalysis in Electrochemical Energy Conversion . . . 55
4.2. Hydrogen Oxidation Reaction . . . 56
4.3. Oxygen Reduction Reaction . . . 58
4.4. Electro-organic Oxidation . . . 61
4.5. Sintering of Supported Metal Crystallites . . . 63
5. Porous Gas Diffusion Electrodes . . . 64
5.1. Models . . . 64
5.2. Current–Potential Relations and Current and Potential Distributions . . . 71
5.3. Extent of Utilization of Total Surface Area of Supported Catalysts . . . 82
5.4. Surface Area Measurements . . . 83
5.5. Transient Techniques to Study Porous Electrode Phenomena . . . 85
6. Fuel Cell Systems: Applications, Performance, and Economics . . . 89
6.1. Types of Applications of Fuel Cells . . . 89
6.2. Fuel Cells for Electric and Gas Utility Application . . . 90
6.3. Fuel Cells for Transportation . . . 106
6.4. Fuel Cells for Space Applications . . . 109
6.5. Important Parameters Determining Overall Efficiency and Cost . . . 110
References . . . 116

3. Electrochemical Energy Storage

Karl Kordesch

1. Introduction . . . 123
1.1. The Need for Energy Storage . . . 123

1.2. Energy Storage Technologies 124
2. The Theory of Galvanic Cells 126
2.1. Electrode Potentials 126
2.2. The Current–Potential Relation 139
2.3. Complete Galvanic Cells 141
2.4. The Galvanic Cell as Energy Converter 145
3. Electrochemical Storage Systems 146
3.1. Introductory Remarks 146
3.2. Rechargeable Batteries—Conventional Technology 148
3.3. Rechargeable Batteries—Future Systems 158
3.4. Primary Batteries 165
3.5. Fuel Cells 169
3.6. The Limits of Electrochemical Energy Storage (The "Super Battery") 174
4. Summary and Outlook 179
4.1. Industrial–Economical Aspects 179
4.2. Research Objectives 182
Appendix 185
References 187

4. Primary Batteries—Introduction

M. Barak

1. General Features 191
1.1. Early Developments 191
1.2. Applications of Primary Batteries 192
1.3. Basic Principles 193
1.4. Kinetic Aspects of Electrode Reactions 196
1.5. Discharge-Voltage Characteristics 197
2. Classification of Primary Cells and Batteries 198
3. Some Properties of Cathodes, Anodes, and Electrolytes 199
3.1. Cathodes 199
3.2. Anodes 199
3.3. Electrolytes 202
4. Performances of Primary Cells 203
4.1. Theoretical Considerations 203
4.2. Practical Outputs of Primary Cells 205
References 205

5. Primary Batteries—Leclanché Systems

Akiya Kozawa

1. Introduction 207
2. Progress in Performance 207
3. Major Technical Changes 209
4. Chemical Reactions in the Cell 212
5. New Cells and Future Study Areas 215
References 217

6. Primary Batteries—Alkaline Manganese Dioxide–Zinc Batteries

Karl Kordesch

1. Introduction . . . 219
2. The History of the Alkaline MnO_2–Zinc Cell . . . 220
3. Electrochemistry of the Alkaline MnO_2–Zinc System . . . 220
4. Primary Alkaline MnO_2–Zinc Cells . . . 223
   4.1. Cell Designs . . . 223
   4.2. Performance Data . . . 226
   4.3. Physical Characteristics . . . 227
5. Secondary Alkaline MnO_2–Zinc Cells . . . 227
References . . . 230

7. Primary Batteries—Sealed Mercurial Cathode Dry Cells

Samuel Ruben

1. Introduction . . . 233
2. Cell Structures . . . 235
3. Cell Discharge Characteristics . . . 238
4. Internal Resistance of the Zn–HgO Cell during Discharge . . . 240
5. Mercury Voltage Reference Cell . . . 240
6. Rechargeable HgO Cells . . . 241
7. Zinc Mercuric Dioxysulfate Cell . . . 243
8. Cell Structures for Zinc–Mercuric Dioxysulfate Cells . . . 244
Suggested Reading . . . 244

8. Primary Batteries—Lithium Batteries

Marvin L. Kronenberg and George E. Blomgren

1. Introduction . . . 247
2. Solid Cathode Cells . . . 248
   2.1. Electrolyte Solution Considerations . . . 248
   2.2. Electrode and Cell Constructions . . . 250
   2.3. Specific Systems . . . 251
3. Liquid Cathode Cells . . . 263
   3.1. Electrolyte Solution Properties . . . 264
   3.2. Discharge Data on Liquid Cathode Cells . . . 267
   3.3. Anode Delay Phenomena . . . 273
   3.4. Safety Considerations . . . 274
4. Summary and Future Possibilities . . . 274
References . . . 275

9. Primary Batteries—Solid Electrolytes

John H. Kennedy

1. Introduction . . . 279
2. Conduction Mechanisms in Solid Electrolytes . . . 280
   2.1. Ionic Defects in Crystals . . . 280

2.2. Determination of Conduction Mechanism 282
2.3. Conductivity in Crystals Containing Excess Lattice Sites 285
2.4. Electronic Conductivity 287
3. Interface Effects in Solid Electrolyte Cells 289
4. Silver-Ion-Conducting Electrolyte Batteries 290
5. Lithium Iodide Electrolyte Batteries 295
6. Beta-Alumina Electrolyte Batteries 298
Selected Reading 301
References 302

10. Secondary Batteries—Introduction

James McBreen

1. Classification, General Features, and Intercomparisons 303
1.1. Introduction 303
1.2. Battery Features 304
1.3. Battery Applications 305
1.4. Characteristics and Classification of Secondary Batteries 305
1.5. Other Intercomparisons 312
2. New Ambient Temperature Batteries 314
2.1. The Zinc–Nickel Oxide Battery 314
2.2. The Zinc–Manganese Dioxide Battery 318
2.3. The Zinc–Chlorine Battery 320
2.4. The Zinc–Bromine Battery 322
2.5. The Zinc–Air Battery 324
2.6. The Iron–Air Battery 325
2.7. The Hydrogen–Nickel Oxide Battery 326
2.8. The Hydrogen–Silver Oxide Battery 329
2.9. The Hydrogen–Oxygen Battery 330
2.10. The Hydrogen–Halogen Battery 331
2.11. The Redox Battery 331
2.12. The Lithium–Organic Electrolyte Battery 334
References 335

11. Secondary Batteries—New Batteries: High Temperature

Elton J. Cairns

1. Introduction 341
2. Cells with Solid Electrolytes 343
2.1. The Sodium–Beta-Alumina–Sulfur Cell 344
2.2. The Sodium–Sodium-Glass–Sulfur Cell 349
2.3. The Sodium–Beta-Alumina–Antimony Trichloride Cell 353
2.4. The Sodium–Beta-Alumina–Sulfur Chloride Cell 353
3. Cells with Molten-Salt Electrolytes 354
3.1. The Lithium-Aluminum–Lithium Chloride-Potassium Chloride–Iron Monosulfide Cell 355
3.2. The Lithium-Silicon–Lithium Chloride-Potassium Chloride–Iron Disulfide Cell 360

3.3. The Calcium-Silicon–Molten Halide–Iron Disulfide Cell 366
4. Conclusions 368
References 368

12. Secondary Batteries—Lead–Acid Batteries

D. Berndt

1. History 371
2. General Theory 371
2.1. The Basic Electrochemical Reactions 372
2.2. Discharge Performance 376
2.3. Charging Performance 377
3. The Actual Appearance of Lead–Acid Batteries 379
3.1. Electrode Designs 380
3.2. Design of Cells and Batteries 381
Selected Reading 384

13. Secondary Batteries—Nickel–Cadmium Battery

Ferdinand von Sturm

1. Introduction 385
2. Thermodynamics and Kinetics 386
3. Materials, Electrodes, and Cells 389
3.1. Materials 389
3.2. Electrode Types 390
3.3. Cell Types 392
4. Technical Performance 396
4.1. Charge–Discharge Characteristic 396
4.2. Charge Retention 399
4.3. Cycle Life 401
4.4. Maintenance 401
4.5. Energy Density and Efficiency 401
5. Application 403
References 404

14. Secondary Batteries—Silver–Zinc Battery

Ferdinand von Sturm

1. Introduction 407
2. Thermodynamics and Kinetics 408
3. Electrodes and Cells 411
3.1. Electrodes 411
3.2. Cell Types 412
4. Technical Performance 415
4.1. Charge–Discharge Characteristic 415

4.2. Charge Retention . . . 416
4.3. Cycle Life . . . 416
4.4. Maintenance . . . 417
4.5. Energy Density and Efficiency . . . 417
5. Application . . . 418
References . . . 418

15. Electrochemical Power for Transportation

Elton J. Cairns and Earl H. Hietbrink

1. Introduction . . . 421
1.1. Historical Background . . . 422
1.2. Modern Transportation Needs . . . 423
1.3. Environmental and Energy Utilization Issues . . . 425
2. Electric Transportation Vehicles . . . 435
2.1. Automobiles . . . 436
2.2. Commercial Electric Vehicles . . . 447
3. Electrochemical Power Source Requirements . . . 453
3.1. Vehicle Propulsion Power Calculations . . . 456
3.2. Battery Power Requirements . . . 460
3.3. Battery Energy Requirements . . . 462
3.4. Durability and Cost Requirements . . . 462
4. Identification of Candidate Power Sources for Electric Vehicles . . . 464
4.1. Battery Performance . . . 464
4.2. Battery Durability . . . 468
4.3. Battery Cost . . . 471
4.4. Fuel Cells . . . 473
5. Electrochemical Power Source Technology . . . 474
5.1. Ambient Temperature Batteries . . . 474
5.2. High-Temperature Batteries . . . 488
5.3. Fuel Cells . . . 493
6. Summary and Concluding Remarks . . . 495
References . . . 498

16. A Hydrogen Economy

J. O'M. Bockris

1. History . . . 505
2. Hydrogen Economy and the Time Scale . . . 506
3. Three Possible Energy Futures during the Coming Century . . . 507
3.1. Coal . . . 508
3.2. Nuclear Hydrogen . . . 508
3.3. Coal–Nuclear Future . . . 508
4. A Solar–Hydrogen Economy . . . 508
5. The Necessity of Beginning the Development of a Hydrogen Economy Several Decades before the Ending of the Fossil Fuel Supply . . . 509
6. The Relationship of Hydrogen to Coal . . . 509

7. The Method of Obtaining Hydrogen on a Massive Scale 510
7.1. Hydrogen from Coal 510
7.2. Biomass 511
7.3. Hydroelectric Plants and the Electrolysis of Water 511
7.4. Hydrogen from Wind Power 511
7.5. Hydrogen from the Kinetic Energy of Natural Streams of Water in the Earth 511
8. The Manufacture of Hydrogen from Solar Energy 512
9. Methods of Decomposing Water 512
10. Electrochemical Decomposition of Water 513
10.1. Classical Electrolyzers 513
10.2. Modern Electrolyzers 514
10.3. Electrolysis of Thermal Systems 515
11. Decomposition of Water by Light 515
12. Hydrogen at High Temperatures 515
13. The Cost Aspect of the Production of Hydrogen 516
13.1. Time Scale 516
13.2. Cost and Price 517
13.3. Large- and Small-Scale Prices 517
13.4. The Cost of Electrochemical Processes in the Production of Hydrogen 517
13.5. The Production of Hydrogen from Coal 519
14. Applications of a Hydrogen Economy 519
14.1. Transmission 519
14.2. Transduction 519
15. Storage of Energy 520
15.1. Reservoirs 520
15.2. Liquefaction 520
15.3. Alloys 521
16. Safety Aspects of Hydrogen as a Fuel 521
16.1. Hydrogen in Transport and Housing 522
16.2. Industry 522
16.3. Pollutional Aspects 522
17. The Hydrogen Economy as the Cheapest Economy 523
18. Electrochemical Technology from Hydrogen Economy 525
18.1. Transportation 525
18.2. Industry 525
References 525

Index 527

1

Electrochemistry and the 21st Century

J. O'M. BOCKRIS

1. Time Scale

It is important in a chapter of this kind to define the time scale considered If a time scale is sufficiently long, everything is indistinct and eventually of lessened interest, whereas with a sufficiently short time scale, everything is a direct extrapolation of the present. For this discussion an ideal time scale would be long enough so that considerations would initiate augmented research support. Such a scale is approximately one generation, i.e., something discussed at a given time tends to become reality in a time of "a few decades," some 15–50 years ahead. The thoughts discussed in this chapter concern matters stretching out into this time period during which the creeping increase of atmospheric CO_2 with its effects on the climate (associated with the reliance on fossil fuels) will become manifest (Figure 1).[1]

It is of interest to refer in this context to an article entitled "Electrochemistry, the Underdeveloped Science," written in 1965.[2]

2. Electrochemistry as "The Other Chemistry"

The principal aspect of electrochemistry which makes it different from other branches of physical chemistry is the ubiquity of its applications.

J. O'M. BOCKRIS • Department of Chemistry, Texas A & M University, College Station, Texas 77843.

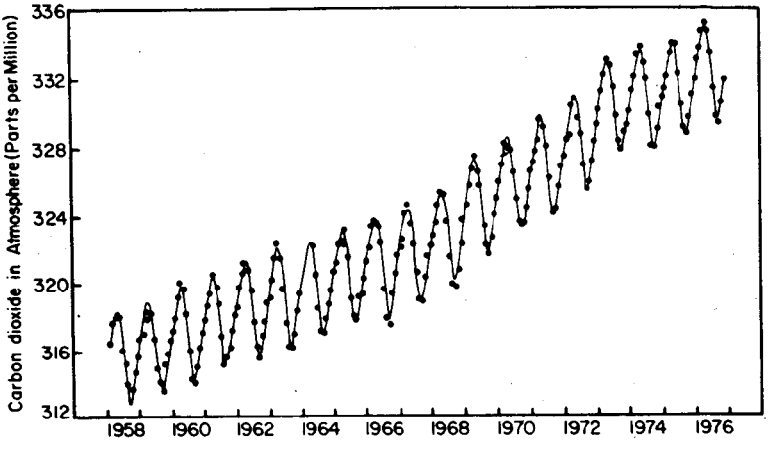

Figure 1. The cyclical increase in CO_2. Climatic modification will follow a continuation of the present trend and be significant before the year 2030.

Batteries, fuel cells, extraction metallurgy, pollutional cleanups, textile manufacture, geological movements, the conservation of materials, tranquilizer mechanisms, and the clotting of blood are all processes in which electrochemistry is the core of much of the scientific underlay.

Electrochemistry theory provides the basis of colloid chemistry. The extraction of metals, except ferrous metals, involves electrochemistry. Engineering is interlaced with electrochemistry, in particular, the electrochemistry of conservation, which may determine whether a machine will last for one year or many decades. Electrochemistry plays a vital role in biological mechanisms concerning the stability of blood in contact with metals, the passage of current through nervous membranes, the growth of bones, etc.

Many more life processes are electrochemical than were once thought to be. The basic idea taught implicitly to students concerned with reaction mechanisms, i.e., that mechanisms of reactions occur by the collision of two molecules, may be the exception rather than the rule among reaction mechanisms in nature.

For example, some reactions which are apparently collisional have been established as being reactions which involve the coupled transfer of charge to and from different sites on the same substrate. The reduction of titanium tetrachloride by magnesium to titanium and magnesium chloride, earlier regarded as a thermal reaction, is, in fact, a reaction in which the magnesium (suspended in molten salts) dissolves anodically and titanium is deposited upon it by means of interfacial charge exchange.

In a different field, one may offer an example of the spreading of cracks through metals. The older explanation involved the concentration of high local

stress with the stretching of bonds. More recently, the model has become that of a typical electrochemical situation involving moisture films, anodic and cathodic reactions, local coupled electrochemical cell reactions, etc.

Chemistry is generally considered to be a science of colliding particles without charge exchange. The assumption that this represents the norm of reaction mechanisms in nature may be a misapprehension; many, perhaps the majority, of reactions are surface reactions and involve interfacial charge exchange. The electrochemical aspect of chemistry, rather than being a branch of chemistry, may be, in terms of numbers of reactions to which it applies, the dominating aspect. It may correspond more to reality to speak of electrochemistry and then, as a special case, "thermal" chemistry (meaning homogeneous reactions of a collisional kind, without charge exchange).

3. On the Nature of Electrochemistry

In 1912, Kistyakovsky† defined electrochemistry as a science concerned with the study of phenomena associated with the direct conversion of chemical energy into electrical energy, and electrical energy into chemical energy. Electrochemical science is related to surface science, for most surface science, in practice, takes place at wet interfaces, across from which charge transfer from metal to solution may occur. Material science is closely connected to electrochemistry, insomuch as a major part of material science is the science of corrosion; and corrosion science, at a molecular level, is based upon electrochemical concepts.

However, electrochemical reactions have an even broader context than that engendered by Kistyakovsky's definition, for most real interfaces pertain to situations which involve electrical charge transfer and potential differences; it is difficult to have an interface which is not electrically charged and at which a potential difference does not exist, i.e., all interfacial situations are sites of electrochemical activity. Consideration of this statement allows one to appreciate the breadth of electrochemistry.

The fundamental difference between ("thermal" collisional) chemical and electrochemical reactions is seldom brought out.‡ Chemical reactions involve collision between the molecules concerned. Electrochemical reactions, allowed to take place spontaneously, interchange charges of the reactants with a third body, the substrate; however, the reactants do not contact each other. Electrochemistry is another chemistry.

It might be reasonable to describe the nature of electrochemistry as (1) a ubiquitous branch of science basically concerned with the interfacial exchange

† See Reference 3.

‡ The realization that most spontaneous electrochemical reactions in nature are fuel-cell-type polyelectrode reactions, involving no external sources of power and no *net* electron transfer, is not widespread. It is seldom realized, for example, that photosynthesis is a process based on a series of anodic and cathodic interfacial reactions.

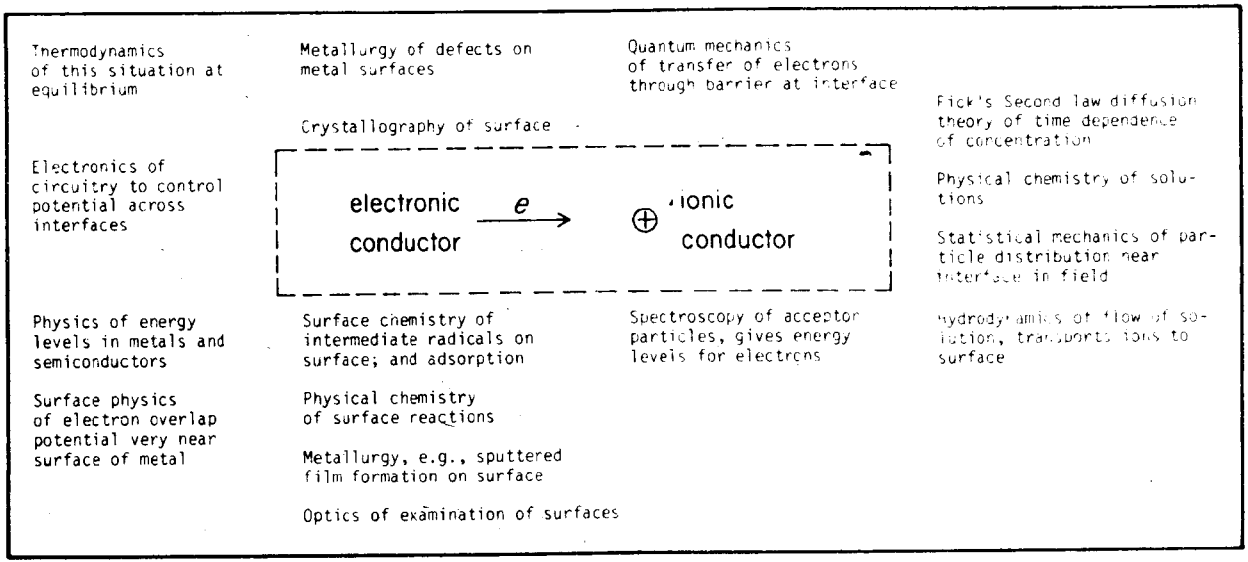
Thermodynamics of this situation at equilibrium
Metallurgy of defects on metal surfaces
Quantum mechanics of transfer of electrons through barrier at interface
Crystallography of surface
Fick's Second law diffusion theory of time dependence of concentration
Electronics of circuitry to control potential across interfaces
electronic conductor
e
ionic conductor
Physical chemistry of solutions
Statistical mechanics of particle distribution near interface in field
Physics of energy levels in metals and semiconductors
Surface chemistry of intermediate radicals on surface; and adsorption
Spectroscopy of acceptor particles, gives energy levels for electrons
Hydrodynamics of flow of solution, transports ions to surface
Surface physics of electron overlap potential very near surface of metal
Physical chemistry of surface reactions
Metallurgy, e.g., sputtered film formation on surface
Optics of examination of surfaces

Figure 2. Electrochemistry and the rest of chemistry.

of electricity and matter with very wide applications to most practical surface phenomena, and (2) the basic science underlying material conservation, energy conversion and storage, and many situations in molecular biology.

4. The Relationship of Electrochemistry to Other Sciences

The relationship of electrochemistry to the rest of chemistry is illustrated in Figure 2.[4]

Electrochemistry is intricately related to other aspects of science. It is based upon the fundamental disciplines of physics and chemistry, the physics of metals and semiconductors, and the surface chemistry of radicals. It is connected to applications of various aspects of science, e.g., metallurgical processes such as cracking, many types of optical devices for the examination of surfaces (Figure 3),[5] and spectroscopy, particularly electron spectroscopy. It involves the application of much hydrodynamic theory.

Electrochemistry appears to be an increasingly interdisciplinary field. For example, it is basic to metallurgy, engineering, biology, geology, etc., and provides essential knowledge of mechanisms of the interfacial aspects of these fields.

Apart from these connections, electrodic electrochemistry is related to thermionics; both are dependent on the passage of electrons across the interface. Another similarity is that between electrodes and their action, and that of catalysts in chemistry.

5. The Currently Expanding World and the Steady State World of the 21st Century

It is necessary to view the development of electrochemistry in the context of the time. Discussion of the nature of the present epoch would include a

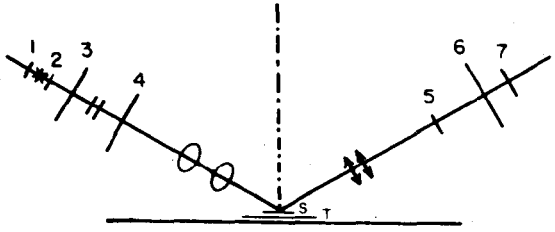

Figure 3. Schematic representation of ellipsometer. 1, Source of light; 2, collimator; 3, polarizer; 4, compensator; S, specimen on the T table; 5, filter; 6, analyzer; and 7, light detector.

Limited Hydrocarbon Supply	+ O_2		⟶	CO_2 + H_2O
Oxide Ores	+	Fossil Fuel Energy	⟶	Metals for Machines
Machines	+	Fossil Fuel Energy	⟶	Affluence
Machines	+	O_2 + Time	⟶	Oxides and Decay

Figure 4. The present growing world.

description of the concept of the transient use of materials, particularly the transient use of the limited fossil fuel cache, its exhaustion within half a century, and the progress of many metals toward exhaustion within a century (Figure 4).

It is unavoidable that a steady state world be attained; the alternative would be disaster. The energy sources must become solar or nuclear fusion. The fate of all materials is recyclization.

Essentially, the nineteenth and twentieth centuries have been times of explosive growth energized by haphazard use of fossil fuels apart from a consciousness of impending exhaustion. The next stage of social development is to attain a steady state, resulting in a stress on the conservational aspect of dealing with materials and their eventual recyclization (Figure 5). Fossil fuels and combustion will no longer be the primary consideration. It is necessary to look forward to the solar and solar-gravitational sources to obtain the energy

Renewable Energy Source	+	H_2O	⟶	Fuel (H_2) + O_2
H_2	+	Fuel Cells	⟶	Electricity + H_2O
Oxide Ores	+	Electricity	⟶	Metals for Machines
Machines			Electricity / H_2 ⟶	Affluence
Machines + O_2	+	Time	⟶	Oxides and Decay
Oxides	+	Electricity on Hydrogen	⟶	Recycled Metals for Machines

Figure 5. The coming steady state (electrochemical) world.

necessary to effect the steady state. Some characteristics of this new era will be:

(1) An increase in energy conversion efficiency.
(2) New fuels to interface with solar and atomic energy.
(3) A stress upon conservation and reduction of the rate of corrosion.
(4) A general recycling of materials, so that they are no longer regarded as coming from mining the earth, but as the result of the steady state conservation in a cycle of production, decay, and reproduction.

The relevance of these characteristics to electrochemical technology arises:

(1) By electrochemical energy conversion, the most efficient conversion of energy to mechanical work can be obtained.
(2) Electrochemistry is the basic science of material conservation.
(3) Although recycling materials can be obtained by many methods, the electrochemical method has one essential advantage, i.e., it adds the variable of potential to concentration and temperature in determining delivery of a certain product.

Electrochemical technology is, thus, a particularly relevant type of technology for the steady state world which must be attained. The polluting and consuming technology of the nineteenth and twentieth centuries worked by combustion and by the conversion of a relatively small quantity of the energy in a fossil fuel—usually less than one quarter—to mechanical useful work. In the steady state situation, electrochemical technology will interface with solar and atomic sources, with hydrogen from water, to effect selective extraction in recycling.

6. On the Media of Energy

From around 1985, when the present fossil fuel sources will fail to meet the world's needs, additional energy will have to come from coal, nuclear, or solar sources. The most economically available sources of solar energy on Earth are summarized in Table 1.[6]

There are few fuels which interface economically with solar and nuclear sources, and the most likely are electricity, hydrogen and, to a lesser extent, methanol.

As an energy source, coal will not be an economic source of synthetic gasoline, which is more expensive than synthetic liquid natural gas. (In 1979 currency the price of the latter will be $4.50/MBTU and the price for the gasoline more than 50% greater.[7])

These considerations do not take into account the role of hydrogen from coal. Hydrogen can be obtained from coal at a first law cost slightly less than the cost of methane, but the effective price is given by the second law cost.

Table 1
Solar Energy from Earth's High-Insolation Areas

Desert	Total area, acres	Annual solar energy input, BTU	Area assumed usable, %	Available production area, acres	Annual energy[a] production, BTU	Energy density, BTU/acre-yr
North Africa	1.92×10^9	6.1×10^{19}	15	2.8×10^8	9.1×10^{18}	3.2×10^9
Arabian Peninsula	3.2×10^8	1.1×10^{19}	30	9.6×10^7	3.3×10^{18}	3.4×10^9
Western and Central Australia	3.8×10^8	1.0×10^{19}	25	9.5×10^7	2.5×10^{18}	2.6×10^9
Kalahari	1.2×10^8	3.5×10^{18}	50	6.0×10^7	1.7×10^{18}	2.8×10^9
Thar (N.W. India)	6.4×10^7	1.8×10^{18}	50	3.2×10^7	9.0×10^{17}	2.8×10^9
Mojave (S. Calif.)	6.6×10^6	2.6×10^{17}	20	1.3×10^6	5.2×10^{16}	3.9×10^9
Vizczino (Baja Calif.)	3.8×10^6	1.2×10^{17}	25	9.5×10^5	3.0×10^{16}	3.1×10^9
Total/average	2.8×10^9	8.8×10^{19}	31 av.	5.6×10^8	1.7×10^{19}	3.1×10^9 av.

[a] A 10% conversion efficiency is used.

Hydrogen is 1.5 times† more efficient than gasoline and 1.3 times† more efficient than methane when used to energize an internal combustion engine, so the cost of hydrogen per unit of distance in a vehicle will be less than the cost of other fuels from coal. Therefore it will not be possible to refuse the choice of hydrogen.

Consequently, it seems unavoidable that natural oil and natural gas will be replaced by hydrogen from coal and then, more gradually, hydrogen from nuclear and solar sources via water.

Hydrogen is the fuel which interfaces best with electrochemical energy converters, so that the new methods of producing energy in the coming century will favor electrochemical energy conversion technology.

7. Present Electrochemical Industry

In a review of the electrochemical industry in the 1960s, Wenglowski[8] represented the composition of the electrochemical industry (Figure 6).[8] Electrowinning and refining is the main element followed by surface finishing, batteries, and capacitors and finally, material conservation. Electrowinning and refining, including aluminum, account for about 50% of the industrial contribution.

With respect to volume of business, the principal U.S. corporations which use electrochemical methods are General Motors (electroplating and storage batteries), the Aluminum Company of America (production of aluminum), and the United States Steel Company (production of tin-plate).

The total size ($ of product) of the electrochemical industry, as a function of all U.S. manufacturing, is approximately 3% and growing faster than the average U.S. manufacturing industry.

In relation to the chemical industry, however, the electrochemical industry is 35–45% of the total. Thus the electrochemical industry is more than one-third of the chemical industry. On the other hand, there are some 1000 Ph.D.'s awarded in chemistry each year in the U.S.A., only 10 of which are electrochemical Ph.D. graduates.

8. Difficulties of Our Present Society[9]

Pollution of the environment is still a danger to our society even though the fears of the early 1970s may have been temporarily lessened. Pollution in cities such as Tokyo and London is not as bad as it was at the beginning of the 1970s. However, while fossil fuels continue to be used as the principal energy source, pollution will be present and will tend to increase in the latter part of the century as the coal contribution to the energy mix increases.

† The precise amounts depend on the driving cycle.

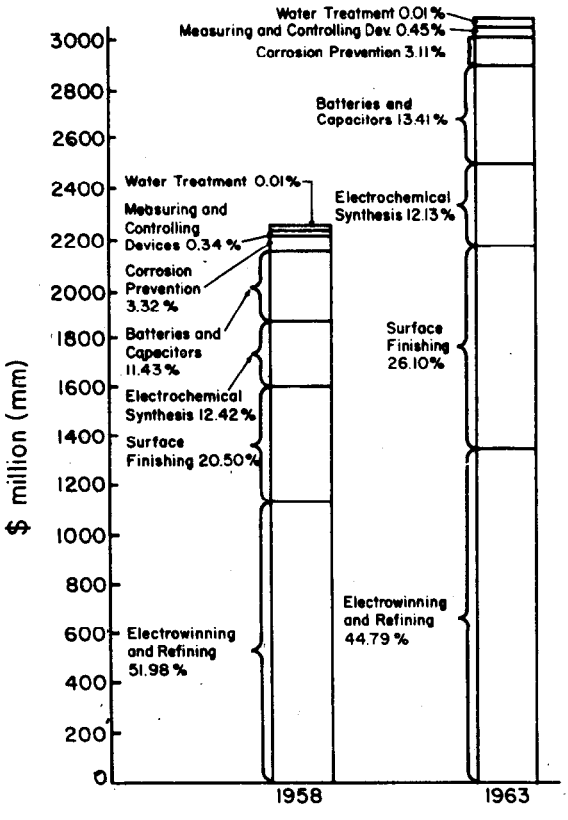

Figure 6. Composition of the electrochemical industry by-product types, 1958 and 1963.

As great a danger to technological society as pollution is that the exhaustion of fossil fuels will begin to be felt before machinery capable of converting renewable energy sources to a usable form has been engineered. Thus the principal problem of renewable resource conversion is the enormous capital and materials investment needed, rather than engineering. The difficulty will increase when the supply of fossil fuel decline.

9. A Latter-Day Coal Age

There will be an interim period of several decades during which we will rely increasingly on coal. Coal is the most likely supplement to the dwindling supplies of gaseous and liquid fossil fuels (Figure 7).[10] However, there will be

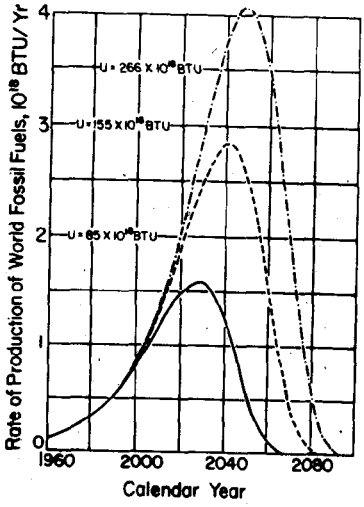

Figure 7. Elliot and Turner's estimation of the total world fossil fuel production rate as a function of time, taking into account the increasing use of coal to cover the shortfall in petroleum and natural gas.

difficulties in extracting the coal at the rate needed. Each year the number of new mines which would have to be opened to extract the amount of coal necessary to replace oil and natural gas would be impractically large, e.g., a new mine would have to be opened each week for many decades. There would thus be a logistical problem.[11]

Secondly, the pollutional difficulties of coal with respect to sulfur are great.[12] The difficulty of extracting sulfur from coal, although not easy, may become practical but the safe disposal of vast amounts of sulfur could prove economically unfeasible.†

Climatic changes due to CO_2 accumulation[12,13] would be an increasing danger if coal were to become the predominant fuel, though these changes would not be felt until the second or third decade of the next century.

10. Near-Future Leads in the Electrochemical Industry

Fuel cells seem to be a certain part of near-future technology.[14] However, hydrogen–air fuel cells produce water, which is currently of use only in space travel. The fuel cell principle[15] could be used with dispatch in the synthesis of many materials, e.g., ethylene dichloride. The by-product, electricity, could be fed into the grid, rather than the wasted heat of reaction. At present, approximately 3/4 of the energy released in manufacturing is released into the atmosphere.

† The sulfur from one year's coal supply (of 5% S content) to a 1000-MW plant[12] would have the size of a typical city block, with a height of around six floors.

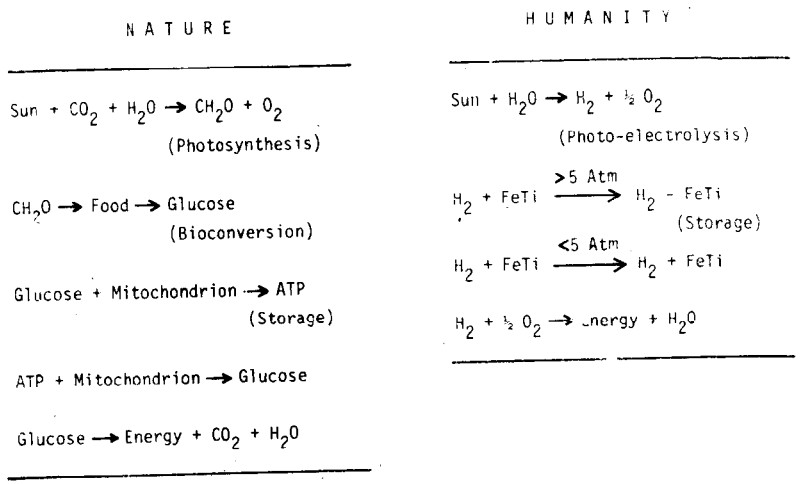
NATURE
HUMANITY
Sun + CO_2 + H_2O → CH_2O + O_2
(Photosynthesis)
CH_2O → Food → Glucose
(Bioconversion)
Glucose + Mitochondrion → ATP
(Storage)
ATP + Mitochondrion → Glucose
Glucose → Energy + CO_2 + H_2O
Sun + H_2O → H_2 + ½ O_2
(Photo-electrolysis)
H_2 + FeTi →(>5 Atm) H_2 - FeTi
(Storage)
H_2 + FeTi →(<5 Atm) H_2 + FeTi
H_2 + ½ O_2 → Energy + H_2O

Figure 8. Solar energy systems: (a) nature, (b) humanity.

An Electrochemical House. Paths for development in a near-future electrochemical technology include (1) hydrogen-piped houses with fuel cell electricity production, (2) rooftop solar-hydrogen production converted to electricity and stored in batteries, (3) rooftop-collected electricity electrolyzing water to produce hydrogen fuel for cars, (4) rooftop production of electricity to reduce atmospheric carbon dioxide which can be constructively used to produce methanol for cars, and (5) in-house treatment of sewage with subsequent oxidation to useful products. Figure 8 compares a synthetic solar energy system with nature's model.

Electrochemical Transportation. Electrochemically driven transport using a hydrogen–air fuel cell with a nickel–hydrogen battery for acceleration will be economical in the near future (using hydrogen from coal), thus removing the principal cause of pollution and health hazards.†

Electrochemical Production of Hydrogen.[20] Insofar as hydrogen becomes a medium of energy for solar and atomic energy sources, it will be produced from water. Many reviews of possible near-future methods of obtaining hydrogen from water exist. Photoelectrochemical methods seem possible.

† This economical change would be one of the greater ones which could be made, retaining many of the advantages, in terms of speed and range, of present cars. Compared with gasoline, efficiency would roughly double. Currently, hydrogen from coal would be around 25% more expensive than gasoline on a first law basis; so, even now, there would be a substantial net decrease in transportation costs achieved by the general introduction of the fuel cell–hydrogen combination to run transportation.

Other electrochemical methods could involve processing sewage in a fuel cell by using an oxygen cathode.

For house wastes, disposal could occur in this manner, with the in-house manufacture of useful products. For example, in a fuel cell mode, sewage and trash could be converted to CO_2, which, in turn, could be converted to methanol, with the addition of roof-produced solar electricity, or to foods, with the aid of the Schlegel-suggested bacteria.[23]

Electrochemical Recycling. The attraction of electrochemical recycling involves the availability of potential as an extra controlling variable. This would enhance the selectivity of the removal of a material from a mixture. Car bodies could be advantageously recycled in this fashion.[24]

Electrochemical Conservation. Electrochemical conservation will be an increased part of electrochemical industry. Our throw-away society will be converted to a cyclical one as the cost of newly mined material becomes sufficiently high. Conservation (anticorrosion) will become increasingly important. The conservation of materials has a predominantly electrochemical basis.

Electrochemical Energy Conversion. Fuel cells[25] are an important aspect of the electrochemistry of the future. The primary problem is the lifetime of the electrocatalyst. The cost of fuel cells is nominally some $400/kilowatt, but the comparative meaning of this statement is not clear unless the lifetime of the catalyst can be defined.

It is necessary to carry out further fundamental work on electrocatalysis. Techniques for *in situ* observation of radicals on electrode surfaces must be developed. Potentials of zero charge on metals and semiconductors must be extensively determined. The analysis of adsorbed intermediates must occur.

It is essential to locate[26] the regions of optimum effect of the electrocatalyst within the porous matrix; for example, noble metal catalyst material may be more useful in present fuel cells, if it is distributed with reference to current distributions. Materials research on fuel cell components must be carried out at a more mechanistic level than in the past.

Fuel cell efficiency would be increased if hydrogen were the fuel.[27] Methanol and hydrazine have lower i_0's in their electrochemical oxidation reactions to CO_2. Overpotential (proportional to $\log i/i_0$) is equivalent to reduced efficiency and is the electrochemical analog of Carnot efficiency loss.

In the time period concerned, the opportunities for electrochemical energy conversion in industry are good. The fundamental principle of reduction of efficiency loss is on the side of the fuel cell, and it seems that, as energy conservation becomes important, fuel cells and electrogenerative cells should prosper.

A twofold increase of efficiency may not be enough if the increase in capital costs is too much, compared with what is offered by older convertors. It is desirable to apply defense department accounting, rather than marketplace accounting, to the development of new energy supply equipment and, hence, to

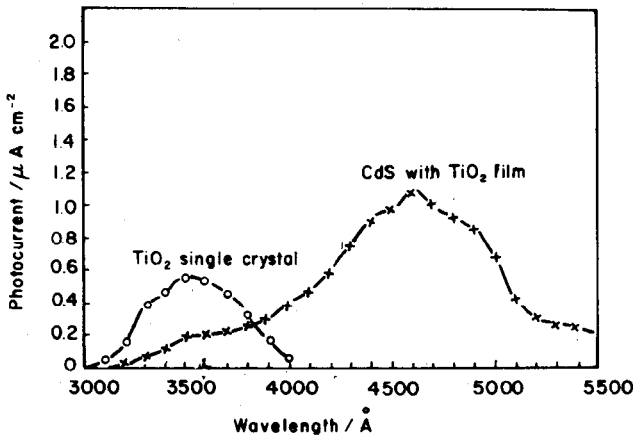

Figure 9. The effect of cladding on photoelectrochemical energy conversion.

the progress of that part of electrochemical technology which is associated with the new energy supply.

At the present time, electrochemical energy conversion via the photoelectrochemical decomposition of water is delayed by lack of stability of the electrodes. It may be that *cladding* is the future of this kind of system (Figure 9).[28]

Electrochemistry and light should be regarded as a new field (Figure 10).[29]

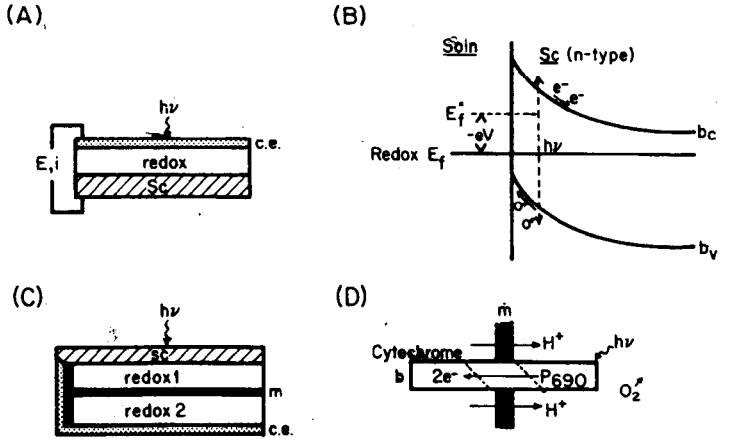

Figure 10. Electrochemistry and light: converters in a new field.

11. Biomedical Applications[30]

The breadth of potential application of electrochemical science in biology is so extensive that it is difficult to describe it fully. At the first symposium on electrochemistry and biology in medicine in 1953, Shedkovsky stated the following:

> The living cell is not only an assembly of chemical compounds. It is an oriented, dynamic system of complex materials in constant attraction with its environment, manufacturing many compounds no chemist has been able to synthesize, electrochemical in many, if not all, of its functions.

An electrodic version is in Figure 11.[31]

Table 2 shows some of the parts of electrochemistry in the biomedical sciences.

Membrane Potentials. Much bioelectrochemistry has been associated with membrane potentials. The most famous theory is that of Hodgkin and Katz.

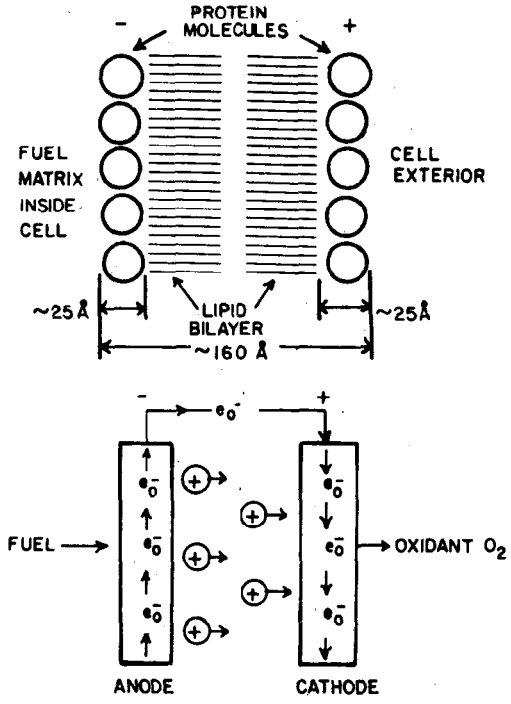

Figure 11. A simplistic electrodic model for the electrochemical aspects of cells.

Table 2
Electrochemistry in the Biomedical Sciences—Some Areas of Active Research

Electrophysiology	Energy metabolism	Cellular chemistry	Clinical medicine, surgery, and dentistry	Biomedical engineering
1. Rest potentials across membranes 2. Action potentials 3. Transport of ions and neutral molecules across membranes 4. Bilayer lipid membranes 5. Nerve conduction, excitation, and impulse 6. Synaptic and ephatic transmission 7. Neuromuscular functions 8. Neuroskeletal phenomena	1. Electron transfer and energy conservation 2. Phases, membranes, and electron transfer 3. Oxidative phosphorylation	1. Contributions of chemical groups to surface charge 2. Antigen–antibody reactions	1. Intravascular thrombosis 2. Bone healing and growth 3. Acupuncture 4. Iontophoresis 5. Cancer	1. Inactivation of pathogens 2. Microbial detection 3. Blood-gas determinations 4. Specific ion electrodes 5. Enzyme electrodes 6. Biochemical fuel cells 7. Energy sources for pacemakers and artificial hearts

Table 3
Anti-K_i^+/K_o^+ Evidence against the Diffusion Potential Theory[a]

I. Varied K_o^+ and did not obtain the expected results
  1. Ling, various old data
  2. Stampfli, node of Ranvier
  3. Tasaki, nerve fibers
  4. Schoffeniels, electroplate
II. Varied K_i^+ and did not obtain the expected results
  5. Grundfest, nerve fibers
  6. Baker, Hodgkin, and Shaw; Baker, Hodgkin, and Meves, nerve fibers
  7. Tasaki, Watanabe, and Takenaka; Tasaki and Shimamura; Tasaki and Takenaka; Tasaki, nerve fibers
  8. Falk and Gerard, muscle fiber
  9. Ling, soaked muscle
III. Natural variation of K_i^+/K_o^+
  10. Blinks, marine algae, *Valonia* and *Halicystis*
IV. Varied Ca_o^{2+} and other cations. All lower the emf
  11. Naitoh and Eckert
V. K_i^+ is bound to cytoplasmic material
  12. Nasonov; Aleksandrov; Tarusov; Troshin; Ling; Eisenman; Fischer and Hooker; Jahn; Dunham and Child; Cope; Ling

[a] From Jahn.[33] References for original papers may be obtained from Reference 33.

The evidence against this theory of membrane potentials is illustrated in Table 3.[33]

Thus when the potassium concentration outside the cell is varied, the potentials differ from those calculated by equations based on the membrane theory. Other difficulties exist as well.

More modern theories have been formulated for membrane potentials. Some of these are associated with electrodic aspects.[34]

The Metabolic Processes of Membranes. Mitchell's[35] theory for electrochemical reactions at membranes has been awarded a Nobel prize and involves some complicated processes concerned with proton transfers through membranes by carriers. His mechanism is summarized in Figure 12.[36]

A more explicitly electrodic theory, which has a more scientific basis, is also offered[36] in Figure 12. The essence of the difference in these two theories is that, in Mitchell's model, there are supposedly reversible electrochemical changes occurring at the membrane–solution interface, whereas, in fact, it is unlikely that processes carried out at rates in the region of those *observed in* metabolic processes will still be reversible. A purely electrode kinetic process, taking into account irreversibility in overpotential, seems to be a more competitive way of expressing the metabolic process.

The mechanisms of both Mitchell and of Bockris *et al.* are electrochemical.

Ion Transport through Membranes. Biological membranes are complex in structure and difficult to use in investigations. How do carriers help

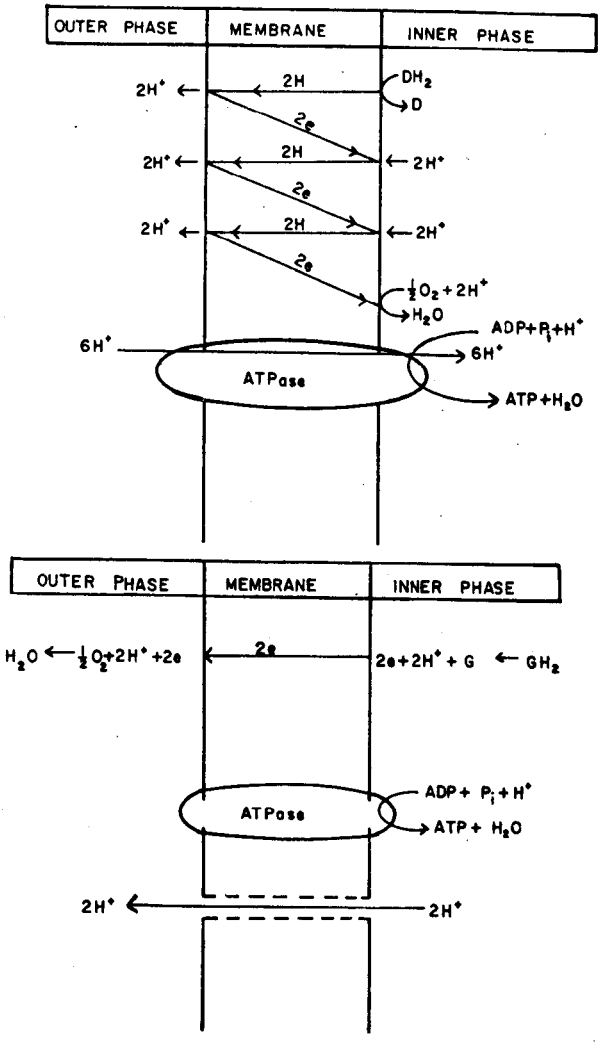

Figure 12. More detailed alternatives for metabolic functions. Top, Mitchell; bottom, Bockris and Tunnulli.

the transport of ions across membranes? An answer has been given by McLaughlin and Eisenberg.[37] The antibiotics valinomycin and actin are neutral carriers. Some antibiotics facilitate the transport of ions by other mechanisms. They cause an increase in the size of pores in the membranes. Antibiotics (e.g., gramicidin) produce discreet conduction steps across the membrane.[38]

Electron Transfer Reactions of Hemoproteins. Electron transfer reactions of hemoproteins have recently been studied by Jordan.[39]

Electrochemistry in Immunology. Immunology is the study of antigen–antibody reactions. Mathot, Rothen, and Cassals pioneered investigations in immunoelectroadsorption.[40] An antigen is first adsorbed on a metal slide. The slide is then dipped in a solution of metal–serum; owing to the immunological reactions, there is adsorption of antibodies from the solution onto the metal slide. The change in thickness of the film on the metal slide, measured by ellipsometry, indicates the extent of the immunological reaction (Figure 3).[5]

Thrombosis. Sawyer, Srinivasan, and co-workers[41–45] have demonstrated a correlation between thrombogenic properties of materials and their potential. If the material is more negative than −0.6, clotting will not take place upon it. Thus only corrodable metals and alloys are nonthrombogenic; noble ones are thrombogenic. This is a good example of what might be called "the negative principle."

There are correlations between the effect of drugs on the surface-charge characters through the vascular system and their anticoagulant properties. Both Srinivasan[46,47] and Stoner[48] have contributed to this field (Figures 13[49] and 14[48]).

Electrochemical reactions play a part in the complex coagulation factor; here, the ellipsometric techniques used by Sawyer and Srinivasan to detect the first platelet layers are useful.

Modification of rejection may also be improved by electrochemical considerations (Figure 15).[50]

Electrochemical Inactivation of Pathogens. An electrochemical process has been developed which is capable of destroying viruses.[51,52]

Electrochemical Destruction of Tumors. Rosenberg and Van Camp[53,54] have shown that when electric current is passed between platinum

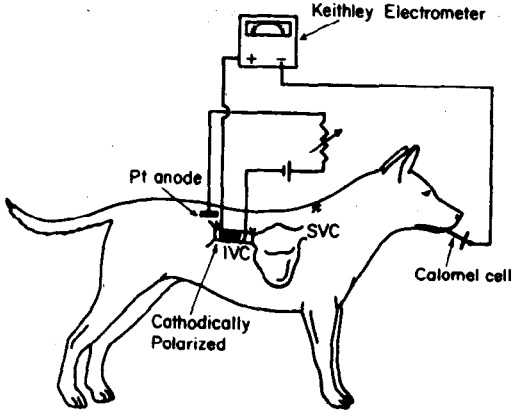

Figure 13. An arrangement for maintaining a copper prosthesis in a dog.

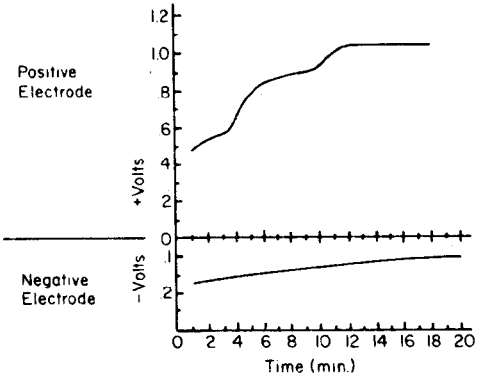

Figure 14. Potential–time relations in blood plasma. When the electrode is spontaneously negative, it changes little with time. When it is positive, it changes much, indicating thrombotic action.

electrodes in some cultures, cells did not divide, but continued to grow and form long filaments. With this background in mind, preliminary experiments were carried out on tumors responsive to electric currents.[55] Tumor destruction may be associated with the formation of HO_2^- (Reference 56) during the electrochemical reduction of oxygen.

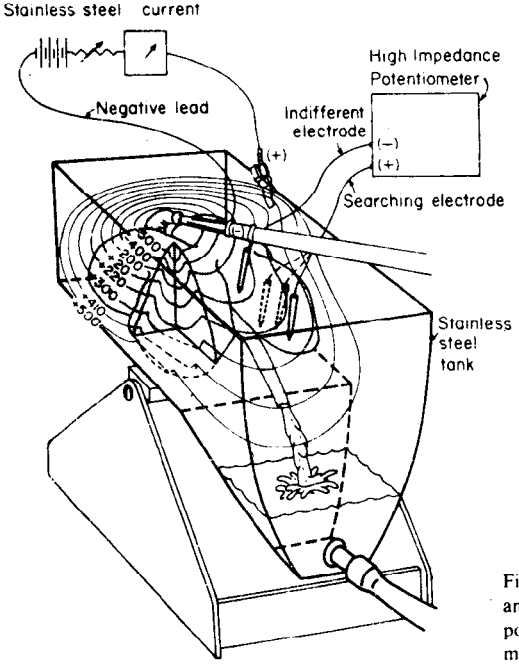

Figure 15. Addition of a battery, ammeter, and resistance modifies the potential of the surface of liver cells to modify rejection.

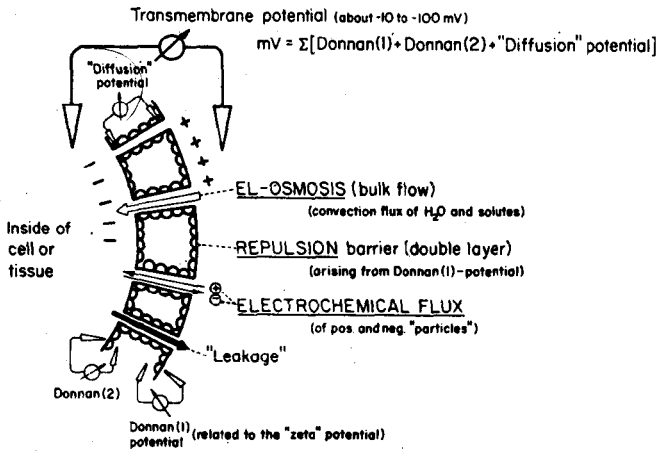

Figure 16. Some electrochemical events near a cell wall.

Some events at cell walls are shown in Figure 16.[57]

Biofuel Cells. The concept here is that one could use glucose and oxygen in the blood to keep the fuel cell working and, thus, produce electricity in the body which could power heart pacers or even a pump for the heart.[58,59,93]

Neurophysiology. In this field, the electrochemical view is central, but controversial. The new electrochemical view of such matters, electrode processes instead of concentration cells, has many commendable qualities. A gap in communication exists between the large group of electrophysiologists and clinicians (numbering hundreds of thousands) and the small group of electrochemists trained in modern concepts (numbering perhaps around one thousand). Nernst's equation and membrane potentials are known to the clinicians, but the Butler–Volmer equation and the concept of overpotential remain unknown.

Energy Metabolism. How is energy converted from that of the biochemical reaction in metabolism to a form which can be used by the organism? Szent-György[60] was the first to stress the role of electron transfer. The next step is to apply the electron transfer concept to free energy metabolism in terms of an electrochemical fuel cell, which may bring growth in understanding.

Photoinduced processes[61] for the biological production of hydrogen seem to be incipient (Figure 17).[62]

Healing. One of the more challenging problems in electrochemistry today is that of understanding the electrochemical mechanisms which control healing processes. A new era was opened by the experiments of Rosenberg and others[53,54] in cell division: The electrochemical mechanisms are not known. Pilla and Bassett[63] have recently shown that oscillating magnetic fields have therapeutic effects.

Homogeneous Test System for Light-Induced H_2 Production

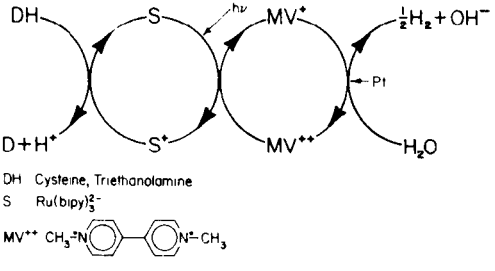

Figure 17. Scheme for photo-induced processes involving cysteine and ruthenium bipyridyl.

Medical Engineering. The development of glucose-driven pacemakers and improvements in renal dialysis are among numerous innovations which will be implemented in the near future. Electrochemical principles are involved in the choice of prosthesis.

12. The Electrodeposition of Materials from High-Temperature Melts

There are interesting areas here. Some have been investigated by Inman and Williams.[64]

1. *The recovery of metals from waste materials and unusual ores.* Refractory metals would be dissolved in a molten oxide solvent and recovered by electrodeposition. Processing a slag would be an illustration of this.

2. *Electrochemical processes at high temperatures.* Richardson has drawn attention to the disparity in the rates of the range of metallurgical processes. The electrowinning of aluminum occurs at 0.00005 ton m^{-3} min^{-1}. In an iron blast furnace, the rate is 0.004 ton m^{-3} min^{-1}.

There has been much attention focused on these facts in recent years, and a number of cell designs have been evolved. These have not yet been applied to high-temperature electrochemistry. For example, the development of bipolar electrodes for aluminum electrowinning is encouraging. The fluidized bed reactor developed by Fleischman is a good and important aspect.

3. *Direct reduction of sulfide ores to metals.*[64,65] Molybdenum production from molybdates might be viable. The anodic dissolution of metal sulfides in an aqueous medium is gaining importance. Sulfur is produced from the sulfide anode, releasing metal ions into the solution. Metal is extracted at the cathode. The alternative process, which utilizes a sulfide cathode to form the metal and release sulfide ions into the solution, is slow in aqueous media.

13. Mineral Processing

The innovative work of D. F. A. Koch and colleagues in the Australian CSIRO organization should be stressed. It is based on the studies of Ian Walk. There are many electrochemical aspects concerned with the field which have been brought out.

One example is the electrochemical model for the *in situ* oxidation of a nickel sulfide ore body. The oxidation of the ore occurs below the water table with the transfer of electrons at the air–water interface by the electronically conducting ore body. Reduction taking place at this interface is the reduction of oxygen. Oxidation leads to a series of oxidation products which depend upon depth and upon the oxidation potential (Figure 18).[66] It may be possible to predict the type of mineralization to be expected from a knowledge of the structure of the ore body.

Mining. Mining operations can be improved by applying electrochemistry in the preparation of drill tips which are spark free, thus minimizing the ignition of the ore. Schlain[67] has made progress in this area. This idea could be extended to the deposition of harder abrasive materials. For example, a range of deposits of zirconium boride on nickel can be made from fused salt deposition.

Beneficiation. The process by which a hydrophobic surface is produced into sulfide ores has been shown to be electrochemical in nature and can be studied by electrode kinetics. Two electrochemical reactions are involved—a

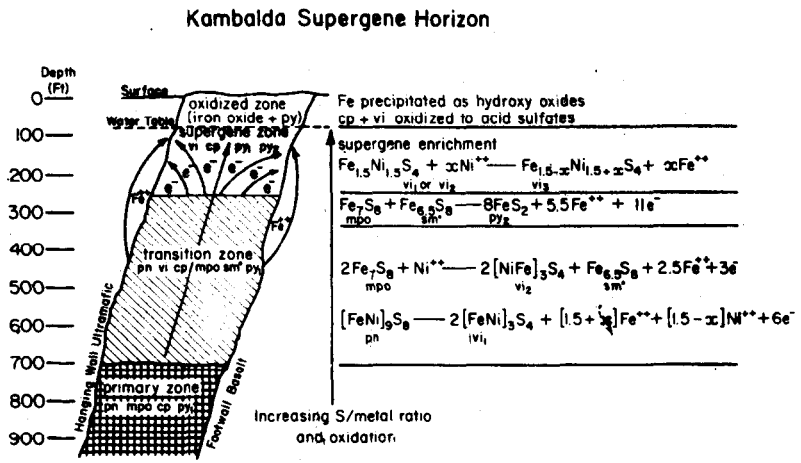

Figure 18. Electrochemical model for the *in situ* oxidation of a NiS ore body.

xanthate ion is oxidized, and oxygen is reduced[68]:

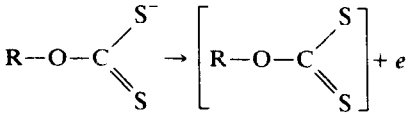

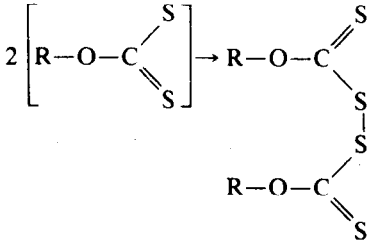

Empirical developments of flotation techniques have been successful in concentrating sulfides. Flotation will be applied to difficult ores. The problem of mineral liberation from the gangue must be overcome.

Processing. Pioneering studies[69,70,71] in the structure of liquid silicates have now developed into an understanding of how to make melts. The coordination complexes are now understood, and these will help to procure processes which do not produce sulfur dioxide. Thus, for example, the treatment of copper sulfides has received the greatest attention. The direct electrolysis of sulfides to form metal at the cathode and sulfur at the anode has been used commercially for nickel.

Summarizing Remarks on Mineral Processing in Electrochemistry. The extraction of materials from ores will be progressively more difficult. Probably half a century remains before recycling becomes essential. Meanwhile, it will become harder to obtain minerals which can be extracted easily; and here, electrochemistry sometimes becomes advantageous because of its extra selectivity in separation.

Furthermore, environmental considerations lead to the rejection of careless mineral extraction. Kuhn[72] says that the red mud produced during aluminum extraction at the bauxite-to-aluminum stage threatens the Mediterranean.

Electrochemistry offers a relatively clean technology in mineral processing. Such futuristic possibilities as the direct application of electricity from wind, nuclear, or solar power to ores which may be ground and the metal extracted in an electrochemical cell without a separate leaching process, are already past the initial discussion stage.

14. Electrocatalysis[73]

The future efficiency (hence, economics) of processes in electrochemical industry will depend upon electrocatalysis, not only with respect to the i_0 and, therefore, overpotential at a given i, but also with respect to lifetime.

For electrocatalysis at bare metals, the situation is affected by the electronic structure of the electrodes (Figure 19).[74] For oxygen reduction the exchange current density increases with the number of unpaired electrons, e.g., gold–palladium alloys. In fuel cell applications, small grains of Teflon-bonded platinum black is normal. How does the air-formed oxide differ from that produced anodically? Can a reactive surface be stimulated into highly controlled anodic growth?

Spillover Theories in Electrocatalysis. The theory by Bockris and McHardy[75,76] enables the interaction of two substances. For example, a fragment of tungsten bronze crystal on the underlying catalyst may act synergistically. Furthermore, in oxygen reduction, electron transfer to oxygen appears to be fastest upon a platinum catalyst (Figure 20),[76] and the subsequent radical reaction is faster upon the tungsten bronze substrate containing traces of platinum.

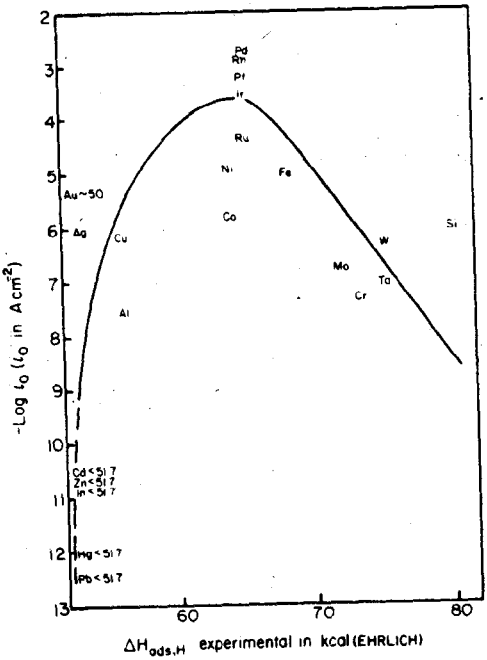

Figure 19. Although electrochemical catalysts are increasing semiconducting oxides, the effect of electronic structure is clearly seen in the log i_0–$\Delta H_{ads,H}$ relation.

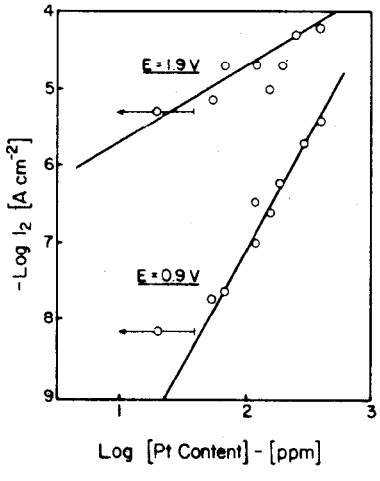

Figure 20. Log-log plots of catalytic activity vs. Pt concentration for oxygen evolution (1.9 V) and oxygen reduction (0.9 V), respectively.

The radicals "spill over" from the Pt onto the tungsten bronze substrate. If the substrate is not there, the radicals do not undergo such rapid subsequent reactions, so that the decomposition reaction of the radicals themselves (to water) becomes the rate-determining step (Figure 21).[76]

Conclusions Concerning the Future of Electrocatalysis. Since adsorption of a substance changes with its electronic character, it is reasonable to expect adsorption onto the substrate to have an effect. Electronic factors are important, but should not be considered apart from geometric factors. It would be interesting to investigate the effect of the deposition of a catalyst atom on the properties of supporting material. Ion implantation is a technique suited to give controlled dispersion of an electrocatalyst.

Titanium is the cheapest of the valve metals. Interesting electrodes often consist of deposits on this metal, e.g., deposits of ruthenium. From the hundred

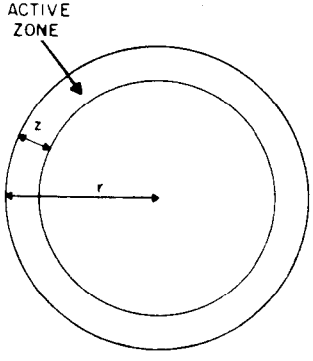

Figure 21. The spill-over model in the interpretation of the synergism of Pt tungsten bronzes.

elements in the periodic table, oxides of manganese, lead, cobalt, and tin seem to be of recurrent interest. Beer† patented titanium nitride as an electrode. Is there a future in this direction for non-noble metal anodes in acid solutions?

15. Material Conservation[78]

The future of humanity depends upon conservation and prevention of corrosion almost as much as it depends upon the replacement of finite fuel sources by machinery to convert renewable resources to useful fuels. The exhaustion of ores will mean recyclization and conservation of materials. Many essential metals will be exhausted within the time period covered in this chapter. Nuclear reactors require materials with increased corrosion resistance. The possibility of using fusion at all depends upon the solution of immense materials problems. Progress has not begun because of the absence of a suitable neutron source.

Many new concepts have been put forward by Mattson.[78]

One of the improvements in dealing with the electrochemistry of conservation will be computer-based retrieval of data. Stored information such as electrode kinetic constants will be available on an international basis by computer methods.

Electrochemical methods,[78] including the impedance technique, will play an increased role. Stress corrosion cracking, atmospheric corrosion, and wet and high-temperature corrosion will be of interest, along with studies of passivity. Construction materials consisting of high-strength–low-alloy steels, aluminum, titanium, and metal matrix composites will be advanced.

Control mechanisms of the future will have to involve nondestructive and remote sensing of corrosion. Polarization-resistance methods will prove useful. There should be an electrochemical technique for the determination of atmospheric corrosion rates. Accoustical methods can sometimes detect stress corrosion cracking in an early stage.

Electrochemical protection methods, cathodic or anodic, are important to develop. As indicated by Mattson[78] there is a decrease in interest in inhibitors which seem to be too risky sometimes. They decrease, but also increase, corrosion rates.

Quick, reliable nondestructive test methods are needed. New techniques[78] would permit the painting of steel underwater without prior cleaning. Aluminization could be an interesting alternative to zinc protection for steel.

16. Electro-organic Chemistry

As atomic and solar sources of energy come into action, an increasing proportion of energy available for chemical processes will be electrical.

† See Reference 77.

Electrochemical methods have advantages in this circumstance. The cost of energy will cause existing chemical processes to be examined in terms of the production of electricity as a by-product, a process which can be carried out electrochemically.

Environmental aspects will be of prime importance. Electrochemical methods are alternatives which contribute less noise and less thermal and chemical pollution than do the corresponding nonelectrochemical processes.

The versatility of electrochemical processes will give weight to their consideration. It is possible to get a different product from simple changes of potential in the same reactor.

Reduction of carbon dioxide must be mentioned as an interesting process for study. It may give rise to carbon monoxide, formic acid, formate, formaldehyde, and methanol and could have a profound influence on syntheses in the organic chemical industry.

Electropolymerization[79,80] appears to have an encouraging future. Although the electrode acts as an initiator, some electrode-dependent characteristics in the composition of polymers have been suggested. Economic factors make this one of the industrial frontiers of electrochemistry.

17. High-Temperature Electrolytes

One extremely interesting high-temperature electrolyte process is that of steam electrolysis (Figure 22).[81] It seems that in U_3O_8–Y_2O_3, Bevan, Badwall, Pound,[82] and others have found an electronically conducting electrode of great interest for high-temperature work.

Future applications of high-temperature electrolytes to technology include the use of melts as reaction media. Homogeneous reactions of high-temperature processes in which the gas phase is in contact with an inorganic melt have a substantial future.

An extention of the range of temperatures and pressure over that normally available may introduce new variety into the area. Gordon[83] draws attention to the positive side of fused organic salts, which have low melting points.

A melt can act as a catalyst. An alternative is to replace the fluid as the bed of solid material with a molten salt of high thermal conductivity. For example, the production of vinyl chloride by the chlorination of ethane in a zinc chloride–potassium chloride melt is an example of reactions where metals are obtained, compared with the use of the solid. Redox equilibria involving oxide ions are alternatives to proton transfer equilibria because of the attractive electrostatic environments for transition states.

Ionic melts may become important in hydrocarbon cracking. Halide melts at high temperatures have been used since 1959 for this purpose, and they offer advantages over solid state catalysts. Hydrocarbon cracking of coal and coal

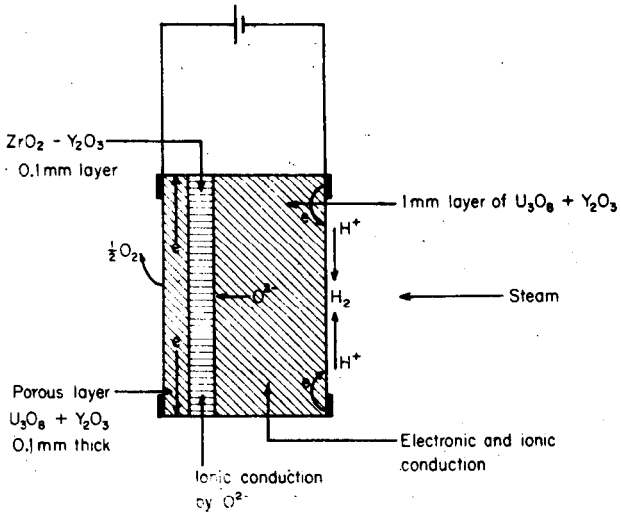

Figure 22. The high-temperature electrolysis of steam to hydrogen, using U_3O_8–Y_2O_3 as an electronically conducting electrode and ZrO_2–Y_2O_3 as the electrolyte.

extracts to produce high-octane gasoline in molten chlorides at 3500 psi H_2 and temperatures of 430°C is highly efficient.[84]

Finally, molten salt waste-disposal systems should be mentioned. They form an improved sewage treatment system,[85] and the molten salt reactor offers advantages over the fluidized bed incinerators. When organic wastes are not biodegradable, the molten salt incinerator may be useful, for it will have no end product except carbon dioxide.

The molten salt will affect our technology considerably; and, eventually, when the energy problem diminishes, the plentiful availability of solar and nuclear energy must, to use Tomlinson's phrase,[86] "color the spectacles with which high temperature processes are viewed."

18. Electrochemistry of Cleaner Environments

Electrodialysis.[87,88] Many electrodialysis stacks are now used for the purification of liquids. For example, copper cyanide may be thus removed from waste liquors.[89]

Electroflotation.[90,91] Electroflotation is used, for example, for scouring liquors from yarn or for dealing with abattoir wastes, etc.[92]

The use of this technique is widespread and includes application to effluents in the lead industry and to manganese-containing slurries.

Electrochemical Treatments.[92] Electrophoresis, electro-endosmosis, and electrofiltration are all methods which exemplify applications of electrochemistry in purification procedures.

Cathodic Deposition of Metals.[92] Metals are broken down into three groups[93]: (1) gold, silver, copper, tin, cadmium, zinc, mercury, arsenic, and antimony; (2) nickel, cobalt, and chromium (difficult deposition); and (3) aluminum and titanium (deposition is not possible).

19. Electrochemistry for a Better World[94]

It is relevant to summarize the overall situation.

The Energy Industries. Society in the 21st century will rely on nuclear, solar, and wind energy and perhaps geothermal sources, as well as coal, if the pollutional character of the latter can be alleviated. Energy will be in the form of electricity and hydrogen.

While fossil fuel energy is available, fuel cells will find application.[95] They will be based upon the carbonate or acid system. Technological and cost problems associated with the molten carbonate fuel cells will be less important than the problems of development of high-temperature solid oxides.

Electrolyzers will be important.[94] A more recent design of electrolyzers is shown in Figure 23.[96] There is a need for surface-catalyzed nickel, operating at the thermoneutral potential, at 70 bar and 130°C and with KOH-resistant separators.

A stable fluorinated, sulfonated acid membrane is important.

Low-temperature electrolysis will supply hydrogen at about 30% efficiency, if there is no nuclear source, or 38% using a high-temperature source.

Thermochemical reactions will probably not be used, since they do involve Carnot cycles and are no more efficient than is the production of electrical energy by means of a heat engine.

Transportation.[97] For short-distance, urban or rural travel, the fuel cell battery vehicle will dominate. If hydrogen is piped over long distances, the battery vehicle will be at a disadvantage. Fuel cells may find a place in heavy intercity road vehicles when railways are impractical. However, rail systems will return to importance and be electrically driven, for they give a far lower cost per passenger mile than other methods.

Electrochemical systems will count for most of the transportation of the time period we are talking about.

A related area, in which electrochemistry will be of prime importance, is that of telecommunications which depend upon batteries. The batteries which are likely for traction are given in Table 4.[94]

High-temperature batteries are in the early stage of development and are illustrated in Figure 24.[94]

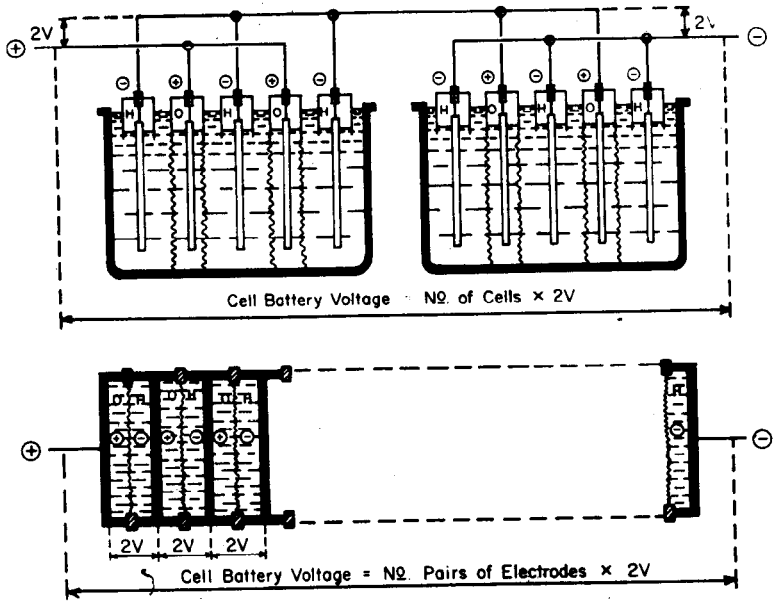

Figure 23. Two examples of simple electrolyzers.

Alternative battery concepts[94] involve use of solid materials with liquid or solid electrolytes. Concepts involving iron sulfide in union with lithium in a chloride eutectic are of interest, as are nickel–zinc chloride systems.

Fuel Cells and Transportation. Fuel cells, hydrogen or metal–air type, are attractive from the viewpoint of convenience, because they can be

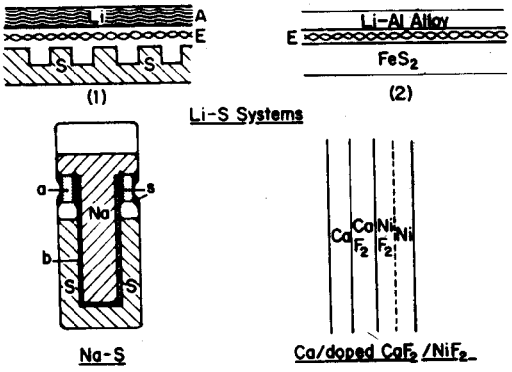

Figure 24. High-temperature batteries in an early stage of development.

Table 4
Ambient-Temperature Secondary Cells for Traction

Couple	Relative cost	Wh/kg (1-hr rate)	Peaking capability[a]	Cycle life	Efficiency	Problems
Pb/PbO_2	1	30	+	~500	~60	Poor energy density
Ni/Zn	3	65	++	500+		Zn cycle life
Ni/Fe	3	40	+	1000+	~50	Poor energy density
Ni/H_2	>3	65	++	2000+	~65	Cost (H_2 electrode, pressure vessel)
O_2/Zn (a)	High	120	++	500+[b]	50	Zn cycle life; cost (O_2 electrode, pressure vessel)
O_2/Zn (b)	?1–2[b]	100	–	500+[b]	~40	Zn cycle life, O_2 electrode, efficiency, carbonation
O_2/Fe	?1–2	70	–	1000+	<30	Very poor efficiency, O_2 electrode, carbonation
Cl_2/Zn	?	?110	++	?	65	Materials

[a] ++, Very good; +, good; –, poor.
[b] Future.

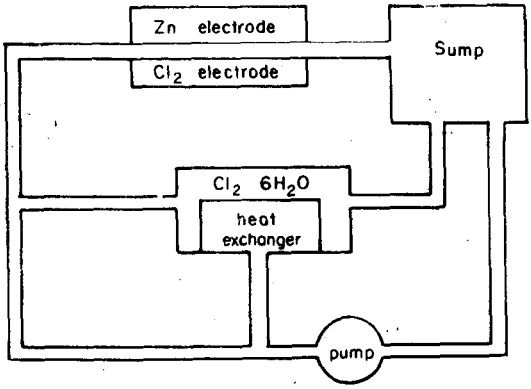

Figure 25. A version of the zinc–chlorine fuel cell.

replenished. They must go about 200 km between charges and allow a car to have a cruising speed of 80 km/hr, with short distances at 100 km/hr.

Zinc–chlorine systems go a long way to meet these requirements.

Some relevant fuel cells are illustrated in Figure 25.[98]

Industrial Processes. Since the media of energy in the future will consist of electricity from hydrogen, electrolytic processes will replace many thermal processes. Electrochemical processes can eliminate the energy required for separation of constituent ores and the energy loss associated with rejection of slag material. Iron ores will be reduced by hydrogen when this is cheaply available from coal (or via the solar-hydrogen route). The spongy iron thus produced will separate from mineral matter in electrochemical reactors. Electroflotation will be increasingly used.

Electrochemical processes will be important in the field of organic synthesis because of high yield, a wider free energy range, and fewer reaction steps.

Electrochemistry in the Life Sciences. Implanted fuel cells, which use compounds from the blood such as glucose, give the possibility of permanent control devices to influence health. The most ambitious objective is a biological fuel cell which would drive a mechanical pump to replace the heart.[94,99]

Electrochemistry can be used for understanding biological processes. On this basis, a relation between electrochemistry and biochemistry becomes clear, particularly in photosynthesis and the respiratory cycle. Biochemical energy conversion probably proceeds by electrochemical mechanisms.[34]

Summary. (1) Electrochemistry introduces a new principle—the absence of Carnot efficiency loss (Figure 26).[100] The consequent indications for energy conversion in transportation and industry are considerable.

(2) Electrochemical applications would tend to allow recycling and cleaner extractions than do chemical methods. An economy based on hydrogen

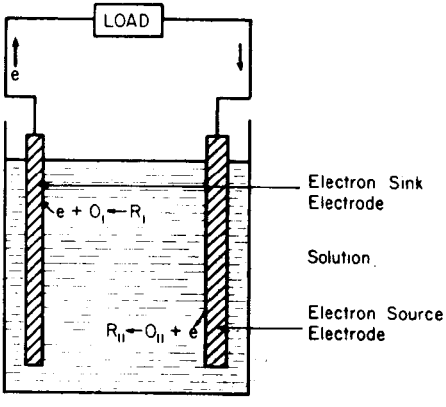

Figure 26. The electrochemical energy converter (fuel cell). Conversion of energy in it does not suffer the Carnot loss.

as a fuel source represents a particularly desirable foundation for future technology.

(3) Electrochemistry is the basis for conservation of materials in air.

(4) Electrochemical processes underlie many interfacial biological processes.

(5) Some (perhaps many) naturally occurring processes seem to take place via fuel-cell-type local electrochemical reactions. Electrochemistry is "the other chemistry." It is speculatively suggested that, numerically, electrochemical reactions in nature outweigh chemical reactions.

(6) Tens of percent of the chemical industry is electrochemical. Less than 1% of new Ph.D. chemists are electrochemists.

20. Borderline Phenomena

There are many borderline phenomena which are sources of confusion for classical scientists, who usually demand that, to be credible, a phenomenon must be reproducible in the laboratory at will. Some sporadically observed phenomena are now being accepted into science, at least as far as phenomenology is concerned; and one of them, telepathy, is accepted as a fact by most scientists, although models are blank. An article on "remote viewing" has been published in *Nature*.[101]

Biological systems operate by a series of electrochemical mechanisms. The relevance to information transfer over long distances is that these electrochemical systems (biological systems) interact with magnetic fields. This has been demonstrated directly by Pilla and Bassett.[63]

Thus the basis of many cyclical phenomena in which biological phenomena follow the variation of, e.g., sun spots and other cyclical happen-

ings in the surrounding space, may lie in considering biological cells as electrochemical entities and relating their behavior to the magnetic and electrical variations in the environment.

21. Lack of Training in Electrochemistry

Electrochemistry is a large basic interdisciplinary area with great relevance to near-future technology. Training remains extremely limited. The average engineer is not yet conscious of electrochemical reactions and would be hard-put to define "overpotential." The solution to this problem lies in articles which can make people aware of the economic and social reasons for turning to electrochemical methods. Such a realization would in turn eventually influence the availability of education and training in electrochemistry.

References

1. G. M. Woodwell, *Sci. Am.* **238**(1), 37 (1978).
2. J. O'M. Bockris, *J. Electroanal. Chem.* **9**, 408 (1965).
3. L. I. Antropov, *Theoretical Electrochemistry*, Mir Publishers, Moscow (1972), p. 5.
4. J. O'M. Bockris and A. K. N. Reddy, *Modern Electrochemistry*, Vol. 1, Plenum Press, New York (1970), p. 27.
5. J. O'M. Bockris, A. Damjanovic, and W. E. O'Grady, *J. Colloid Interface Sci.* **34**(3), 390 (1970).
6. J. O'M. Bockris and L. Handley, *Energy Research*, Vol. 2, John Wiley and Sons, New York (1978), p. 296.
7. L. Lessing, in *Chemistry in the Environment*, Freeman, San Francisco (1973), p. 159.
8. G. Wenglowski, in *Modern Aspects of Electrochemistry*, Vol. 4, J. O'M. Bockris, ed., Plenum Press, New York (1966), pp. 251–306.
9. J. O'M. Bockris, ed., in *Trends in Electrochemistry*, Plenum Press, New York (1977), pp. 1–6.
10. M. A. Elliot and N. C. Turner, paper presented to the American Chemical Society, Boston (1972).
11. J. O'M. Bockris, *Energy: The Solar-Hydrogen Alternative*, Australia and New Zealand Book Co., Sydney (1975), p. 33.
12. J. O'M. Bockris, *Energy: The Solar-Hydrogen Alternative*, 2nd ed., Halstead Press, New York (1980), Chap. 4.
13. K. Sekihara, in *Environmental Chemistry*, J. O'M. Bockris, ed., Plenum Press, New York (1977), pp. 285–311.
14. J. O'M. Bockris and S. Srinivasan, *Fuel Cells*, McGraw-Hill, New York (1969), pp. 625–632.
15. J. O'M. Bockris and A. K. N. Reddy, *Modern Electrochemistry*, Vol. 2, Plenum Press, New York (1970), p. 1366.
16. J. O'M. Bockris, *Energy: The Solar-Hydrogen Alternative*, Australia and New Zealand Book Co., Sydney (1975), pp. 89–92, 259.
17. A. J. Appleby, in *Electrochemistry. The Past Thirty and the Next Thirty Years*, Harry Bloom and Felix Gutmann, eds., Plenum Press, New York (1977), p. 53.
18. A. J. Appleby, in *Trends in Electrochemistry*, J. O'M. Bockris, ed., Plenum Press, New York (1977), pp. 71–73.
19. J. O'M. Bockris, *Search* **4**, 144 (1973).

20. J. O'M. Bockris, ed., *Trends in Electrochemistry*, Plenum Press, New York (1977), pp. 79–109.
21. A. T. Kuhn, in *Electrochemistry of Cleaner Environments*, J. O'M. Bockris, ed., Plenum Press, New York (1972), pp. 123–128.
22. R. M. E. Diamant, in *Environmental Chemistry*, J. O'M. Bockris, ed., Plenum Press, New York (1977), pp. 95–119.
23. H. G. Schlegel, ed., *Fermentation Advances*, Academic Press, New York (1969).
24. J. O'M. Bockris and J. McHardy, University of Pennsylvania, 1971, patent submitted.
25. J. O'M. Bockris, ed., *Environmental Chemistry*, Plenum Press, New York (1977), pp. 605–615.
26. J. O'M. Bockris and B. D. Cahan, *J. Chem. Phys.* **50**, 1307 (1969).
27. J. O'M. Bockris, ed., in *Environmental Chemistry*, Plenum Press, New York (1977), pp. 583–604.
28. J. O'M. Bockris and K. Uosaki, *Energy* **1**, 95 (1976).
29. A. J. Appleby, in *Trends in Electrochemistry*, J. O'M. Bockris, ed., Plenum Press, New York (1977), p. 67.
30. S. Srinivasan, G. L. Cahen, Jr., and G. E. Stoner, in *Electrochemistry. The Past Thirty and the Next Thirty Years*, Harry Bloom and Felix Gutmann, eds., Plenum Press, New York (1977), pp. 57–84.
31. M. Del Ducca and K. Fucsoe, *Int. J. Sci. Technol.* **1** (March, 1965).
32. A. L. Hodgkin and B. Katz, *J. Physiol.* **108**, 37 (1949).
33. T. L. Jahn, *Bioelectrochem. Bioenerget.* **1**, 441 (1974).
34. J. O'M. Bockris and S. Srinivasan, *Nature* **215**, 197 (1967).
35. P. Mitchell, *Nature* **191**, 144 (1961).
36. J. O'M. Bockris and M. S. Tunuli, *J. Electroanalyt. Chem.* **3**, 139 (1979).
37. S. McLaughlin and M. Eisenberg, *Ann. Rev. Biophys. Bioeng.* **4**, 335–366 (1975).
38. S. B. Hladky and D. A. Haydon, *Nature* **225**, 451 (1970).
39. J. Jordan, in *Proceedings of a Workshop in Bioelectrochemistry, Princeton, New Jersey*, October 10–14, 1971, A. A. Pilla, ed., National Science Foundation, Washington, D.C. and ESB Inc. Technology Center, Yardley, Pennsylvania (1971), pp. 103–122.
40. C. Mathot, A. Rothen, and J. Cassals, *Nature* **202**, 1181 (1964).
41. P. N. Sawyer, ed., *Biophysical Mechanisms in Vascular Homeostasis and Intravascula Thrombosis*, Appleton-Century-Crofts, New York (1965).
42. S. Srinivasan and P. N. Sawyer, *J. Colloid Interface Sci.* **32**, 456 (1970).
43. S. Srinivasan, L. Duic, N. Ramasamy, P. N. Sawyer, and G. E. Stoner, *Ber. Bunsenges. Phys. Chem.* **77**, 798 (1973).
44. P. N. Sawyer and S. Srinivasan, *Bibl. Anat.* **12**, 106 (1973).
45. N. Ramasamy, J. T. Keates, S. Srinivasan, and P. N. Sawyer, *Bioelectrochem. Bioenerget.* **1**, 244 (1974).
46. S. Srinivasan and B. R. Weiss, in *Colloid Dispersions and Micellar Behavior*, K. L. Mittal, ed., ACS Symposium Series No. 9, American Chemical Society, Washington, D.C. (1975), Chap. 24.
47. S. Srinivasan and P. N. Sawyer, in *Electrochemical Bioscience and Bioengineering*, H. T. Silverman, I. F. Miller, and A. J. Salkind, eds., Electrochemical Society, Princeton, New Jersey (1973), pp. 17–36.
48. S. Srinivasan, G. L. Cahen, Jr., and G. E. Stoner, in *Electrochemistry. The Past Thirty and the Next Thirty Years*, Harry Bloom and Felix Gutmann, eds., Plenum Press, New York (1977), p. 79.
49. E. Gileadi, B. Stanczewski, A. Parmeggiani, T. R. Lucas, M. Ranganathan, S. Srinivasan, and P. N. Sawyer, *J. Biomed. Mat. Res.* **6**, 489 (1972).
50. P. N. Sawyer, B. Stanczewski, N. Ramasamy, D. V. Raman, W. Wrzlewicz, I. Parsa, J. Pindyck, S. L. Kountz, and K. Butt, *J. Electrochem. Soc.* **123**(10), 1446 (1976).
51. G. E. Stoner, U.S. Patent 3,725,226.

52. G. E. Stoner, G. L. Cahen, Jr., and J. Parcells, presented at the Spring Meeting of the Electrochemical Society, Toronto, Canada, May 1975; *J. Electrochem. Soc.* **122**, 106C (1975).
53. *Medical World News* 40U (May 7, 1971).
54. B. Rosenberg and L. Van Camp, private communication, 1975.
55. S. Srinivasan, A. Ofodile, T. R. Lucas, E. C. Ateyeh, E. Ahrens, S. Jacobson and R. Redner, unpublished.
56. H. L. Gray, *Am. J. Roentgenol.* **85**, 803 (1961).
57. T. Teorell, in *Biophysical Mechanisms in Vascular Homeostasis and Intravascular Thrombosis*, P. N. Sawyer, ed., Appleton-Century-Crofts, New York (1965), pp. 19–29.
58. J. R. Rao and G. Richter, *Naturwissenschaften* **61**, 200–206 (1974).
59. J. R. Rao, G. Richter, F. von Sturm, E. Weidlich, and M. Wenzel, *Biomed. Eng.* **9**(3), 98–103 (1974).
60. A. Szent-Györgyi, *Bioelectronics*, Academic Press, New York (1968).
61. G. Neil, D. J. D. Nicholas, J. O'M. Bockris, and J. F. McCann, *Int. J. Hydrogen Energy* **1**, 45–58 (1976).
62. K. Kalayanasundaram and M. Grätzel, *Helv. Chim. Acta* **61**(256), 2730 (1978).
63. A. Pilla and B. Bassett, Gordon Conference, Santa Barbara, California, 1979.
64. D. Inman and D. E. Williams, in *Electrochemistry. The Past Thirty and the Next Thirty Years*, Harry Bloom and Felix Gutmann, eds., Plenum Press, New York (1977), pp. 273–284.
65. F. Habashi, *Miner. Sci. Eng.* **3**(3), 3 (1971).
66. M. R. Thornber, Newcastle Conference 1972, Australasian I.M.M., 1972, pp. 51–58.
67. D. Schlain, F. X. McCawley, and C. Wyche, *J. Electrochem. Soc.* **116**, 1227 (1969).
68. D. F. A. Koch and B. J. Welch, in *Electrochemistry. The Past Thirty and the Next Thirty Years*, Harry Bloom and Felix Gutmann, eds., Plenum Press, New York (1977), p. 302.
69. J. O'M. Bockris and D. C. Lowe, *Proc. R. Soc. London Ser.* A **226**, 423 (1954).
70. J. O'M. Bockris, J. D. Mackenzie and J. A. Kitchener, *Trans. Faraday Soc.* **51**, 1734 (1955).
71. J. W. Tomlinson, J. L. White and J. O'M. Bockris, *Trans. Faraday Soc.* **52**, 299 (1956).
72. A. T. Kuhn, in *Electrochemistry. The Past Thirty and the Next Thirty Years*, Harry Bloom and Felix Gutmann, eds., Plenum Press, New York (1977), p. 311.
73. A. Damjanovic and A. T. Ward, in *Electrochemistry. The Past Thirty and the Next Thirty Years*, Harry Bloom and Felix Gutmann, eds., Plenum Press, New York (1977), pp. 89–116.
74. G. Ehrlich, in *Proceedings of the Third Congress on Catalysis*, W. M. H. Sachtler, C. G. A. Schuit, and P. Zwietering, eds., North-Holland, Amsterdam (1965); *J. Chem. Phys.* **31**, 1111 (1959).
75. J. McHardy and J. O'M. Bockris, *J. Electrochem. Soc.* **120**, 53 (1973).
76. J. McHardy and J. O'M. Bockris, *J. Electrochem. Soc.* **120**, 61 (1973).
77. A. T. Kuhn, in *Electrochemistry. The Past Thirty and the Next Thirty Years*, Harry Bloom and Felix Gutmann, eds., Plenum Press, New York (1977), p. 170.
78. E. Mattson, in *Electrochemistry. The Past Thirty and the Next Thirty Years*, Harry Bloom and Felix Gutmann, eds., Plenum Press, New York (1977), pp. 239–256.
79. James W. Johnson, in *Electrochemistry. The Past Thirty and the Next Thirty Years*, Harry Bloom and Felix Gutmann, eds., Plenum Press, New York (1977), pp. 257–263.
80. G. Parravano, in *Organic Electrochemistry*, M. Bazier, ed., Marcel Dekker, New York (1973), pp. 947–974.
81. J. Bevan, H. Singh, and J. O'M. Bockris, unpublished.
82. J. Bevan, S. Badwall, and B. Pound; cf. S. Badwall, Ph.D. thesis, Flinders University, 1978.
83. J. E. Gordon, in *Techniques and Methods of Organic and Organometallic Chemistry*, Vol. I, D. B. Denney, ed., Marcel Dekker, New York (1969).
84. C. W. Zielke *et al.*, *Ind. Eng. Chem. Proc. Res. Dev.* **8**(4), 546 (1969).
85. L. Lessing, *Fortune*, 138 (July 1973).
86. J. W. Tomlinson, in *Electrochemistry. The Past Thirty and the Next Thirty Years*, Harry Bloom and Felix Gutmann, eds., Plenum Press, New York (1977), p. 348.

87. J. O'M. Bockris, ed., *Electrochemistry of Cleaner Environments*, Plenum Press, New York (1972).
88. A. T. Kuhn, ed., *Industrial Electrochemical Processes*, Elsevier, Amsterdam (1971).
89. Environmental Protective Administration Investigation of Treatment of CN Waste by ED, U.S. Government EPA Grant Project 12010 DFS to RAI Corp.
90. J. O'M. Bockris and B. E. Conway, eds., *Modern Aspects of Electrochemistry*, Vol. 8, Plenum Press, New York (1972).
91. A. T. Kuhn, *Chem. Proc. (London)* **20**, 9–12 (June 1974); **20**, 5–7 (July 1974).
92. A. T. Kuhn, in *Electrochemistry. The Past Thirty and the Next Thirty Years*, Harry Bloom and Felix Gutmann, eds., Plenum Press, New York (1977), pp. 355–371.
93. B. R. Surfleet, paper presented at the Symposium on Electrochemical Methods for Environmental Control, University of Salford, 1973.
94. A. J. Appleby, in *Electrochemistry. The Past Thirty and the Next Thirty Years*, Harry Bloom and Felix Gutmann, eds., Plenum Press, New York (1977), pp. 373–392.
95. J. O'M. Bockris and S. Srinivasan, *Fuel Cells*, McGraw-Hill, New York (1969), pp. 357–411.
96. A. K. Stuart, paper presented at the American Chemical Society Symposium on Non-Fossil Fuels, Boston, 13 April 1972.
97. J. O'M. Bockris, *Energy: The Solar-Hydrogen Alternative*, Australia and New Zealand Book Co., Sydney (1975), pp. 282–301.
98. P. C. Symons, Extended Abstracts, Conference on Electrolysis for Power Sources, Society for Electrochemistry, Brighton, England, December 13–14, 1973.
99. A. J. Appleby, D. Y. C. Ng, and H. Weinstein, *J. Appl. Electrochem.* **1**, 79 (1971).
100. J. O'M. Bockris, *Pure Appl. Chem.* **47**, 30 (1976).
101. R. Targ and H. E. Puthoff, *Nature* **252**(5476), 602–607 (1974).

2

Electrochemical Energy Conversion—Principles

B. V. TILAK, R. S. YEO, and S. SRINIVASAN

1. Introduction

1.1. Historical Background of Fuel Cells

The history of fuel cells, since their discovery by Sir William Grove in 1839 and until the early fifties, has been covered in great detail in several publications.[1-10] The main impetus to fuel cells was in the late fifties when known solar, nuclear, and chemical conversion systems were being considered as power sources for NASA's space programs. These were rated with respect to weight, reliability, safety, power capability, and tolerance to the mission environmental profile. The fuel cell system ranked best, which resulted in the development of the General Electric solid polymer electrolyte fuel cells for the Gemini Space Program and the Pratt and Whitney alkaline (Bacon-type) fuel cell for the Apollo flights in the sixties. The potential advantages of fuel cells stimulated an enthusiastic research and development program on fuel cells for terrestrial applications, in addition to space applications. However, because of the high cost of fuel cells, noble metal requirements, and short life, the interest in fuel cells for terrestrial applications declined in the late sixties. Fuel cell

B. V. TILAK • Hooker Chemical Corporation, Research Center, Grand Island, New York 14072. **R. S. YEO and S. SRINIVASAN** • Department of Energy and Environment, Brookhaven National Laboratory, Upton, New York 11973.

activity was revived in the early seventies and was greatly enhanced in 1973 after the energy crisis, mainly for electric power generation.

1.2. The Energy Conversion Methods: Advantages and Disadvantages of Fuel Cells Over Other Methods

One of the forms of energy most frequently required is electricity, which should be obtained from one of the primary energy sources—chemical, nuclear, solar, or gravitational. The conventional methods of energy conversion, apart from hydroelectric, involve the intermediate conversion of heat to mechanical energy, the efficiency of which is Carnot limited. The space program stimulated an examination of direct energy conversion methods (i.e., thermoelectric, thermionic, photovoltaic, magnetohydrodynamic, and fuel cells), from the point of view of the requirements of simplicity, reliability, and lessened weight. The main advantage of fuel cells over all other methods of energy conversion is that chemical energy is converted directly to electrical energy, and its efficiency is not limited by Carnot's theorem. Thus the demonstrated efficiencies of fuel cells are considerably higher than those of other energy conversion methods (Table 1). The other advantages of fuel cells include (i) simple operation compared to other energy conversion devices, (ii) clean, quiet operation (the exhaust gases from fuel cells are not noxious and are non pollutant), (iii) adaptability to operate over any desired temperature range, (iv) siting flexibility because of modularity (cells can be made in any shape or size), and (v) multifuel capability.

1.3. Types of Fuel Cells and the Most Promising Systems

Several types of fuel cells have been or are being investigated at the present time. These may generally be classified as shown in Figure 1, with a

Table 1
Demonstrated Efficiencies[a] of Direct Energy Conversion Devices

Energy converter	% Efficiency
Thermoelectric	10
Thermionic	22
Photovoltaic	18
Magnetohydrodynamics	60
Low-temperature fuel cells	60
High-temperature fuel cells	60
Gas turbines	30
Internal combustion engines	30
Diesel engines	40

[a] Highest efficiencies reported for energy converters.

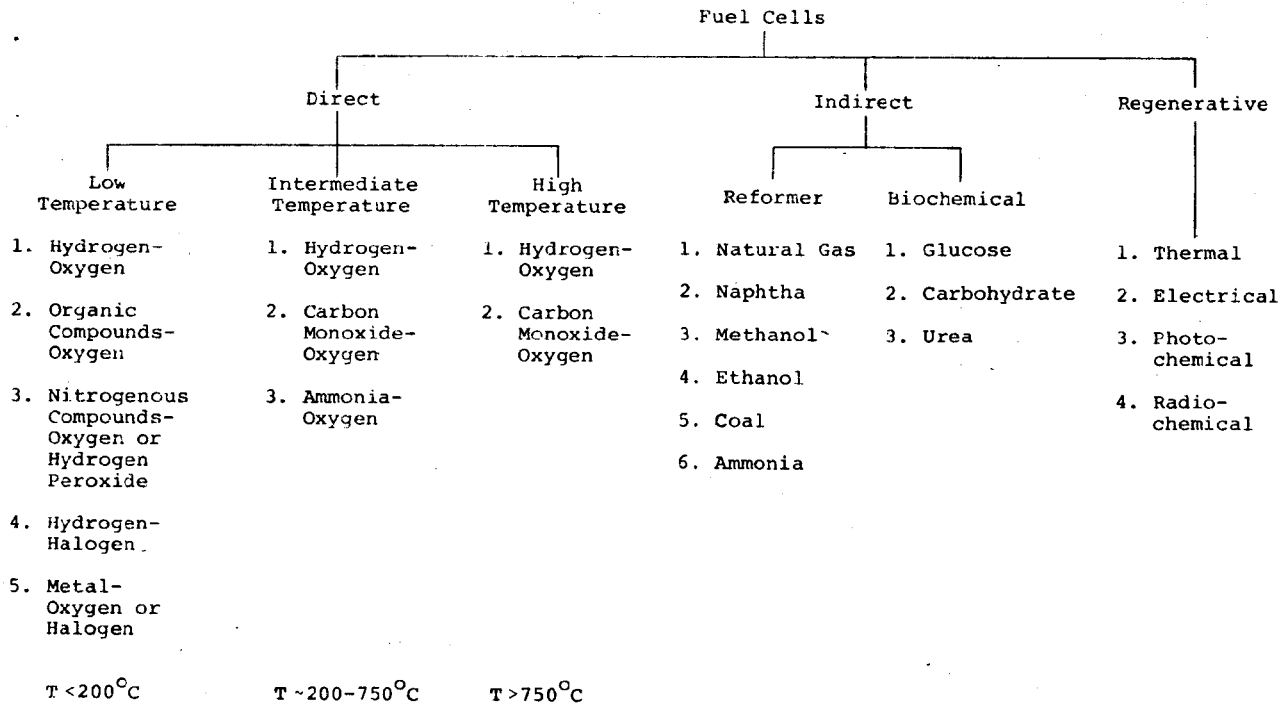

Figure 1. Classification of fuel cells.

broad distinction between direct and regenerative fuel cells, which are similar to primary and secondary batteries. A third type is the indirect fuel cell, under which one may categorize reformer and biochemical fuel cells. A subdivision, under the direct type, may be based on the temperature at which the fuel cell operates, the scheme adopted being: low <200°C, medium 200–750°C, and high >750°C. A variety of fuels have been tested and their classification is also shown in Figure 1. Oxygen, either pure or as in air, is the oxidant in practically all fuel cell systems. In a few cases, halogens or hydrogen peroxide play this role. A classification, not shown in Figure 1 is the type of electrolyte. The promising electrolytes are acid (H_3PO_4, RSO_3H), alkali (KOH), molten carbonate (Li^+, K^+, Na^+, CO_3^{2-}), and solid oxide (ZrO_2–Y_2O_3).

The essential criteria, which have to be examined, in considering fuel cells for space or terrestrial applications are (i) efficiency, (ii) power/weight ratio, (iii) power/volume ratio, (iv) life expectancy, (v) cost, and (vi) reliability. All these factors, except perhaps cost, are important for space applications, whereas for terrestrial power generation and transportation applications, efficiency, cost, and life expectancy are of greatest concern.

The hydrogen–oxygen fuel cells, with a solid polymer electrolyte or alkaline electrolyte, have been demonstrated to be the most promising systems for space applications. For electric utility power generation, hydrogen(derived from natural gas, petroleum, or coal)–air fuel cells with phosphoric acid, molten carbonate, or solid electrolyte are the strong contenders. Because of problems connected with low catalytic activities, direct hydrocarbon–air fuel cells have a low chance of success. For transportation applications, it is necessary to convert the chemical energy of petroleum-derived or coal-derived fuels to mechanical energy, directly or via electricity. The only type of energy converter in which the efficiency is not Carnot limited for converting chemical energy to mechanical energy is the fuel cell, coupled with a motor. For this application, the fuel will desirably be in a liquid form (e.g., methanol), and the power plant will probably consist of a reformer and an acid (H_3PO_4 or RSO_3H) fuel cell.

1.4. Role of Electrochemical Energy Conversion in Efficient Utilization of Primary Energy Sources

The primary energy sources are (i) fossil fuels, (ii) nuclear energy, (iii) solar energy, and (iv) gravitational energy. The energy crisis of 1973 has surfaced the realization of the dwindling reserves of the fossil fuels (petroleum, natural gas, and coal). There is a great awareness at the present time of the need to use fossil energy in the most efficient manner, be it for electric utility power generation, for providing thermal energy (heating, hot water, process heat), or for transportation. For electric utility power generation, a system consisting of a fuel conditioner, fuel cell (with phosphoric acid, molten carbonate, or solid oxide as electrolyte), and power conditioner is projected to have the highest efficiency

for utilization of fossil energy. The total energy concept with a fuel cell (i.e., for the fuel cell to provide electricity and heat) appears to be an attractive scheme for energy conservation of fossil fuels, particularly for apartment buildings, industries, and shopping centers.

Nuclear power plants will provide electricity at an increasing level, particularly in countries which lack fossil fuels. However, from an environmental point of view, large nuclear power plants will be located in remote sites, and non-nuclear power plants will provide the necessary electric power in dispersed sites in cities and towns. A scheme, which shows promise, will be to electrolyze water and transmit hydrogen via pipelines to the dispersed sites for utilization in fuel cells. Since this hydrogen will be free of CO_2 contamination, alkaline fuel cells are potentially suitable for this application. A similar scheme is probably applicable for load-levelling purposes with nuclear and hydroelectric power plants. Generally, energy storage systems will have to be coupled with solar power plants (solar–steam, photovoltaic, and windmills), and the hydrogen scheme proposed with nuclear power plants shows considerable promise for these systems. Another scheme, which is currently being investigated to produce electricity, is with ocean thermal power plants. Hydrogen produced in water electrolyzers coupled with these power plants, would be transmitted to land via pipelines for use in fuel cells to produce electricity.

One of the major energy users is the transportation sector, e.g., 30% in the U.S. The overall efficiency for energy utilization using conventional engines is only about 10%. From the point of view of energy conservation of petroleum and coal reserves, the fuel cell, coupled with a motor, has the highest projected efficiency for conversion of chemical energy of the fuel to mechanical energy. Comparison of vehicular efficiencies assuming coal to be the primary energy source yields for an IC (internal combustion) engine, 9%; diesel, 10%; battery, 15%; fuel cell–battery, 20%.

1.5. The Relevant Electrochemical Principles in Electrochemical Energy Conversion

The heart of the fuel cell system is the electrochemical cell, which converts the chemical energy of the fuel to electrical energy. The electrochemical principles, which govern the performance of the fuel cell, are thermodynamic and electrode kinetic in origin. One is thus concerned with the thermodynamics and the electrode kinetics of the reactions occurring at the electrode–electrolyte interfaces and with the transport processes through the electrolyte and in the electrode. These subjects are dealt with in Sections 2 and 3 of this chapter. One of the major problems which has retarded the development of fuel cells is associated with the low electrocatalytic activity with gaseous fuels and oxidants (cf. batteries, where the electrode reactions are rapid), compounded by a progressive fall in the performance caused by electrode poisoning or loss in surface area. These aspects are dealt with in Section 4 of

this chapter. A topic of vital interest to fuel cells is porous electrodes—without such types of electrodes, it would have been impossible to develop fuel cells with the desired power densities for space and terrestrial applications. Models for porous gas diffusion electrodes, potential and current distribution in such electrodes, and use of transient methods to obtain active areas and investigate electrode kinetics in porous electrodes are presented in Section 5. Section 6 is devoted to the system aspects of the most promising fuel cell systems from an electrochemical point of view (emphasizing the influence of electrochemical parameters on fuel cell systems performance), for electric utility, transportation, and space application.

2. Thermodynamic Aspects

2.1. Reversible Potentials and Open-Circuit Potentials of Fuel Cells

A single electrochemical cell constitutes the basic unit of a fuel cell system (see Figure 2 for a view of a single hydrogen–air phosphoric acid fuel cell developed by United Technology Corporation), where under reversible conditions, the free energy change (ΔG) of the reaction

$$H_2(g) + 1/2O_2(l) \rightarrow H_2O(l) \tag{1}$$

is converted into electrical energy. This free energy change is related to the reversible potential of the cell by the equation

$$\Delta G = -nFE_r \tag{2}$$

where E_r is the reversible potential of the electrochemical cell in which reaction (1) is at equilibrium and n refers to the number of electrons taking part in the overall interfacial reaction. If the activities of the reactants and products in their standard states [see Eq. (1), where g signifies gas and l liquid] are unity, Eq. (2) can be rewritten as

$$\Delta G^\circ = -nFE_r^\circ \tag{3}$$

where ΔG° and E_r° refer to the standard free energy changes and standard reversible potentials, respectively, for reaction (1). The thermodynamic data for a number of fuel cell reactions at 25°C and 150°C (see Table 2) shows that the nitrogenous fuels and the hydrogen–oxygen fuel cells have higher reversible potentials than the organic–oxygen systems. Thus the reversible potential for the hydrazine–oxygen fuel cells is over 1.5 V; however, the observed open-circuit potentials are lower presumably due to the decomposition of hydrazine to nitrogen and hydrogen near the electrode. The open-circuit potentials of the hydrogen–oxygen fuel cells are about 200 mV less than the reversible potentials because of the difficulty of attaining the

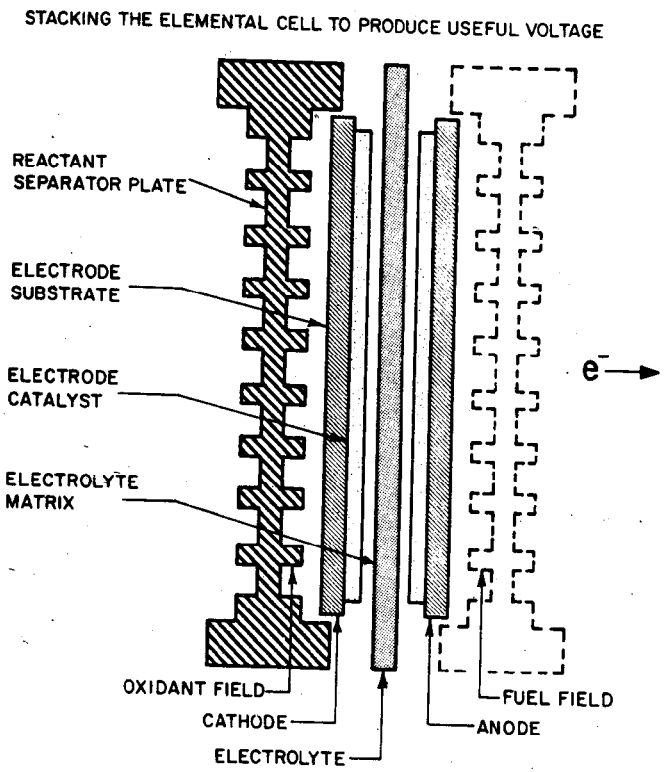

Figure 2. Single cell in hydrogen–air phosphoric acid fuel cell system developed by United Technologies Corporation. (With permission from United Technologies Corporation.)

reversible potential for the oxygen electrode reaction, which in turn is due to mixed potentials being set up by the competing electrode reactions, such as oxide formation, on the electrocatalyst.

2.2. Temperature and Pressure Coefficients of Reversible Potentials

By definition,

$$\left(\frac{\partial \Delta G}{\partial T}\right)_p = -\Delta S \qquad (4)$$

Hence

$$\left(\frac{\partial E}{\partial T}\right)_p = \frac{\Delta S}{nF} \qquad (5)$$

Table 2
Thermodynamic Data for Some Fuel Cell Reactions[a,(7)]

Reaction	$\Delta G°$, kcal mol^{-1}	$\Delta H°$, kcal mol^{-1}	n	Δn	$E_r°$, V	$\partial E_r°/\partial T$, mV/°C	$\partial E_r/\partial \log P$, mV	ε_i
Temperature, 25°C								
$H_2 + 1/2O_2 \rightarrow H_2O$	−56.69	−68.32	2	−1.5	1.229	−0.84	45	0.830
$CH_4 + 2O_2 \rightarrow CO_2 + 2H_2O$	−195.50	−212.80	8	−2	1.060	−0.31	15	0.919
$C_2H_6 + 7/2O_2 \rightarrow 2CO_2 + 3H_2O$	−350.73	−372.82	14	−2.5	1.087	−0.23	10.7	0.941
$C_3H_8 + 5O_2 \rightarrow 3CO_2 + 4H_2O$	−503.93	−530.61	20	−3	1.093	−0.19	9	0.950
$C_4H_{10} + 13/2O_2 \rightarrow 4CO_2 + 5H_2O$	−656.74	−687.99	26	−3.5	1.095	−0.17	8	0.955
$C_5H_{12} + 8O_2 \rightarrow 5CO_2 + 6H_2O$	−809.48	−845.17	32	−4	1.097	−0.16	7.5	0.958
$C_8H_{18}(g) + 25/2O_2 \rightarrow 8CO_2 + 9H_2O$	−1268.43	−1317.46	50	−5.5	1.100	−0.14	6.6	0.963
$C_8H_{18}(l) + 25/2O_2 \rightarrow 8CO_2 + 9H_2O$	−1265.87	−1307.54	50	−4.5	1.098	−0.12	5.4	0.968
$C_{10}H_{22}(g) + 31/2O_2 \rightarrow 10CO_2 + 11H_2O$	−1574.42	−1632.35	62	−6.5	1.101	−0.13	6.3	0.965
$CH_3OH(g) + 3/2O_2 \rightarrow CO_2 + 2H_2O$	−168.05	−182.61	6	−1.5	1.215	−0.35	15	0.920
$CH_3OH(l) + 3/2O_2 \rightarrow CO_2 + 2H_2O$	−167.91	−173.67	6	−0.5	1.214	−0.13	5	0.967
$NH_3 + 3/4O_2 \rightarrow 1/2N_2 + 3/2H_2O$	−85.04	−91.44	3	−1.25	1.225	−0.31	25	0.930
$N_2H_4 + O_2 \rightarrow N_2 + 2H_2O$	−143.83	−148.69	4	−1	1.560	−0.18	15	0.967
$C + 1/2O_2 \rightarrow CO$	−32.81	−26.42	2	+0.5	0.711	+0.46	−15	1.240
$C + O_2 \rightarrow CO_2$	−94.26	−94.05	4	0	1.022	0	0	1.002
$CO + 1/2O_2 \rightarrow CO_2$	−61.45	−67.63	2	−0.5	1.333	−0.44	15	0.909
$Li + 1/2Cl_2 \rightarrow LiCl(g)$	−58.00	−53.00	1	0.5	2.515	−0.72	−30	1.094

Temperature, 150°C								
$H_2 + 1/2O_2 \rightarrow H_2O$	−52.94	−58.142	2	−0.5	1.14799	−0.25	21	0.911
$CH_4 + 2O_2 \rightarrow CO_2 + 2H_2O$	−191.29	−191.42	8	0	1.03702	0	0	0.999
$C_2H_6 + 1/2O_2 \rightarrow 2CO_2 + 3H_2O$	−346.99	−340.66	14	0.5	1.07491	+0.04	−3	1.019
$C_3H_8 + 5O_2 \rightarrow 3CO_2 + 4H_2O$	−499.54	−487.82	20	1	1.08324	+0.05	−4.2	1.024
$C_4H_{10} + 13/2O_2 \rightarrow 4CO_2 + 5H_2O$	−651.94	−634.29	26	1.5	1.08747	+0.06	−4.9	1.028
$C_5H_{12} + 8O_2 \rightarrow 5CO_2 + 6H_2O$	−804.98	−781.19	32	1	1.09099	+0.07	−5.4	1.030
$C_8H_{18} + 25/2O_2 \rightarrow 8CO_2 + 9H_2O$	−1263.72	−1221.70	50	3.5	1.09614	+0.08	−5.9	1.034
$C_{10}H_{22}(g) + 31/2O_2 \rightarrow 10CO_2 + 11H_2O$	−1569.62	−1515.37	62	4.5	1.09796	+0.08	−6.2	1.036
$NH_3 + 3/4O_2 \rightarrow 1/2N_2 + 3/2H_2O$	−47.28	−77.28	3	0.25	0.6835	−0.96	−7.1	0.612
$C + 1/2O_2 \rightarrow CO$	−36.09	−26.31	2	0.5	0.782	0.47	−21	1.372
$C + O_2 \rightarrow CO_2$	−94.36	−94.08	4	0	1.02309	0	0	1.003
$CO + 1/2O_2 \rightarrow CO_2$	−58.26	−67.77	2	−0.5	1.26335	−0.46	21	0.860
$Li + 1/2Cl_2 \rightarrow LiCl(g)$	−81.38	−52.01	1	0.5	3.52942	+2.84	−42	1.565

[a] Thermodynamic data are presented for the oxidation of one mole of fuel.

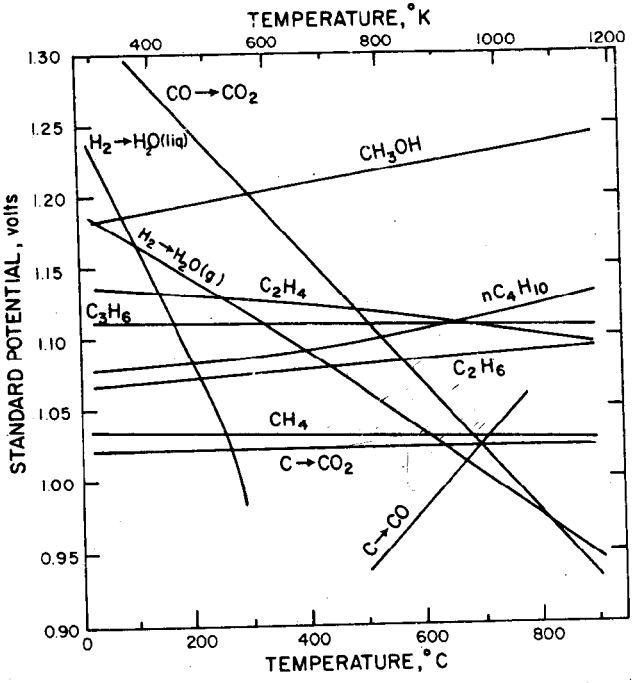

Figure 3. Temperature dependence of standard reversible potentials for selected fuel cell reactions. [With permission from the author: G. H. J. Broers, Central Technical Institute, T.N.O., The Hague, The Netherlands, File No. DA-91-591-EUC-1023 (1959).]

Thus the temperature coefficient of the reversible potential can be calculated using Eq. (5) from a knowledge of the entropy change for the cell reaction. (See Table 2 for the temperature coefficients of the reversible potentials for the various types of fuel cell reactions at 25 and 150°C.) Table 2 shows the temperature coefficient to be (i) negative for all cell reactions involving reduction in the number of gas molecules (Δn) when going from reactants to products (i.e., ΔS is negative for such cases), (ii) zero when Δn is zero ($\Delta S = 0$), and (iii) positive for positive Δn (ΔS is positive for this condition). Temperature dependence of the standard reversible potentials for selected fuel cell reactions of interest is shown in Figure 3.

The thermodynamic reversible potential is also a function of pressure:

$$E_{r,p} = E_{r,p_0} - \frac{\Delta nRT}{nF} \ln \frac{P}{P_0} \tag{6}$$

or

$$E_{r,p} = E_{r,p_0} - \frac{1}{nF} \int_{P_0}^{P} \Delta V \, dp \tag{7}$$

where ΔV is the volume change for the reaction and $E_{r,p}$ and E_{r,p_0} are the cell potentials at total pressures of P and P_0, respectively, assuming that the gaseous reactants and products obey the ideal gas laws. Pressure coefficients $(\partial E_r/\partial \log P)$ for various reactions are presented in Table 2.

2.3. Expressions for Efficiencies of Fuel Cells

The overall efficiency of a fuel cell (ε_0) is given by

$$\varepsilon_0 = \varepsilon_i \varepsilon_v \varepsilon_f \tag{8}$$

where ε_i is the thermal or intrinsic maximum efficiency, ε_v the voltage efficiency, and ε_f the Faradaic efficiency. The component efficiencies are represented by

$$\varepsilon_i = \frac{\Delta G}{\Delta H} \tag{9}$$

$$\varepsilon_v = \frac{E}{E_r} \tag{10}$$

and

$$\varepsilon_f = \frac{I}{I_m} \tag{11}$$

where ΔH is the enthalpy change for the fuel cell reaction, E is the fuel cell voltage when the current drawn from the cell is I, and I_m is the theoretically expected current output from the cell assuming reactants are converted completely to the products, according to the overall fuel cell reaction. The Faradaic efficiency is analogous to current efficiency in "driven" electrochemical cells and is generally unity. However, owing to (i) parallel electrochemical reactions, (ii) chemical reactions of reactants, catalyzed by the electrodes, or (iii) direct chemical reaction of two electrode reactants, the Faradaic efficiency can be lower than unity. If $\varepsilon_f = 1$ and $E = E_r$ (i.e., reversible conditions) the overall efficiency is the intrinsic maximum possible efficiency (ε_i), and is a measure of the ratio of the useful work output to the enthalpy change for the reaction. Values of ε_i for the various fuel cell reactions, presented in Table 2, are close to unity for all fuel cell reactions, which is not so with the theoretical efficiencies of other energy conversion devices. For the cases in which the entropy change of the reaction is positive, the intrinsic maximum efficiency exceeds unity. The main goals in electrochemical energy conversion operations are to achieve values of ε_v and ε_f close to unity. As stated earlier, while the second goal is relatively easy, the first one appears difficult.

2.4. Heat Changes under Reversible Conditions

The total energy released in a chemical reaction is the enthalpy change (ΔH). However, it is only the free energy change of the reaction (even under reversible conditions), which is converted to electrical energy. Hence, that part of the energy which cannot be converted to electrical energy [$(\Delta H - \Delta G) = T\Delta S$] is liberated as heat if ΔS is negative or absorbed from the surroundings when ΔS is positive. There are other reasons for heat generation in cells, i.e., irreversibilities of reactions, mass transfer problems, ohmic resistances and, these aspects are discussed in Section 3.5.

3. Electrode Kinetic Aspects

3.1. Dependence of Cell Potential and of Differential Cell Resistance on Current

The basic equation, characterizing the performance of a fuel cell, describes the dependence of the cell potential (E) on the cell current as follows:

$$E = E_r - \eta_{c,\text{act}} - \eta_{a,\text{act}} - \eta_{c,\text{conc}} - \eta_{a,\text{conc}} - IR_i \tag{12}$$

In the above equation, E_r is the reversible potential for the cell, η_{act} and η_{conc} terms represent the activation and concentration overpotentials at the respective electrodes (a for anode and c for cathode), and IR_i is the ohmic overpotential. For simplicity, one may assume a planar electrode configuration and conditions when η_{act} and η_{conc} are expressed by the following equations:

$$\eta_{\text{act}} = -\frac{RT}{\alpha} \ln i_0 + \frac{RT}{\alpha F} \ln \frac{I}{A} \tag{13}$$

$$\eta_{\text{conc}} = -\frac{RT}{nF} \ln \left(1 - \frac{I}{Ai_L}\right) \tag{14}$$

In Eqs. (12)–(14), I represents the cell current, R_i the internal resistance of the cell, i_0 the exchange current density, A the area of the electrodes, and i_L the limiting current density.

Substituting Eqs. (13) and (14) for the activation and concentration overpotentials at each of the electrodes into Eq. (12) results in the dependence of the cell potential on the cell current. A typical plot of cell potential vs. cell current, illustrating the regions of control by various types of overpotentials, is presented in Figure 4.

Differentiating Eq. (12) with respect to current leads to the following expression for the differential resistance of the cell as a function of current:

$$\frac{dE}{dI} = -\frac{RT}{\alpha_c FI} - \frac{RT}{\alpha_a FI} - \frac{RT}{nF(A_c i_{L,c} - I)} - \frac{RT}{nF(A_a i_{L,a} - I)} - R_i \tag{15}$$

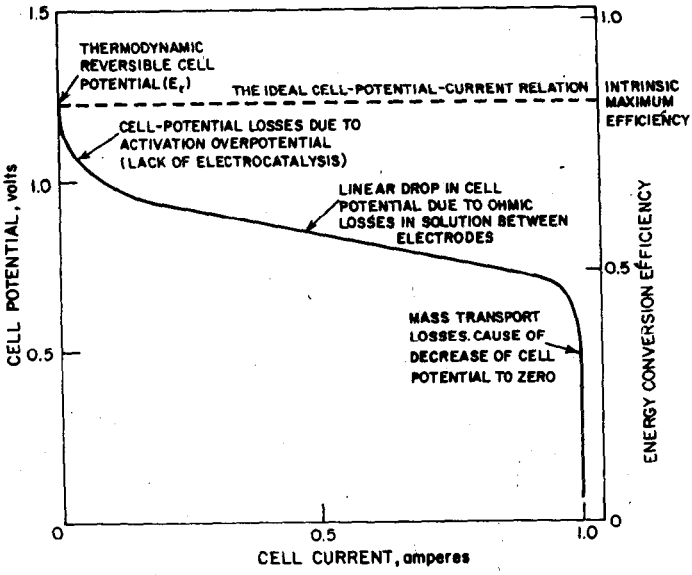
1.5
1.0
0.5
0
0.5
1.0
CELL POTENTIAL, volts
CELL CURRENT, amperes
ENERGY CONVERSION EFFICIENCY
THERMODYNAMIC REVERSIBLE CELL POTENTIAL (E_r)
THE IDEAL CELL-POTENTIAL-CURRENT RELATION
INTRINSIC MAXIMUM EFFICIENCY
CELL-POTENTIAL LOSSES DUE TO ACTIVATION OVERPOTENTIAL (LACK OF ELECTROCATALYSIS)
LINEAR DROP IN CELL POTENTIAL DUE TO OHMIC LOSSES IN SOLUTION BETWEEN ELECTRODES
MASS TRANSPORT LOSSES CAUSE OF DECREASE OF CELL POTENTIAL TO ZERO

Figure 4. Typical plot of cell potential versus current for fuel cells illustrating regions of control by various types of overpotentials.[7] (With permission from McGraw-Hill Book Company.)

From Eq. (15), it is clear that at low current densities, the major contribution to the differential resistance is from the activation overpotential losses, as indicated by the sharp drop in cell potential with increasing current (Figure 4). As the current is increased, the importance of the first two terms on the right-hand side of Eq. (15) decreases and R_i dominates the differential resistance, as exhibited by the linear region in Figure 4. When the current approaches the limiting current at one of the electrodes, the differential resistance is controlled by mass transfer limitations resulting in a rapid decrease of the cell potential. Under ideal conditions, i.e., when all the overpotential losses are zero, one would expect a straight line parallel to the x axis as indicated by the dotted line in Figure 4. The cell potential–current density behavior in fuel cells with porous electrodes is very similar to that shown in Figure 4 depicting the three regions. However, the equations for cells with porous gas diffusion electrodes would be much more complex than Eq. (15). (See Section 5 for a description on porous electrode kinetics.)

3.2. Dependence of Efficiency on Current Density

The expression for the overall efficiency (ε_0) of a fuel cell, assuming $\varepsilon_f = \varepsilon_v = 1$, can be written as follows:

$$\varepsilon_0 = -\frac{nFE}{\Delta H} \tag{16}$$

By combining Eqs. (12)–(14) with Eq. (16), it can be shown that the efficiency varies with current density in the same manner as the cell potential–current density relation described in Figure 4.

3.3. Dependence of Power on Current Density

The power (P) of a fuel cell is given by

$$P = EI \tag{17}$$

where

$$I = Ai \tag{18}$$

Qualitatively, one can forecast the nature of the P–i curve by examining the behavior at low and high current densities. Thus at low current densities, $i \to 0$ and at high current densities, $E \to 0$. Hence, P approaches zero values at both ends, while at intermediate values of i, P assumes a maximum value as illustrated in Figure 5 for the type of E–I relationship in Figure 4. In most typical fuel cells, owing to the sophisticated construction of the porous gas diffusion electrodes the limiting current density is not reached even at current

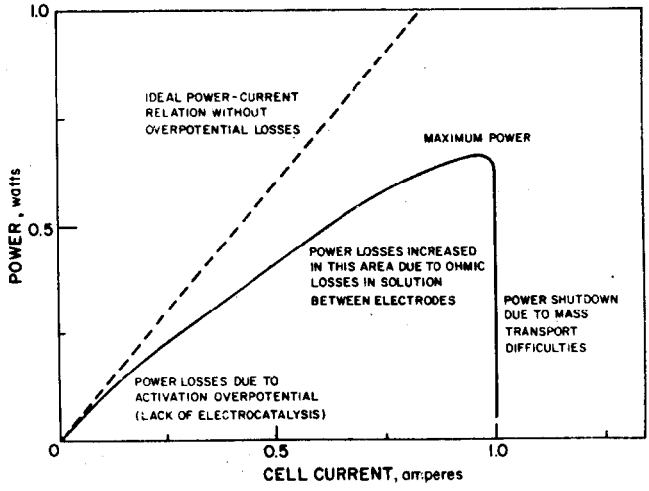
1.0
0.5
0
POWER, watts
IDEAL POWER-CURRENT RELATION WITHOUT OVERPOTENTIAL LOSSES
MAXIMUM POWER
POWER LOSSES INCREASED IN THIS AREA DUE TO OHMIC LOSSES IN SOLUTION BETWEEN ELECTRODES
POWER SHUTDOWN DUE TO MASS TRANSPORT DIFFICULTIES
POWER LOSSES DUE TO ACTIVATION OVERPOTENTIAL (LACK OF ELECTROCATALYSIS)
0.5
1.0
CELL CURRENT, amperes

Figure 5. Typical plot of power versus current density for fuel cells, illustrating regions of control by various types of overpotentials.[7] (With permission from McGraw-Hill Book Company.)

densities as high as 500 mA cm^{-2}, and the cell potential–current density relation is linear. In such cases, the power–current density relation tends to be parabolic.

3.4. Expressions for Maximum Power in Limiting Cases

It is not possible to derive an analytical expression for maximum power in the most general case when all forms of overpotential, i.e., activation, concentration, and ohmic, are present, except under the two limiting conditions described below.

Case (1): Linear Cell Potential–Current Density. The equation for the cell potential as a function of current density is given by

$$E = E_r - mi \tag{19}$$

where m is a constant and essentially represents the ohmic loss. Hence

$$P = i(E_r - mi) \tag{20}$$

From Eq. (20), which shows the P–i variation to be parabolic, the conditions for the maximum i and P can be deduced as

$$i_{max} = \frac{E_r}{2m} \tag{21}$$

$$E_{max} = \frac{E_r}{2} \tag{22}$$

and

$$P_{max} = \frac{E_r^2}{4m} \tag{23}$$

Thus the maximum power density is realized when the cell potential is equal to one-half of the reversible potential. Quite often, the open-circuit potential is less than the reversible cell potential, because of competing reactions. Therefore the maximum power is obtained when the cell potential is equal to one-half of the open-circuit potential.

Case (2): Semilogarithmic Cell Potential–Current Density Relation. When concentration and ohmic overpotentials are negligible and activation overpotential predominates in the entire current density range, the cell potential is related to the current density by

$$E = E_r + a - b \ln i \tag{24}$$

where b is the sum of the numerical values of the Tafel slope for the anodic and cathodic reaction; hence

$$P = i(E_r + a - b \ln i) \tag{25}$$

From Eq. (25), the maximum current density (i_{max}) and power (P_{max}) can be shown to be expressed by

$$\ln i_{max} = (E_r + a - b)/b \tag{26}$$

$$P_{max} = b \exp[(E_r + a - b)/b] \tag{27}$$

At P_{max}, the cell potential (E_{max}) is given by

$$E_{max} = b \tag{28}$$

Thus the cell potential at the maximum power density has a value equal to the sum of the Tafel slopes for the anodic and cathodic reactions.

3.5. Heat Generation

The heat generation in fuel cells (Q) is expressed by the equation

$$Q = -(4.18\ T\Delta S/nF)i + i\Sigma\eta + i^2R \tag{29}$$

The first term on the right-hand side arises from the entropy change of the reaction in the fuel cell. [For example, with a hydrogen–oxygen fuel cell operating at 25°C, ΔH is about -68 kcal mol^{-1}, while $\Delta G = 56$ kcal mol^{-1}. Hence the difference $T\Delta S$ (of -12 kcal mol^{-1}) is given off as heat even if the cell functions reversibly.] The second term represents the heat generated due to the irreversibilities of the fuel cell reaction caused by the slowness of electrode reactions and mass transfer limitations. The third term represents the heat produced by the ohmic losses in the cell. Since this heat is a "waste" energy, the overall efficiency would be reduced. To achieve increased efficiency of utilization of a fuel (e.g., natural gas, petroleum, or coal), this heat should be used in another part of the process, e.g., for the reformer or gasification reactions and/or for thermal energy (see Section 6). The latter idea of a total energy concept (i.e., treating the fuel cell as a device producing electricity and heat) enhances the value of fuel cells from an energy conservation point of view (see Section 6 for a more complete discussion).

3.6. The Ideal Electrode Kinetic Parameters for Fuel Cells

The desired characteristics for fuel cell systems, whether they be for space or terrestrial applications, are high overall efficiencies and high power densities. By achieving such goals, one is able to reduce capital costs, operating costs, maximize conservation of fossil fuels, and increase power densities with respect to weight and volume. The heart of the fuel cell system is the electrochemical

cell which governs the performance. To attain high efficiencies and power densities, it is essential to reduce activation, concentration, and ohmic overpotentials to a minimum. Activation overpotential is reduced by discovering better electrocatalysts, use of electrodes with a high surface area, and operation at high temperatures. The greatest advance in fuel cell technology has been achieved by using porous gas diffusion electrodes, which have a high porosity and high surface area. Thus not only activation overpotential but also concentration overpotential is decreased significantly. For further reductions in concentration overpotential, higher operating pressures may be helpful. Ohmic overpotential is reduced by minimizing interelectrode spacing (the best examples are the General Electric solid polymer electrolyte fuel cell and the Westinghouse solid electrolyte fuel cells) and by using highly conductive electrolytes (e.g., trifluoromethane sulfonic acid), electrodes, and current collectors.

From a practical point of view, the aim of hydrogen–air fuel cell (the most advanced and promising fuel cell) research is to achieve current densities of at least 200 mA cm^{-2} (considerably higher values, such as over 500 mA cm^{-2} are necessary for transportation and space applications) at cell potentials of over 0.75 V. To reach these goals, electrocatalysts with exchange current densities of over 10^{-3} A cm^{-2} on planar electrode configurations, limiting current densities of greater than 10^{-4} A cm^{-2} at planar electrodes, and specific resistivities of less than 1 Ω cm are essential. Some of the recent developments, aimed at realizing these objectives, are discussed in the following sections.

4. Electrocatalysis

4.1. Major Role of Electrocatalysis in Electrochemical Energy Conversion

Activation overpotential is the main cause of efficiency losses in fuel cells operating at temperatures of less than 200°C. In Table 3 are shown the most recent performance characteristics of some fuel cells. The hydrogen–air cells with acid or alkaline electrolytes are in the most advanced state of development. In these cells, while the hydrogen overpotential is relatively low, the oxygen overpotential is the predominant cause for the departure of the cell potential from the reversible value at desired current densities. Methanol–air fuel cells are particularly attractive for transportation applications. However, some breakthrough is needed to increase the power density by a factor of 10 for methanol–air fuel cells if they are to be used as the power source in electric vehicles. The low performance of the methanol–air fuel cell is due to high overpotentials for both the methanol oxidation and oxygen reduction reactions. Since hydrogen is not a primary fuel, considerable effort was expended in the sixties to develop direct hydrocarbon–air fuel cells for electric utility and

Table 3
Importance of Electrocatalysis in Electrochemical Energy Conversion, Storage, and Conservation

Energy conversion—fuel cells

System	Current density, mA cm^{-2}	Cell potential, V	% Efficiency
H_2—air, acid electrolyte	200	0.65	43
H_2–oxygen, alkaline electrolyte	400	0.8	55
Methanol–air	50	0.5	38

Energy storage—secondary batteries

System	% Efficiency, electric → electric
Fe–air	25
Zn–air	~40

Energy conservation

System	Reversible potential, V	Cell potential, V
Chloralkali cell	2.2	3.8
Electrowinning of Zn	2.0	4.1

transportation power generation. Because of the inefficiencies of the hydrocarbon oxidation and the high requirements for noble metal contents in the electrodes, there was general agreement that it will be most beneficial to pursue the indirect route, viz., produce hydrogen by the reformer reaction and consume it in a hydrogen–air fuel cell. In the remaining subsections, the progress made in investigations of (i) electrocatalysis of the hydrogen, oxygen, and organic electrode reactions, including particle size effects and poisoning problems, and (ii) sintering mechanisms will be summarized.

4.2. Hydrogen Oxidation Reaction

The mechanism of the hydrogen ionization reaction has not been studied as extensively as that of the hydrogen evolution reaction, but in recent years, there has been an increasing emphasis on the former, particularly with the renewed interest in fuel cells.[11–13] In acid electrolytes, platinum is still by far the best electrocatalyst, though there is some promise for finding non-noble metal catalysts. The mechanism of the hydrogen ionization reaction is not necessarily the reverse of the hydrogen evolution reaction, because the hydro-

gen evolution reaction occurs, for instance, on most transition metals in the region of potentials, where these metals are covered with at least a monolayer of adsorbed hydrogen atoms, whereas in the potential region of the oxidation reaction, the coverage with adsorbed hydrogen is less than a monolayer.

The mechanism of electro-oxidation of hydrogen on platinum in phosphoric acid has been extensively investigated[11–15] and it was concluded that the dual-site dissociation of H_2 on Pt is the rate-determining step. It has also been shown that the slow step for the H_2/O_2 exchange reaction on Pt is the same as for the hydrogen ionization reaction on this metal. The exchange current density for hydrogen oxidation on Pt in 85% phosphoric acid at 160°C is 140 mA cm^{-2}, with limiting current densities of greater than 10^4 mA cm^{-2}. The reaction mechanisms on smooth Pt, unsupported Pt, and Pt supported on carbon are the same, the rates being dependent only on the roughness factor. The main problems with the hydrogen electrode in this most advanced fuel cell are the poisoning and sintering problems. Carbon monoxide and sulfur impurities are deadly poisons. Carbon monoxide adsorbs on the electrode surface, thereby reducing the reaction rate for the hydrogen oxidation reaction. The reduced current (i_{CO}) in the presence of CO may be expressed by

$$\frac{i_{CO}}{i_{H_2}} = (1 - \theta_{CO})^2 \tag{30}$$

where i_{H_2} is the current in the absence of CO. Assuming i_{H_2} is the limiting current density of hydrogen oxidation in the absence of CO, and that a current density of 300 mA cm^{-2} is desired for the fuel cell operation, the maximum tolerable CO coverage (θ) on the surface is 0.83. The surface coverage of CO decreases with increase of temperature, which in turn improves the anode behavior in the presence of CO (Figure 6). Though carbides, phosphides of ruthenium, and rhodium have been reported to enhance CO tolerance,[16,17]

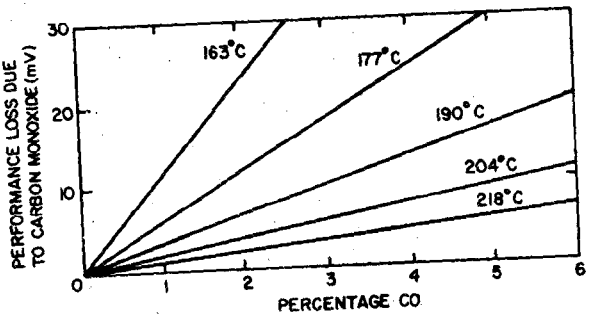

Figure 6. Effect of CO content and temperature on hydrogen ionization reaction on Pt (loading 0.35 mg/cm^2) at a current density of 269 mA/cm^2 in 99% H_3PO_4.[15] (With permission from the author and *J. Electrochem. Soc.*)

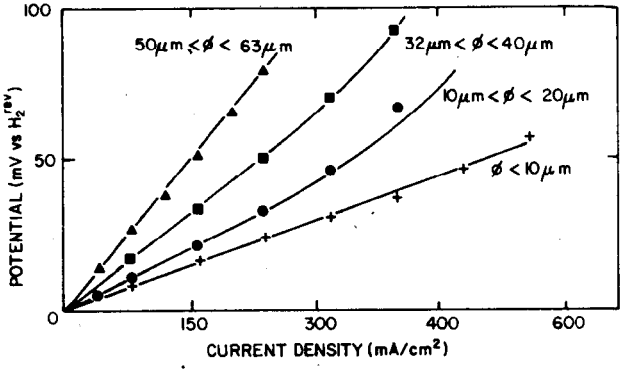

Figure 7. Current density–potential relations (*IR* free) for the hydrogen ionization reaction on Raney Ni–Ti electrodes in 6 *N* KOH at 80°C showing the influence of particle size[22] (∅ refers to particle diameter; catalyst loading 100 mg/cm^2). (With permission from the authors and *J. Electrochem. Soc.*)

incorporation of these materials has not helped in realizing low overvoltage and long life. At a temperature of 190–200°C, 1% CO can be tolerated with Pt catalysts. While the CO poisoning problem is decreased, sintering effects become dominant at high temperatures (see also Section 4.5).

A large number of phosphides, arsenides, selenides, and tellurides, of Fe, Co, and Ni, were investigated as hydrogen electrodes in sulfuric acid as the electrolyte at temperatures of less than 100°C, and CoP_3 was found to be most promising, having least sensitivity to CO poisoning (considerably less than Pt).[18,19] Tungsten carbide was also found to be tolerant to CO; however, the rate constant for hydrogen oxidation on this material was less than on Pt by two orders of magnitude.[20,21]

In alkaline solutions, there is no need for use of noble metal catalysts. Raney nickel is unstable for hydrogen oxidation in alkaline solution. However, Ti containing Raney nickel shows superior performance from the point of view of electrocatalytic activity and stability.[22] A possible explanation lies in increased *d*-band vacancy caused by the addition of Ti to Raney nickel. The performance of this electrocatalyst depends on the grain size and the operating current density (Figure 7).

4.3. Oxygen Reduction Reaction

The oxygen reduction reaction is as important to fuel cells as it is to life. The enzymatic route appears to have more success than the electrocatalytic route. The complexities of this electrocatalytic reaction arise from the following reasons: (i) instability of most metals and alloys in the region of potentials where the reaction occurs in acid and in alkaline solutions, (ii) relatively slow

reaction rates (with i_0 of the order of 10^{-10} A cm^{-2}) compared to other electrode reactions, (iii) competing reactions such as oxide formation altering the substrate characteristics, and (iv) generation of H_2O_2 as an intermediate or in a parallel reaction in many cases.

The irreversible cathode is the main cause for the performance limitation in the most advanced fuel cell, i.e., the phosphoric acid fuel cell. However, considerable progress has been made over the last 10 years.[14] For instance, the noble metal loading has been reduced from over 10 mg cm^{-2} in the sixties to about 0.5 mg cm^{-2} (Pt on carbon support) at the present time. The performance of the electrode for various platinum loadings, shown in Figure 8, suggests a linear relationship between current density for oxygen reduction at a constant potential and the noble metal content. The Tafel slope for oxygen reduction on Pt in highly purified phosphoric acid is surprisingly independent of temperature (Figure 9). A crystallite size effect has been observed in that there is a definite decrease of catalytic activity with increase of surface area (Figure 10). Furthermore, an increase of Tafel slope is observed with a decrease of the surface area both on supported and unsupported catalysts.

One of the problems connected with the oxygen reduction reaction is the energy required to dissociate the O–O bond. The ideal case will be one in which the electrocatalyst favors the dissociative adsorption of oxygen. An area which needs extensive investigation is the mechanism of corrosion of the platinum catalyst and carbon support when the potential at the oxygen electrode exceeds 0.85 V versus the reversible hydrogen electrode. The other platinum group metals as well as alloys of noble metals are not as active as Pt for oxygen reduction. Carbon, activated by addition of transition metals such as Mn, Fe, Co, Ni, and heating in ammonia, have been tested as electrocatalysts for

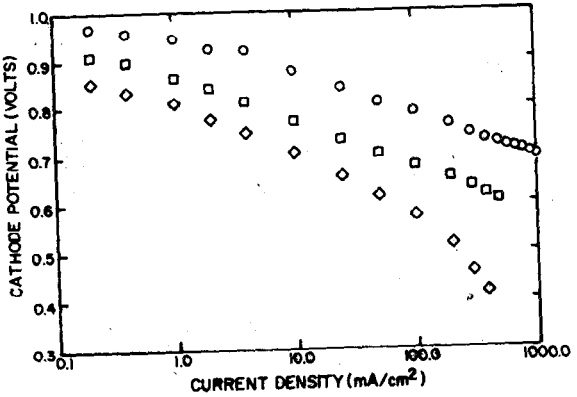

Figure 8. Cathode performance[15] on oxygen for various loadings of Pt supported on Vulcan XC-72 at 160°C in 96% H_3PO_4. ○, 0.25 mg/cm^2; □, 0.025 mg/cm^2; ◇, 0.0025 mg/cm^2. (With permission from the author and *J. Electrochem. Soc.*)

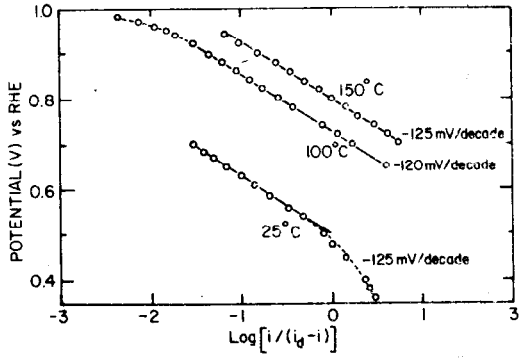

Figure 9. Tafel lines for the O_2 reduction reaction on Pt in highly purified 85% H_3PO_4 as a function of temperature[25] (i is current density, i_d cathodic diffusion limiting current density.)

oxygen reduction.[23] Though the electrocatalytic activity by this activation procedure was enhanced over the untreated carbon, the electrodes were short lived because of the instability of carbon. Metal chelates, sulfides, and thiospinels were examined for their usefulness as oxygen electrodes.[24] The three macrocyclic complexes tetraazaannulene, tetraphenylporphyrin, and cobalt phthalocyanin, showed relatively high activities for oxygen reduction. The catalytic activity of the chelate can be increased by increasing the electron density in the center of the chelate. Since the chelates have been found to

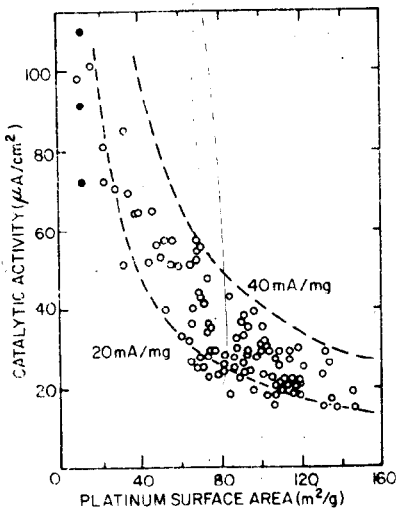

Figure 10. Catalytic activity[15] for O_2 reduction as a function of Pt surface area at 177°C in 99% H_3PO_4. ●, Pt black blended with carbon support; ○, Pt supported on Vulcan XC-72; E = 0.9 V. Dotted lines represent constant activities per unit mass. (With permission from the author and *J. Electrochem. Soc.*)

degrade in a few days under fuel cell operating conditions, efforts are underway to stabilize the chelates by polymerization.[25]

Finding oxygen electrodes for alkaline media is an easier proposition than for acidic environments. Activated carbon electrodes show good performance. One of the most promising electrocatalysts in alkali is (Bi, Ni, Ti) doped Ag containing 11.5% Hg.[26] Using this catalyst as an air electrode, the hydrogen–air fuel cell voltage, although decreased from 750 to 700 mV over 600 hr, remained constant over longer periods of time.

Some attempts have been made to draw correlations between electrocatalytic activities of oxides for oxygen reduction and their magnetic properties.[27] Nickel oxide is antiferromagnetic and has a Neel temperature of 250°C, which is decreased as the surface area per gram increases. Above the Neel temperature, oxygen is chemisorbed side-on, enhancing direct reduction to water, while below this temperature, end-on adsorption of oxygen favors peroxide formation during reduction. Nickel cobalt oxide with a spinel structure, corresponding to the composition $NiCo_2O_4$, shows a high catalytic activity for oxygen reduction.[28] Ring-disk studies show that reduction of O_2 proceeds directly to OH^- in contrast to HO_2^- formation on simple oxides.[29] Like spinels, perovskites also are potentially useful catalysts for oxygen reduction. With the perovskite, $La_{0.5}Sr_{0.5}CoO_3$, the open-circuit potential in an oxygen-saturated potassium hydroxide solution at 170°C approached the reversible potential for the reaction.[30]

4.4. Electro-organic Oxidation

Since hydrogen is not a primary fuel, there was a great stimulation in the sixties to develop direct hydrocarbon–air or alcohol–air fuel cells. The published literature[2-9] in the field is voluminous, but because even the simplest hydrocarbon (CH_4) oxidation reaction occurs by an eight-electron transfer reaction, while the simplest alcohol (CH_3OH) gives up six electrons to its electrode during its oxidation to CO_2, one can envision such oxidation reactions taking place in a large number of steps involving several intermediates and yielding some by-products. It is, however, striking that even with the liquid hydrocarbons like decane, "cold combustion" in electrochemical cells (i.e., at temperatures less than 200°C) has been demonstrated in contrast to the high temperatures (>400°C) required for their gas phase "hot combustion."

Electro-oxidation of organic fuels involve at least six intermediate electron transfer and chemical steps. It is somewhat of a coincidence that the most frequently occurring rate-determining step is the chemical reaction of an organic radical near (two or three steps) the beginning of the series of the partial reactions with an adsorbed OH radical.[7] There is little work in progress on the direct oxidation of hydrocarbon fuels, the main problems being connected with their low reactivity and high noble metal requirements for the

electrocatalysts. The indirect route (reformer/fuel cells) shows considerably greater promise and such fuel cell systems are in the state of large-scale development. Apart from the electrode material, the electrolyte seems to play an important role in hydrocarbon oxidation. For example, the exchange current density for propane oxidation on Pt in trifluoromethane sulfonic acid is considerably higher than in phosphoric acid.[31] Furthermore, carbon monoxide is electro-oxidized on Pt in this electrolyte and is not a poison as in other electrolytes.[32]

Methanol is the most electroactive organic fuel but its activity is considerably less than that of hydrogen. For fuel-cell-powered vehicles, it is the ideal fuel, whether used directly or indirectly in the electrochemical energy converter. The fuel cell technologist's dream is to use it directly in the fuel cell because fuel cell power plant design and construction would be greatly simplified.

Methanol, being a liquid fuel and quite soluble in aqueous electrolytes, does not cause concentration overpotential problems as with hydrogen, oxygen, and the hydrocarbons. The problems connected with methanol oxidation are mainly due to (i) slowness of the electrode reactions of methanol and its intermediates, (ii) poisoning of the electrode surface by the intermediate(s), (iii) formation of formaldehyde and formic acid as by-products on a number of electrocatalysts, and (iv) an unaccountable loss of 0.4 V at open-circuit potentials or at extremely low current densities.

There has been some progress in increasing the activity for methanol oxidation with modified Pt catalysts. The incorporation of Ru, Sn, Re, and Mo into Pt catalyst enhances methanol oxidation.[33–36] Redox mechanisms involving different oxidation states of these metals have been proposed. In a number of the studies with such types of catalysts, the oxidation reaction rates of formaldehyde and formic acids are also higher than with unmodified platinum catalysts. Metals which have high hydrogen overpotentials, such as Pb, Bi, and Cd, present as ad-atoms on Pt surfaces promote the oxidation of methanol and its intermediates.[37]

During electro-oxidation of methanol, formaldehyde, and formic acid, a dehydrogenated residue of composition COH was found on the electrode surface—as determined using electrochemical and radiotracer techniques[38–40]—in both acid and alkaline electrolytes. A similar species is formed during electroreduction of CO_2[38] as well as in gas phase oxidation of methanol.[41] Water plays an important role in methanol electro-oxidation. The promotion of OH adsorption may help in the removal of the COH species. It has been suggested that with Pt–Ru[42] and Pt–Os[43] catalysts, Pt adsorbs the organic (COH) and the Ru or Os adsorbs the OH species, the latter occurring at a lower potential than on Pt. This may help account for the increased catalytic activity. Conversely, tungsten carbide has zero activity for methanol oxidation since it strongly adsorbs OH inhibiting adsorption of the organic intermediate.[44,45]

4.5. Sintering of Supported Metal Crystallites

One of the modes of loss of activity of fuel cell electrodes is associated with the phenomenon of sintering[15,46–48] of the small metal catalyst particles, used for fabricating the high-surface-area structures. Sintering results in the loss of effective surface area and, hence, shrinkage in the electrode dimensions, loss of structural integrity, porosity, etc. Figure 11 illustrates the loss of surface area (of ~40–50 m^2/g) observed[48] with carbon-supported platinum electrodes in concentrated H_3PO_4 at 190°C, as á function of time.

The driving force for the sintering of small metal particles is the excess free energy of the particles over that of the solid material. Theoretical descriptions of the sintering process are intended to account for the mechanism of transport of metal across the support and growth of large supported metal crystallites at the expense of small particles. It may be noted that the pore structure of the catalyst and the interactions between the metal and the support will tend to stabilize the metal dispersed on the support. The stability is greater in a reducing atmosphere than in an oxidizing medium.

There are essentially three models proposed for interpreting[49–50] the growth of metal crystallites due to the sintering of supported catalysts. A classification of these models can be made in terms of two modes of growth: "noninhibited" [(i) Ruckenstein–Pulvermacher model,[51,52] involving particle migration, collision, and coalescence, (ii) Flynn–Wanke model,[53,54] assuming atom escape, diffusion, and recapture], and "inhibited" [Wynblatt and Gjostein's model,[50] wherein each new layer of atoms added to the particle inhibits the continuing growth of metal crystallites].

In this section are presented some of the factors [50] which will lead to the retardation of crystallite growth when sintering occurs via the noninhibited growth mechanisms. For a detailed discussion of the various theories, the reader is referred to References 49–54. When the metal particles are small and particle migration is rate controlling, the growth rate is proportional to $D_s\eta_0$, where D_s refers to the diffusion coefficient of metal monomers on the particle surface and η_0 to the average particle density of the initial dispersion. Hence by

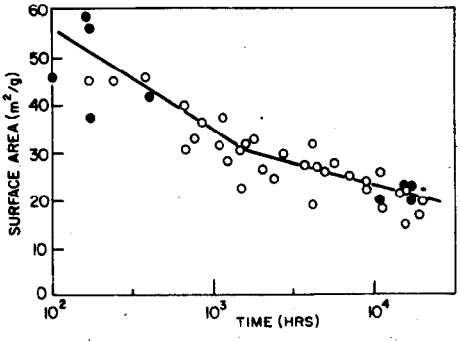

Figure 11. Surface area loss[15] with time at 190°C for Pt supported on Vulcan XC-72; ○, determined electrochemically; ●, determined using transmission electron microscope. (With permission from the author and *J. Electrochem. Soc.*)

decreasing the particle density in the initial dispersion, D_s will be lowered, resulting in greater stability of the supported crystallites. Based on D_s values, the stability of catalytically active noble metals with respect to growth should increase:

$$Ag < Au < Pd < Rh = Pt < Ru < In < Os$$

Alloying of a metal with one higher in the series should offer increased stability according to the above model.

When the metal particles are larger and interparticle migration by monomer diffusion on the substrate is the rate-determining step, the growth rate is controlled by the energy difference (H_{ps}) between the monomer on the substrate and a monomer on the particle. Since H_{ps} increases with increasing melting point of the particle, the series presented above is applicable for these conditions in a reducing medium. However, under oxidizing conditions, H_{ps} can be greatly reduced by the formation of easily volatalized oxide species. Hence the stability series, determined by the enthalpy change of the reaction $M(s) + O_2(g) \rightarrow MO_2(g)$, is

$$Os < Ru < Ir < Pt < Pd = Rh$$

Formation of mixed oxides with higher members in this series results in stabilization of the small metal particles. Other factors enhancing stability are substrate morphology and increased particle wetting.

Stabilization is inherent in the "inhibited" mode of growth with high step energies and low temperatures favoring small particle sizes. Step energy increases with increasing melting point of the metal particle, whereas adsorption of impurities tends to lower the step energy.

Some of the results reported with nickel- and platinum-based porous electrode structures in a fuel cell environment are presented in Table 4. These studies show that sintering effects can be greatly minimized by alloying or by choosing appropriate supports on which the surface mobility of the atoms or crystallites is not energetically favored. Progress in understanding the energetics and kinetics involved in the sintering process should lead to developing better preparation techniques and compositions having superior sintering resistance, which, in turn, will improve the long-term performance of fuel cell electrodes.

5. Porous Gas Diffusion Electrodes

5.1. Models

An electrochemical energy conversion device (be it a battery or a fuel cell) employs porous electrodes, which offer high specific surface area, thereby enhancing the rate of otherwise kinetically slow electrochemical reactions (e.g.,

Table 4
Sintering Effects in Porous Electrode Operations

Electrode	Some techniques adopted to minimize sintering
1. Porous nickel anode in molten carbonate fuel cells	Performance improved by incorporating[55] Ag particles in porous nickel or by using Ni–Cr alloys[56] as the anode material.
2. Au in alkaline fuel cells for O_2 reduction	Au blacks sinter at 70 to 120°C. Alloying Au black with Pt, Ni, Rh, or Cu was claimed[57] to decrease the sintering rate of Au black.
3. Au on supported catalysts	Activation energy for sintering[58] on C in vacuum is 30 kcal/mol and on SiO, the value is 35 kcal/mol. Au on SiO support sinters at a lower rate than on carbon support.
4. Pt on carbon support in hot concentrated H_3PO_4	Sintering of Pt particles was retarded with peroxidized carbon support.[59] Sintering can be controlled by the type of carbon used. Activated charcoal seems to provide the best characteristics of a support for Pt in hot concentrated H_3PO_4 solutions.[60]

O_2 reduction) and permitting realization of high power density per unit volume. Three types of porous structures, often encountered in practical applications, include (i) flooded battery, (ii) porous metal black, and (iii) highly porous Teflon-bonded metal black electrodes. Both (i) and (ii) are generally two-phase systems involving solid and liquid reactants, whereas (ii) and (iii) often feature the complexities of three-phase systems with solid, liquid, and gas participating in the electrochemical reaction. The three-phase systems—gas diffusion electrodes—constitute the essential components of electrochemical energy conversion devices.

Electrodes of type (ii)—hydrophilic electrodes—are usually prepared from a mixture of catalyst particles and pore-forming reagents, which are removed at a later stage to provide an average particle radius ranging from 0.1 to 1 μm. These electrodes are comprised of a single metal component. On the other hand, structures of type (iii)—hydrophobic electrodes—belong to a multicomponent system composed of catalyst (e.g., Pt crystallites), hydrophobisizer [e.g., polytetrafluoroethylene (PTFE)], current collector, and a binder; these composites are made by sintering metal particles with PTFE.

The structural and performance characteristics of the hydrophobic and hydrophilic electrodes depend on the preparation technique and mode of operation, and some of the typical features observed[61–63] with these electrodes are presented in Table 5. Any theoretical description of the performance characteristics of these real systems would involve a detailed knowledge of the structural features of the internal surface of the porous matrix, the material, and the phenomenological components of the system.[64]

Table 5
Typical Features of Hydrophilic and Hydrophobic Electrodes

Property	Hydrophilic electrodes	Hydrophobic electrodes
1. Dependence of electrochemical activity on the pressure drop (ΔP) between gas and electrolyte	Increases with ΔP rapidly and reaches a plateau.	Almost none; activity increases with increasing Teflon content up to <50% and then decreases.
2. Parameters influencing the electrode performance	Average radius of the gas pores, specific area of the catalyst, and average liquid porosity.	Radius of the catalyst particles (~100 Å), radius of the Teflon particles (~1000 Å), porosities of the catalyst and Teflon particles, liquid porosity, effective electrolyte conductivity, specific area of the catalyst.
3. Wetting characteristics	All the catalyst particles are wetted.	Not all the catalyst particles are wetted. It is a function of Teflon concentration and method of fabrication.
4. Pore structure	One type of gas pore ($r = 0.1-1$ μm) is present.	Two types of gas pores (pore of inner space between hydrophilic and hydrophobic walls and hydrophobic pores with small chains of porous agglomerates of PTFE) are present. The later play a significant role; also gas pores with $r = 25-200$ Å make a significant contribution to the electrochemical activity.
5. Electrolyte supply	Average radius of gas pores is greater than the liquid pores; few microns thick electrolyte film present on the surface of gas pores.	Macroporosity has no effect on performance. Electrochemical activity increases with micropore volume
6. Thickness	Order of magnitude larger than that of hydrophobic electrodes.	Depends on the mode of preparation.

5.1.1. Structural Details of the Internal Surface of the Porous Matrix

A porous body can be viewed as an ensemble of catalyst particles with voids or pores distributed in a random or ordered fashion. The parameters required to characterize a real porous electrode system—pore diameter being one of them—do not assume unique values, and are always distributed around their average values. This is true even for a single particle material like platinum black, for which at least two effective radii, representing particle distribution and particle composition, are needed for describing this agglomerate. More parameters become essential in the case of practical systems in view of the additional nonhomogeneities such as dual porosity, particle size, porosity of the hydrophobic material (e.g., Teflon), and degree of wetting, introduced by the various methods of preparation of porous electrodes.

5.1.2. Material and Phenomenological Components of the System

The overall performance of a porous electrode is governed by the interplay of the various material and phenomenological components described in Figure 12. The catalyst particles, gaseous and/or liquid reactants, and the electrolyte, interacting in a region whose geometry is complex, form the material components of the porous electrode system. The phenomenological features include, among others, finite rate of charge transfer, mass transport of reactants, products (and intermediates), adsorption, migration to the catalytic sites, etc. All of these create polarization effects which offset the advantages of using a porous structure. Thus, operating with a high-surface-area medium generates its own problems.

An exact theoretical analysis of porous electrode operations is a monumental task because of the following factors: (1) lack of precise knowledge of the structural details, (2) nonlinear, multidimensional and coupled equations describing the mass transport and potential distributions, and (3) problems involved in defining the operating regimes, e.g., three-phase boundaries, the so-called zone of electrochemical activity. To circumvent the pursuit of these complexities, idealizations of various types have been employed. For example, for purposes of theoretical analysis, porous structures can be idealized to consist of parallel, cylindrical pores. To avoid mathematical complexity, the multidimensional nonlinear equations can be simplified. The local geometry is again rendered simple by choosing mathematically manageable structures (or models).

Several models have been proposed for describing porous operations[7,10,65–75] and these models may be classified into three groups: (i) homogeneous, (ii) quasihomogeneous, and (iii) discrete or statistical models (see Figure 13). The "diverse" character of the various models, proposed in the literature, stems primarily from the myriad of designs of porous gas diffusion

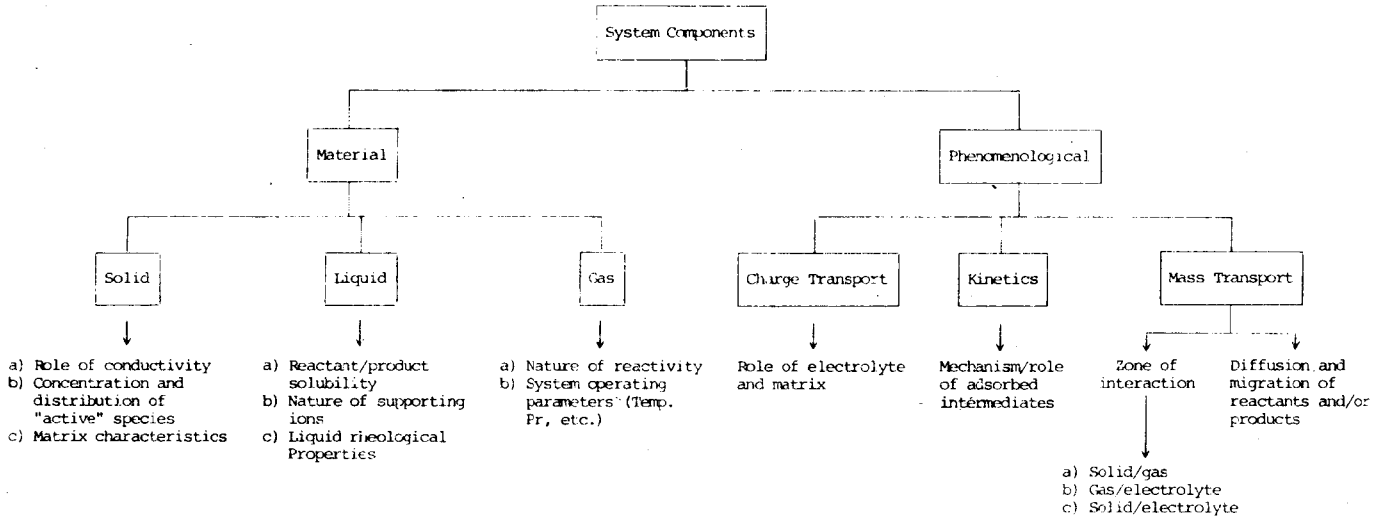

Figure 12. Material and phenomenological components involved in porous electrode operations.

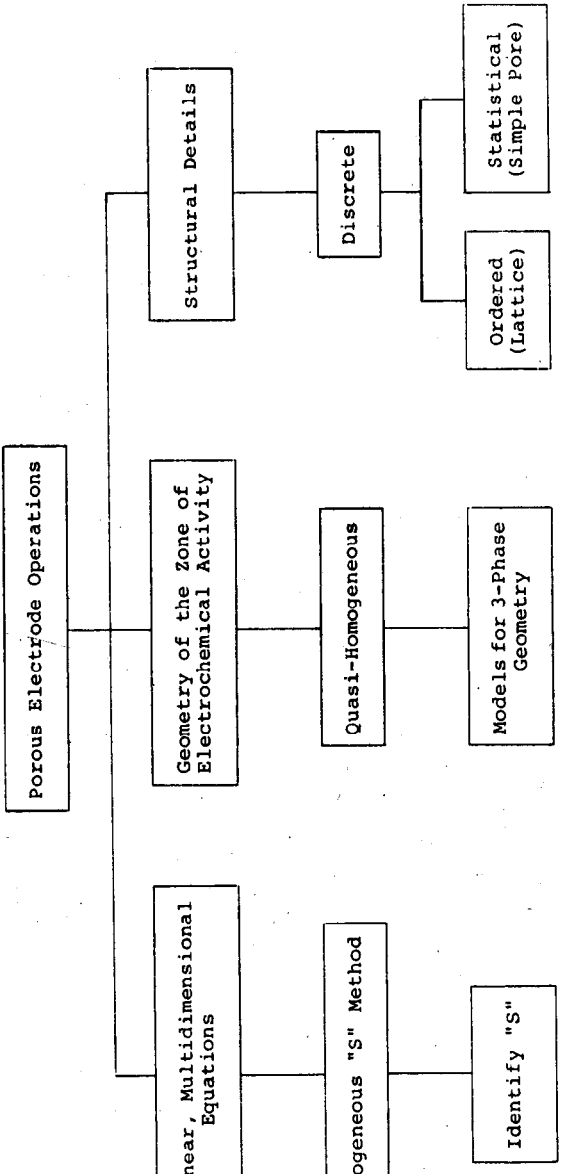

Figure 13. Porous electrode descriptions.

electrodes, controlling factors (e.g., mass transport or activation controlled) and operating regimes (e.g., temperature, pressure, nature of electrolyte, etc.). Thus a specific model may not be applicable for an arbitrary choice of variables but may be valid for certain carefully chosen conditions.

1. *Homogeneous Models.* Here, the interconnected multiphase system is treated as a single homogeneous phase by replacing the distributed heterogeneous sources/sinks by appropriate homogeneous or volume entities. This avoids precise definition regarding the structural details of the porous matrix and also the geometry of the zone of the electrochemical activity. Homogenization is achieved in the elementary flooded model by assuming a local current density–overpotential (i–η) relationship and transforming the surface sources to volume sources by replacing i by Si (S signifying the specific surface of the matrix in cm^2/cm^3) and setting up the differential equations. This procedure can be justified since the electrochemical reaction takes place, though at different rates, along the entire surface of the porous medium and is valid[74,75] if the pore radii are small compared with other characteristic dimensions. S can be identified as the total internal surface for flooded porous electrodes. However, its precise meaning depends on the reaction mechanism. Thus, for gas-filled electrodes, S can be set equal to the total internal surface (up to 80% gas content[65]), and can reflect macroporosity,[65,66] if wetting by macropores is possible. In the case of three-phase systems, S may be calculated[67,68] in terms of the common area between gas and liquid, by judiciously considering the mechanism and active areas.

The parameter S is a geometric characteristic dependent on the gas pressure, via the critical radius, that controls the extent of flooding of the pores. It can be defined[64] in terms of the structural and equilibrium properties of the porous medium alone. Hence the mathematical procedures used for flooded porous electrode systems can be applied to gas diffusion electrodes by properly reidentifying S and through appropriate constitutive relationships.

2. *Quasihomogeneous Models.* For this class of models, the current density–overpotential relationships are deduced by modeling the three-phase boundary regions (and the phenomena occurring therein) and relating these results to the pore structures elucidated through homogenization and a knowledge of the boundary distributions. Variations in this class of models are mainly due to the vast number descriptions (see References 7, 10, 69–75 for a review of these models) possible in modeling the zone of electrochemical activity and the porous electrode structures.

3. *Statistical Models.*[64] Instead of ignoring the structure of the porous matrix, one may idealize it by adopting simple concepts such as single-pore or lattice (or cell) models.

In the single-pore approach, one may assume that the porous structures are made up of noninteracting pores characterized by two parameters—radius of the solid capillary and distance parameter representing the packing of these solids. Taking into account the pore(s) geometry, one may solve

the boundary value problem and subsequently develop ensemble-averaged parameters.

The interconnected pore medium can also be described by cell or lattice modeling wherein, as in a cascade process, each lattice influences the flux adjacent to it. Probabilistic factors would be involved in this type of formalism.

5.2. Current–Potential Relations and Current and Potential Distributions

In this section, the salient results obtained using simple-pore, thin-film, and cylindrical pore models are outlined to highlight the nature of current–voltage relationships and the current (and potential) distribution patterns in the pore. For a critical discussion of the various treatments and details, the reader should consult References 7, 10, and 69–75.

5.2.1. Simple-Pore Model[76]

When all forms of polarization are present, the differential equation describing the potential variation in the pore (Figure 14) is given as

$$\frac{d^2\eta}{dz^2} = \frac{2i_0}{\rho r_2}\left\{\frac{C}{C_0}\exp\left(\beta\eta\frac{F}{RT}\right) - \exp\left[-(1-\beta)\eta\frac{F}{RT}\right]\right\} \tag{31}$$

where η is the overpotential, C, C_0 the surface and bulk concentration of the reactant respectively, z the distance coordinate, r_2 the pore radius, β the symmetry factor, F the Faraday constant, T the temperature, R the gas constant, and ρ is the specific conductance of the electrolyte. Solution of Eq. (31) with the boundary conditions

$$\eta = \eta_0 \qquad \text{at } z = 0 \tag{32}$$

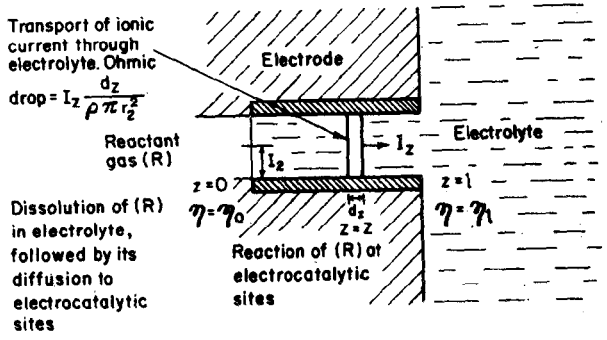

Figure 14. A schematic of a simple-pore model.[76] (With permission from *J. Chem. Phys.*)

and

$$i = \rho\pi r_2^2 \frac{d\eta}{dz} \qquad \text{at } z = 0 \tag{33}$$

results in the following relationships for the current distribution and total current per pore (i_t):

$$\frac{i_z}{i_t} = \left[\left(\frac{dc}{d\alpha}\right)_{\alpha=\alpha_1} - \frac{dc}{d\alpha}\exp\left(\frac{mx}{2}\right)\right] \Big/ \left(\frac{dc}{d\alpha}\right)_{\alpha=\alpha_1} \tag{34}$$

where

$$\frac{dc}{d\alpha} = 1 - \exp(-2y_0)\,\frac{K_1(\alpha_2)I_1(\alpha) - I_1(\alpha_2)K_1(\alpha)}{K_0(\alpha_1)I_1(\alpha_2) + I_0(\alpha_1)K_1(\alpha_2)} \tag{35}$$

$$x = \frac{z}{l} \tag{36}$$

$$\alpha = 2\left[\frac{a}{bm^2}\exp(y_0 + mx)\right]^{1/2} \tag{37}$$

$$a = \frac{i_0 l^2 F}{\rho r_2 RT} \tag{38}$$

$$b = \frac{DnF^2 C_0}{2\rho RT} \tag{39}$$

$$y_0 = \frac{\eta_0 F}{2RT} \tag{40}$$

$$m = \frac{lFi_t}{2\pi r_2^2 \rho RT} \tag{41}$$

In the above equations, η_0 is the overpotential at $z = 0$, n is the number of electrons transferred in the overall reaction, i is the current, l the pore length, i_z the total current generated from $z = 0$ to $z = z$, i_t the total current generated from $z = 0$ to $z = l$, α_1, α_2 are values of α evaluated at $z = 0$ and $= 1$, respectively, and K's and I's are Bessel functions of the indicated orders:

$$i_t = -2\pi r_2^2 \rho \frac{RT}{lF}[ab\exp(y_0)]^{1/2}\left(\frac{dc}{d\alpha}\right)_{\alpha=\alpha_1} \tag{42}$$

Since Eqs. (34) and (42) are complex, one may examine the polarization behavior under some limiting conditions.

5.2.1.1. Activation–Concentration Overpotential Control (Neglecting Ohmic Polarization)

The current density distribution and the total current, under these conditions, are expressed by the relationships

$$\frac{i_t - i_z}{i_t} = \left\{ \sum_{n=1}^{\infty} \frac{\sinh[(l-z)\alpha_n]}{\alpha_n(h^2+\alpha_n^2)\cosh l\alpha_n} \right\} \Big/ \sum_{n=1}^{\infty} \left[\frac{\tanh l\alpha_n}{\alpha_n(h^2+\alpha_n^2)} \right] \tag{43}$$

and

$$i_t = 4\pi i_0 \left[\exp\left(\frac{\beta\eta F}{RT}\right) - \exp\left(-\frac{(1-\beta)\eta F}{RT}\right) \right] \sum_{n=1}^{\infty} \frac{h \tanh l\alpha_n}{\alpha_n(h^2+\alpha_n^2)} \tag{44}$$

where α's are the roots of the Bessel function equation

$$\alpha r_2 J_1(\alpha r_2) - h r_2 J_0(\alpha r_2) = 0 \tag{45}$$

and

$$h = \frac{i_0}{DnFC_0} \exp\left(\frac{\beta\eta F}{RT}\right) \tag{46}$$

when $hr_2 \ll 1$, i.e., when the local activation current density is much smaller than the limiting current density due to radial diffusion,

$$\frac{i_z}{i_t} = \frac{\sinh K - \sinh[K(1-x)]}{\sinh K} \tag{47}$$

and

$$i_t = \frac{\pi r_2^2 DnFC_0}{l}[1 - \exp(-2y_0)]K \tanh K \tag{48}$$

where

$$K^2 = \frac{a}{b}\exp(y_0) \tag{49}$$

The current variations along the length of the pore deduced according to Eq. (47), in Figure 15, indicate the significant role of mass transfer. Thus at high values of K, the degree of utilization of the pore decreases owing to a decrease in C_0 or an increase in η_0, i_0, D, l. Under these conditions, $\tanh K = 1$ and

$$\frac{i_z}{i_t} = 1 - \exp(-Kx) \tag{50}$$

and

$$i_t = \frac{\pi r_2^2 DnFC_0 K}{l}[1 - \exp(-2y_0)] \tag{51}$$

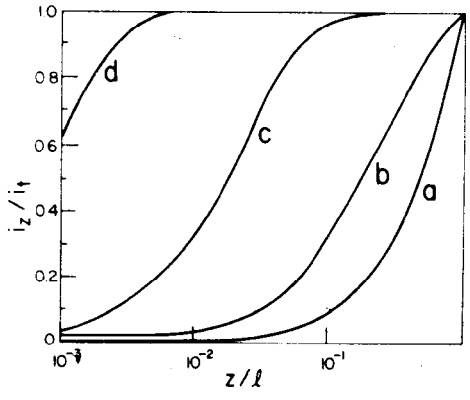

Figure 15. Current–distribution relations for the case of simple-pore model with all forms of polarization present as a function of K. Curve a: $K = 1$, $i_0 = 10^{-12}$ (A cm^2), $\eta_0 = 0.10$ (volts). Curve b: $K = 3.8$, $i_0 = 10^{-9}$, $\eta_0 = 0.10$. Curve c: $K = 40.5$, $i_0 = 10^{-12}$, $\eta_0 = 0.65$; $K = 40.5$, $i_0 = 10^{-6}$, $\eta_0 = 0.01$. Curve d: $K = 122.0$; $i_0 = 10^{-9}$, $\eta_0 = 0.65$. $DnFC_0 = 10^{-7}$ for all cases. (With permission from *J. Chem. Phys.*[76])

Equations (50) and (51) show that the penetration depth—a measure of the degree of participation of the pore in generating the current—decreases exponentially with distance and that the Tafel slope will be $2RT/\beta F$, which is twice the normal value of the Tafel slope observed for planar electrodes.

When K assumes small values, i.e., at low values of i_0, η_0 and at high values of the product $DnFC_0$, $\tanh K = K$ and therefore

$$\frac{i_z}{i_t} = x \tag{52}$$

and

$$i_t = \frac{\pi r_2^2 DnFC_0 K^2}{l}[1 - \exp(-2y_0)] \tag{53}$$

For this situation, the current density distribution in the pore is uniform and the Tafel slope is given by $RT/\beta F$ as observed on planar electrodes for rate-determining discharge-type reactions.

Under diffusion-controlled conditions, i.e., at large values of the term hr_2, the expression for the limiting current ($i_{t,l}$) appears:

$$i_{t,l} = 4\pi DnFC_0 r_2 \tag{54}$$

Figure 16 depicts the current–voltage relationship showing changes in slope corresponding to the limiting situations described above.

5.2.1.2. Activation–Ohmic Control

When the rate of the backward reaction becomes negligible in comparison to the forward rate,

$$\frac{i_z}{i_t} = \frac{\tan Ax}{\tan A} \tag{55}$$

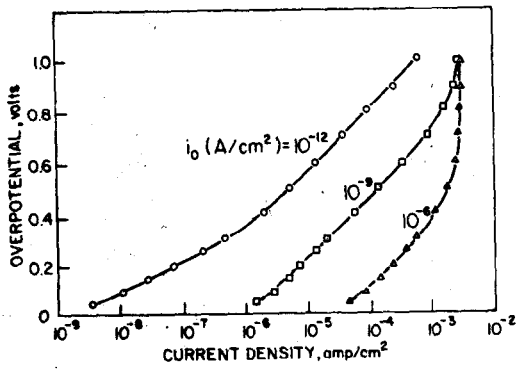

Figure 16. Overpotential–current density relationship[17] for the simple-pore model. Values of $DnFC_0$ and ρ are the same as in Figure 15. (With permission from *J. Chem. Phys.*)

where

$$A = \frac{a^{1/2}}{2} \exp\left(\frac{\gamma_0}{2}\right) \tag{56}$$

and

$$i_t = \frac{4RT\rho\pi r_2^2}{lF} A \tan A \tag{57}$$

The potential variation along the pore length is expressed by the following equation:

$$\eta_z - \eta_0 = \frac{4RT}{F} \ln \sec Ax \tag{58}$$

For small values of A (i.e., $A \leq 0.2$)

$$\frac{i_z}{i_t} = x \tag{59}$$

and

$$i_t = \frac{\rho\pi r_2^2 4RT}{lF} A^2 \tag{60}$$

This case corresponds to uniform current distribution realized through low i_0 values at low η_0 as well as for high r_2 and ρ values. The Tafel slope for this case is the same as observed on planar electrodes ($RT/\beta F$) for slow discharge reactions.

When $A \geq 1.4$, i.e., for high values of A, the current–voltage relationship can be expressed as

$$\ln i_t = \frac{\beta \eta_t F}{2RT} + \frac{1}{2} \ln \frac{8 i_0 RT \rho \pi_1^2 r_2^2}{F} \tag{61}$$

According to Eq. (61), the Tafel slope should be equal to $2RT/\beta F$ with reactions having high i_0 values at high η_0 and for low ρ and r_2.

Figure 17 illustrates the current distribution variations for the limiting cases discussed here.

A comparison of the expressions for current distribution and the current–voltage relationships obtained under various conditions show the following noteworthy features:

a. With low i_0 systems and at low η values, uniform current density distribution is expected and the Tafel slope is $RT/\beta F$ under ohmic-activation conditions.

b. At high η, the current density distribution is nonuniform and the Tafel slope is $2RT/\beta F$ for ohmic-activation and activation-concentration overpotential-controlled conditions, the main difference being that all the current is generated in the vicinity of the gas–electrolyte interface for activation-concentration overpotential control, whereas for ohmic-activation control, current is mainly generated at the opposite end (i.e., near $z = l$ in Figure 14).

5.2.2. Thin-Film and Dual-Porosity Models

While the simple-pore model is a naive description of a real porous matrix, experiments with partially submerged electrodes have showed that the electrode reaction takes place mainly in a region where the electrolyte forms a thin

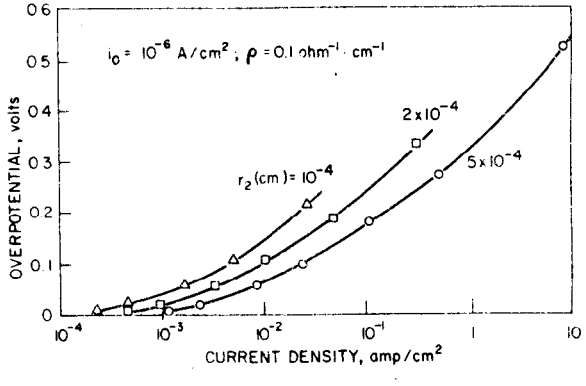

Figure 17. Overpotential-current density relationships under ohmic-activation conditions for a two-phase porous electrode.[17] (With permission from McGraw-Hill Book Company.)

meniscus and a film at the electrode–gas interface. This facilitates molecular diffusion of the gaseous reactant through the thin film of the electrolyte. For various geometries of meniscus and film, mathematical analyses have been carried out by several authors (see References 7, 10, 69–75, and 77–80 for a comprehensive discussion).

A comparison[77] of the results of the simple-pore model with the theoretical calculations performed using a finite thin-film model show non-uniform current–density distribution at low overpotentials for the latter model. This arises owing to ionic conduction through a finite thickness of the film, whereas in the simple-pore description, the entire pore is used. Unlike the simple-pore model, even with low i_0 reactions and at small overpotentials, there is an effect due to ohmic overpotential in the case of the thin-film model.

The applicability of the thin-film models for describing porous electrode systems seems to have a restricted scope.[79]

Most real systems (e.g., Bacon electrode, JUSTI DSK electrode) have a dual-porosity structure, in which the bulk electrolyte meniscus is stabilized at a junction between coarse- and fine-porosity layers. Evidence of thin films on nonwetting surfaces is again difficult to envisage, unless it is assumed that these films are formed at wettable micropores.

The dual-porosity model has been treated by several authors[62,81] and, here we briefly present Pshenichnikov's model,[66,82] which treats a porous electrode as containing both wide and narrow pores—the wide ones being filled with gas but having their walls covered with a solution film, and the narrow ones being flooded. According to this model, the current is proportional to $(p\phi)^{1/2}$, where p is the total perimeter of the gas-filled areas and ϕ refers to the total cross section of the solution-filled pores. p and ϕ are experimentally accessible, and vary with gas pressure. Increase in gas pressure leads to an increase in ϕ and a decrease in p, and hence the electrode performance (i.e., current) has a maximum at a given pressure. Figure 18 shows a comparison of the theoretical

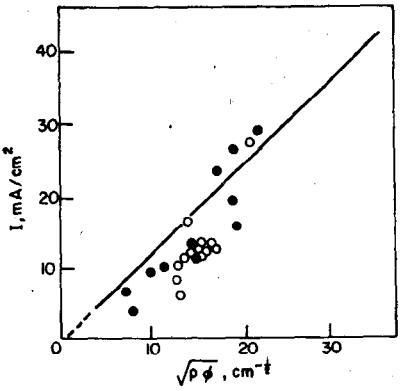

Figure 18. Electrochemical activity[66] as a function of $(p\phi)^{1/2}$. ○: $r = 1.5\ \mu m$, $\Delta P = 600$ torr; ●: $r = 3\ \mu m$, $\Delta P = 300$ torr. (With permission from the author and the Consultants Bureau.)

variation of total current vs. $(p\phi)^{1/2}$ with the experimental results obtained during the oxidation of H_2 on nickel electrodes.

5.2.3. Models for Hydrophobic Electrodes

The biporous model discussed in Section 5.2.2 seems applicable for hydrophilic-type systems. However, for describing hydrophobic electrodes, the "biporous approach" seems inadequate[62] to explain the observed phenomena.

Several models have been proposed for the hydrophobically treated electrodes and these models may be classified into three basic types[83] (see Figure 19). In the first category (model I in Figure 19), the hydrophobic gas pores are formed by agglomerates of PTFE in a hydrophilic medium consisting of catalyst particles and separated by the electrolyte. In model II, the hydrophilic pores are formed by agglomerates of catalyst located in a hydrophobic medium consisting of PTFE particles with the space occupied by gas. It may be noted that the first category of models may be transformed into the second by increasing the amount of PTFE in the coating. These two descriptions assume that the catalyst particles are not present in the gas pores and that PTFE is absent from the liquid pores. More complex variations of these models have been considered by Chirkov (see, for example, Reference 84). The last category of model (model III) assumes a material whose activity is proportional to the specific surface of catalyst per unit volume—the contact angle at the

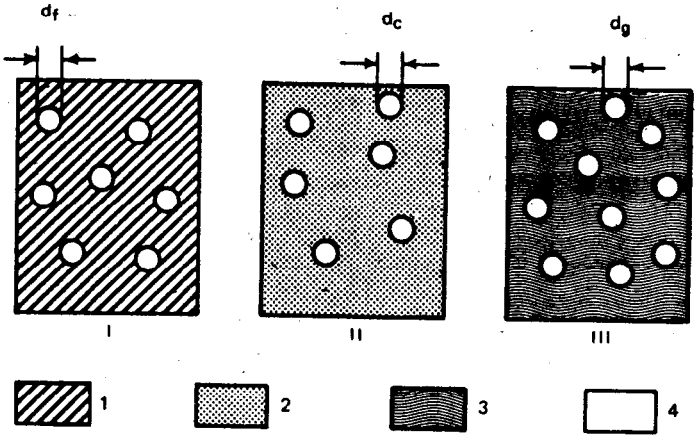

Figure 19: Models[83] of hydrophobically treated electrodes; d_f is the mean size of pores by PTFE, d_c the mean size of liquid pores formed by the catalyst, and d_g the mean size of the gas pores formed by the homogeneous mixture of the catalyst and PTFE. (1) catalyst; (2) PTFE; (3) uniform mixture of catalyst + PTFE; (4) gas. (With permission from the authors and the Consultants Bureau.)

boundary of the liquid being determined by the PTFE concentration at the surfaces of the gas pores.

5.2.3.1. Flooded Agglomerate Model

This model, introduced by Giner[85,86] in an attempt to explain the dependence[92] of the electrochemical activity on the agglomerate size of catalyst particles (see Figure 20), assumes that the catalyst particles (forming the flooded agglomerate and flooded with the electrolyte) are bonded together by Teflon binder, which creates the hydrophobic gas channels. As the current is drawn, gas diffuses through these channels, dissolves in the electrolyte contained in the agglomerates, and reacts at the available catalytic sites. Assuming the absence of transport limitations in the gas phase and kinetic limitations in the process of gas dissolution, a theoretical analysis was performed and experimentally tested. Performance characteristics of a Teflon-bonded Pt electrode (Pt loading ~20 mg/cm^2) acting as an oxygen cathode in 30% KOH at 80°C were studied.

The theoretical calculations showed the current to be significantly affected by decreasing the agglomerate radius (r_0) from 10^{-3} to 10^{-4} cm under diffusion conditions (see Figure 21A). Further decrease below 1 μm was found to have no influence on the performance. The current densities calculated for $i_0 = 5 \times 10^{-7}$ A/cm^2 and agglomerate sizes $r_0 \leq 10^{-4}$ cm are in close agreement with those determined experimentally. The effect of microporosity on current is not pronounced at small values of the characteristic agglomerate size. Thus the performance behavior is controlled by internal diffusion limitations with large agglomerates, and optimal utilization of the catalyst is expected when the catalyst is at the periphery of the agglomerate.

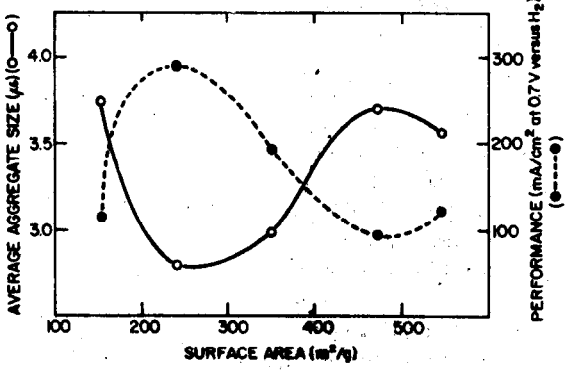

Figure 20. Influence of agglomerate size on the electrochemical activity of graphite during oxygen reduction.[92] (With permission from the authors and *Nature*.)

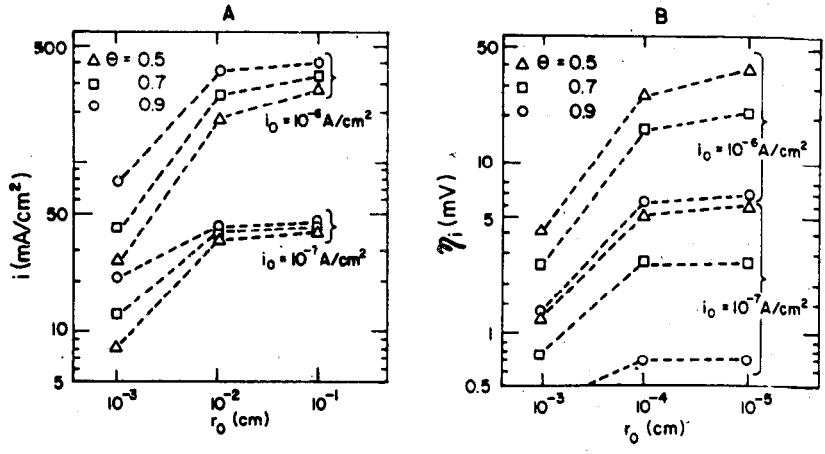

Figure 21. Effect[85] of r_0, i_0, and microporosity (θ), at 300-mV polarization on (A) measurable current density and (B) internal ohmic drop (η_i). (With permission from the authors and *J. Electrochem. Soc.*)

Figure 21B shows the effect of agglomerate size, microporosity, and i_0 on the internal ohmic drop (η_i), which becomes significant at low r_0 and high i_0 values.

When the utilization of the catalyst across the thickness of the electrode (transversal) and along the radius of the flooded agglomerate (radial) is high, as achieved with $r_0 = 10^{-5}$ cm and $i_0 = 10^{-7}$ A/cm², the Tafel behavior is normal, with a slope of $RT/\beta F$. However, if the radial utilization of the agglomerate is poor, a linear relationship (with a Tafel slope of $2RT/\beta F$) is predicted.

5.2.3.2. Cylindrical Gas Pore Model

The main parameter determining the distribution of gas and liquid and the electrochemical activity of hydrophilic electrodes is the pressure difference between the gas and the solution. However, in the case of hydrophobized electrodes, the performance characteristics depend on the degree of hydrophobilization. Thus as the Teflon concentration is increased, the electrochemical activity goes through a maximum at a Teflon concentration of 30–35% (see Figures 22 and 23).

Burshtein *et al.* suggested a model[87–90] to explain the above observation by proposing gas-filled circular cylinders of radius r, arranged in a regular manner, with walls composed of a mixture of PTFE and catalyst, moistened with the electrolyte. Neglecting the backward rate and gas diffusion through the electrolyte film, the polarization distribution equation was solved for the

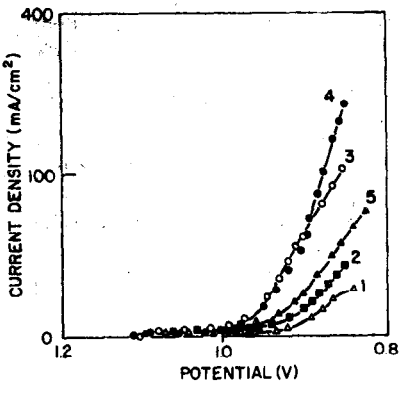

Figure 22. Polarization curves[88] for oxygen reduction at hydrophobized electrodes containing various amounts of Teflon (wt %); (1) 5; (2) 10; (3) 20; (4) 35; (5) 50. (With permission from the authors and the Consultants Bureau.)

total current density (i_t), expressed by Eq. (62), which was found to be in good agreement with experiment (see Figure 23):

$$i_t = \left[\frac{4RT\bar{x}\nu_1}{F^{1/2}r}(\eta\bar{D}C_0S_cV_c)^{1/2}\int_{\bar{\eta}_\Delta}^{\bar{\eta}_0}\exp\left(\frac{\bar{\eta}}{2}\right)\psi(\bar{\eta})\,d\bar{\eta}\right]^{1/2} \tag{62}$$

where

$$\bar{\eta} = \frac{\eta F}{RT} \tag{63}$$

$$\psi = \frac{I_1(l'/l_d)K_1(r/l_d) - I_1(r/l_d)K_1(l'/l_d)}{I_1(i/l_d)K_0(r/l_d) + I_0(r/l_d)K_1(l'/l_d)} \tag{64}$$

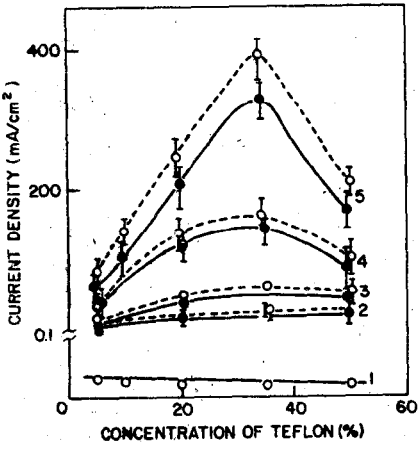

Figure 23. Electrochemical activity[88] of hydrophobic electrodes as a function of Teflon concentration at various values of overpotential (mV); (1) 5; (2) 100; (3) 150; (4) 200; (5) 250. The continuous lines represent experimental data and the dashed lines to the calculated values. (With permission from the authors and the Consultants Bureau.)

K_1, K_0, I_1, I_0 are Bessel functions of pure imaginary argument, r is the radius of the gas cylinder, $\bar{x}$ the effective conductivity of the electrolyte, $\bar{\eta}_\Delta$ the electrode polarization on the gas side, $\bar{D}$ the effective diffusion coefficient, $\bar{S}_c$ the specific surface of the catalyst, v_c the volume fraction of the catalyst in the mixture, ν_1 the gas porosity, l_d the characteristic diffusion length, and l' is half the mean distance between the gas pores.

Thus, at low Teflon concentrations, the proportion of gas porosity, ν_1, is small over the entire pore volume and the active layer is filled with the electrolyte. This results in (internal) diffusion control and hence the current is small. As the Teflon concentration is increased to ~20–35%, the gas porosity increases which, in turn, shifts the control from diffusion to activation, thereby enhancing the electrochemical activity. Further increase in Teflon concentration results in lowered electrochemical activity due to decrease in effective conductivity, $\bar{x}$, and the catalyst surface per unit volume.

The descriptions of porous electrode operations, mentioned in this section, in no way describe all phenomenological features (see Table 5) observed with gas diffusion electrodes. Rigorous approaches, not ignoring the fine structure of the porous matrix, interphase boundaries, and other attendant phenomena such as mass transfer, adsorption, etc., are still not available and are much awaited. It may be pointed out that most of the published models are essentially phenomenological descriptions (see Figure 13) and a "unified" description with limiting situations corresponding to the present models could probably provide a deeper insight in understanding the porous electrode operations.

5.3. Extent of Utilization of Total Surface Area of Supported Catalysts

The degree of utilization of the catalyst is one of the important parameters and is essential for optimization purposes, especially in view of the expensive catalyst materials used for preparing gas diffusion electrodes, which suffer from polarization losses mainly caused by finite conductivity of the electrolyte, matrix and diffusion of reactants, and products. Hence the less the current is controlled by the transport of reactants (and/or products) to the catalyst sites, the more efficient the surface of the catalyst can participate in the electrochemical reaction.

The degree of utilization, q, is defined[91] as the ratio of the transport-controlled current density, i_m, to the ideal current density:

$$q = \frac{i_m}{i_d} = \frac{I_p}{i_d S'} \tag{65}$$

i_m can be estimated from the measured current, I_p (A/g), at a given overpotential, and from the specific surface, S' (cm^2/g) of the catalyst.

Obviously, the relationship of q to the characteristic porous electrode parameters depends on the specific model, the choice of which depends on the type of the system under study. For simple-pore models, q has been shown[91] to be expressed by the relationship

$$q = \frac{\lambda}{l} \tanh \frac{l}{\lambda} \tag{66}$$

where

$$\lambda = \left(\frac{nFr_2DC_0}{2i_0}\right)^{1/2} \exp\left(\frac{-\beta\eta F}{RT}\right) \tag{67}$$

λ signifies the penetration depth of the current.

According to Eq. (66), the electrode is best utilized with small pore lengths at low polarization, and for low exchange current density reactions (see Figure 24A). Pore diameter also influences the degree of utilization as seen in Figure 24B. Thus, by proper choice of pore dimensions, it is possible to optimize the electrode structure to realize maximum activity at low catalyst loadings. Ohmic resistance in the catalyst and support also influences the degree of utilization, and the reader is referred to the original article[91] for additional details (see also References 85 and 86 for a discussion of the radial and depth utilization factors for the flooded agglomerate model).

5.4. Surface Area Measurements

Surface area, porosity, exchange current density, diffusion coefficient of the reactants (and/or products) within the porous matrix are some of the relevant parameters characterizing the performance (and failure!) of porous electrodes. Thus "surface area" calculated from the double-layer capacitance

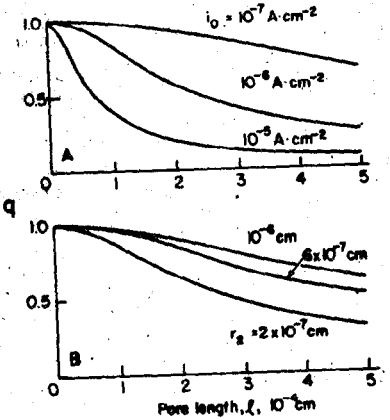

Figure 24. Degree of utilization[91] of a catalyst pore (q) as a function of pore length (l): A, for varying i_0 at $\eta F/RT = 4$; B, for varying pore radii at $\eta F/RT = 1$. (With permission from the authors and Pergamon Press.)

is known to provide a reliable estimate of the *effective surface area* participating in the electrochemical reaction. A knowledge of the exchange current density, on the other hand, yields information regarding the influence of geometric factors (e.g., crystallite size[12]) on the intrinsic rate of the electrochemical reactions. These parameters have previously been estimated using various transient techniques such as current step,[93] potential step,[94] linear sweep voltammetry,[95] and low-frequency ac impedance.[96]

Analysis[97] of these various techniques indicates that most of the difficulties associated with evaluating the double-layer capacity stem from the interference of Faradaic reactions and lack of an independent estimate of the resistance of the electrolyte in the pores, both of which tend to complicate the data analysis. These complications are normally "avoided" by selection of experimental conditions, such that the influence of a Faradaic reaction is minimized. Electrolyte resistance within the pores is usually estimated and/or neglected in these treatments.

These difficulties are overcome, to a large extent, by using the exponential relaxation technique.[97] Assuming the elementary flooded model and linear i–η relationship (neglecting diffusion and adsorption pseudocapacitance), the potential response to an exponentially decaying current pulse [i.e., $\Delta i(t) = \Delta i \exp(-t/\tau)$] can be expressed by the relationship

$$\eta(t) = -R_0 i(t)\left(\frac{\exp[-t(B - 1/\tau)] - 1}{\beta'(B - 1/\tau)} + \left\{\frac{2}{\beta'}\sum_{n=1}^{\infty}\frac{(-1)^n \cos n\pi(1-x)}{(A - 1/\tau)}\exp[-t(A - 1/\tau)]\right\}\right) \tag{68}$$

where

$$A = \frac{n^2\pi^2 + \alpha'}{\beta'} \tag{69}$$

$$B = \frac{\alpha'}{\beta'} \tag{70}$$

$$\alpha' = \frac{R_0 S \ln Fi_0}{RT} = \frac{R_0}{R_T} \tag{71}$$

where τ is the time constant of the exponentially decaying pulse, R_0/R_T is the ratio of the electrolyte resistance in the pores to the charge transfer resistance;

$$\beta' = R_0 C_T \tag{72}$$

where $R_0 C_T$ is the time constant associated with the charging of the double layer;

$$R_0 = \frac{l}{\rho A} \tag{73}$$

where A is the cross-sectional area;

$$C_T = SC_d l \tag{74}$$

where C_T is the total differential capacity, S is surface area of the porous electrode per unit length, and C_d is the differential capacity per cm^2.

The potential response exhibits a maximum due to the opposing character of the increasing tendency of potential with time and the decreasing nature of the input function. The coordinates of this maximum are related:

$$\frac{\eta_m}{\Delta i\tau} = \frac{1}{C_T}\exp\left(-\frac{\alpha' t_m}{\beta'}\right)\theta_3 \exp\left(-\frac{\pi^2 t_m}{\beta'}\right) \tag{75}$$

where $\theta_3(X)$ is the Jacobian θ function defined as $\sum_{n=0}^{\infty} \varepsilon_n X^{n^2}$ ($\varepsilon_n = 1$ for $n = 0$; $\varepsilon_n = 2$ for $n > 0$).

When $t_m \gg \beta'/\pi^2$, an approximation that is valid for $\beta \to 0$ (i.e., when the control is shifted from R_0 to R_T), is

$$\frac{\eta_m}{\Delta i\tau} = \frac{1}{C_T}\exp\left(-\frac{\alpha'}{\beta'} t_m\right) \tag{76}$$

A plot of $\ln(\eta_m/\Delta i\tau)$ vs. t_m should yield a straight line of slope $\alpha'/\beta' = 1/R_T C_T$ and intercept $1/C_T$. From C_T, S can be estimated assuming an ideal double layer capacity of $\sim 20\ \mu F/cm^2$ in the cathodic region and 30–40 $\mu F/cm^2$ in the anodic region. This technique has been tested using a sintered nickel plaque in 4 M NaOH at 25°C.

Figure 25A depicts the input current profile $i(t) = \Delta i \exp(-t/\tau)$ in which $\Delta i = 0.77\ mA/cm^2$ and $\tau = 826$ msec. The corresponding potential response is also presented in Figure 25B. These input–output profiles indicate the qualitative behavior previously discussed, i.e., presence of a maximum in the potential transient, the locus of which is dictated by the input parameters and electrode properties.

All the experimentally determined η_m–t_m pairs for the nickel plaque system are plotted in Figure 26 as $\ln(\eta_m/\Delta i\tau)$ vs. t_m. The linearity, predicted by the theory, is apparent for values of $t_m > 50$ msec. From the intercept of Figure 26, C_T is estimated to be 6.7 mF. The slope yields a value of the charge transfer resistance, $R_T = 63.9\ \Omega$. This R_T value corresponds to an exchange current density of $\sim 1\ \mu A/cm^2$, in general agreement with the published data.[98,99]

5.5. Transient Techniques to Study Porous Electrode Phenomena

Unlike the steady state techniques, transient studies can provide information because of the extra parameter, viz., time, available to the experimenter. Time-dependent phenomena can be examined by using either pulse or impedance measurements. These aspects as related to porous electrodes have

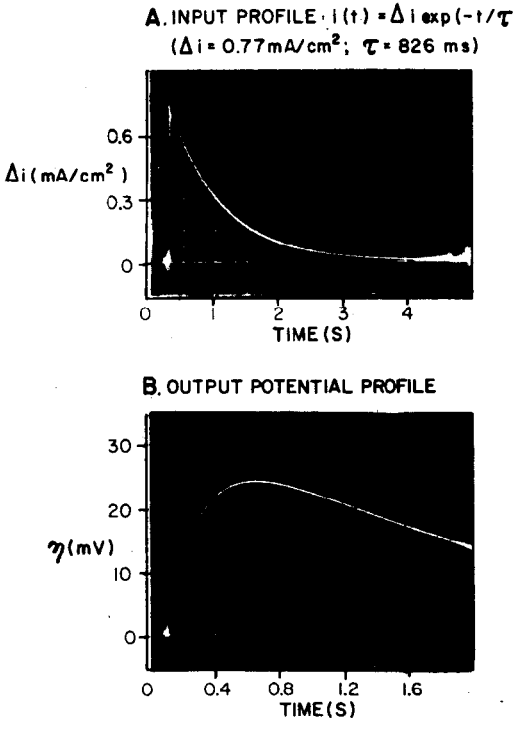

Figure 25. Experimental input current and output potential profiles for Ni plaque–NaOH system.[104]

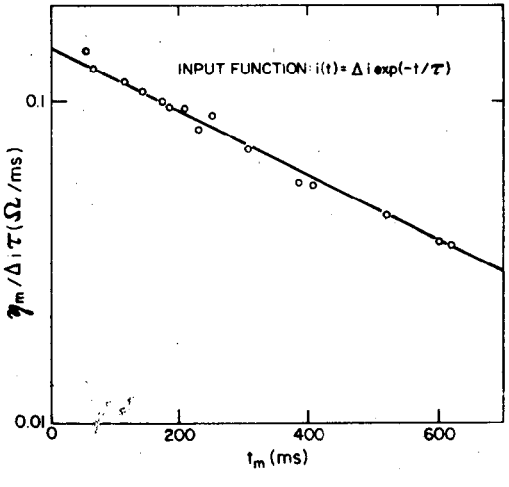

Figure 26. Plot of $\eta_m/\Delta i\,\tau$ vs. t_m for the Ni plaque–NaOH system.[97] (With permission from *J. Electrochem. Soc.*)

been comprehensively treated by deLevie[74] and are not presented here. However, some generalities associated with the transient techniques, based on a recent parametric analysis[100] of linear perturbation techniques are outlined in this section. This analysis carried out in a time or frequency axis (parametric domain) showed that the role of input parameters, occurring through the input voltage on the current profile, lies in the ability of "force" specific features, e.g., a maximum, inflection point, change of polarity, etc., in the output response profile, which can be conveniently employed to arrive at the parameters characterizing the interfacial processes. This approach was extended to show, for example, how two-parameter current-controlled functions[101-103] would provide response characteristics, unique in the ease of data analysis and experimental design. In this treatment, the theoretical equivalency of all relaxation techniques is stressed with emphasis placed on the ease of data acquisition which makes one technique "better" than others for a given system.

5.5.1. Transient Response under Ohmic-Activation Conditions

Output response to various forms of current or potential-controlled input profiles are available[74,104] in the literature. Of these, the exponential relaxation technique seems to be more promising for determining the overall double-layer capacity and charge transfer resistance (see Section 5.4 for details).

5.5.2. Transient Response under Activation and/or Diffusion Conditions

Grens and Tobias,[105] Rangarajan,[106] and Alkire *et al.*[107] (see Reference 74 for a discussion of the earlier work) examined the dynamic response of porous electrodes for diffusion-controlled conditions. The treatment of Grens and Tobias and Alkire *et al.* involves numerical analysis of the convective-diffusion transport equations relevant to the homogeneous models of porous electrodes. Some results,[104] valid under diffusion-limited conditions that would provide information on *in situ* values of diffusion coefficients and effective electrolyte conductance appropriate for the porous medium under study are presented here. When diffusion, whether it be in the bulk or in the pores, becomes the rate-controlling process, as at sufficiently large times (and also $\rho \to 0$, $R_0/R_T \to 0$, and $\theta_4 \sim \theta_4^0 \to \infty$), the current–time behavior in a galvanostatic experiment under linear polarization conditions, can be shown to be given by

$$\eta(t) \sim iR_0\left(\frac{X_0^2}{\{\frac{1}{2} - (\theta_3/2X_0)[(X_0^2/\theta_3) - 1]^2\}} \times \frac{1 - \exp\{-[(D/L^2)(\theta_3 - X_0^2)]t\}}{(\theta_3 - X_0^2)}\right) \tag{77}$$

where X_0 is the nonzero root of

$$\tanh X + X\left(\frac{X^2}{\theta_3} - 1\right) = 0 \tag{78}$$

and

$$\theta_3 = \frac{\nu_r S i_0 E L^2}{nFC_r^v D'}, \qquad \theta_4^0 = \frac{DL}{D'\delta} \tag{79}$$

where D is the diffusion coefficient in the bulk, D' is the diffusion coefficient in the pores, δ is the diffusion layer thickness, ν_i is the stoichiometric reaction coefficients of species i, and C_i^v is the equilibrium concentration of the species i ($i = r$ for reactant and $i = p$ for product) and

$$E = 1 + \frac{\nu_p C_r^v}{\nu_r C_p^v} \tag{80}$$

The time required for the potential to reach steady state, τ_s, for the above conditions can be approximated[106]:

$$\tau_s \approx \left(3X_0 \coth \frac{X_0}{\theta_3}\right)\frac{L^2}{D} \tag{81}$$

When the input function is $i(t)$ equal to $\Delta i \exp(-t/\tau)$, the corresponding potential response is expressed by the relationship

$$\frac{\eta(t)}{R_0} \sim \frac{i(t)Y_0^2}{(\theta_3/a') - (Y_0^2/a') - (1/\tau)} \times \frac{1 - \exp\{-[(\theta_3/a') - (Y_0^2/a') - (1/\tau)]t\}}{a'\{\frac{3}{2} - (\theta_3/2)[(Y_0^2/\theta_3) - 1]^2\}} \tag{82}$$

where Y_0 is the dominant nonzero root of

$$\tanh Y + Y\left(\frac{Y^2}{\theta_3} - 1\right) = 0 \tag{83}$$

and $a' = L^2/D$.

The coordinates of the maximum in the potential transient are related as shown in the following equation:

$$\frac{\eta_m}{\Delta i \tau} \sim \frac{Y_0^2}{a'\{\frac{3}{2} - (\theta_3/2)[(Y_0^2/\theta_3) - 1]^2\}} \exp\{-[(\theta_3/a') - (Y_0^2/a')]t_m\} \tag{84}$$

Thus, from an evaluation of τ_s or from a plot of $\ln(\eta_m/\Delta i\tau)$ vs. t_m, it is possible to obtain estimates of θ_3 which are related to the diffusional characteristics of the porous electrode–electrolyte system.

6. Fuel Cell Systems: Applications, Performance, and Economics

6.1. Types of Applications of Fuel Cells

6.1.1. Space

It is well known that the first important application for fuel cells was in a series of space missions, including the Gemini,[108] the Apollo,[109,110] Skylab, and Apollo–Soyuz link-up missions. Multikilowatt advanced fuel cells are being developed for the NASA Space Shuttle,[111] Biosatellite, and other high-altitude Aerostat programs. In addition, the same basic cell design as in the General Electric solid polymer electrolyte fuel cell[112,113] is being used (a) in the water electrolysis mode to generate oxygen for spacecraft and submarine life support systems, and (b) in an oxygen concentrator mode (which combines an air-breathing fuel cell cathode with an electrolysis anode, so that the net power for producing pure oxygen is reduced) to generate oxygen for the crew in combat aircraft.[114,115]

6.1.2. Military

The fuel cell, as a versatile ground power unit, also appears to be attractive for terrestrial and military applications. Thus the hydrazine–air fuel cell has been employed by the U.S. Army for battery charging, etc., and Engelhard[116-118] phosphoric acid fuel cells of 12 and 750 W have been employed as a long-life power source for telecommunication relays, offshore navigational aids, etc. As for underwater applications, a 20-kW hydrogen–oxygen unit has been built by Pratt & Whitney Aircraft for the U.S. Navy for the propulsion of the Deep Submergence Search Vehicle.

Fuel cells offer special advantages as buoy power sources where light weight and small volume are desired. Self-contained fuel cell power units of 1.8 and 44 kWh for buoy applications, developed by General Electric for the U.S. Navy, are designed to operate continuously for three months and one year, respectively, at peak power levels of 8 and 500 W and can be readily sized to several hundred kilowatts. A secondary peaking battery is included in the system for applications where high pulses are required for short time periods.

6.1.3. Transportation

Apart from space and military uses, another potential application of fuel cells is for powering transportation vehicles. An advantage of fuel cells over internal combustion (IC) engines as a mobile power source is that fuel cells have higher torque characteristics and efficiencies at lower speeds, whereas the reverse is the case with IC engines.[120] The fuel cell is the only energy

conversion device which is non-Carnot limited and hence has the greatest potential of achieving the highest efficiency for utilization of the chemical energy of a fuel. Since higher torque at lower speeds is desirable and air pollution effects are minimal, fuel-cell-powered vehicles show promise of replacing conventional vehicles.

6.1.4. Utility

Fuel cells are being developed for electric and gas utility applications because of the many attractive features including high energy conversion efficiency, flexibility, and minimal disturbance to the environment.[119] As a result, fuel cell power plants are ideal for on-site service, close to the point of energy demands, permitting effective utilization of waste heat. In this way, over 80% of the energy value of the fuel can be used, which leads to significant resource savings.

Large-megawatt power plants are suitable for central power generation. The waste heat from the fuel cell can be used for fuel conditioning, and even for coal gasification when a high-temperature fuel cell is employed. On the other hand, the smaller-kilowatt power plants are ideal for service at substation level or even near to the users, such as for apartment buildings, industry sites, and shopping centers. A fuel cell, coupled with a heat pump, not only supplies all necessary electricity, but also provides thermal energy (space heating–cooling, hot water, process heat). This *on-site total energy concept* will be discussed in Section 6.2.2.3.

Fuel cells also find application in electric utility load leveling and peaking when hydrogen is used as the medium to store energy and transport energy to the site (see Section 1.4). Other applications include on-site fuel resource conservation in electrolytic industries, e.g., chloralkali industry.[121]

6.2. Fuel Cells for Electric and Gas Utility Application

6.2.1. The Advantages of the System

For terrestrial power generation applications, efficiency, cost, and useful life are essential. In a time when utility plant costs are high, construction lead times long, and future power demand uncertain, the major attraction towards fuel cells is their versatility, which stems from the physical, operating, and fuel flexibilities associated with the fuel cell power plants.

6.2.1.1. Physical Flexibility

A typical fuel cell power plant consists of three basic units (see Figure 27): fuel processor (or conditioner), fuel cell, and power conditioner. These units are essentially modular in nature and can be connected in parallel or in series to meet additional power demands. This inherent modularity in turn permits standardization so that they can be factory built and rail/truck-transported to

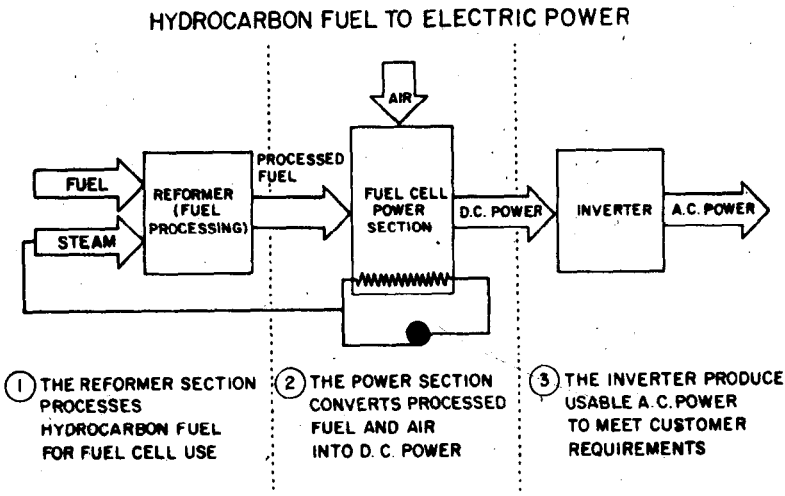
HYDROCARBON FUEL TO ELECTRIC POWER
AIR
FUEL
STEAM
REFORMER (FUEL PROCESSING)
PROCESSED FUEL
FUEL CELL POWER SECTION
D.C. POWER
INVERTER
A.C. POWER
1 THE REFORMER SECTION PROCESSES HYDROCARBON FUEL FOR FUEL CELL USE
2 THE POWER SECTION CONVERTS PROCESSED FUEL AND AIR INTO D.C. POWER
3 THE INVERTER PRODUCES USABLE A.C. POWER TO MEET CUSTOMER REQUIREMENTS

Figure 27. Basic segments of a typical fuel cell power plant.[122]

the plant site. This results in lower cost, shorter plant construction lead time, and greater flexibility in plant size.

6.2.1.2. Operating Flexibility

The fuel cell system (in various sizes) could serve at any point in a utility system, from a central power station to the consumer site. Siting close to the point of electricity demand can reduce energy losses associated with transmission and distribution (about 8–10% of power transmitted), besides saving the capital cost of transmission lines (about $50–$100/kW). Additional fuel savings through effective use of waste heat usually discarded in central generating systems can be readily effected. It should be noted here that the fuel cell power plants, ranging in power output from <100 to >1000 kW, have an efficiency (see Figure 28A) comparable[122] to the best large central steam plants and, at part load operation, the efficiency of fuel cells increases (see Figure 28B), unlike the conventional generation systems. Furthermore, fuel cells can also provide "instant response," generating electricity from the moment they are switched on.

6.2.1.3. Fuel Flexibility

Fuel flexibility is another advantage of fuel cell systems since fuel processors already accept a variety of hydrocarbon fuels, including light distillates, natural gas, methanol, and high-, medium-, and low-Btu gases† with a

† Natural gas or high-Btu gas (mainly methane) has a heating value of about 1000 Btu/ft^3 or 200 kcal/mol; low-Btu gas of less than 500 Btu/ft^3 and usually less than 150 Btu/ft^3. Gas in the 300–500-Btu/ft^3 range is often called medium- or intermediate-Btu gas.

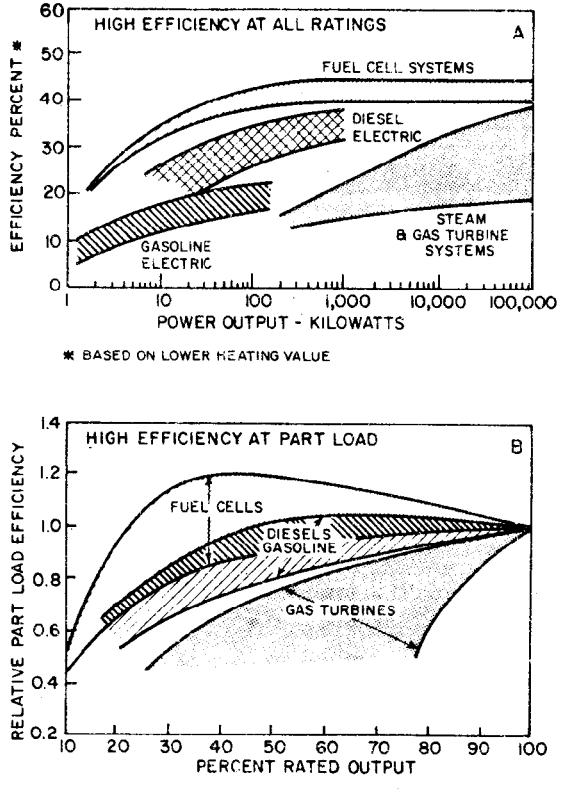

Figure 28. Fuel economy vs. efficiency at (A) full load and (B) part load operation (from Reference 122).

possibility of using synthetic fuel products from the nation's more plentiful coal supplies.

6.2.1.4. Environmental Impact

Environmental considerations such as low water requirements, limited emissions, and quiet operation help make fuel cell plants an attractive power option. Where fossil fuel and nuclear plants require large quantities of water for cooling, fuel cells (which generate less heat) can be air cooled by low-speed fans. Furthermore, since fuel cells do not involve a combustion process, emissions from their operations are significantly lower than emissions from conventional plants, and well within[122] the present EPA requirements (see Table 6).

Table 6
Comparison of Emissions from Fuel Cells and Other Modes of Power Generation[122]

Emission	Gas-fired central station[a]	Oil-fired central station[a]	Coal-fired central station[a]	Experimental fuel cells[b]
Particulates[c]	0.1	0.1	0.1	0.0000029
NO_x[c]	0.2	0.3	0.7	0.013–0.018
SO_2[c]	No requirement	0.8	1.2	0.000023
Smoke (% opacity)	20	20	20	Negligible

[a] Federal standards (effective August 17, 1971).
[b] York Research Corporation, Y-7309, April 1970.
[c] lbs/10^6 Btu heat input.

The range of sizes, the modularity, and the environmental advantages make the fuel cell system an attractive candidate for power generation in a variety of utility applications. Multimegawatt fuel cell power plants will be dispersed within electric utility networks to complement large-scale systems to cater to the needs of small private and public utilities. Small-size fuel cells will be sited at building locations to provide integrated electric and thermal service for commercial and industrial complexes (see Section 6.2.2.3).

6.2.2. Power Plant Characteristics

Economic and logistic analyses indicate that the size unit for dispersed power generation which would provide the greatest benefit would be approximately 27 MW. The large-megawatt-size power plants designed for on-site service are capable of continuously operating at any output power level from 1/4 load to rated load, supplying up to 10% overload. The small (typically 40 kW) power plants, capable of operating continuously at any output electrical power level from zero to rated load, can supply up to 40% overload for periods of up to one second to accommodate consumer transients.

6.2.2.1. Overall Efficiency

The performance characteristics of a fuel cell power plant can be best judged by three important parameters, which are defined as follows (see Reference 119 for a thorough discussion of various other factors involved in describing the fuel cell power plant operations):

$$\text{Overall efficiency} = \frac{\text{power output}}{\text{HHV of coal required to produce the fuel}} \quad (85)$$

Power plant efficiency

$$= \frac{\text{power output at grid voltages}}{\text{HHV of fuel (e.g., high-Btu gas) fed to the power system}} \tag{86}$$

$$\text{Thermodynamic efficiency} = \frac{nFE}{\text{HHV of fuel}} \tag{87}$$

E refers to the average cell voltage, F to 23.06 kcal/eV, n to number of electrons transferred, and HHV to the higher heating value (heat of combustion, at 25°C) of the fuel.

It is interesting to note that Eq. (87) becomes Eq. (16) by replacing HHV of the fuel by ΔH. That is to say, the thermodynamic efficiency of a fuel cell power plant is represented by the overall efficiency of the cell alone.

The power plant efficiency is also expressed in terms of heat rate (HR) of the power plant as

$$\text{HR} = V_{\text{fuel}} \cdot (\text{HHV}) \cdot P_{\text{dc}}/P_{\text{ac}} \tag{88}$$

where V_{fuel} refers to the fuel rate (see below), P_{dc} to the nominal dc power rating in megawatts, and P_{ac} to the net ac power output in megawatts. V_{fuel} is expressed by the relationship

$$V_{\text{fuel}} = A/nFEf_{\text{H}_2}f_{\text{fuel}}B \tag{89}$$

where A is a constant and B refers to moles of hydrogen produced per mole of fuel gas, f_{H_2} to hydrogen utilization (see Section 6.5.6), and f_{fuel} to the fraction of fuel gas used for fuel conversion.

The smaller the heat rate, the more efficient the system is. Thus a heat rate of 9000 Btu/kWh (HHV) is equivalent to an efficiency of 40.6% (LHV, lower heating value). The heat rate goal [123] of the present fuel cell power plant is 7500 Btu/kWh with naphtha and 7100 Btu/kWh with methanol as the starting fuel. A nominal heat rate curve is shown in Figure 29. The break in the curve reflects the point of transition from operation with the normal high-flow turbocompressor for pressurizing the process air to a special low-flow turbocompressor used to obtain good efficiency at lower power for spinning reserve.

Thermodynamic efficiency is a function of the overall cell voltage (E) which is related to overvoltages as expressed by Eq. (12). Thus the operating cell performance is governed by the current–voltage characteristics at the individual porous gas diffusion electrodes and is a function of reactant and gas composition and utilization, operating temperature, pressure, etc. As discussed in Section 5 there is no adequate description of real porous electrode systems and, hence, various idealizations have been employed to predict the local current–voltage relationship (see References 119, 124, 125 for details).

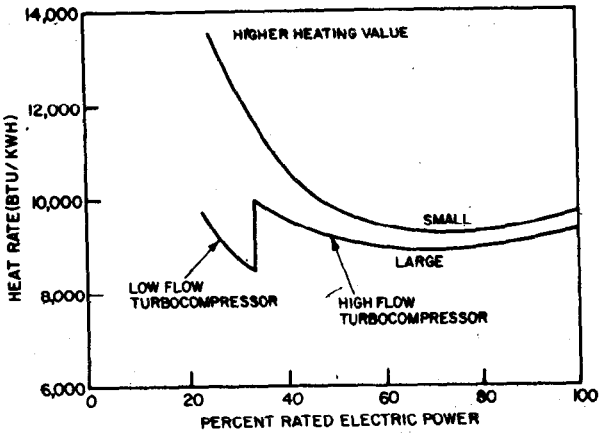

Figure 29. Fuel consumption in first generation fuel cell power plants.[123] (With permission from the authors and United Technology Corporation.)

6.2.2.2. *Waste Heat Recovery and Utilization*

Besides electricity, fuel cells release a large amount of heat due to thermodynamic and electrochemical inefficiencies in the cells (see Sections 2.4 and 3.5 and Reference 126 for a discussion on thermal phenomena in fuel cells). This waste heat can be recovered without influencing the generation efficiency, since fuel cells convert energy electrochemically. The amount of waste heat produced is proportional to the amount of electricity generated and inversely related to the operating efficiency. Hence more heat is produced in the fuel cell power plant operating at full load than at part load. Typical heat balance curves[123] with small and large fuel cell power plants using the lower heating value of fuel shows (see Figure 30) that the amount of heat recovered is a function of water return temperature.

Assuming part-load operation when less waste heat is available, for a fuel input of 7830 Btu/kWh (LHV), the electricity produced will correspond to 3413 Btu/kWh, whereas the sensible heat will be 4417 Btu/kWh, of which ~40% is suitable for high-grade heat (process steam at 15–60 psig) and 50% is low-grade heat suitable for heating water at 160°F. Ten percent of the sensible heat is unrecoverable as it is lost to the surroundings.

At 60% recovery efficiency for the waste heat, 2650 Btu/kWh of waste heat could be provided for use, although the demand for this heat may be different from what is available from the power plant. Estimates based on a coincidence factor of 70% indicate that 1855 Btu of heat will be used for every kWh of electric energy produced by the fuel cell power plant. This is equal to 2473 Btu of fossil fuel used at 75% efficiency by conventional methods for

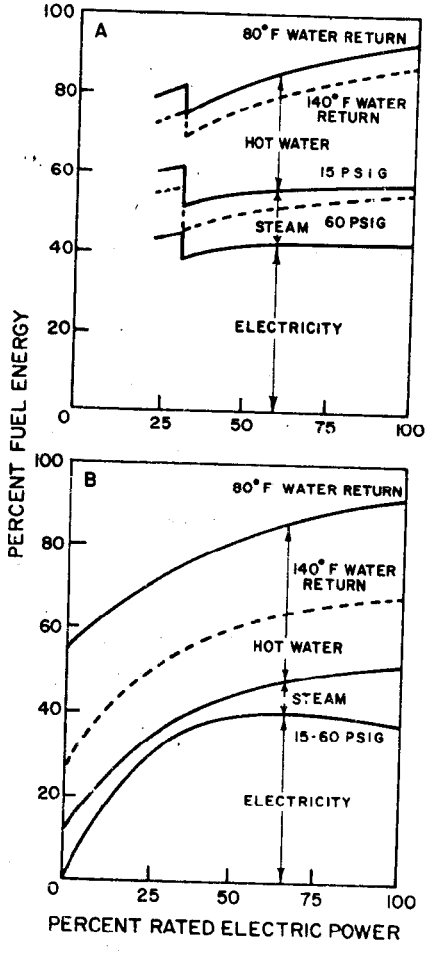

Figure 30. Fuel cell power plant heat balance for (A) large and (B) small on-site power plants.[123] (With permission from the authors and United Technology Corporation.)

production of heat or steam. Thus primary fuel savings of 2473 Btu/kWh or 1.13×10^3 millions of barrels/day oil equivalent (B/DOE) and resource savings of 1.33×10^3 B/DOE per 10^9 kWh generated can be achieved by waste heat recovery.

6.2.2.3. On-Site Total (or Integrated) Energy Concept

Fuel cell power plants of ~40 kW are being envisaged for use in apartment and industrial buildings.[119,122] At present, fuel cells convert natural gas to electricity at 40% efficiency (LHV) and the waste heat (5120 Btu/kWh) can be

recovered to produce heat (3456 Btu/kWh) for domestic hot water requirements and then, depending on the season, directly for space heating or indirectly via an absorption chiller for air-conditioning. To satisfy higher thermal demands, additional electricity is generated for the thermal load (for resistance heating or to power heat pumps† or compression chillers). This is termed the *on-site total energy concept.*[122]

The fuel input requirement and, hence, the system efficiency is a function of (a) fuel cell efficiency, (b) coefficient of performance (c.o.p.) of the heat pump, (c) waste heat availability and recovery efficiency, and (d) the ratio of thermal to electric load requirements. While the heat recovered by the heat exchanger is dependent on the fuel cell efficiency and the recovery efficiency, the heat recovered by the heat pump is determined by the electricity input and the c.o.p. of the heat pump, which depends on the mode of operation (heating or cooling), ambient temperature, and equipment size and type.

It is of interest to note that the c.o.p. of a heat pump for this type of application is 2.5 and that the ratio of thermal energy to electricity demand (dependent on the building type or industrial process) varies from 0.5 to 4.0 for office buildings, 0.5 to 8.0 for hotels, and from 3 to 11 for apartment buildings.

Assuming a ratio of 4.5 for the thermal energy to electricity demand,[122] the energy balance of a fuel cell and fuel cell–heat pump energy system is shown in Figure 31. It is seen that, while the system efficiency is 80% without the heat pump, an integrated fuel cell–heat pump energy system can result in more than 100% efficiency. Thus 40% of the fuel can be saved when using a fuel cell–heat pump total energy system instead of the gas-fired furnace to address the given thermal needs.

6.2.3. Fuel Processors and Fuels

Fuel processors for the 27-MW and 40-kW fuel cell systems were originally designed to steam reform naphtha and natural gas, respectively. The current trend[127] is to broaden the fuel processing capability to include widely used fuel oils in the larger fuel cell systems, and methanol and naphtha in the smaller fuel cell systems.

Most fuel cells now operate using hydrogen which is currently derived economically from natural gas and oil by a reforming process which is an endothermic reaction. The endothermic heat required for the water–gas reaction (which can take place internally or externally to the fuel cell) can be provided using the high-grade waste heat from the fuel cell power plant, especially the high-temperature molten carbonate or solid electrolyte cell. Besides, the steam requirements for the reaction can be satisfied by recovering the water from the fuel cell reaction as shown in Figure 27.

† A heat pump is essentially an air-conditioning system which, when operated in reverse, efficiently transforms electricity into heat.

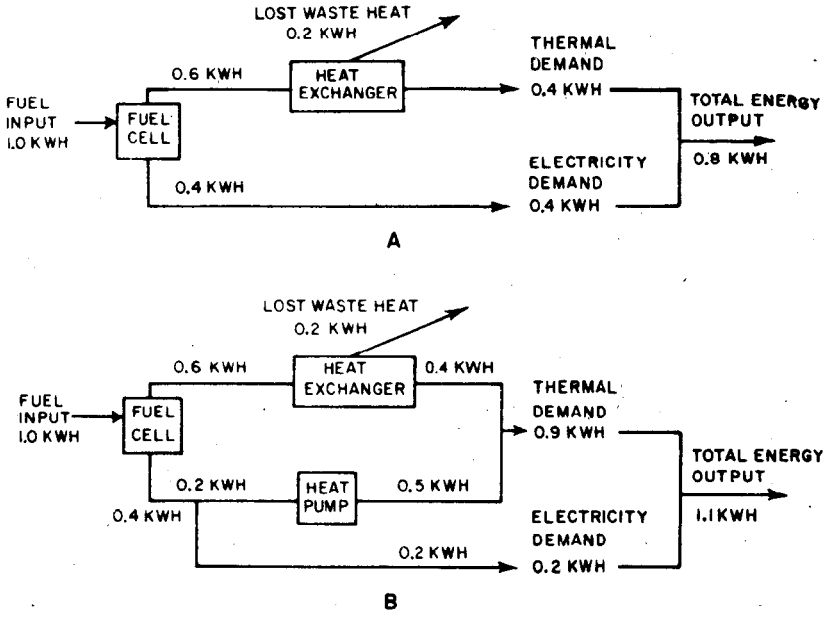

Figure 31. Fuel cell integration energy system at thermal to electricity demand ratio of (A) 1.0 and (B) 4.5 (from Reference 122).

Natural gas and oil are becoming more expensive and less available for power generation and, hence, the U.S. government has embarked on an ambitious program to increase the country's use of its coal (accounting for 85% of its fossil fuel resources) by coal gasification. The advantages of this scheme are removal of sulfur at the gasification stage, almost complete absence of particulates in the synthetic gas produced, the possibility of using gas in an advanced power cycle to achieve efficiencies of 50%, and a significant reduction of nitrous oxides. In coal gasification, the water–gas reaction is an endothermic process and, conventionally, about 30% of the coal feed is burned within the gasifier using oxygen (from an oxygen plant) to supply this endothermic heat. The solid electrolyte fuel cell power plant is a unique candidate when coal is employed as the fuel, since the waste heat can be used directly for the water–gas reaction during the coal gasification process, saving ~30% of the coal feed, and permitting the elimination of the oxygen plant.

6.2.4. Fuel Cell–Power Generation Systems—Their Performance

Fuel cell power-generation systems, grouped in four distinct classes differentiated by electrolyte used in the fuel cells (see Table 7), are (1) acid

Table 7
Components of Cells for Four Different Fuel Cells[110][a]

Fuel cell	Anode	Cathode	Electrolyte (thickness in mm)	Temperature of operation, °C	Cell voltage, V; current density, mA/cm^2
Phosphoric acid	C catalyzed by Pt (1 mg/cm^2)		99 wt % H_3PO_4 immobilized in a matrix (0.5)	190	0.8; 200
Alkaline	C catalyzed by Pt[b] (1 mg/cm^2)	C catalyzed by Ag[b] (5 mg/cm^2)	30 wt % KOH (0.5)	70	0.8; 100
Molten carbonate	Porous Ni	Lithiated NiO	Alkali aluminate + molten alkali carbonates (1.0)	650	0.7; 200
Solid electrolyte	Ni–ZrO_2 Cermet	In_2O_3–$PrCoO_{3-x}$ with Cr_2O_3 interconnection	$(ZrO_2)_{1-x}(Y_2O_3)_x$(0.04)	1000	0.84; 400

[a] Voltage degradation at constant power output: 5%; useful life: 36 months.
[b] Prospects are good for developing alkaline fuel cells with much lower noble metal loadings or with substitutes for noble metals as electrocatalysts.

type, including phosphoric acid (first generation), sulfuric acid, and solid polymer electrolyte; (2) alkaline type; (3) molten carbonate type (second generation); and (4) solid electrolyte type (third generation). (See References 7, 119, and 125 for a discussion on other fuel cell systems.)

6.2.4.1. Phosphoric Acid Fuel Cells

Fuel cells utilizing phosphoric acid electrolytes are in the most advanced state of development, relative to other fuel cell systems, for utility application. The best available estimates of cost and life are available only for the phosphoric acid fuel cell system. Those fuel cells typically employ[128] 85–100% aqueous phosphoric acid, immobilized in a matrix, as the electrolyte at an operating temperature in the range 175–200°C.

The major functional components of the dc module (see Figure 32) are the fuel and air processing subsystems, a fuel cell power section, and a thermal management subsystem.

Air entering one of the compressors, shown at the upper left in the schematic, is compressed to 35 psig before being fed to the cathode (a low-flow turbocompressor will be used below 35% of rated power and the high-flow unit at all other power requirements) and is mixed with water which is evaporated from the cathode gas space. This hot and moist cathode effluent stream then passes through a regenerator and a liquid-cooled condenser, where it is cooled sufficiently to condense the water required for use in the fuel processing

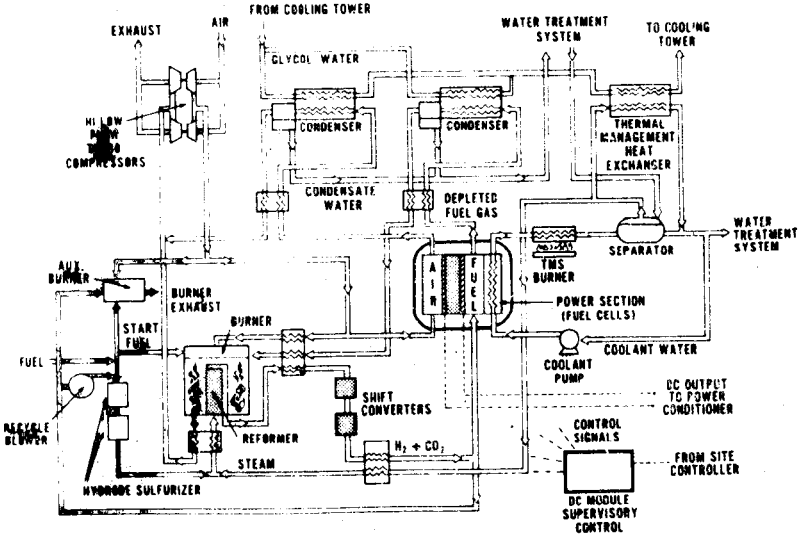

Figure 32. First generation phosphoric acid fuel cell power plant schematic. (With permission from United Technology Corporation.)

subsystem. The cathode exhaust stream, combined with the hot reformer-burner effluent, provides the energy to drive the turbine of the turbocompressor unit.

Power plant process fuel is sometimes burned in the auxiliary burner to add energy to the gas stream before it enters the turbine. The system components are matched such that, at rated output power of the plant, the energy in the gas stream is sufficient to power the turbine. As the power plant output level is reduced, the energy available in the gas stream decreases. Since the turbine requires a near-constant energy input as the output power is reduced, process fuel is burned to make up for the small energy deficit at part power.

At the bottom left of the schematic, naphtha fuel (which has been pressurized by a pump) is mixed with hydrogen-rich gas from the fuel processor exit stream. The mixture passes through a hydrotreater (hydrodesulfurizer), where sulfur compounds are removed. The clean fuel is then mixed with steam from the power section waste heat. The fuel–steam mixture passes into the reformer where it is processed to a mixture of hydrogen, carbon dioxide, carbon monoxide, and water vapor. The carbon monoxide and the water are then further converted to hydrogen and carbon dioxide in two shift converters operating successively at lower temperatures. The low-temperature shift converter reduces the carbon monoxide concentration to less than 1%. The processed fuel next flows to the anode cavities in the fuel cell power section, where hydrogen is extracted for the electrochemical reaction. The anode effluent gas stream passes through a regenerator and condenser where it is cooled to condense additional water for power section cooling and steam generation. The anode exhaust stream then enters the reformer burner, where the dilute hydrogen is burned to provide heat for the reforming process and is combined with the cathode exhaust stream before entering the turbine.

6.2.4.2. Alkaline Fuel Cells

Alkaline cells offer higher performance than phosphoric acid cells. The cell voltage (0.8 V) is higher than that (0.7 V) of the acid cell because of the observed lower cathodic overpotentials in the alkaline cell. The cathodes do not require noble metals, which results in a substantial reduction in cost when compared to the acid cells. A further advantage of alkaline cells is that nickel, which is stable in the cell environment, can be used for fabrication of electronically conductive components (e.g., electrodes, current collectors). In contrast, acid systems are restricted to expensive materials, such as graphite, tantalum, or niobium.

Carbon dioxide, in air or in fuel gas, fed to the cell causes a rapid carbonation of the electrolyte and loss of performance. Consequently, a carbon dioxide scrubber is necessary, prior to the cell inlet, to prevent this problem. At present, the energy required for carbon dioxide removal is rather high and, hence, the efficiency advantage of the alkaline fuel cell, resulting from lower

cathodic polarization, is almost totally negated by the efficiency penalty associated with elimination of carbon dioxide from the air and fuel gas streams.[129] Estimated overall system efficiencies for alkaline fuel cell power systems, using carbonaceous gas as a fuel, are similar to those for acid systems, about 35–40%. If the carbonation problem can be overcome without significantly increasing capital costs and reducing overall efficiency, alkaline fuel cells will be attractive for large-scale power generation.

6.2.4.3. Molten Carbonate Fuel Cell

The molten carbonate fuel cell employs[128] a mixture of alkali metal carbonates in a ceramic particulate matrix as the electrolyte and porous nickel based electrodes as anodes and cathodes. The half-cell reactions in this cell are

$$H_2 + CO_3^{2-} \rightarrow H_2O + CO_2 + 2e \quad \text{(anodic reaction)} \tag{90}$$

$$CO + CO_3^{2-} \rightarrow 2CO_2 + 2e \quad \text{(anodic reaction)} \tag{91}$$

$$\tfrac{1}{2}O_2 + CO_2 + 2e \rightarrow CO_3^{2-} \quad \text{(cathodic reaction)} \tag{92}$$

The molten carbonate fuel cell power plant has several significant advantages over a system using acid cells because of the higher power density at higher voltages than with the acid cell. The fuel processor is simpler since the cell is tolerant to carbon monoxide and the reforming process can occur within the fuel cell. As a result, reformer and shift converter are not required. Higher efficiency is achieved because the reforming process absorbs heat, which would be supplied *in situ* by heat produced at the electrodes of the cell. Although a commercial reformer operates at a higher temperature than does the molten carbonate cell, the large electrode area within the cell and the probable slower through-put per unit area makes internal reforming efficient.

In addition, water is removed only at the anode of the molten carbonate cell rather than at both electrodes, permitting the use of smaller and lower-cost condensers and simplifying the control system. Furthermore, the cell operation at high temperature (600–750°C) is conducive to the use of process air for cooling (the lower-temperature acid cells require a separate coolant loop). In large systems, it is anticipated that increased efficiency can result by recovering waste heat in order to generate steam for use in a steam turbine or as process steam.[130] Since the highest efficiency plants would be large, the turbogenerator plant costs can be minimized.

6.2.4.4. Solid Electrolyte Fuel Cell

The solid electrolyte cell is essentially a H_2–O_2 fuel cell with a solid, ceramic oxide material serving as the electrolyte—the mechanism of ionic conduction being oxygen ion transport via anion defects in the solid oxide crystal lattice.

High-temperature (~1000°C) solid electrolyte fuel cells have many advantages over other types of fuel cells[131,132] as there are no liquids involved

and, hence, the problems associated with pore flooding and maintenance of a stable three-phase interface are totally avoided. In addition, the electrolyte composition is invariant and independent of the composition of the fuel and oxidant streams, and activation polarization losses are negligible.

Fuel cell power plants using solid electrolyte cells are projected to have a high overall system efficiency through integration with a fuel processing system. As with the molten carbonate fuel cells, the cell is tolerant to carbon monoxide, and the reforming process can take place in the cell; the fuel processing system for a solid electrolyte cell is thus simplified relative to the requirements for an acid cell system.

Carbon dioxide is not required as a cathode reactant and, therefore, the solid electrolyte cell offers a somewhat simpler power plant system than the molten carbonate cell. Also, the higher operating temperature facilitates waste heat rejection and integration with other power plant functions. Furthermore, the solid electrolyte cell power plant has a unique advantage when coal is employed as a fuel in that the waste heat generated can be employed to gasify coal, thus providing fuel gas for the fuel cells. Thermal coupling leads to high overall efficiencies for the power system and, practical efficiencies of greater than 60% are considered possible.[132] This efficiency is significant, as this type of power system employs coal rather than natural gas, methanol, or naphtha as a fuel.

6.2.4.5. Capital Costs and Electricity Costs of Fuel Cell Power Plants

The typical capital costs, overall system efficiencies, and electricity costs of fuel cell power plants, based on parametric assessment by Westinghouse,[128] are listed in Table 8 and a comparison of the capital cost breakdown for all four fuel cell systems is given in Figure 33. The difference between the sum of the material and site labor costs for the major components and the total direct costs of the power plant is expressed as a balance of the plant. The indirect costs, which include the interest during construction, escalation, and contingency charges, and the profit and owner costs, were calculated similarly and represent

Table 8
Comparison of Fuel Cell Power Plants with Various Electrolytes[128]

System	Capital cost, $/kW$_e$	Overall system efficiency, %	Electricity cost (COE), mills/kWh	Projected lowest COE, mills/kWh
Phosphoric acid	350–450	24–29	42–50	High 30
Alkaline	450–700	26–31	46–61	Low 40
Molten carbonate	480–650	32–46	38–70	Low 30
Solid electrolyte	420–950	26–53	35–61	High 20

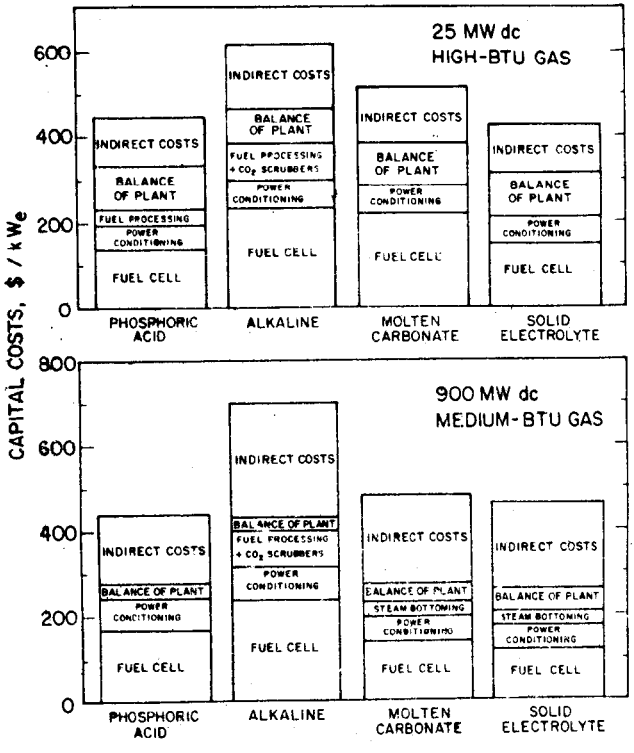

Figure 33. Capital cost breakdown of fuel cell systems (from Reference 128).

the difference between the total capital and total direct costs. (See also References 119 and 133 for a detailed discussion.)

6.2.4.6. Integration of a Fuel Cell with Coal Gasifier and Steam Bottoming Cycle

One of the systems with a potential for high efficiency is the molten carbonate fuel cell power plant containing both a gasifier and a steam bottoming cycle[128,134,135] (see Figure 34 for a schematic of the system). The low-Btu gasifier subsystem converts coal to clean hydrogen-rich gaseous fuel (synthetic gas) required by the fuel cell. The low-Btu fuel gas exits the gasifier at 1310 K. The desulfurizer uses a total of ~4.6% of the cleaned fuel gas, and the remainder of the cleaned fuel gas is fed to the fuel cell at 918 K. Since the desulfurizer and the fuel cell operate at 922 K, the fuel gas at the exit of the gasifier must be cooled from 1310 K. Part of the sensible heat removed from

the gasifier synthesis gas is required for reheating steam for the steam turbine bottoming cycle and the other for generating steam used by the gasifier itself.

Turbocompressors and the steam bottoming cycle share the fuel cell waste energy. The turbocompressors supply compressed air to the gasifier and to the fuel cell catalytic burner at the cathode inlet. As shown in the fuel cell part of the schematic in Figure 34, the cathode vent gas is expanded through these turbines and some of it is recirculated back to the cathode, during which some of its sensible heat is transferred to the bottoming cycle in the steam boiler superheater. Recirculation serves to control the fuel cell temperature as well as to conserve, in the system, considerable thermal energy still left in the gas after it has transferred thermal energy to the steam bottoming cycle. In addition, the gas which is expanded in the turbine transfers heat to the bottoming cycle feed water in the economizer and deaerator. Finally, this steam is fed back to the stack carrying the water generated in the fuel cell.

The steam bottoming cycle operates at 2400 psig/811 K, and throttle conditions with single reheat to 811 K, at a condenser pressure of 50.8 mm of mercury. As noted earlier, the steam cycle receives heat from the turbocompressor exhaust gas and from the raw fuel gas upstream of the desulfurizer, while the steam cycle assumes no turbine steam extraction for regenerative feed water heating. Instead, the feed water is heated by recovering the usable waste heat in the turbocompressor exhaust gas. The steam turbine power output is 222 MW_e.

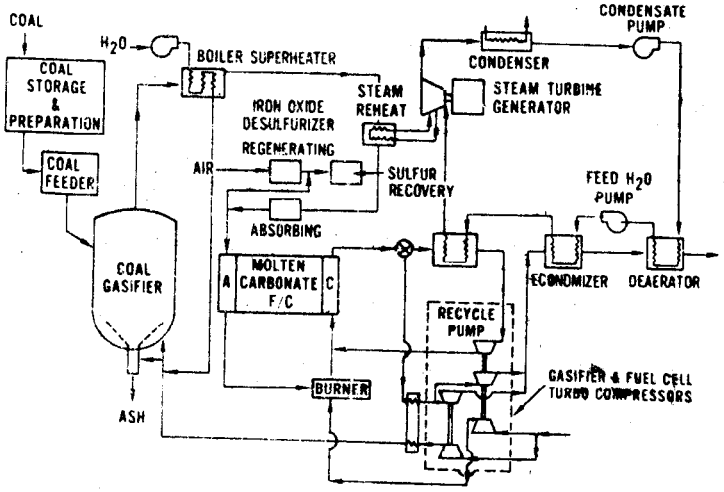

Figure 34. Schematic of integrated coal gasifier–molten carbonate fuel cell power plant. (With permission from United Technology Corporation.)

Table 9
Summary of Low-Btu Gasifier–Molten Carbonate Fuel Cell–Steam System Performance[134]

Net power output, MW_e	635
Auxiliary power requirements, MW_e	16.4
Transformer losses, MW_e	2.6
Fuel cell ac output, MW_e	432
Steam-bottoming-cycle output, MW_e	222[a]
Efficiencies, percent	
Overall energy	49.6
Thermodynamic	53.6[b]
Fuel cell/inverter	45.0[c]
Steam bottoming cycle	40.0[a]
Gasifier–cleanup subsystem	89.5
Power-steam auxiliary power requirement	98.1
Gasifier system auxiliary power requirement	99.3
Transformer	99.6

[a] Not including effect of boiler feed pump.
[b] Gross power from fuel cell and steam cycle divided by fuel gas HHV and sensible heat.
[c] Fuel cell ac output divided by fuel gas HHV.

The gasifier–fuel cell air turbocompressors use the waste thermal energy of the fuel by expanding the fuel cell exhaust to perform three important functions. First, they compress process air to 150 psia for the cathode of the fuel cell. Second, air at 235 psia for the gasifier is provided. Finally, the turbocompressors provide shaft power to the cathode recycle compressor. As shown in Figure 34, the recycle stream removes fuel cell waste heat of high grade and transfers this heat to the boiler superheater of the bottoming cycle. The split between recycle flow and turbine inlet flow is ~2–1. The thermal energy in the exhaust from the turbocompressors is used by the economizer and the deaerator of the bottoming cycle.

Figure 35 illustrates the energy flows[134,135] between subsystems which are in the form of electrical power and heat transfer through heat exchangers from one fluid to another. The subsystem outputs and efficiencies in Table 9 (see Table 10 for cost estimates) show that thermal integration of the system results in a high overall efficiency. If a gas turbine is used instead of a steam turbine for the bottoming cycle, the overall efficiency and the cost will be lower. These aspects are discussed further in Section 6.5.3.

6.3. Fuel Cells for Transportation

For transportation applications, it is essential to convert the chemical energy of petroleum-derived or coal-derived fuels to mechanical energy, directly or via electricity. The projected vehicular efficiencies for utilization of

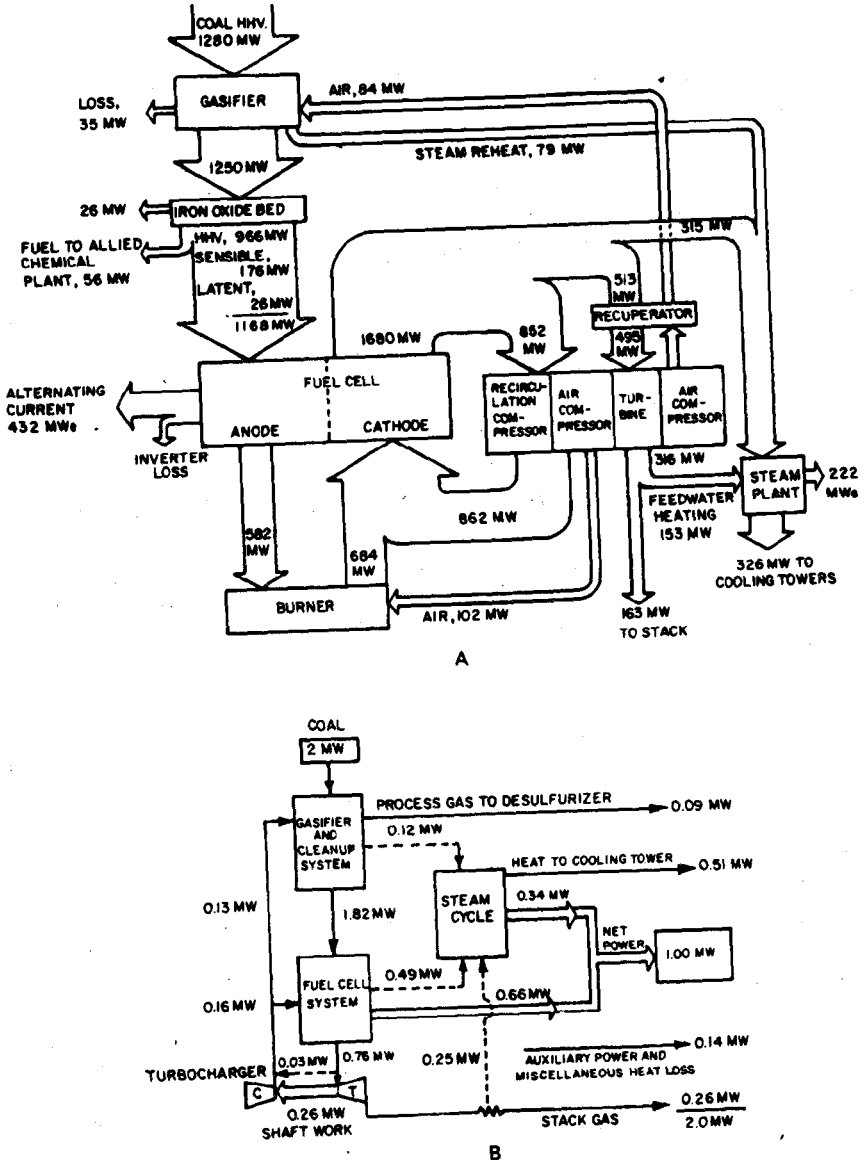

Figure 35. (A) Energy flow diagram for low-Btu gasifier–molten carbonate–steam bottoming system (net power output: 635 MW_e; auxiliary power and transformer loss: 19 MW) (from Reference 134). (B) Approximate energy flow scheme (from Reference 135).

Table 10
Summary of Low-Btu Gasifier–Molten Carbonate Fuel Cell–Steam System Costs[a,(134)]

Power plant capital cost, $/kW$_e$	595
Cost of electricity (with 0.65 capacity factor), mills/kWh:	
Capital	18.8
Fuel (at $1 per million Btu for coal)	6.9
Operation and maintenance	3.3
	29.0

[a] Estimated time of construction, 5 years; estimated date of first commercial service, 1985–1990.

coal-derived fuels (see Table 11) show the distinct advantage of the fuel cell–battery hybrid vehicles.[136,137] In addition, the fuel cells are efficient at part-load operation in contrast to heat engines. Variation of specific power with specific energy for fuel cells (see Figure 36) shows the similarity[137] of fuel cells, more to a heat engine than a battery, yielding about 30 W/lb. However, for fast start-up and acceleration, the specific energy demands are ~80 W/lb. Hence, it appears necessary to hybridize a fuel cell with a battery for vehicular applications.

The important performance criteria for vehicular applications are the power density, efficiency, life, and cost. The capital costs of fuel cells should be of the order of $50/kW. Five types of fuel cells, which appear to be promising candidates for applications in the transportation sector, include four fuel cell

Table 11
Comparison of Vehicular Efficiencies Assuming Coal as Primary Energy Source[136]

Power plant	Component efficiency, %	Overall efficiency, %
IC engine		
Diesel		8.8
Battery		9.9
Coal to electricity	35	
Transmission and distribution	85	
Battery	70	
Motor	75	
Overall		15.7
Fuel cell–battery hybrid		
Coal to methanol	70	
Fuel cell	45	
Motor	75	
Overall		23.7

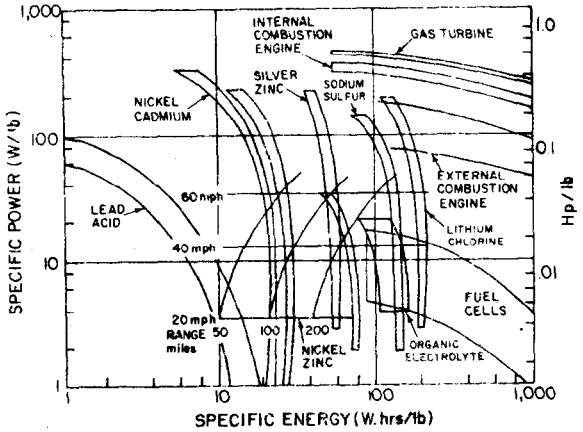

Figure 36. Specific power vs. specific energy for various energy producers.[137]

systems in which hydrogen is the fuel and air is the oxidant with phosphoric acid, a solid polymer (Nafion), potassium hydroxide, or aqueous trifluoromethane sulfonic acid (TFMSA) serving as the electrolyte. The fifth, where some breakthrough is needed to increase the power densities in the cell by at least a factor of 5, is the direct methanol–air fuel cell.

6.4. Fuel Cells for Space Applications

The need for lightweight power production in space led to the awakening of interest in fuel cells. The electrical power needed for space applications varies from a few watts (for communication and weather satellites) to 100 kW (for manned space laboratories), with long life as a requisite.

Owing to the cost of putting a pound of substance into space (around $10,000 per pound), the weight/energy ratio of the energy conversion system is an important factor and is favorable in the case of fuel cells. Figure 37A shows the energy/weight ratio dependence[8] on the mission duration for some of the energy conversion devices, assuming that the devices operate at a power level of 1 kW. From similar figures constructed for different power levels, the regions of applicability[1,140] of the various energy conversion devices for space missions of varying duration and requiring different power outputs (see Figure 37B—"Map of Balkans") shows that fuel cells are best for space missions ranging from a few hours to a month and for power levels of up to 100 kW.

The advanced electrochemical systems, regenerative H_2–O_2 fuel cells with a power density of 100 W/kg or over, appear to be promising for space applications.

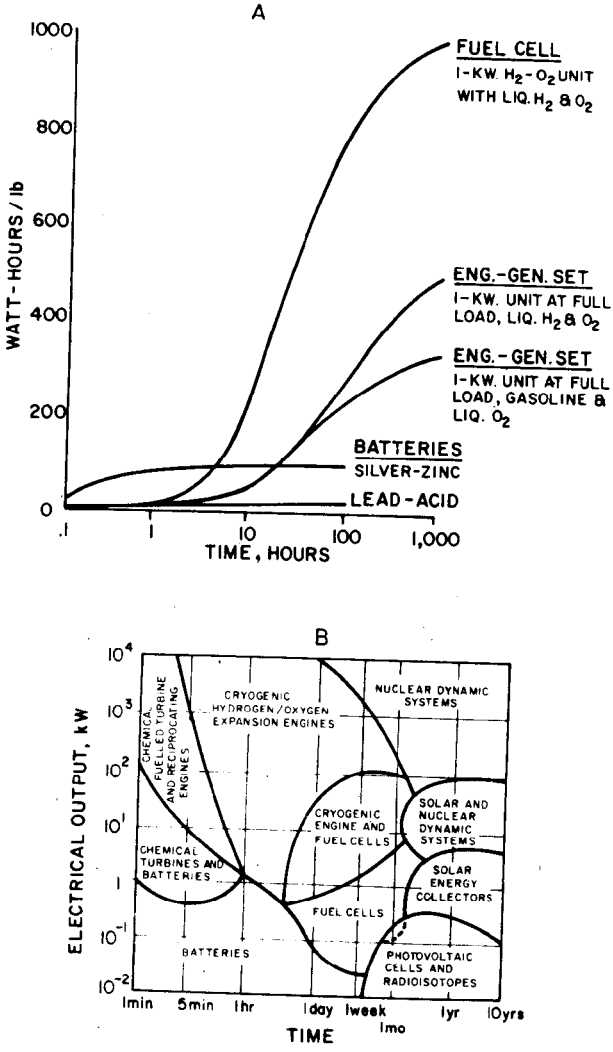

Figure 37. (A) Power-weight ratios[8] for fuel cells, batteries, and engine generator sets. (With permission from the author and Academic Press.) (B) Map of Balkans.[140]

6.5. Important Parameters Determining Overall Efficiency and Cost

The fuel cell is the heart of the power plant, controlling the overall power plant efficiency, power plant capital, and maintenance costs. The efficiency of

the fuel cell can affect the capital costs since it determines (i) the quantity of fuel (hence the type of fuel cell) which must be processed in the fuel processor and (ii) the quantity of heat which must be rejected from the cell, and can be improved by increasing the cell operating voltage or W/ft^2 at a given voltage. However, this leads to an increase in the capital costs for all the cases considered in Section 6.2.

A recent Energy Conversion Alternatives study[128] shows that for the same system, fuel cell useful life, power density, use of a waste heat recovery system, and fuel type are of importance for efficiency improvement and/or electricity cost reduction, while the other factors do not effect overall efficiency and cost significantly.

6.5.1. Fuel Cell Useful Life

The importance of fuel cell subsystems useful life (see Figure 38) on COE (cost of electricity) is most pronounced for the high-temperature molten carbonate and solid electrolyte systems,[128] and is least pronounced for the phosphoric acid system. The acid and alkaline systems have a sizeable salvage value due to their platinum loading. Therefore the COE is dictated by the cell useful life.

6.5.2. Power Density

The fuel cell power density, i.e., power output per unit electrode area, also affects the cost[128] of the power plant. The cost per kilowatt of the fuel cell

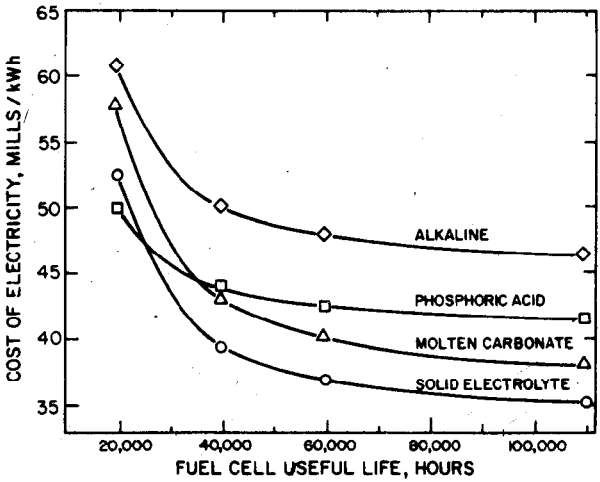

Figure 38. Effect of useful life of fuel cell subsystem on the cost of electricity. Costs were calculated assuming the use of medium-Btu gas for the solid electrolyte system and high-Btu gas for the acid, alkaline, and molten carbonate systems (from Reference 128).

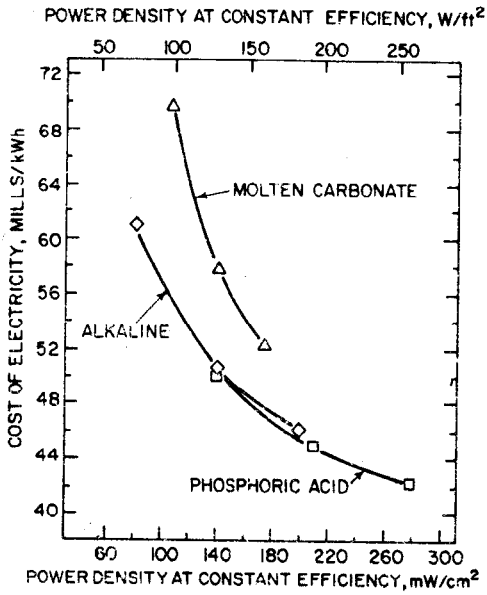

Figure 39. Dependence of cost of electricity on power density at constant efficiency (from Reference 128).

module alone is about inversely proportional to the power density (see Figure 39), since the capital cost of the cell stack is proportional to the total area of the cell. Increasing power density at the same efficiency implies advances in technology and is feasible by increasing the current density and accepting a cell voltage reduction (because of increased ohmic and concentration polarization losses). This results in an increased fuel charge, which serves to offset the reductions in the capital and O&M (operation and maintenance) portions of the COE. Another complication of operation at a higher power density was reported by Kordesch[138] for alkaline fuel cells, wherein the fuel cell subsystem should be frequently replaced resulting in higher O&M cost. Thus the cell power density is determined by a cost-efficiency trade-off.

6.5.3. Waste Heat Recovery System

The heat produced by the high-temperature solid electrolyte or molten carbonate cell is more than sufficient for heating the fuel and oxidant to the cell temperature. The excess heat is of high grade and can be used for (i) steam conversion, (ii) the bottoming cycle to produce additional electricity, (iii) thermal coupling of a coal gasifier with the fuel cell, and (iv) fuel cell power plant coupled with an oxygen plant where the excess heat is ideal for the

Table 12
Comparison of Power Plant Characteristics[135]

Characteristic	Steam turbine bottoming	Gas turbine bottoming
Overall thermal efficiency, %	50	45
Heat rate, Btu/kWh	6850	7580
Power plant rating, MW	635	145–578
Power plant lead time, years	5	4
Capital cost, $/kW	595	575[a]
Busbar cost,[b] mills/kWh	29	30
Water requirements, gal/kWh	0.4	0.07
Relative gaseous Emissions/10^6 Btu	1.0	1.0

[a] At 578 MW
[b] At 0.65 capacity factor and $1/$10^6$ Btu coal.

operation of the steam turbine drive for the compressor. (The steam turbine drive converts the available energy to shaft work with an efficiency of ~40%.)

Two bottoming cycle options are available for utilizing waste heat to produce useful power. The vent gases from the fuel cells, at elevated temperature and pressure, may be expanded through a gas turbine generator unit or used to raise high-pressure, superheated steam, which is utilized in conventional steam-turbine generator equipment. It is reported that[135] high power plant efficiencies can be achieved with a steam bottoming cycle, since this system makes better use of waste heat. The gas turbine bottoming cycle system, however, has attractive features in terms of increased modularity, which can provide high power plant availability, short lead times, and hence low capital cost. The performance and economic characteristics of the power plants using these two bottoming cycles are shown in Table 12.

6.5.4. Fuel Type

The power density and overall efficiency of the fuel cells are affected by the type of fuel used. Thus when the fuel is methanated (high-Btu) gas, a reforming step becomes necessary, while with medium-Btu fuel for high power, such as a 900-MW plant, the steam–methane reformer is not required; this results in a reduced capital cost of the power plant, greater efficiency, and 25% gain in overall energy efficiency.

Another factor which affects the power plant cost is the requirements placed on the quality of gas delivered to the cell stack from the fuel processor. Methane, H_2S, and NH_3 are the typical impurities which could enter the cell from advanced fuel processors operating on distillate fuel oils or coal.

6.5.5. Oxidant Type

The current density of acid, alkaline, and molten carbonate fuel cells is enhanced (about twofold) by changing the oxidant from air to oxygen, owing to reduced concentration polarization at the cathodes. A similar effect is observed with the solid electrolyte fuel cell. However, a dedicated oxygen plant is required for supplying O_2 to the fuel cells.

With near-ambient-pressure air as the oxidant, the optimum operation temperature of the solid polymer electrolyte fuel cell is approximately 75°C. Because the air streams must be presaturated to ensure membrane stability, higher temperatures cause excessive dilution of the oxygen in the air stream by water vapor. Operating temperatures of up to 150°C are possible with O_2.

The performance and heat rate of the phosphoric acid fuel cell are currently limited by cathode polarization, which can be reduced by using various redox couples. Three possible approaches[139] involve (i) attaching the redox material directly to the cell cathode, (ii) incorporating the redox material into a solution with the electrolyte, and (iii) using an intermediate cathode reactant which is regenerated external to the cell. However, the resulting system efficiencies are low due to the additional energy requirements for regeneration.

6.5.6. Fuel and Oxidant Utilization

Reactant utilization is defined as the ratio of the reactant consumed by the cell to the reactant supplied to the cell. Thus, in the case of the molten carbonate cell where CO is shifted to H_2 *in situ*, fuel utilization can be estimated from the ratio of H_2 consumed in the cell to the sum of H_2 + CO supplied to the cell, and is a measure of the system efficiency (since it indicates the mole or volume percent of $H_2 + CO$ in the fuel gas which is electrochemically consumed). Hence reactant utilization, which is usually $<100\%$, is related to the cell performance, determining the variation of reactant partial pressure over the cell which affects both the ideal and operating cell voltage. Consequently, a trade-off must be made between efficiency and cell performance while establishing fuel utilization, which is 85% for a theoretical power plant design—oxygen and CO_2 utilizations being 50% and 26%, respectively.

6.5.7. Catalyst Loading

Non-noble metals are used as the electrocatalyst for the molten carbonate and solid electrolyte fuel cells and, hence, electrode costs are lower than for phosphoric acid fuel cells. For the acid fuel cells, noble metals are used as the electrocatalysts and the current trend is in the direction of achieving optimal performance at minimal catalyst loadings. Alkaline fuel cells can be constructed without use of noble metal catalysts.

6.5.8. Fuel Cell Plant Rating

Owing to the modular nature, no economy of scale was assumed for the fuel cell subsystems. Any economic benefits, therefore, should be realized from the other subsystems, as exemplified with the integrated coal gasifier fuel cell power plant with a steam bottoming cycle.

6.5.9. Electrolyte Thickness

The ohmic loss in the electrolyte is determined by the electrolyte thickness and, in the case of phosphoric acid fuel cells, reduction in thickness from 0.50 to 0.25 mm resulted in an increase of cell voltage from 0.70 to 0.71 V. Thus cost and efficiency are not significantly altered by reduced electrolyte gap.

6.5.10. Voltage Degradation

Terminal voltage decreases by ~5% at constant power at the end of a useful life and, hence, degradation specification is important in determining power-conditioning costs.

6.5.11. Operating Temperature and Pressure

Operating temperature plays a significant role in determining overall efficiency of the fuel cell system power plant. However, in practice, fuel cell efficiency increases (via reduction in overpotential losses) at higher temperatures, under which conditions corrosion rates increase. Hence the choice of operating temperature should be based on a trade-off between ideal cell voltage, cell polarization, and endurance.

Operating at a pressure of 150 psia is expected to result in better cell performance than operating at atmospheric pressure. At these high pressures, methane production is kept low in the gasifier.

6.5.12. Cell Configuration

Cell stack configuration, which reduces the number of cell components (hence lower manufacturing costs), can significantly reduce the cost and also result in improved cell performance since elimination of components reduces the contact resistance within the cell stack.

6.5.13. Environmental Regulations

Stricter controls (see Table 7) on emissions from conventional power plants lead to a substantial increase in capital cost at reduced efficiency. However, EPA regulations hardly affect the fuel cell power plant operations.

Acknowledgments

This work was performed under the auspices of the U.S. Department of Energy. The authors wish to thank United Technologies Corporation and Energy Research Corporation for the valuable material supplied during the preparation of this chapter.

References

1. S. W. Angrist, *Direct Energy Conversion*, Allyn and Bacon, Englewood Cliffs, New Jersey (1964).
2. S. L. Chang, *Energy Conversion*, Prentice-Hall, Englewood Cliffs, New Jersey (1963).
3. H. A. Liebhafsky and E. J. Cairns, *Fuel Cells and Fuel Batteries*, John Wiley & Sons, New York (1968).
4. K. R. Williams, *An Introduction to Fuel Cells*, Elsevier, Amsterdam (1966).
5. W. Vielstich, *Fuel Cells—Modern Processes for the Electrochemical Production of Energy* (translated by D. J. G. Ives), John Wiley & Sons, New York (1970).
6. E. Justi and A. Winsel, *Fuel Cells—Kalte Verbrennung*, Steiner, Wiesbaden (1962).
7. J. O'M. Bockris and S. Srinivasan, *Fuel Cells—Their Electrochemistry*, McGraw-Hill, New York (1969).
8. W. Mitchell, *Fuel Cells*, Academic Press, New York (1963).
9. D. R. Adams, P. Y. Cathou, R. E. Gaynor, R. D. Jackson, Jr., J. H. Kirsch, L. L. Leonhard, G. S. Lockwood, Jr., W. P. Warnock, and R. E. Wilcox, Jr., *Fuel Cells—Power for the Future*, Fuel Cell Research Associates, Cambridge, Massachusetts (October 1960).
10. C. Berger, ed., *Handbook of Fuel Cell Technology*, Prentice-Hall, Englewood Cliffs, New Jersey (1968).
11. A. J. Appleby, Electrocatalysis, in *Modern Aspects of Electrochemistry*, B. E. Conway and J. O'M. Bockris, eds., Vol. 9, Plenum Press, New York (1974), p. 369.
12. P. Stonehart and P. N. Ross, The commonality of surface processes in electrocatalysis and gas-phase heterogeneous catalysis, *Catal. Rev. Sci. Eng.* **12**(1), 1 (1975).
13. B. D. McNicol, Electrocatalysis, *Catalysis* **2**, 243 (1978).
14. A. P. Fickett, Fuel cell electrocatalysis—Where have we failed, in *Proceedings of the Symposium on Electrode Materials and Processes for Energy Conversion and Storage*, Vol. 77-6, J. D. E. McIntyre, S. Srinivasan, and F. G. Will, eds, The Electrochemical Society, Princeton, New Jersey (1977), p. 546.
15. H. R. Kunz, The state-of-the-art of hydrogen–air phosphoric acid electrolyte fuel cells, in *Proceedings of the Symposium on Electrode Materials and Processes for Energy Conversion and Storage*, Vol. 77-6, J. D. E. McIntyre, S. Srinivasan, and F. G. Will, eds., The Electrochemical Society, Princeton, New Jersey (1977), p. 607.
16. F. von Sturm, Electrocatalytic oxidation of non-noble metal catalysts, in *Proceedings of the Symposium on Electrode Materials and Processes for Energy Conversion and Storage*, Vol. 77-6, J. D. E. McIntyre, S. Srinivasan, and F. G. Will, eds., The Electrochemical Society, Princeton, New Jersey (1977), p. 247.
17. H. Behret, H. Binder, and G. Sandstede, Inorganic and organic non-noble metal containing electrocatalysts for fuel cells, in *Proceedings of the Symposium on Electrocatalysis*, M. W. Breiter, ed., The Electrochemical Society, Princeton, New Jersey (1974), p. 303.
18. G. Luft, K. Mund, G. Richter, R. Schulte, and F. von Sturm, New electrocatalysts for acid fuel cells, *Siemens Forsch, Entwicklungsber.* **3**, 177 (1974).

19. K. Mund, G. Richter, R. Schulte, and F. von Sturm, Electrokatalyse an Phosphiden der Eisengruppe und Einigen Ternaren Verbindungen, *Ber. Bunsenges, Phys. Chem.* **77**, 839 (1973).
20. H. Böhm and F. A. Pohl, Wolframcarbid, ein Elektrokatalysator für saure Brennstoffzellen, *Wiss. Ber. AEG-Telefunken*, **41**, 46 (1968).
21. K. von Benda, H. Binder, A. Kohling, and G. Sandstede, Electrochemical behaviour of tungsten carbide electrodes, in *From Electrocatalysis to Fuel Cells*, G. Sandstede, ed., University Washington Press, Seattle (1972), p. 87.
22. K. Mund, G. Richter, and F. von Sturm, Titanium-containing Raney nickel catalyst for hydrogen electrodes in alkaline fuel cell systems, *J. Electrochem. Soc.* **124**, 1 (1977).
23. H. H. Boehm, Oxygen electrode, German patent 2,202,898 (1973).
24. H. Behret, H. Binder, W. Clauberg, and G. Sandstede, On the mechanism of electrocatalytic oxygen reduction with special reference to metal chelates, in *Proceedings of the Symposium on Electrode Materials and Processes for Energy Conversion and Storage*, Vol. 77–6, J. D. E. McIntyre, S. Srinivasan, and F. G. Will, eds., The Electrochemical Society, Princeton, New Jersey (1977), p. 519.
25. E. B. Yeager, Improved cathodes for phosphoric acid fuel cells, EPRI EM-505, Research Project 634-1, Final Report, June, 1977.
26. K. Hohne, Air electrodes for hydrogen–air fuel cells with alkaline electrolyte, *Siemens Forsch. Entwicklungsber.* **5**, 266 (1976).
27. H. L. Bevan and A. C. C. Tseung, The electrochemical reduction of oxygen on high surface area lithium doped oxides, *Electrochim. Acta* **19**, 201 (1974).
28. A. M. Trunov, V. A. Presnov, M. V. Uminskii, O. F. Rakityanskaya, T. S. Bakutina, and A. I. Kotseruba, Oxygen reduction at semi-conductor catalysts—V. Investigation of physical and electrochemical properties of mixed nickel–cobalt oxides, *Sov. Electrochem.* **11**, 509 (1975).
29. R. Kh. Burshtein, V. S. Vilinskaya, M. R. Tarasevich, and N. G. Bulavina, Electrocatalytic properties of oxide catalysts on a carbon carrier, *React. Kinet. Catal. Lett.* **4**, 159 (1976).
30. A. C. C. Tseung and H. L. Bevan, A reversible oxygen electrode, *J. Electroanal. Chem.* **45**, 429 (1973).
31. A. A. Adams and H. J. Barger, Jr., A new electrolyte for hydrocarbon air fuel cells, *J. Electrochem. Soc.* **121**, 987 (1974).
32. G. W. Walker, H. J. Barger, Jr., and A. A. Adams, The oxidation of carbon monoxide in $CF_3SO_3H \cdot H_2O$, *Electrochem. Soc. Ext. Abstr.* **75–1**, 102 (1975).
33. H. Binder, A. Köhling, and G. Sandstede, Platinum catalysts modified by adsorption or mixing with inorganic substances, in *From Electrocatalysis to Fuel Cells*, G. Sandstede, ed., University of Washington Press, Seattle (1972), p. 59.
34. J. A. Shropshire, Flow coulometry, *J. Electroanal. Chem.* **9**, 90 (1965).
35. M. M. P. Janssen and J. Moolhuysen, Platinum–tin catalysts for methanol fuel cells prepared by a novel immersion technique, by electrodeposition, and by alloying, *Electrochim. Acta.* **21**, 861 (1976).
36. B. D. McNicol, R. T. Short, and A. G. Chapman, Methanol electro-oxidation catalysts, *J. Chem. Soc. Faraday Trans. 1* **72**, 2735 (1976).
37. R. R. Adzic, D. N. Simic, A. R. Despic, and D. M. Drazic, Electrocatalysis by foreign metal monolayers: Oxidation of formic acid on platinum, *J. Electroanal. Chem.* **65**, 587 (1975).
38. V. E. Kazarinov, V. N. Andreev, and G. Ya. Tysyachnaya, Carbon monoxide and carbon dioxide chemisorption products on platinized platinum, *Electrokhimiya* **8**, 927 (1972).
39. A. Capon and R. Parsons, The oxidation of formic acid at noble metal electrodes—Part III. Intermediates and mechanism on platinum electrodes, *J. Electroanal. Chem.* **45**, 205 (1973).
40. Yu. B. Vasilev, V. S. Bagotskii, and O. A. Khazova, General scheme for chemisorption, electroxidation, and electroreduction processes of simple organic substances at platinum group metals, *Sov. Electrochem.* **11**, 1406 (1975).
41. Y. Nishiyama and H. Wise, Surface interactions between chemisorbed species on platinum: Carbon monoxide, hydrogen, oxygen, and methanol, *J. Catal.* **32**, 50 (1974).

42. M. Watanabe and S. Motoo, Electrocatalysis by ad-atoms—Part II. Enhancement of the oxidation of methanol on platinum by ruthenium ad-atoms, *J. Electroanal. Chem.* **60** 267 (1975).
43. M. Watanabe, T. Suzuki, and S. Motoo, Electrocatalytic activities of noble metal alloys for the oxidation of fuels—IV. Electrocatalytic activities of rhodium–ruthenium, rhodium–osmium, platinum–rhodium and platinum–iridium alloy blacks for the oxidation of methanol and sodium formate, *Denki Kagaku* **40**, 210 (1972).
44. V. Sh. Palanker, R. A. Gajyev, and D. V. Sokolsky, On adsorption and electro-oxidation of some compounds on tungsten carbide; their effect on electro-oxidation, *Electrochim. Acta* **22**, 133 (1977).
45. G. Schulz-Ekloff, D. Baresel, and J. Heidemeyer, Influence of competitive adsorption of water and fuel on the activity of anodes in fuel cells, *Collect. Czech. Chem. Commun.* **36**, 928 (1971).
46. K. Kinoshita, J. A. S. Bett, and P. Stonehart, Effects of gas- and liquid-phase environments on the sintering behavior of platinum catalysts, in *Sintering and Catalysis*, G. C. Kuczynski, ed., Plenum Press, New York (1976).
47. K. Kinoshita, Effects of sintering on porous fuel cell electrodes, paper presented at the 151st Electrochemical Society Meeting, Philadelphia, 1977.
48. Y. C. Pan and G. Ciprios, Phosphoric acid catalyst sintering, in National Fuel Cells Seminar, San Francisco, California, Extended Abstracts, p. 79, July 11–13, 1978.
49. J. C. Schlatter, Sintering of supported metals, *Mat. Sci. Res.* **10**, 141 (1975).
50. P. Wynblatt and N. A. Gjostein, Supported metal crystallites, *Prog. Solid State Chem.* **9**, 21 (1975).
51. E. Ruckenstein and B. Pulvermacher, Kinetics of crystallite sintering during heat treatment of supported metal catalysts, *AIChE J.* **19**, 356 (1973).
52. E. Ruckenstein and B. Pulvermacher, Growth kinetics and the size distributions of supported metal crystallites, *J. Catal.* **29**, 224 (1973).
53. P. C. Flynn and S. E. Wanke, A model of supported metal catalyst sintering—I. Development of model, *J. Catal.* **34**, 390 (1974).
54. P. C. Flynn and S. E. Wanke, A model of supported metal catalyst sintering—II. Application of model, *J. Catal.* **34**, 400 (1974).
55. A. C. C. Tseung, Inhibition of sintering in molten carbonate fuel cell anodes, *J. Appl. Electrochem.* **1**, 279 (1971).
56. B. S. Baker, S. Abens, and D. Rigney, Molten carbonate fuel cells—A technical philosophy, ERDA/EPRI Seminar, Palo Alto, California, June 29–July 1, 1976).
57. M. S. Freed and R. J. Lawrence, Development of gold alloy catalyst cathode for alkaline fuel cells, paper presented at the 147th Electrochemical Society Meeting, Toronto, 1975.
58. W. Phillips, E. Desloge, and J. Skofronick, A mechanism to account for observed morphological changes in discontinuous gold films following deposition, *J. Appl. Phys.* **39**, 3210 (1968).
59. K. F. Blurton, H. R. Kunz, and D. R. Rutt, Surface area loss of platinum supported on graphite, *Electrochim. Acta.* **23**, 183 (1978).
60. G. Ciprios, Y. C. Pan, and S. C. Fung, Catalyst sintering in phosphoric acid electrolyte, ERDA/EPRI Seminar, Palo Alto, California, June 29–July 1, 1976.
61. Yu. G. Chirkov, Difference between hydrophobic and hydrophilic electrodes—I. Effect of pore corrugation, *Sov. Electrochem.* **8**, 1480 (1972).
62. Yu. G. Chirkov, Difference between hydrophobized and hydrophilic electrodes—II. Biporous model, *Sov. Electrochem.* **10**, 1710 (1974).
63. Yu. G. Chirkov, Difference between hydrophobized and hydrophilic electrodes—V. Role of electrode structure, *Sov. Electrochem.* **11**, 503 (1975).
64. S. K. Rangarajan, Theory of porous electrode operations, *Curr. Sci.* **40**(8), 175 (1971).
65. O. S. Ksenzhek, Mechanism of the functioning of porous electrodes, *Fuel Cells—Their Electrochemical Kinetics*, V. S. Bagotskii and Yu. B. Vasilev, eds., Consultants Bureau, New York (1966).

66. A. G. Pshenichnikov, Some aspects of the performance of porous gas diffusion electrodes, *Fuel Cells—Their Electrochemical Kinetics*, V. S. Bagotskii and Yu. B. Vasilev, eds., Consultants Bureau, New York (1966).
67. V. S. Markin, A. A. Chernenko, Yu. A. Chizmadzhev, and Yu. G. Chirkov, Aspects of the theory of porous gas diffusion electrodes, *Fuel Cells—Their Electrochemical Kinetics*, V. S. Bagotskii and Yu. B. Vasilev, eds., Consultants Bureau, New York (1966).
68. K. M. Mehta and V. K. Venkatesan, A probability model for a non-uniform gas porous electrodes, *Trans. SAEST* **11**, 411 (1976).
69. L. G. Austin, The electrochemical theory of fuel cells, in *Handbook of Fuel Cell Technology*, C. Berger, ed., Prentice-Hall, Englewood Cliffs, New Jersey (1968).
70. M. Eisenberg, Electrochemical energy conversion, in *Physical Chemistry—An Advanced Treatise*, Vol. IXB, *Electrochemistry*, H. Eyring, ed., Academic Press, New York (1970).
71. V. S. Bagotskii and Yu. B. Vasilev, eds., *Fuel Cells—Their Electrochemical Kinetics*, Consultants Bureau, New York (1966).
72. Yu. A. Chizmadzhev, V. S. Markin, M. R. Tarasevich, and Yu. G. Chirkov, *Macrokinetics of Processes in Porous Media* (in Russian), Nauka, Moscow (1971).
73. M. Breiter, *Electrochemical Processes in Fuel Cells*, Springer-Verlag, New York (1969).
74. R. deLevie, Electrochemical responses of porous and rough electrodes, *Adv. Electrochem. Electrochem. Eng.* **6**, 329 (1967).
75. Yu. A. Chizmadzhev, Some problems of the theory of porous gas electrodes, *Sov. Electrochem.* **2**, 1 (1966).
76. S. Srinivasan, H. D. Hurwitz, and J. O'M. Bockris, Fundamental equations of electrochemical kinetics at porous gas-diffusion electrodes, *J. Chem. Phys.* **46**, 3108 (1967).
77. S. Srinivasan and H. D. Hurwitz, Theory of a thin film model of porous gas-diffusion electrodes, *Electrochem. Acta* **12**, 495 (1967).
78. J. O'M. Bockris and B. D. Cahan, Effect of a finite-contact-angle meniscus on kinetics in porous electrode systems, *J. Chem. Phys.* **50**, 1307 (1969).
79. L. G. Austin, M. Ariet, R. D. Walker, G. B. Wood, and R. H. Comyn, Simple-pore and thin-film models of porous gas-diffusion electrodes, *I&EC Fund.* **4**, 321 (1965).
80. E. A. Grens, R. M. Turner, and T. Katan, A model for analysis of porous gas electrodes, *Adv. Energy Conv.* **4**, 109 (1964).
81. E. A. Grens, II, Analysis of operation of porous gas electrodes with two superimposed scales of pore structure, *I&EC Fund.* **5**, 542 (1966).
82. A. G. Pshenichnikov, Mechanism for the operation of a hydrophilic porous-gas electrode, *Sov. Electrochem.* **6**, 644 (1970).
83. A. G. Pshenichnikov, Yu. I. Kryukov, R. Kh. Burshtein, I. I. Astakhov, and V. V. Surikov, Models for porous hydrophobically treated electrodes, *Sov. Electrochem.* **12**, 1183 (1976).
84. Yu. G. Chirkov, Capillary equilibrium in hydrophobized electrodes, IV. Model of differently sized grains: $r_c > r_p$, *Sov. Electrochem.* **8**, 358 (1972).
85. J. Giner and C. Hunter, The mechanism of operation of the Teflon bonded gas diffusion electrode: A mathematical model, *J. Electrochem. Soc.* **116**, 1124 (1969).
86. J. Giner, The structure of hydrophobic gas-diffusion electrodes, in *From Electrocatalysis to Fuel Cells*, G. Sandstede, ed., University of Washington Press, Seattle (1972).
87. R. Kh. Burshtein, A. V. Dribinskii, M. R. Tarasevich, Yu. A. Chizmadzhev, and Yu. G. Chirkov, Mechanism of current generation of water repellent gaseous diffusion electrodes. I., *Sov. Electrochem.* **7**, 1762 (1971).
88. R. K. Burshtein, A. V. Dribinskii, M. R. Tarasevich, Yu. A. Chizmadzhev, and Yu. G. Chirkov, Mechanism of current generation in hydrophobized gas diffusion electrodes. II. Dependence of the electrochemical activity on the hydrophobizing agent in the active layer, *Sov. Electrochem.* **8**, 195 (1972).
89. Yu. G. Chirkov, Difference between hydrophobized and hydrophilic electrodes. III. Cylindrical gas pore model, *Sov. Electrochem.* **11**, 36 (1975).
90. Yu. G. Chirkov and Yu. A. Chizmadzhev, Mechanism of current generation in water proofed electrodes, *Trans. SAEST* **7**, 11 (1972).

91. K. Mund and F. von Sturm, Degree of utilization and specific effective surface area of electrocatalysts in porous electrodes, *Electrochim. Acta* **20**, 463 (1975).
92. A. D. S. Tantrum and A. C. C. Tseung, Structure and performance of hydrophobic gas electrodes, *Nature* **221**, 167 (1969).
93. F. A. Posey and T. Morozumi, Theory of potentiostatic and galvanostatic charging of the double layer in porous electrodes, *J. Electrochem. Soc.* **113**, 176 (1966).
94. W. Tiedemann and J. Newman, Double-layer capacity determination of porous electrodes, *J. Electrochem. Soc.* **122**, 70 (1975).
95. L. G. Austin and E. G. Gagnon, The triangular voltage sweep method for determining double-layer capacity of porous electrodes. Part 1. Theory, *J. Electrochem. Soc.* **120**, 251 (1973).
96. J. McHardy, J. M. Barris, and P. Stonehart, Investigation of hydrophobic porous electrodes. 1. Differential capacitance by a low frequency ac impedance technique, *J. Appl. Electrochem.* **6**, 371 (1976).
97. B. V. Tilak, C. G. Rader, and S. K. Rangarajan, Techniques for characterizing porous electrodes. I. Determination of the double-layer capacity, *J. Electrochem. Soc.* **124**, 1879 (1977).
98. J. O'M. Bockris and S. Srinivasan, Elucidation of the mechanism of electrolytic hydrogen evolution by the use of H–T separation factors, *Electrochim. Acta* **9**, 31 (1964).
99. O. S. Abramzon, S. F. Cherynshov, and A. G. Pshenichnikov, Specific surface areas of exchange currents of the hydrogen ionization and evolution reaction for different nickel catalysts, *Sov. Electrochem.* **12**, 1520 (1976).
100. S. K. Rangarajan, On linear relaxation methods, *J. Electroanal. Chem.* **41**, 459 (1973).
101. S. K. Rangarajan, An exponential relaxation technique— theory, *J. Electroanal. Chem.* **41**, 491 (1973).
102. G. Prabhakara Rao and S. K. Rangarajan, A new relaxation method for studying electrode reactions, *J. Electroanal. Chem.* **41**, 473 (1973).
103. G. P. Rao, S. K. Lakshmanan, and S. K. Rangarajan, Decreasing current ramp technique for the study of fast electrode reactions, *J. Electroanal. Chem.* **62**, 273 (1975).
104. B. V. Tilak, C. G. Rader, and S. K. Rangarajan, Insights into the determination of the double-layer capacity of porous electrodes, paper presented at 70th Annual Meeting of A.I.Ch.E., November 13–17, 1977.
105. E. A. Grens, II, and C. W. Tobias, Analysis of the dynamic behaviour of flooded porous electrodes, *Ber. Bunsenges. Phys. Chem.* **68**, 236 (1964).
106. S. K. Rangarajan, Theory of flooded porous electrodes—I. Galvanostatic transients and generalized impedance, *J. Electroanal. Chem.* **22**, 89 (1969).
107. R. Alkire and B. Place, Transient behaviour during reactant depletion in porous electrodes, *J. Electrochem. Soc.* **119**, 1687 (1972).
108. J. H. Russell, Gemini fuel cell system, in *Proceedings of the 19th Power Sources Conference*, PSC Publications Committee, New Jersey (1965), pp. 35–38.
109. C. C. Morrill, Apollo fuel cell System, in *Proceedings of the 19th Power Sources Conference*, PSC Publications Committee, New Jersey (1965), pp. 38–41.
110. A. C. Ching, A. P. Gillis, and F. M. Plauche, Fuel cell powerplant operation in Apollo spacecraft, in Proceedings of the 7th Intersociety Energy Conversion Engineering Conference, 1972, paper No. 729064, pp. 368–372.
111. W. E. Rice and D. Bell, Status of Shuttle fuel cell technology program, in Proceedings of the 7th Intersociety Energy Conversion Engineering Conference, 1972, paper No. 729067, pp. 390–395.
112. L. E. Chapman, The solid polymer electrolyte fuel cell for the Space Shuttle orbiter, in Proceedings of the 7th Intersociety Energy Conversion Engineering Conference, 1972, paper No. 729076, pp. 466–471.
113. J. F. McElroy, Solid polymer electrolyte (SPE) fuel cell technology program, Final Technical Report for NASA/JSC, October 1975.

114. W. A. Titterington and A. P. Fickett, Electrolytic hydrogen fuel production with a solid polymer electrolyte, in Proceedings of the 8th Intersociety Energy Conversion Engineering Conference, paper No. 739020, August 1973, pp. 574–579.
115. L. J. Nuttall and W. A. Titterington, General Electric's solid polymer electrolyte water electrolysis, in Conference on the Electrolytic Production of Hydrogen, City University, London, February 1975).
116. M. F. Collins, Life test of a 200 W ammonia–air fuel cell system, in *25th Power Sources Symposium*, PSC Publications Committee, New Jersey (1972), pp. 162–164.
117. M. F. Collins, R. Michalek, and W. Brink, Design parameters of a 300 watt ammonia–air fuel cell system, in Proceedings of the 7th Intersociety Energy Conversion Engineering Conference, 1972, paper No. 729006, pp. 32–36.
118. O. J. Adlhart. The phosphoric acid fuel cell—a long life power source for the low to medium wattage range, in Proceedings of the 7th Intersociety Energy Conversion Engineering Conference, 1972, paper No. 729163, pp. 1097–1101.
119. R. Noyes, ed., *Fuel Cells for Public Utility and Industrial Power*, Noyes Data Corporation, Park Ridge, New Jersey (1977).
120. G. Szego, Economics, logistics, and optimization of fuel cells, Institute for Defence Analysis Research Paper, 1965, p. 208.
121. United Technologies, Inc., Connecticut, Final Report for "On site fuel cell resource conservation in industrial process applications", FCR 0439, October 3, 1977.
122. Power Systems Division, United Technology Corporation, National benefits associated with commercial application of fuel cell power plants, ERDA 76-54, UC-93, February 1976.
123. P. Bolan and L. M. Handley, First generation fuel cell powerplant characteristics, paper presented at Fuel Cell Workshop at Sarasota, Florida, November 14–17, 1977.
124. M. Eisenberg, Design and scale-up considerations for electrochemical fuel cells, *Adv. Electrochem. Electrochem. Eng.* 2, 235 (1966).
125. H. J. R. Maget, The ion exchange membrane fuel cell, *Handbook of Fuel Cell Technology*, C. Berger, ed., Prentice-Hall, Englewood Cliffs, New Jersey (1968).
126. B. S. Baker, D. Gidaspow, and D. Wasan, Thermal phenomena in fuel cells and batteries, *Adv. Electrochem. Electrochem. Eng.* **8**, 63 (1971).
127. J. A. Cusumano and R. B. Levy (Catalytica Assoc., Inc.), Assessment of fuel processing alternatives for fuel cell power generation, EPRI Report EPRI EM-570 (Research Project 919-1) (October 1977).
128. C. J. Warde, R. J. Ruka, and A. O. Isenberg, Fuel cells, energy conversion alternatives study (ECAS), Westinghouse Phase I—Final Report, NASA CR-134941, Vol. XII, 1976.
129. A. P. Fickett, Electric Power Research Institute, in Alkaline Fuel Cell Discussions at the EPRI Catalyst Workshop, January 1975.
130. A. B. Hart and G. J. Womack, *Fuel Cells*, Chapman and Hall, London (1967).
131. T. L. Markin, Limiting problems in the development of a high temperature solid oxide electrolytic fuel cell, in Proceedings of the 18th International Symposium on Power Sources, Brighton, England, paper No. 3, pp. 31–42, September 1972.
132. Final Report, Project fuel cell, Research and Development Report No. 57, Office of Coal Research, Department of the Interior, Washington, 1971.
133. J. Verstraete, D. Lefevre, R. Lefort, and J. Henry, Fuel cell economics and commercial applications, in *Handbook of Fuel Cell Technology*, C. Berger, ed., Prentice-Hall, Englewood Cliffs, New Jersey (1968).
134. M. Warshay and R. K. Burns, Molten carbonate fuel cell/steam system, in Evolution of phase II conceptual design, implementation, and assessment resulting from the energy conversion alternatives study (ECAS), Section 4.6, NASA TMX-73515, April 1977.
135. J. M. King, Integrated coal gasifier/molten carbonate fuel cell powerplant conceptual design and implementation assessment, Energy conversion alternatives study (ECAS), United Technology Phase II Final Report, NASA CR-134955, FCR 0237 (1977).

136. S. Srinivasan, J. McBreen, and B. McCormick, Program plan for the development of fuel cell technology for vehicular application, September 15, 1977.
137. Proceedings of the Fuel Cell Powered Vehicle Workshop, B. McCormick, S. Depp, S. Srinivasan, J. McBreen, I. L. Harry, A. Voelker, C. Pax, D. Hamilton, W. Kerwin, and B. S. Baker, eds., Los Alamos Scientific Laboratory, Los Alamos, New Mexico, August 1978.
138. K. V. Kordesch, Carbon electrodes, in Proceedings of the Conference on Fuel Cell Catalysis Workshop, EPRI Special Report, SR-13, pp. 101–106, August 1975.
139. J. M. King, Jr., Advanced technology fuel cell program, EPRI EM-335 (Research Project 114-1), October 1976.
140. I. R. McNab, Power conversion in space, in Research Programme on Magnetoplasmadynamic Power Generation, Tech. Summary Report, December 1, 1962 to March 31, 1964, Part 3: Theoretical (AD602383); Washington, D.C., Office of Technical Services, U.S. Department of Commerce, 1964.

3

Electrochemical Energy Storage

KARL KORDESCH

1. Introduction

1.1. The Need for Energy Storage

Fossil fuels contain stored chemical energy produced through the action of sunlight over past geological eras in a compact and conveniently convertible form. Unfortunately, the supply will only last a few more generations at the fast-rising rate of use. Renewable resources such as sunlight, wind, or the kinetic energy of the ocean waves have the problem of variability. Technology must therefore use devices which can store the energy generated when supply exceeds demand, for use at a later time or a different location.

Nuclear fuels, fossil fuels, solar and geothermal energy, even the temperature gradient of the ocean can be used to generate electricity, but the consumer and industry need energy at different levels, and difficulties arise when a fluctuating amount of energy should be supplied efficiently. The typical demand load of the utilities, as an example, varies so much during the day, over the weekend, and seasonally, that the capacity of the electric power system needs to be much larger than the average capacity used. As a result, expensive, rarely utilized equipment must be kept available to be pressed into service when required.

KARL KORDESCH • Institute for Inorganic Chemical Technology, Technical University of Graz, 8010 Graz, Austria.

The use of a flashlight for a short time is a storage problem on a small scale; the operation of an automobile (gasoline or even battery powered) is a storage problem for medium quantities of energy to be released on demand.

The purpose of storage devices is to match the production of energy with the consumer's needs. The choice of an efficient storage device is becoming more and more important because we can no longer afford to waste energy of any kind. A suitable storage system is also a means to provide flexibility at lower cost.

The storage of massive amounts of energy is an inherent requirement of modern technology, but not all types of storage are equal in cost, efficiency, or convenience. A selection between storage technologies is timely because it can help to bridge successfully the gap between the present fossil fuel period and the future nuclear–solar era which may use a universal energy transport and storage system based on chemicals (hydrogen, methanol, etc.). Such scenarios and models have been discussed extensively.[1] To gain the proper perspective, several methods of energy storage will be shortly reviewed before electrochemical systems will be presented. The interconnections with other storage means are necessary because there is no practical system known which can store electricity as such. Only a plate capacitor may come close to a direct storage device, but for electricity to be stored in larger amounts it must be converted into another form of energy first, then stored and finally reconverted again. This rather complicated process is accepted because electricity is the most convenient and universally useful form of energy available to us.

1.2. Energy Storage Technologies

Energy storage methods may be classified into the following groups[2]:

Mechanical (physical) methods: hydro-pumped-storage facilities; compressed air; flywheel energy storage; superconductive magnets.

Thermal (physical and chemical) methods: heat, capacity storage (liquids, solids); reaction heat storage (chemical recombination).

Electrochemical (chemical) methods: galvanic cells, batteries (primary and secondary); chemical storage (after electrolysis); converters (fuel cells).

1.2.1. Hydropumped-Storage Technology

Energy is stored by pumping water from a lower to a higher elevation. Pumping and generating can be accomplished by the reversal of a dual-action system. In the U.S.A. plants have been built in sizes from a few megawatts to 1000 MA (10,000 MWh). The overall efficiency for a cycle is in the range of 66–75% and the storage capacity (kWh/kW) ranges from 8 to 24 hr. Reliability is generally 85% considering normal out-times and maintenance. The turn-around times are 5–40 min from generating to pumping and 1–5 min from

shut-down to full load. The useful life is 50 years (tax rating). Underground pumped storage in bedrock caverns down to 800 m below ground is being considered.

1.2.2. Compressed Air Storage

This method is an old concept but plans have not been implemented until recently. About two-thirds of the power generated by the hot-gas expansion in a turbine is absorbed by the compressor. Separate compressed air storage could therefore improve the peak power capability of a plant greatly. The compression could be done by the water flowing down in off peak times, or, in a pumped hydroplant, by creating pressure in the underground storage reservoir. Heating of the compressed supply air (even by fossil fuel) results in further efficiency improvements. The largest conventional gas turbines are rated at 100 MW; with separate compressed air storage, the same units can produce 300 MW.

1.2.3. Flywheel Energy Storage

The kinetic energy of the rotating mass stores the electrical energy used to produce the spinning of the wheel. Most application studies to date have been concerned with vehicle or space power systems. Basic concepts include ganged wheels on a common shaft, feeding a variable frequency field machine. Energy densities of 25–30 Wh/kg can be achieved with constant stress steel, 90–110 Wh/kg with brush-boron fibers, and 130–140 Wh/kg with graphite (Thornel) epoxy composites as materials for the flywheel. Subsystems (not included in the figures) require special bearings, supports, and vacuum and control systems.

1.2.4. Superconducting Magnet Energy Storage (SMES)

Electrical energy is stored in a magnetic field produced by a circulating current in the windings of a superconducting electromagnet. The efficiency of SMES devices is usually high but the losses in the refrigeration system (operating temperature: 1.8 K) are about 20%. The system is in very early stages of development.

1.2.5. Thermal Energy Storage (TES)

The energy must be in a form to be used in a heat engine, and the storage temperatures must be high. The thermal energy can be stored in a chemical which undergoes a phase change like in a melting salt or simply in a hot fluid (oil). Especially suited are fused salts, e.g., a mixture of 46% LiF, 44% NaF, and 10% MgF_2 melts at 632°C and has a latent heat of 205 cal/g (857 J/g). LiH

has about three times the capacity. For comparison: a lead–acid battery has a capacity of 30 cal/g (125 J/g). However, the conversion is subject to Carnot's law in the case of the heat cycle. Liquid sodium is also a promising heat storage material, particularly with nuclear plants.

1.2.6. Thermochemical Storage

This concept involves energy storage in the heat of decomposition and recombination of reversible reactions. An example is the SO_2–SO_3 system, which has a storage capacity of 295 cal/g (1233 J/g) and operates at 724°C. It is proposed for solar-collector gas cooling. The reaction can be turned on by a catalyst (V, Pt). Of course, a heat content pipeline filled with the components of the $CH_4 + H_2O$ reaction (CO and $3H_2$) would have very low losses on transport at ambient temperature, but produce 1756 cal/g (7340 J/g) on recombination. Fuel cell operation opens even more intriguing versions.

1.2.7. Chemical Storage and Electrochemical Conversion

A potentially important example of the combination of storage as chemicals and electrochemical conversion is the process of electrolyzing water to hydrogen and oxygen and totally recombining the gases in a fuel cell. Electrolysis is a commercially proven method; so is the storage of H_2 as compressed or liquefied gas. Metal hydride storage is a recent technology. Fuel cell batteries are now in the megawatt design stage.

1.2.8. Electrochemical Storage in Batteries

On a large scale, only lead–acid batteries are available, placing this method on about third place after hydropumped storage and thermal storage. Advanced batteries, as they are under development now, may become competitive for utility purposes in situations where the credits of battery performance are large and represent advantages over other systems.

Smaller-scale applications, like in consumer and vehicle use, batteries are not replaceable by the other systems because of the inherent simplicity of battery use and instant power availability.

2. The Theory of Galvanic Cells

2.1. Electrode Potentials

Electrode potentials can be used to determine the chemical potentials (Gibbs free energies, free enthalpies) of substances; they are expressed in volt-faradays (per mole) or in joules. With known temperature coefficients the

heat content (enthalpy) becomes available. The opposite calculations are equally important, experimental thermochemical data can be applied to elucidate electrochemical processes under conditions which may be difficult to establish or simply are not known yet.

Electrode potentials and temperature coefficients can be used to calculate equilibrium constants. Deviations from the standard conditions can be calculated with the help of the Nernst equation. All these interrelations are called *thermodynamics of galvanic cells.*

However, it must be stressed that thermodynamic data can not tell us anything about the charge transfer, the overpotential, or indicate how fast a reaction will proceed or even, if it will proceed at all. Thermodynamics is only applicable for equilibrium conditions. It is fruitless for kinetics.

From the failure of thermodynamics to predict actual electrode or cell performances it should not be construed that thermodynamics is wrong. Just the contrary: it is *always* right, as long as we do not ask kinetic questions. A comparison may be useful: a triangle always has 180°, as long as one does not leave plane geometry.

Vetter[3] was the first strong proponent for kinetics treatment of electrode processes. He pointed out that the actual mechanisms involve more than the formation of a potential difference determined by the activities related to a standard hydrogen electrode. Especially oxide electrodes must be treated on a nonstoichiometric basis. Phase boundaries are important and must be established between different metals and electrode surfaces and electrolytes, often containing ions of different valencies.

Bockris and Reddy[4] and other modern electrochemists established "ionics" and "electrodics" as parts of electrochemical science based on quantum mechanics and solid state theory. Academician A. Frumkin was one of the pioneers of the "new" trend, away from the once all-important Nernst equation.

However, we must also admit that in the practical world of battery technology the empirical experimentalist can show a higher "batting average" than the pure scientist. The reason is simply that we do not have enough data to define a certain electrode situation in a real cell. We must live currently with approximations and use the known "laws" to the best of our knowledge. This is fortunate, since it provides many chances to invent new, unpredicted things and offers a challenge to the scientist and engineer as well.

The electrode potentials are listed in tables relating to the specific chemical elements or compounds; they are expressed in volts and indicate the maximum electrical energy obtainable from the reaction of that element or compound with hydrogen. Latimer,[5] De Bethune,[6] Pourbaix,[7] Ives and Janz,[8] and Hampel[9] have published such compilations.

In the following examples it will be shown how thermodynamic data can be used to calculate principal cell characteristics. Table 1 lists a selected number of half-cell potentials.

Table 1
Standard Potentials ($E°$) and Temperature Coefficients ($dE°/dT$) of Electrodes at 25°C

Electrode	Half-reaction	$E°$, V	$dE°/dT$, mV/K
Li^+; Li	$Li^+ + e = Li$	−3.045	−0.59
K^+; K	$K^+ + e = K$	−2.925	−1.07
Ba^{2+}; Ba	$Ba^{2+} + 2e = Ba$	−2.90	−0.40
Sr^{2+}; Sr	$Sr^{2+} + 2e = Sr$	−2.89	−0.23
Ca^{2+}; Ca	$Ca^{2+} + 2e = Ca$	−2.87	−0.21
NA^+; Na	$Na^+ + e = Na$	−2.7141	−0.75
Mg^{2+}; Mg	$Mg^{2+} + 2e = Mg$	−2.37	+0.18
Al^{3+}; Al	$Al^{3+} + 3e = Al$	−1.66	+0.53
Ti^{2+}; Ti	$Ti^{2+} + 2e = Ti$	−1.63	—
OH^-, H_2; Pt	$2H_2O + 2e = 2OH^- + H_2(g)$	−0.8281	−0.80
Zn^{2+}; Zn	$Zn^{2+} + 2e = Zn$	−0.7631	+0.10
I^-, TlI; Tl	$TlI + e = Tl + I^-$	−0.753	−0.20
Br^-, TlBr; Tl	$TlBr + e = Tl + Br^-$	−0.658	−0.31
Cl^-, TlCl; Tl	$TlCl + e = Tl + Cl^-$	−0.557	−0.49
Fe^{2+}; Fe	$Fe^{2+} + 2e = Fe$	−0.440	+0.05
Cr^{3+}, Cr^{2+}; Pt	$Cr^{3+} + 3 = Cr^{2+}$	−0.41	—
Cd^{2+}; Cd	$Cd^{2+} + 2e = Cd$	−0.4019	−0.09
SO_4^{2-}, $PbSO_4$; Pb	$PbSO_4 + 2e = Pb + SO_4^{2-}$	−0.3553	−0.99
Tl^+; Tl	$Tl^+ + e = Tl$	−0.3363	−1.31
Ni^{2+}; Ni	$Ni^{2+} + 2e = Ni$	−0.250	+0.31
I^-, AgI; Ag	$AgI + e = Ag + I^-$	−0.1524	−0.33
Pb^{2+}; Pb	$Pb^{2+} + 2e = Pb$	−0.1288	−0.38
$I^-Hg_2I_2$; Hg	$Hg_2I_2 + 2e = 2HG + 2I^-$	−0.0405	+0.02
H^+, H_2; Pt	$2H^+ + 2e = H_2(g)$	0.0000	0
UO_2^{2+}, UO_2^+; Pt	$UO_2^{2+} + e = UO_2^+$	+0.05	+0.58
Br^-, AgBr; Ag	$AgBr + e = Ag + Br^-$	0.0711	−0.49
Br^-, Hg_2Br_2; Hg	$Hg_2Br_2 + 2e = 2Hg + 2Br^-$	0.1392	−0.15
Cu^{2+}, Cu^+; Pt	$Cu^{2+} + e = Cu^+$	0.153	+0.07
Cl^-, AgCl; Ag	$AgCl + e = Ag + Cl^-$	0.2224	−0.66
Cl^-, Hg_2Cl_2; Hg	$Hg_2Cl_2 + 2e = 2Hg + 2Cl^-$	0.2681	−0.31
Cu^{2+}; Cu	$Cu^{2+} + 2e = Cu$	0.337	+0.01
$C_2O_4^{2-}$, $Hg_2C_2O_4$; Hg	$Hg_2C_2O_4 + 2e = 2Hg + C_2O_4^{2-}$	0.4166	—
Cu^+; Cu	$Cu^+ + e = Cu$	0.521	−0.06
I_2, I^-; Pt	$I_2 + 2e = 2I^-$	0.5346	−0.13
I_3^-, I^-; Pt	$I_3^- + 2e = 3I^-$	0.5356	−0.19
SO_4^{2-}, Hg_2SO_4; Hg	$Hg_2SO_4 + 2e = 2Hg + SO_4^{2-}$	0.6153	−0.83
Fe^{3+}, Fe^{2+}; Pt	$Fe^{3+} + e = Fe^{2+}$	0.771	+1.19
Hg_2^{2+}; Hg	$Hg_2^{2+} + 2e = 2Hg$	0.789	−0.31
Ag^+; Ag	$Ag^+ + e = Ag$	0.7991	−1.00
Hg^{2+}, Hg_2^{2+}; Pt	$2Hg^{2+} + 2e = Hg_2^{2+}$	0.920	+0.10
Br^-, Br_2; Pt	$Br_2 + 2e = 2Br^-$	1.0652	−0.61
H^+, O_2; Pt	$4H^+ + O_2 + 4e = 2H_2O$	1.229	−0.85
Mn^{2+}, MnO_2; Pt	$MnO_2 + 4H^+ + 2e = Mn^{2+} + 2H_2O$	1.23	−0.61
Tl^{3+}, Tl^+; Pt	$Tl^{3+} + 2e = Tl^+$	1.25	+0.97
$Cr_2O_7^{2-}$, Cr^{3+}; Pt	$Cr_2O_7^{2-} + 14H^+ + 6e = 2Cr^{3+} + 7H_2O$	1.33	—

Table 1 (continued)

Electrode	Half-reaction	$E°$, V	$dE°/dT$, mV/K
Cl^-, Cl_2; Pt	$Cl_2 + 2e = 2Cl^-$	1.3595	−1.25
Pb^{2+}, PbO_2; Pt	$PbO_2 + 4H^+ + 2e = Pb^{2+} + 2H_2O$	1.455	−0.25
Au^{3+}; Au	$Au^{3+} + 3e = Au$	1.50	—
MnO_4^-, Mn^{2+}; Pt	$MnO_4^- + 8H^+ + 5e = Mn^{2+} + 4H_2O$	1.51	−0.64
Ce^{4+}, Ce^{3+}; Pt	$Ce^{4+} + e = Ce^{3+}$	1.61	—
Au^+; Au	$Au^+ + e = Au$	1.68	—
$SO_4^{2-}, PbSO_4, PbO_2$; Pb	$PbO_2 + SO_4^{2-} + 4H^+ + 2e = PbSO_4 + 2H_2O$	1.6852	+0.35
MnO_4^-, MnO_2; Pt	$MnO_4^- + 4H^+ + 3e = MnO_2 + 2H_2O$	1.695	−0.67
F^-, F_2; Pt	$F_2 + 2e = 2F^-$	2.87	—

Example 1: Energy Output of a Cell. The standard potential of the chlorine electrode is listed as 1.359 V, referring to the standard hydrogen electrode at 25°C. The half-cell reaction for the chlorine electrode is the following:

$$Cl_2 + 2e^- = 2Cl^- \tag{1}$$

The cell in which such an electrode reaction is occurring must contain the reference:

$$(-)Pt|H_2, H^+\|Cl^-, Cl_2|Pt(+) \tag{2}$$

In the writing of these equations the Stockholm convention drafted by the International Union of Pure and Applied Chemistry (IUPAC) is followed (Yeager and Salkind[110]). The Comité International de Thermodynamique et de Cinétique Électrochimiques (CITCE) convention introduced relative electrode tensions. Fortunately it arrived at the same electrode sign (+1.359 V) but placed the standard hydrogen electrode on the right.

The chemical equation describing the process is

$$Cl_2 + H_2 = 2H^+ + 2Cl^- = 2HCl \tag{3}$$

It means that 70.9 g of chlorine react with 2.016 g of hydrogen to form 72.916 g of hydrochloric acid. In accordance with thermodynamics the cell produces a maximum electric energy of 2 faradays × 1.3595 V or 2.719 V-faradays or 262.349 kJ (62.773 kcal) per mole. One faraday corresponds to 96487 Asec or 26.8 Ahr mol. One volt-faraday is 96.487 kJ or 23.061 kcal/mol. The chlorine–hydrogen cell produces 2 × 26.8 Ah at 1.359 V or 72.8 Wh/mol. This value agrees well with actual measurements.

Example 2: Thermodynamic Data from Potentials. Thermodynamic data can be calculated from cell potentials and temperature coefficients. The

relations to be used are

$$\Delta G^\circ = -nFE^\circ = \Delta H^\circ - T\Delta S^\circ \tag{4}$$

$$\Delta H^\circ = -nFE^\circ + nFT(dE/dT) \tag{5}$$

$$\Delta S^\circ = nF(dE/dT) \tag{6}$$

The cell $Pt|H_2|HCl|AgCl|Ag$ has a measured potential at 25°C of 0.2224 V, it is described by the reaction

$$AgCl + 1/2H_2 = Ag + H^+ + Cl^- \tag{7}$$

whereby all activities are set to be 1 M (and $PH_2 = 1$ atm). With $n = 1$ the free energy difference $\Delta G^\circ = 96{,}487 \times 0.2224 = -21{,}458$ J/mol. The measured temperature coefficient is -0.655 mV/K and ΔS° becomes -62.2 J/K (-14.9 cal/K) per mole. ΔH° calculates to -40 kJ/mol (-9.6 kcal/mol). Specific heat values ΔC_p° can be calculated from the isothermal temperature coefficient d^2E°/dT^2, and the difference $C_p - C_v$ is the gas constant R.

Example 3: The Potential of the Oxygen Electrode. Thermodynamical data can provide cell potentials which have not been measured, for instance for the reaction of hydrogen with oxygen in a fuel cell:

$$2H_2 + O_2 = 2H_2O(aq.) \tag{8}$$

The reaction is represented by the equation

$$O_2 + 4H^+ + 4e^- = 2H_2O \text{ in acidic solution} \tag{9}$$

and by

$$O_2 + 2H_2O + 4e^- = 4OH^- \text{ in alkaline solutions} \tag{10}$$

ΔG° has been determined from ΔH° and ΔS° data as -474.33 kJ/mol. This value results in a potential of 1.229 V for Eq. (9) and 0.401 V for Eq. (10); the difference is the potential of the acid–alkali cell under standard conditions: 0.82 V. The reason that this voltage of the H_2–O_2 cell has not been measured is that the $4e^-$ process represents a splitting of the O=O bond, which is energetically not favored; consequently the electrode reaction proceeds via the $2e^-$ peroxide mechanism:

$$O_2 + H_2O + 2e^- = HO_2^- + OH^- \tag{11}$$

with a standard potential of -0.076 V (with some uncertainties). Combined with a standard hydrogen electrode the cell potential calculates to about 0.75 V. In actual cells the voltage is ~1.05 V. This big discrepancy was certainly not expected from thermodynamic data, but fortunately the true mechanism has been sufficiently well established so that thermodynamics can have a second go around to improve the agreement between the findings.

In real cells the peroxide is rapidly decomposed by oxide-surface catalysis and the standard concentration (activity) of 1 M is never achievable. Experimentally, the peroxide concentration is below the (analytically easy to determine) value of 10^{-8} M and may well reach 10^{-10}–10^{-12} M.

One can now apply the Nernst equation to correct for the deviation from the standard condition and the result is

$$E = 0.75 - \frac{0.059}{2} \log \frac{a_{HO_2^-} a_{OH^-}}{a_{H_2O} p_{O_2}} \tag{12}$$

If we set the activities for OH^-, H_2O equal to 1 M and p of O_2 equal to 1 atm, a value of 10^{-10} M results for the peroxide activity when the cell potential is 1.05 V, or vice versa. The difference of 0.3 V in the first theoretical prediction is now explained. The change from the $4e^-$ process to the actual $2e^-$ process in the reaction mechanism of the oxygen electrode has other implications which thermodynamically could not have been predicted. The dependance of the potential on the O_2 gas pressure changed from 15 to 29 mV per magnitude. Similarly, the dependance on the pH value changes from 59 to 29 mV per activity decade of the OH^- ions.

Figure 1 pictures the equilibrium potentials of both, the O_2 and oxygen peroxide, in relation to those of hydrogen and cadmium. Such diagrams are named after Pourbaix,[7] who arranged such data in an atlas of electrochemical equilibria. The authors responsible for Figure 1, von Döhren and Euler,[11] use the CITCE convention in writing their equations.

Example 4: Metal Oxide Cathodes. To what extent thermodynamics can predict the potentials of metal oxide–metal cells will be shown in this example.

The reaction of manganese dioxide with zinc in alkaline solution is (in summary) represented by the following equation:

$$2MnO_2 + Zn = ZnO + Mn_2O_3 \tag{13}$$

The thermodynamic data for the participating substances are $\Delta H°$: MnO_2, −518 kJ/mol; Zn, 0 kJ/mol; ZnO, −346 kJ/mol; and Mn_2O_3, −953 kJ/mol. $\Delta S°$: MnO_2, 53 J/mol K; Zn, 38 J/mol K, ZnO, 43 J/mol K; and Mn_2O_3, 110 J/mol K. $\Delta H°$ for the reaction is −264 kJ/mol and $\Delta S°$ is 62 J/mol K. $\Delta G°$ according the Eq. (4) results in −280 kJ/mol, which value corresponds to a cell potential of 1.46 V (n = 2).

Figure 2 is a composite of two Pourbaix diagrams from the atlas, that of zinc and that of MnO_2, joined at the hydrogen–pH line with a slope of 59 mV per magnitude change. The diagram was also somewhat simplified (Kordesch[12]).

Figure 2 enables one to estimate the potentials in the acidic and neutral region (area of the Leclanché cell) and the alkaline electrolyte domain. The accuracy is relatively good, considering the necessary amount of information which has to be included in the solid state portions of the diagram. The real

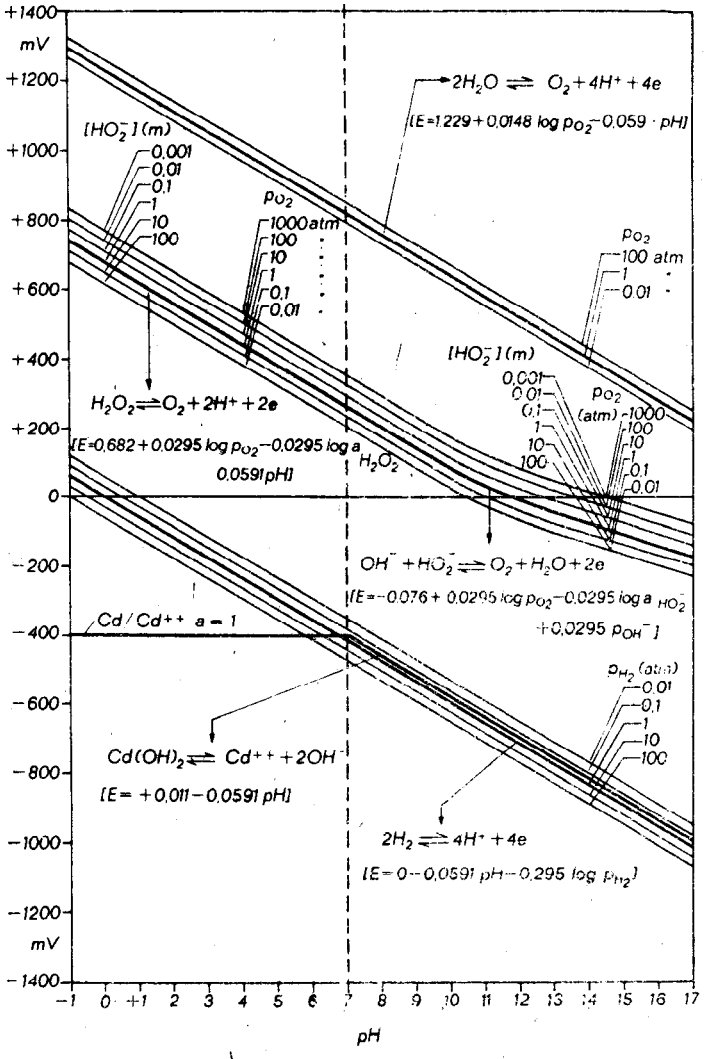

Figure 1. Pourbaix diagram of the oxygen, peroxide, hydrogen, and cadmium electrodes.

activities of the electrolytes at the interfaces can only be guessed. The alkaline MnO_2–Zn cell with 9 *M* KOH electrolyte and with δ-MnO_2 as active material has an open-circuit voltage of 1.65 V. β-MnO_2 has a potential of 0.1 V less.

On the metal oxide side the diagram can be made more accurate if one describes the varying potential of the MnO_2 electrode as a function of the

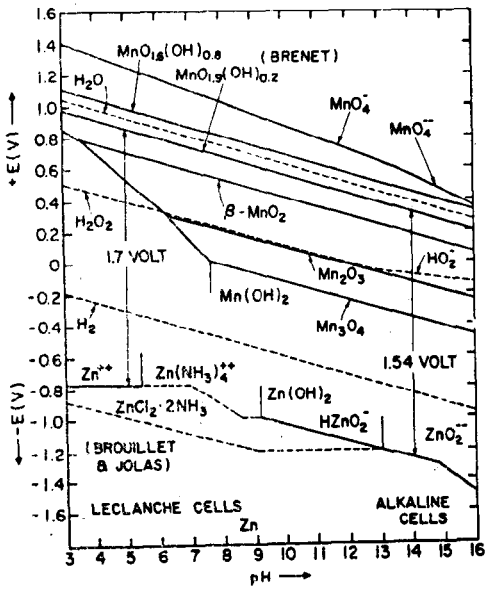

Figure 2. Simplified Pourbaix diagram of the MnO_2–Zn cell showing electrode potentials as functions of pH.

Mn^{3+}/Mn^{4+} distribution in the solid electrode. Actually, large efforts have been made to explain the thermodynamics of oxide electrodes for cases where the oxide is not in contact with its parent material and in contact with a solution containing ions of the same metal but of different valency (Vetter[13]). For the cathodes of Leclanché MnO_2 batteries the case metal oxide (homogeneous phase)/inert conductor (carbon)/ion transfer to the electrolyte has been discussed in opposition to the case of a heterogeneous phase system by Huber.[14] He pointed out that attention must be paid to the fact that thermodynamic equilibrium can only be attained if the reactions across the phase boundaries are not inhibited, which is not assured. For the case of alkaline MnO_2 batteries, thermodynamics has been abandoned and a solid homogeneous metal oxide system with the capability to take up protons (from water) into the structure gradually, has been proposed by Kozawa[15]—it is the only mechanism which also describes the potential change on discharge satisfactorily. It is obvious that kinetics is participating already! Still we can calculate equilibrium potentials and describe the potential as a function of the x in MnO_x by a Nernst-type equation as follows:

$$E = E' - \frac{RT}{F} \ln \frac{Mn^{3+}\ \text{solid}}{Mn^{4+}\ \text{solid}} \tag{14}$$

Figure 3 shows the curve describing the potential as a function of the x in MnO_x from $x = 2$ to $x = 1.5$, the homogeneous phase. After $MnO_{1.5}$ the

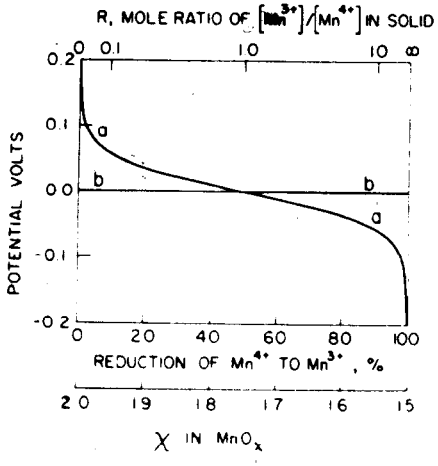

Figure 3. Calculated equilibrium potential versus x in MnO_x for a homogeneous phase reduction (curve a). [Curve b represents Eq. (15).]

mechanism changes and further reduction of the MnOOH to $Mn(OH)_2$ takes place in a heterogeneous process in which the electrolyte participates in a solution phase. In simplified form it can be written as

$$MnOOH \rightarrow Mn(OH)_4^- + e^- \rightarrow Mn(OH)_4^{2-} \rightarrow Mn(OH)_2 \qquad (15)$$

At the beginning and at the end we find distinct solid phases but the reduction occurs in the liquid phase with the carbon participating as an electron transfer means. The potential does not change during the heterogeneous process.

Figure 4 shows the whole reduction curve. It can be compared with the phase diagram of ice/water on heating (Kozawa and Powers[16]).

Heterogeneous reductions of metal oxides are frequent in galvanic cells: the Ag_2O and the HgO systems are good examples. If we write the equation

$$HgO + H_2O + 2e^- = Hg + 2OH^- \qquad (16)$$

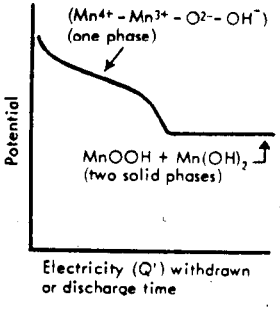

Figure 4. Electrode potential of the MnO_2 system on discharge.

and calculate the equilibrium potential with the Nernst equation we can state

$$E = E^\circ - \frac{RT}{2F} \ln \frac{a_{Hg} a^2_{OH}}{a_{HgO} a_{H_2O}} \tag{17}$$

As a result, the potential does not change much, even if the ratios HgO to Hg change considerably: the curve is flat, not S-shaped as in Figure 3.

Summarizing the teaching of Example 4 it is realized that the [Eq. (13), overall] thermodynamic calculation gave a nearly correct answer but no indication of the mechanism by which the metal oxides change or establish their potential.

Example 5: Anodes and Electrolytes. The Pourbaix diagrams of Figures 1 and 2 show also the potentials of metal electrodes, Cd and Zn. The case of the zinc is rather complicated because this metal forms many complexes in alkaline solution. The standard potential for zinc is calculated from the equation

$$Zn^{2+} + 2e^- = Zn, \qquad E^\circ = -0.76 \text{ V} \tag{18}$$

The zinc potential should then be independant of pH and follow the Nernst relation:

$$E = -0.76 + 0.029 \log a_{Zn^{2+}} \tag{19}$$

However, since this metal forms zincate ions, the potential follows:

$$E = 0.441 - 0.118 \text{ pH} + 0.029 \log (ZnO_2^{2-}) \tag{20}$$

Besides, zinc forms a solid phase zinc oxide or hydroxide, and in this case the potential follows:

$$E = -0.439 - 0.059 \text{ pH} \tag{21}$$

The ZnO can also interact with the MnO_2 and form hetaerolite, resulting in a higher voltage because of the removal of reaction species.

The interactions in concentrated electrolytes can be partly explained by the Debye–Hückel theory but in practice activity coefficients $\delta\pm$ must be taken from tables (Robinson and Stokes[17]).

As an example: 40% KOH is ~10 *M*, 11.9 *m*, has a pH value of 16.6 and $\delta\pm$ is 10.5 at 25°C. In acidic electrolytes the correction figures are not as large as in alkaline solutions. However, solubility equilibria can play an important role in the establishment of potentials. In the lead–acid battery system the equilibrium of lead, lead oxide, and lead sulfate and its change with pH is useful for the judgment of self-discharge and passivation effects.

Figure 5 shows the Pourbaix diagram of the lead–acid system.

Figures 6a and 6b present Pourbaix diagrams for the system Pb–H_2O–H_2SO_4 for two combined sulfate activities, 6a for unity and 6b for an activity

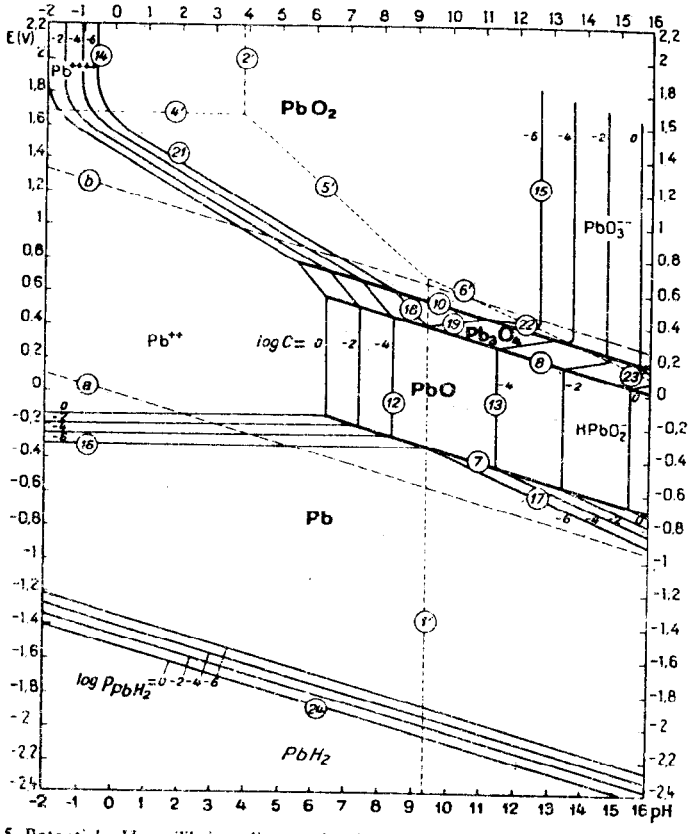

Figure 5. Potential-pH equilibrium diagram for the system lead-water at 25°C (Pourbaix[7]).

sum of 10^{-7} (Ruetschi and Angstadt[18]). The significance of such thermodynamic equilibria is their contribution to the knowledge of possible situations. Without a thorough understanding of the ways they are established in the electrode system, they could not help much.

Example 6: Lead–Acid Battery. The reaction patterns may be considered as a part of electrode thermodynamics if a cell in its equilibrium state is considered. The reactions in a lead–acid battery are the following:

$$\text{Anode:} \quad Pb + HSO_4^- \underset{\text{charge}}{\overset{\text{discharge}}{\rightleftharpoons}} PbSO_4 + H^+ + 2e^- \qquad (22)$$

$$\text{Cathode:} \quad PbO_2 + 3H^+ + HSO_4^- + 2e \rightleftharpoons PbSO_4 + 2H_2O \qquad (23)$$

$$\text{Overall:} \quad Pb + PbO_2 + 2H^+ + 2HSO_4^- \rightleftharpoons 2PbSO_4 + 2H_2O \qquad (24)$$

The half reactions are based on the electrolyte dissociation into H^+ and HSO_4^- ions, which is closer to reality than the complete dissociation. The anodic reaction has an $E°$ of 0.303 V and the cathodic reaction an $E°$ of −1.267 V. The total reaction $\Delta G°$ is −372 kJ/mol and the corresponding potential is 1.93 V. In 35% H_2SO_4 (specific gravity 1.265) the cell potential is 2.1 V.

Figure 7 shows the reaction pattern of the anode (a and b).

Figure 8 shows the reaction pattern of the cathode (a and b). Both patterns include a solid state reaction (a) and a reaction including an ionic species (b) (Berndt[19]).

So far, only cell potentials have been discussed. Once a load is applied to a cell, kinetics becomes the other important factor. The highest voltage is of no use without a current flow.

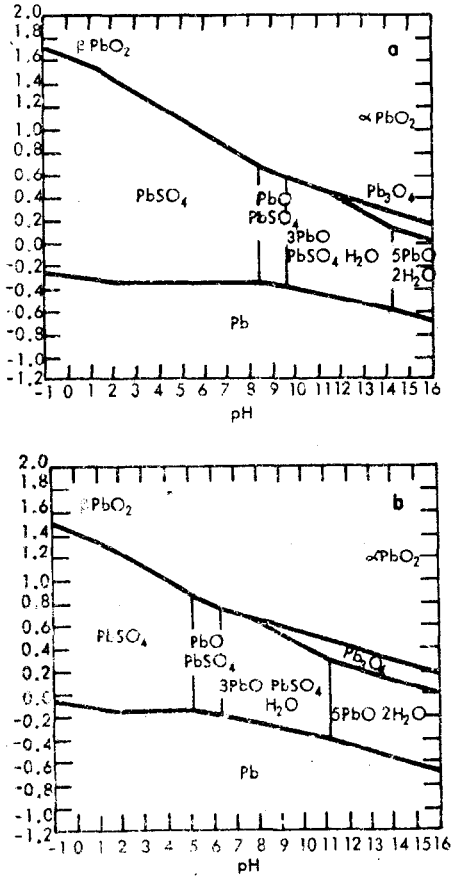

Figure 6. (a) Potential-pH diagram of the system $Pb-H_2O-H_2SO_4$ for $(a_{SO_4^{2-}} + a_{HSO_4^-}) = 1$. (b) Potential-pH diagram of the system $Pb-H_2O-H_2SO_4$ for $(a_{SO_4^{2-}} + a_{HSO_4^-}) = 10^{-7}$ (corresponding to complete acid exhaustion in the pores of the plate).

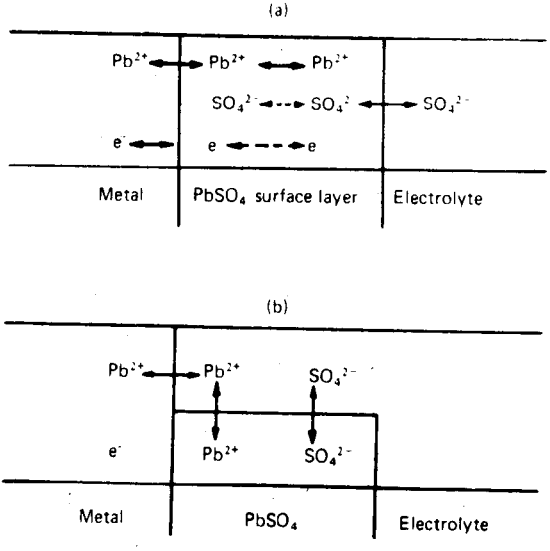

Figure 7. Schematic reaction pattern of the Pb–$PbSO_4$ electrode. (a) Solid state reaction, (b) reaction with solved Pb^{2+} ions.

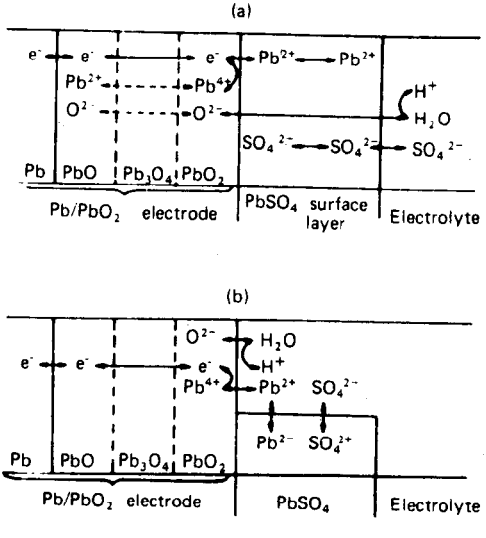

Figure 8. Schematic reaction pattern of the $PbSO_4$–PbO_2 electrode. (a) Solid state reaction, (b) reaction with solved Pb^{2+} ions.

2.2. The Current–Potential Relation

In 1905 J. Tafel discovered the relationship between the current an electrode produces and the difference between the potential under load and no-load condition. The relation is simply

$$\eta = a + b \log i \tag{25}$$

where a and b are constants. In a semilogarithmic plot the relationship is represented by a straight line. The importance lies in the fact that this equation tells us how much one must change the potential to get a certain current density. The name for this potential difference is *overpotential* (η). One can consider two types of electrode reactions, in one case the electrochemical cell is driven by an outside source of potential. As an example we can split water into hydrogen and oxygen by an outside power source: such a cell is a substance producer. In a similar way we can plate a metal on a conductive support. The opposite process occurs in a fuel cell when hydrogen and oxygen interchange electrons with their electrodes and spontaneously produce water. This is called a self-driving system, or an energy producer. To be correct, both types are substance producers, only that the self-driving type has the advantage of producing energy too.

It is now obvious that the term *overpotential* can be applied in both directions, depending on the sign we move away from the equilibrium condition (at which no current is flowing), and electrodes may be "charged" or "discharged." To speak in more defined terms: if the overpotential is negative, then there is a net emission of electrons to the solution (de-electronation) and if the overpotential is positive, then the electrode accepts electrons from the solution (electronation).

The Tafel equation, Eq. (25), can also be written in a different form:

$$i = A \exp(B\eta/RT) \tag{26}$$

The significance of this exponential relationship is that small changes in potential can cause tremendous changes in the current, which is the expression of the electrochemical reaction rate. Such potential changes can be done deliberately by changing the applied voltage.

The explanation for that sensitive behavior lies in the structure of the double layer (Bockris and Reddy[4]; Bockris and Drazic[20]). It can be shown that 10^{-6} mol of electrons per m^2 can change the reaction rate by a factor of 10^5. Double layer capacities are in the order of 0.1 F/m^2 and electrochemical field strengths are in the order of 10^9 V/m. This is very unique for electrochemical double layers because the distance is one or two water molecules and no dielectricum which could break down is there.

The Tafel equation is actually a special case (for large η) of the Butler–Volmer equation:

$$i = i_0\{\exp[(1-\beta)F\eta/RT] - \exp(-\beta F\eta/RT)\} \tag{27}$$

which has been derived from basic assumptions about a simultaneous existence of anodic and cathodic current densities which at the equilibrium potential produce the *exchange current density*. The latter is a characteristic value for each individual electrode system ($\eta = 0$ provides i_0).

Figure 9 shows the overpotential–current density diagram for an electrode reaction. The full line is the net current density curve which is anodic if η is positive.

The special case of the Butler–Volmer equation for very small values of the overpotential (<5 mV) is represented by the linear relation

$$\eta = (RT/i_0F)i \tag{28}$$

Since RT and F are constants, the exchange current density i_0 determines the slope of the line, a way of determining that value experimentally.

Figure 10 shows the two cases Tafel relation and linear dependance in two diagrams (a and b).

The third case, $\eta = 0$, represents the Nernst equation applicable to a thermodynamic equilibrium.

The relation of the exchange current density with the electrode material is a factor in electrocatalysis; different metals (Au, Pd, alloys) used for the catalysis of the oxygen reduction show different Tafel slopes.

In corrosion science, the value of i_0 may be presented as the inverse of an "electrode resistance," determining the speed of the corrosion process.

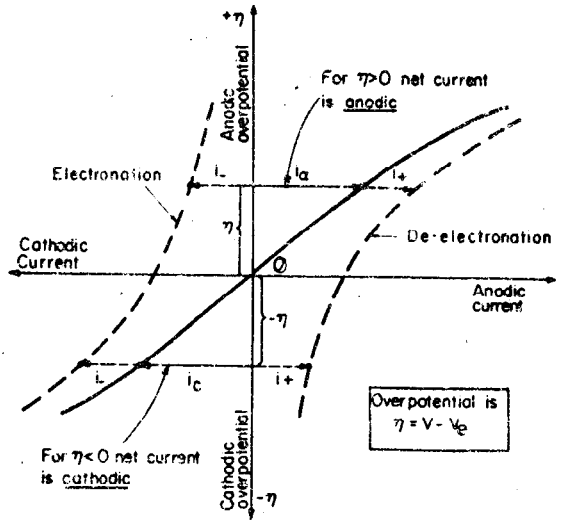

Figure 9. Overpotential-current density diagram for an electrode reaction (Bockris and Drazic, 1972).

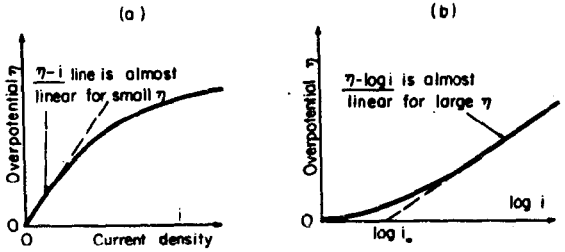

Figure 10. Overpotential as a function of current density. (a) Small, (b) large overpotentials (Bockris and Drazic[20]).

The slope η versus $\log i$ may help in deciding rate-determining steps. Example: hydrogen evolution reaction (30 *or* 120 mV).

2.3. Complete Galvanic Cells

The thermodynamic or equilibrium potential is the highest voltage a "self-driving" cell can have and, inversely the starting voltage a "driven" cell can have. The overvoltages on each electrode are always in the opposite direction; that means they represent always losses (reducing the output of the energy producing cell or reducing the effectiveness of the driving power source in case of cell "charging"). The term *overvoltage* (in technical literature also called cell polarization) is usually understood as a cumulative name for different kinds of voltage losses caused by the electrode reaction; specifically it should be divided into the overvoltage due to the charge transfer at the interface and the overvoltage (polarization) caused by mass transfer processes. The voltage loss which occurs owing to the resistance of the electrolyte and other conductors in the cell as a result of the current flow (*IR* loss) should not be called overvoltage in order to avoid ambiguity.

Figure 11 shows, as an example, the voltage–current diagram of a hydrogen–oxygen fuel cell. The linear characteristic of the *IR*-voltage difference is distinguished from the S-shaped curves of the voltage difference due to overvoltage (polarization) effects. In this particular case the effects are due to diffusion and concentration phenomena. It should be noted that the thermodynamically determined potential of 1.23 V is not reached in the no-load condition. The term *activation overvoltage* has been used in this connection, but considering the discussion of the "true" electrode mechanism as was expressed in Eq. (11), we may just accept the facts and not coin a new name with a different meaning. As a matter of fact, at higher temperatures the difference between the peroxide and oxygen potential gets smaller. In technical cells the varying "open-circuit potentials" are often caused by mixed potentials (impurities).

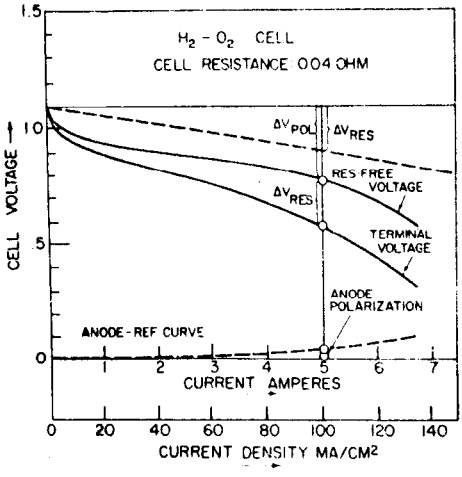

Figure 11. Voltage–current diagram of a H_2–O_2 fuel cell. Anodic and cathodic overvoltage and resistance loss are shown schematically.

O_2 gas electrodes proved to be excellent vehicles to discuss the behavior of mass-transport-limited electrodes (electrode kinetics) and the show cases for electrocatalysts in action (Bockris and Srinivasan,[21] Sandstede,[22] Breiter[23]). We may also use them for Example 1.

Example 1: Gas Diffusion Electrodes. Figure 12 snows graphically how it is possible to separate the *IR*-voltage drop from the other kinds of cell polarization (overvoltages). An alternating current bridge would be able to determine the ohmic resistance components in the cell, under load or no load condition. An oscilloscopic measurement during an on- or off-switching of the load could also give the information, based on the principle that the voltage change due to a current interruption or due to the closing of the circuit is "instantaneous," at least compared with the speed of mass transport processes; capacitance effects need special consideration. In a simple manner, a halfway rectified alternating current can supply the pulses, and the voltage measurements made between the current-on periods would be free of the ohmic resistance voltage drop (or gain, on charge). Such instrumentation was developed for the study of technical batteries (Kordesch and Marko[24]). As can be seen from Figure 12 the "slow" and "fast" electrode processes can be separated to the benefit of the cell designer who wants to optimize their relative magnitude. The remaining characteristic voltage differences caused by the production of electrical energy can be either calculated or determined by different measurements.

The electrolyte concentration effect, partly ohmic, partly appearing as a pH change in the adjacent pore structure of the electrode, can be determined by water vapor pressure (relative humidity) measurements behind the electrodes.

The gas diffusion pressure drop is accessible from independent determinations of the porosity and tortuosity of the electrode body. The Fick equation can be used with good accuracy with pure gases; with gases containing inerts the counterdiffusion of the other species must be considered, so that the limiting current density for the mass transport of oxygen becomes a logarithmic function of the mole fraction of the nonreactive components (Eisenberg[25]). A detailed discussion of the effects of hydrodynamics and mass transfer on the rate processes of electrochemical cells has been published as early as 1947 by Levich,[26] later by Tobias *et al.*[27] and Ibl.[28] The use of limiting-current experiments for the determination of electrode characteristics from the mass transport point of view (electrolyte and gas supply to the reaction zone) proved to be valuable for the development of high-current-density fuel cell electrodes (Kordesch[29]).

In Figure 12 there is also a voltage difference (polarization) ascribed to the Tafel equation. In the case of the oxygen electrode operating as peroxide-producing generator, the catalyst has the purpose to remove this reaction product as fast as possible. The catalytic actions of carbon, silver, spinels, and platinum are different, resulting in different exchange currents and Tafel slopes (Kordesch[30]).

In large battery systems considerations for static electrolytes must be replaced by a description of the behavior of the boundary layer under forced convection, even turbulence. Thermal gradients also cause some stirring. The limiting current is firstly proportional to the bulk concentration, but secondly

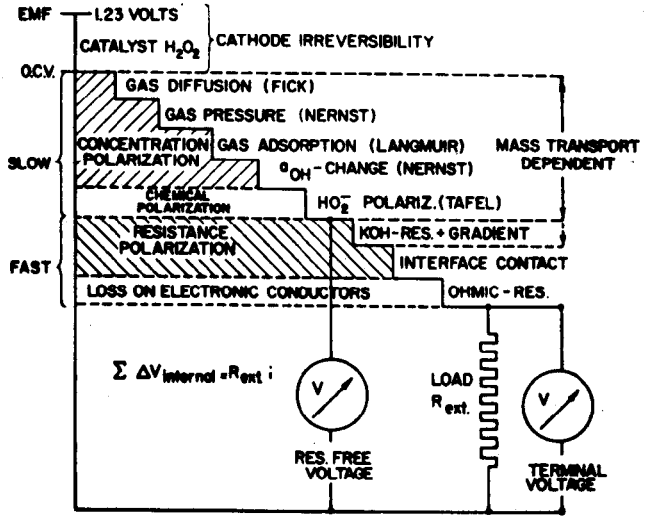

Figure 12. Schematic diagram, picturing the various types of overvoltages in a cell under load.

inverse proportional to the diffusion layer thickness: Fick's first law applies also here:

$$i_{\text{lim}} = nFDc_{\text{bulk}}/d_{\text{layer}} \tag{29}$$

This equation is also very important in charging cells. If the cell is forced by an outside source to pass current faster than the diffusion limits permit the electrodes to produce the charged species, hydrogen will evolve from the aqueous electrolyte. Stirring can change that limit by a magnitude.

Adsorption plays a very important role in the electrochemistry of galvanic cells. The isotherms of Langmuir, Frumkin and Tempkin describe ionic adsorption on electrodes. Bockris, Devanathan, and Müller[31] modified the theory to fit the experimental data better. A primary and secondary water layer and specifically adsorbed anions were introduced into the metal-solution interface to represent the actual situations better. Gas adsorption on large surfaces (active carbon and catalysts like Pt-black) is the first step of interaction for oxygen or hydrogen electrodes under load (see Figure 12). "Electrosorption" of neutral species is important in the electrochemical oxidation of organic "fuels" (Gileadi *et al.*[32]).

The "work function" has been a rather potent physical concept. It was introduced to metal interfaces in electrochemistry recently. A comprehensive literature review was published by Trasatti.[33]

Example 2: Smooth Electrodes, Porous Electrodes. Electrochemical kinetics can be applied to all types of electrode systems; it is just more difficult in practical batteries to analyze the problems. However, the concept of the exchange current density shall be used to make important estimates.

It may be assumed that in a technical battery an electrode overvoltage of 0.05 V is permitted at a current flow of 1.0 A. If we use the Butler–Volmer relation [Eq. (27)] for a large η the expression becomes

$$\eta = b \log (i/i_0) \tag{30}$$

The slope of this Tafel equation shall be 0.12, therefore i_0 will be about 0.4 A/cm^2. This value is about right for the zinc electrode in a Leclanché cell of the R-20 (D) size. Should an electrode system not exhibit a sufficiently large exchange current density, then the surface area must be increased. This may be applied to the mixture of MnO_2 with carbon to increase the working interface. The use of zinc powder in alkaline cells is necessary for the same reason (in zincate-saturated KOH the zinc passivates easily).

Example 3: Low-Temperature–High Temperature Batteries. As big an influence as surface area has in practically used electrodes (note, that in equilibrium thermodynamics the activity of a solid is unity, regardless of the surface or shape), equally important is the influence of temperature on the rates at which a process goes from state A to state C over the energy "hill" B. In 1887 van't Hoff and later in 1889 Arrhenius pointed out that the logarithm of the

specific rate constant was a linear function of the reciprocal of the absolute temperature. The equation is

$$k = A\, e^{-\Delta G^{\ddagger}/RT} \tag{31}$$

$\Delta G^{\ddagger}$ is the critical energy to get over the energy barrier. It is also called the *activation energy*. Generally it is observed in two classes: large values of 20–100 J/mol and low values of 10–20 J/mol. The large activation energies are typical for processes controlled by reaction kinetics, the others characterize diffusion-controlled processes. In the first case the increase in temperature or a catalyst may help, in the second stirring.

2.4. The Galvanic Cell as Energy Converter

At the present time, electrical energy production on a large scale is done by converting the heat evolved from a chemical reaction (oxidizing a fuel by burning it) into mechanical energy (steam turbine) from which it is again converted into electricity (generating plant). Physically, the evolved heat (enthalpy change of the reaction) causes an increase in the translational energy of gases which are either the reaction products (internal combustion engine) or the working fluids (water, steam). In all cases the conversion act is the collision of the gas molecules with the driven member (piston, turbine wheel) of the mechanical device used. However, not all the translational energy is transferred, the remaining heat is contained in the heat energy of the exhausted gas. A simple derivation of the conversion efficiency is the following.

The translational energy of a mole of gas at the high (source) temperature T_1 is given by $3RT_1/2 = W_{in}$, the energy of the leaving gas is $3RT_2/2$, with T_2 as the sink temperature. The amount converted to useful work is the difference:

$$W_{conv} = \frac{3R(T_1 - T_2)}{2} \tag{32}$$

Dividing this value by W_{in}, we obtain the efficiency of the Carnot cycle, namely,

$$\text{eff}_C = (T_1 - T_2)/T_1 \tag{33}$$

The efficiency can only be unity if T_2 is absolute zero.

The efficiency of a reversibly operating galvanic cell can be expressed by

$$\text{eff}_{rev} = \frac{\Delta G}{\Delta H} = 1 - \frac{T\Delta S}{\Delta H} \tag{34}$$

ΔS may be larger, equal or smaller than zero, depending on the reaction, but in all cases it is small compared to the ΔH, and therefore the efficiency is close to unity. As examples, the efficiency and emf values of some fuel cell reactions are tabulated in Table 2. There is no mistake in the value of 1.24 for the oxidation of carbon to CO; the reaction would take heat from the surroundings, if it could

Table 2
Efficiency Values and emf of Some Fuel Cell Reactions

Reaction	Temperature, °C	Efficiency	emf
$H_2 + \frac{1}{2}O_2 \rightarrow H_2O$ (aq.)	25	0.83	1.23
$H_2 + \frac{1}{2}O_2 \rightarrow H_2O$ (gas)	25	0.94	1.19
$H_2 + \frac{1}{2}O_2 \rightarrow H_2O$ (gas)	700	0.78	1.00
$C + \frac{1}{2}O_2 \rightarrow CO$	25	1.24	0.71
$C + O_2 \rightarrow CO_2$	25	1.00	1.03
	700	1.00	1.03
$CH_4 + 2O_2 \rightarrow CO_2 + 2H_2O$	25	0.92	1.04
	700	0.90	1.04

be made to at 25°C. Heat engines operating at a source temperature of 500°C and an exhaust temperature of 30°C have only a Carnot-efficiency of 0.59 for the ideal engine. Practical values are 0.4 for modern steam power plants, 0.3 for large diesel engines, and 0.2 for Otto motors.

It is important to note that heat engines become more efficient at higher temperatures, while fuel cells usually show the opposite behavior as a result of the Gibbs–Helmholtz equation:

$$\Delta G = \Delta H + T\frac{\partial nFE}{\partial T}p = \text{const} \tag{35}$$

$\partial E^\circ/\partial T$ for the hydrogen–oxygen reaction is $-0.8\,\text{mV/K}$. Of course, the efficiency of galvanic cells is lowered by the electrode overvoltages and the voltage drop across the internal resistance as soon as current is delivered.

The actual thermal efficiency of a cell is obtained by counting all the efficiency factors (even losses like gas escaping from the electrodes through the pore system must be considered) and relating the thermal energy input (heat value of the fuel) to the equivalent of the electric power delivered at the terminals. Practical values are in the 60% range. Fuel cell conversion is therefore far superior to the heat engine.

3. Electrochemical Storage Systems

3.1. Introductory Remarks

A short discussion of terminology is necessary to relieve some existing confusion. An electrochemical arrangement consisting of two electrodes, an electrolyte, and a container or mounting device is called a cell. It may be a laboratory cell in a beaker or a completely sealed industrial product sold to the consumer. If there is more than one cell in series or parallel, the arrangement becomes a battery. With additional hardware (controls, pumps, safety devices)

it is commonly called a system; however, "galvanic system" often just means "cell."

Rechargeable batteries are also named accumulators or secondary batteries. They are distinguished from primary batteries by the feature of electrical rechargeability. Significantly, both accumulators and primary batteries contain all the chemical reactants within the cell boundaries. Contrary to this, fuel cells are chemical converter systems (generators) which have the capability to convert the energy of chemicals stored outside of the cells into electricity. The latter point is very important because the capacities of fuel cell systems are dependent only on the size of their fuel and oxidizer tanks (like the range of a car depends on the size of the gasoline tank).

Rechargeable batteries have a single-cycle capacity, which is the capacity of the charged battery (all chemicals converted to the higher state) delivered once, like a primary battery. Primary cells are usually systems which have irreversible electrode reactions; they are in most cases discarded after use.

Counting all the cycles a battery is capable of giving above a prescribed energy minimum (or service time minimum) leads to a value of cumulative energy, a figure of merit which can also be combined with the cost of the battery to the purchaser.

The word *capacity* is often used. It has in this context nothing to do with electrostatic charges. Ah capacity is the number of Ah which can be delivered per unit weight or volume. It is directly related to the coulombic storage density, which is the maximum amount of electricity which can be produced by a formula weight (mole) or unit weight or volume. The energy density is coulombic storage density (Ah capacity) multiplied by the cell voltage. There are maximum, ideal values if the theoretical numbers are used, and technical values if the real measured data are used. The units Wh/kg or Wh/liter are often given for a commercial unit in consideration of a specified application. The numbers may change for different power densities, expressed in W/kg or W/liter.

In battery technology there are also the quotients capacity/time in frequent use. Their dimension: A. The Ah capacity available from the battery to a certain minimum voltage level depends on the current which is withdrawn; at a high load the battery delivers far less than at a small load; the same is true for different temperatures. The value $C/5$ therefore is the current which discharges a battery completely in 5 hr; $C/0.5$ or $2C$ means discharge (or charge) in one-half of an hour. The significance of these numbers is that they are to a large extent independent of size or weight considerations, but extremely characteristic for the system. A battery for an electric vehicle, for instance, must have a $C/3$ capability (battery output to operate the vehicle for 3 hr at a given speed). A radio battery needs only a $C/100$ discharge rate, a torpedo battery requuires perhaps a $20C$ performance.

To illustrate the problem of varying capacity under different load conditions, the specific energies of several battery systems (all weighing 300 kg) are

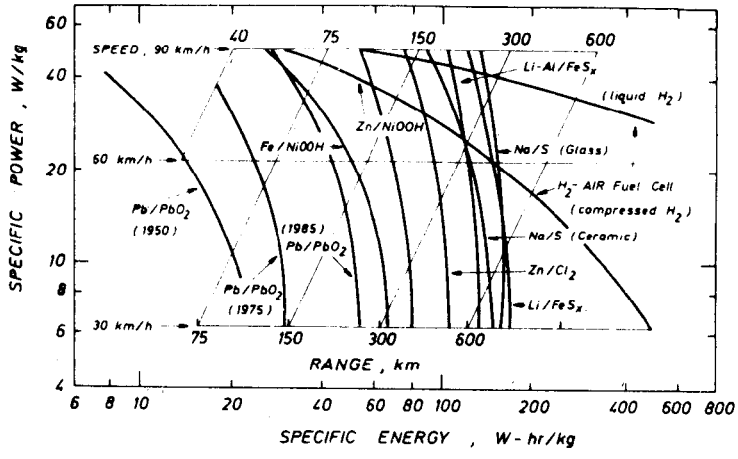

Figure 13. Specific power and specific energy diagram for the lead–acid battery and advanced systems. A grid of the projected ranges of a 1300-kg automobile with a 300-kg battery at different speeds is drawn in.

plotted against their specific power output in Figure 13. An overlayed grid marks the projected range an electric automobile of 1.3-ton weight could travel at certain speeds. The $C/3$ rate is just feasible for 1975-built lead–acid batteries, providing a range of about 120 km at 40 km/hr; it is hoped that in 1985 it may be a $C/2$ rate corresponding to 120 km at 60 km/hr. The diagram also shows the tremendous difference which fuel cell batteries would mean to vehicle propulsion (Kordesch[34]).

As a general rule of thumb it should also be mentioned that technical batteries, manufactured on a large scale, can only be counted on to deliver about one-fourth of the calculated maximum energy of their electrode systems.

3.2. Rechargeable Batteries—Conventional Technology

3.2.1. The Lead–Acid Cell

It took approximately 60 years from the time of Volta's discovery of the galvanic cell in 1800 for its application to Planté's electric storage battery. His cells consisted of lead sheets wound spirally in a cylindrical configuration separated by rubber strips or linen separators. The lead was electrochemically formed into the Pb/PbO_2 couple. Progress continued steadily, first under the influence of the invention of the dynamo for battery charging, and after 1900 industrial growth, together with the use of lead–acid batteries in electric automobiles, established the technology. The utilization for traction and as a starter battery in gasoline-powered cars called for more improvements. Today

Table 3
A Summary of Highlights in Development of the Lead–Acid Battery

1860	Planté reduced the lead–acid system to practice using formed lead sheet plates.
1881	Faure developed the pasted plate structure.
1883	Tudor developed extended area (spun) lead plates.
1880–1890	Grids are first designed into the lead–acid battery; antimonial alloys are first used.
1882	Gladstone and Tribe's double sulfate theory.
1890–1900	Wood separators are used.
1900–1910	Lead dust and leady oxides as raw materials; "iron-clad" plate structure designed (hard rubber and asbestos).
1914–1920	Rubber separators; the role of expanders on capacity was first defined.
1927–1937	Porous ebonite and microporous rubber used as battery separators.
1935	Lead–calcium grid alloys first introduced for applications requiring low rates of self-discharge (float)
1948–1950	Cellulosic and synthetic fiber bonded separators; lower density pastes (active material) introduced usage.
1965	Maintenance-free batteries for portable devices.
Mid-1960s	Lightweight construction, plastic battery cases; high automation of the production and battery assembly processes; high-efficiency (low-IR) designs.
1970s	New applications: water-activated and maintenance-free batteries for automotive use; increased emphasis on traction batteries.

the lead–acid battery industry is a business enterprise with production values in the range of several billions of dollars annually worldwide.

Table 3 summarizes the highlights of the development of the lead–acid battery (Weissman[35]).

The improvement between 1920 and 1960 represents a cutting in half of the weight of lead needed to manufacture a 6-V, 100-Ah battery (from 15 to 7.5 kg) and an increase in the service life from about 20 to 30 months between 1940 and 1960. Over the last 20 years the weight of an automobile battery again decreased by about 25% and the service life rose to 5 years. As far as material utilization is concerned only marginal improvements can be expected in the future, but cycle life under higher current densities and at deep discharge conditions is worth looking at, especially with respect to electric vehicles. Hermetical sealing and overcharge capability are the goals for small lead–acid batteries, partly already achieved, but with serious compromises in capacity.

Figure 14 shows the weight analysis of a typical starter battery (SLI stands for starting, lighting, ignition).

Figure 15 presents a schematic of the discharge process in a lead–acid cell (Bockris and Drazic[20]).

The overall electrochemical reaction can be written as follows:

$$2PbSO_4 + 2H_2O \underset{\text{discharge}}{\overset{\text{charge}}{\rightleftharpoons}} Pb + PbO_2 + 2H_2SO_4 \tag{36}$$

In Figures 7 and 8 of Section 2.1 a more detailed electrode mechanism was pictured.

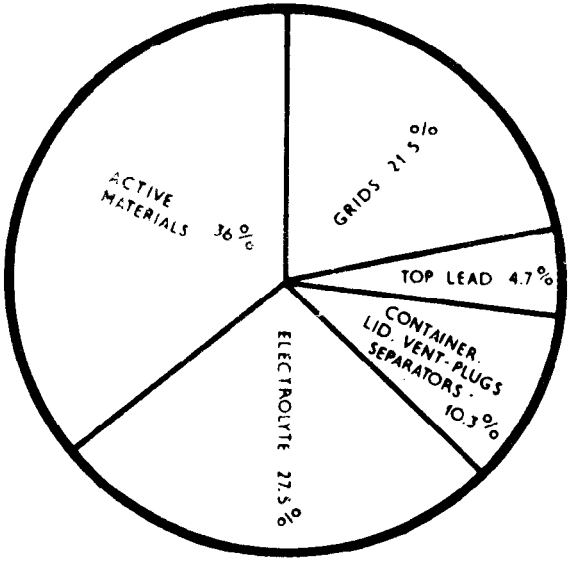

Figure 14. Weight analysis of a typical SLI battery.

Figure 16 shows the current–capacity diagram of a typical 100-Ah SLI battery. It can be seen that the temperature of operation and the discharge rates determine the output of the battery.

In the manufacturing process, a lead oxide paste consisting of PbO and/or Pb_3O_4 mixed with sulfuric acid is pasted onto a grid (usually a Pb–Sb alloy) and charged ("formed") in H_2SO_4. Porous PbO_2 is formed on the positive plate and spongy lead on the negative plate. PbO_2 and Pb are good conductors (4×10^{-3} and 2×10^{-5} Ω cm. respectively.) $PbSO_4$, the discharge product on both sides is an insulator. Sulfuric acid is used up when the cell is discharged and the state of charge can therefore be determined by measuring the specific gravity. "Battery acid," 35% H_2SO_4 has a specific weight of 1.260 at 20°C. The capacity of a lead acid battery with this acid is 120 Ah/liter [Eq. (36)]; the practical values depend on cell construction and discharge rates.

3.2.1.1. What Is "New" in Lead–Acid Technology?

The improvements mentioned before were for those of the most widely used type, the automobile SLI battery. Lightweight containers and through-the-wall connectors made the batteries much lighter. Low maintenance was achieved by changing from antimony grid alloys to calcium alloys; gassing was reduced by this measure and water replenishment became less frequently

necessary. Production of the Ca-alloy grids is more difficult and needed years of development to establish a large-scale manufacturing process.

Big strides were also made in stationary batteries. They are now produced in sizes up to 15,000 Ah and have a service life up to 25 years. In the Bell Telephone System there are an estimated total of over one million cells in the capacity range of 180–1680 Ah in service for dc filtering of rectified ac, instantaneous power reserve for outages (milliseconds to minutes), and extended reserves for periods of 3–48 hr.

In the small-cell groups the biggest advantage was gained by immobilizing the electrolyte and, after even longer development period it was finally possible to seal acidic cells.

Figures 17a and 17b show the construction of a spirally wound D-size cell (Gates Rubber Corp.[36]). The cell has excellent high current capabilities owing

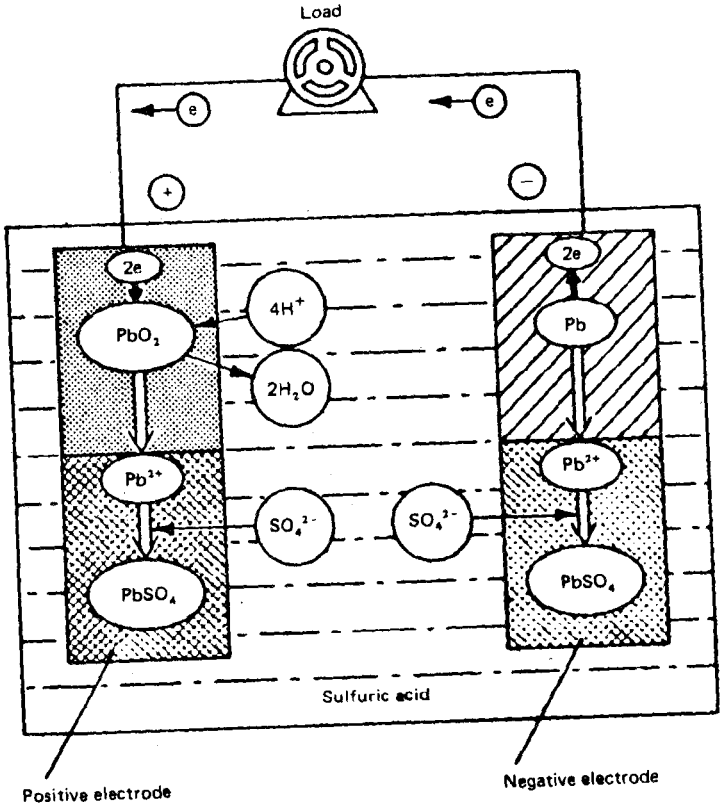

Figure 15. The discharge process in a lead–acid cell.

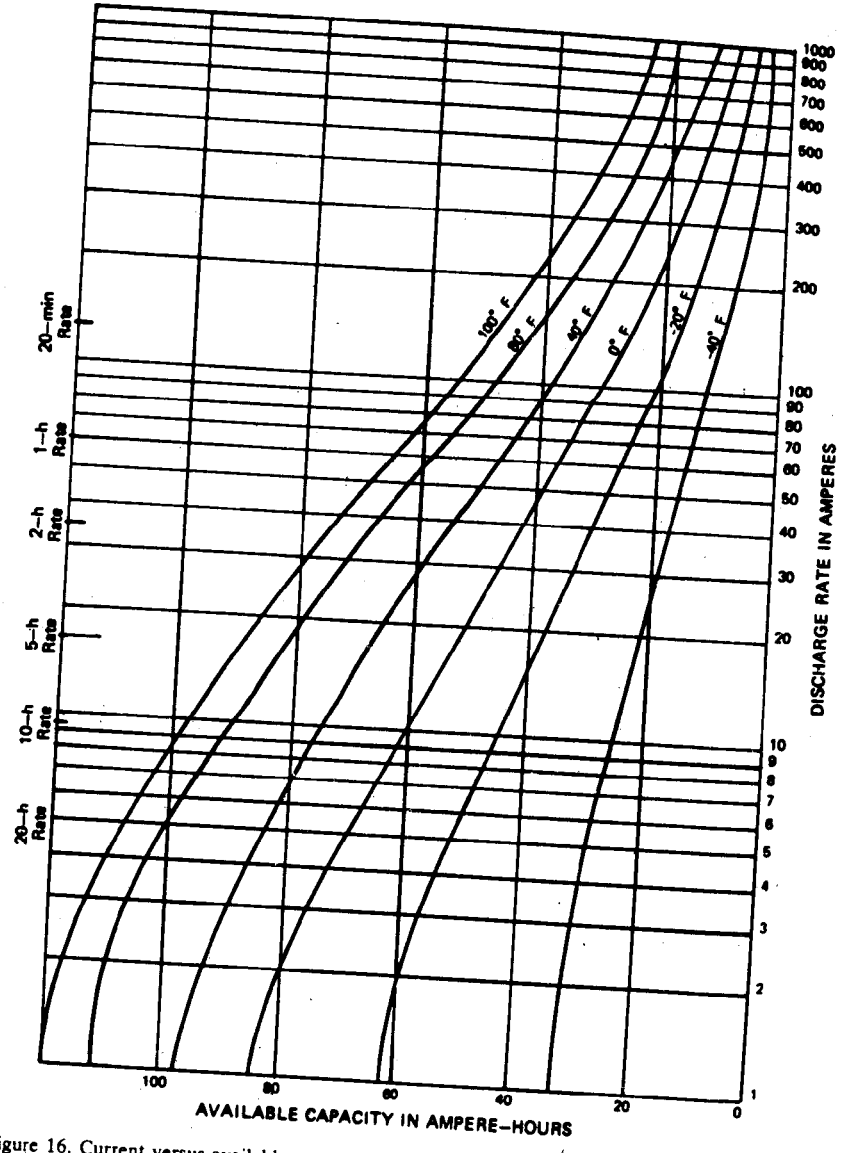

Figure 16. Current versus available capacity at various temperatures for a typical 100-Ah 3LI battery (Weissman[35]).

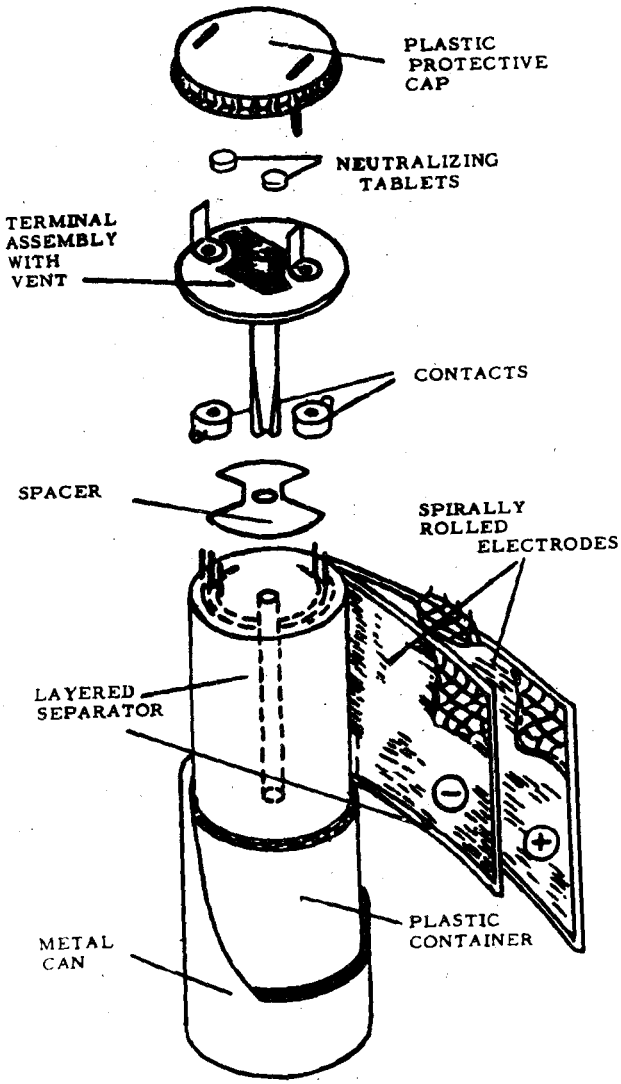

Figure 17a. Construction of a D-size lead–acid cell (Gates Rubber Co., 2.5 Ah at the $C/5$ rate).

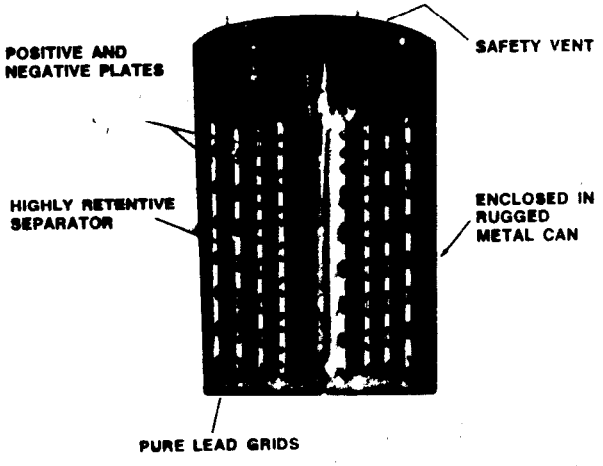

Figure 17b. Cut through an actual D-size lead–acid cell (courtesy of Gates Rubber Co.).

to the large electrode surfaces but only a relatively low active material usage (20–30%) because of electrolyte limitation, on purpose, to make the cell capable of being overcharged and deep discharged.

The use of the oxygen recombination cycle, with a "starved electrolyte condition," was not as easy as with Ni-oxide–cadmium cells because the gas recombination rates are far smaller between oxygen gas and lead: it involves an ionic cycle.

The cycle life of SLI batteries—if deep discharged—is in the 100–500 range. (The shallow cycles of the vehicle applications with a generator providing immediate recharge go into the 100,000 range.) The cycle life of an industrial or traction battery is between 1500 and 5000.

3.2.1.2. Why Do Lead–Acid Batteries Fail?

Figure 18 shows the failure modes of batteries removed from service in the years 1962 versus 1970 (Battery Council International—BCI[37]).

3.2.1.3. Future Improvements

Near-future improvements are just a continuation of already existing trends in battery technology:

1. Lower specific current densities by making plates thinner and increasing their number.
2. Lower cell resistance: better grid designs, intercell connectors, bipolar plates, closer electrode spacing.

3. Construction changes: lightweight grids (Al, C?), plastic containers, redesign of terminals.
4. Better electrolyte utilization: optimal plate porosity, circulation of electrolyte, temperature control.
5. Better charge and discharge efficiency by modifications of plate composition, new alloys, special additives.
6. Increase of cycle life through better plate support, lower electrolyte concentration, higher plate porosity.

Of course, some of these points conflict with each other; optimization is therefore required.

Information about manufacturing details is not always freely published; many processes are considered proprietary. Fortunately this has changed. The by now classical book of Vinal[38] has now been followed by modern treatises about lead–acid batteries (Bode,[39] Weissman,[35] Collins[40]).

The lead–acid battery was and still is the "workhorse" of the electrochemical rechargeable storage systems. Its economy is not surpassed by any other system yet.

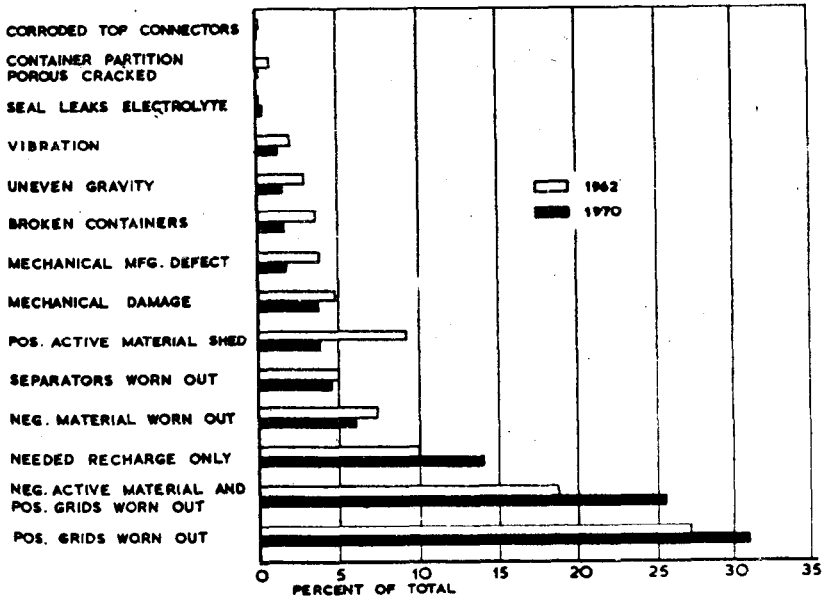

Figure 18. Failure modes of batteries removed from service (BCI, 1970).

Table 4
The Energy Densities, Power Densities, and Cycle Life of Rechargeable Batteries (Existing Technology)

Battery	Energy density, Wh/kg	Power density, W/kg	Cycle life, cycles
Lead–acid	20–35	20–175	300–2000
Nickel–iron	20–25	65–90	2000–5000
Nickel–cadmium	25–45	200–600	2000–5000
Silver–zinc	50–175	200–400	100–200
Nickel–zinc	60–70	100–200	200–300

However there are systems with a higher energy density, power density, and cycle life, but they cost more.

Table 4 compares other commercial storage battery systems with the lead–acid battery. In the following sections the four alkaline storage battery types mentioned in Table 4 will be discussed briefly. Extensive literature is available (Falk and Salkind[41]).

3.2.2. The Nickel–Iron Battery

Nickel–iron batteries were first introduced by Edison in 1900 and, after some correction of initial deficiencies this battery system has been manufactured almost without any changes until today.

The normal reaction in a well-cycled battery can be described as:

$$2NiOOH + Fe + H_2O \underset{\text{charge}}{\overset{\text{discharge}}{\rightleftharpoons}} 2Ni(OH)_2 + Fe(OH)_2 \qquad (37)$$

The negative active material is prepared from pure iron and consists of a fine powder with a high surface area. It forms a stable oxide Fe_3O_4 mixed with α-iron and is further mixed with nickel flakes to give it more conductivity.

The positive active material is similar to that used in nickel–cadmium batteries. The electrolyte is usually a mixture of potassium and lithium hydroxide. LiOH helps to maintain the capacity.

Nickel–iron batteries have an excellent cycle life and the system was preferentially used in mining locomotive–traction applications. Today it may find a new field of application in electric vehicles for over the road use (Salamon and Krämer[42]). In this recent development a special sintered iron electrode is used, which shows a low gassing characteristic and a charge behavior which makes the iron electrode better compatible with a nickel oxide cathode.

3.2.3. The Nickel–Cadmium Battery

The reaction mechanism in Ni–Cd cells has been studied extensively with respect to sintered-type electrodes; however, the mechanism applies to pocket cells as well:

$$2NiOOH + Cd + 2H_2O \underset{\text{charge}}{\overset{\text{discharge}}{\rightleftharpoons}} 2Ni(OH)_2 + Cd(OH)_2 \qquad (38)$$

An unknown in this equation is the exact amount of adsorbed water at the nickel electrode.

The positive electrodes are prepared by impregnation and conversion techniques from nickel salts. The material for the negative electrode is usually coprecipitated with iron and nickel to maintain the finely divided state of the Cd. The pocket electrodes were developed by Jungner as early as 1896; later, Edison decided to use tubular electrodes for positive plates and flat plates for negative plates. While Ni–Cd batteries (the "open" type) are sometimes used for traction purposes because of their long-life properties, they are generally too expensive for large-scale applications. The hermetically sealed Ni–Cd batteries are widely used in small portable devices (tape recorders, radios) where their feature of being overchargeable makes them suitable for rather uncritical customer use. Figures 19a and 19b present the schematic of the Ni–Cd mechanism on overcharge and deep discharge.

3.2.4. The Silver–Zinc Cell

This system is also manufactured in the "open" and sealed version. The most valued property is the high energy density, which is 3–6 times that of the first three systems in Table 4. The disadvantage is the poor cycle life of the zinc electrode and the high cost of the silver electrode. The discharge curve shows two steps, corresponding to the two types of silver oxides available. The discharge mechanism is heterogeneous in nature [Eq. (17)]. The reactions are

$$Ag_2O_2 + H_2O + 2e^- \rightarrow Ag_2O + 2OH^- \qquad (39)$$

$$Ag_2O + H_2O + 2e^- \rightarrow 2Ag + 2OH^- \qquad (40)$$

A special system, taking its place between the Ni–Cd and the Ag–Zn system, is the silver–cadmium battery. It combines their advantages, but has the disadvantage of a low voltage.

3.2.5. The Nickel–Zinc Cell

The Ni–Zn cell is a relatively new development. With an open-circuit potential of 1.7 V and a theoretical energy density of 375 Wh/kg and a currently achieved energy density of 60–70 Wh/kg, about 300 cycles are

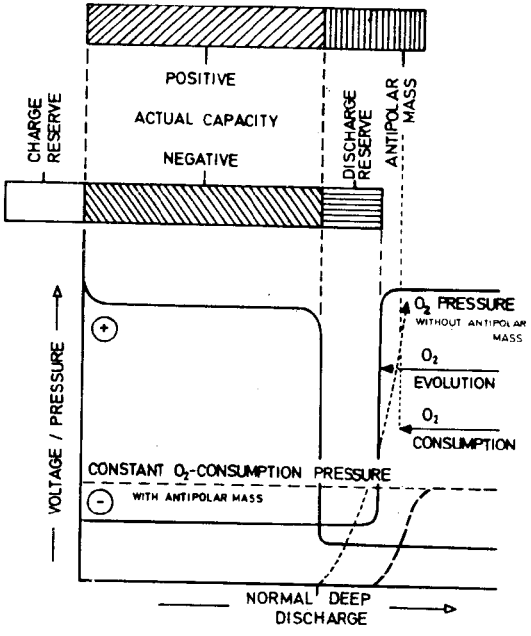

Figure 19a. Characteristics of a hermetically sealed Ni–Cd cell on normal discharge and deep discharge.

obtainable. The cycle life is limited by the zinc electrode, which has a tendency to produce zinc dendrites which short the cell. The overall reaction is

$$2NiOOH + Zn + 2H_2O \underset{\text{charge}}{\overset{\text{discharge}}{\rightleftharpoons}} 2Ni(OH)_2 + Zn(OH)_2 \qquad (41)$$

Batteries have been developed for vehicle propulsion and represent the next generation in efforts to increase the range of electric cars twofold (Schwartz[43]). A battery with a similar cycle life but featuring far less expensive components is the rechargeable alkaline MnO_2–Zn cell (Kordesch[12]).

3.3. Rechargeable Batteries—Future Systems

Table 5 lists several battery systems which are being considered as future electrochemical storage devices surpassing the present conventional batteries by a factor of 3–5.

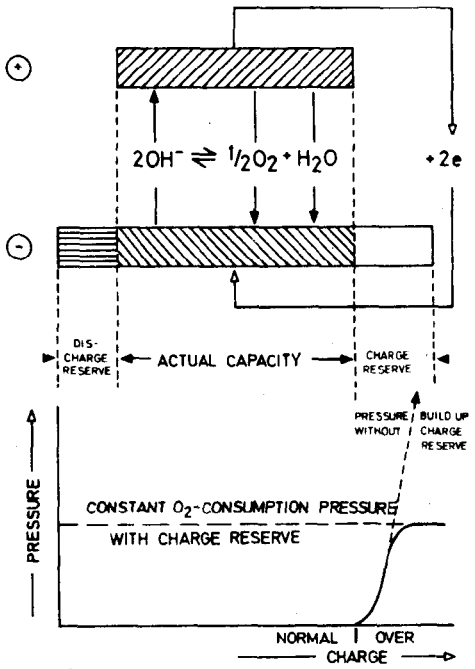

Figure 19b. Characteristics of a hermetically sealed Ni–Cd cell on overcharge.

3.3.1. Metal–Air Systems

Among high-energy batteries the zinc–air battery has been the subject of particular attention. The advantages of zinc are reactivity, low cost, and a reasonable rechargeability. The theoretical value for the specific energy content is 1050 Wh/kg. Primary air–zinc cells are "old" technology; such applications as signal lights and navigational aids are widely found. During the last 15 years (with the improvement of air electrodes for fuel cells) high-current air electrodes have emerged. Rechargeability became possible through special electrode structures which were not damaged by the oxygen evolved during charging (Elbert[44]). Also, circulating electrolyte systems avoided problems with the zinc deposition (Caprioglio and Porter[45]).

Figure 20 shows the principal processes during air–zinc cell discharging and charging. The problem of CO_2 removal from the air is a serious restriction for alkaline air cells; if not done, the pores system plugs prematurely and the current drops. *Zinc–oxygen* cells (closed system) do not suffer from that problem.

Instead of zinc, cadmium was tried, with some success, but the low voltage of that system prohibited its effective use. The combination of air electrodes

Table 5
Future Batteries for Energy Storage

System	Projected performance		Problem areas
	Wh/kg	W/kg	
Conventional type			
Nickel–iron	44	110	Weight
Nickel–zinc	66	220	Cost, life
Metal–gas			
Iron–air	88	66	Life
Zinc–air	88	66	Life, complexity
Nickel–hydrogen	66	110	Volume
Zinc–oxygen	110	110	Life, cost
Cadmium–oxygen	66	66	Life, cost
Alkali metal–high temperature			
Sodium–sulfur (β-alumina)	176	220	Life of separator
Sodium–sulfur (glass)	176	220	Glass stability
Lithium alloy–metal sulfide	165	220	Corrosion, materials
Lithium–chlorine	110	220	Cycle life
Other systems			
Zinc–bromine	66	110	Life
Zinc–chlorine hydrate	165	110	Accessories, life
Fuel cells (Air–H_2)	Tank limited	110	Catalyst cost, H_2 supply
(O_2–H_2)	Tank limited	220	Cost, H_2 and O_2 supply

with iron rechargeable electrodes has gained some more attention recently, with the development of better iron electrodes (Cnobloch *et al.*[46]). *Aluminum–air* cells have been studied extensively because the low equivalent weight of Al ($3e^-$) gives that system an advantage over any other room temperature aqueous system. Energy storage systems up to two kW have been built, but the rechargeability is not satisfactory, the reaction products must be removed mechanically. Aluminum corrosion problems are also high (hydrogen

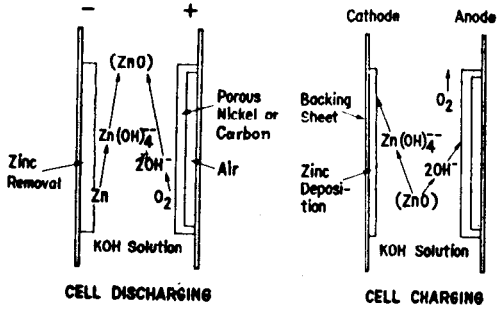

Figure 20. Air–zinc cell discharge and charge process.

evolution). Theoretically at least the Al–air (O_2) battery is still a promising project for future developments (Zaromb,[47] Despic *et al.*,[48] Ruch[49]). *Sodium–air* and *lithium–air* systems using the alkali metal–water electrode are powerful systems recently developed by Lockheed (Halberstadt,[50] Littauer[51]).

3.3.2. Metal-Oxide–Hydrogen Systems

These sealed cells have been developed for comunication requirements (COMSAT) because the cycle life of the combinations nickel oxide–hydrogen or silver oxide–hydrogen turned out to surpass that of any other system. Solar cell charging in relatively short intervals (90 min) takes advantage of the high cycle life and is not limited by the comparatively high self-discharge rates of these systems (Dunlop *et al.*[52]). Low-cost commercial systems (D-size cells) seem possible (Kordesch and Cieszewski.[53]

Table 6 presents a comparison between different metal oxide–gas systems. The top combination, hydrogen and oxygen, has the highest energy density, in principle, but actual realization of this value has not been successful in spite of many attempts. Cross-leakage of the two gasses is the main problem.

Figure 21 shows the construction of a nickel oxide–hydrogen battery.

3.3.3. Alkali-Metal–High-Temperature Cells

The Sodium–Sulfur System

The Ford Motor Co. has been carrying out research on sodium–sulfur cells since 1966 with the objective of developing an electric vehicle battery. The

Table 6
Metal (Oxide)–Gas Systems[a]

System	Theoretical		Actual		
	Voltage, E	Energy density, Wh/kg	Voltage, V	Energy density, Wh/kg	Number of cycles achieved
Hydrogen–oxygen	1.229	3652	0.88	44–110	200
Zinc–oxygen	1.645	1078	1.30	110–220	200
Cadmium–oxygen	1.210	506	0.85	55–95	500
Nickel oxide–H_2	1.358	389	1.25	55–93	2000
Silver oxide–H_2	1.398	523	1.10	60–132	600

[a] Note: These systems use compressed hydrogen or oxygen in a sealed system. Metal hydride storage gives better volume efficiency (Earl and Dunlop[54]).

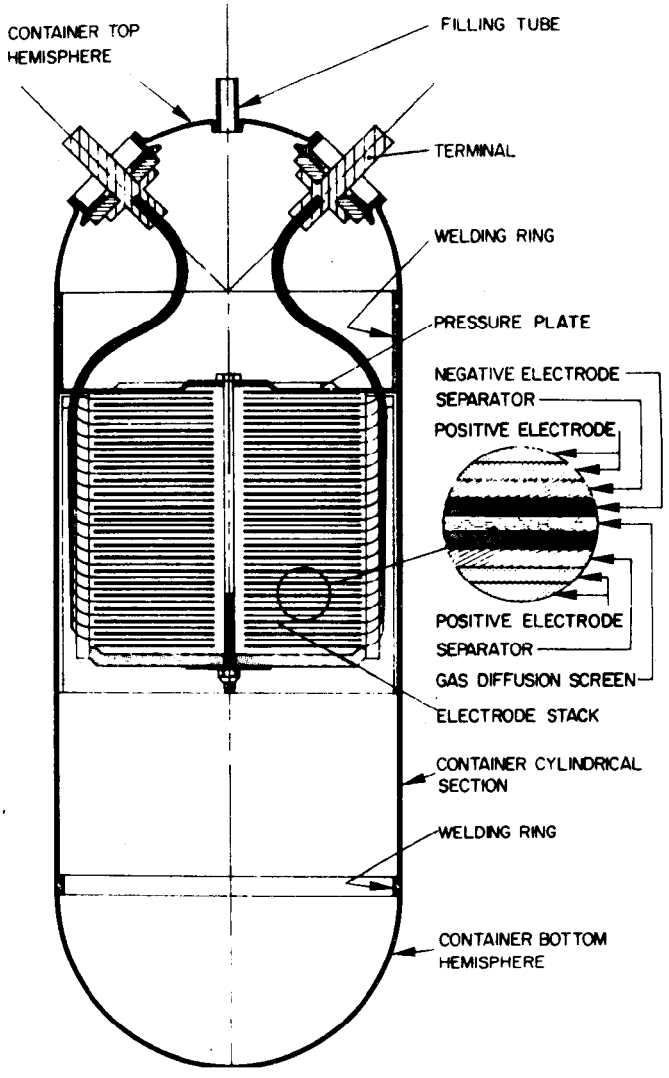

Figure 21. Nickel oxide–hydrogen cell construction (COMSAT).

principle is to separate the molten reactants, sodium and sulfur by a sodium-ion-conducting membrane of β-alumina. Graphite felt makes the sulfur conductive. The reaction products are polysulfides. Means of minimizing cracking and increasing the life of the ceramic membrane were found after years of development. In a somewhat modified form, this battery system is

considered to be suitable for large-scale energy storage. The main points are the low cost of the reactants and the high power density of the sodium–sulfur battery, operating at 350°C.

The goal for energy density was stated at 80 Wh/kg and the power density as 280 W/kg (Weiner[155]).

Figure 22 shows the schematic of a Na–S power cell. A different approach was taken by the Dow Chemical Co. They developed a sodium-ion-conducting glass in the form of hollow fibers as the separator between sodium and sulfur. A large sodium sulfur battery program was supported by British Rail and the batteries were tested in a Bedford van to prove road worthiness.

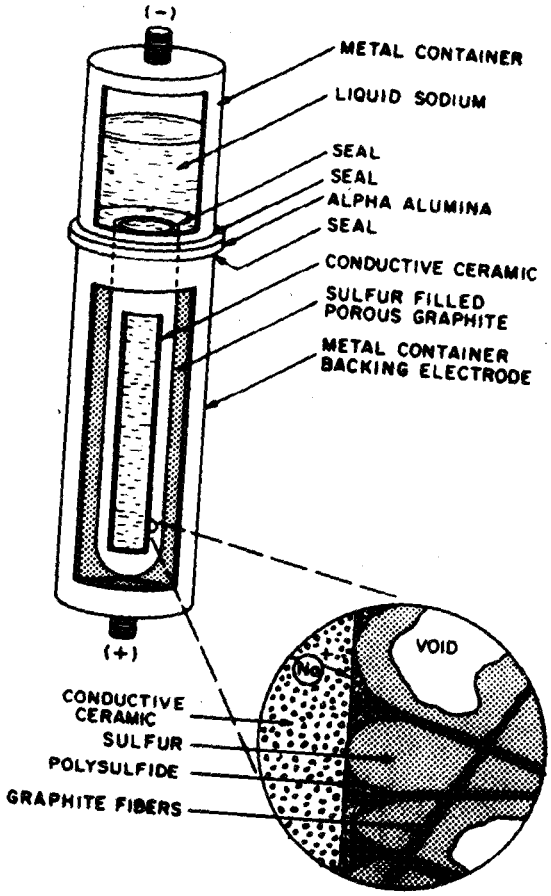

Figure 22. Construction of a sodium–sulfur cell (Ford Motor Co.).

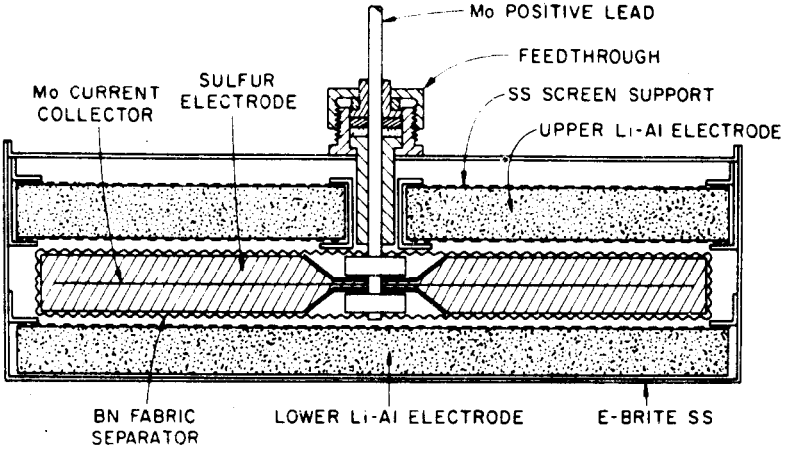

Figure 23. LiAl–sulfur cell construction (Argonne Natl. Laboratory).

High-temperature lithium systems development started in 1962, and by 1968 most systems had changed to lithium-alloy–metal-sulfide systems for safety and easier operation. The electrolytes were LiCl–KCl eutectica. A survey of the advanced battery status at that time has been given by Yao and Birk[56]; Figure 23 shows such a cell.

Summarizing the best data on LiSi–FeS_2 cells, it was was stated that 1000 cycles at a depth of discharge of 80% and an energy density of 180 Wh/kg were demonstrated in 1977, a big improvement over the previous 300 cycles.

3.3.4. The Zinc–Chlorine Hydrate System

Zinc can be plated out of zinc chloride solutions and a rechargeable system using a nonalkaline electrolyte is considered to be a big step forward. Air electrodes perform very poorly in neutral electrolytes; therefore chlorine was chosen as a substitute. Chlorine hydrate, $Cl_2 \cdot 6H_2O$, which can be prepared by bubbling chlorine gas into water under cooling, is a useable chlorine storage. The energy density is theoretically very high: 830 Wh/kg. A prototype system was used to propell a Vega automobile with a 200-V, 100-A power plant. This system is also under serious consideration as a large utility energy storage system (Birk[57]).

The *zinc–bromine* system has a theoretical energy density of 430 Wh/kg. The bromine reacts on carbon or titanium electrodes.

3.4. Primary Batteries

The available primary battery systems will not play any major role in a large-scale electrochemical storage scenario, but the place of these batteries on the industrial manufacturing scene is quite important. As examples, the yearly production of primary manganese dioxide cells in 1970 was valued at about 260 million dollars in the U.S.A. alone. The value of lead–acid starter batteries was 475 million dollars in the same year. Also, small batteries made a tremendous leap forward in volume production and value, mainly owing to the progress of the electronic and solid state industry. The alkaline manganese dioxide primary battery, for instance, had a growth rate of 15% annually; the nonaqueous batteries, which practically did not exist in 1970, are now entering the market. The lead–acid battery production grew slower, essentially with the pace of the automobile industry, as far as the SLI battery was concerned. Industrial and "golf cart" batteries increased very much in numbers. However, the numbers alone do not tell the whole story: lead–acid batteries are on the lowest level of the profit margin (only the large-scale production methods are assuring some return on investment), while the primary batteries are in a far better position, therefore capable of putting more funds into new research and development.

With the energy crisis, large storage battery installations with improved batteries are needed. This may be the chance for new systems to get developed. Of course, these will be rechargeable systems, but it has happened already that some primary batteries have become secondary systems. The air cells, silver cells, and sodium cells are examples. The alkaline MnO_2–Zn battery is also a candidate to become a good rechargeable system. In the nonaqueous area, rechargeability could revolutionize the battery industry; because of the very high energy densities compared to the aqueous systems (mainly the voltage makes the difference: 3–4 V versus 1–2 V per cell), multiple cell systems become simpler.

The future aspects of electric vehicles are also strongly tied in with the battery industry's capability to produce the new systems which research is now suggesting. Also, the underdeveloped nations have a staggering need for batteries!

Table 7 shows a primary cell comparison with respect to shelf life, low-temperature performance, and energy density per kg and per dm^3 (liter).

Extensive literature about primary batteries can be found in Heise and Cahoon,[58] Huber,[14] Kordesch,[12] and Brodd *et al.*[59]

Research and development efforts to increase the capacity and life of primary cells is going on in four major directions:

Air Cells. The use of air as an oxidizing agent allows the designer a maximum space for the anode, for instance a powered zinc electrode in an alkaline electrolyte. Such cells were known before World War I and resulted in

Table 7
Primary Cell System Comparison

Characteristic	Cell types				
	Leclanché	MnO_2–Zn alkaline	HgO–Zn	MnO_2–Mg	Li–SO_2
Shelf life[a]					
Storage temperature					
20°C	1–2 Yrs.	2–3 Yrs.	3–4 Yrs.	5–7 Yrs.	10 Yrs
50°C	1 Mo.	2 Mos.	4 Mos.	7 Mos.	12 Mos.
Wh/kg[b] at 20°C	43	57	88	80	200
Wh/dm^3 at 20°C	100	140	270	200	400
Low-temperature capacity (percent of 20°C)					
0°C	15%	35%	5%	70%	100%
−6°C	5%	15%	0%	58%	96%
−30°C	0%	3%	0%	23%	85%
−40°C	0%	0%	0%	0%	60%

[a] Time in years or months that a cell will provide a minimum of 75% of its initial capacity at room temperature.
[b] The energy density figures vary considerably with load. The values given above are for low current densities; at high current densities the Leclanché and HgO system are poor performers, which is also expressed in the low-temperature data.

large cells for signal service. Only recently has this system been applied to miniature cells. The reason is clear (in hindsight): as long as larger currents were demanded from air cells, the air access had to be good. This meant drying out, carbonating the electrolyte, or wetting up at high air humidity, all cell-destroying processes. Cells for calculators or electric watches need only very small currents, therefore the air access can be very much restricted and the problems were largely eliminated (Biddick *et al.*[60]).

Figure 24 shows the construction of a miniature hearing aid cell as it was produced about 10 years ago, with a limited market success, because the currents needed were too high for the air-restricted cathodes (Brodd *et al.*[59]).

Cells with Organic Electrolytes. These systems were also investigated extensively a decade or two ago (Morehouse[61]). Currently they have achieved attention again because their energy density is very high. In this case the voltage is relatively low, but the organic molecules provide may electrons per equivalent reaction. Figure 25 shows the discharge curves of several organic cathodes. Some of the rechargeable organic materials, like chloranil, may be used in secondary cells if a high voltage anode can be designed. The potential is just under that of an air electrode, therefore an internal "hybrid" can be designed, with the air electrode recharging the organic material during idle times (Sandstede[62]).

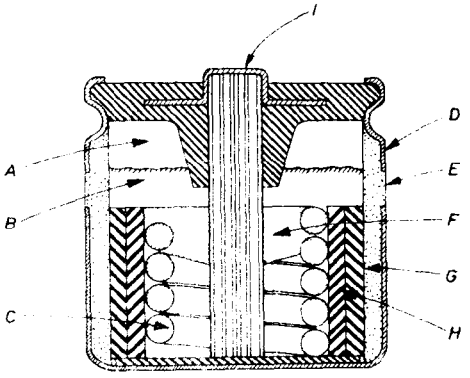

Figure 24. Cut through an alkaline air-zinc cell (Eveready 1002 E). A, Expansion space; B, electrolyte paste; C, zinc spiral; D, steel can; E, air opening; F, zinc powder; G, carbon electrode (+); H, separator; I, brass collector cap (−).

Nonaqueous Lithium Batteries. These are the newest types of primary batteries, with some of the systems showing promise of rechargeability. There are two groups: with organic electrolytes and with inorganic electrolytes. The first group needs a cathode (e.g., CuO) and an anode (e.g., Li). The second group needs the anode (Li) but only an inert conductor (carbon) as the current collector on the positive side: the electrolyte itself is oxidizing. One example is SO_2 dissolved in an inorganic salt solution (KBr in an organic solvent), another is the use of $SOCl_2$ mixed with $LiAlCl_4$ as a "liquid cathode." Capacity: 0.8 Wh/cm^3 (Dey[63]). While these latter systems are in the development

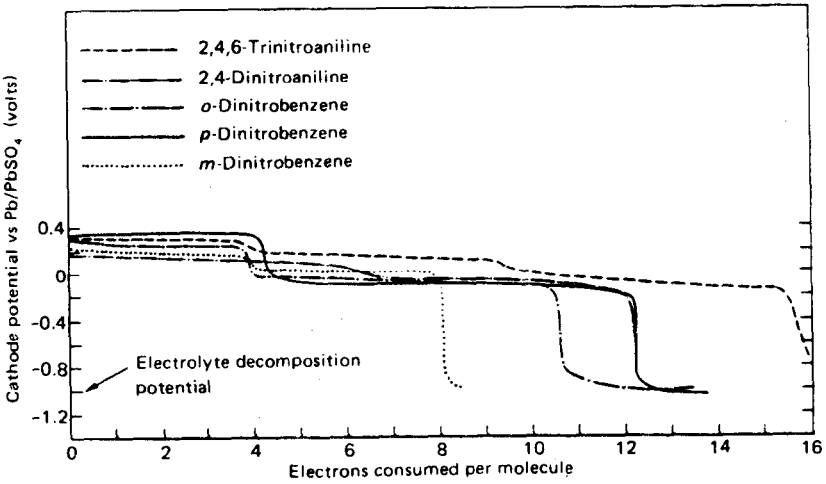

Figure 25. The capacity of organic compounds is higher than that of inorganic substances because of the large numbers of electrons consumed per molecule.

stages, the SO_2 systems have already captured the military market for use in Northern countries (Rosansky and Chodosh[64]).

Figure 26 shows a graphical display of the energy densities of nonaqueous cells with lithium anodes.

Rechargeability was reported with lithium cells containing cathodes made from di-, tri- and tetraselenides of niobium (Broadhead,[65] Murphy *et al.*[66]).

Solid State Batteries (*operating at room temperature*). The ideal cell for small current densities and practically unlimited life should be a solid state system. An example for such a cell is the combination $Ag|KAg_4I_4CN|3I_2$ with perylene as a charge-transfer complexing agent (Mrgudich and Louzos[67]). The rechargeability of such a system was reported by Scrosati and Torroni.[68]

Solid state electrolytes for high-temperature cells have been discussed before, in connection with the sodium–sulfur cell.

Summary. Concerning the recent developments in the field of nonaqueous and solid state cell components, it can be said that these new directions may completely change the electrochemical storage devices as we know them today. At the present time the low transference numbers and the high resistivities seem to be obstacles at room temperatures. However, the picture changes rapidly at higher temperatures; the exploration of the intercalated structures for solid electrodes like halogenes in graphite or the dichalcogenides of the group IV and V transition metals (Worrell and Nagelberg[69]) has made rapid progress.

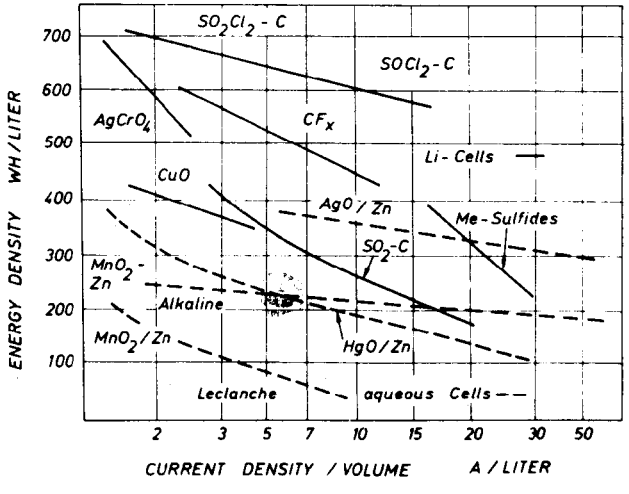

Figure 26. Comparison of nonaqueous Li cells with the MnO_2 and HgO cells. The energy density depends strongly on the current density.

3.5. Fuel Cells

3.5.1. Introduction

"A fuel cell is an electrochemical cell which can continuously change the chemical energy of a fuel and oxidant to electrical energy by a process involving an essentially invariant electrode–electrolyte system" (NEMA[70]). This definition is placed ahead of the necessarily short treatment of fuel cells, which are now in their "fourth cycle" to put into technical reality what Grove[71] discovered and Ostwald[72] envisioned as an electrochemical device, more efficient than the heat engine (see Section 2.4). Grove electrolized water and then used the evolved gases to produce electricity. He realized that he needed more cells to effect electrolysis again, applying the voltage of several of the H_2–O_2 cells in series. This is essentially the electrochemical storage technology which was discussed in Section 1.2.7 as an important variation of some future energy supply options.

The expectations were high around the turn of the century when Jacques[73] published a popular article about electricity directly from coal in Harpers Magazine. Haber and Brunner[74] and Nernst[75] in Germany, Noel[76] in France, and Jungner[77] in Sweden were the believers in fuel cells in Europe. Also, Edison[78] played with the fuel cell idea, but was not successful in that endeavour. An excellent collection about the early times of galvanic fuel elements was published by Euler.[79] He found a patent by Scharf[80] which showed a filter-press-type battery for two gases in an illustration which could have come out of a modern design laboratory, with all the details of manifolding and contacting as we know it now.

However, these expectations failed, mainly due to operating difficulties and material problems. The "second cycle" of fuel cell efforts is best represented by the school of Baur and Tobler,[81] who ended their work with the statement that a direct coal burning cell is not feasible and that the best chances are with a galvanic cell operating on gases (H_2, air) at room temperatures. Still, Bischoff and Justi[82] were considering a direct coal burning cell with a Cu/CuO–air electrode.

The findings of Davtyan[83] with respect to the "Nernst mass" (a solid electrolyte based on ZrO_2 and Y_2O_3) were the starting points for Broers and Ketelaar[84] in the construction of their very successful high-temperature molten carbonate cells, operating on CO and H_2. They used porous electrodes and a matrix electrolyte. In the middle 1950s the "third period" had begun, but not only with new ideas in the high-temperature field; fuel cells were also designed for high-pressure operation at medium temperatures and at low pressures in liquid electrolytes. All with "diffusion gas electrodes." The principle of increasing the interface, to establish a three phase zone: Gas–porous–conductor–liquid electrolyte was finally technically applied after it was actually known for many years (Naray-Szabo[85]) and used in small carbon–air/zinc cells (Heise and Schumacher[86]).

The dual-porosity nickel electrode of Bacon,[87] the Raney-nickel electrode of Justi *et al.*,[88] and the catalyzed carbon electrode of Kordesch and Marko[89] may be considered representative for the nearly simultaneous rising of fuel cell efforts all over the world. Bacon's fuel cell was developed into the most successful application of H_2–O_2 fuel cells, the power source for the Apollo spacecraft which went to the moon. Justi's work was continued in West Germany and has finally resulted in the present Siemens A.G. H_2–O_2 battery. The carbon electrode development of Kordesch at Union Carbide Corp. produced air-breathing military batteries using hydrazine or Zn, and were used in an electric vehicle which demonstrated the feasibility of a hybrid propulsion system (lead–acid battery and H_2–air fuel cell).

It is not possible to write here an abbreviated survey which would recognize all the work which went into fuel cells during the period 1950–1975. A historical paper entitled "25 Years Fuel Cells" was published in 1978 by the Electrochemical Society in connection with the 75th anniversary of its founding in 1902 (Kordesch[90]). There are also many books available which allow the study of the fuel cell developments in details.

To help the reader find fuel cell papers collected in books or symposia (series) proceedings, especially those which are not separately reported in *Chemical Abstracts*, a fuel cell bibliography has been added to this work, listing the general battery bibliography of the last two decades (as far as symposia are concerned). The order is chronological. The list appears as the Appendix.

After 1970 work on fuel cell systems was reduced drastically with the ending of the lavish support of space programs in the U.S.A. Since most of the developments were government subsidized, work at private companies was also abandoned. The only group which continued at a high level of effort was the TARGET program (Team to Advance Research for Gas Energy Transformation, Inc.) led by Pratt & Whitney Aircraft Division (now United Technologies Corp.). It was supported by money from the utility companies (gas and electric power companies), which agreed to develop the acidic (phosphoric acid) fuel cell system. This system is the only one which can operate on impure fuel gases, as (for instance) are produced in a hydrocarbon converter or coal gas converter. Since this system requires a high level of noble metal catalyst, it was not considered favorably in the "third period" of fuel cell development. It started the "fourth cycle" of fuel cell development, which by 1977 had started getting wide attention in connection with the energy crisis.

Until about 1975 the main emphasis on fuel cells was from the viewpoint of energy conversion. In recent years the aspect of using fuel cells in connection with electrolysis units to store energy has become equally important.

3.5.2. The Classification of Fuel Cell Systems

In the following a survey of the many different types of fuel cell systems is given. Beside the companies which constructed the actual batteries, the names of the principal investigators are shown.

A. *High-Temperature Cells*

A.1. Molten Carbonate Cells

Pittsburgh Consolidation Coal Co. (Gorin, Recht)
Texas Instruments, Inc. (Trachtenberg)
Institute of Gas Technology (Baker)
General Electric Co. (Douglas)
Union Carbide Corporation (Kronenberg)
Central Technical Institute, T.N.O., Holland (Broers)
Sondes Place Research Inst., Great Britain (Tantram, Chambers)
Gaz de France, France (Salvadori)

A.2. Solid Electrolyte Cells

Westinghouse (Weissbart, Archer, Zahradnik)
Brown Boveri A.G., West Germany (Böhme)
Battelle Inst. Frankfurt, West Germany (Baukal)
Battelle Institute Geneva, Switzerland (Tannenberg)
University of Grenoble, France (Deportes)
University of Nagoya, Japan (Takahashi)
Ural Institute of the Academy of Science, UdSSR (Palguev)

B. *Medium-Temperature Cells*

B.1. Hydrogen–Oxygen Cells (*Pressurized*)

Marshall's Flying School, England (Bacon)
Patterson-Moos Research Laboratory, Leesona Corp. (Moos)
Pratt & Whitney Div., United Aircraft Corp. Apollo Project (Morrill, Podolni)

B.2. Methanol Cell

General Electric Co. (Cairns)

C. *Low-Temperature Fuel Cells*

C.1. With Carbon Electrodes

Union Carbide Corp. (Kordesch)
Comp. General d'Electricité, France (Jaquelin)

C.2. With Platinum Black Electrodes

American Cyanamide Co. (Haldeman)
General Electric Co. (Grubb, Niedrach)
Englehard Ind. (Adelhart)

C.3. Porous Metal Electrodes

Varta A.G., West Germany (Justi, Winsel)
Siemens A.G., West Germany (von Sturm, Cnobloch)
ASEA, Sweden (Lindström)
Allis Chalmers Manufacturing Co. (Kirkland, Platner)
Electric Storage Battery Co. (Ruetschi)

C.4. With Tungsten Carbide Electrodes

AEG, West Germany (Pohl, Böhm)
Battelle Inst. Frankfurt, West Germany (Binder, Sandstede)

C.5. Ion Exchange Membrane Cells

General Electric Co., Gemini Project (Liebhafski, Maget, Oster)

C.6. Matrix—Phosphoric Acid Cell

Pratt & Whitney Div., United Aircraft Corp., TARGET program (Stonehart, Vogel, Lundquist, Podolni)
United Technologies Corp., Power Systems Div., ERDA-DOE (continuation of TARGET program, 1976)
Engelhard Ind. (Adelhart)
Energy Research Corp. (Baker)
Union Carbide Corp. (Scarr, Kordesch)

C.7. Hydrazine Fuel Cells

Union Carbide Corporation (Kordesch)
Allis Chalmers Mfg. Co. (Tompter, Anthony, Jasinski)
Monsanto Chem. Co. (Salathe)
Electrochimica Corp. (Eisenberg)
Electric Power Storage Co., England (Gillibrand, Lomax)
University of Bonn, West Germany (Vielstich)
Alsthom, France (Warszawski) Two-phase system
Moscow Power Institute, UdSSR. (Korovin)

C.8. Methanol Fuel Cells (*Acidic and Alkaline Electrolytes*)

Esso Res. and Engineering Co. (Heath)
Exxon and Alsthom combined, France. Two-phase system R&D
Shell Research, England (Williams, Gregory)
General Electric Co. (Gilmann, Breiter)
Allis Chalmers Mfg. Co. (Wynveen)
Gould National Co. (Biddick, Douglas)

C.9. Formiates (and Glycols, etc.)

University of Braunschweig, West Germany (Justi, Winsel)
University of Bonn, West Germany (Vielstich)
Allis Chalmers Mfg. Co. (Grimes)

C.10. Direct Hydrocarbon Fuel Cells

Esso Research and Engineering Co. (Heath)
General Electric Co. (Breiter, Gilman, Grubb, Niedrach, Cairns)
Battelle Institute Frankfurt, West Germany (Binder, Köhling)
California Research Corp. (Schlatter)
Tyco Laboratories (Brummer, Giner)

D. Other Systems

D.1. Redox Cells

General Electric Co. (Carson)
NASA (Thaller, Reid)

D.2. Biochemical Cells

Magna Corporation (Perry, Rohrback)
Melpar, Inc., Philco Corp., Marquart Corp.

D.3. Regenerative Fuel Cells

Pratt & Whitney (Podolny)
General Electric Co. (Gilman, Niedrach)
Xerox Corporation (Klein)

D.4. Thermally Regenerative Cell (Lithium–Hydrogen)

MSA Corporation (Shearer)

D.5. Photochemically Regenerative Cell

Philco Corporation (Zaromb, Kalhammer)

D.6. Nuclear Regenerative Cell

Union Carbide Corporation (Bennett)

D.7. Nitric Acid Regenerative Cell

Esso Research and Engineering Co. (Shropshire, Tarmy)

D.8. Sodium Amalgam Cell

Kellogg Co. (Yeager)

E. Indirect (Fuel Converter) Cells

E.1. Ammonia as Fuel

Engelhard Ind. (Adelhart)
Varta A.G., Germany (Winsel)

E.2. Internal Hydrocarbon Conversion (catalytic)

Leesona Moos Laboratories (Moos) with Pd–Ag membrane
Battelle Institute, Columbus (Hardy) with reforming anode

E.3. External Fuel Reforming

Institute of Gas Technology (Baker)
Pratt & Whitney Div., United Aircraft (Bartosh)
Allis Chalmers Manufacturing Co. (Kirkland)
Esso Research and Engineering Co. (Heath)
Union Carbide Corporation (Rothfleisch)
Shell Co., England (Williams)
U.S. Army, Ft. Belvoir (Frysinger)

Figures 27–33 show fuel cells from the described groups: A (Figure 27); B (Figures 28, 29); C (Figures 30, 31); D (Figure 32); E (Figure 33).

3.6. The Limits of Electrochemical Energy Storage (The "Super Battery")

The storage capability of an electrochemical system is determined by its voltage and the weight of one equivalent (96,500 C). If one plots the specific energy (Wh/kg) versus the g-equiv., then a family of lines is obtained which makes it possible to select a "super battery." The limits of electrochemical storage are indicated too.

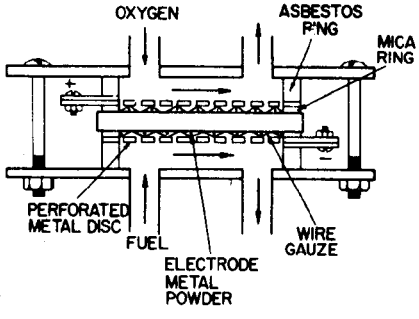

Figure 27. The high-temperature fuel cell of Broers.

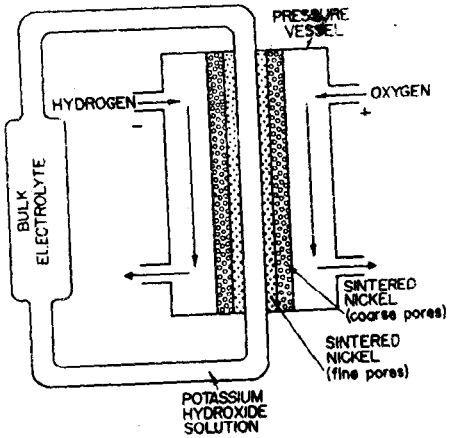

Figure 28. Principal design of the Bacon fuel cell systems.

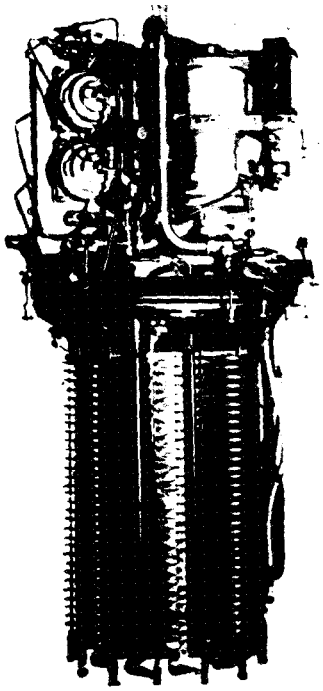

Figure 29. Apollo command and service module (Pratt & Whitney, Div. of United Aircraft Co.).

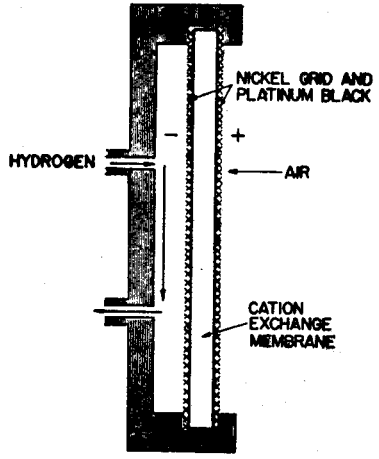

Figure 30. Ion exchange membrane H_2–air fuel cell (General Electric Co.).

In Figure 34 the theoretical limits of the specific energies of lead–acid cells, Ni–Cd, Ni–Zn, and Ni–Fe cells, the only commercially available systems today, are found in the right lower corner of the diagram. The high-energy systems currently under development are in the center. The limits are on the top. The highest energy densities are found with high-temperature systems and nonaqueous systems, not with aqueous, ambient temperature systems.

The technologically available energy densities are only a fraction of the theoretical values (for comparison, see Figure 13). The system Na–S, for instance, lists with 800 Wh/kg in Figure 34, with only 200 Wh/kg in Figure 13. This is about the expected ratio between theoretical data and practical batteries.

However, it should also be considered that "time to develop" is an important factor. The curves in Figure 35 show the gradual improvements of the "old" systems with the years. Probably the same can be expected from the "new" systems. The secondary version of a primary system can have a higher or lower energy density (for one discharge) due to a change in design emphasis (maximal capacity or highest cycle life).

The improvement trend is still strong but somehow these curves will reach a plateau, sooner with the developed systems. Among all systems the fuel cells will have the highest possible values if air operation is considered, and because they do not contain their energy within the confines of the cells (plates, electrolyte, etc.) but in a separate tank, which under all conditions is a more efficient storage device, they must come out on top of all systems with respect to energy density.

It should be noted that for the sake of a realistic data comparison the fuel cell systems in Figures 13 and 35 have had the necessary fuel included in the

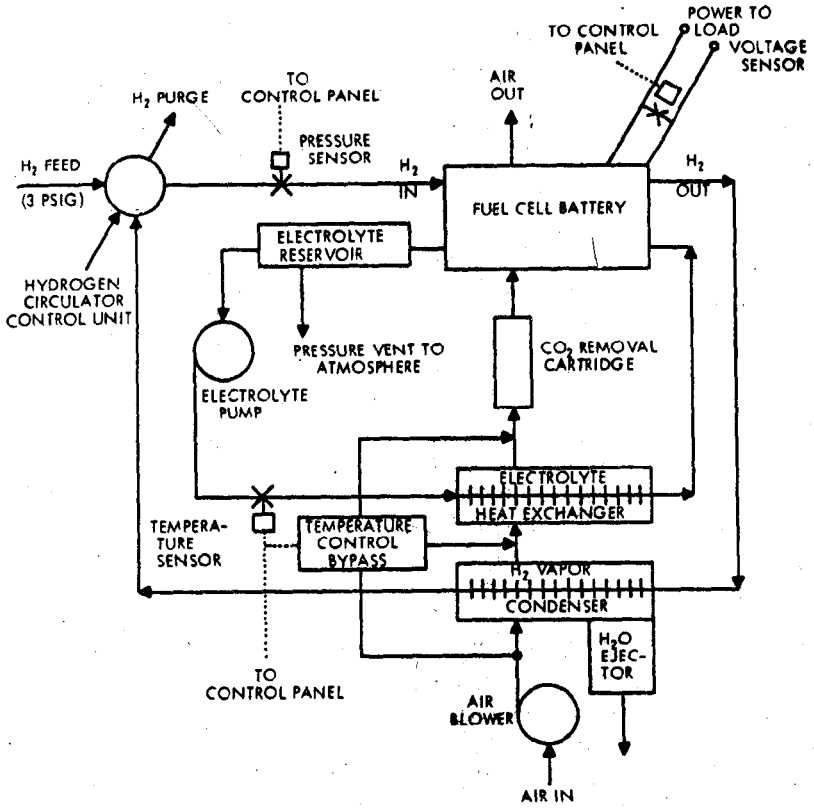

Figure 31. Complete hydrogen–air fuel cell system (Union Carbide Corp.).

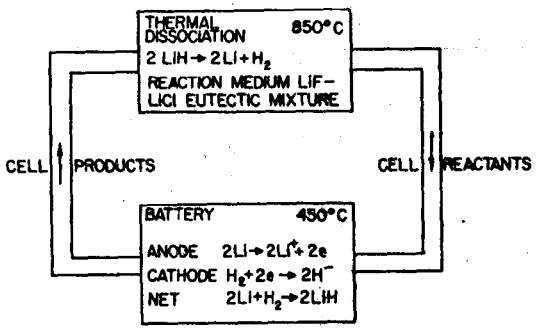
THERMAL DISSOCIATION 850°C
2 LiH → 2Li + H_2
REACTION MEDIUM LiF–LiCl EUTECTIC MIXTURE
CELL PRODUCTS
CELL REACTANTS
BATTERY 450°C
ANODE $2Li \rightarrow 2Li^+ + 2e$
CATHODE $H_2 + 2e \rightarrow 2H^-$
NET $2Li + H_2 \rightarrow 2LiH$

Figure 32. A thermally regenerative system (MSA Corp.).

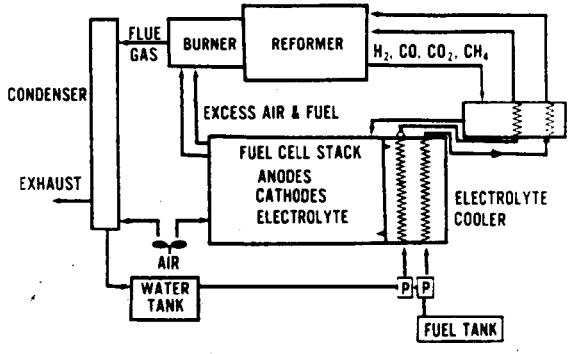

Figure 33. Hydrocarbon converter and fuel cell system (U.S. Army).

weight figures. In reality this is not so; the fuel is supplied externally, like gasoline to a car, in "unlimited" amounts.

In Section 1.2.7 the combination of water electrolysis and fuel cell was described as the way to combine chemical and electrochemical storage methods. Electrolyzer designs have been improved considerably in the last 10 years (Gregory[105]), which will result in higher efficiencies and lower cost in the

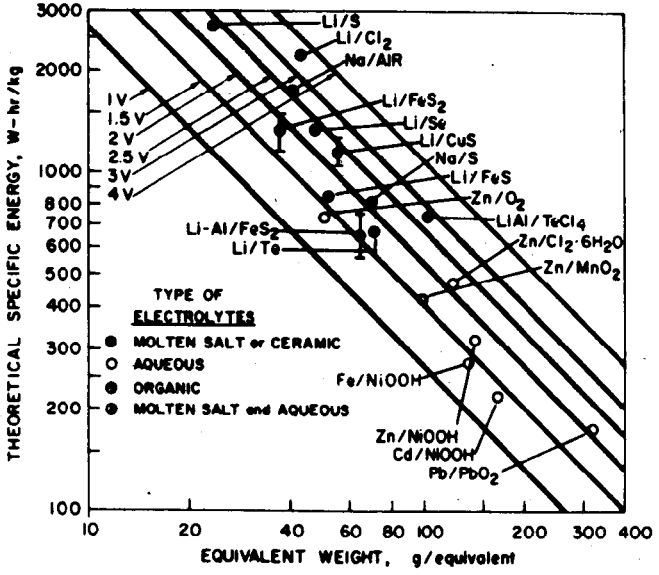

Figure 34. Theoretical specific energy plotted against the equivalent weight. The present commercial battery systems are in the lower right corner (Yao and Birk[56]).

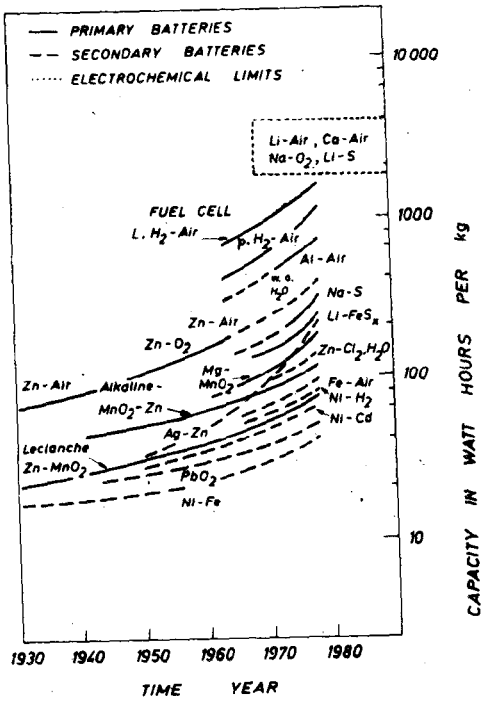

Figure 35. Improvement of battery systems between 1930 and 1977 and the capabilities of advanced systems.

future. At the present time the fuel cell–electrolyzer combination is projected to be higher in cost than the other storage devices (Kalhammer[93]). Hydrogen from coal is a well-worked-out chemical process, and hydrogen directly from a nuclear reactor through the use of the heat to decompose water via many intermediate steps is a much researched area (DeBeni and Marchetti[91]). The author is therefore of the opinion that the future super battery for energy storage need not be a system requiring extreme material usage and special operational parameters, but a combination of well-established principles (the most important being chemical storage and transmission) and of a low-cost fuel cell system using hydrogen and air, or perhaps another suitable choice, like methanol and air, fitting a future unified energy scenario.

4. Summary and Outlook

4.1. Industrial–Economical Aspects

For electrochemical energy storage there seem to be two large areas of future applications. One is the need for load leveling in the electric utility

industry, the other is the use of batteries in electric vehicles. In both applications the economic picture is important. In the field of small power users (portable equipment) the costs are not so much decisive as the requirement of safety and convenience. The production numbers are also very large in this third area, including the primary battery applications.

Figure 36 shows the effect of using a load-leveling device on the weekly load curve of an electric power company. It was estimated that the total market for storage batteries in 1985 could be as high as 3.7 billion dollars if the cost of the battery were approximately $210/kW (Birk[92]). However, few options (if any at all, besides lead–acid) are available to satisfy such a market. On the other hand, the projected increase in power demand (7% per year) may not happen, so that a longer time span will be available to develop better suitable systems.

Table 8 gives a survey of the projected characteristics and the status of some energy storage systems (Kalhammer *et al.*[93]). Since the advanced battery systems are still in the development stage, they will need to be tested. A facility to do that is being built near Princeton, New Jersey, sponsored by the Department of Energy (DOE) and the Electric Power Research Institute (EPRI). It will accommodate batteries of up to 2-MW capacity (*EPRI Journal*[94]). The tests will begin with blocks of improved lead–acid batteries. As new systems come along they will be included.

The batteries needed for the use in electric vehicles differ from the systems for load leveling in power density requirements. For acceleration at least 100–200 W/kg are required to operate a vehicle in a comparable way to present-day large cars, but considering a moderation in the size of future cars 100 W/kg may be sufficient; an energy density of 100 Wh/kg is needed to stay within the weight limits. A small 1200-kg car needs an electric motor with at least 10-kW output; e.g., operating it for 3 hr requires 30 kWh. A battery which could deliver that energy would weigh 300 kg, one-fourth the weight

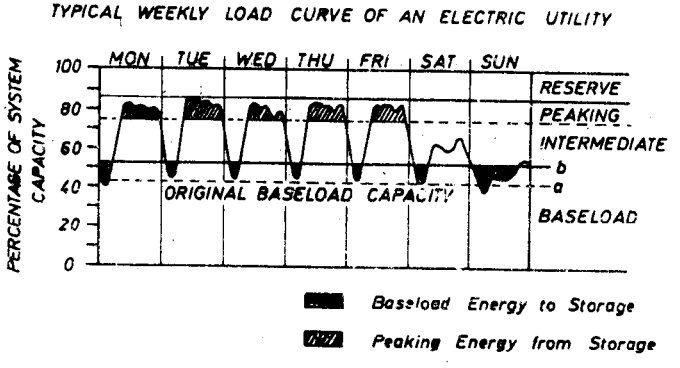

Figure 36. (a) Daily and weekly variations of the load curve of an electric utility. (b) The effect of adding energy from storage.

Table 8
Projected Characteristics and Status of Energy Storage Systems

Type	Round trip efficiency, %	Capital costs		Energy density, kWh/m^3	Development stage
		C_p, \$/kW	C_s, \$/kWh		
Mechanical					
Pumped hydro	67–75	100–140	2–15	1.0	Existing application; engineering studies for underground
Compressed air–gas turbine system	65–75	100–200	4–20	3–13	First commercial demonstration 1977
Flywheels	70–85	70–100	100–300	13–55	Initial development
Thermal					
Steam (pressure vessel)	70–80	150–250	30–70	Up to 30	Historical installations; engineering studies of modern systems
Hot oil	65–80	150–250	10–20		
Batteries					
Lead–acid	60–75	60–100	70–80	30–55	State of the art
Advanced aqueous	60–75	60–100	30–40	30–80	Small prototypes
High temperature	70–80	60–100	30–50	55–130	Laboratory cells
Redox	60–70	100–200	15–35	13–50	Conceptual and laboratory studies
Chemical					
Hydrogen (electrolysis plus fuel cell)	35–55	400–600	5–30	Supply limited only	Advanced development of subsystems

of the car (a good rule of thumb). It must be noted, however, that present lead–acid batteries are only capable of a fraction of that required performance, while a fuel-cell-powered vehicle has fulfilled those requirements using a hydrogen–air battery (Kordesch[95]).

An intermediate solution to the electric vehicle propulsion problem may be the construction of hybrid vehicles, for instance a combination of a motor generator with a lead–acid battery. Tests of such vehicles have proven their high-performance capabilities (Kordesch,[96] Volkswagen,[97] Unnewehr[98]). The disadvantage of such dual-power propulsion systems is cost and added complexity. The reduced pollution aspect is important.

From the standpoint of efficiency, the electric vehicle which is operated from a rechargeable battery is not much better in overall conversion of the chemical energy of the fuel into mechanical energy than the combustion engine because the losses of the central powerplant amount to about 60%. The recharging cycle is, at best, 64% efficient. The electric motor may be 85% efficient. A small diesel engine may have the same overall figure of merit for fuel utilization. The decisive difference is the shift from the critical oil-based fuel to coal or nuclear fuel. There are also environmental gains.

Efficiency improvements are only possible by using fuel cells as direct energy converters, avoiding the heat engine (steam turbine) losses. As suitable fuel we may consider hydrogen directly or any convertible fuel like methanol or ammonia.

However, coming back to the cost picture, a fuel cell system for an electric vehicle cannot be priced above approximately one-fourth the price of the car: this may be $2000 for a 20-kW system, which amounts to $100/kW. This is roughly one-tenth of what any equipment for utility peak power supply costs. The same consideration is true for any battery; therefore the chances are better for developing a new system for utility uses. On the other hand, a powerplant must have a life of at least 20 years, while a battery for a car needs only to last about five years, and that on intermittent duty only. An automotive engine has only to operate for 5000 hr to propel the vehicle over 200,000 km (5000 hr amounts to a little over one-half of a year). This argument allows a lower cost design standard.

The industrial use of primary batteries is rather limited, except maybe in solid state devices with extremely low power consumption, which may soon have the electrochemical storage of power permanently attached to the circuitry. The same is true for medical devices, e.g., heart pacers which should have the longest possible service and highest reliability. In a watch battery the customer pays $6000 for a kWh.

4.2. Research Objectives

The development of technical electrochemical storage devices was not guided by scientific discoveries like basic "ionics" or "electrodics" but rather

by practical requirements and market situations. It would be unrealistic to expect a rapid change, but the necessity to improve batteries and the competitive pressure of a more and more sophisticated industry has called on electrochemists to become deeply involved with the fundamentals of their technology.

Thermodynamics shows which cell system would have the highest voltage. The table of standard potentials (Table 1) lists lithium and fluorine at opposite ends. The Li–F_2 cell would have a potential of 6 V. Certainly such a cell is very difficult to build, but research has been able to find the next best couples: the combinations of Li with the fluorides of carbon, copper, cobalt, and nickel in nonaqueous electrolytes (see Figure 26), which produce potentials in the range from 3.5 to 3.0 V. Energy density figures are in the 1.5-kW/kg range for the ideal cells. This energy content is doubled in couples with organic cathodes; they have lower voltages, but exchange many electrons per reaction equivalent (see Figure 25). A calcium–metadinitrobenzene cell should produce about 3 kWh/kg. Such a system has not been designed yet, but magnesium organic cells were manufactured.

It can be said that in the last decade electrochemists have had a good look at the table of standard potentials and have tried couples which were considered impossible a few years ago. Li–cells with SO_2, sulfuryl, and thionyl-chlorides as "liquid"–carbon cathodes are technological breakthroughs, but their 100-year-old predecessor, the zinc–chromic-acid–carbon cell should have been an earlier reminder that such systems exist in principle. Probably it needed the discovery that nonaqueous electrolyte mixtures can be reasonably good conductors (with a changed concept of ionic transport) to overcome the "aqueous hurdle."

Currently electrochemists are looking to the oddest combinations of the elements in the periodic table and are coming up with some surprises after mixing the substances with graphite. Carbon fluoride and the sulfur compounds of the heavy metals are examples.

Far more scientific knowledge seems to guide the ways of the solid state researchers who are trying their concepts (which were so fantastically successful in electronics) in the field of energy conversion and storage. There is one obvious big difference: in solid state electronics minimal quantities of charges are necessary to build or break barriers. It is a "gate function" not a large quantity "storage function" which is performed. A storage battery will have to be concerned with chemical equivalents. This shall not minimize the possible effect of solid state knowledge on the improvement of batteries, but just the opposite: the biggest impact could be in the field of reaction kinetics and in the area of electrocatalysis. It has been pointed out how important the situation on an interface is, how sensitive the double layer reacts to relatively small amounts of electricity (Section 2.2).

The progress in electrochemistry is still following the pattern of a young, not yet mature science: practical findings and surprising inventions are *followed*

by scientific confirmation. Empirical research and immediate applications are closer in nature than basic science and product manufacturing. It is a difference in the ways of logical thinking (principle oriented versus purpose oriented) and a subconscious value grading which keeps the disciplines apart. In reality none is "worth more" than the other because results can only be achieved in cooperation. The basic scientific knowledge, however, should come ahead of the manufacturing "know how."

That the sequence is often turned around by commercial edict is a characteristic of our times. Research objectives are *demanded* by technology; it is a simple question of economy to explore first "what is needed," even if this need is only a competitive market situation in trivial things and certainly not affecting the future of humanity (like energy supply).

Electrochemical energy conversion and storage are certainly two of the critical objectives with which technology must deal. The role which batteries and especially fuel cells might play was discussed. There are indeed large efforts going on.

The state of the art of the hydrogen–air–phosphoric-acid fuel cells has reached 40-kW-size units, and megawatt powerplants are being built (Kunz[99]). This in spite of the fact that the problems of catalyst degradation are poorly understood. Under the pressure of such a situation advances in the field of electrocatalysis are made. The difficulty is that the otherwise elegant methods of surface physics and techniques like LEED, UPS, XPS, and Auger studies cannot be applied to electrodes *in situ* (Yeager[100]).

In the case of the hydrogen electrode and Pt catalysts there are decades of basic research work available. The reaction mechanism and the limiting steps are known; "only" the actual interface details are missing. However, in the case of the oxygen electrode the mechanism of the irreversible peroxide reaction is still puzzling and embarrassing because we lose 0.2 V per cell before we even put a load on.

There is promising work being done too. It seems the chemisorption of oxygen on the carbon depends strongly on the orientation of the layers, and theoretically there should be a way to bypass the HO_2^- intermediate (Tseung[101]).

Unfortunately, technology does not wait for research to solve problems, if the solutions do not come along in time.

The phosphoric acid fuel cell program may be relegated to the past and hopes set on the high-temperature systems again, a full circle in developmental efforts. It might have to be that way; solutions must be found one way or another (Fickett[102]).

The foregoing discussions may sound pessimistic, but they are not necessarily so; the purpose was to show that any scientific endeavor is nowadays under time pressure, and electrochemistry is no exception. Research objectives are to be set, either by an individual if he is part of the "free" academic community or by the management of the industrial concern one is part of. By planning for a certain result it must be made sure that the budgeting is right too,

and the commensurate supply of people, materials, and outside help must be assured by the planner.

Electrochemical conversion and storage is now in that situation: governmental and large-scale industrial help is ready. If the opportunity is missed, then basic research is on its own again.

It is important that the young people at our universities and technical institutes realize this challenge!

Acknowledgment

I wish to thank the "Fonds zur Förderung der wissenschaftlichen Forschung," Vienna, Austria, for the support of this paper.

Appendix: Bibliography on Fuel Cells

L. G. Austin, *Fuel Cells, A Review of Government-Sponsored Research, 1950–1964*, by NASA SP-120, Office of Technology Utilization, Washington (1967).

G. T. Young, ed., *Fuel Cells*, Rheinhold Publishing, New York. Vol. 1: Symposium of American Chemical Society, 1959, published 1960; Vol. 2: Symposium of American Chemical Society (1961), published 1963.

H. H. von Döhren and K. J. Euler, eds., *Brennstoffelemente*, Varta Fachbuchreihe, Vol. 6, VDI Verlag, Düsseldorf (1961).

E. W. Justi and A. W. Winsel, *Kalte Verbrennung-Fuel Cells*, Franz Steiner Verlag, Wiesbaden (1962); English translation, Pergamon, New York (1965).

W. Mitchell, Jr., ed., *Fuel Cells*, Academic Press, New York (1963).

V. S. Bagotskii and Yu B. Vasil'ev, eds., *Toplivne Elementy* (Fuel Cells), Academy of Sciences of the USSR, Moscow, 1964. English translation, Consultants Bureau, New York (1966).

B. S. Baker, ed., *Hydrocarbon Fuel Cell Technology*, Academic Press, New York (1965).

Odile Block, ed., Publications de l'Institute Francais du Petrole, *Les Piles à Combustible*, Collection No. 6, Editions Technip, Paris (1965).

R. F. Gould, ed., *Fuel Cell Systems*, Advances in Chemistry Series 47, American Chemical Society, Washington, D.C. (1965).

W. Vielstich, *Brennstoffelemente-Fuel Cells*, Verlag Chemie, Weissheim/Bergstr., 1965; English translation, John Wiley & Sons, London (1970).

K. R. Williams, *An Introduction to Fuel Cells*, Elsevier, Amsterdam (1966).

A. B. Hart and G. J. Womak, *Fuel Cells*, Chapman & Hall, London (1967).

K. Schwabe and E. Winkler, eds., *Proceedings of the International Fuel Symposium*, Dresden in 1967; Vol. 49, Abh. d. Sächs, Akad. d. Wiss., Leipzig, Academie Verlag, Berlin (1968).

C. Berger, ed., *Handbook of Fuel Cell Technology*, Prentice-Hall, Englewood Cliffs, New Jersey (1968).

H. A. Liebhafsky and E. J. Cairns, *Fuel Cells and Fuel Batteries*, John Wiley & Sons, New York (1968).

J. O'M. Bockris and S. Srinivasan, *Fuel Cells, Their Electrochemistry*, McGraw-Hill, New York (1969).

M. W. Breiter, *Electrochemical Processes in Fuel Cells*, Springer Verlag, New York (1969).

R. F. Gould, ed., *Fuel Cell Systems II*, Advances in Chemistry Series 90, American Chemical Society, Washington, D.C. (1969).

G. Sandstede, ed., *From Electrocatalysis to Fuel Cells*, Battelle Seattle Research Center, University of Washington Press, Seattle (1972).

K. V. Kordesch, "Power Sources for Electric Vehicles" (pp. 339–443), in *Modern Aspects of Electrochemistry*, Vol. 10, J. O'M. Bockris and B. E. Conway, eds., Plenum Press, New York (1975).

United States Army, Proceedings, 1956–1976; 10th–12th Annual, Research & Development Conferences, Signal Corps Engineering Laboratories (1956 through 1958); 13th–22nd Annual Power Sources Conference, J. S. Army Signal Research & Development Laboratories, Ft. Monmouth, New Jersey, (1959 through 1968); 23rd Power Sources Conference (1969) and 24th Power Sources Symposium (1970), PSC Publication Committee, Red Bank, New Jersey; 25th–27th Biennial Power Sources Symposium, PSC Publication Committee, Red Bank, New Jersey (1972, 1974, 1976).

United States Army Electronics Laboratory, Washington, D.C., *Status Reports on Fuel Cells*: 1st, by B. R. Stein (1959); 2nd, B. R. Stein and E. M. Cohen (1960); 3rd, by H. F. Hunger *et al.* (1962); 4th, by F. R. Franke and H. F. Hunger (1962); 5th, by S. J. Bartosh *et al.* (1965); 6th, by G. R. Frysinger *et al.*, Final (1967). (Reports 3–6 were published by the U.S. Army Electronics Command, Forth Monmouth, New Jersey).

C.I.T.C.E. Proceedings of the Comité International de Thermodynamique et de Cinétique Electrochimiques, named I.S.E. (International Society for Electrochemistry) from 1971 on: 1959 (11th) Vienna, 1960 (no meeting), 1961 (12th) Brussels, 1962 (13th) Rome, 1963 (14th) Moscow, 1964 (15th) London–Cambridge, 1965 (16th) Budapest, 1966 (17th) Tokyo, 1967 (18th) Schloss Elmau (no Fuel Cells), 1968 (19th) Detroit, 1969 (20th) Strasbourg, 1970 (21st) Prague, 1971 (22nd) Dubrovnik (no Fuel Cells), 1972 (23rd) Stockholm, 1973 (24th) Munich, 1974 (25th) Brighton, 1975 (26th) The Hague, 1976 (27th) Zürich, 1977 (28th) Varna, 1978 (29th) Budapest.

ECS Fuel Cell Symposia, Extended Abstracts, Electrochemical Society—Battery Division: October 1961, Detroit; October 1962, Boston; October 1963, New York; October 1964, Washington, D.C.; October 1966, Philadelphia; October 1968, Montreal; October 1970, Atlantic City; October 1976, Las Vegas; May 1977, Philadelphia.

D. H. Collins, ed., Biennial Proceedings, 1962–1976, Joint Services of the Electrical Power Sources Committee; *Batteries*, 3rd Symposium (Bournemouth, 1962), Pergamon, New York (1963); *Batteries II*, 4th Symposium (Brighton, 1964), Pergamon, New York (1965); *Power Sources 1* (Brighton, 1966), Pergamon, New York (1967); *Power Sources 2* (Brighton, 1968), Pergamon, New York (1969); *Power Sources 3* (Brighton, 1970), Oriel, Newcastle upon Tyne (1971); *Power Sources 4* (Brighton, 1972), Oriel, Newcastle upon Tyne (1973); *Power Sources 5* (Brighton, 1974), Academic, New York (1975); *Power Sources 6* (Brighton, 1976) Academic, New York (1977).

Proceedings of the Fuel Cell Symposia, New Orleans, Louisiana, March 1963 and in Buffalo, New York, May 1963, American Institute of Chemical Engineers, in CEP-Manual: *Fuel Cells*, by AICE, New York (1963).

Societe d'étude de recherches et d'applications (S.E.R.A.I.) and COMASCI, International Symposia on Fuel Cells, Brussels, June 1965; June 1967; June 1969. Proceedings 1969 published by Presses Academiques Europeennes, Bruxelles, Belgium (1969).

I.E.C.E.C., Proceedings of Intersociety Energy Conversion Engineering Conferences (published by the host-organization of the particular year: 1st: Los Angeles, California, 1966, 2nd: Miami Beach, Florida, 1967, 3rd: Boulder, Colorado, 1968, 4th: Washington, D.C., 1969 (Index 66–69), 5th: Las Vegas, Nevada, 1970, 6th: Boston, Massachusetts, 1971, 7th: San Diego, California, 1972, 8th: Philadelphia, Pennsylvania, 1973, 9th: San Francisco, California, 1974, 10th: Newark, Delaware, 1975, 11th: State Line, Nevada, 1976, 12th: Washington, D.C., 1977, 13th: San Diego, California, 1978.

Proceedings of the Symposium on "Power Systems for Electric Vehicles," U.S. Dept. of Health, Education, and Welfare, Columbia University and Polytechnic Institute of Brooklyn, April 1967, in Public Health Service Publication No. 999-AP-37 (1967).

Fuel Cells, a Bibliography, TID-3359 (June 1977), U.S. Energy Research & Development Administration.

National Fuel Cell Seminar Abstracts, June 21–23, 1977, Boston, Dynatrend Inc. (1977); July 11–13, 1978, San Francisco, July 26–28, 1979, Bethesda, Courtesy Associates, Inc. (1978, 1979).

References

1. J. O'M. Bockris, *Energy: The Solar–Hydrogen Alternative*, John Wiley & Sons (1975).
2. EPRI-ERDA, Electric Power Research Institute, EPRI-EM-264, project 225 and Energy Research and Development Adm., ERDA # (11-1)-2501, Final Report, Vol. 2, 1976. An assessment of energy storage systems suitable for use by electric utilities.
3. K. J. Vetter, *Electrochemical Kinetics*, Academic Press, New York (1967). In German: Springer, Berlin (1961).
4. J. O'M. Bockris and A. K. Reddy, *Modern Electrochemistry*, Vols. 1 and 2, Plenum Press, New York (1970).
5. W. M. Latimer, *Oxidation Potentials*, Prentice-Hall, Englewood Cliffs, New Jersey (1952).
6. A. J. De Bethune, Electrode potentials, in Encyclopedia of Electrochemistry, C. A. Hampel, ed., Reinhold, New York (1964).
7. M. Pourbaix, *Atlas of Electrochemical Equilibria*, Pergamon Press, New York (1966).
8. D. J. G. Ives and G. J. Janz, *Reference Electrodes, Theory and Practice*, Academic Press, New York (1961).
9. C. A. Hampel, ed., *Encyclopedia of Electrochemistry*, Reinhold, New York (1964).
10. E. Yeager and A. J. Salkind, *Techniques of Electrochemistry*, Wiley Interscience, New York (Vol. 1, 1972, Vol. 2, 1973, Vol. 3, 1977).
11. H. H. von Döhren and K. J. Euler, *Brennstoffelemente*, Vol. 6, Varta Fachbuchreihe, Frankfurt (1970).
12. K. V. Kordesch, Alkaline manganese dioxide zinc cells, in *Batteries*, Vol. 1, *Manganese Dioxide*, K. V. Kordesch, ed., Marcel Dekker, New York (1974).
13. K. J. Vetter, *J. Electrochem. Soc.* **112**, 959 (1963).
14. R. Huber, The Lechanché cell, in *Batteries*, Vol. 1, *Manganese Dioxide*, K. V. Kordesch, ed., Marcel Dekker, New York (1974).
15. A. Kozawa, Electrochemistry of manganese dioxide, in *Batteries*, Vol. 1, *Manganese Dioxide*, K. V. Kordesch, ed., Marcel Dekker, New York (1974).
16. A. Kozawa and R. A. Powers, *J. Electrochem. Soc.* **113**, 870 (1966).
17. R. A. Robinson and R. H. Stokes, *Trans. Faraday Soc.* **45**, 612–624 (1949).
18. P. Ruetschi and R. T. Angstadt, *J. Electrochem. Soc.* **111**, 1323 (1964).
19. E. Berndt, in *Power Sources 2*, D. H. Collins, ed., Pergamon Press, New York (1970), pp. 17–31.
20. J. O'M. Bockris and D. Drazic, *Electrochemical Science*, Taylor and Francis, London (1972).
21. J. O'M. Bockris and S. Srinivasan, *Fuel Cells, Their Electrochemistry*, McGraw-Hill, New York (1969).
22. G. Sandstede, *From Electrocatalysis to Fuel Cells*, Batelle Seattle Research Center, University of Washington Press, Seattle, Washington (1971).
23. M. W. Breiter, *Electrochemical Processes in Fuel Cells*, Springer-Verlag, New York (1969).
24. K. Kordesch and A. Marko, *J. Electrochem. Soc.* **107**, 480 (1960).
25. M. Eisenberg, in *Advances in Electrochemistry and Electrochemical Engineering*, Vol. 2, C. Tobias, ed., Interscience, New York (1962), Chap. 5.
26. B. Levich, *Discuss. Faraday Soc.* **1**, 37 (1947).
27. C. W. Tobias *et al.*, *J. Electrochem. Soc.* **99**, 359c (1952).
28. N. Ibl, *Helv. Chim. Acta* **1**, 117 (1959).
29. K. V. Kordesch, *Electrochim. Acta* **16**, 597 (1971).
30. K. V. Kordesch, in *Handbook of Fuel Cell Technology*, C. Berger, ed., Prentice-Hall, Englewood Cliffs, New Jersey (1968), pp. 359–421.
31. J. O'M. Bockris, M. A. V. Devanathan, and K. Müller, *Proc. R. Soc. London Ser. A* **274**, 55 (1963).
32. E. Gileadi *et al.*, *Interfacial Electrochemistry*, Addison-Wesley, Reading, Massachusetts (1975).

33. S. Trasatti, in *Advances in Electrochemistry and Electrochemical Engineering*, Vol. 10, H. Gerischer and C. W. Tobias, eds., J. Wiley & Sons, New York (1977).
34. K. V. Kordesch, The electric automobile, in *Batteries*, Vol. 2, *Lead Acid Batteries and Electric Vehicles*, K. V. Kordesch, ed., Marcel Dekker, New York (1977), Chap. 2.
35. E. Y. Weissman, in *Batteries*, Vol. 2, *Lead Acid Batteries and Electric Vehicles*, K. V. Kordesch, ed., Marcel Dekker, New York (1977), pp. a–200.
36. Gates Rubber Corp., Battery Application Manual, Gates Energy Products, Inc., Denver, Colorado (1976).
37. Battery Council International, Technical Committee Report, 1970.
38. C. W. Vinal, *Storage Batteries*, 4th ed., John Wiley & Sons, New York (1955).
39. H. Bode, *Lead Acid Batteries*, John Wiley & Sons, New York (1977).
40. D. H. Collins, ed., Special Issue: Lead Acid Batteries, *J. Power Sources*, **2**, No. 1 (1977).
41. S. U. Falk and A. J. Salkind, *Alkaline Storage Batteries*, John Wiley & Sons, New York (1969).
42. K. Salamon and G. Krämer, *Electrotech. Z.* **1**, 69–74 (1977).
43. H. J. Schwarz, NASA Tech. Memo TM-X-71471, Electric Vehicle Battery Res. & Dev., 1973.
44. R. J. Elbert, U.S. Patent 3,556,856 (1971).
45. G. Caprioglio and J. T. Porter, in *Advances in Battery Technology*, Vol. 3, *Symposium, The Electrochemical Society, S. California–Nevada Section*, The Electrochemical Society, Princeton, New Jersey (1967), pp. 86–100.
46. H. Cnobloch, *Power Sources 5*, D. H. Collins, ed., Academic Press, New York (1975), pp. 261–282.
47. S. Zaromb, in *Power System for Electric Vehicles, Symposium at Columbia University*, U.S. Dept of H.E.W., Washington, D.C., pp. 245–253.
48. A. R. Despic *et al.*, *Power Sources 6*, D. H. Collins, ed., Academic Press, New York (1976), pp. 361–368.
49. J. Ruch, Abstract No. 42, Electrochemical Society Meeting, Atlanta, Georgia, 1977.
50. H. J. Halberstadt, 8th Intersociety Energy Conversion Engineering Conference, Philadelphia, Paper No. 739008, 1973.
51. E. L. Littauer, Reports of Lockheed Palo Alto Research Laboratory and Lawrence Livermore Laboratory, 1977.
52. J. D. Dunlop, G. Van Ommering, and M. W. Earl, *Power Sources 6*, D. H. Collins, ed., Academic Press, New York (1976).
53. K. V. Kordesch and S. J. Cieszewski, *Power Sources 6*, D. H. Collins, ed., Academic Press, New York (1976), pp. 249–258.
54. M. W. Earl and J. D. Dunlop, *26th Power Sources Symposium*, PSC-Publication Committee, Red Bank, New Jersey (1974), pp. 24–27.
55. S. A. Weiner, Proceedings of the Symposium and Workshop on Advanced Battery Research and Design, Argonne Natl. Laboratory, Electrochemical Society, Chicago Section.
56. N. P. Yao and J. R. Birk, 10th Intersociety Energy Conversion Engineering Conference, Paper No. 759166, 1975.
57. J. R. Birk, Electric Power Research Institute, Presentation at the Engineering Foundation Conference on Energy Storage, Pacific Grove, California, 1976.
58. G. W. Heise and N. C. Cahoon, in *Primary Battery*, Vol. 1, John Wiley & Sons, New York (1971); Vol. 2 (1976).
59. R. J. Brodd, K. V. Kordesch, and A. Kozawa, 25 Years of Primary Batteries, Review, *J. Electrochem. Soc.* **125**, 271c–283c (1978).
60. R. E. Biddick, J. W. Cretzmeyer, and D. L. Douglas, *Power Sources 5*, H. D. Collins, ed., Academic Press, New York (1975), pp. 411–424.
61. C. K. Morehouse, Proceedings of the 12th Annual Battery Research & Development Conference, Atlantic City, New Jersey, 1958.

62. G. Sandstede, *From Electrocatalysis to Fuel Cells*, Battelle Seattle Research Center, University of Washington Press, Seattle (1972), pp. 333–343.
63. A. N. Dey, *Electrochim. Acta* **21**, 377, 855 (1976).
64. M. G. Rosansky and S. M. Chodosh, 27th Power Sources Symposium, PSC-Publication Committee, Red Bank, New Jersey (1976), pp. 72–77.
65. J. Broadhead, *Power Sources 4*, D. H. Collins, ed., Oriel, Newcastle (1973), pp. 469–482.
66. D. W. Murphy, F. A. Trumbore, and J. N. Carides, Abstract No. 70, Electrochemical Society Meeting, Las Vegas, Nevada, 1976.
67. J. N. Mrgudich and D. V. Louzos, in *The Primary Battery*, Vol. 1, G. W. Heise and N. C. Cahoon, eds., John Wiley & Sons, New York, (1971), pp. 385–398.
68. B. Scrosati, M. Torroni, and A. D. Butherus, *Power Sources 4*, D. H. Collins, ed., Oriel Press, Newcastle (1973), pp. 453–466.
69. W. L. Worrell and A. S. Nagelberg, Proceedings of the Symposium and Workshop on Advanced Battery Research and Design, Argonne National Laboratory, Electrochemical Society, Chicago Section, 1976, pp. B2–12.
70. NEMA Standard, Publication No. CV-I, National Electrical Mfgs. Assoc., New York, 1968.
71. W. R. Grove, *Philos. Mag.* **3**, 14, 127 (1839).
72. W. Ostwald, *Z. Elektrochem.* **1**, 122 (1894).
73. W. W. Jacques, *Harpers Magazine* **96**, 559, 144–150 (1896).
74. R. Haber and L. Brunner, *Z. Elektrochem.* **10**, 697–713 (1904).
75. W. Nernst, German Patent No. 259,241 (1912).
76. P. G. L. Noel, French Patent No. 350,111 (1904).
77. E. W. Jungner, British Patent No. 15,727 (1906).
78. T. A. Edison, U.S. Patent No. 435,688 (1890).
79. J. Euler, *Aus der Fruhzeit der galvanischen Brennstoffelemente*, Varta Publikation, Frankfurt (1966).
80. P. Scharf, German Patent No. 48,446 (1888).
81. E. Baur and T. Tobler, *Z. Elektrochem.* **36**, 169 (1933).
82. K. Bischoff and E. Justi, *Jahrbuch Akad. Wiss. Lit.* (*Mainz*), 250.
83. O. K. Davtyan, *Bull. Acad. Sci. USSR Sci. Tech.* **107**, 125 (1946).
84. G. H. J. Broers and J. A. A. Ketelaar, *Fuel Cells*, G. J. Young, ed., Reinhold, New York (1960), pp. 78–108.
85. V. St. Naray-Szabo, *Z. Elektrochem.* **33**, 15, 107 (1912).
86. G. W. Heise and E. A. Schumacher, *Trans. Electrochem. Soc.* **62**, 385 (1932).
87. F. T. Bacon, *Beama Journal* **6**, 61 (1954).
88. E. Justi, A. Winsel, and W. Scheibe, German Patent No. 1,019,361 (1954).
89. K. Kordesch and A. Marko, *Osterr. Chem. Z.* **52**, 125 (1951).
90. K. V. Kordesch, 25 Years of Fuel Cells (1951–1976), *J. Electrochem. Soc.* **125**, 77c–91c (1978).
91. G. DeBeni and C. Marchetti, *Euro. Spectra* **9**, 46–50 (1970).
92. J. R. Birk, Presentation at the Battery Council International, (BCI) Mexico City, Mexico, 1976.
93. F. R. Kalhammer, J. R. Birk, and J. W. Pepper, World Electrochemica Congress, Moscow, USSR, 1977.
94. *EPRI Journal*, Official Start of the BEST Facility (December 1977), p. 15.
95. K. V. Kordesch, Power sources for electric vehicles, in *Modern Aspects of Electrochemistry*, Vol. 10, J. O'M. Bockris and B. E. Conway, eds., Plenum Press, New York (1975), pp. 339–443.
96. K. V. Kordesch, in *Batteries*, Vol. 2, *Lead Acid Batteries and Electric Vehicles*, K. V. Kordesch, ed., Marcel Dekker, New York (1977), pp. 201–413.
97. Volkswagen, The city-taxi project, *Electric Vehicle News* **5**(3), 14–15 (1976).

98. L. E. Unnewehr *et al.*, Engine-Electric Vehicular Drives, 11th Intersociety Energy Conversion Engineering Conference, Paper No. 769063, 1976.
99. H. R. Kunz, Abstract No. 389, Spring Meeting of the Electrochemical Society, Philadelphia, 1977.
100. E. Yeager, Abstract No. 334, Spring Meeting of the Electrochemical Society, Philadelphia, 1977.
101. A. C. C. Tseung, Abstract No. 337, Spring Meeting of the Electrochemical Society, Philadelphia, 1977.
102. A. P. Fickett, Abstract No. 378, Spring Meeting of the Electrochemical Society, Philadelphia, 1977.
103. EPRI, Electric Power Research Institute, IPRI-EM-256, Project No. 788-1, Final Report, Vol. 1, 1976.
104. A. Fleischer and J. J. Lander, *Zinc–Silver Oxide Batteries*, John Wiley & Sons, New York (1971).
105. D. P. Gregory, in *Modern Aspects of Electrochemistry*, Vol. 10, J. O'M. Bockris and B. E. Conway, eds., Plenum Press, New York (1975), pp. 239–288.
106. K. V. Kordesch, *J. Electrochem. Soc.* **118**, 815 (1971).

4

Primary Batteries—Introduction

M. BARAK

1. General Features

1.1. Early Developments

I do not intend to trace in this chapter the discovery and historical development of primary batteries. Those interested in these aspects will find a detailed authoritative account in books on this subject.[1,2] Some salient features are, however, worthy of note, since these indicate fundamental principles involved and ways in which basic problems have been approached, often by purely empirical methods. An outstanding feature of the primary battery is that its discovery around the turn of the eighteenth century was closely identified with the birth and the growth of the science of electrochemistry. This science and the power sources related to it will always be associated with the discoveries of the Italian scientist Volta (1800), who gave his name to the "voltaic pile" and the "volt." The voltaic pile was constructed of disks of the electrochemically dissimilar metals silver and zinc, interleaved with absorbent paper saturated with the electrolyte, and provided the only source of direct current at that time. Devices of this kind enabled Nicholson and Carlisle to demonstrate the electrolysis of water (1800) and Faraday to derive his quantitative laws (1834) on which the whole science of

M. BARAK • Consulting Chemist and Engineer, 61 Folders Lane, Burgess Hill, Sussex RH15 0DY, England.

electrochemistry is based. Using similar principles and the metals copper and zinc, Daniell (1836) produced his two-fluid cell, in which the cathode was immersed in copper sulfate solution and the anode in dilute sulfuric acid, the two electrolytes being separated by a porous partition. This arrangement considerably reduced polarization of the cathode by hydrogen, and the resulting standing losses and cells of this type found wide applications for several years in telegraph and railway signaling installations, being finally superseded by Leclanché wet cells, Lalande copper oxide–zinc cells, and air-depolarized zinc–air cells.

Many different combinations of electrodes and electrolyte were then tested. Polarization of the cathode by films of hydrogen gas was a major problem and experiments were made with a variety of oxide depolarizers, which reacted with the hydrogen as it was formed. Lead dioxide and manganese dioxide were found to be among the most effective, particularly the latter, which was used first by Zamboni (1812) and later by Leclanché. In 1866, Leclanché launched his "wet" battery, in which the manganese dioxide was packed around the carbon current collector in the cathode, a solution of ammonium chloride served as the electrolyte, and a zinc rod or plate, sometimes amalgamated with mercury, formed the anode. This proved so successful that Leclanché set up a manufacturing plant in Brussels and within a year or two proudly claimed that there were over 20,000 of his wet batteries in service in telegraph and railway signaling installations in Western Europe.

The next major step forward, following some earlier work by Zamboni and taken by Leclanché and Gassner (1888), was to immobilize the electrolyte in a paste made with starch or other absorbent materials, and this "dry" assembly, which contained no free liquid, could be more or less completely closed. The final important step was to make the zinc anode in the form of a can which served the double function of the anode and the container for all of the other elements of the cell, contact between the anode and the cathode pack being prevented by wrapping the latter in a sheath of absorbent paper.

The dry battery rapidly achieved great commercial popularity and this was stimulated by the invention of the flashlight or hand torch. By 1900 the annual production rate in the United States alone was reported to be around two million cells, and 20 times that number only ten years later. Primary battery production is now a major manufacturing industry in most of the industrialized countries of the world.

1.2. Applications of Primary Batteries

Up to about the time of the second World War the Leclanché dry battery was almost the only small portable power source available and its main use was in torches and lamps of different types, portable radio equipment, instruments, and so on. The war stimulated the search for power sources with greater power and capacity and capable of operation over a much wider range of temperature.

Research and development efforts expanded then and later led to a deeper understanding of the basic principles of voltaic cells; equipped with this knowledge, workers began to tailor special electrochemical systems to the particular power and energy demands of the various commercial consumer and industrial equipment. This in turn stimulated the dry battery manufacturers to improve their products, leading to a line of what are often known as "premium" batteries. At the same time the discovery and development of solid state transistors, and the introduction of miniaturized circuitry, revolutionized the electronics industry and opened up new uses for the lower-powered energy sources.

Primary batteries are now used in a wide variety of both consumer products and industrial equipment. At one extreme, there are the minute hearing aids, so small that they can be secreted, almost unnoticed behind the ear, or the medical devices, some little larger than an aspirin tablet, which may be implanted in the body to signal internal conditions, such as the acidity of the stomach or to stimulate the beating of the heart in a pacemaker. Moving up the scale in size are many types of specialized equipment, including watches, portable radio and walkie-talkie communication sets, tape recorders, small calculators, dry shavers, polarized and cine cameras, photoflash apparatus, toys, flashlights and lighting equipment of all types, air–sea rescue beacons, and many other devices, which fall into the omnibus class of cordless electrical appliances.[3,4]

Cells and batteries for these applications take a wide variety of shapes and sizes from small disk-shaped button cells to large rectangular laminated packs, in addition to the well-known cylindrical types, commonly used in flashlights. The approximate volumetric power density of the batteries used in a number of these applications, expressed in terms of W/dm^2 is shown in Figure 1.[5] For purposes of comparison, values are also shown for the standard lead–acid storage battery used for automobile starting, lighting, and ignition (SLI) service.

1.3. Basic Principles

The term *battery* is sometimes loosely applied to what is in reality a single electrochemical or voltaic cell. Strictly speaking, a battery is an assembly of cells. Voltaic cells convert the energy evolved during certain chemical reactions into low-voltage, direct current electricity. These devices may therefore be regarded as electrochemical energy converters. Each cell contains three major components, a positive electrode or "cathode," a negative electrode or "anode," and an electrolyte, and all three components are intimately involved in the electrochemical reactions which take place during discharge and in secondary reversible cells, during charge.

Note that this terminology for the electrodes is based on the discharge process and is the reverse of the convention usually applied to an electrolytic

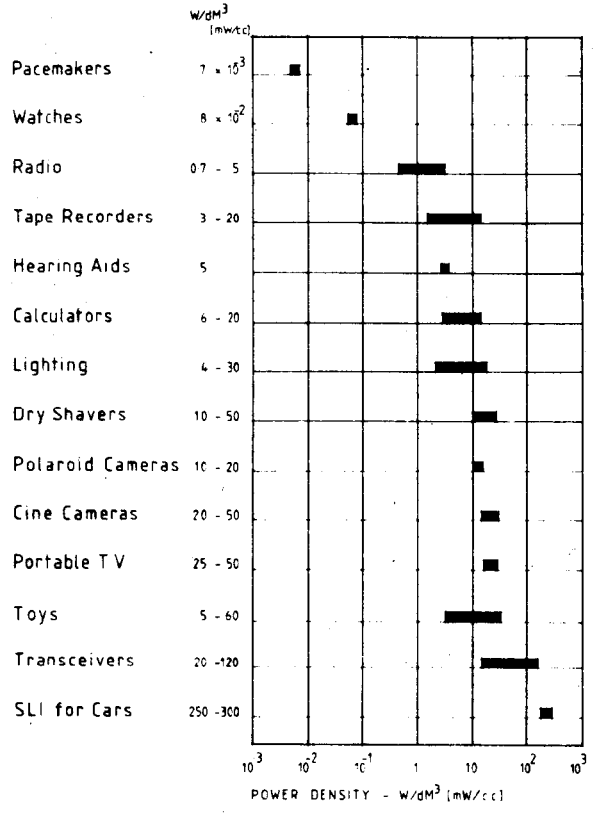
W/dM3 [mW/cc]
Pacemakers 7 x 10^3
Watches 8 x 10^2
Radio 0.7 - 5
Tape Recorders 3 - 20
Hearing Aids 5
Calculators 6 - 20
Lighting 4 - 30
Dry Shavers 10 - 50
Polaroid Cameras 10 - 20
Cine Cameras 20 - 50
Portable TV 25 - 50
Toys 5 - 60
Transceivers 20 -120
SLI for Cars 250 -300
10^3 10^2 10^-1 1 10 10^2 10^3
POWER DENSITY - W/dM3 [mW/cc]

Figure 1. Applications for primary batteries—approximate power density requirements.[5] [Courtesy of SAFT Co. (U.K.).]

cell, where the current is fed into the cell through the positive anode and out through the cathode.

With some exceptions, described later, the electrodes and the electrolyte are for the most part inorganic in origin.

Each electrode exerts its own characteristic potential to the electrolyte and this represents the emf of the reversible redox reaction involved. (Lists of the standard reversible potentials of elements and compounds in acid and alkaline electrolytes are given in various textbooks.) These thermodynamic reduction potentials are quantitatively defined by the Nernst equation:

$$E = E_0 - \frac{RT}{nF} \ln \frac{f(a_1)}{f(a_2)} \qquad (1)$$

where E is the potential of either the cathode or the anode, E_0 is the corresponding standard potential, $f(a_1)$ and $f(a_2)$ are functions of the activity coefficients of the ions in the reduction and oxidation stages of each electrode, n represents the number of electrons involved, F is the Faraday constant (96,500 C), R is the gas constant, and T the absolute temperature.

The potential of each electrode E_0 is related thermodynamically to the Gibbs free energy change, ΔG, by the expression

$$\Delta G = -nFE_0. \tag{2}$$

The free energy change, ΔG, differs from the heat of the reaction, to which it is related by the expression

$$\Delta G = \Delta H - T\Delta S \tag{3}$$

where ΔS is the entropy factor, and the efficiency of the whole process is then given by the equation

$$\frac{\Delta G}{\Delta H} = 1 - \frac{T\Delta S}{\Delta H} \tag{4}$$

Since under ambient conditions $T\Delta S$ is small compared with ΔH, the efficiency is close to 1.

The open-circuit cell voltage is given by the difference between the potentials of the cathode and the anode:

$$E = E_c - E_a \tag{5}$$

It is obviously an advantage to use a couple, having electrode potentials as widely spaced numerically as possible, hence the efforts to develop cells with lithium anodes ($E_0 = -3.0$ V) and fluoride cathodes ($E_0 = +2.85$ V), for which the theoretical open-circuit voltage would be around 6 V. With some exceptions, these voltaic cells can be stored in a state of quasiequilibrium, sometimes for long periods without any loss of capacity. The desired chemical reactions are instantly started simply by closing the external circuit, when an electric current flows from the cathode to the anode, signifying a movement of electrons in the reverse direction. During the discharge process, the cathode is reduced by electrons, released by the oxidation of the anode, and carried across the intervening layer of electrolyte by the electrically charged ions which it contains. With most voltaic cells, the overall process of discharge is reversible, that is, the chemical compounds can be regenerated to a greater or lesser extent by charging with a direct current passed through the cell in the reverse direction. In some systems, this discharge–charge cycle can be repeated a large number of times without any significant fall in the capacity of the cell; such systems are known as "secondary" batteries or "accumulators." In others, the recharging process is less efficient and the compounds either cannot be reformed at all or, if they can, to only a limited degree. In these cases when the

cell or battery is fully discharged, it is more economical to discard it, and batteries of this type are referred to as "primary" batteries. As mentioned above, both primary and secondary batteries store energy and, although the term *storage battery* is often reserved for secondary batteries, or accumulators, it is equally applicable to primary batteries.

The electrochemical reactions which take place during discharge and, in the case of secondary batteries during recharge, are combined reduction–oxidation or "redox" processes, and in this respect they bear some resemblance to the combustion processes in which coal or petroleum products are burned in air. In the latter case, however, the free energy change manifests itself almost entirely as heat. As indicated by Eq. (4) above in electrochemical cells the bulk of the free energy is released as electrical energy. Depending on the rate at which this energy is used, that is, on the rate of the discharge, there are some losses as heat, but these are generally limited to less than 30% of the total amount, which is thermodynamically available.

1.4. Kinetic Aspects of Electrode Reactions

O/C values in Table 1 apply only under equilibrium conditions, when the exchange currents between electrode and electrolyte are extremely small. When the steady state is interrupted by discharge or charge, with the release of electrons into the external circuit, work is performed at each electrode. The electrode potentials change numerically from the equilibrium values by an amount known as the "overpotential" or "overvoltage." Since the function of voltaic cells is to supply energy (watt-hours) or power (watts) to do useful work, the current–voltage relationships are of prime importance. The vector causing the fall in voltage is usually referred to as "polarization" and, as has been indicated by Kortum and Bockris[6] and others, this may be divided into three broad categories:

(a) Activation polarization, which is a measure of the energy required to initiate the electron transfer reactions.

(b) Concentration polarization, arising from changes in the concentration of the reacting species in the electrodes and the electrolyte and operated against the forces of diffusion, which tend to equalize the conditions at the electrode–electrolyte interface.

(c) Resistance polarization, caused partially by the change in the concentration of the electrolyte due to factor (b) and also to the formation on the surface of the electrode of solid reaction products which have a higher electrical resistivity than the substrate of the active mass itself.

The relation between the overvoltage (n) and the current density (I) on the electrode is represented by the empirical equation, first devised by Tafel:

$$n = a - b \log I \tag{6}$$

where a and b are constants, b being defined by the expression $2.303RT/\alpha F$. α, the so-called transfer coefficient, represents the reciprocal of the number of electrons involved in the reactions. The validity of this relationship has been well established. Values for b vary between 0.07 and 0.19, the mean being around 0.12, which is the value when the transfer coefficient is 0.5, corresponding to a two-electron transfer reaction. The value of a, which represents the overvoltage when the current density is unity, varies according to the electrode.

1.5. Discharge-Voltage Characteristics

When a cell is discharged, for reasons mentioned, there is an immediate fall in the cell voltage. Depending on the rate of the discharge, i.e., the current density, the voltage may fall at a fairly uniform rate until the effects of polarization become predominant, when there is a sudden change in voltage with time. Figure 2 shows typical discharge-voltage curves for some primary cells. The sudden point of inflection at the end of some of these curves indicates that little useful energy in the form of W-h can be obtained by continuing the discharge beyond what is usually called the "knee" of the curve. This point of inflection is more pronounced when cells are discharged at constant current rather than through a fixed resistance. In the latter case the current falls with the voltage and the curves are smoother. The curves also become steeper as the rate of discharge increases, as is evident from the curves for the Leclanché cells.

The relation between the current density, $I(\mathrm{A/cm^2})$, and the duration of the discharge, t(min), is given by the empirical expression, originally deduced by Peukert (1897):

$$tI^n = k \tag{7}$$

where n and k are constants, characteristics of the system under consideration. This expression may also be written as $n \log I = \log k - \log t$, giving a linear

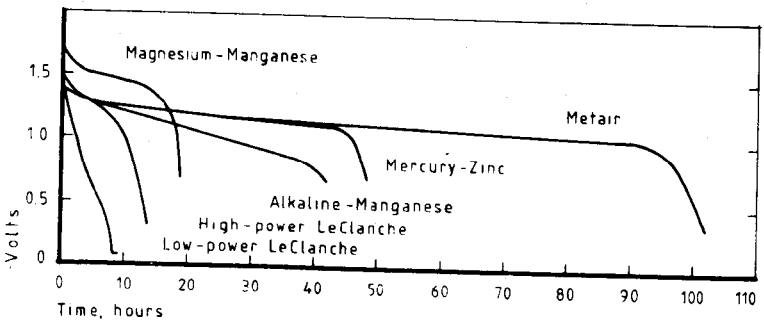

Figure 2. Typical discharge-voltage curves of D-size primary cells at 250 mA.[7]

relation between log I and log t, with n equal to the slope of the graph. Values of n generally fall around 1.30/1.40. The value of k varies according to the system. If two values of the current and the duration of the discharge to a standard final voltage are known, it is possible to derive corresponding outputs for any rate of discharge.

2. Classification of Primary Cells and Batteries

There are several ways in which primary batteries could be classified, e.g., by anode or cathode, type of service, whether for equipment calling for high or low rates of discharge, and so on. As far as the service is concerned, it is difficult to make clear distinctions, since, in many cases different systems are used for the same application. Probably the most satisfactory classification is by electrolytes, since this lays stress on the most outstanding differences between different cells.

Table 1 lists primary batteries classified in this way. The following points should be noted.

a. Some systems, which have been used extensively in the applications listed, are no longer in demand. The technology is, however, still available and manufacture could be resumed at short notice. They have therefore been included. They are marked N/D.

b. With some systems, the electrolyte is stored in a separate container, usually integral with the cell or battery elements, and the unit is primed by piercing the electrolyte container just before use. These batteries are referred to as "reserve" or "self-priming" batteries.

c. Some systems are primed either by admitting water or by dipping the whole unit in water. This applies particularly to systems primed with seawater. They are usually referred to as "water-activated" (W/A) batteries.

d. Thermal batteries are primed by igniting an external pyrotechnic heat source, usually consisting of a mixture of a metal powder and chromate or perchlorate. The heat melts the eutectic electrolyte and the discharge starts at once. These systems have a long shelf life and give high current drains for periods of a few minutes, with outputs of 1–2 kWmin.

e. Ammonia-vapor-activated batteries are also heat activated, the ammonia vapor then released, is absorbed by the thiocyanate electrolyte, and the discharge begins. These systems also have a long shelf life. Classes d and e have few, if any commercial applications, but they have found useful service in specialized military equipment.

f. Standard Clark and Weston cells are not used as sources of energy or power, but they fulfill a unique and very important role in providing a standard of reference for the unit of electromotive force.

g. Fuel cells are not included in the table, although they are technically primary power sources, since the oxidant and fuel are continuously consumed

during each discharge and cannot be regenerated. They differ from voltaic cells, however, in that the active masses of the cathode and the anode are stored outside the reaction vessel and fed into the reaction zone as the discharge proceeds. They will be dealt with in a separate section.

3. Some Properties of Cathodes, Anodes, and Electrolytes

3.1. Cathodes

As indicated in Table 1, the majority of the cathodes are metallic oxides. Their role is to provide the oxidant for the electrochemical oxidation of the anode, which takes place during the discharge. They should therefore accept electrons readily, and in the process the metals are reduced to a lower valency state by a reaction of the type

$$C_xO_y + H_2O + 2e = C_xO_{y-1} + 2OH^- \tag{8}$$

The metals of which these oxides are composed all exhibit more than one valency and readily pass from a higher to a lower valency state. In the case of the oxides of silver and copper, they may be reduced to the metallic state by the discharge process.

All have one or two electrons in the outer shell and, in some cases, electrons are available from unfilled *D* orbitals.

In the air depolarized systems, oxygen serves as the cathode. In this case the gas must be passed over a catalyst, such as silver or platinum, suitably distributed throughout the porous current collector, and this results in the following reaction:

$$O_2 + 2H_2O + 4e = 4OH^- \tag{9}$$

Other anions, such as sulfur and the halogens fluorine, chlorine, bromine, and iodine, all of which are electron acceptors, can therefore perform an oxidizing function and serve as cathodes in the systems listed in Table 1.

In general the products of the discharge reaction have a relatively low electrical conductivity, and current collectors are necessary to conduct the electrons into the reaction zones. These sometimes also serve the dual role of supports for the active mass and take a variety of forms, e.g., carbon rods or plates, metallic grids, and meshes of all types, distributed throughout the active mass in a manner designed to keep the internal resistance of the electrode to a minimum.

3.2. Anodes

As indicated in the table, anodes are metals, which are corrodable in the electrolyte to varying degrees and thereby provide "fuel" for the redox

Table 1
Classification of Primary Batteries

Designation or application	Electrodes: Cathode	Electrodes: Anode	Electrolyte	O/C emf, V	References
		1. *Aqueous electrolyte—solutions of inorganic salts*			
"Dry" Leclanché	MnO_2	Zn	$NH_4Cl/ZnCl_2$	1.50	8, 9, 10
Air depolarized	O_2	Zn	$NH_4Cl/ZnCl_2$	1.40	10, 11
Torpedo W/A[a]	AgCl	Mg	NaCl; seawater	1.30	8, 12
High power W/A	Cl_2[b]	Al alloy	$AlCl_3$ + NaCl; seawater	2.10	13, 14
Radar-Sonde W/A N/D[c]	Cu_2Cl_2	Mg	NaCl or KCl	1.20	8
Meteorological balloon W/A N/D	PbO_2	Mg	NaCl or KCl	1.80	8
		2. *Aqueous electrolyte—solutions of alkali or acid*			
Alkaline manganese					
"Premium" Leclanché	MnO_2	Zn	KOH	1.50	15
Military applications	MnO_2	Mg	KOH	1.65	15
Mercury–zinc,					
Rubens–Mallory	HgO	Zn	KOH	1.30	8, 16, 17
Mercury–indium	HgO	In/Bi	KOH	1.16	18
Air depolarized	O_2	Zn	KOH	1.40	17, 19, 20
Lalande–Chaperon N/D	CuO	Zn	NaOH	1.10	21, 22, 23
Torpedo:RD fuze	PbO_2	Pb	$HClO_4$ (reserve)	1.95	25, 26
Lifeboat radio N/D	PbO_2	Zn	H_2SO_4 (reserve)	2.20	8

		3. *Nonaqueous electrolytes*			
Panasonic high energy (Japan)	$(CF_x)_n$	Li	Propylene carbonate with $LiClO_4$	2.80	27, 28
Lithium (GTE)	$SOCl_2$	Li	Thionyl chloride ($SOCl_2$) with $LiCl$–$AlCl_3$	3.60	29, 30
Lithium (Mallory)	$SOCl_2$	Li	Acetonitrile or polypropylene carbonate with $LiClO_4$	2.95	31, 32, 33, 34
Lithium (SAFT)	CuO	Li	Propylene carbonate with $LiClO_4$	2.35	35
		4. *Solid electrolyte*			
Iodide cell	RbI_3	Ag	Rubidium silver iodide ($RbAg_4I_5$)	0.66	36
		5. *Molten salt electrolyte*			
Thermal batteries	Chromates	Ca or	KCl + LiCl		
Military applications	Fe_2O_3	Mg or Li	300 to 600°C	0.80	37, 38
		6. *Ammonia vapor activated* (AVA)			
Military applications	V_2O_5 or	Mg or	(NH_3)		
	PbO_2 or	Zn	KCNS or LiCNS	1.50	
	*m*DNB[d]	Mg			39, 40
		7. *Standard cells—aqueous electrolytes*			
Clark cell	Hg	Zn	Sat. aq. $HgSO_4$ plus $ZnSO_4$	1.457	41
Weston cell	Hg	Cd	Sat. aq. $HgSO_4$ plus $CdSO_4$	1.018	

[a] Water activated.
[b] Trichlorotriazinetrione.
[c] No longer in demand.
[d] Metadinitrobenzene.

reaction. In the general case, this may be represented by the equation

$$A + 2OH^- = A(OH)_2 + 2e \quad (10)$$

Metallic anodes meet the criterion of having a high electrical conductivity. As in the case of cathodes, however, the interface between the anode and the electrolyte becomes polarized by the products of the discharge reaction and the electrical conductivity of these boundary layers therefore steadily falls. Problems of mass transport also increase as the current density increases and it is usual, particularly in batteries, which are expected to sustain heavy currents to extend the surface area as much as possible by making the electrodes porous. In such cases, as for the cathode, a metal grid may serve as both a support for the active mass and a current collector.

3.3. Electrolytes

The electrons, exchanged in the chemical processes, are carried across the intervening layer of electrolyte by the electrically charged ions which it contains. In these processes some of the ions are discharged and deposited on one or other of the electrodes. To perform its function efficiently, therefore, the electrolyte must have a high concentration of ions and these should preferably have high mobilities. Water is a very suitable medium. It dissociates into the very mobile hydrogen and hydroxyl ions:

$$H_2O \rightleftharpoons H^+ + OH^- \quad (11)$$

The hydrogen ion or proton is an electron acceptor and the hydroxyl ion is an electron donor. As noted above, these are the basic requirements for reduction and oxidation. The degree of ionization of pure water is, however, too low and this must be increased by the addition of acids, bases, or salts. As indicated in Table 1, aqueous solutions of this kind form by far the most widely used electrolytes, and they have the added advantage of satisfying the criteria at ambient temperatures.

Molten salts also possess many of the requirements, particularly high ionic conductivity, and are used in some primary cells, notably fuel cells, and cells having as anodes the metals calcium or lithium, which react explosively with water and cannot therefore be used with aqueous electrolytes. For this reason also, some nonaqueous organic electrolytes have recently come into service, but their low electrical conductance, which may be increased by additions of salts such as lithium perchlorate, limits their use. Some solid electrolytes have minimal electronic but adequate ionic conductivity. One example is cited in Table 1.

Table 2
Properties of Cathodes

Active material	Mass density, g/ml	Equivalent weight, g/Faraday	Energy density, /Ah/kg
MnO_2	5.0	43.5	616
HgO	11.0	108	248
CuO	6.0	72	312
PbO_2	9.4	120	223
NiOOH	7	91	295
Ag_2O	7	62	432
AgCl	5.6	144	156
$CuCl_2$	3	67	400
S	2	16	1675
O_2	—	8	3350
Cl_2	—	35.5	755
F_2	—	19	1410
Br_2	3.1	80	355

4. Performances of Primary Cells

4.1. Theoretical Considerations

Weight and volume are crucial factors in portable battery systems and considerable efforts are expended annually on research and development to reduce the weight of existing cells and to find new lightweight systems. The parameters under constant review are the "energy density" and the "power density." In terms of weight, these comprise the watt-hours per kilogram and the watts per kilogram, respectively and, in terms of volume, the watt-hours per dm^3 and watts per dm^3. Two factors are involved, firstly the capacity in ampere-hours or the current in amps at any given rate of discharge, and secondly, the mean voltage of the system at the particular rate of discharge. Tables 2 and 3 show the relevant properties—the mass density and the

Table 3
Properties of Anodes

Active material	Mass density, g/ml	Equivalent weight, g/Faraday	Energy density, Ah/kg
Pb	11.3	104	258
Cd	8.7	56	480
Zn	7.1	33	812
Mg	1.7	12	2230
Na	0.97	23	1170
Li	0.53	7	3830

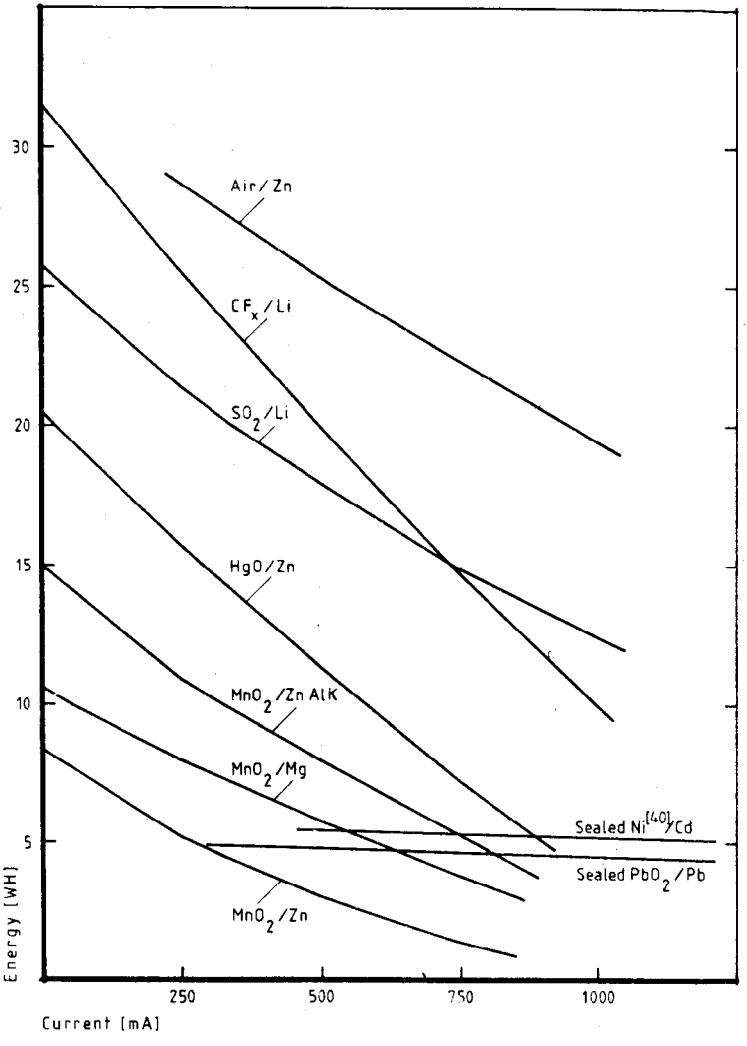

Figure 3. Outputs of D-size primary cells at different rates of continuous discharge [Courtesy of SAFT Co. (U.K.).]

theoretical energy density of the active materials used in cathodes and anodes, respectively.

Outstanding features of these two tables are the high energy densities of cathodic oxygen, sulfur, and the halogens, and anodic magnesium and lithium,

and the relatively low energy densities of both the cathodic and anodic materials used in the conventional lead–acid and alkaline storage batteries.

As mentioned above, the voltage of the couple must also be taken into account and as this is represented by the difference between the potentials of the two electrodes, it is an advantage to use a couple, having electrode potentials as widely spaced as possible.

4.2. Practical Outputs of Primary Cells

Figure 3 shows the outputs in terms of watt-hours of a number of primary cells on continuous discharge at different rates. For purposes of comparison, values are also shown for rechargeable nickel–cadmium and lead–acid sealed cells. An interesting feature of these curves is that, while the rechargeable cells show increasing advantages at the higher rates of discharge, at the lower rates, the primary systems have higher energy densities.

References

1. G. W. Vinal, *Primary Batteries*, 2nd ed., John Wiley and Sons, New York (1951).
2. G. W. Heise and N. C. Cahoon, eds., *The Primary Battery*, Vol. 1, John Wiley and Sons, New York (1971).
3. M. Barak, *J. R. Soc. Arts* **116**, 815 (1968).
4. A. I. Harrison and K. Peters, in *Power Sources 3*, D. H. Collins, ed., Oriel Press, Newcastle (1970), pp. 211–225.
5. Private communication from the SAFT Co. (UK) Ltd., 1974.
6. G. Kortum and J. O'M. Bockris, *Textbook of Electrochemistry*, Vol. 2, Elsevier, New York (1962).
7. Energy Conversion Ltd., Metair Catalogue, 1972.
8. M. Barak, *IEE Rev.* **117**, 1561–1584 (1970).
9. M. Barak, *Electron. Power*, 288–296, (August/September 1972).
10. A. M. Bredland, J. W. Paulson, T. G. Messing, and B. Bergum, Design and performance of novel thin plate Leclanché battery, paper presented at the 10th International Power Sources Symposium, Brighton, England, 13–16 September 1976.
11. Catalogue of Le Carbone (GB) Ltd., Portslade, Sussex, Great Britain, 1976.
12. J. P. Harivel, J. Doll, R. S. Cattle, and R. T. Gale, in *Power Sources 4*, D. H. Collins, ed., Oriel Press, Newcastle (1972), pp. 51–61.
13. L. J. Pearce and R. Holland, in *Power Sources 4*, D. H. Collins, ed., Oriel Press, Newcastle (1972), pp. 63–77.
14. A. Gibson, L. J. Pearce, and D. C. P. Birt, in *Power Sources 5*, D. H. Collins, ed., Academic Press, London (1974), pp. 447–464.
15. J. J. Murphy, *Chem. Technol.*, 487–494 (August 1971).
16. P. Ruetschi, *Power Sources 4*, D. H. Collins, ed., Oriel Press, Newcastle (1972), pp. 381–400.
17. G. W. Heise and N. C. Cahoon, eds., *The Primary Battery*, Vol. 1, John Wiley and Sons, New York (1971), pp. 207–223.
18. G. W. Heise and N. C. Cahoon, eds., *The Primary Battery*, Vol. 1, John Wiley and Sons, New York (1971), pp. 173 and 174.
19. E. R. Musgrave and G. W. Walkiden, in *Power Sources 3*, D. H. Collins, ed., Oriel Press, Newcastle (1970), pp. 511–523.

20. H. R. Espig and D. F. Porter, in *Power Sources 4*, D. H. Collins, ed., Oriel Press, Newcastle (1972), pp. 327–345.
21. H. R. Espig, J. W. Cretzmeyer, and R. S. Melrose, Commercial zinc–air batteries, paper presented at the 10th International Power Sources Symposium, Brighton, England, 13–16 September 1976, p. 13.
22. L. Langrish, A primary reserve type zinc–air battery for military manpack applications, paper presented at the 10th International Power Sources Symposium, Brighton, England, 13–16 September 1976, p. 9.
23. R. E. Biddick, J. W. Cretzmeyer, and D. L. Douglas, *Power Sources 5*, D. H. Collins, ed., Academic Press, London (1974), pp. 411–424.
24. G. W. Heise and N. C. Cahoon, eds., *The Primary Battery*, Vol. 1, John Wiley and Sons, New York (1971), pp. 191–206.
25. C. J. Bushrod and N. A. Hampson, *Trans. Inst. Met. Finishing* **48**, 131 (1970).
26. N. A. Hampson and C. J. Bushrod, *J. Appl. Electrochem.* **4**, 1 (1974).
27. M. Fukuda and T. Iijima, in *Power Sources 5*, D. H. Collins, ed., Academic Press, London (1974), pp. 713–728.
28. R. G. Gunther, in *Power Sources 5*, D. H. Collins, ed., Academic Press, London (1974), pp. 729–740.
29. D. Linden, N. Wilburn, and E. Brooks, *Power Sources 4*, D. H. Collins, ed., Oriel Press, Newcastle (1972), pp. 483–491.
30. J. J. Auborn and N. Marincic, in *Power Sources 5*, D. H. Collins, ed., Academic Press, London (1974), pp. 683–694.
31. Per Bro, R. Holmes, N. Marincic, and H. Taylor, in *Power Sources 5*, D. H. Collins, ed., Academic Press, London (1974), pp. 703–712.
32. A. N. Dey and Per Bro, Primary Li/$SOCl_2$ cells 111. The effect of the electrolyte and electrode variables on the energy density and the voltage delay, paper presented at the 10th International Power Sources Symposium, Brighton, England, 13–16 September 1976.
33. E. D. Wilmar, Experience with the use of lithium primary batteries for military field operation, paper presented at the 10th International Power Sources Symposium, Brighton, England, 13–16 September 1976, p. 14.
34. A. N. Dey, *Electrochim. Acta* **22**(11), 885–860 (1976).
35. G. Lehmann, G. Gerbier, A. Brych, and J.-P. Gabano, in *Power Sources 5*, D. H. Collins, ed., Academic Press, London (1974), pp. 695–701.
36. G. W. Heise and N. C. Cahoon, eds., *The Primary Battery*, Vol. 1, John Wiley and Sons, New York (1971), pp. 414–418.
37. D. Bush and A. Baldwin, in *Power Sources 5*, D. H. Collins, ed., Academic Press, London (1974), pp. 581–594.
38. G. C. Bowser, D. Harney, and F. Tepper, A high energy density molten anode thermal battery, paper presented at the 10th International Power Sources Symposium, Brighton, England, 13–16 September 1976, p. 10.
39. G. W. Heise and N. C. Cahoon, eds., *The Primary Battery*, Vol. 1, John Wiley and Sons, New York (1971), pp. 360–369.
40. C. G. Elzinga and C. G. Vermeulen, in *Power Sources 5*, D. H. Collins, ed., Academic Press, London (1974), pp. 603–616.
41. G. W. Heise and N. C. Cahoon, eds., *The Primary Battery*, Vol. 1, John Wiley and Sons, New York (1971), pp. 433–477.

5

Primary Batteries—Leclanché Systems

AKIYA KOZAWA

1. Introduction

The purpose of this chapter is to summarize the recent progress in performance and technology of Leclanché-type MnO_2–Zn dry cells including zinc chloride electrolyte cells. Major reactions in the cells are also summarized. The basic wet-type Leclanché cell, a MnO_2–Zn cell using NH_4Cl solution, was invented around 1868 by G. Leclanché, and shortly after a dry cell version of the cell system using an immobilized electrolyte was invented by C. Gassner in Germany,[2] by S. Yai in Japan, and by Helessens in Denmark.[3] Since then, dry cells have been produced commercially in large quantities for more than 100 years. Although the basic chemicals used for the anode and the cathode as well as the size of the cells remained unchanged since the early 1900s, the performance has been greatly improved, particularly in the past 25 years.[4,5] The improvements are mainly attributed to use of electrolytic manganese dioxide (EMD) instead of natural MnO_2 ore and use of a paper-lined construction with $ZnCl_2$ electrolyte instead of NH_4Cl electrolyte.

2. Progress in Performance

Figure 1 shows a summary of dry cells on the market today. Figure 2 shows the performance in the following three tests: (a) 2.25-Ω continuous discharge,

AKIYA KOZAWA • Battery Products Division, Union Carbide Corporation, Cleveland, Ohio 44101.

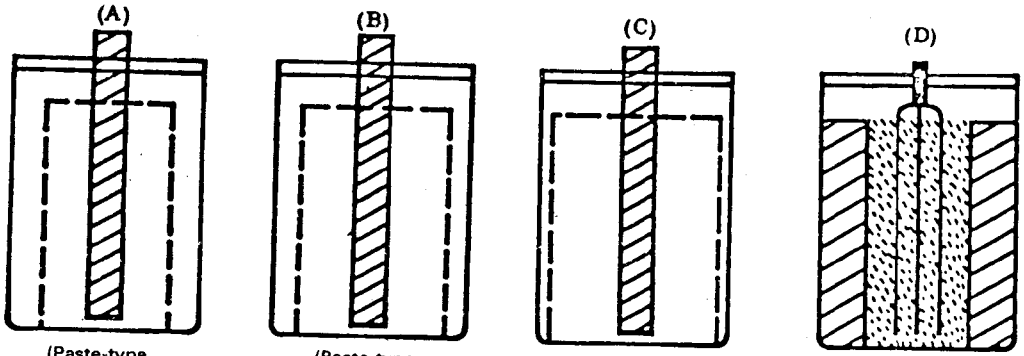

	(A) (Paste-type natural ore cell)	(B) (Paste-type EMD cell)	(C) (Paper-lined EMD cell)	(D) (Alkaline MnO_2–Zn cell)
Commercial production	1900–present	1960–present	1970–present	1965–present
Kind of MnO_2	Natural ore	EMD	EMD	EMD
Amount of MnO_2 in the cathode g (AH)	21 g (6.5 Ah)	23 g (7 Ah)	25 g (8 Ah)	39 g (12 Ah)
Zn anode: Amount of Zn (Ah)	Can: 14 g (12 Ah)	Can: 18 g (15 Ah)	Can: 21 g (17 Ah)	Powder: 14 g (12 Ah)
Electrolyte	$NH_4Cl + ZnCl_2$	$NH_4Cl + ZnCl_2$	$ZnCl_2$	KOH
Carbon	A.B. 4 g	A.B. 3 g	A.B. 6 g	Graphite: 4 g
Cell weight	85 g	96 g	105 g	123 g
Energy density (Wh/cm^3)	0.08	0.12	0.15	0.21

Figure 1. Technical progress in MnO_2–Zn primary cells: Comparison of D-size (R20) cells. D-size (U.S.A.) = R20 (International) = SUM-1 (Japan). D-size cell: Outside diameter including the jacket is about 3.4 cm and the height is about 6 cm. The diameter of the zinc can is 3 cm and the height of the zinc can is 5 cm. The total volume of the cell is about 53 cm^3. The total volume of the zinc can is about 37 cm^3. A.B. = Acetylene black.

(b) 2.25-Ω LIF test (discharge for 4 min once an hour, 8 hr/day), and (c) 25-Ω test (discharge for 4 hr/day. A, B, C, and D in Figure 2 correspond to those in Figure 1. For the purpose of comparison, alkaline cells are included in Figure 1.

While the 2.25-Ω continuous test is not a realistic test of a consumer use, it does demonstrate the remarkable progress in the cell performance. Such a dramatic improvement (shown in Figure 2) is not only due to the greater amount of MnO_2 used in a cell, but also due to the improved utilization of MnO_2. The 2.25-Ω LIF test is a somewhat more realistic test to evaluate practical performance in lighting use. In this test, the MnO_2 utilization is about 50% for cells of type A (natural MnO_2 ore) and 70–85% for cells of type B, C, and D (EMD cells). The 25-Ω test is a light drain test which is intended to simulate discharge capacity for radio application. In this test the MnO_2 utilization reaches 85–90% in EMD cells, whereas the utilization of natural ore is only 60%. From these data we can see that a key material in dry cell performance is the MnO_2 in the cathode.

3. Major Technical Changes

Major technical developments responsible for the great performance improvements, shelf life, and leakage characteristics in the past 25 years are as follows:

(a) Use of EMD instead of Natural MnO_2 ores.
(b) Improved cell sealing which minimizes moisture loss and oxygen ingress during storage.
(c) Change of electrolyte from $NH_4Cl + ZnCl_2$ solution (type A, B) to $ZnCl_2$ solution (type C) or to KOH solution (type D). Figure 3 shows the range of composition.
(d) Change of a starch separator layer of 1–2-mm-thick layer as in type A and B cells to a thin coated paper separator as in type C cell.

Use of EMD instead of natural MnO_2 ore provides the high closed circuit voltage during discharge because EMD has much higher voltage and less polarization as shown in Figure 4. It was pointed out by Kozawa[9] that polarization of MnO_2 evaluated in KOH solution is useful to evaluate polarization of MnO_2 in Leclanché cells.

The cathode mix of dry cells is a mixture of MnO_2 powder and acetylene black (see composition in Figure 1) containing sufficient electrolyte for ionic conduction. Moisture loss from the cell and oxygen ingress due to a poor seal structure at the top of the cell, will increase the ionic *IR* drop and reduce the discharge capability. Seal improvements in modern dry cells is an important factor in the great improvement of the shelf life. Today's dry cells of type B and

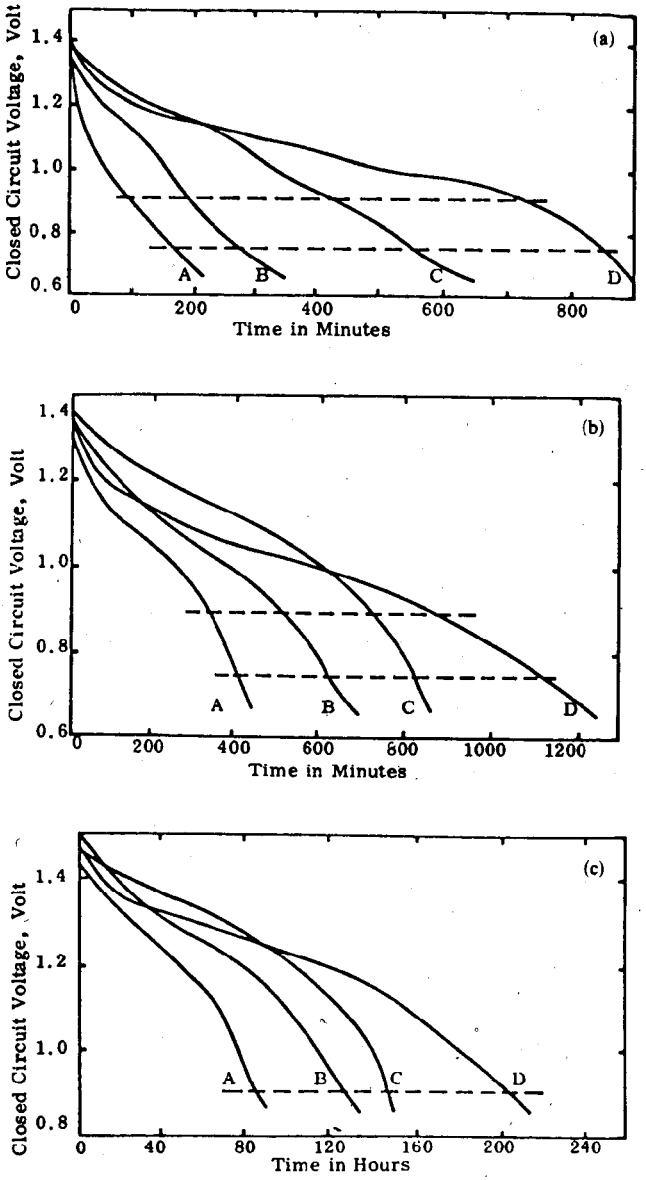

Figure 2. Performance of D-size cells. (a) Discharge curves of D-size cells on 2.25 Ω continuous test at 21°C. (b) Discharge curves of D-size cells on 2.25 Ω LIF test at 21°C. (c) Discharge curves of D-size cell through 25 Ω, 4 hrs per day at 21°C.

Data for Figure 2a

Curve	Discharge time to 0.9 V	Ah	U (%)[a]	Discharge time to 0.75 V	Ah	U (%)
A	95 min	0.79	12.2	162 min	1.26	19.5
B	190 min	1.60	22.5	274 min	2.16	30.4
C	435 min	3.71	47.7	557 min	4.44	57.1
D	735 min	6.21	59.5	855 min	6.75	64.7

[a] U, utilization based on the one-electron reaction $MnO_2 + H_2O + e^- \rightarrow MnOOH + OH^-$.

Data for Figure 2b

Curve	Discharge time to 0.9 V	Ah	U (%)	Discharge time to 0.75 V	Ah	U (%)
A	340 min	2.82	43.7	415 min	3.21	49.7
B	520 min	4.33	60.6	625 min	4.86	68.5
C	730 min	6.15	79.0	820 min	6.45	82.9
D	880 min	7.40	70.9	1120 min	8.79	84.2

Data for Figure 2c

Curve	Discharge time to 0.9 V	Ah	U (%)
A	84 hrs	3.91	60.5
B	127 hrs	6.07	85.5
C	147 hrs	7.03	90.4
D	204 hrs	9.63	92.2

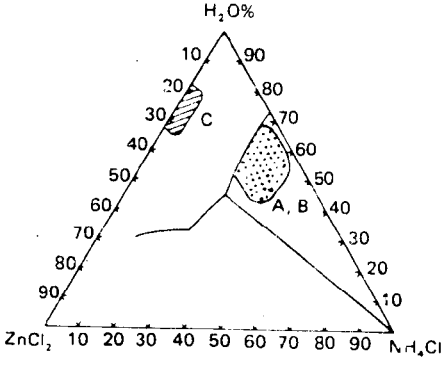

Figure 3. Electrolyte composition used for dry batteries. A, B; Leclanché cells of types A and B in Figure 1. C: $ZnCl_2$ cell of type C in Figure 1.

C will not lose the discharge capacity more than 5–7% per year when stored at room temperature.[6]

Use of $ZnCl_2$ solution, instead of $NH_4Cl + ZnCl_2$ solution, improves the leakage characteristics of the cell as will be discussed later in the discussion on the cell reactions.

Use of a paper-lined separator construction (type C cell), instead of a starch construction (type A and B cells), not only reduces the *IR* drop considerably, but also provides more space for active ingredients, i.e., MnO_2. These technical aspects of $ZnCl_2$-type (type C cell) cells were summarized and compared to NH_4Cl cells in a recent review by Kobayashi.[6]

4. Chemical Reactions in the Cell

The basic reactions of MnO_2 in NH_4Cl, $NH_4Cl + ZnCl_2$, and KOH solutions were studied by Kozawa, Powers, and Yeager[7,8] using H_2O and D_2O. It was established by their work that MnO_2 discharges in two steps (see Figure 4), the first step being a one-phase solid redox system having an S-shaped potential decrease, and the second step being the two-phase solid discharge having a constant potential. The main discharge reaction in the useful life of dry cells is the first step reaction [Eq. (1)] as pointed out recently[9].

$$MnO_2 + H_2O + e^- \rightarrow MnOOH + OH^- \qquad (1)$$

Although Eq. (1) gives us an impression that the original structure of MnO_2 is converted to a different structure of MnOOH, the actual reaction proceed by injection of electrons and protons into the MnO_2 lattice without changing its original MnO_2 structure.[7,8] This unique reaction takes place because both protons and electrons can move fairly freely in the MnO_2 structure. We can see

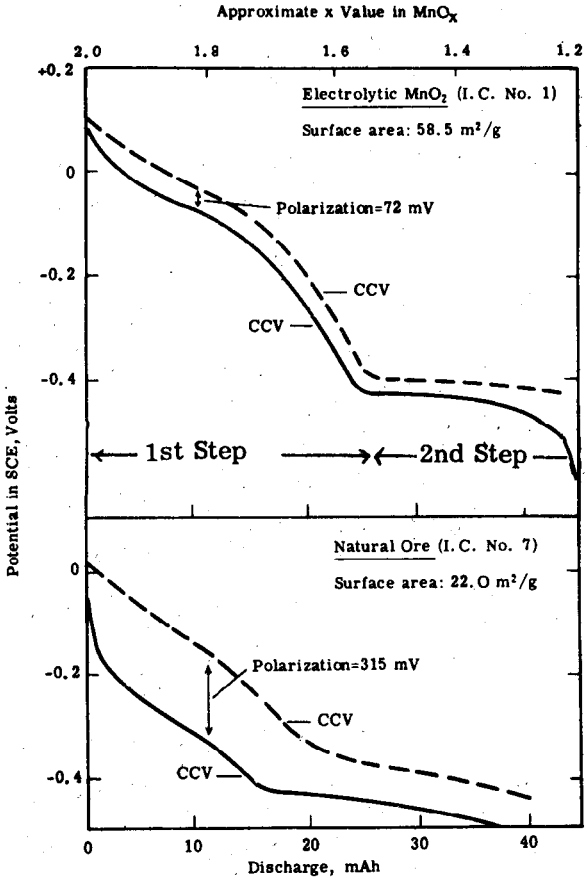

Figure 4. Polarizations of EMD and natural MnO_2 ore (I.C. = International Common samples; see Table 1).

this unique point by comparing to an ordinary battery reaction (two-phase solid reaction) such as $PbO_2 + H_2SO_4 + e \rightarrow PbSO_4 + H_2O$. In the two-phase reactions, which include most battery reactions in the anode and cathode, two distinctly different solids (PbO_2 and $PbSO_4$ in the example above) coexist in the system and the open-circuit voltage remains constant regardless of the depth of discharge. Understanding the presence of these two types of reactions for batteries is very important and useful.[10]

We can write the main reactions in the cell as follows:

A. Potential-producing electrochemical reactions

i. Cathode:

$$MnO_2 + H_2O + e^- \rightarrow MnOOH + OH^-$$

ii. Anode

$$Zn \rightarrow Zn^{2+} + 2e$$

B. Precipitation reaction in the cathode or separator layer

i. In $ZnCl_2$ cells (type C in Figure 1).

$$Zn^{2+} + OH^- + ZnCl_2 \rightarrow ZnCl_2 \cdot 4Zn(OH)_2$$

ii. In NH_4Cl cells (type A and B in Figure 1):

$$Zn^{2+} + OH^- + NH_4Cl \rightarrow Zn(NH_3)_2Cl_2$$

C. Overall cell reactions

i. In $ZnCl_2$ cells:

$$8MnO_2 + 8H_2O + ZnCl_2 + 4Zn = 8MnOOH + ZnCl_2 \cdot 4Zn(OH)_2$$

ii. In NH_4Cl cells:

$$2MnO_2 + 2NH_4Cl + Zn = 2MnOOH + Zn(NH_3)_2Cl_2$$

The zinc anode produce Zn^{2+} ions (a mixture of complex ions $[ZnCl_4]^{2-}$, $[Zn(OH)_x(H_2O)_yCl_2]$, etc). The zinc ion solution of low pH (0–4) diffuses through the separator layer and moves into the cathode as shown in Figure 5. Since the cathode reaction produces OH^- ions, the acidic zinc solution produces precipitates: $ZnCl_2 \cdot 4Zn(OH)_2$ or $Zn(NH_3)_2Cl$ as a typical solid material. The precipitates are actually a mixture of a few solid compounds depending on the discharge condition and the electrolyte composition. When the discharge rate is high, Zn^{2+} ions tend to accumulate to form a concentrated zinc solution of very low pH (0 or less). Under this condition, water moves from

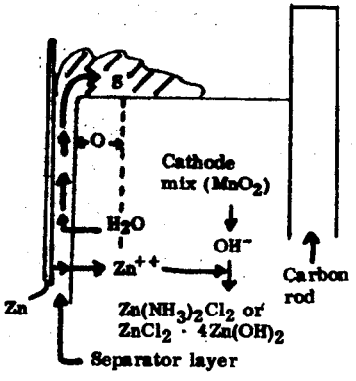

Figure 5. Reaction products in cells. S: Concentrated zinc solution called "spew." O: Outer layer of the cathode, where crystalline $Zn(NH_3)_2Cl_2$ precipitates.

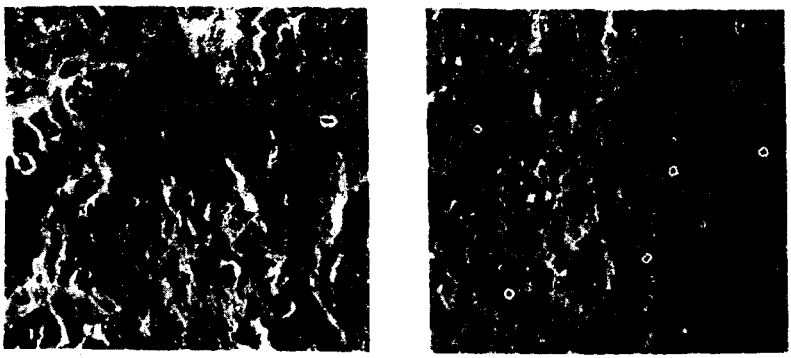

Figure 6. Precipitate material in the cathode of Leclanché and $ZnCl_2$ cells.

the cathode to the zinc anode instead of the movement of the zinc solution into the cathode. When water moves into the zinc solution near the Zn anode, often the zinc solution is pushed up into the upper air space of the cell (see Figure 5). Under some conditions of use, this may result in leakage as the gases produced in the cell are vented.

In the Leclanché cells, often the crystalline precipitate of $Zn(NH_3)_2Cl_2$ forms in the outer zone (O of Figure 5) of the cathode. This crystalline precipitates prevent the diffusion of the zinc solution into the cathode and also it increases the *IR* drop considerably. In the zinc chloride cells, the precipitate $ZnCl_2 \cdot 4Zn(OH)_2$ seems to be porous and allow ionic conduction even at high rate discharges. This was discussed by Kobayashi *et al.*[6] and they showed photos of the two compounds (Figure 6). Kobayashi *et al.*[6] also pointed out that in zinc chloride cells, the amount of H_2O in the cathode is important since it is a reactant and it also provides a medium of ionic conduction. They found a relation between the cell performance and the water content as shown in Figure 7. It clearly shows that the cell output depends on the H_2O content.

Many chemists were puzzled that addition of 10–20% $ZnCl_2$ to NH_4Cl solution or use of pure 20–25% $ZnCl_2$ solution instead of NH_4Cl solution, increase the discharge capacity, since $ZnCl_2$ is a discharge product. Kozawa pointed out in 1957 that the essential function of $ZnCl_2$ is the pH buffer action (prevent pH increase due to OH^- produced from MnO_2).[11] The MnO_2 potential is a function of pH: $E = E' - 0.059$ pH and the potential decrease when the pH increases.[17]

5. New Cells and Future Study Areas

In recent years there has been one new configuration of Leclanché cell on the market, the thin battery[13] used in a Polaroid film pack. Continued activity

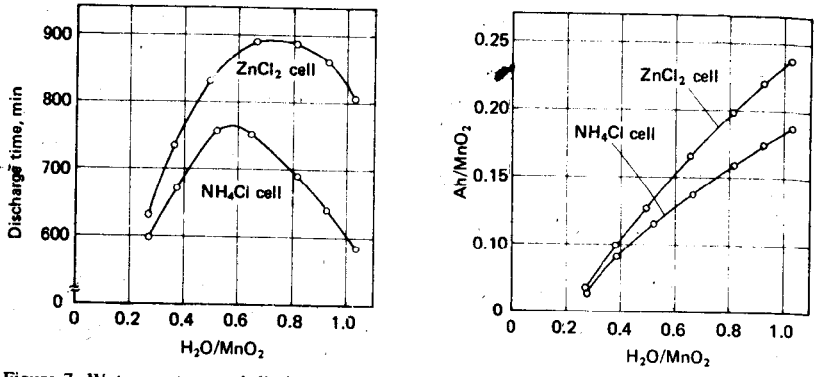

Figure 7. Water content and discharge capability of D-size (R20) $ZnCl_2$ cell at 4 Ω continuous discharge test to 0.9 V.[6]

also exists in terms of MnO_2–Zn cells with other electrolytes, e.g., a thin cell using $Zn(ClO_4)_2$ as electrolyte.[12]

Since manganese dioxide is a key material in Leclanché and $ZnCl_2$ as well as alkaline MnO_2 cells, an organized investigation of battery activity of MnO_2 was started in 1970 by the U.S. Electrochemical Society (Cleveland Section

Table 1
I.C. MnO_2 Samples Available from The Electrochemical Society Office[14]

Samples	Nature of sample	Source	Amount in the sample bottle
I.C. No. 1	Electrolytic MnO_2 made by Ti anode	Japan	About 1 kg
I.C. No. 2	Electrolytic MnO_2 made by Pb anode	Japan	About 1 kg
I.C. No. 3	Electrolytic MnO_2 made by C anode	Japan	About 1 kg
I.C. No. 4	Electrolytic MnO_2	LaPile Leclanché, France	About 1 kg
I.C. No. 5	Chemically prepared MnO_2	Japan Metals & Chemicals Co.	About 1 kg
I.C. No. 6	Beta MnO_2	A reagent grade chemical	500 g
I.C. No. 7	Natural MnO_2 ore	Ghana Ore	About 1 kg
I.C. No. 8	Chemically prepared MnO_2	Sedema, Belgium	About 1 kg
I.C. No. 9	Electrolytic MnO_2 (coarse grade)	Kerr-McGee Corp, U.S.A.	About 1 kg
I.C. No. 10	Electrolytic MnO_2	Kerr-McGee Corp, U.S.A.	About 1 kg
I.C. No. 11	Chemical MnO_2 made by chlorate process	Kerr-McGee Corp, U.S.A.	About 100 g
I.C. No. 12	Chemical MnO_2	Sedema, Belgium	About 1 kg
I.C. No. 13	Natural MnO_2	Comilog	About 1 kg

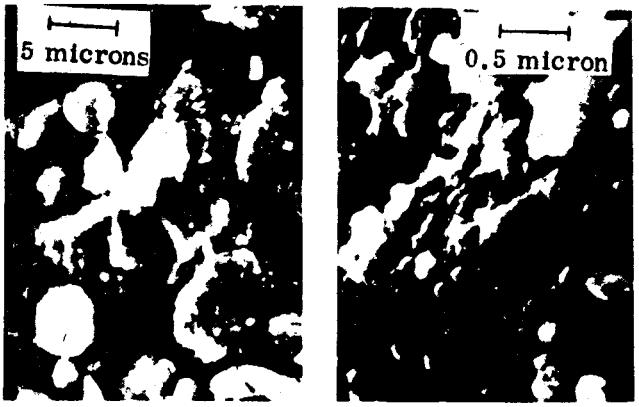

Figure 8. SCM photograph of EMD.

and Battery Division) by distributing I.C. (International Common) MnO_2 samples. The most active and useful MnO_2 for dry cells is EMD at this time. EMD has surface area in a range 40–50 m^2/g, and average pore size of 40–50 Å and average particle size is 10–20 μm. Although EMD is a highly porous solid powder, its density is 4.3 g/cm^2 and can be packed into limited spaces better than other MnO_2 powders. Table 1 shows the 12 I.C. MnO_2 samples available from the I.C. Sample Office for studies under international cooperation. All the physical, chemical, and electrochemical data of these I.C. MnO_2 samples are compiled in a book.[14] Figure 8 shows an SCM photograph of EMD. Specific research areas are summarized by the I.C. MnO_2 Sample Office.[15,16] Electrochemical reactions of MnO_2 are summarized in a review by Ruetschi *et al.*[18] and A. Kozawa.[19]

References

1. G. W. Heise, in *The Primary Battery*, Vol. 1, G. Heise and N. C. Cahoon, eds., John Wiley and Sons, New York (1971), Chap. 1.
2. C. Gassner, German Patent 37,748 (1886).
3. K. Takahashi, in *New Batteries*, S. Yoshizawa, ed., Tokyo Denki Daigaku Press, Tokyo (1978), Chap. 2, p. 18.
4. A. Kozawa, in *Progress in Batteries and Solar Cells*, Vol. 1, A. Kozawa and K. V. Kordesch, eds., JEC Press, Cleveland (1978), Chap. 54, pp. 249–260.
5. R. J. Brodd, A. Kozawa, and K. V. Kordesch, *J. Electrochem. Soc.* **125**, 271c (1978).
6. S. Kobayashi, J. Asaoka, A. Ohta, and J. Miyoshi, *Nat. Tech. Rept.* **24**, 256 (1978).
7. A. Kozawa and J. F. Yeager, *J. Electrochem. Soc.* **112**, 959 (1965); **405**, 113 (1966); **115**, 1003 (1968).
8. A. Kozawa and R. A. Powers, *J. Electrochem. Soc.* **113**, 870 (1966); **115**, 122 (1968); *Electrochem. Tech.* **5**, 535 (1967).

9. A. Kozawa, in *Power Sources 7*, J. Thompson, ed., Academic Press, New York (1979).
10. A. Kozawa and R. A. Powers, *J. Chem. Educ.* **49**, 587 (1972).
11. A. Kozawa and K. Sasaki, *Denki Kagaku* (*J. Electrochem. Soc. Japan*) **25**, 322 (1957).
12. Matsushita Electric Co., in *Progress in Batteries and Solar Cells*, Vol. 2, JEC Press, Cleveland (1979).
13. U.S. Patent 4,105,831 (August 8, 1978).
14. A. Kozawa and R. J. Brodd, in *Manganese Dioxide Symposium, Vol. 1, 1975, Cleveland*, The I.C. Sample Office, Cleveland, Ohio.
15. The I.C. Sample Office, in *Progress in Batteries and Solar Cells*, Vol. 1, A. Kozawa and K. V. Kordesch, eds., JEC Press, Cleveland (1978), p. 241.
16. The I.C. Sample Office, in *Progress in Batteries and Solar Cells*, Vol. 2, A. Kozawa and K. V. Kordesch, eds., JEC Press, Cleveland (1979), p. 101.
17. N. C. Cahoon, in *Primary Batteries*, Vol. 2, N. C. Cahoon and G. W. Heise, eds., John Wiley & Sons, New York (1975), Chap. 1, p. 40.
18. P. Ruetschi, R. Giovanoli, and P. Burki, in *Manganese Dioxide Symposium, Vol. 1, 1975, Cleveland*, The I.C. Sample Office, Cleveland, Ohio, p. 12.
19. A. Kozawa, Electrochemistry of MnO_2 and MnO_2 batteries, the U.S. Office of ECS of Japan, Cleveland, Ohio.

6

Primary Batteries—Alkaline Manganese Dioxide–Zinc Batteries

KARL KORDESCH

1. Introduction

One of the most important changes in the characteristics of the MnO_2–Zn dry cell as known before the 1960s[1] occurred when caustic electrolytes were introduced to the technology of this system on a large scale. The current-carrying capability, capacity, and shelf life increased considerably, and today this type of galvanic cell is the mainstay of the radio transceiver, cassette recorder, toy, and flashlight business in all battery applications where a higher load is needed continuously.

When compared to the long development time of the Leclanché cell[2] or the lead–acid battery,[3] the system is still young, and many avenues for improvement are open from the standpoints of the scientist, the developer, and the marketer. The rechargeability of this low-cost alkaline system is a field for investigation that has not been fully explored technically.[4] Because of the likelihood of a future materials "crunch," a throw-away battery (as is now common) seems to be an unbearable waste.

KARL KORDESCH • Institute for Inorganic Chemical Technology, Technical University of Graz, 8010 Graz, Austria.

2. The History of the Alkaline MnO_2–Zinc Cell

A galvanic element containing a plate consisting of manganese dioxide and carbon and a tin plate immersed in sodium hydroxide solution was probably the first cell to use MnO_2 as a "depolarizer" in an alkaline electrolyte.[5] Yai[6] obtained a U.S. patent for a "wet" alkaline cell with potassium hydroxide solution as the electrolyte. The first "dry cells" of the alkaline MnO_2 version were patented by Achenbach.[7,8] The "dry" stood for "a gelatinous filling" of KOH or NaOH immobilized with starch or with 10% MgO as filler. Heil[9] used sodium hydroxide in his cells. Patents by Ruben[10–12] using zinc anode technology that employed large-surface electrodes in zinc-oxide-containing electrolytes were especially applicable.[13] Herbert[14,15] developed the "crown cell" during the 1950s, so-called because of the bottle-cap-like crimping of the cell container. A steel can was used as the current collector and support for the MnO_2–graphite mixture which was pressed into a pellet. The zinc was contacted by tin-plated steel. Absorbent separators or the addition of a gelling agent were the means for immobilizing the electrolytes. From today's point of view, these cells were low-current-density cells, and were used for powering small radios.

The decade of 1960–1970, which may be called the "modern age of the alkaline MnO_2–Zn cell," brought a large number of innovations and improvements. Essential contributions involved the changes to the MnO_2 sleeve-type cell (outside cathode in steel can) and use of the powder zinc anode. Within a few years the industry succeeded in coming up with an efficient cell design, and special binders and conductive additives for the MnO_2 mix were introduced. High-porosity-powder zinc anodes proved essential for the high efficiency of zinc utilization. A treatize on alkaline MnO_2–Zn batteries was published by Kordesch[16] pointing to their increasing importance in the primary battery market.

3. Electrochemistry of the Alkaline MnO_2–Zinc System

The overall reaction of MnO_2 with zinc can be expressed by the equation

$$2MnO_2 + Zn \rightarrow ZnO + Mn_2O_3 \tag{1}$$

with a Gibbs free energy ΔG° of -2.77×10^5 J (-66.2 kcal). For alkaline cells, the cell reactions may be written in the following ways:

$$Zn + 2OH^- = ZnO + H_2O + 2e \tag{2a}$$

$$2MnO_2 + H_2O + 2e = Mn_2O_3 + 2OH^- \tag{2b}$$

$$Zn + 2MnO_2 = ZnO + Mn_2O_3 \tag{2c}$$

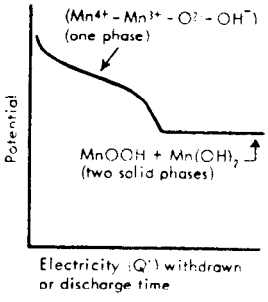

Figure 1. Homogeneous and heterogeneous discharge of manganese dioxide.

Walkley[17] points to the fact that it makes little difference whether the product is the oxide or the hydroxide; the same applies to the formation of zincate. Thermodynamic data can be found in Latimer,[18] Pourbaix,[19] and the Tables of Physical and Chemical Constants.[20]

The reduction of MnO_2 can occur in either a homogeneous or in a heterogeneous reaction. The shape of the discharge curve can tell us what type of reaction is going on, i.e., in a single-phase system the potential changes continuously while the reaction is taking place, while in a two-phase system the potential remains unchanged. Figure 1 shows this behavior. In the homogeneous phase (from MnO_2 to $MnO_{1.5}$) the discharge product is not formed as a new separate phase.[21] Figure 2 presents schematically the discharge of the system (Mn^{4+}, Mn^{3+}, O^{2-}, OH^-). The electrons and protons originating from the water molecules are introduced into the ionic crystal of the MnO_2 according to the equation

$$MnO_2 + H_2O + e \rightarrow MnOOH + OH \qquad (3)$$

As the discharge process proceeds, the concentrations of Mn^{3+} and OH^- in the lattice increase, and in the open-circuit condition both of these species become distributed homogeneously throughout the oxide lattice.[22–25]

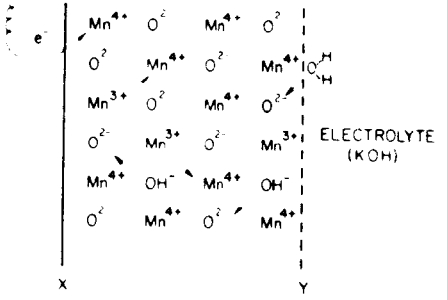

Figure 2. Proton transfer into the homogeneous phase.

The electrode potential at any equilibrium state of the oxide electrode in the homogeneous phase can be expressed as follows:

$$E = E^{\circ} - \frac{[Mn^{3+}]\,\text{solid}}{[Mn^{4+}]\,\text{solid}} \tag{4}$$

if $[OH^-]$ and $[H_2O]$ are assumed constant.

However, as the discharge goes on, the original MnO_2 lattice expands. The ionic radius of OH^- (1.53 Å) is greater than that of O^{2-} (1.40 Å), and Mn^{3+} (0.62 Å) is larger than Mn^{4+} (0.52 Å).

The further reduction of MnOOH to $Mn(OH)_2$ has the characteristic of a two-phase system in that the discharge curve is reasonably flat.[26] The homogeneous reaction mechanism of MnO_2 is rather unique, the only others being V_2O_5 and RuO_2. Ag_2O, PbO_2, and HgO discharge heterogeneously and for that reason do not show the "recuperation" which is so characteristic for MnO_2. Boden, Venuto, Wisler, and Wylie[27,28] studied the discharging and charging of manganese dioxide electrodes in KOH. They found that the amorphous product of the first step was reconvertible to MnO_2. The reversible discharge–charge reaction (for the first step, amorphous phase) was written as follows:

$$MnO_2 + nH^+ + ne \rightarrow MnO_{2-n}(OH)_n \tag{5a}$$

or

$$MnO_2 + nH_2O + ne \rightarrow MnO_{2-n}(OH)_n + nOH \tag{5b}$$

The quantity of electricity withdrawn and consumed is almost equal so long as the discharge does not go beyond $MnO_{1.55}$. At a discharge state of $MnO_{1.46}$, the diffraction peaks which are characteristic for Mn_3O_4 are found, and the rechargeability becomes less efficient. Electrodes discharged to $MnO_{1.29}$ show a rapid increase of the charge voltage and produce a large quantity of irreversible Mn_3O_4.

Kang and Liang[29] found that the higher the concentration of KOH, the more difficult it was to reoxidize the electrode back to MnO_2. Ohira and Ogawa[30] determined the cycle life as a function of the depth of discharge in 7 *M* KOH. McBreen[31] applied low-rate sweep voltametry (25 μV/sec) as a means of cycling MnO_2 electrodes concurrently with X-ray diffraction examination of the reaction products at different potentials. It should be noted that structural information on γ-MnO_2 was usually derived from X-ray powder data.[32] Unfortunately, the better defined the crystal structure, the less useful the MnO_2 becomes in galvanic cells. Ruetschi[33] lists selected structural data for manganese oxides and reaction products and shows that the electrochemical reaction mechanism is closely linked to the structure. In the homogeneous phase, γ-MnO_2 (nsutite) is reduced to MnOOH; the protons entering the structure lead to an expansion of the lattice, and graphite (α-MnO_2) is formed.

The potential decreases when the interior of the γ structure becomes less accessible. Isostructuralism (ramsdellite-groutite) accounts for the ease of proton migration via hydrogen bonds through the tunnels between the double chains of linked $[MnO_6]$ octahedra.[34]

The oxidation and dissolution of zinc in alkaline solutions have been extensively studied, and literature has been reviewed quite recently.[16,35–37]

Screening methods for selection of suitable separators were developed and compiled in a summary publication by Air Force Propulsion Laboratory.[38] These tests were concerned with dimension stability, tensile strength, electrolyte retention, pore-size determination, electrical resistance, stability against oxidants, electrolyte diffusion, and zinc penetration.

4. Primary Alkaline MnO_2–Zinc Cells

4.1. Cell Designs

The construction features of the MnO_2 bobbin and Zn can, as used in Leclanché cells, were not satisfactory for alkaline cells because of mass transport limitations in the massive cathode and because of passivation which occurred easily at smooth zinc surfaces. A new cathode (a sleeve inside the cell container) assured a thin MnO_2 electrode with improved diffusion properties, and the zinc powder anode provided the large area needed to overcome the passivation tendency of the zinc.

Figure 3 shows the construction of a typical cylindrical alkaline MnO_2–Zn cell.[39] The cathode is composed of 70–80% MnO_2 mixed with 7–10% graphite and 1–3% acetylene black as additional conductor. In some cells a binder material (e.g., 6% Portland cement and fibers) is utilized to increase strength.[40,41] The cathode is usually lined with a separator sandwich consisting of two types of separator materials, one having good absorption of KOH (next to the cathode) and one for preventing zinc penetration (nonwoven fabric). The gelled zinc powder anode is inserted into the separator basket and contacted by the collector assembly (brass tongues). In Figure 4, the components needed to produce the D-size Eveready cell are shown in an assembly line (schematic) outlay.

The seal is a very important part of alkaline cell manufacture; it means the difference between a laboratory cell and a marketable battery. Gassing in an alkaline cell is at such a low level that the cell can be hermetically sealed (thereby providing long shelf life). However, cells can be inadvertently abused, i.e., heated overcharged (by reverse insertion into a series cell combination) or short circuited. This requires that a safety vent be provided to prevent a pressure buildup. The use of Na-carboxymethylcellulose (Na-CMC) gelled electrolyte has remedied some of the difficulties arising from free liquid surplus within the powder zinc structure.[42,43]

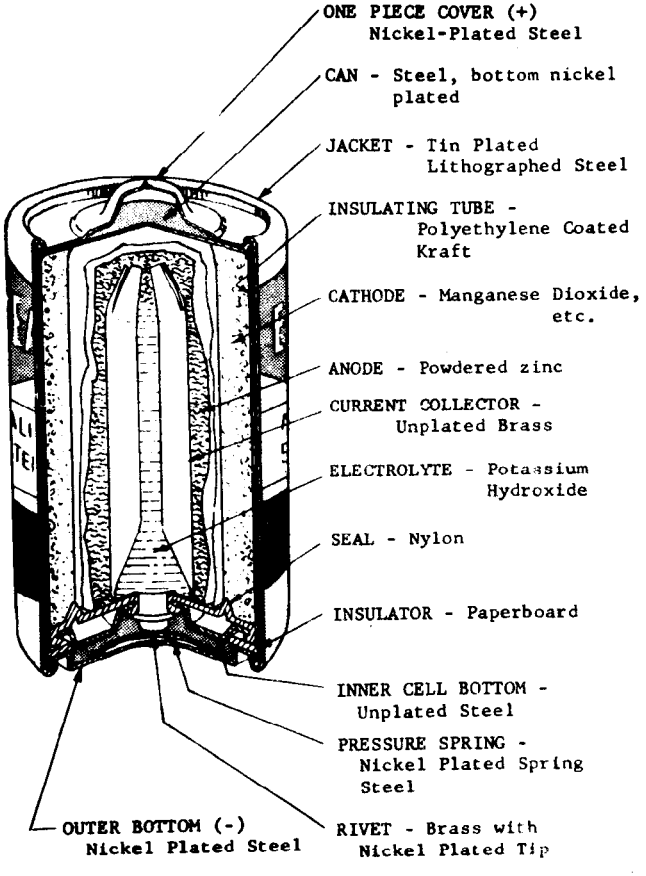
ONE PIECE COVER (+)
Nickel-Plated Steel
CAN - Steel, bottom nickel plated
JACKET - Tin Plated Lithographed Steel
INSULATING TUBE - Polyethylene Coated Kraft
CATHODE - Manganese Dioxide, etc.
ANODE - Powdered zinc
CURRENT COLLECTOR - Unplated Brass
ELECTROLYTE - Potassium Hydroxide
SEAL - Nylon
INSULATOR - Paperboard
INNER CELL BOTTOM - Unplated Steel
PRESSURE SPRING - Nickel Plated Spring Steel
OUTER BOTTOM (-) Nickel Plated Steel
RIVET - Brass with Nickel Plated Tip

Figure 3. Sectional view of an alkaline MnO_2 D-size cell (courtesy of Union Carbide Corporation).

Powder zinc of a certain mesh size (usually between Nos. 20 and 100) is amalgamated and mixed into a KOH "gel" consisting of 30–45% KOH containing 5–8% Na-CMC and some zinc oxide. The so-called "homogeneous" gel anode is a compromise between good electronic conductivity and maximum pore volume with optimized zinc particle size (30–200 mesh). Figure 5 relates the percent by volume (or weight) of zinc to the resistivity of an electrolyte–metal-powder paste.[44]

The construction of a miniature (button-type) cell is shown in Figure 6. These small cells have been made for many years for hearing aid or watch battery applications with HgO or Ag_2O as cathode. Recently, MnO_2 has been considered as an inexpensive replacement. Modern digital watches need only

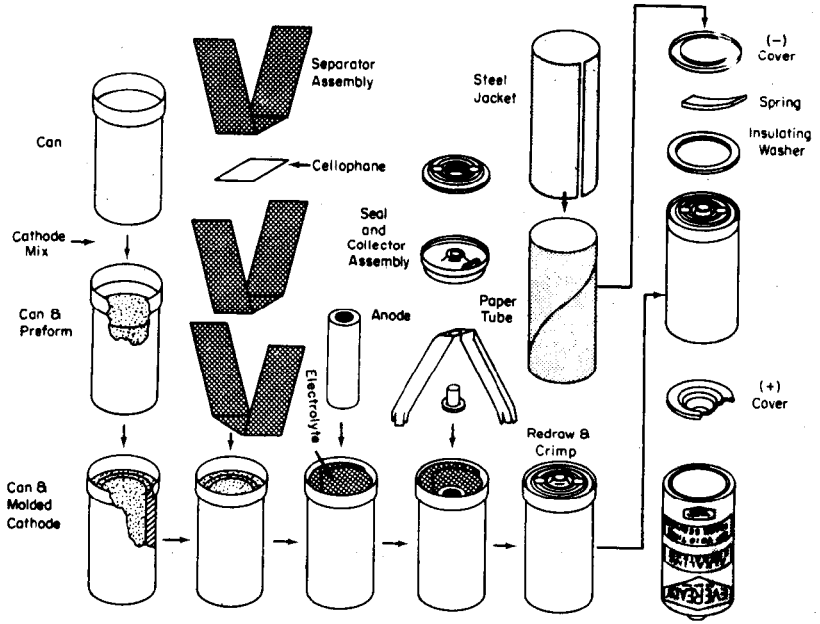

Figure 4. Assembly of a D-size alkaline MnO_2–Zn cell (courtesy of Union Carbide Corporation).

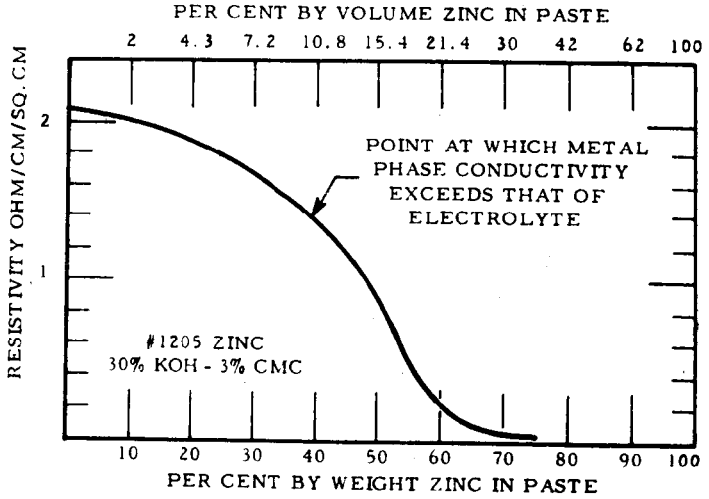
PER CENT BY VOLUME ZINC IN PASTE
2 4.3 7.2 10.8 15.4 21.4 30 42 62 100
RESISTIVITY OHM/CM/SQ.CM
2
1
POINT AT WHICH METAL PHASE CONDUCTIVITY EXCEEDS THAT OF ELECTROLYTE
#1205 ZINC
30% KOH - 3% CMC
10 20 30 40 50 60 70 80 90 100
PER CENT BY WEIGHT ZINC IN PASTE

Figure 5. Resistivity of electrolyte–metal-powder pastes.

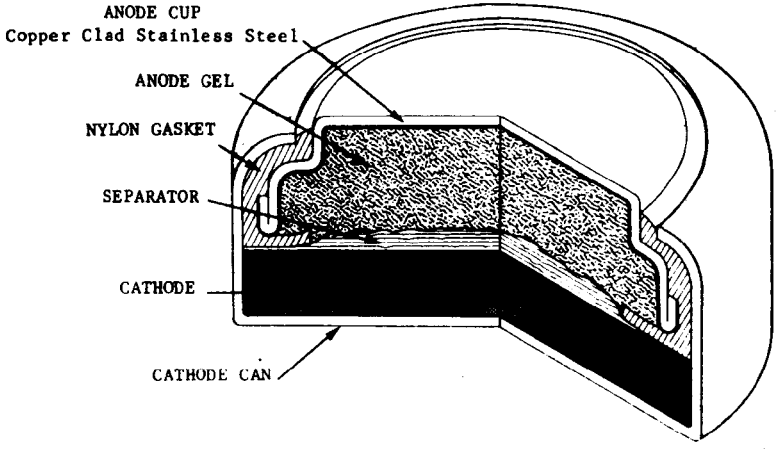

Figure 6. Construction of a miniature cell (courtesy of Union Carbide Corp.).

microamperes to operate and milliamperes in flash currents to light up the LEDs (*l*ight *e*mitting *d*iodes). LCDs (*l*ight-*c*ollecting *d*isplays) need even less current.

4.2. Performance Data

Alkaline MnO_2 cells have been produced to meet a wide range of performance objectives; for details the reader is advised to consult the technical brochures of various manufacturers, e.g. Eveready.[45] Some consumers, for instance, insist on high-temperature shelf life (for summer storage and transportation) and require a higher amalgamation level to lower zinc corrosion. Judgment of cell quality is very difficult because it includes many features, depending on application of the battery. A low-resistance battery designed for a very high current output must be formulated differently than one serving as a low-current–intermittent-duty power source; the latter can contain less conductive material (graphite) and thus more active MnO_2 material.

In radios and tape recorders, alkaline cells usually last twice as long as carbon–zinc (Leclanché) cells; their performance is better due to the lower internal resistance and a less sloping discharge curve (see Figure 7). Service capacity remains relatively constant when discharge schedules are varied; the typical "recovery need" of a Leclanché cell is hardly noticeable. For service at very low or very high temperatures the alkaline cell is superior also. Small appliances represent a rapidly growing application for alkaline cells; this includes electric typewriters, toys, handtools, and portable TV sets. Primary batteries should not be charged or disposed of by fire because any excessive

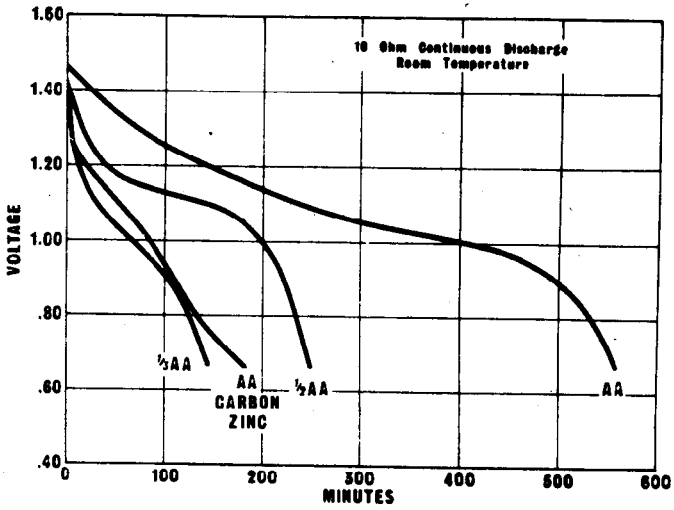

Figure 7. Discharge curves of miniaturized alkaline MnO_2–Zn cells (sizes AA, 1/2 AA and 1/3 AA) compared with the characteristic of a full size (AA) Leclanché cell.

pressure increase can cause a rapid closure failure and this may lead to injury or damage. Other abuse conditions (i.e., shorting, continuous heavy discharge, high-temperature storage, high humidity, and temperature cycling are taken care of by the cell design. The shelf life of alkaline MnO_2–zinc batteries is excellent. After one-year storage at room temperature or after three months at 50°C, these batteries can be expected to supply in excess of 90% of their rated capacity.

4.3. Physical Characteristics

The size, capacity, current, dimensions, weight, and volume of some representative alkaline MnO_2–zinc primary cells are shown in Table 1.

5. Secondary Alkaline MnO_2–Zinc Cells

The technological differences between primary and secondary cells are not great. Use of the same cell design and production equipment for both primary and rechargeable systems is responsible for the relatively low cost of rechargeable alkaline MnO_2 batteries. One of the main problems in rechargeable cells is slow disintegration of the cathode during cell cycling. On discharge, the volume increases and the cathode structure breaks apart if it is not well supported

Table 1
Physical Characteristics of Alkaline MnO_2–Zinc Cells

Cell size[a]	Capacity, ~Ah	Suggested current, A	Diameter, mm	Height, mm	Weight, g	Volume, cm^3
N	0.5	0.08	11.43 ±0.13	28.45 ±0.27	9.64	3.12
½-AA	0.6	0.06	14.30	27.61	11.34	4.44
AAA	0.6	0.10	10.16 ±0.13	44.07 ±0.26	11.34	3.61
AA	1.5	0.15	14.28	50.01	21.26	7.87
½-D	3.0	0.30	34.14	30.56	59.54	26.22
C	4.0–5.0	0.50	25.80 ±0.13	49.02 ±0.26	66.34	25.70
D	8.0–10.0	0.65	34.14	61.11	127.58	51.96

[a] These U.S. cell sizes correspond to the following International E.C. numbers (L = alkaline): N, LR1; 1/2 AA, none; AAA, LRO3; AA, LR6; C, LR14; D, LR20.

inside the steel can. High molding pressures are used for that reason. Outside-sleeve cathodes withstand the dimensional changes that occur during cycling better than central-bobbin cathodes. Addition of special binders to MnO_2–graphite mixes has been used to improve the coherence of the cathodes (steel wool or graphite-coated "Dynel" fibers). Mixing with butadiene–styrene emulsions (latex) has resulted in stronger, more flexible cathodes. Painting a mixture of $Mn(NO_3)_2$ solution and graphite powder on the collector surface and heating to 250–300°C is said to improve rechargeability also.

It is very detrimental to the rechargeability of the alkaline MnO_2 cathode to be discharged more than 50%, therefore a voltage-controlled cut at 0.9 V is recommended. The simplest method is to reduce the zinc amount and to limit the cell capacity anodically[46]; however, this leads to rapidly receding anode capacities. Another method is the use of low-normality KOH to force the zinc anode into premature passivation.[47]

A requirement for good rechargeability is the existence of a structure onto which the zinc can be plated. Tin- or silver-plated copper mesh as substrates can provide a large replating surface. In a sealed system, a zinc-limited balance must be maintained to prevent generation of hydrogen during overdischarge.

A way to combine the requirements of a large-surface collector and the zinc capacity limitation is described by Kordesch.[48] In this case, copper or lead powder is mixed with the zinc powder to provide a large residual surface after anode discharge.

Only fibrous separators are used in presently marketed rechargeable alkaline MnO_2–zinc cells. Oxygen which is produced during charge or overcharge cannot be transported through membrane-type separators! Overcharge problems are encountered if the cell is already fully charged and remains

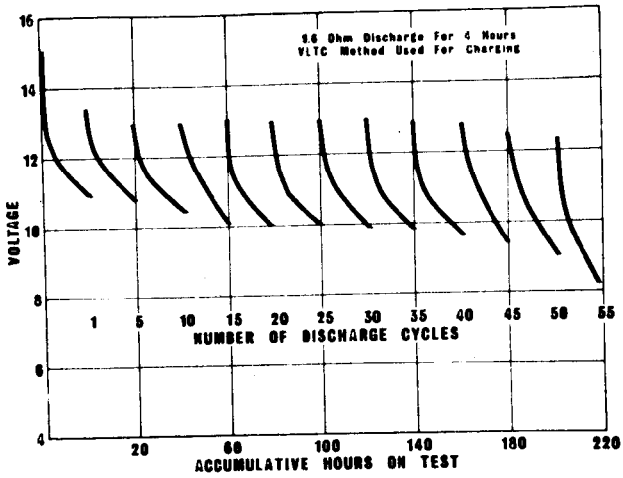

Figure 8. Typical discharge characteristics of Eveready No. 561 rechargeable battery. Discharge is shown for every first and every fifth cycle.

connected to the charging equipment. Oxygen which is produced at the cathode should reach the large-surface zinc anode to form zinc oxide. This cycle, similar to the overcharge process in hermetically sealed Ni–Cd batteries, can theoretically continue forever if the separator system is gas permeable. The oxygen recombination cycle in the presence of a membrane can be made possible by providing an internally exposed anode surface.[49]

Figure 8 shows the discharge characteristics of a 15-V rechargeable TV battery (containing 10 "G" cells in series) with a rated cycle capacity of 5 Ah.

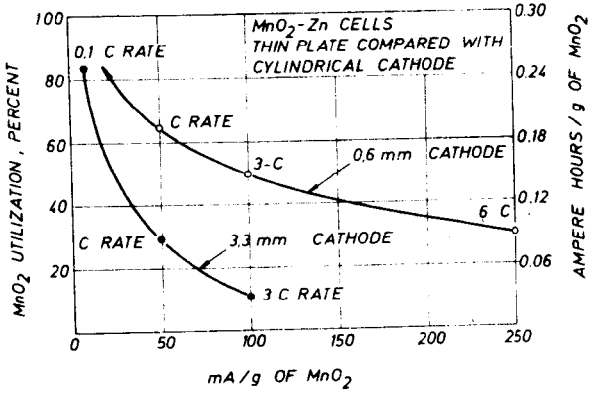

Figure 9. Comparison of the performance of a thin (0.6-mm) MnO_2 electrode with the output a regular (3-mm) cylindrical cathode.

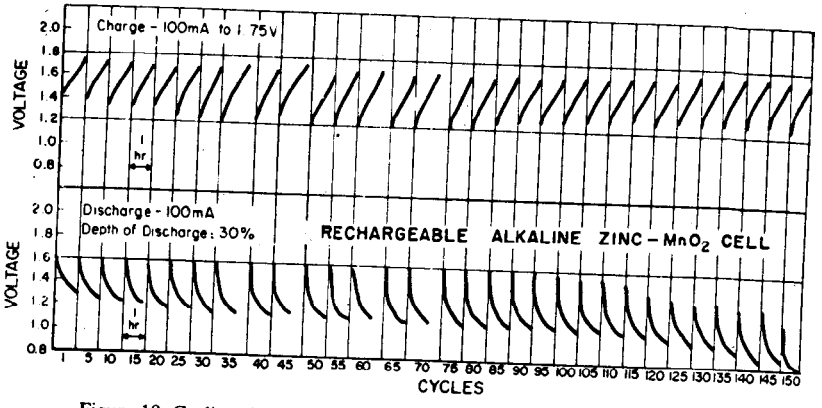

Figure 10. Cycling characteristics of thin electrode alkaline MnO_2–Zn cell.

Discharge curves are shown for each fifth cycle, each curve representing a 4-hr discharge across a 9.0-Ω resistor. During its lifetime (approximately 55 cycles), about 3000 W-h have been stored and delivered. Since the battery weighs only 2.75 kg (6 lb), the energy density of this system can be stated as 227 Wh/kg (500 Wh/lb), which is at least 20 times higher than that of the primary alkaline MnO_2–zinc cell.[39]

The charging procedure affects cycle life very much. The so-called voltage-limited–taper-current charging method with a set voltage limit (1.75 V/cell) is recommended. The charging time should also be limited. An important factor is the energy product (current × time) removed per cycle and the voltage level at which it is withdrawn. Figure 9 shows the performance of thin electrodes which can be used in plate cells or in rolled (spiral) electrode cells.[50] Plastic binders like polysulfones or methacrylates are used to produce very coherent electrode structures. Therefore cycling of that type of alkaline MnO_2–Zn cells is much improved (see Figure 10).

Acknowledgment

I wish to thank my former colleague Dr. Akiya Kozawa at Union Carbide Corporation Technical Center, Parma, Ohio for his very valuable contributions.

References

1. G. W. Heise and N. C. Cahoon, eds., *The Primary Battery*, Wiley, New York (1971).
2. R. Huber, Leclanché batteries, in *Batteries*, Vol. 1, *Manganese Dioxide*, K. V. Kordesch, ed., Marcel Dekker, New York (1974), pp. 1–239.
3. E. Y. Weissman, Lead acid batteries, in *Batteries*, Vol. 2, *Lead Acid Batteries and Electric Vehicles*, K. V. Kordesch, ed, Marcel Dekker, New York (1977).

4. S. Uno Falk and A. J. Salkind, in *Alkaline Storage Batteries*, Wiley, New York (1969).
5. G. Leuchs, German Patent 24,552 (1882).
6. S. Yai, U. S. Patent 746,227 (1903).
7. E. Achenbach, German Patent 261,319 (1912).
8. E. Achenbach, German Patent 279,911 (1913).
9. A. Heil, U.S. Patent 1,195,677 (1916).
10. S. Ruben, U.S. Patent 2,422,045 (1947).
11. S. Ruben, U.S. Patent 2,542,574 (1951).
12. S. Ruben, U.S. Patent 2,576,266 (1951).
13. M. Bolen and B. H. Weil, Literature search on dry cell technology, U.S., Signal Corps Engineering Labs, Ft. Monmouth, New Jersey, Special Report No. 27, State Engineering Experimental Station, Georgia Institute of Technology, Atlanta, Georgia.
14. W. S. Herbert, *J. Electrochem. Soc.* **99**, 190C (1952).
15. W. S. Herbert, U.S. Pat. 2,650,945 (1953).
16. K. V. Kordesch, Alkaline manganese dioxide–zinc batteries, in *Batteries*, Vol. 1, *Manganese Dioxide*, K. V. Kordesch, ed., Marcel Dekker, New York (1974), pp. 241–384.
17. A. Walkley, *J. Electrochem. Soc.* **99**, 209C–214C (1952).
18. W. Latimer, *The Oxidation States of the Elements and Their Potential in Aqueous Solutions*, 2nd ed., Prentice-Hall, Englewood Cliffs, New Jersey (1952).
19. M. Pourbaix, *Atlas of electrochemical equilibria*, in *Aqueous Solutions*, rev. ed., Pergamon, New York (1966).
20. Tables of Physical and Chemical Constants, in *Thermodynamics of Inorganic Compounds*, Longman Group, London (1973), Chap. 2.10.
21. A. Kozawa, Electrochemistry of manganese dioxide, in *Batteries*, Vol. 1, *Manganese Dioxide*, K. V. Kordesch, ed., Marcel Dekker, New York (1974), pp. 385–519.
22. J. P. Brenet, in *Proceedings of the 8th Meeting of C.I.T.C.E.*, Madrid, Butterworth, Washington, D.C. (1956), p. 394.
23. A. Kozawa and R. A. Powers, *J. Electrochem. Soc.* **113**, 870 (1966).
24. A. Kozawa and R. A. Powers, *Electrochem. Technol.* **5**, 533 (1967).
25. A. Kozawa and R. A. Powers *J. Electrochem. Soc.* **115**, 122 (1968).
26. J. P. Gabano, B. Morignat, and J. F. Laurent, in *Power Sources 1*, D. H. Collins, ed., Pergamon, New York (1967), p. 49.
27. D. Boden, C. J. Venuto, D. Wisler, and R. B. Wylie, *J. Electrochem. Soc.* **114**, 415–417 (1967).
28. D. Boden, C. J. Venuto, D. Wisler, and R. B. Wylie, *J. Electrochem. Soc.* **115**, 333 (1968).
29. H. Y. Kang and Ch. C. Liang, *J. Electrochem. Soc.* **115**, 6 (1968).
30. T. Ohira and H. Ogawa, *Natl. Tech. Rep.* **16**, 209 (1970).
31. J. McBreen, in *Power Sources 5*, D. H. Collins, ed., Academic, New York (1974), p. 525.
32. H. Bode, A. Schmier, and B. Berndt, *Z. Elektrochem.* **66**, 586 (1962).
33. P. Reutschi, in *Manganese Dioxide Symposium, Vol. 1, Cleveland*, 1975, A. Kozawa and R. J. Brodd, eds., The Electrochemical Society, I.C. Sample Office, Cleveland, Ohio (1975), pp. 12–46.
34. R. J. Burns and V. M. Burns, in *Manganese Dioxide Symposium, Vol. 1, Cleveland*, 1975, A. Kozawa and R. J. Brodd, eds., The Electrochemical Society, I.C. Sample Office, Cleveland, Ohio (1975), pp. 306–327.
35. T. P. Dirkse, in *The Zinc–Silver Oxide Battery*, A. Fleischer and J. J. Lander, eds., Wiley, New York (1969), Chap. 3.
36. R. V. Bobker, *Zinc in Alkaline Batteries*, The Society for Electrochemistry, Univ. of Southampton, England, Joseph Lucas, Ltd., London (1972), p. 212.
37. R. J. Brodd and V. E. Zilionis, in *The Electrochemistry of the Elements*, Vol. 5, A. Bard, ed., Marcel Dekker, New York (1976), Chap. 1.
38. J. E. Cooper and A. Fleischer, Characteristics of separators for alkaline silver oxide–zinc secondary batteries, Air Force Aero Propulsion Laboratory, Dayton, Ohio (1965).
39. H. P. Keating, Advances in Battery Technology Symposium, Southern California–Nevada Section of the Electrochemical Society, pp. 115–140.

40. P. A. Marsal, K. V. Kordesch, and L. F. Urry, U.S. Patent 2,960,558 (1960).
41. K. V. Kordesch and R. F. Stark, U.S. Patent 3,113,050 (1963).
42. B. H. King, U.S. Patent 2,593,893 (1952).
43. K. Kordesch and A. Marko, Brit. Patent 704,90[illegible] (1953).
44. J. L. S. Daley in *Proceedings of the 15th Annual Power Sources Conference*, P.S.C. Publications Committee, Red Bank, New Jersey (1961), p. 96.
45. *Eveready (1975) Battery Engineering Data*, a customer advisory brochure, published by the Union Carbide Corp., New York (1975).
46. Y. Amano *et al.*, U.S. Patent [illegible]30,496 (1970).
47. N. A. Hampson, M. J. Tarbox, J. F. Lilley, and J. P. G. Farr, *Electrochem. Technol.* **2**, 309–313 (1964).
48. K. V. Kordesch, U.S. P[illegible]2,752 (1962).
49. K. V. Kordesch, U.S. P[illegible]8,642 (1966).
50. K. V. Kordesch and A. [illegible], U.S. Patent 3,945,847 (1976).

7

Primary Batteries—Sealed Mercurial Cathode Dry Cells

SAMUEL RUBEN

1. Introduction

The type of battery suitable for a given application is no longer a matter of cell geometry, as it has been in the past, but one of an electrochemical system that will operate most effectively for a particular use. The size of the cell is related more to the total capacity or energy developed for the load range, and not as limited in respect to the rate of discharge. This was highlighted in 1941 by the advent of large-scale military use of transreceivers and miniaturized equipment where more exacting requirements were encountered. There were three requirements, namely, maximum electrical capacity per unit volume, maximum storage life under varying ambient temperature, and as constant discharge voltage as possible.

In 1941, the only commercially available dry cell system for portable communication equipment was the Leclanché cell system, commonly known as the zinc carbon cell. The development of the sealed zinc–mercuric oxide cell provided a dry battery system that could meet the requirements unfilled by the Leclanché system. A number of fundamental factors were found necessary to produce a sealed zinc–mercuric oxide alkaline cell and overcome the limitations met with in the early attempts to use HgO as a cathodic reactant. They were as follows:

SAMUEL RUBEN • Ruben Laboratories, New Rochelle, New York 10801.

1. High-density cathode;
2. Anodes having an adequate ratio of effective electrode areas to cathode coulombic capacity;
3. Alkali-resistant and absorptive barrier spacer of a submicroporous material in contact with the cathode;
4. A compressible electrolyte-retaining spacer;
5. An alkaline electrolyte containing a saturated zincate ion component;
6. Quantitative balance between anode and cathode coulombic capacities;
7. An anode contactor of nonelectrolytically consumable but amalgamatable metal insulated from the cell container by an elastomeric plastic grommet;
8. A cell container composed of a passive metal in contact with the cathode;
9. A sealed structure provided by crimping the container against the insulated anode contactor.

The combination of these factors provides a cell having internal chemical stability within an air-tight seal with freedom from atmospheric effects, pressures, or humidity.

The cell system and reactions could be expressed as

$$\mathrm{Zn}\,|\,\mathrm{Zn(OH)_2(s)},\ \mathrm{KOH(aq)},\ \mathrm{HgO(s)}\,|\,\mathrm{Hg}$$

The overall reactions for two faradays are

$$\mathrm{Zn} + \mathrm{H_2O} + \mathrm{HgO} \rightarrow \mathrm{Zn(OH)_2} + \mathrm{Hg}$$
$$\Updownarrow$$
$$\mathrm{ZnO} + \mathrm{H_2O}$$

Since the basic reactions at the electrodes are the oxidation of the zinc, $\mathrm{Zn} - 2e^- \rightarrow \mathrm{Zn}^{2+}$, and the reduction of mercuric oxide at the cathode, $\mathrm{Hg}^{2+} + 2e \rightarrow \mathrm{Hg}$, and since water appears at both electrodes, there is no significant change in KOH or $\mathrm{H_2O}$ content. Chemical analysis and X-ray diffraction patterns indicate a deposition of a crystalline form of zinc oxide on the anode and mercury on the cathode as end products.

The electrode potentials are as follows. The half cell potential in reference to the hydrogen electrode, expressed by the Nernst equation, is $E = E^\circ - (RT/nF) \ln Q$, where Q is the product of the activities (a) of the resulting substances divided by the activities of the reacting substances, each raised to that power whose exponent is the coefficient of the substances in the chemical equation. Applying this, we have the following.

Anode:

$$E_{\mathrm{Zn,Zn^{2+}}} = E^\circ_{\mathrm{Zn}} - (RT/nF) \ln a_{\mathrm{Zn^{2+}}}$$

Since the activity product $(a_{Zn^{2+}})(a_{OH^-})^2$ is 4.5×10^{-17}, the OH^- molality is 7.7, the activity coefficient is 3.75, and $n = 2$, at 25°C and $\log_{10}$, we get

$$E_{Zn,Zn^{2+}} = 0.76 - 0.0296 \log \frac{4.5 \times 10^{-17}}{(28.9)^2} = 1.332 \text{ V}$$

Cathode:

$$E_{HgO,OH^-} = E^\circ_{Hg} + (RT/nF) \log a^2_{OH^-}$$

$$E_{Hg} = Hg + 2OH^- \rightleftharpoons HgO + H_2O + 2e = -0.098$$

HgO/OH^- activity = 1; $n = 2$;

$$E_{Hg,OH^-} = E^\circ_{Hg} + (RT/F) \log a_{OH^-} = 0.098 + 0.0592 \log 28.9 = -0.012 \text{ V}$$

$$E_{cell} = E_{Zn,Zn^{2+}} - E_{HgO,OH^-} = 1.332 - (-0.012) = 1.344 \text{ V}$$

which is in close agreement with observed commercial cell potentials.

In order to have a sealed structure that would not develop excessive gas pressure after complete reduction of cathodic reactant, a balanced relation of equivalent coulombic capacities of anode and cathode is required. This is accomplished by using a nonconsumable anode contactor which serves as the top closure of the sealed cell, made of an amalgamatable metal such as tinned steel or copper. Since the deposition potential of hydrogen in the electrolyte is 0.898 V and the hydrogen overvoltage of the steel container is 0.15 V, the sum of both is less than the zinc potential in the zincated electrolyte of 1.332 V. Therefore there will be hydrogen gas generated at the cathode as long as there is no zinc available. The same principle has been applied to sealed alkaline cells with other cathodic reactants such as manganese or silver oxides. For balance, 1.295 g zinc requires 4.07 g mercuric oxide per ampere-hour.

2. Cell Structures

The sealed zinc mercuric oxide alkaline cell is manufactured in three basic structures: (i) the wound anode type, (ii) the flat pressed powdered cathode and anode type, and (iii) the cylindrical pressed powdered electrode type. These three types of structures are shown, respectively, in Figures 1, 2, and 3. The wound anode type (Figure 1) has its anode composed of a corrugated zinc strip with a paper absorbent wound in an offset manner so that it protrudes at the other end. The zinc is amalgamated with mercury (10%), and the paper impregnated with the electrolyte, which causes it to swell and produce a positive contact pressure. The other necessary details of construction are apparent in Figure 1. In the pressed powder cells (Figures 2 and 3), the zinc powder is preamalgamated prior to pressing into shape, and its porosity allows electrolyte impregnation with oxidation in depth when current is discharged. A

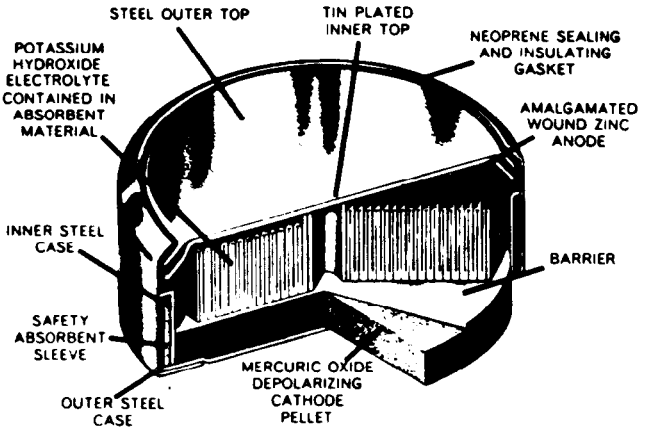

Figure 1. Wound anode and pressed powder cathode.

double-can structure is used in the larger-sized cells, the space between the inner and outer containers providing passage for any gas generated in a cell not properly balanced in relation to the stoichiometric requirements of anode to cathode weights, or the presence of impurities in the anode material. The

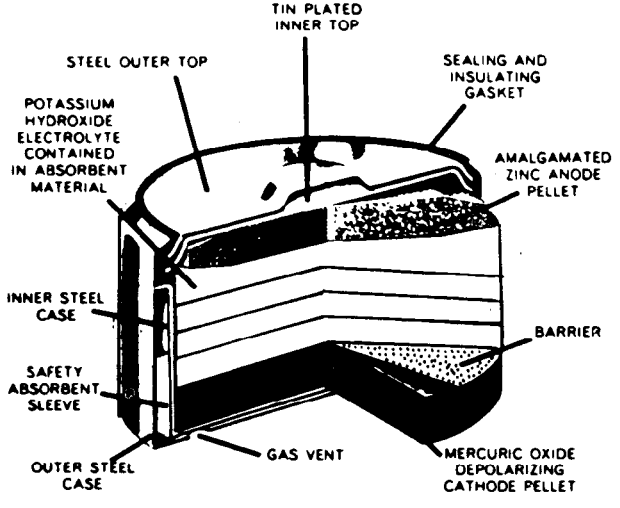

Figure 2. Pressed powder anode and cathode.

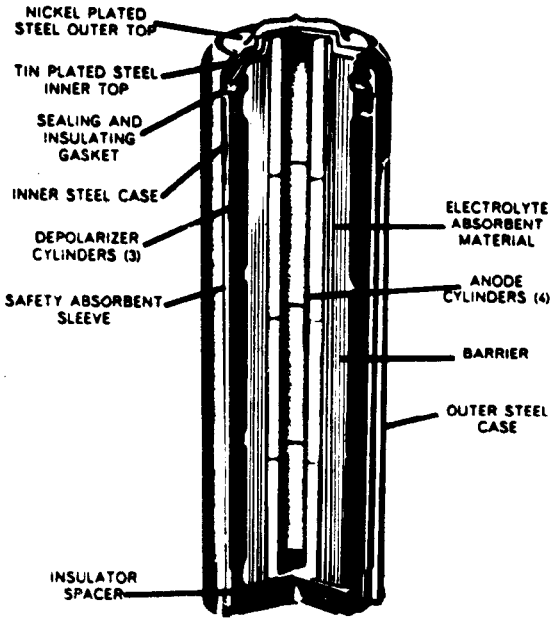

Figure 3. Cylindrical pressed powder anode and cathode structure.

construction is such that if excessive gas pressures are experienced the compression of the upper part of the grommet by internal pressure allows the gas to escape into the space between the two cans. A paper tube surrounds the inner can so that any liquid carried by discharging gas will be absorbed, maintaining a leak-resistant structure. Release of excessive gas pressure automatically reseals the cell. Tables 1, 2, and 3 are the mechanical and

Table 1
Wound Anode Cells

Type #	Maximum diameter, cm	Height, cm	Weight, g	Rated capacity, mAh
RM 640	1.587	0.965	9.68	360
RM 3	2.498	1.37	22.56	1,500
RM 1438	3.71	1.003	36.22	2,700
RM 1450	3.71	1.36	51.80	4,500
RM 2550	6.58	1.394	165.20	13,000

Table 2
Flat Pressed Powder Cells

Type #	Maximum diameter, cm	Height, cm	Weight, g	Rated capacity, mAh
RM 312	0.87	0.34	0.59	36
RM 575	1.143	0.33	1.4	100
RM 675	1.143	0.54	2.24	160
RM 630	1.549	0.58	4.76	350
RM 640	1.574	1.104	7.84	500
RM 4R	3.02	1.66	40.88	3,400

electrical specifications of representative cells embodying the respective structures of Figures 1, 2, and 3.

The type designation "RM"† is used in the industry to identify Zn–HgO cells.

3. Cell Discharge Characteristics

The general characteristic of the Zn–HgO system is noted in Figure 4. This figure illustrates an equilibrium period (T_2) representing practically 97% of the cell life when the current drain is relatively low; e.g., for an RM-1 cell at 1-mA drain, voltage is constant (at 98% of no-load potential) within less than $\frac{1}{2}$% during this period. At higher level drains such as 20 mA, the potential will vary by ±2% from 90% of no-load level and the equilibrium period is approximately 67% of cell life. Larger cells, or groups of smaller cells in parallel, would show longer equilibrium period characteristics for equivalent rates of drain. Since the current density per unit of electrode area determines the equilibrium

† RM is a contraction of the names Ruben and Mallory, the inventor and principal manufacturer, respectively.

Table 3
Cylindrical Pressed Powder Cells

Type #	Maximum diameter, cm	Height, cm	Weight, g	Rated capacity, mAh
RM 24	1.0	4.396	14.0	900
RM 601	1.59	2.857	34.16	1,800
RM 3R	2.489	1.651	28.56	2,200
RM 502	1.358	4.90	30.44	2,400
RM 401	1.133	2.844	11.20	800
RM 1R	1.579	1.638	12.04	1,000
RM 12R	1.519	4.959	30.88	3,600
RM 42R	2.922	6.032	148.33	14,000

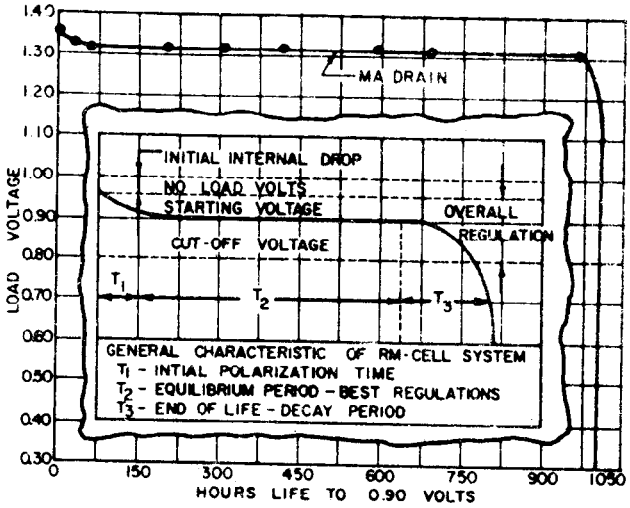

Figure 4. General discharge characteristics of Zn–HgO alkaline system. RM-1 cells: drain, 1 MA; load, 1350 Ω.

period, it is obvious that in the proper cell design the voltage may be as constant as desired (for any predetermined equilibrium period) to meet the demands of any particular circuit. The electrical and mechanical specifications for the RM-1 cell are 1.580-cm diameter, 1.638-cm height, 1.960-cm^3 volume, 12.191-g weight, and 1000-mAh capacity. The voltage discharge curves for the RM-1 cell at various loads vs. time are shown in Figure 5.

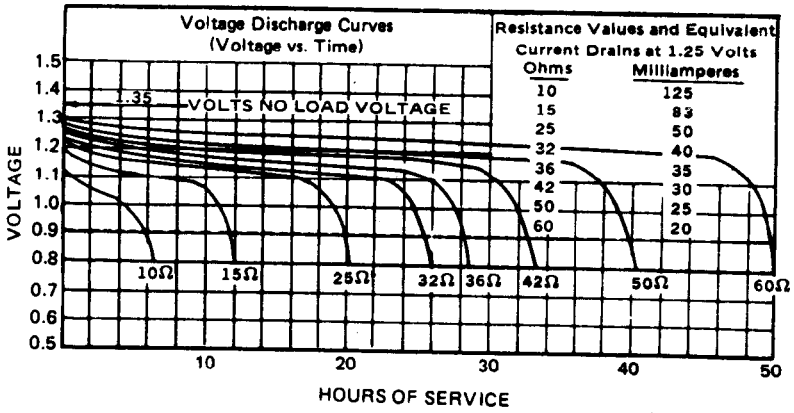

Figure 5. Variation of cell capacity with load.

4. Internal Resistance of the Zn–HgO Cell during Discharge

The maintenance of low internal resistance or impedance is an important characteristic of the mercuric oxide cell. Analysis of the factors which are responsible for this desirable characteristic are as follows:

I. Cathode mix of HgO plus graphite compressed at high pressures such as 180 kg/cm^2;
II. Direct reduction of the semiconductor HgO to the metal Hg, maintaining a low cathode resistance;
III. Anodes designed with enough effective area to allow complete oxidation in depth;
IV. Electrolyte composition and conductivity remaining relatively constant with use of cell;
V. Low heat of formation of HgO;
VI. Rapid ion diffusion at electrodes, which does not impose a rigid limit of discharge current density.

This latter factor is one of the important ones in the mercuric oxide cell. The ions immediately adjacent to the cathode must be discharged in order for current to flow through the circuit. When the electrons are produced by ionization of the zinc anode ($Zn - 2e^- \rightarrow Zn^{2+}$) and discharged to the cathode ($2e^- + Hg^{2+} \rightarrow Hg$) through the circuit, direct reduction takes place.

It has been found that current densities below 1.5 A/dm^2 of cathode surface are conducive toward obtaining maximum cell efficiency and high terminal voltages, since current densities of such magnitude do not excessively deplete the concentration of HgO at the effective cathode surface. The value of 1.5 A/dm^2 was observed with cells designed for general use. However, this value increases with electrodes having higher porosities. The growth of the deposited ZnO on the anode is responsible for a decreased rate of ion discharge at low temperatures. The relation of discharge characteristics of cells having anode areas designed specifically for low temperatures is shown in Figure 6.

The relation of cell impedance to discharge time is shown in Figure 7, and while it refers to an RM-625 cell, the specifications of which are 1.549-cm diameter, 0.592-cm height, 1.115-cm^3 volume, 3.969-g weight, and 350-mAh capacity, it is the characteristic discharge form of all Zn–HgO cells. The rapid rise in ac resistance at end of discharge is indicative of the complete oxidation of the Zn anode.

5. Mercury Voltage Reference Cell

The unusually fixed and reproducible potential of the Zn–HgO cell has led to its development as a voltage reference battery. As shown in Figure 8, this

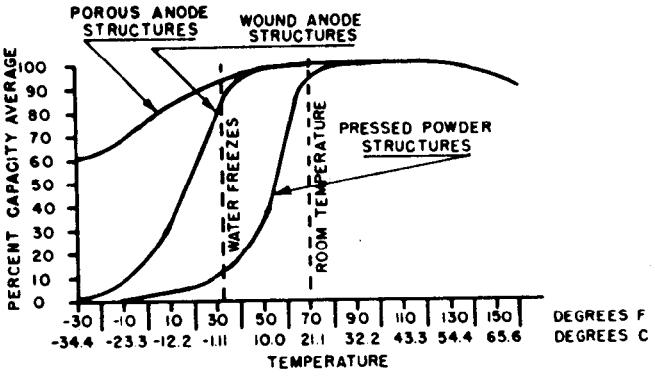

Figure 6. Percent capacity of cell with temperature

type of voltage reference is stable over a wide range of temperature (−50 to +50°C) and has the advantage of being able to withstand accidental overloads which may be experienced in a measurements laboratory.

6. Rechargeable HgO Cells

The problem of mercury conservation has necessitated the development of a rechargeable Zn–HgO cell. Since the electrochemical reactions are completely reversible, $Zn + HgO \rightleftharpoons ZnO + Hg$, new requirements were

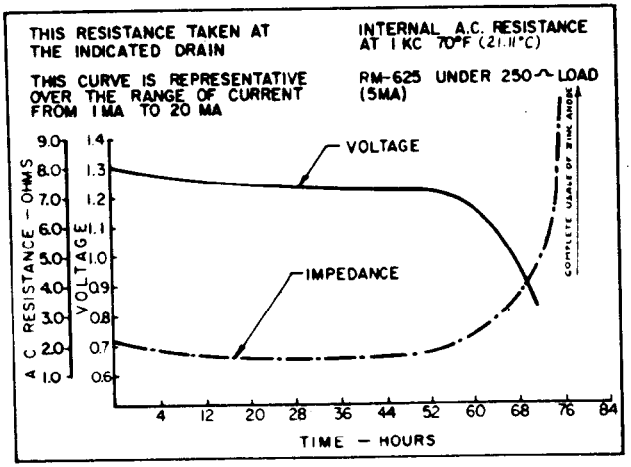
THIS RESISTANCE TAKEN AT THE INDICATED DRAIN
THIS CURVE IS REPRESENTATIVE OVER THE RANGE OF CURRENT FROM 1 MA TO 20 MA
INTERNAL A.C. RESISTANCE AT 1 KC 70°F (21.11°C)
RM-625 UNDER 250Ω LOAD (5MA)
VOLTAGE
IMPEDANCE
COMPLETE USAGE OF ZINC ANODE
A C RESISTANCE - OHMS
9.0 8.0 7.0 6.0 5.0 4.0 3.0 2.0 1.0
VOLTAGE
1.4 1.3 1.2 1.1 1.0 0.9 0.8 0.7 0.6
4 12 20 28 36 44 52 60 68 76 84
TIME — HOURS

Figure 7. Internal ac resistance of cell during discharge with time.

introduced to allow electrodes and separators to remain in an operable condition during cycling. The cathode requirements were met when silver powder was substituted for the graphite content in the semiconductive mercuric oxide cathode. This provided means for immobilizing in place the Hg formed during discharge, forming an amalgam and preventing the formation of large mobile mercury globules. It serves to maintain wide distribution of, and continuous contact to, the reduced mercury. This function is twofold. The first is to allow reconversion in depth of the mercury to mercuric oxide. The second is that the silver allows a readily controllable means for avoiding overcharging. The recharging potential of 1.35 V is maintained until all of the cathode's Hg component is oxidized. If the charge is continued beyond this point the silver component becomes oxidized to Ag_2O, causing a rapid rise in potential from 1.35 to 1.6 V. If continued even further, the potential would rise to 1.82 V as the Ag_2O is converted to AgO. If charging were to continue even further, oxygen gas would be produced. The differential potential (0.25 V) allows a relay or semiconductive device to disconnect the charger, thereby preventing formation of colloidal silver or cathode gas. The cyclic performance of a rechargeable Zn–HgO cell is related to the ionic conductivity of the cathode barrier or spacer, which must be a more oxidation-resistant microporous material than that applied to primary cells, and have a filter action for colloidal silver. Our laboratory experience has been that a ceramic barrier produced by

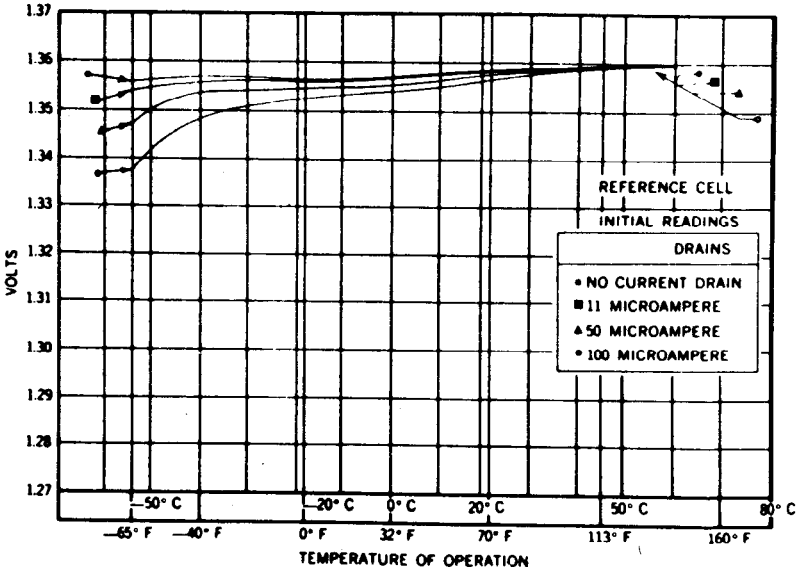

Figure 8. Voltage of Zn–HgO reference cell with ambient temperature.

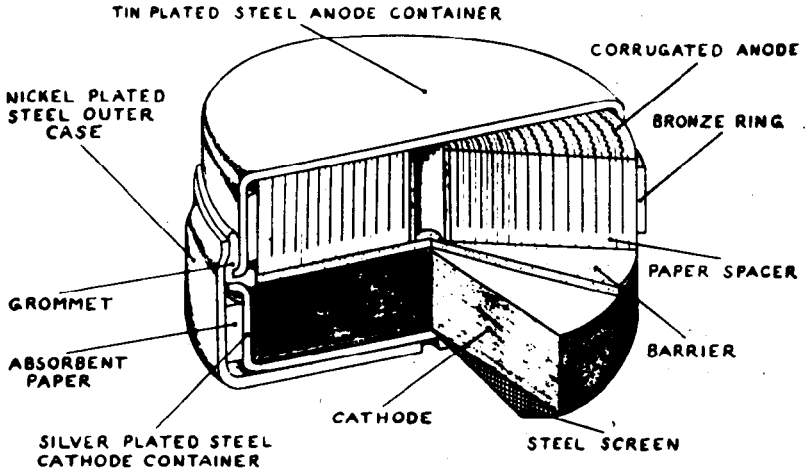

Figure 9. Rechargeable Zn–HgO cell structure.

the compression and sintering of a disk of magnesium oxide gave us the greatest number of cycles without change in cell characteristics. The structure of the rechargeable cell anode differs from that of the primary cell, as shown in Figure 9.

It provides a continuous contact to the zinc oxide formed at the anode so as to allow reduction to zinc or deposition of plated zinc at the anode surface. In the wound anode structure the anode consists of a bronze strip electroplated with an amount of zinc adequate to provide a balanced cell. When the pressed powder type of structure is used, silver powder is added to the zinc amalgam. The silver powder amalgamates and serves as a continuous contacting network for contact to the zinc oxide produced at the anode.

7. Zinc Mercuric Dioxysulfate Cell

Another mercurial cathode system has been developed for lower current requirements which has some of the desirable flat voltage discharge characteristics of the zinc–mercuric oxide alkaline cell, while allowing the use of the less expensive conventional dry cell construction. In the past, attempts have been made to use mercury compounds in the cathode of a nonalkaline dry cell, but these have failed because of inherent limitations of the materials used. In the Zn–$HgSO_4 \cdot 2HgO$ cell, which might be termed the mercury–zinc carbon cell, the cathode reactant is the basic mercuric sulfate, or mercuric dioxysulfate, and the electrolyte is a zinc sulfate solution in which the cathode

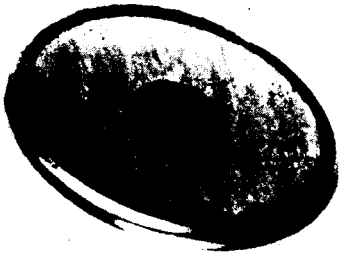

Figure 10. Wafer structure $Zn–HgSO_4 \cdot 2H_2O$ nonalkaline cell.

is stable. The anode is amalgamated zinc. The electrochemical system in the presence of an aqueous solution of zinc sulfate can be expressed as $Zn–ZnSO_4–HgSO_4 \cdot 2HgO + C$, with an overall reaction on discharge as $3Zn + HgSO_4 \cdot 2HgO \rightarrow ZnSO_4 + 2ZnO + 3Hg$. The potential of the cell is 1.36 V. The theoretical capacity of $HgSO_4 \cdot 2HgO$ is 0.2204 Ah/g, and the practical capacity of the carbon mix is 0.15 Ah/g.

8. Cell Structures for Zinc–Mercuric Dioxysulfate Cells

While this system can be used in a standard dry cell structure, one of the important characteristics of the zinc–mercuric dioxysulfate electrochemical system is that it allows the use of stainless steel containers for contact to the cathode. This has permitted production of thin wafer-type cells of the structure shown in Figure 10.

The case is a shallow stainless steel cup, the cathode a pressed disk of mercuric dioxysulfate, Shawinigan carbon, and zinc sulfate solution containing 1% potassium dichromate as an inhibitor, in contact with the bottom of stainless steel. The spacer is a laminate of paper and cellophane which separates the cathode from the amalgamated zinc disk anode. The anode has a polyethylene grommet around its edge, insulating it from the cathode container which is crimped against it for sealing of the cell. The electrical and dimensional specifications of the WD-5 wafer-type cell are 2.54-cm diameter, 0.272-cm height, 1.376-cm^3 volume, and 4.9-g weight. Initial flash currents are in the order of 0.5 A, capacity is 230 mAh, with a 1000-hr impedance of 10 Ω.

Suggested Reading

M. Friedman and C. E. McCauley, The Ruben cell, *Trans. Electrochem. Soc.* **92**, 195–215 (1947).
E. C. Potter, *Electro-Chemistry*, Macmillan, New York (1956), pp. 375–377.
A. G. Garrett, *Batteries of Today*, Research Press, Dayton, Ohio (1957), pp. 84–87.
G. Milazzo, *Electro-Chemistry*, Elsevier, Amsterdam (1964), pp. 645–647.

C. A. Hampel, *Encyclopedia of Electrochemistry*, Reinhold, New York (1964), pp. 74, 75, 83–84.
S. Ruben, Zinc mercuric dioxysulfate dry cell, *J. Electrochem. Soc.* 2, 77–79 (1959).
S. Ruben, International Committee for Electrochemistry, Thermodynamics and Kinetics (CITCE) 17th Meeting, Tokyo, 1966.
G. Heise and C. N. Cahoon, eds., *The Primary Cell*, Wiley, New York (1971).
S. Ruben, *The Evolution of Electric Batteries in Response to Industrial Needs*, Dorrance, Philadelphia (1978), pp. 51–65.

8

Primary Batteries—Lithium Batteries

MARVIN L. KRONENBERG and GEORGE E. BLOMGREN

1. Introduction

Lithium is a unique metal because of its large negative standard potential and low equivalent weight. As a result, batteries made with lithium as an anode show great promise for wide use as energy sources and have already seen service in advanced applications. Electrochemists have long recognized these attributes of lithium, but the extreme reactivity of the metal with the atmosphere and most solvents retarded development. However, in 1958, W. S. Harris[1] discovered that lithium was stable with cyclic esters and butyrolactone. Furthermore, he found that a number of lithium salts had high solubility in these solvents and the resulting electrolyte solutions had reasonable conductivity for battery purposes. These results coupled with the need developing at that time for batteries of high specific energy because of the U.S. space program gave great impetus to the study and development of lithium batteries. This chapter describes the characteristics and battery construction of the most promising lithium battery systems resulting from the efforts since the late 1950s. Only primary battery systems with liquid electrolytes at room

MARVIN L. KRONENBERG and GEORGE E. BLOMGREN • Battery Products Division, Union Carbide Corporation, Cleveland, Ohio 44101. Dr. Kronenberg's present address: CEN, Argonne National Laboratory, Argonne, Illinois 60439.

temperature are treated here, although lithium–solid electrolyte systems and lithium–molten salt systems are being extensively investigated at present. Other room temperature, liquid electrolyte systems which have been advanced are described in comprehensive reviews by Jasinski[2] and Besenhard and Eichinger.[3,4] A more limited review is given by Dey.[5]

The chapter is divided into two main sections on solid cathode cells and liquid cathode cells. Most of the earlier lithium battery work was done on conventional solid cathode cells and a number of high-energy systems are described. Much recent work has concentrated on systems in which the electrolyte solvent performs as both the ion carrier for electrolytic conduction as well as the active cathode material. Several of these systems are described in the Section 3 on liquid cathode cells.

2. Solid Cathode Cells

Because of the lithium stability problem, the electrolyte solution phase generally consists of an organic solvent–inorganic salt for solid cathode cells. This introduces new problems with regard to the interface between the solid cathode active material and the electrolyte solution. The analogous interface with aqueous solutions has been studied for many years with electrochemical and physical–chemical methods, but there is little information about the organic solutions. As a result, most workers have approached the battery problems empirically and changed solvents until finding appropriate combinations that make the system work. We will discuss in this section the properties that are known for the electrolyte solutions and the particular solutions that have been found to be useful for each solid cathode considered.

2.1. Electrolyte Solution Considerations

There are a number of criteria for excellence of an electrolyte solution for lithium cells, but the one of paramount importance is stability and compatibility with lithium and its associated electrode structure. This definition includes stability under intermittent discharge situations and the absence of corrosion couples between lithium and the metal current collector, lead wire, contacting cell case, etc. While it was thought at one time that some electrolyte solutions were unreactive with lithium it is now generally believed that all or nearly all electrolyte solutions react at least to some slight extent with the lithium metal surface. Thus successful electrolyte solutions must show metastability with lithium for long storage periods even at elevated temperatures. This metastability may come from reaction of the lithium surface with the electrolyte solvent resulting in the formation of a thin product layer which inhibits further reaction. Good evidence for this mechanism has been obtained with electrochemical measurements by Scarr[6] and SEM studies by Dey[5] for

propylene carbonate. Liquid cathode electrolyte solutions discussed in Section 3 are also known to provide metastability by this mechanism. Metastability can be very sensitive to impurities and every effort should be made to remove water and Bronsted acid impurities for fundamental studies.

Table 1 gives the physical properties of a number of the most widely used solvents which have shown adequate metastability with lithium. The table shows a wide range of properties. However, numerous studies have been carried out on solvent mixtures in order to achieve properties intermediate to those of the pure solvents. Many of these mixtures have interesting effects. For example, because of the opposite effects of viscosity and dielectric constant on conductivity, higher conductivities are obtained from $LiClO_4$ in tetrahydrofuran–propylene carbonate mixtures than from $LiClO_4$ in either of the pure solvents.[7]

Other criteria of importance for the electrolyte are adequate conductivity for the expected current drains, stability and compatibility with cathode materials, low solubility for cathode active materials, compatibility with materials of cell construction, and high cathode activity.

The conductivity requirement implies high salt solubility as well as minimal ion-pairing effects, i.e., the use of strong electrolytes. Because of low anion solvation with aprotic solvents, solubility usually occurs only for salts with relatively large, monovalent anions. Thus the commonly used solutes are the perchlorates, hexafluorophosphates, hexafluoroarsenates, tetrafluoroborates, and tetrachloroaluminates of the alkali metals. Even in the best conducting of the organic solvent solutions, however, the conductivities are one to two orders

Table 1
Physical Properties[a] of Some Commonly Used Solvents

Solvent	Melting point, °C	Boiling point, °C	Viscosity, cP	Dielectric constant	Density, g/cm³
γ-Butyrolactone	−43	202	1.75	39.1	1.13
1,2-Dimethoxyethane (DME)	−58	83–84	0.455	7.20	0.859
Dimethyl formamide (DMF)	−61	158	0.796	36.71	0.9443
Dioxolane	−95[b]	78[b]	—	7.13[c]	1·0600 (20°C)[b]
Ethylene carbonate (EC)	39–40	248	1.85 (40°C)	89.6 (40°C)	1.3218 (39°C)
Methyl formate (MF)	−99.0	31.50	0.3298	8.5 (20°C)	0.97421 (20°C)
Propylene carbonate (PC)	−49	241	2.53	64.4	1.19
Sulfolane	28.86	–	9.87 (30°C)	43.29	1.262 (30°C)
Tetrahydrofuran (THF)	−65[b]	65.0	0.46	7.39	0.880

[a] Data at 25°C except as noted from G. J. Janz and R. P. T. Tomkins, *Nonaqueous Electrolyte Handbook*, Vol. I, Academic Press, New York (1972).
[b] *Handbook of Chemistry and Physics*, Chemical Rubber Co., Cleveland (1969).
[c] A. Venkateswaran, J. R. Easterfield, and D. W. Davidson, *Can. J. Chem.* **45**, 884 (1967).

of magnitude less than aqueous solutions of the same salts. As a result, the thick porous electrodes and large electrode spacings commonly used for aqueous batteries, e.g. dry cells, are usually not found in nonaqueous battery designs.

Cathode compatibility has usually been found to be a matter of cathode solubility. For example, much early work focused on copper halide cathodes, particularly CuF_2, because of their high theoretical specific energy. Unfortunately, however, these compounds were found to have too high solubilities in all of the electrolytes tested. This resulted in migration of copper ions to the anode followed by displacement in solution by lithium and copper metal deposition on the anode with deleterious effects. It is possible for solutes and solvents to be oxidized by cathode materials, although there is not an extensive literature on the subject. This is probably because such materials are often also incompatible with lithium and do not get past the first screening test. For example, aldehydes and alcohols can be oxidized by MnO_2 or PbO_2, but are obviously unsuitable with lithium. Thiocyanate anions are also known to be oxidized by the above oxides so are not suitable as electrolyte salts with these cathodes. A note of caution should be added about the still widespread use of $LiClO_4$ as an electrolyte salt. Thermal and impact detonations have been reported for organic solvent solutions with this electrolyte in batteries.[8,9] Thus extensive testing should precede any use of these potentially hazardous solutions.

Each electrolyte solution has its own compatibility problems with materials of cell construction. However, there are a number of materials which have been found to be inert in many organic solvent solutions. Noncellulosic separators such as microporous rubber and polypropylene are usually used to avoid the problems of adsorbed water and the OH groups of cellulosics which react with lithium. Nickel and stainless steel are preferred over soft iron or other metals for case materials, although aluminum is sometimes used. Most workers use stainless steel, nickel, or aluminum as current collectors and carbon or graphite as a conductive additive for cathodes.

Few publications have appeared regarding cathode activity, although some work has focused on mechanisms of cathode reactions, as noted in the sections on individual cell systems. Even though many nonaqueous electrolytes are poorly conducting, cell rates often seem to be limited by slow kinetics of the cathode reactions rather than mass transport of ions in the electrolyte solution. This problem will undoubtedly be the subject of future investigations as the field of lithium batteries develops commercially and scientifically.

2.2. Electrode and Cell Constructions

Most workers in lithium batteries have used similar constructions for the anode. An expanded metal or wire screen made of nickel, stainless steel, or aluminum and containing a welded wire or tab for external contact is pressed into a sheet or foil of lithium, the thickness of which is determined by the

capacity requirement and cell construction. This step is easily accomplished because of the softness of lithium metal.

Cathode constructions vary according to cell type and current requirements. High-rate cells require extended area electrodes. Therefore a well-mixed paste consisting of cathode-active material, conductive additive, and a binder such as a fluorocarbon–water emulsion is spread across an expanded metal or wire screen (having a welded wire or tab for external contact), heated mildly to evaporate the water from the emulsion, and then heated more strongly to sinter the binder. Lower-rate cells can be made as button cells or round cells. In the button cells, the lower half of the can is usually filled with a mix similar to that for high-area electrodes, sometimes pressed to densify the mix and finally heated for evaporation and sintering. The binder is sometimes eliminated from the mix. Low-rate round cells have been made for copper oxide cells (see Section 2.3.2) by pressing a dry mix against the sides of the cylindrical can and placing the anode in the cell center.

Most high-rate cells have been assembled by placing one thin separator sheet between electrodes and another on top of one electrode, winding the stack of long thin electrodes in a spiral, and placing the spiral in a cylindrical can. One tab is welded onto the can and the other to an outside terminal. If the cell is to be hermetically sealed, the other terminal comes into the cell through a glass-to-metal feedthrough in the cover. This may be a fillport or another tube may serve as the electrolyte fillport. The cover is then welded to the can, and electrolyte is brought into the cell by vacuum filling through the fillport. Plastic-sealed cells usually have a plastic gasket between can and cover, the electrolyte is added, and the can is crimped over the gasket and cover. There is only sparse information in the literature as yet about the relative merits of these two methods.

Button cells are assembled by placing a separator disk on the cathode, connecting the anode to the cover, usually by a screen welded to the top, and sealing by means of a plastic gasket after electrolyte filling or sealing by means of a glass-to-metal feedthrough as discussed for high-rate cells.

Low-rate round cells have not been discussed in much detail, but presumably both types of seals could be used for these cells as well. The anode may be a lithium rod or thick lithium sheet bent around a collector rod or cylindrically shaped screen, which in turn is connected to the cell cover.

Certainly, one would like to use hermetic seals for all lithium cells on technical grounds; but the plastic-sealed cells are less costly. Whether economics or long-term stability weighs more heavily in the balance remains to be seen.

2.3. Specific Systems

The specific solid cathode lithium batteries discussed in this chapter involve the following cathodes: $(CF_x)_n$, CuO, MnO_2, Ag_2CrO_4, V_2O_5, CuS,

and MoO_3. An almost bewildering array of other cathodes have been reported in the scientific and patent literature, but at this time the above cathodes appear to be most advanced and are either in commercial applications already or in an advanced state of development. Because of the large negative potential of the lithium electrode, most cathode materials can provide at least a 1.5-V couple so performance, cost, energy density, and specific energy will be important criteria used to decide which lithium batteries will ultimately be successful.

2.3.1. Li–Carbon Fluoride Cells

A highly developed cathode material used in lithium cells is a polymeric, covalent carbon fluoride compound designated as $(CF_x)_n$. The x value varies from about 0.7 to 1.3 and is subject to approximate control. It is prepared by the direct fluorination of graphite, carbon black, or other forms of crystalline carbon.[10–15] As fluorination progresses, the normal, planar graphite structure becomes puckered and the fluorine atoms form a layer above and below the carbon atoms. The use of this fluorocarbon as a cathode material in lithium batteries was first proposed by Watanabe and Fukuda.[16]

Prior to the use of $(CF_x)_n$ as a cathode material, another carbon fluorine compound, tetracarbon monofluoride (approximate composition C_4F) was used as a battery cathode by Braeuer.[17] Tetracarbon monofluoride is quite different structurally from $(CF_x)_n$. C_4F has unpuckered rings, shorter interlayer spacings, and is less thermally stable than $(CF_x)_n$. The two compounds are prepared at different temperatures and C_4F is not directly convertible to $(CF_x)_n$ by increasing the fluorine content. The electrochemical capacity of C_4F is only 0.4 Ah/g compared to 0.86 Ah/g for $(CF_x)_n$ (where $x = 1$).

Commercial cells use material having an x value close to 1.0. At this fluorine level, the color is almost white, while fluorine-poor preparations are grey or black. Electronic conductivity decreases with increasing fluoride content so that the white preparations that have the highest coulombic capacity are virtually nonconducting.

Lithium cells using $(CF_x)_n$ cathodes have been produced commercially in Japan for several years by the Matsushita Electric Co., Ltd.[18–20] and for military use in the U.S.A. principally by Eagle Pitcher[21,22] and Yardney Electric.[23] Cathodes for C-size cells or larger are generally made by pressing a cathode mix consisting of $(CF_x)_n$, carbon, and fluoroplastic binder into a titanium or nickel metal grid.

The commercial C-size cell uses $LiBF_4$ in butyrolactone as electrolyte and a spirally wound configuration with the flexible cathode and lithium anode grid separated by nonwoven polypropylene, all contained in a Ni-plated steel can. Discharge characteristics for a C-size cell of this type under 8-, 20-, and 50-Ω loads at 20°C are given in Figure 1.[19] The cathode efficiency was about 90% under the 50-Ω load and 80% with the 8-Ω load. After a slight decrease, the discharge voltage is relatively flat in the 2.4–2.7-V range depending on the

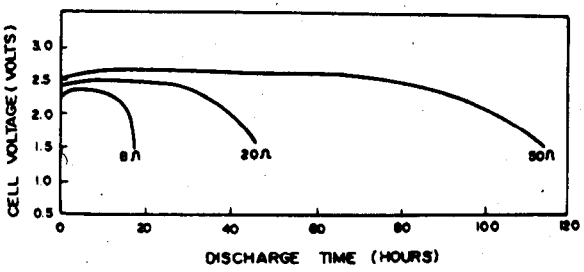

Figure 1. Discharge characteristics of the LR-C, Li-$(CF_x)_n$ battery at 20°C (Reference 19). (Reprinted by permission.)

load. Specific energy as a function of temperature at a constant 8-Ω load for this same size cell is given in Figure 2.[19] It is seen that the specific energy is relatively high, ranging from about 150 to over 300 Wh/kg in the temperature range of −20 to 50°C. Excellent results have also been reported in pressed pellet button cells,[19] which may find the widest applications for this type of cell owing to the small quantities of $(CF_x)_n$ used and the relatively high projected cost of this material.

The initial open-circuit voltages (OCVs) of Li–CF_x cells range from about 2.8 to 3.3 V depending on the CF_x source and electrolyte used. Since the reversible emf of $(CF)_n$ vs. Li has been calculated at over 4 V vs. lithium,[24]

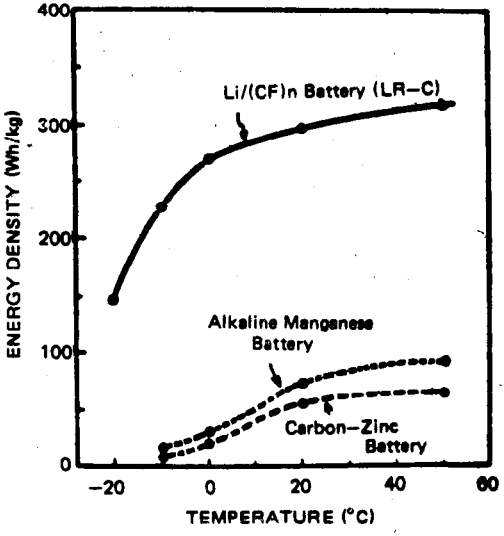

Figure 2. Energy densities of the LR-C, Li-$(CF_x)_n$ battery as a function of temperature compared with conventional C-size batteries: Li-$(CF_x)_n$, 8 Ω continuous; alkaline manganese, 4 Ω continuous; Carbon–Zinc, 4 Ω intermittent (30 m/d) loads (Reference 19). (Reprinted by permission.)

alternate proposals have been made to explain the lower OCVs and operating potentials.[25-28] Whittingham[26] proposed that an intermediate ternary compound of composition Li_yCF_x is formed during the discharge, whereas Tiedemann[25] and Hunger[27,28] attribute the voltage discrepancy to mixed potentials resulting from anodic solvent reactions coupled with cathodic reduction of the fluorocarbon.

2.3.2. Li–CuO Cells

This system was reported on by G. Lehmann *et al.*[29] and has been produced in AA-size cells in limited quantities by SAFT in France. The cell uses an "inside-out" construction similar to alkaline Zn–MnO_2 cells. Copper oxide used for the cathode mix was prepared by thermal oxidation of copper powder. The cathode is made by mixing copper oxide with graphite and shaping it into hollow cylindrical cathodes by a cold-pressing method and forced into contact with the inside wall of nickel-plated steel cans. Pure lithium strip welded into a cylindrical rolled sheet of tin-plated steel is used as the internal anode. Several layers of nonwoven polypropylene are used as a separator and the electrolyte contains $LiClO_4$ salt dissolved in a cyclic ether such as dioxolane or THF.[30,31] Cell discharge characteristics as a function of various loads for AA-size cells at ambient temperature are given in Figure 3.

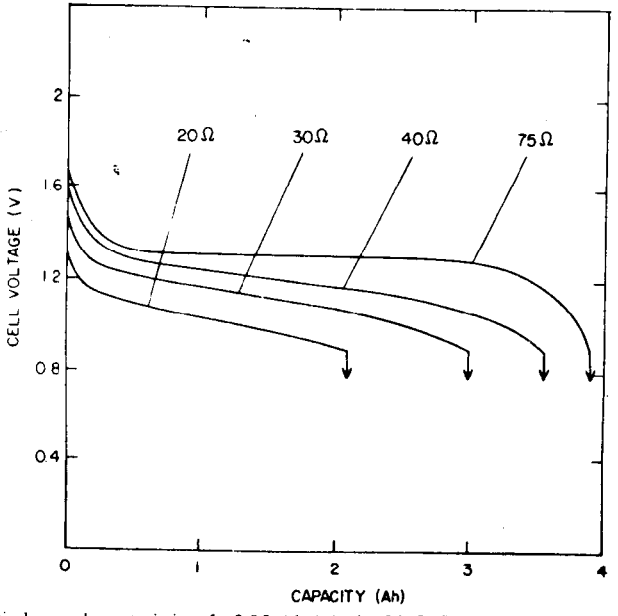

Figure 3. Discharge characteristics of a 3.95-Ah AA-size Li–CuO cell at various loads (Reference 29). (Reprinted by permission.)

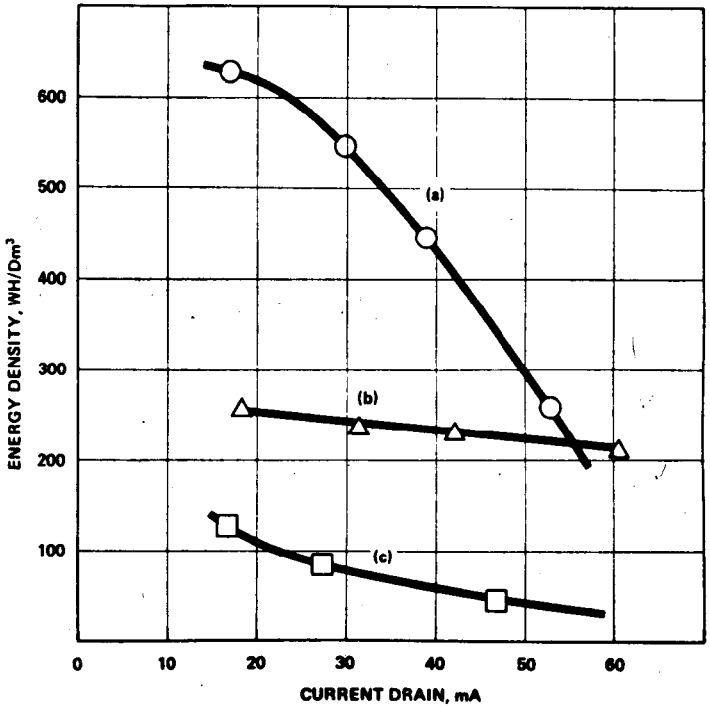

Figure 4. Energy density of AA-size Li–CuO cells (a), alkaline MnO_2 cells (b), and carbon–zinc cells (c), as a function of current under continuous load (Reference 29). (Reprinted by permission.)

It is seen that the voltage plateau at low to moderate drain rates is in the 1.0–1.4-V range, although the open-circuit voltage is about 2.4 V. The potential calculated from thermodynamic data for a one-electron discharge to Cu_2O and Li_2O also occurs at about this same potential. After one equivalent of discharge, the cathode mix was found to contain a mixture of Cu, Cu_2O, and CuO. Matsuda *et al.*[32] found similar mixtures upon discharging Li–CuO cells in $LiClO_4$–PC electrolytes. However, a material balance and complete discharge mechanism has not been reported for either solvent system.

Figure 4 is an energy density comparison of continuously discharged Li–CuO, Zn–KOH–MnO_2, and Leclanché cells as a function of drain rate. The Li–CuO cells have significantly higher energy densities at low and moderate drain rates than these aqueous cell systems showing an optimum of about 600 Wh/dm^3 at low rates.

Recently improved performance and efficiency have been reported for a 1/2-AA size by Broussely *et al.*[33] Cell operation between 1.4- and 0.9-V cutoff for this size cell have a capacity of 1.14 Ah at the 6.5-mA rate

(1.75-mA/cm^2). This corresponds to an efficiency of over 85%. Even at a 25-mA drain rate (7.6 mA/cm^2) the capacity was 0.53 Ah, which corresponds to a discharge efficiency of 40%. This is a very substantial improvement over the 2–3% efficiency at this drain rate previously reported. The improved performance and efficiency is attributed to a new but not specified separator material.

2.3.3. Li–MnO_2 Cells

There have been several references to the use of MnO_2 as a cathode material for nonaqueous, lithium cells.[28,34–36] The results, however, were not encouraging enough to consider commercial development due to a reported capacity equivalence significantly less than one electron per MnO_2 formula weight,[28,34,35] or loss of capacity and gassing on storage.[36] More recently, these limitations have been overcome, with good stability and efficiencies of over 90% at low drain rates, by H. Ikeda and co-workers.[37–39] This has resulted in commercialization of the nonaqueous Li–MnO_2 system by Sanyo Electric Co., Ltd.[40]

Improved performance and stability upon storage is attributed to heat treatment of the MnO_2. Using analytical and electrochemical methods, Ikeda and co-workers[37] have shown that heating electrolytic MnO_2 yields γ phase between ambient temperature and 250°C, γ-β intermediate phase between 250 and 350°C, and β phase for temperatures above 350°C. The best combination of performance and storage stability is obtained when the MnO_2 is heat treated at about 400°C.

A number of sizes of Li–MnO_2 cells in flat-type and cylindrical configuration are produced commercially. Table 2 summarizes the various sizes and

Table 2
Specifications of Sanyo Li–MnO_2 Cells[a]

Type	Model No.	Outside diameter, mm	Total height, mm	Weight, g	Capacity, mAh
Flat (button)	LF-A	7.9	3.6	0.5	30
Flat (button)	LF-C	11.6	5.4	1.5	130
Flat (button)	LF-D	15.7	6.1	2.9	225
Flat (button)	LF-1/2V	20.0	3.2	2.6	170
Flat (button)	LF-1/2W	24.5	2.8	4.0	200
Flat (button)	LF-1/2WH	24.5	2.8	4.0	160
Flat (button)	LF-1/3W	24.5	2.0	3.0	120
Round	LR-b	7.9	7.2	0.9	50
Round	LR-AA	14.5	50.0	17.5	1500
Round	LRC	26.0	50.0	53.0	5000

[a] Data from Reference 39.

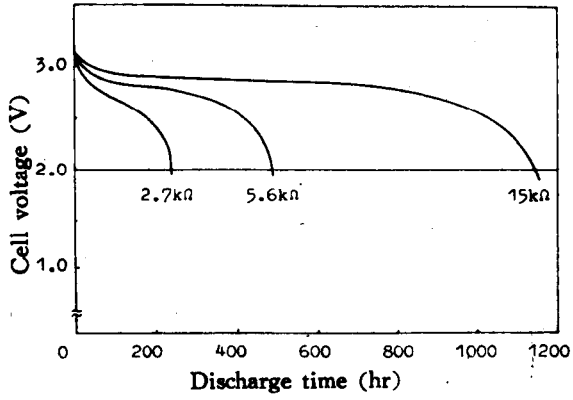

Figure 5. Discharge curves of LF-1/2W, Li–MnO_2 cells with various loads (Reference 39). (Reprinted by permission.)

capacities currently available.[39] The preferred electrolyte used in both types is 1 *M* $LiClO_4$ in a 1:1 PC–DME mixture. The flat-type cell is available in two varieties—one using a pressed powder molded electrode for low-rate applications, and the other a paste-type thin electrode for high-rate applications. The anode and cathode in the paste-type cell are doubled up providing a large surface area. Stainless steel cans are the preferred containers for both cylindrical and flat cells.

Discharge characteristics for the three cell types at various loads[39] are given in Figures 5–7. The nominal capacities are 200, 160, and 5000 mAh for the pressed powder (LF-1/2W), paste type (LF-1/2Wh), and round cell

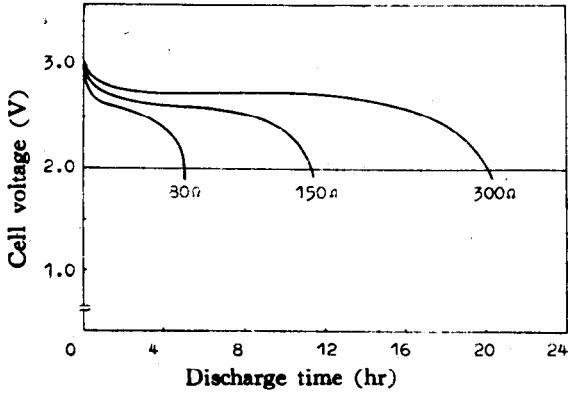

Figure 6. Discharge curves of LF-1/2WH, Li–MnO_2 cells with various loads (Reference 39). (Reprinted by permission.)

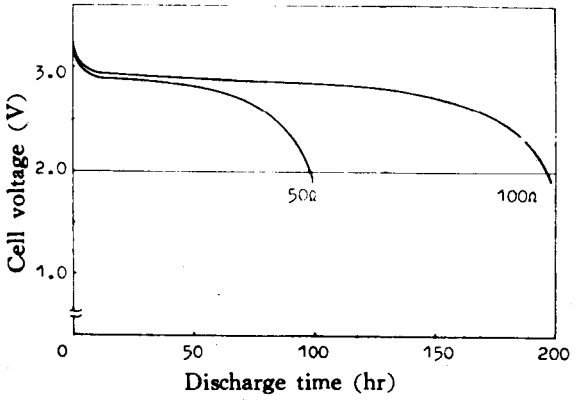

Figure 7. Discharge curves of round cell, LR-C, Li–MnO_2, with various loads (Reference 39). (Reprinted by permission.)

(LR-C), respectively. It is seen that the double anode and cathode construction of the paste-type flat cell permits higher drain rates than the pressed powder cathode cell, with some sacrifice of optimum capacity. At low drain rates, the discharge curve slopes only slightly, providing service in the 2.7–2.8-V range for about the first 75% of the discharge capacity.

The expected products of Li_2O and Mn_2O_3 for a one-electron discharge of a Li–MnO_2 cell are not observed in X-ray diffraction analysis.[37] Also, the cell potential calculated from thermodynamic data is 2.69 V for these products, significantly lower than observed experimentally. These facts coupled with analytical data correlating the quantity of lithium found in the cathode with degree of discharge, led Ikeda and co-workers[37] to propose a mechanism wherein lithium cations diffuse into the MnO_2 lattice upon discharge. Equation (1) describes the proposed mechanism:

$$Li + Mn(IV)O_2 \rightarrow Mn(III)O_2(Li^+) \qquad (1)$$

2.3.4. Li–Ag_2CrO_4 Cells

This couple is the basis of a low-drain-rate cell with good shelf life characteristics developed by SAFT[41,42] and P. R. Mallory and Co.[43,44] It has been marketed by SAFT for use in pacemakers and in electronic watches.

Cell construction and performance have been described in detail[41] for a button cell designated at WM15. The general constructional details for this cell, which is designed to deliver 120 mAh at very low drain rates, is given in Figure 8. Discharge capacity as a function of drain rate for 62- and 15-kΩ loads are given[41] in Figure 9. It was found that there was a significant reduction in

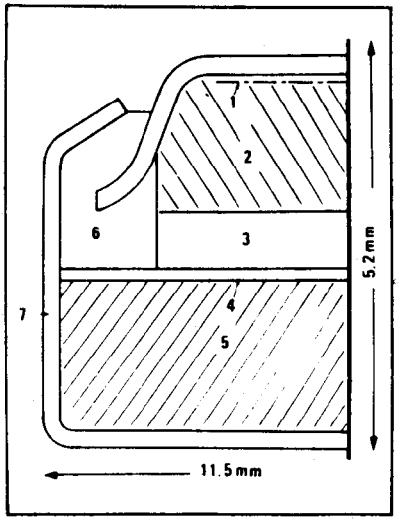

Figure 8. Construction details of a Li-Ag_2CrO_4 button cell (Reference 41). (Reprinted by permission.)

capacity with a 15-kΩ load. The electrolyte was $LiClO_4$ in an unspecified organic solvent.

The excellent storage capability at elevated temperature was demonstrated with only small capacity losses in the 45–100°C range after one month storage.

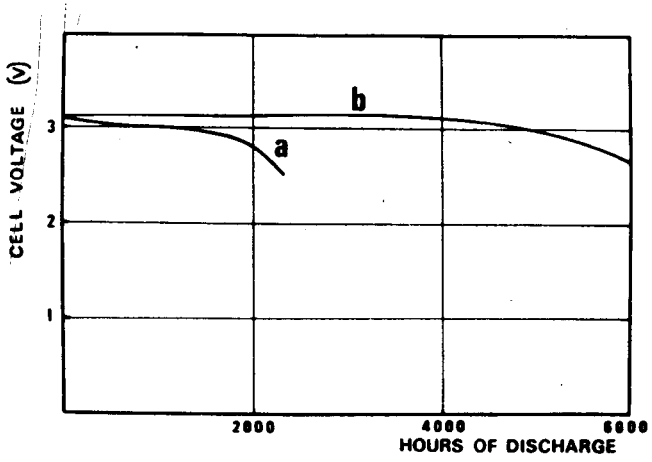

Figure 9. Discharge characteristics of a WM15 Li-Ag_2CrO_4 cell at loads of (a) 62 kΩ and (b) 150 kΩ (Reference 41). (Reprinted by permission.)

The cell balance for the button cell described above was negative limited to involve only a two-electron reduction:

$$2Li + Ag_2CrO_4 \rightarrow Li_2CrO_4 + 2Ag \quad (2)$$

Further reduction of Li_2CrO_4 occurs at more negative potentials than the Ag_2CrO_4 reduction of the silver component. The mechanism for the overall reaction, Eq. (2), is believed to be more complicated than the straightforward reduction of Ag(I). Messina *et al.*[45,46] showed that, even though mass transport problems are severe, the electrochemical process can be broken down into two consecutive steps: (1) the reduction of Cr(VI) to Cr(V) and (2) the reoxidation of Cr(V) to Cr(VI) by Ag(I), which yields the overall reaction products.

2.3.5. Li–V_2O_5

The Li–V_2O_5 cell provides a moderate-drain-rate, high-voltage system that has been developed by the Livingston Electric Corporation (now a division of Honeywell Corp.) primarily for military applications[47–50] and by P. R. Mallory and Co., Inc.[36,51] Cell construction and performance data have been released[47] for a DD-size cell, which has the same diameter as a D cell but twice the length. Because of the high-initial-discharge voltage of about 3.3 V, it is intended to be equivalent to two aqueous electrolyte D cells in series. Much of the present work[48–50] appears to be in the development of reserve cells in which the electrolyte is encapsulated in a frangible sealed tube in the center of the cell.

The DD cell uses multiple parallel plates of lithium anodes and pressed powder V_2O_5-based cathodes separated by porous polypropylene separators. The lithium anode current is collected by a central metal rod. Cathodes are isolated from the central rod by insulating rings and are press fit to the cell case wall. The poor electronic conductivity of V_2O_5 requires the use of a conductive powder such as graphite in addition to the binder which is the normal component of a pressed powder cathode mix. The electrolyte with this cell construction was reported to be a solution of $LiAsF_6$ and $LiBF_4$ in methyl formate solvent. This electrolyte has been found to be thermally unstable in the cell environment, however,[50] which has led to the reserve cell approach. Salts such as $LiClO_4$ or $LiBF_4$ with solvent mixtures containing propylene carbonate and tetrahydrofuran have also been used with the Li–V_2O_5 system.[51]

Figure 10 shows a typical, ambient temperature, multistep discharge curve for 20-mA drain on a DD cell.[47] At low drain rates, Li–V_2O_5 cells deliver coulombic capacity equivalent to about three electons per V_2O_5 unit, but specific reactions attributed to each step are not known in detail. Whittingham[52] has postulated that the first voltage plateau (above 3.0 V) may be due to the diffusion of lithium ions into the V_2O_5 lattice to form LiV_2O_5. The mechanism of the first reaction step was reviewed and it was shown that the

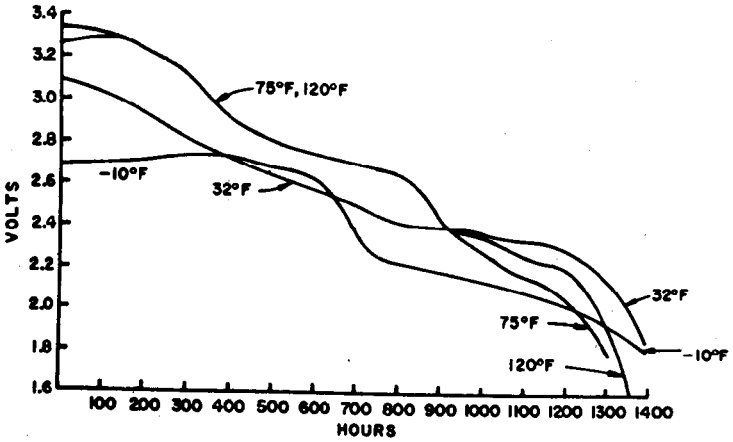

Figure 10. Discharge curves of DD-size Li–V_2O_5 cells at 20 mA and various temperatures (Reference 41). (Reprinted by permission.)

purity of the starting material is critical to the performance of the cell at the high voltage level.[53]

2.3.6. Li–CuS Cells

The use of metallic sulfides as the oxidizing agent in lithium cells using saturated aliphatic amines in the organic solvent was mentioned as a patent claim by Herbert and Ulam in the early 1960s.[54] Later, specific references to lithium–copper sulfide cells were made in the patent literature[55,56] and technical literature[57,58] by Gabano and co-workers of SAFT and in the patent literature by Wuttke of DuPont.[59] Mixtures of cyclic and straight-chain ethers are used as the main solvent components of the electrolyte with $LiClO_4$ as the preferred salt. CuS has good electronic conductivity so no conducting additive is needed in cathode preparations. Cathodes are generally made by mixing cupric sulfide powder with a Teflon binder and cold pressing it into a nickel-plated steel strip. After a curing step, it is separated from a lithium strip by nonwoven polypropylene. After appropriate tabs are inserted it is placed as a coiled element into a nickel-plated steel can.[58]

Discharge data[58] for D-size cells are given in Figure 11 at loads ranging from 1 to 10 Ω. The two-step discharge that is apparent at the high-resistance loadings has been attributed to the two-stage reduction of Cu^{2+} to metallic copper. However, Eichinger and Fritz[60] have shown that the second discharge step is solvent dependent and does not occur in propylene carbonate. Moreover in solvents such as DMF, the second plateau is larger than the first, giving an overall two-electron efficiency of more than 100%. Their results

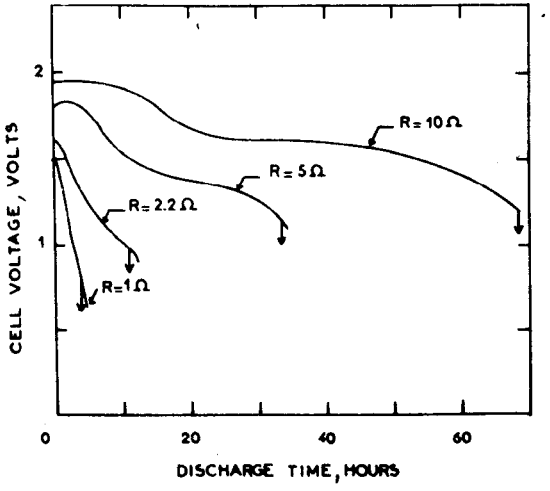

Figure 11. Discharge curves of 13 Ah D-size Li–CuS cells at various loads (Reference 58). (Reprinted by permission.)

support direct discharge of CuS to copper without a defined, stable Cu_2S intermediate. The second plateau is attributed to solvent or solvent impurity reduction. The specific energy at ambient temperature discharge ranges from about 100 Wh/kg at high drain rates to 300 Wh/kg at low rates. The best performance reported, at very low drain rates, corresponded to a volumetric energy density of 470 Wh/dm^3, which compares favorably to the Zn–HgO system, which has the best volumetric energy density (350 Wh/dm^3) in aqueous electrolytes for the D-size cell.[58]

2.3.7. *Li–MoO_3 Cells*

Knapp[34] carried out studies in the mid-1960s on the use of MoO_3 in organic solvent lithium cells. He concluded that useful cells could be made with several of these cathode materials, but ranked CrO_3, metadinitrobenzene, $HgSO_4$, and sulfur as better cathode materials than MoO_3. Other investigators[61–63] became interested in the discharge behavior of Li–MoO_3 cells because of the relatively high energy density and the apparently high coulombic capacity based on an anticipated capacity of 2 faradays per MoO_3 unit. Later workers[36,64–67] showed that only 1.5 faradays per MoO_3 unit are obtained in the discharge.

The Li–MoO_3 system has been tested in 0.41-cm-high by 1.1-cm-diameter button cells by Margalit[66] and in D-size cells by Dampier[65] at ESB Inc. The finished cathode in the button cell contained 85% or more of MoO_3

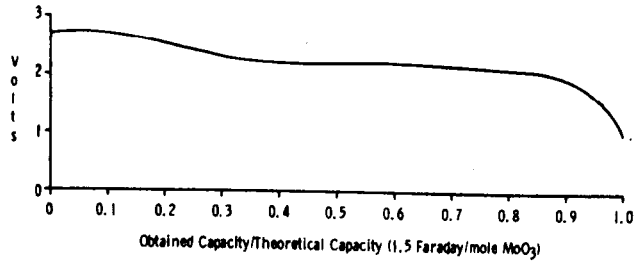

Figure 12. Discharge curve of a Li–MoO_3 cell at 35°C and 15.0 kΩ load; 577 hr of discharge (Reference 66). (Reprinted by permission.)

and the balance was carbon powder, because of the very low electronic conductivity of MoO_3, and a fluorocarbon binder. The salt was $LiAsF_6$ and the solvent γ-butyrolactone. Figure 12 gives a discharge curve for the button cell at 35°C and 15-kΩ load.[66] The cells show two plateaus and deliver about one-third of their capacity in the first discharge step, which amounts to about 1.5 faradays per MoO_3 unit at these low currents.

Besenhard and Schollhorn[67] studied the discharge of MoO_3 cathodes in several different salt–solvent combinations and found the redox reaction not very dependent on the nature of the anion, but strongly dependent on the size and nature of the cation present in solution. Bare cations are believed to be taken up into the interlayer space between MoO_3 planes during discharge. The normal distance of 6.93 Å between planes is increased to 7.85 Å when Li^+ ions are present.

DiPietro *et al.*[68] found that cathodes could be made without added carbon if the substoichiometric Mo_8O_{23} (a low-resistivity semiconductor) was used in place of MoO_3. The high voltage plateau was found to deliver only 1 faraday per MoO_3 unit, however.

3. Liquid Cathode Cells

A number of liquid cathodes for lithium cells have been evaluated, but this chapter will deal only with those systems which have been carried to the cell development stage. The Li–SO_2 system, invented by Maricle and Mohns[69] of American Cyanamid, was the first liquid cathode to be developed since early work in the battery art. It has had much study and development devoted to it and is already a commercial reality. Li–$SOCl_2$ and Li–SO_2Cl_2 cells, pioneered independently by Blomgren and Kronenberg,[70] A. Heller and co-workers,[71] and Behl *et al.*[104] have been shown to have outstanding specific energy and energy density. However, only the Li–$SOCl_2$ system is commercially available at present.

3.1. Electrolyte Solution Properties

The solvent must perform two roles in a liquid cathode cell. First, it must provide an ionization medium which allows good ionic conduction in the electrolyte solution with the usual physical properties required of an electrolyte solution. Second, it must perform as the cathode active material. These two roles place severe demands on the physical and electrochemical properties.

3.1.1. Physical Properties

The ideal physical properties are as follows. The solvent should have a low melting point and high boiling point to permit battery operation under conditions actually encountered in practice. The solvent should have high salt solubility (greater than 1 M) for at least some salts which are compatible with anode-active material, electrodes, and construction materials; a dielectric constant high enough to permit good ionization and dissociation of the electrolyte salt, and low viscosity of the solution to allow good ion mobility. The solvent should have a reasonably low vapor pressure to ensure that gas pressure will not cause venting of the cell owing to expected or normal abusive handling. The solvents must be thermally stable towards decomposition throughout the range of temperatures expected for operation of the cell. The solvent itself must be chemically and electrochemically stable or metastable towards anode-active materials, electrode materials, and materials of cell construction throughout the expected temperature range, except of course for the desired reduction of the solvent at the cathode collector. The desired cathodic reduction reaction should proceed with as high specific energy and energy density as possible without severe rate limitations or passivation mechanisms which prematurely limit the capacity of the cell. These very stringent requirements will be discussed in turn for the various liquid phase oxidants which have been used, and the degree to which the ideal properties have been approached will be considered.

Table 3 gives physical properties for the solvents under discussion. Obviously, the high vapor pressure and low boiling point of sulfur dioxide are the most serious limitations of the physical properties of this solvent. The other two solvents have useable liquid ranges. Sulfur dioxide has a moderate dielectric constant which permits reasonable ionization of electrolyte salts. Sulfuryl chloride and thionyl chloride have low dielectric constants, but the low viscosities allow reasonable conductivities to be obtained when bulky anion salts of lithium are used as electrolytes. $LiAlCl_4$ is a particularly satisfactory salt for these solvents. SO_2 and $SOCl_2$ are more stable to thermal decomposition than SO_2Cl_2.

Table 4 gives conductivity results of various salts in several of the solvents of interest. The combination of higher dielectric constant and improved solvation properties imparted by the acetonitrile–propylene carbonate (AN–PC) mixture added as cosolvent to SO_2 results in a high solubility of LiBr (the

Table 3
Physical Properties for Solvents for Liquid Cathode Cells[a]

Substance	Melting point, °C	Boiling press, °C	Density,[b] g/cm^3
Sulfur dioxide (SO_2)	−75.46	−10.02	1.3695
Sulfuryl chloride (SO_2Cl_2)	−54.1	69.4	1.6570
Thionyl chloride ($SOCl_2$)	−104.5	75.8	1.629

	Dielectric[c] constant	Viscosity,[b] cP	Vapor pressure,[c] torr
Sulfur dioxide (SO_2)	14.1	0.291	2454
Sulfuryl chloride (SO_2Cl_2)	9.15[d]	0.674	106.5
Thionyl chloride ($SOCl_2$)	9.25	0.603	96.65

[a] All data from *Gmelins Handbuch der Anorganischen Chemie*, Vols. 9B1 (1953) and 9B3 (1963), Verlag Chemie, GmbH, Weinheim.
[b] 25°C.
[c] 20°C.
[d] 22°C.

solubility of LiBr in SO_2 at 0°C, is only 6×10^{-3} M[72]) and extremely high conductivity for a nonaqueous solution. The relatively high conductivity of $SOCl_2$ solutions of various salts must be a result of the low viscosity of the solvent. For $AlCl_3$–$SOCl_2$ solutions, however, the low conductivity observed must result from poor ionic dissociation. $AlCl_3$ in $SOCl_2$ is an unsatisfactory electrolyte in any case as it has been found to cause rapid corrosion of lithium

Table 4
Electrical Conductivities of Electrolyte Solutions for Liquid Cathode Cells

Solvent	Reference	Electrolyte	Concentration, mol/liter	Specific conductance, $\times 10^3$ cm^{-1}
50 wt% SO_2: 40 wt% (3 AN: 1 PC volume ratio)	73	LiBr	10 wt%	60
$SOCl_2$	71	$LiAlCl_4$	1.0	14.6
$SOCl_2$	71	$LiAlCl_4$	2.0	20.4
$SOCl_2$	85	$LiAlCl_4$	2.8	20
$SOCl_2$	85	$LiAlCl_4$	4.0	15
$SOCl_2$	71	$LiSbCl_6$	1.0	12.5
$SOCl_2$	[a]	$AlCl_3$	3.93	0.841
SO_2Cl_2	71	$LiAlCl_4$	1.0	7.4

[a] E. B. Rosser, The Application of Thionyl Chloride as a Parent Solvent, Solubility and Conductance of Aluminum Chloride in Thionyl Chloride, Ph.D. thesis, Case Western Reserve University, Cleveland (1952).

in a mixture containing 1 *M* $LiAlCl_4$ and 10% $AlCl_3$.[5] While all of these conductivities are low by aqueous solution standards they are adequate to produce reasonable currents in batteries with a small separation between electrodes as will be seen in the cell results discussed later. It is of interest that liquid phase oxidant cells, unlike many solid oxidant cells, undergo a change in the conductance of the solution as the cell is discharged because the composition of the liquid phase changes owing to removal of solvent oxidant and appearance of the reduced product. Thus in SO_2 cells Bro *et al.*[73] have shown that the conductivity passes through a maximum as SO_2 is removed from the electrolyte during discharge and that an optimum conductivity situation may be selected by adjusting the salt and organic cosolvent concentrations.

3.1.2. Electrochemical Properties

Maricle and Mohns[69] discussed the overall cell reaction for Li–SO_2 cells in their patent, but did not present any evidence to support the mechanism. The rather complex reaction mechanism for the reduction of SO_2 in an organic solvent was well studied in a paper by Martin and Sawyer,[74] which may be consulted for reference to earlier work. These authors showed by means of electrochemical techniques and uv spectroscopy that the initial one-electron reduction of SO_2 to form the negative free radical SO_2^- is followed by several chemical reactions. The free radical may either associate with unreacted SO_2 or dimerize to form dithionite ion. The dithionite may either associate with SO_2 to form a complex which is reducible at much more negative potentials or precipitate (especially in the presence of alkali ions). The rates of these various reactions appear to be sensitive to the particular cosolvent which is chosen. Bro *et al.*[73] found by chemical analysis of cathodes of discharged Li–SO_2 cells that the sole reaction product was lithium dithionite, which agreed with the postulate of Maricle and Mohns[69] and expectations from the dilute solution studies[74] when a lithium salt is used as the electrolyte.

The reduction of $SOCl_2$ and SO_2Cl_2 have been studied by Blomgren *et al.*[75] by electrochemical methods and chemical analysis of cell reaction products. SO_2Cl_2 reduction was shown to occur through parallel paths by a rather complex mechanism. The initial step is a one-electron reduction as for SO_2, followed by a side reaction (undoubtedly small) to form some $SOCl_2$ and a second one-electron reduction to form SO_2 and LiCl. At more negative potentials the SO_2 is reduced to dithionite and the dithionite to thiosulfate. All of the above materials, with the exception of thionyl chloride, were determined as products by chemical analysis, and a mass balance was obtained.

The reduction mechanism of $SOCl_2$ is considerably more controversial. Blomgren *et al.*[75] believed the reduction proceeds through an initial one-electron reduction step followed by a disproportionation to form SO_2 and an S_2Cl_2 intermediate (detected by low-temperature gas chromatography). Reduction of S_2Cl_2 was believed to occur to form sulfur and LiCl. The presence

of SO_2, S, and LiCl was proven by chemical analysis and again a mass balance was obtained. Dey,[76] on the other hand, proposed a two-electron reduction to an SO intermediate which decomposes to S and SO_2 or may form polymeric sulfur–oxygen compounds.[5] Such polymeric materials have not been observed analytically, but their presence could account for the slower than predicted pressure increase in discharging cells as discussed by Schlaikjer *et al.*[77] These interesting systems will no doubt be the subject of much further study.

The anode reaction mechanism has not been thoroughly studied, but the overall reaction is clearly lithium ion dissolution for all of the systems under discussion. The unique feature of the anode, of course, is that it does not react vigorously with the solvent. In all of the systems, exposure of the anode to the electrolyte solution is accompanied by the formation of a thin layer of corrosion product. As the exposure time is increased the thickness of the layer increases and the porosity of the layer decreases. This is the origin of the anode delay or passivation effect which is seen as an initial voltage suppression for the cell followed by a more or less rapid recovery to the normal closed-circuit voltage seen with fresh cells. This effect will be further discussed in Section 3.3.

3.2. Discharge Data on Liquid Cathode Cells

In this section, direct comparisons of discharge data will be limited to fresh cells since the lithium passivation that occurs in storage does not appear to be completely predictable and controllable at this time, although considerable progress has been reported on defining and controlling passivation.

In order to compare results reported by various laboratories, we will discuss discharge results from AA, C, or D cells whenever possible. Energy density comparisons will be made using 7.9 cm^3 for the AA cell, 24.9 cm^3 for the C cell, and 52.5 cm^3 for the D cell.

3.2.1. Li–SO_2 Cells

Li–SO_2 cells are useful for high-rate applications and are usually constructed with the "jelly roll" configuration to maximize anode and cathode area. A schematic diagram[78] of a cell design for this type of cell is shown in Figure 13. This design uses a steel can which contacts the lithium anode and an aluminum top that contacts the current collector for the SO_2 cathode. Anodes were constructed by rolling lithium foil in a copper metal grid. Cathodes were 0.9 mm thick and measured 38 by 165 mm and were made by spreading carbon paste onto an expanded aluminum grid. The resulting porosity after drying was about 80%. The foil electrodes were separated by porous polyethylene and rolled together. The total active area of the electrodes in this slightly larger than C-size cell was 126 cm^2 including both sides of the electrodes. Completed cells weighed 41 g and occupied a volume of 22.6 cm^3. The electrolyte was 1.8 *M* in

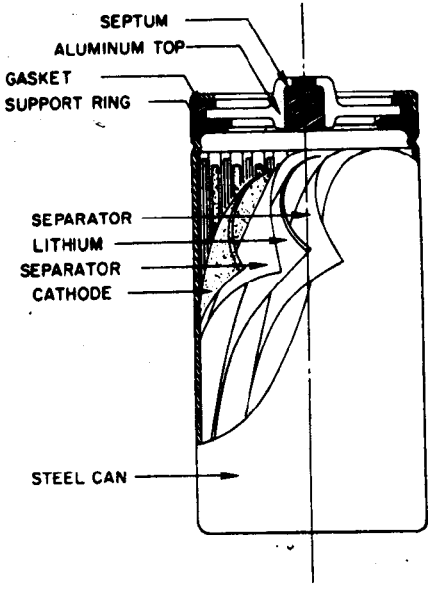

Figure 13. Diagram showing construction details of a Li–SO_2 cell (Reference 78). (Reprinted by permission.)

LiBr and contained sulfur dioxide, acetonitrile, and propylene carbonate in the volume ratio 23 : 10 : 3.

Typical discharge curves for Li–SO_2 D-size cells at ambient, elevated, and subambient temperatures are given[79] in Figure 14. The rise in cell voltage shortly after cells are placed on load is attributed to a recovery from lithium passivation. This recovery occurs within several minutes or less. At this

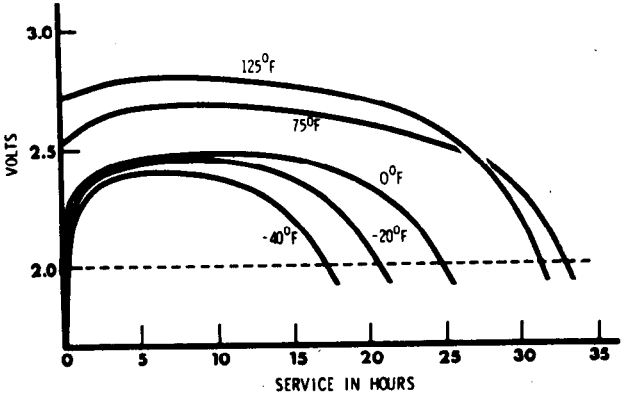

Figure 14. Discharge curves at 0.250 A of Li–SO_2 D-size cells at various temperatures (Reference 79). (Reprinted by permission.)

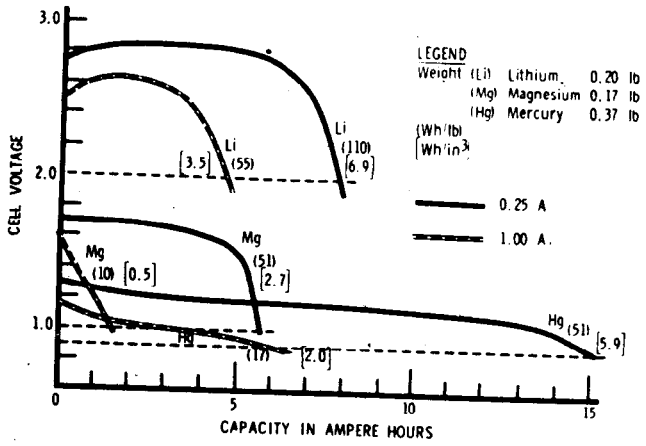

Figure 15. Comparison of Li–SO_2, Mg–MnO_2, and Zn–HgO D cells at 23.5°C (Reference 79). (Reprinted by permission.)

relatively low drain rate (0.25 A), the low-temperature performance is relatively good with more than 50% of the room temperature performance obtained at −40°C and over 70% at −17.8°C.

Room temperature discharge performance for Li–SO_2 D cells compared to Mg–MnO_2 and Zn–HgO cells at drain rates of 0.25 and 1.0 A are given[79] in Figure 15. It is seen that the lithium cells have the highest energy densities for the three systems on both a volume and weight basis. The Zn–HgO and Mg–MnO_2 cells are bobbin cells and exhibit the relatively poor performance at high current density normally associated with this type of cell.

Figure 16 gives the specific energy for D-size Li–SO_2 cells as a function of load and temperature in the range of −40°C to 49°C. While there is a wide variation in performance level over these ranges, it is seen that a significant utilization is still possible at heavy loads and temperatures as low as −40°C. In fact, the specific energy at −40°C is comparable to that of a mercury cell at room temperature.

3.2.2. Li–$SOCl_2$ Cells

Most lithium–thionyl chloride cells have used a spiral wound configuration similar to that described for Li–SO_2 cells. Materials of construction, however, are limited to fluorocarbon plastics, glass, nickel, and stainless steel. This is primarily due to the corrosive nature of the solution, which contains 0.5–1.8 *M* $LiAlCl_4$ in thionyl chloride. Lithium sheet pressed into expanded nickel screen is used as the cathode collector. Anode and cathode are separated by glass filter papers, and fluorocarbon plastic disks are used as insulators.

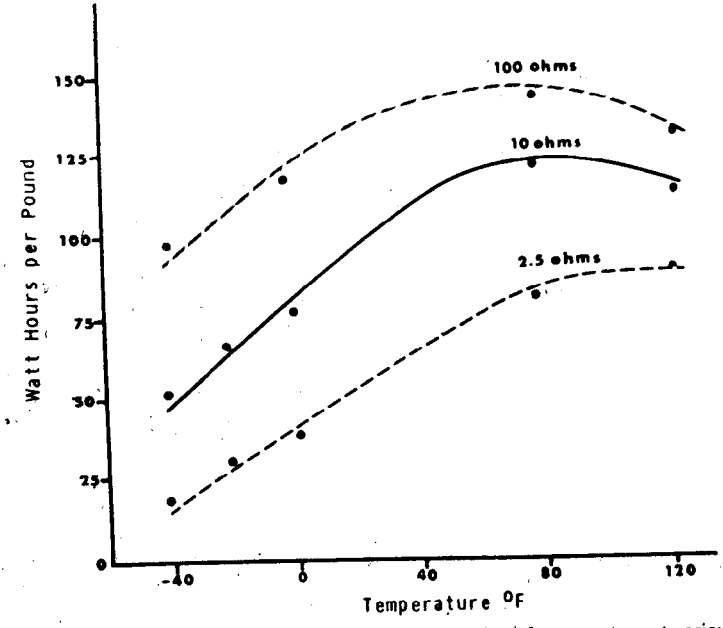

Figure 16. Specific energy of the Li-SO_2 system as a function of temperature at various loads (Reference 80). (Reprinted by permission.)

For moderate- and low-drain applications, "bobbin" cells[81] and button cells[82] have been proposed. The bobbin cell consisted of a central "bobbin" cathode with a lithium sheet anode pressed to the inside wall of the nickel cell container. The button cells were made in two sizes, 0.210 in. high by 0.455-in. diameter and 0.120 in. high by 1.256-in. diameter and were hermetically sealed with glass to metal seals. Internal construction details were not described.

Typical ambient temperature discharge curves for freshly prepared D cells[83] using a spiral wound configuration at various constant currents are given in Figure 17. Cell voltages are relatively flat over the course of the discharge with voltage plateaus at about 3.5, 3.2, and 2.8 V for 0.1-, 1.0- and 3.0-A drain rates, respectively. It is seen that cell capacity significantly decreases with drain rate—from about 12 Ah at the 0.1-A rate to about 8 Ah at the 3.0-A rate.

Table 5 summarizes ambient temperature discharge information from several sources for three sizes of Li-$SOCl_2$ cells of the spiral wound type. The energy density ranges from about 366 Wh/dm^3 at high drain rate to over 1000 Wh/dm^3 at low rates. This is about ten times the average energy density for Leclanché cells, four times that of alkaline cells, and about 1.5 times that of

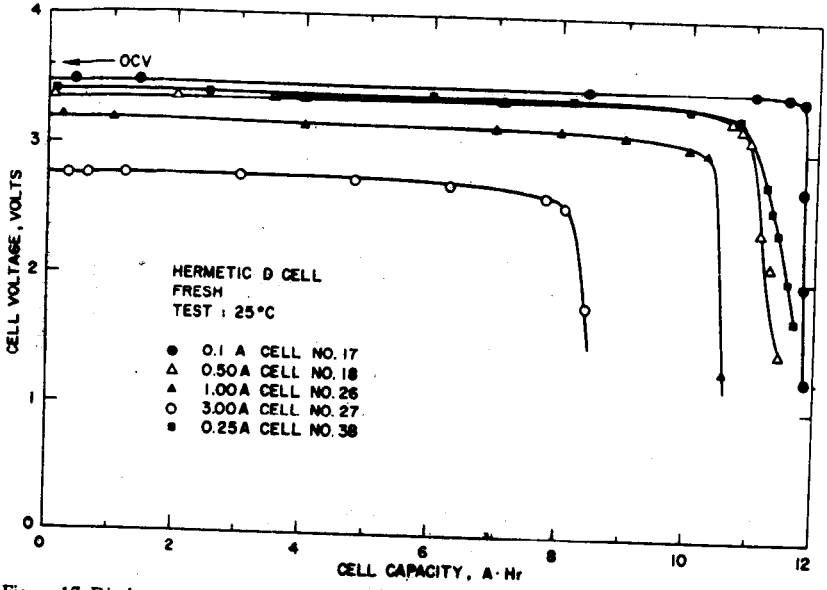

Figure 17. Discharge curves of fresh Li–$SOCl_2$ D-size cells at various constant currents (Reference 83). (Reprinted by permission.)

Li–SO_2 cells. A further optimization with D cells[87] led to a low drain energy density of 1240 Wh/dm^3 (20 Wh/in.^{3}) with specific energy of 660 Wh/kg (300 Wh/lb).[87] Figure 18 shows the energy density and specific energy as a function of current for D cells optimized for rate or for energy density. These

Table 5
Comparison of Room Temperature Discharge Results for Fresh AA, C, and D Spiral Wound Cells

Cell size	Reference	Discharge current, A	Discharge capacity, Ah	Plateau cell potential, V	Energy density, Wh/dm^3
AA	81	0.06	1.20	3.35	513
AA	81	0.30	1.20	3.15	482
AA	85	0.02	2.23	3.53	1025
AA	85	0.20	1.69	3.39	744
AA	85	1.0	0.94	3.04	366
C	84	0.10	5.2	3.40	708
C	84	0.30	4.7	3.30	622
C	84	1.0	3.9	3.20	500
D	83	0.1	11.9	3.40	769
D	83	1.0	10.3	3.20	628
D	83	3.0	8.3	2.75	433

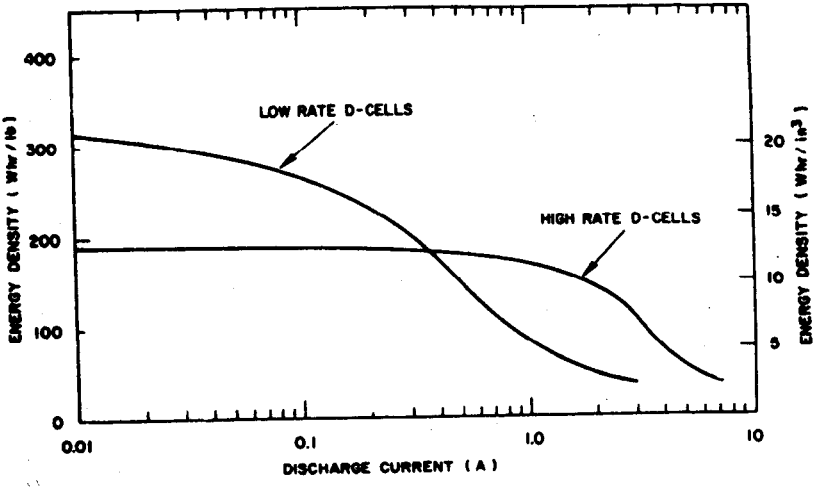

Figure 18. Energy densities and specific energies of high- and low-rate types of Li–$SOCl_2$ D-size cells (Reference 87). (Reprinted by permission.)

remarkable results show the inherent superiority of the liquid cathode battery concept for these important properties.

The results for button cells[82] showed similar excellent performance. The energy density of the smaller cells was 915 Wh/dm^3 (15 Wh/in.^{3}), while the larger cells were capable of pulse-type operation with 40-mA, 2-sec-duration pulses.

The bobbin cells[81] showed a somewhat sloping discharge curve for AA cells and a more steeply sloping curve for D cells. The slope to the discharge curve was attributed to a porous electrode effect of the relatively thick porous carbon cathodes. Higher energy density was obtained from these cells than from comparable spiral wound cells, nevertheless.

3.2.3. Li–SO_2Cl_2 Cells

Relatively little sealed cell discharge data has been published for this system even though it is a higher-voltage, and possibly higher-energy-density, system than Li–SO_2 or Li–$SOCl_2$. Heller[88] compared AA-size cells with $SOCl_2$ and SO_2Cl_2 liquid cathodes at a current of 0.03 A and found that the sulfuryl chloride cell discharged at an average voltage level of about 0.3–0.4 V higher than the corresponding thionyl-chloride-based cell. For the data shown, the energy density was approximately 752 Wh/dm^3 for the Li–$SOCl_2$ cell and 885 Wh/dm^3 for the Li–SO_2Cl_2 cell.

At higher drain rates the sulfuryl chloride cell has shown significantly higher coulombic capacities than thionyl chloride based cells. At a current density of 26 mA/cm^2 (anode), a Li–$SOCl_2$ cell gave about 360 mAh of capacity compared to a 600-mAh capacity for a Li–SO_2Cl_2 cell of the same size.[85]

Auborn and Marincic[81] also obtained higher capacities for AA cells with SO_2Cl_2 compared to $SOCl_2$ at both high and low rates.

Gilman[89] indicated that the larger liquid range of $SOCl_2$ compared to SO_2Cl_2 (Table 3) made $SOCl_2$ a more favorable candidate for development.

3.3. Anode Delay Phenomena

The fact that lithium does not dissolve significantly in the presence of liquid phase oxidants unless the cell is under an external load is attributed to the presence of a protective film. In fresh cells this protective layer does not interfere with cell discharge under normal conditions. However, the film increases in thickness with time and its growth is accelerated with increasing temperature.

In SO_2 cells the film is believed to be mostly dithionite,[69] and in the presence of oxyhalides, mostly LiCl.[5] In the case of oxyhalides, the LiCl film also appears to form over the nickel or stainless steel–anode support screen, preventing excessive solvent reduction on these surfaces.[90]

The delay in attaining the normal operating voltage may vary from seconds to even hours depending on storage and test conditions. In general the results are erratic and not completely predictable. Cells generally do not exhibit significant loss of capacity on storage due to the delay phenomena. It is primarily the initial rate capability that is reduced.

Much detailed data have been reported on anode delay phenomena as a function of storage time, temperature, salt concentration, and subsequent discharge temperature for Li–$SOCl_2$ cells. Several remedies such as addition of excess $AlCl_3$,[5] SO_2 additions,[5] electrolyte purification,[90] polymeric anode coatings,[91] anode pretreatment with calcium,[92] use of clovoborate salts,[93] and new electrolyte salts[94] have been suggested and hold promise that this problem will be resolved.

Recent studies by Peled[95] indicated that anodic protection for Li–$SOCl_2$ cells may be due to the creation of a very thin compact film which conducts lithium ions, but not electrons. Anode delay would then be a result of a creation of a thick porous film.

Relatively little has been written about anode delay phenomena in Li–SO_2 cells, but one work[96] indicates that similar phenomena occur with this system except at higher storage temperatures and longer storage times than Li–$SOCl_2$ cells. After 72°C storage, delays of 7–80 sec were experienced at high currents, and considerable scatter in the data was observed.

3.4. Safety Considerations

Sulfur dioxide, thionyl chloride, and sulfuryl chloride are not flammable but have high toxic ratings for skin irritation, for ingestion, and for inhalation. Organic cosolvents used with SO_2 cells are flammable, however. Thionyl chloride gives HCl and SO_2 and sulfuryl chloride yields HCl and H_2SO_4 in the presence of moist air. Extended exposure to vapor concentrations above 20 ppm for any of these materials is highly irritating to the upper respiratory tract.

The use of oxyhalide cells at high rates, short-circuit conditions, or forced overdischarge has occasionally led to thermal runaways and explosions. Explosions may be caused by the reaction of molten lithium (mp 180°C) with molten sulfur product (mp 120°C).[87] Considerable progress has been made in reducing cell instability by the use of low-pressure vents[83,97] and by reducing the rate capability of cells by using bobbins instead of spiral wound cells.[98] S_2Cl_2 which dissolves considerable sulfur has also been used[99] as an additive to prevent the direct contact of lithium and solid sulfur.

Li–SO_2 cells have also shown the presence of instability leading to explosions in some cases. Shah[100] has shown that the electrolyte salt and the cosolvents lead to instability, particularly in the presence of water contaminants. DiMasi[101] observed explosions in cells with an excess of Li compared to SO_2. Kilroy and Dallek[102] observed violent reactions with cell components and product combinations with differential scanning calorimetry. Proper cell balance[101] and low-pressure vents[103] appear to be helpful in alleviating the instability problems in active primary batteries, while a new electrolyte may be required for reserve cell applications.[100]

4. Summary and Future Possibilities

A large number of lithium battery systems have been discussed in this chapter. Each of the systems is either in use today in competition with aqueous batteries or in an advanced state of development with potential applications in view. We believe that there will be other systems brought to at least the stage of development of the systems discussed here because of the ease of obtaining relatively high voltages with use of lithium anodes. The competition with aqueous batteries has been joined, but the eventual emergence of large-scale production and ready availability of lithium batteries depends on economic, performance, and safety factors. Some of these factors are more difficult to establish than the purely technical matters, which have already shown lithium batteries to be superior to aqueous systems in many applications. The use of lithium batteries in many military applications is almost assured because of the lesser role of economics in the cost–performance trade-offs. We anticipate that much of the study in the near future will deal with the development of

production methods to produce batteries reliably and establish quality standards and costs. Obviously, the success of lithium batteries in commercial and to some extent military applications will depend on the results of such studies.

References

1. W. S. Harris, Ph.D. thesis, University of California, Berkeley, 1958.
2. R. Jasinski, *High Energy Batteries*, Plenum Press, New York (1967).
3. J. O. Besenhard and G. Eichinger, *J. Electroanal. Chem.* **68**, 1 (1976).
4. G. Eichinger and J. O. Besenhard, *J. Electroanal. Chem.* **72**, 1 (1976).
5. A. N. Dey, *Thin Solid Films* **43**, 131 (1977).
6. R. F. Scarr, *J. Electrochem. Soc.* **117**, 295 (1970).
7. R. Jasinski, in *Advances in Electrochemistry and Electrochemical Engineering*, Vol. 8, P. Delahay and C. W. Tobias, eds., Interscience, New York (1971), p, 253.
8. R. Jasinski and S. Carroll, *J. Electrochem. Soc.* **117**, 218 (1970).
9. B. M. L. Rao, G. H. Newman, R. W. Francis, and L. H. Gaines, in Extended Abstracts, Electrochemical Society Fall Meeting, Atlanta, 1977, paper No. 7.
10. O. Ruff and O. Bretschneider, *Z. Anorg. Allg. Chem.* **217**, 1 (1934).
11. W. Rüdorff and G. Rüdorff, *Z. Anorg. Allg. Chem.* **253**, 281 (1947).
12. W. Rüdorff, in *Advances in Inorganic Chemistry and Radiochemistry*, Vol. 1, H. J. Emeleus and A. G. Sharpe, eds., Academic Press, New York (1959), p. 230.
13. N. Watanabe and K . Kusmen, *Denki Kagaku* **35**, 19 (1967).
14. R. J. Logow, R. S. Bodachape, J. L. Wood, and J. L. Margrave, *J. Chem. Soc. Dalton*, 1268 (1974).
15. D. T. Meshri and W. E. White, in Extended Abstracts, ISE 24th Meeting, Brighton, England, 1974, p. 251.
16. N. Watanabe and M. Fukuda, U.S. Patent 3,536,532 (October 27, 1970); 3,700,502 (October 24, 1972).
17. K. H. M. Braeuer, in Extended Abstracts, Electrochemical Society Spring Meeting, New York, 1969, paper No. 164.
18. M. Fukuda and T. Iijima, in *Power Sources 5*, D. H. Collins, ed., Academic Press, New York (1975), p. 713.
19. M. Fukuda and T. Iijima, in *Record of the 10th Intersociety Energy Conversion Engineering Conference*, Institute of Electrical and Electronics Engineers, New York (1975), p. 413.
20. M. Fukuda and T. Iijima, *Denki Kagaku* **44**, 543 (1976).
21. J. Giltner, U.S. Army Electronics Command Contract No. DAAB07-73-C-0269, Report No. ECOM-73-0269-F, July 1975.
22. D. Linden, N. Wilburn, and E. Brooks, in *Power Sources 4*, D. H. Collins, ed., Oriel Press, Newcastle, England (1973), p. 483.
23. R. G. Gunther, in *Power Sources 5*, D. H. Collins, ed., Academic Press, New York (1975), p. 729.
24. J. L. Wood, R. B. Bodachape, R. J. Lagow, and J. L. Margrave, *J. Phys. Chem.* **73**, 3139 (1969).
25. W. Tiedemann, *J. Electrochem. Soc.* **121**, 1308 (1974).
26. M. S. Whittingham, *J. Electrochem. Soc.* **122**, 526 (1975).
27. H. F. Hunger and J. E. Ellison, *J. Electrochem. Soc.* **122**, 1288 (1975).
28. H. F. Hunger and G. J. Heymach, *J. Electrochem. Soc.* **120**, 1161 (1973).
29. G. Lehman, G. Gerbier, A. Brych, and J. P. Gabano, in *Power Source 5*, D. H. Collins, ed., Academic Press, New York (1975), p. 695.
30. A. Brych, U.S. Patent 3,871,915 (March 18, 1975).
31. G. Lehman and J. Romnaux, U.S. Patent 3,960,595 (June 1, 1976).

32. Y. Matsuda, K. Teraji, and Y. Tahasu, *J. Electrochem. Soc. (Japan)* **44**, 363 (1976).
33. M. Broussely, Y. Jumel, and J. P. Gabano, in Extended Abstracts, Electrochemical Society Fall Meeting, Atlanta, 1977, paper No. 9.
34. H. R. Knapp, U. S. Army Electronics Command ECOM-2632 (AD 627,215), October 1965.
35. F. W. Dampier, *J. Electrochem. Soc.* **121**, 656 (1974).
36. A. N. Dey, in Extended Abstracts, Electrochemical Society Fall Meeting, Boston, 1973, paper No. 54.
37. H. Ikeda, T. Saito, and H. Tamura, in *Manganese Dioxide Symposium*, Vol. 1, I.C. Sample Office, Cleveland (1975), p. 384.
38. H. Ikeda, T. Saito, and H. Tamura, *Denki Kagaku* **45**, 314 (1977).
39. H. Ikeda, S. Ueno, T. Saito, S. Nakaido, and H. Tamura, *Denki Kagaku* **45**, 391 (1977).
40. H. Ikeda, T. Saito, and H. Tamura, U.S. Patent 4,133,856 (January 9, 1979).
41. G. Lehman, T. Rossinaux, G. Gerbier, and J. P. Gabano, *Power Sources 4*, D. H. Collins ed., Oriel, Newcastle, England (1973), p. 493.
42. G. Lehman and J. P. Gabano, U.S. Patent 3,853,627 (December 10, 1974).
43. A. N. Dey and M. L. B. Rao, in Extended Abstracts, Electrochemical Society Fall Meeting, Boston, 1973, paper No. 53.
44. A. N. Dey, U.S. Patents 3,658,592 (April 25, 1972); 3,947,289 (March 30, 1976).
45. R. Messina, M. Broussely, G. Gerbier, and J. Perichon, *J. Appl. Electrochem.* **8**, 87 (1978).
46. R. Messina, J. Perichon, M. Broussely, and G. Gerbier, *J. Appl. Electrochem.* **8**, 405 (1978).
47. M. Lang, J. R. Backlund, and E. C. Weidner, in *26th Power Sources Symposium*, PSC Publications Committee, Red Bank, New Jersey (1974), p. 37.
48. W. F. Meyers, B. Bell, and J. W. Simmons, U.S. Patent 3,423,242 (January 21, 1969).
49. W. J. Eppley, D. K. Szidon, and C. R. Walk, in *Record of the 10th Intersociety Energy Conversion Engineering Conference*, Institute of Electrical and Electronics Engineers, New York, (1975), p. 418.
50. W. B. Ebner and C. R. Walk, in *27th Power Sources Symposium*, PSC Publications Committee, Red Bank, New Jersey (1976), p. 48.
51. A. N. Dey and B. P. Sullivan, U.S. Patents 3,655,585 (April 11, 1972) and 3,947,289 (March 30, 1976).
52. M. S. Whittingham, *J. Electrochem. Soc.* **123**, 315 (1976).
53. M. M. Merriman and G. C. Vezzoli, *Mat. Res. Bull.* **14**, 77 (1979).
54. D. Herbert and J. Ulam, U.S. Patent 3,043,896 (July 10, 1962).
55. J. P. Gabano and G. Gerbier, U.S. Patent 3,511,716 (May 12, 1970).
56. J. P. Gabano, U.S. Patent 3,542,601 (November 24, 1970).
57. J. P. Gabano, G. Gerbier, and J. F. Laurent, in *22nd Annual Power Sources Conference*, PSC Publications Committee, Red Bank, New Jersey (1969), p. 80.
58. J. P. Gabano, V. Dechenaux, G. Gerbier, and J. Jammet, *J. Electrochem. Soc.* **119**, 459 (1972).
59. K. G. Wuttke, U. S. Patent 3,884,723 (May 20, 1975).
60. G. Eichinger and H. P. Fritz, *Electrochim. Acta* **20**, 753 (1975).
61. L. Campanella and G. Pistoia, *J. Electrochem. Soc.* **118**, 1905 (1971).
62. L. Campanella and G. Pistoia, *J. Electrochem. Soc.* **120**, 383 (1973).
63. J. P. Gabano, Y. Jumel, and J. P. Gomis, in Extended Abstracts, Electrochemical Society Fall Meeting, Boston, 1973, paper No. 55.
64. A. N. Dey, U.S. Patent 3,808,052 (April 30, 1972).
65. F. W. Dampier, *J. Electrochem. Soc.* **121**, 656 (1974).
66. N. Margalit, *J. Electrochem. Soc.* **121**, 1460 (1974).
67. J. Besenhard and R. Schollhorn, *J. Power Sources* **1**, 267 (1976).
68. B. DiPietro, V. Filippeschi, M. Lazzari, G. Pistoia, and B. Scrosati, in *Power Sources 6*, D. H. Collins, ed., Academic Press, New York (1977), p. 527.
69. D. L. Maricle and J. P. Mohns, U.S. Patent 3,567,515 (March 2, 1971).

70. G. E. Blomgren and M. L. Kronenberg, Union Carbide Corp., German Patent 2,262,256 (December 20, 1972).
71. J. J. Auborn, K. W. French, S. I. Lieberman, V. K. Shah, and A. Heller, *J. Electrochem. Soc.* **120**, 1613 (1973).
72. P. J. Elving and J. M. Markowitz, *J. Chem. Educ.* **37**, 75 (1960).
73. P. Bro, H. Y. Kang, C. Schlaikjer, and H. Taylor, in *Record of the 10th Intersociety Energy Conversion Engineering Conference*, Institute of Electrical and Electronics Engineers, New York (1975), p. 432.
74. R. P. Martin and D. T. Sawyer, *Inorg. Chem.* **11**, 2644 (1972).
75. G. E. Blomgren, V. Z. Leger, M. L. Kronenberg, T. Kalnoki-Kis, and R. J. Brodd, in *Power Sources 7*, J. Thompson, ed., Academic Press, New York (1979), p. 583.
76. A. N. Dey, *J. Electrochem. Soc.* **123**, 1262 (1976).
77. C. R. Schlaikjer, F. Goebel, and N. Marincic, *J. Electrochem. Soc.* **126**, 513 (1976).
78. P. Bro, R. Holmes, N. Marincic, and H. Taylor, in *Power Sources 5*, D. H. Collins, ed., Academic Press, New York (1975), p. 703.
79. D. Linden, N. Wilburn, and E. Brooks, in *Power Sources 4*, D. H. Collins, ed., Oriel Press, Newcastle, England (1973), p. 483.
80. E. Brooks, in *Record of the 7th Intersociety Energy Conversion Engineering Conference*, American Chemical Society, Washington, D.C. (1972), p. 71.
81. J. J. Auborn and N. Marincic, in *Power Sources 5*, D. H. Collins, ed., Academic Press, New York (1975), p. 683.
82. H. Taylor, S. Simenas, and C. Ralto, in *Proceedings of the 12th Intersociety Energy Conversion Engineering Conference*, American Nuclear Society, LaGrange Park, Illinois (1977), p. 296.
83. A. N. Dey, *Electrochim. Acta* **21**, 855 (1976).
84. A. N. Dey, *J. Electrochem. Soc.* **123**, 1262 (1976).
85. S. Kashehara and G. Takeshima, *GS News* **35**, 38 (1976).
86. A. N. Dey and P. Bro, in *Power Sources 6*, D. H. Collins, ed., Academic Press, New York (1977), p. 493.
87. A. N. Dey and P. Bro, *J. Electrochem. Soc.* **125**, 1574 (1978).
88. A. Heller, *Nav. Res. Rev.* 17 (May 1975).
89. S. Gilman, in *26th Power Sources Symposium*, PSC Publications Committee, Red Bank, New Jersey (1974), p. 28.
90. G. L. Holleck and M. J. Turchan, in *Record of the 10th Intersociety Energy Conversion Engineering Conference*, Institute of Electrical and Electronics Engineers, New York (1975) p. 449.
91. T. Kalnoki-Kis, U.S. Patent 3,993,501 (November 23, 1976).
92. J. R. Driscoll, U.S. Patent 4,093,784 (June 6, 1978).
93. C. R. Schlaikjer, U.S. Patent 4,020,240 (April 26, 1977).
94. J. P. Gabano and P. Lenfant, in Extended Abstracts, Electrochemical Society Fall Meeting, Pittsburgh, 1978, paper No. 27.
95. E. Peled, in Extended Abstracts, Electrochemical Society Fall Meeting, Atlanta, 1977, paper No. 4.
96. H. Taylor, in *Proceedings of the 12th Intersociety Energy Conversion Engineering Conference*, American Nuclear Society, LaGrange Park, Illinois (1977), p. 288.
97. A. N. Dey, in *27th Power Sources Symposium*, PSC Publications Committee, Red Bank, New Jersey (1976), p. 42.
98. J. F. McCartney, W. H. Shipman, and C. R. Gundersen, in *11th Intersociety Energy Conversion Engineering Conference Proceedings*, American Institute of Chemical Engineers, New York (1976), p. 457.
99. J. J. Auborn and R. D. Bezman, U.S. Patent 3,998,657 (December 21, 1976).
100. P. M. Shah, in *27th Power Sources Symposium*, PSC Publications Committee, Red Bank, New Jersey (1976), p. 59.

101. G. DiMasi, in *27th Power Sources Symposium*, PSC Publications Committee, Red Bank, New Jersey (1976), p. 75.
102. W. P. Kilroy and S. Dallek, *J. Power Sources* **3**, 291 (1978).
103. H. Taylor and B. McDonald, in *27th Power Sources Symposium*, PSC Publications Committee, Red Bank, New Jersey (1976), p. 66.
104. W. K. Behl, J. A. Christopulos, M. Ramirez, and S. Gilman, *J. Electrochem. Soc.* **120**, 1619 (1973).

9

Primary Batteries—Solid Electrolytes

JOHN H. KENNEDY

1. Introduction

All electrochemical cells require that the electrodes be separated by a material called the electrolyte. This material prevents an electronic short circuit but, at the same time, must carry electrical charge within the cell via ions. Although the traditional electrolyte in primary battery cells has been an aqueous ionic solution the electrolyte role may be played by any material which exhibits little or no electronic conductivity and adequate ionic conductivity. In recent years a whole host of nonaqueous battery electrolytes has been developed including molten salts, organic and inorganic liquids, and ionically conductive solids.

All liquid electrolyte cells possess the inherent shortcoming of limited shelf life resulting from corrosion reactions of the electrode materials by the electrolyte solutions. Often these corrosion reactions lead to gas evolution which may damage seals and eventual electrolyte leakage. In addition, the useful temperature range of a liquid electrolyte is limited to between its freezing point and boiling point. It is for these reasons that the development of primary batteries which employ solid electrolytes has been pursued.

JOHN H. KENNEDY • Department of Chemistry, University of California, Santa Barbara, California 93106.

We will now consider how ionic solids can meet the requirements for an electrolyte, namely, high ionic conductivity coupled with low electronic conductivity.

2. Conduction Mechanisms in Solid Electrolytes

2.1. Ionic Defects in Crystals

In the ideal ionic crystal all ions reside on their lattice sites, and the ions will exhibit no mobility. This is essentially true for ultrapure alkali halides at low temperature. However, even these materials will contain vacant lattice sites as the temperature is raised, and a small amount of ionic conductivity will be observed. Because the species involved are charged there must be a concentration of vacant anion sites equivalent to the concentration of vacant cation sites in the pure crystal. This situation is called a Schottky defect, and a chemical equilibrium can be written for its formation using NaCl as an example (Kroger–Vink defect notation):

$$Na^{x}_{Na} + Cl^{x}_{Cl} \rightarrow V'_{Na} + V^{\cdot}_{Cl}, \qquad K_{Sf} = [V'_{Na}][V^{\cdot}_{Cl}] \tag{1}$$

in which Na^{x}_{Na} and Cl^{x}_{Cl} represent neutral (compared to the ideal crystal) sodium and chloride ions on their lattice sites, V'_{Na} represents a negatively charged sodium ion site vacancy, and $V^{\cdot}_{Cl}$ represents a positively charged chloride ion site vacancy. K_{Sf} is the equilibrium constant for the Schottky defect formation.

A second type of defect commonly encountered in ionic crystals leading to ionic conductivity is the Frenkel defect in which an ion on a lattice site moves to an interstitial position. This defect is found in silver halides, and its formation may be expressed as

$$Ag^{x}_{Ag} \rightarrow Ag^{\cdot}_{i} + V'_{Ag}, \qquad K_{Ff} = [Ag^{\cdot}_{i}][V'_{Ag}] \tag{2}$$

in which Ag^{x}_{Ag} represents a neutral (compared to the ideal crystal) silver ion on a silver ion site, $Ag^{\cdot}_{i}$ a positively charged interstitial silver ion, and V'_{Ag} a negatively charged silver ion site vacancy. Note that in the case of a Frenkel defect only one type of ion needs to be mobile and that electroneutrality is maintained by the interstitial and vacancy defect pair.

With the formation of ionic defects the solid may now exhibit ionic conductivity. Three mechanisms for charge transport are usually considered:

(i) Vacancy mechanism in which there is an exchange of a vacancy with a neighboring ion on a normal lattice site.
(ii) Direct interstitial mechanism in which an interstitial ion moves to a neighboring equivalent interstitial site.
(iii) Indirect interstitial (interstitialcy) mechanism in which an interstitial ion displaces an ion on a normal lattice site to a neighboring interstitial site.

The magnitude of the ionic conductivity will depend on the concentration of all mobile species, their charges, and mobilities:

$$\sigma = \sum_i n_i q_i \mu_i \tag{3}$$

Usually only one species predominantly accounts for the ionic conductivity so that the expression simplifies to

$$\sigma = nq\mu \tag{4}$$

Normally a good deal of energy is required to form a defect, e.g., 2.1 eV for a Schottky defect in NaCl, and thus the concentration of defects in a pure crystal will be extremely low at low temperature but will increase rapidly with increasing temperature:

$$K_{Sf} = [V'_{Na}][V^{\cdot}_{Cl}] = x^2 = \exp\left(-\frac{\Delta G_f}{kT}\right) = \exp\left(-\frac{\Delta H_f}{kT}\right)\exp\left(\frac{\Delta S_f}{k}\right) \tag{5}$$

$$x = \exp\left(-\frac{\Delta H_f}{2kT}\right)\exp\left(\frac{\Delta S_f}{2k}\right) \tag{6}$$

in which x represents the mole fraction of defects in the pure crystal (intrinsic defect concentration). The other terms represent the Gibbs free energy, enthalpy, and entropy of formation for the defect. The concentration of mobile species (cm^{-3}) is related to the mole fraction by the expression

$$n = Nx \tag{7}$$

where N is the number of ions per unit volume which then can be combined with Eq. (6) to give

$$n = N\exp\left(-\frac{\Delta H_f}{2kT}\right)\exp\left(\frac{\Delta S_f}{2k}\right) \tag{8}$$

The conductivity will, therefore, depend on the enthalpy and entropy of formation of the defect. However, the conductivity also depends on the mobility, which has its own temperature dependence. When ionic mobility in crystals occurs as a result of random, thermally activated jumps the process can only take place if the ion surmounts a potential barrier. A jump frequency can be associated with this process which is related to ν_0, the vibrational frequency of the ion in the lattice approximately equal to the Debye frequency and the thermodynamic factors for migration, ΔG_m, ΔH_m, and ΔS_m:

$$\nu = \nu_0 \exp(\Delta S_m/k)\exp(-\Delta H_m/kT) \tag{9}$$

The mobility is directly proportional to the jump frequency

$$\mu = Ga^2 q\nu/kT \tag{10}$$

where a is the jump distance and G is a geometric factor depending on the number of equivalent downfield jumps available in the particular crystal

structure. We can now express the conductivity as a function of temperature by combining Eqs. (4), (8), (9), and (10):

$$\sigma = \frac{Ga^2q^2\nu_0 N}{kT} \exp\left(\frac{\Delta S_f}{2k} + \frac{\Delta S_m}{k}\right) \exp\left(-\frac{\Delta H_f}{2kT} - \frac{\Delta H_m}{kT}\right) \tag{11}$$

A more convenient expression is in the form of an Arrhenius-type equation

$$\ln \sigma T = C - (\Delta H_f/2 + \Delta H_m)/kT \tag{12}$$

Equation (12) represents the ionic conduction behavior in the "intrinsic" region where the concentration of mobile species is generated thermally and is normally encountered only at high temperature.

At low temperature the impurities present will generally produce a concentration of defects far greater than the thermal generation. The conductivity will no longer depend on the formation of defects, only the motion of the defects present and the mole fraction, x_D, of these "extrinsic" defects:

$$\sigma = \frac{Ga^2q^2\nu_0 N x_D}{kT} \exp\left(\frac{\Delta S_m}{k}\right) \exp\left(-\frac{\Delta H_m}{kT}\right) \tag{13}$$

The Arrhenius plot form will now be

$$\ln \sigma T = C' - \Delta H_m/kT \tag{14}$$

where C' is a function of the impurity concentration. A plot of $\ln \sigma T$ vs. $1/T$ at low temperature will give the enthalpy of motion, while at high temperature will give the sum of $(\Delta H_f/2 + \Delta H_m)$. This is shown in Figure 1 in which the low-temperature extrinsic region is below 430 K, while the high-temperature intrinsic region is above this temperature. The enthalpies of formation and motion for Frenkel defects can be found by the same method. It should be noted that the factor 2 in $\Delta H_f/2$ depends on the number of defects formed. In the case of Schottky defects formed in alkaline earth fluorides such as CaF_2,

$$Ca^x_{Ca} + 2F^x_F \rightarrow V''_{Ca} + 2V^{\cdot}_F, \qquad K_{Sf} = [V''_{Ca}][V^{\cdot}_F]^2 = 4x^3 \tag{15}$$

where x refers to the mole fraction of calcium ion vacancies. The Arrhenius plot in the intrinsic region will now be

$$\ln \sigma T = C - \Delta H_f/3 + \Delta H_m/kT \tag{16}$$

It is possible then using the equations above to determine the enthalpy of motion and the enthalpy of defect formation by observing the temperature dependence of conductivity in both the low-temperature "extrinsic" region and the high-temperature "intrinsic" region.

2.2. Determination of Conduction Mechanism

In the development of materials useful as solid electrolytes for primary batteries it is usually necessary to determine the conduction mechanism. With

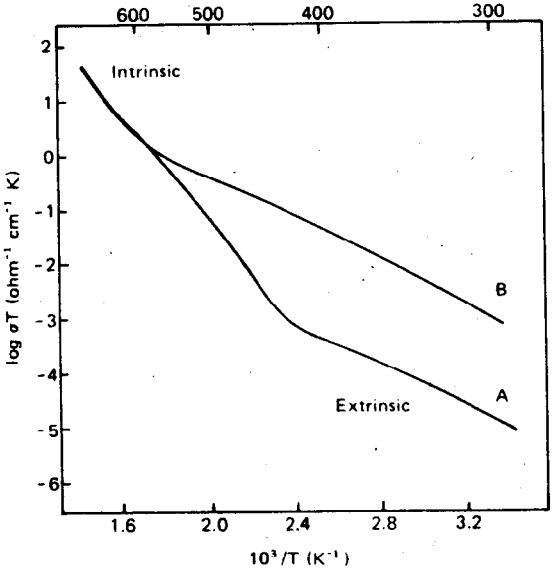

Figure 1. Arrhenius plot of conductivity showing intrinsic and extrinsic regions. Single-crystal AgCl samples: crystal A nominally pure containing 4.8 ppm divalent impurity; crystal B doped with 1200 ppm Cd^{2+}. Taken from Reference 1.

this information the researcher may be able to improve the electrochemical properties by "doping" techniques or by modifying the structure to achieve higher mobilities.

One of the basic questions to be answered for any material which conducts via ionic defects is whether the conduction mechanism involves anions or cations and whether it is predominantly vacancy or interstitial movement of those ions. A transference number experiment can be carried out in which weight changes in the anode and cathode sections of a cell are noted. From this information it is usually elementary to determine if the material is an anion or cation conductor. In general, most solid electrolytes contain small mobile cations such as Ag^+, Na^+, or Li^+ although F^- and O^{2-} conductors are also known. A series of experiments can then be performed in which controlled amounts of aliovalent dopants are added to the pure material. For example, in the case of the anion-conducting $PbBr_2$ a compound of the type MBr such as TlBr can be added or a compound of the type NBr_3 such as $BiBr_3$ can be added. The dopant will change the concentration of vacancies and interstitials according to the following reactions:

$$MBr \rightarrow M'_{Pb} + Br^{x}_{Br} + V^{\cdot}_{Br}$$

$$NBr_3 \rightarrow N^{\cdot}_{Pb} + 2Br^{x}_{Br} + Br'_i$$

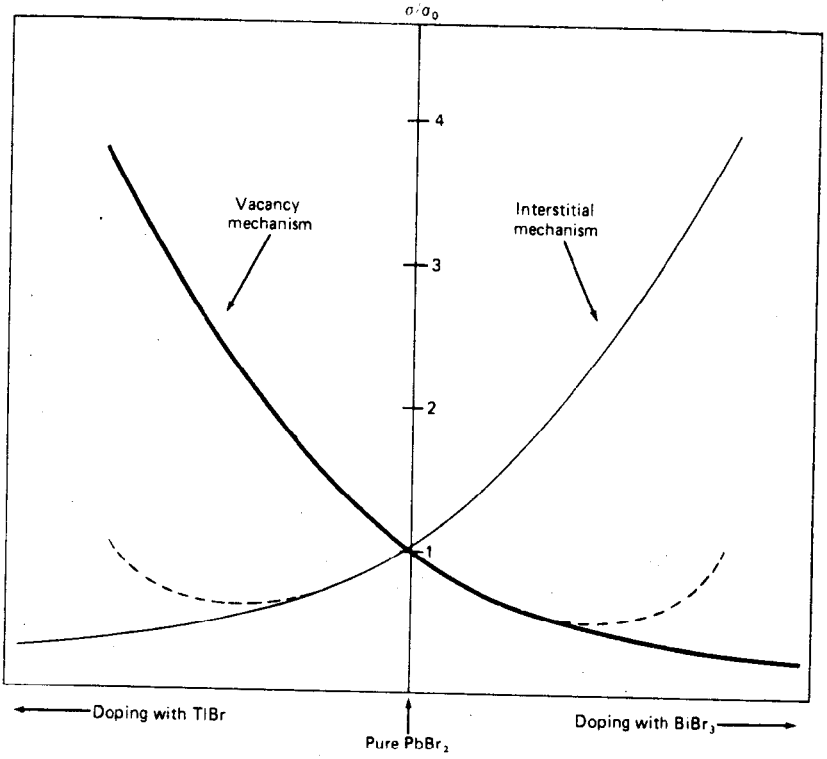

Figure 2. Aliovalent doping effects on conductivity. Dashed lines indicate rise in conductivity which occurs when both interstitials and vacancies conduct but with different mobilities, i.e., the minimum occurs when $n_v\mu_v = n_i\mu_i$.

The MBr dopant leads to an increase in vacancy concentration and by way of the defect equilibrium constant will cause a decrease in interstitial concentration (Figure 2). The NBr_3 dopant, on the other hand, will increase interstitial concentration and decrease vacancy concentration (Figure 2). Schoonman[2] has shown that MBr doping increases conductivity, while NBr_3 doping decreases conductivity, indicating that $PbBr_2$ is predominantly a bromide ion vacancy conductor. It was possible to increase the conductivity of $PbBr_2$ by a factor of 10^2 by adding a mere 0.02% TlBr.

Another example is the very high conductivity exhibited by ZrO_2 stabilized in the cubic form by the presence of 5–20 mol% CaO (CSZ). The addition of CaO increases the concentration of mobile oxide ion vacancies according to

$$CaO \rightarrow Ca''_{Zr} + O^x_0 + V^{\cdot\cdot}_0 \qquad (17)$$

When the aliovalent doping studies indicate the presence of interstitials the defect mechanism must be Frenkel but vacancies could arise from either a Schottky or Frenkel defect formation. One method of determining which type of defect formation is responsible involves measuring volume changes as the temperature is increased. Schottky defects give rise to vacancies equivalent to taking ions from the bulk and placing them on the surface. This will increase the volume assuming no change in lattice spacing. Frenkel defects, on the other hand, involve movement of an ion from a lattice site to an interstitial position and would not increase the volume. Any lattice spacing changes can be corrected for with high-temperature X-ray diffraction data, but even without such data it is generally recognized that a large thermal expansion per mole of ionic defect formed is a strong indication of Schottky defect formation.

For interstitial conductivity there remains the question of direct vs. indirect movement. This question can often be answered by comparing tracer diffusion coefficients, D_t, with diffusion coefficients calculated from conductivity measurements, D_σ, using the Nernst–Einstein equation:

$$D_\sigma = \frac{\sigma RT}{nq^2} \tag{18}$$

where n is the concentration of mobile ions. The two diffusion coefficients differ because of different jump distances between tracer movement and charge movement and the correlation factor, f. The ratio of coefficients is

$$\frac{D_t}{D_\sigma} = \left(\frac{a_t}{a_\sigma}\right)^2 \frac{\nu_t}{\nu_\sigma} f = H_R \qquad \text{(Haven ratio)} \tag{19}$$

where a is the jump distance and ν is the jump frequency. The factor, f, is introduced for tracer jumps because they may not be completely random, e.g., there will be a correlation between successive steps of a particle moving by a vacancy mechanism even if the steps of the vacancies themselves (charge movement) are uncorrelated.[3] In general, it is usually assumed that $\nu_\sigma = \nu_t$, and then a measure of H_R can be used to help elucidate the conduction mechanism. For the vacancy mechanism $a_t = a_0$ and $f \cong 0.3$–0.8, depending on geometrical configuration. Direct interstitial jumps are not correlated ($f = 1$) and $a_t = a_0$ so that $H_R = 1$. On the other hand, when the conduction mechanism is indirect $a_t < a_0$, $f \neq 1$, and $H_R \neq 1$. For example, the Haven ratio for Ag^+-β-alumina has been found to be 0.6,[4] and this has been attributed to an indirect interstitialcy movement of silver ions in the structure.

2.3. Conductivity in Crystals Containing Excess Lattice Sites

Materials which conduct via thermally generated or doped-in defects will normally contain defect concentrations of only 10^{16}–$10^{20}\,cm^{-3}$. This means that even if mobilities were comparable (often not true) conductivities of these

materials will be orders of magnitude lower than concentrated ionic aqueous solutions. Several years ago it was recognized, however, that a few silver compounds such as α-AgI and $RbAg_4I_5$ did exhibit conductivities comparable to aqueous solutions and behaved as though all the silver ions were mobile with mobilities comparable to Ag^+ in water. Detailed crystal structure determinations of these materials have shown that the large anions form an arrangement that provides a number of sites greater than the number of silver cations present. The silver ions are distributed among these many sites in a disordered fashion. In other words, the intrinsic crystal contains "built-in defects," and the concentration of mobile ions is the total concentration of silver ions. For example, AgI undergoes a phase transition at 146°C to form body-centered cubic α-AgI. In this form a unit cell of AgI contains two Ag^+ distributed among a possible 42 available sites. In $RbAg_4I_5$ the 16 silver ions in the unit cell are distributed among 56 available sites.

The β-aluminas represent a class of compounds which exhibit properties between defect conductors and excess lattice site conductors. β-Alumina (ideal formula $NaAl_{11}O_{17}$) has several sites of almost equivalent energy. The material contains excess sodium, and the sodium ions are distributed among the various sites. Because one site (Beevers–Ross) shown in Figure 3b is lowest in energy it is nearly filled (~80%) and is considered to be the normal lattice site. The other positions (anti-Beevers–Ross, mid-oxygen) are classified as interstitial positions if one takes into account the energy difference, or as excess lattice sites

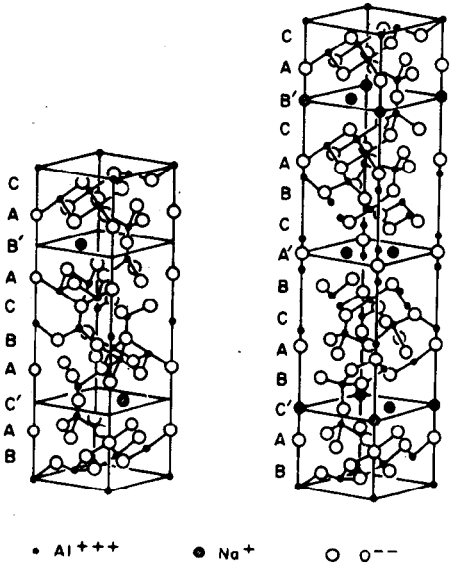

Figure 3a. Structure of β- and β''-alumina showing arrangement of Al^{3+} and O^{2-} ions in "spinel-like blocks" and Na^+ and O^{2-} ions in conduction plane.

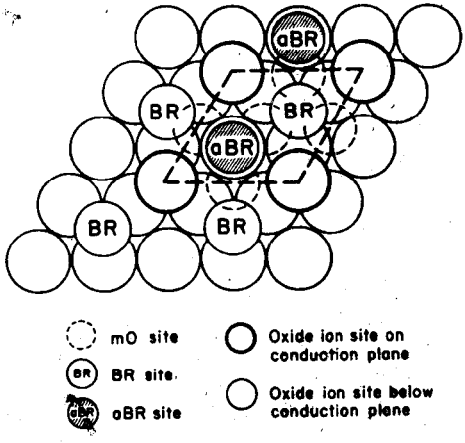

Figure 3b. Arrangement of ions on conduction plane in β-alumina including various sites for mobile Na^+ ions (or other M^+ ions). mO is mid-oxygen site, BR is Beevers–Ross site, aBR is anti-Beevers–Ross site.

if the small energy difference is disregarded. In any case, a large fraction (20–30%) of the sodium ions are mobile and conductivity, especially at elevated temperatures, is comparable to aqueous electrolytes. It should be noted that Na^+–β-alumina can be ion exchanged with other metal ions such as Ag^+, K^+, Rb^+, Tl^+, etc., to yield the corresponding M^+–β-alumina.

β''-Alumina (ideal formula $Na_2MgAl_{10}O_{17}$ when stabilized with magnesium) contains two identical sodium ion sites which would be completely occupied in the ideal crystal. However, it is sodium ion deficient and behaves as though the $\sim 1.7Na^+$ are distributed randomly among the $2Na^+$ sites similar to the silver compounds containing excess lattice sites described above.

2.4. Electronic Conductivity

It was stated earlier that a solid electrolyte useful for batteries must exhibit negligible electronic conductivity. If this were not the case the electrochemical cells would not attain their thermodynamic equilibrium potentials even at open circuit, and the internal short-circuiting would consume electrode materials resulting in short shelf life. It is necessary, therefore, to determine the electronic conductivity of any solid electrolyte before it can be developed for battery applications.

It was also pointed out that the ionic conductivity is sensitive to the presence of impurities, and it is equally true that electronic conductivity will be sensitive to impurities and especially to nonstoichiometry. The band gaps are usually several electron volts (larger than Frenkel or Schottky defect formation energies) so that the intrinsic concentrations of electrons and electron holes will be extremely low in pure ionic compounds. However, deviation from ideal stoichiometry can result in large increases of electronic conductivity. For

example, AgBr containing excess silver would create electron carriers according to the reaction

$$Ag \rightarrow Ag_i + e'$$

Large electronic conductivity effects can be measured by noting potentials, E, observed for electrochemical cells and comparing with the theoretical potential, $E°$:

$$E = E°(1 - t_e) \tag{20}$$

where t_e is the electronic transference number for the solid electrolyte. Low levels of electronic conductivity are best measured using a "blocking" electrode technique developed by Wagner.[5] In this dc polarization technique one electrode is inert and cannot exchange ions with the electrolyte. Thus with a dc signal ionic current becomes "blocked" (decays to zero), and the only current observed when steady state is reached is due to electronic conductivity. The other electrode is reversible with respect to the electrolyte and serves as a reference state for the electrolyte. In the cell

$$-Ag|AgBr|C+$$

C is the blocking electrode and Ag is the reversible electrode. The total electronic current at steady state is given by

$$I = I_e + I_h = \frac{RTA}{LF}\left\{\sigma_e^\circ\left[1 - \exp\left(-\frac{EF}{RT}\right)\right] + \sigma_h^\circ\left[\exp\left(\frac{EF}{RT}\right) - 1\right]\right\} \tag{21}$$

where I_e is the electronic contribution due to electron carriers, I_h is due to elec ron holes, L is the electrolyte path length, and A is the electrode area. The specific conductivities due to electrons and holes in the electrolyte (AgBr in the example) in equilibrium with the reversible electrode (Ag in the example) are denoted by σ_e° and σ_h°, respectively. Generally I_e or I_h predominates so that the electronic current either increases exponentially with increasing applied voltage (hole conductor) or exhibits a current plateau (electron carrier) for the cell type A|AB|M:

$$I_h = \frac{RTA}{LF}\sigma_h^\circ\left[\exp\left(\frac{EF}{RT}\right) - 1\right] \cong \frac{RTA}{LF}\sigma_h^\circ \exp\left(\frac{EF}{RT}\right) \qquad \text{for } EF \gg RT \tag{22}$$

$$I_e = \frac{RTA}{LF}\sigma_e^\circ\left[1 - \exp\left(-\frac{EF}{RT}\right)\right] \cong \frac{RTA}{LF}\sigma_e^\circ \qquad \text{for } EF \gg RT \tag{23}$$

The solid electrolytes used in the primary batteries discussed later all exhibit electronic conductivities many orders of magnitude lower than the ionic conductivities exhibited by these materials. However, it should always be kept in mind that electronic conductivities are normally measured and quoted for pure materials, while an actual battery electrolyte might develop electronic defects during use or storage leading to considerably higher electronic conductivities.

3. Interface Effects in Solid Electrolyte Cells

The discussion in the previous section centered around the requirements that practical solid electrolyte materials must exhibit low electronic conductivity and high ionic conductivity. The latter requirement involves ohmic polarization, one mechanism of energy loss in a galvanic cell. Cells, however, exhibit other types of polarization leading to energy losses which can be even more severe than ohmic polarization. These polarization effects involve the electrode–electrolyte interface, and several studies have focused attention on this phase boundary.[6,7]

A basic difference between a solid electrolyte system and a liquid electrolyte system with typical solid electrodes is that the former involves a solid–solid interface which does not readily allow flow of material to maintain intimate contact during operation of the electrochemical cell. Raleigh[6] studied the Ag–AgX interface and observed larger polarizations in the anodic direction compared to the cathodic direction especially after appreciable charge had been transferred. This was attributed to the dissolution of silver leaving vacant sites on the metal surface and resulting in higher current densities at the remaining electrode–electrolyte contact points. In the extreme the anode completely detached itself from the electrolyte. As might be expected the effect was highly dependent on contact pressure. Kennedy and Chen[8] also observed high polarization during anodic dissolution of silver at both Ag–AgBr and Ag–Ag_3SBr interfaces using three-electrode techniques.

Similar contact problems have been observed with other solid electrolytes. Liang[9] reported a discharge efficiency of >80% at 50 $\mu A/cm^2$ for the cell Li–LiI(doped)–PbI_2. However, when discharged at 500 $\mu A/cm^2$ the cell operated for only 30 min and at this point the lithium anode was completely separated from the electrolyte. Similar to the silver electrolyte cells, an increase in contact pressure caused some plastic flow to take place with a resultant decrease in the interface resistance.

One method of avoiding the solid–solid interface problems is to use liquid electrodes. Several investigators have accomplished this with silver cells by amalgamating the silver.[7,10,11] Raleigh concluded that amalgamation provided a liquid interface in which silver atoms dissolved from the solid silver and then were oxidized to silver ions which could enter the electrolyte phase readily because of the intimate contact involved. The use of liquid electrodes in solid electrolyte cells has been a main feature in the sodium–sulfur battery.[12] The Na(l)–β-alumina–Na_2S_x(l),C cell can operate at current densities of about 1 A/cm^2 with little polarization other than ohmic provided the temperature is above the melting point of the cathode mixture (normal operating temperature is 300°C). Kennedy and Sammells[13] also showed large changes in the Na–β-alumina interface resistance at the melting point of sodium (98°C).

There are, of course, other types of polarization which should be considered. It is interesting to note that since most solid electrolytes have one ion

carrying all the current (transference number equals 1) no classical concentration polarization can exist. Electroneutrality demands that the concentration of the mobile ion remain constant throughout the electrolyte. However, an *activity* polarization could arise if, for example, anodic dissolution of a silver anode occurred more rapidly than the ions could maintain their equilibrium distribution among available sites. The activity of Ag^+ would be higher than at equilibrium and thus the electrode potential would increase. The process would behave in a similar fashion to normal concentration polarization. In fact, a limiting current could be observed at a Ag–AgX interface if anodic dissolution of silver took place so fast that the concentration of available interface sites decreased to zero as shown below:

$$Ag(s) + V_i^x(\text{surface}) \rightarrow Ag_i^{\cdot}(\text{surface}) + e'$$

$$E = E^{\circ}_{Ag^+/Ag} + \frac{RT}{nF} \ln \frac{[Ag_i^{\cdot}]}{[Ag(s)][V_i']}, \qquad E \rightarrow \infty \text{ as } [V_i'] \rightarrow 0 \tag{24}$$

Activation polarization has not been reported for the solid electrolyte cells being developed for primary batteries. This probably indicates that the systems chosen have reasonably high exchange current densities compared to the operating current densities (some solid electrolyte cells only operate at $\mu A/cm^2$ current levels) and that the other losses described above are large enough to mask any small activation polarization effects.

Another requirement of the electrode–electrolyte interface is that the electrode materials must be chemically compatible with the electrolyte. This is especially critical with complex electrolytes such as Ag_3SI or $RbAg_4I_5$ which may not have much thermodynamic stability compared to their components. For example, in the $Ag–Ag_3SI–I_2,C$ cell the following reaction may take place[14]

$$I_2 + Ag_3SI \rightarrow 3AgI + S$$

The electrolyte would eventually be transformed from Ag_3SI in which $\sigma = 10^{-2}\ \Omega^{-1}\ cm^{-1}$ to AgI in which $\sigma = 10^{-6}\ \Omega^{-1}\ cm^{-1}$.

Physical incompatibility can also play a role. The Li–LiI–AgI cell exhibits theoretical open-circuit potentials and can be discharged at reasonable rates. AgI is chemically compatible with LiI, but Liang[15] found that AgI dissolved in the LiI and diffused to the Li anode, resulting in self-discharge. The effect was especially pronounced in a thin-film version of the cell in which the anode–cathode spacing was only 0.0015 cm (Reference 16).

4. Silver-Ion-Conducting Electrolyte Batteries

The field of solid electrolytes developed around the study of silver-ion-conducting materials. It was recognized over 50 years ago that silver halides

were considerably more conductive than the corresponding alkali halides. The extremely high conductivity of $\sim 1\ \Omega^{-1}\ cm^{-1}$ for AgI above its 146°C transition temperature to the cubic α-AgI form was also known early on. This type of research achieved notable success with the development of complex silver salts exhibiting conductivities at 25°C comparable to aqueous solutions. The parent material, $RbAg_4I_5$, discovered by Owens and Argue[17] and Bradley and Greene[18] has a conductivity of $0.27\ \Omega^{-1}\ cm^{-1}$ at 25°.[17] Many analogs have now been synthesized and characterized in which the Rb^+ has been replaced by K^+, NH_4^+, or large organic cations. The properties of several silver salts are summarized in Table 1 and Figure 4. As was pointed out in a previous section the high conductivity of these materials is a result of the excess lattice sites for Ag^+ allowing relatively easy migration for all silver ions, not just a small defect concentration as in the case of alkali and alkaline earth halides.

It is only natural, therefore, that solid state batteries using these highly conductive silver salts would be developed. However, silver compounds, and especially those based on AgI, have low decomposition potentials placing an upper limit on the open-circuit voltage of any galvanic cell which is thermodynamically stable. Almost all batteries using silver-ion-conducting electrolytes have open-circuit voltages of 0.6–0.7 V, and there are a few examples such as those using Ag–Te and Ag–Se couples which have voltages of ~0.2 V.

Table 1
Conductivity of Silver-Ion-Conducting Solid Electrolytes[a]

Substance	Ionic conductivity, $\Omega^{-1}\ cm^{-1}$	Temperature, °C	Activation energy, kJ/mol	Electronic conductivity, $\Omega^{-1}\ cm^{-1}$
α-AgI	2.7	555	4.9	
$RbAg_4I_5$	0.27	24	13.5	10^{-9}
KAg_4I_5	0.21	20	12.5	
QI·*n*AgI,				
where Q = $(CH_3)_4N$				
n = 6.5	0.042	22	16.7	10^{-10}
where Q = $(CH_3)_2(C_2H_5)_2N$				
n = 7	0.064	22	15.1	10^{-10}
where Q = $(C_2H_5)_4N$				
n = 7	0.022	22	23.8	10^{-10}
KCN·4AgI	0.14	25	8.1	
RbCN·4AgI	0.18	25		
Ag_3PO_4·4AgI	0.019	25	15.9	
$Ag_4P_2O_7$·15AgI	0.09	25	13.8	
Ag_2WO_4·4AgI	0.047	25	15.1	
Ag_3SI	0.01	25		10^{-8}
Ag^+–β-alumina	0.0064	23	16.7	$<10^{-8}$

[a] Taken from Liang (1974), Takahashi (1973), and Hladik (1972) (see Selected Reading list).

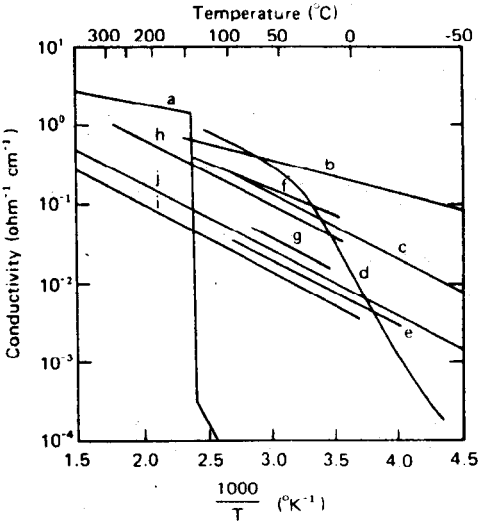

Figure 4. Temperature dependence of the ionic conductivity for several Ag^+-conducting solid electrolytes which contain excess lattice sites: (a) AgI (highly conductive α-AgI form above 146°C); (b) $RbAg_4I_5$; (c) $(CH_3)_2(C_2H_5)_2NAg_7I_8$; (d) $(C_6H_5NH)Ag_5I_6$; (e) β-Ag_3SI; (f) $Ag_{19}I_{15}P_2O_7$; (g) $Ag_7I_4PO_4$; (h) $Ag_6I_4WO_4$; (i) Ag^+-β-alumina; and (j) Na^+-β-alumina for comparison. Taken from Liang (1974) (see Selected Reading list).

The application of such low-voltage systems will be limited to low-energy-storage situations especially when one considers the high equivalent weight of both silver and iodine. On the other hand, the high current densities attainable compared to other solid state batteries and the inherent advantages of solid state battery systems discussed in the introductory section make the silver-based systems attractive for some applications.

The first solid state battery delivering currents of >1 mA/cm^2 at ambient temperatures was the Ag–Ag_3SI–I_2,C system described by Takahashi and Yamamoto.[7,10] A discharge curve is shown in Figure 5. Open-circuit voltages were 0.605 V at −75.8°C to 0.681 V at +60°C, somewhat less than the theoretical value of 0.687 V based on the Gibbs free energy of formation for AgI. Although the authors attributed the discrepancy to uncertainty in the thermodynamic data, Topol[10] showed that Ag–AgI–I_2,C cells did give the calculated open-circuit potential. The lower values observed using Ag_3SI electrolyte may be due to a small amount of electronic conductivity which acts as a partial shorting of the cell. However, the electronic conductivity was found to be only $10^{-8}\ \Omega^{-1}\ cm^{-1}$ using the Wagner blocking technique described in a previous section. One other possibility for the low open-circuit voltages observed would be a low I_2 activity at the cathode.

Current densities of only 0.1 mA/cm^2 could be drawn at 25°C when pure silver was used as the anode in the Ag–Ag_3SI–I_2,C cells. However, the large electrode–electrolyte interface polarization effects at the anode could be decreased dramatically by using a silver amalgam, and current densities of 1 mA/cm^2 could be employed (Figure 5). A thin-film version of the cell was

described by Yamamoto and Takahashi[20] in which 10 mA/cm^2 current densities could be drawn at 29°C. Even at −74°C current densities of 20 μA/cm^2 were attainable.

It was anticipated by the authors that since the low-conductivity AgI reaction product would form at the cathode the cell resistance would increase as the cell discharged. However, little resistance increase was noted after 4 hr at 1 mA/cm^2 (Figure 5), and Takahashi and Yamamoto[10] concluded that the AgI was forming a solid solution with Ag_3SI. It should be noted that polycrystalline AgI films exhibit conductivities considerably greater than bulk single-crystal AgI so that the increase in resistance may have been too small to detect in a short period of time. One other potential problem noted with this cell is the instability of Ag_3SI in the presence of I_2 to form AgI and S noted in a previous section. If this reaction were to proceed the cell would eventually become a Ag–AgI–S cell with a theoretical open-circuit potential of only 0.23 V.

With the advent of MAg_4I_5 solid electrolytes and related compounds several new galvanic cells have been studied. Argue *et al.*[21] described Ag–$RbAg_4I_5$–RbI_3,C cells which operated at current densities up to 40 mA/cm^2 at 25°C (Figure 6). Faradaic efficiencies of 80% could be achieved although specific energies of only 5 Wh/kg were possible because of the low voltage and high equivalent weights of the reactants. Replacement of RbI_3 with $(CH_3)_4NI_9$

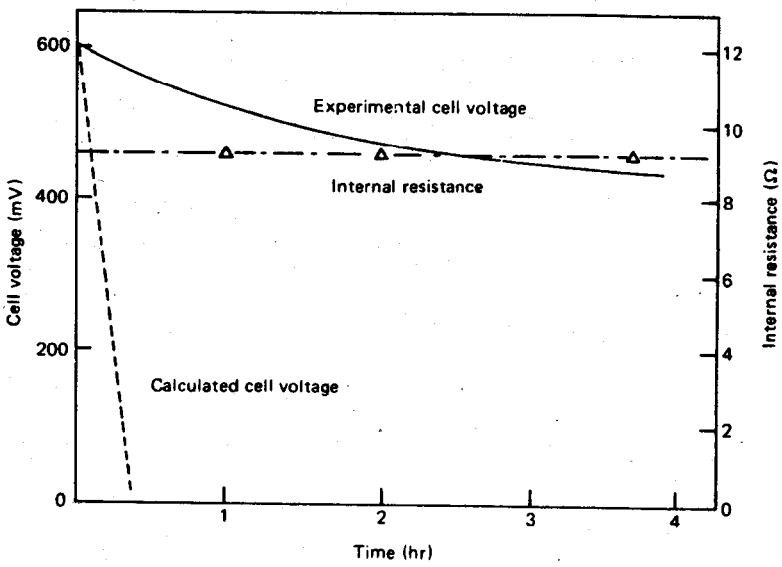

Figure 5. Discharge curve at 1 mA/cm^2 for Ag–Ag_3SI–I_2, acetylene black galvanic cell at 25°C and the change in internal resistance. Taken from Reference 10.

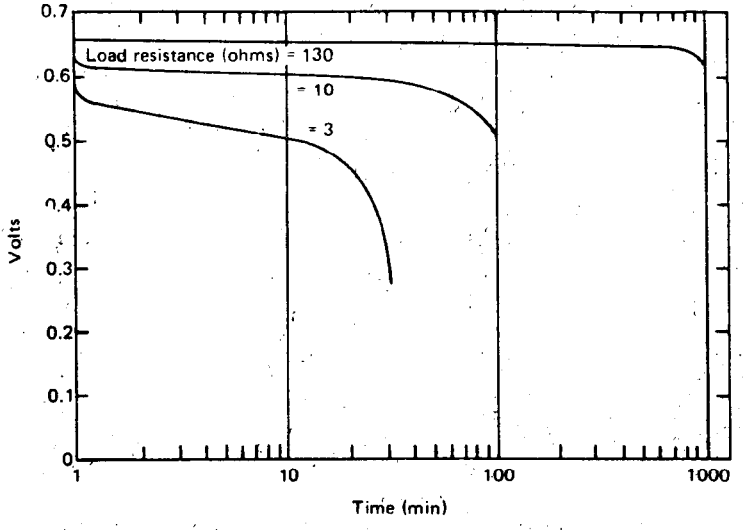

Figure 6. Discharge curves for Ag–Ag_3SI–RbI_3,C galvanic cells at 25°C. Taken from Reference 21

or $(CH_3)_4NI_5$ resulted in a specific energy increase to about 18 Wh/kg. The cells have been proven to exhibit long life with no observed decrease in cell capacity after five years storage at ≤23°C. Cell capacity losses when stored at 71°C were significant but tolerable after five years. Heart pacemaker and military battery applications have been pursued by battery manufacturers.

Since $RbAg_4I_5$ is thermodynamically stable only above 27°C the discharge reaction depended on the temperature. In the cell Ag–$RbAg_4I_5$–RbI_3 the cathode reaction above 27°C was[21]

$$14Ag^+ + 7RbI_3 + 14e^- \rightarrow 3RbAg_4I_5 + 2Rb_2AgI_3$$

while below 27°C the cathode reaction was

$$4Ag^+ + 2RbI_3 + 4e^- \rightarrow Rb_2AgI_3 + 3AgI$$

Disproportionation of the electrolyte itself should occur below 27°C.

$$2RbAg_4I_5 \rightarrow 7AgI + Rb_2AgI_3$$

but the reaction is extremely slow in the absence of moisture.

Polarization losses can be kept minimal by using electrolyte –C– oxidant mixtures as cathode materials and electrolyte –C–Ag mixtures as anode materials.[21] The mixtures create a large contact area for the electrode–electrolyte interface.

Other cathode materials which have been proposed include Te and Se,[22] Rb_2TeI_6,[23] 2-perylene · $3I_2$,[24,25] and several polyiodides.[26]

Several of the $RbAg_4I_5$ systems were fabricated in film form as early as 1971. Takahashi and Yamamoto[27] patented cells of the type $Ag–RbAg_4I_5$ or Ag_3SI–Te or Se in the form of vacuum-deposited films, as well as the more conventional pressed powders. For example, 30-μm-thick $RbAg_4I_5$ was deposited on a 1-cm diameter silver disk followed by a 10-μm–thick Te layer. A 1-μm-thick gold layer was deposited on top to complete the cell. Six of these cells were stacked entirely by vacuum evaporation. At 25°C the open-circuit voltage was 1.2 V, and at 5 mA the operating voltage was 0.9 V. Capacity at 2-mA discharge was 5 mAh. A similar six-cell battery employing vapor-deposited Ag_3SI as the electrolyte and 300-μm-thick vacuum-deposited Te had a capacity of 10 mAh at the 1-mA discharge rate.

A thick-film technique patented by Ervin[23] was used to prepare cells of the type $Ag–RbAg_4I_5–Rb_2TeI_6$,C. The anode was a mixture of silver, carbon, and electrolyte; and electrolyte was also used in the cathode mixture to improve electrode–electrolyte contact. A typical cell was 635 μm thick including nickel alloy and copper back-up plates and had an area of 3.6 cm^2. The cell exhibited an open-circuit voltage of 0.53 V at room temperature and could operate at 0.6 mA for 15 min. The cell could be recharged, and flash currents as high as 300 mA were recorded.

Recently, Bodnaruk *et al.*[28] described thin-film galvanic cells employing $RbAg_4I_5$ electrolyte and Te cathodes. The electrolyte film was prepared by immersing a porous paper base in a Petri dish containing a colloidal solution of $RbAg_4I_5$ in acetone. The open-circuit voltage was 0.18–0.19 V and exhibited internal resistances of 250–350 Ω at 75–150 $\mu A/cm^2$.

Although the outlook for battery applications using silver-based solid electrolytes is not bright because of the low specific energies, these materials may find some use as capacitorlike components in long-time integration (e.g., in warranty devices), timers, or in memory devices.

5. Lithium Iodide Electrolyte Batteries

Although the silver-ion-conducting solid electrolytes exhibit the highest conductivities at ambient temperature, their low decomposition potentials (0.6–0.7 V for AgI-based materials) limit their use in practical batteries. The search for highly conducting materials with a high decomposition potential has not been too fruitful unless one is willing to employ temperatures of 300–1000°C. On the other hand, some applications do not require high current densities but only long-life and good specific energy. One such application is the heart pacemaker battery.

The alkali halides possess high decomposition potentials (typically 3–4 V) but the concentrations of Schottky defects are so low at ambient temperatures that conductivities are impractically low. The highest conductivity for this group is found in LiI, which is about $4 \times 10^{-7}\ \Omega^{-1}\ cm^{-1}$ at 28°C.[29] Schlaikjer

and Liang[29] found that doping with CaI_2 resulted in higher conductivities by increasing lithium ion vacancy concentrations according to the reaction

$$CaI_2 \rightarrow Ca_{Li}^{\cdot} + V_{Li}' + 2I_I^x$$

The maximum conductivity at 28°C was $\sim 1.7 \times 10^{-5}\ \Omega^{-1}\ cm^{-1}$ for LiI containing 2 mol% CaI_2 (Figure 7). However, the conductivity of LiI containing more than 0.4 mol% CaI_2 was not stable with time, which was attributed to a slow precipitation of CaI_2. Results indicated a maximum solubility of only 0.23 mol% CaI_2.

Subsequent studies by Liang[30] on the conductivity of doped LiI showed that stable conductivities of $>10^{-5}\ \Omega^{-1}\ cm^{-1}$ could be obtained by using 35–45 mol% Al_2O_3 mixed with LiI (Figure 8). The effect cannot be attributed to the classical defect equilibria since X-ray diffraction patterns indicated insignificant solubility of Al_2O_3 in the LiI lattice. Normally, doping effects reach their maximum at a few mole percent (Figure 7). The conduction mechanism was shown to be the same as in nominally pure LiI, which conducts via lithium ion vacancies. The activation energy of the conduction process in LiI (Al_2O_3) was 41 kJ/mol, in agreement with the activation energy for the mobility of the lithium ion vacancies in a LiI single crystal. The activation energy in the extrinsic region for pure polycrystalline LiI was also 41 kJ/mol. Liang has suggested that the increased conductivity could be attributed to the creation of V_{Li}' by the dissolution of surface Al_2O_3 molecules in LiI at the LiI–Al_2O_3 interface. Such an interface phenomenon would require high

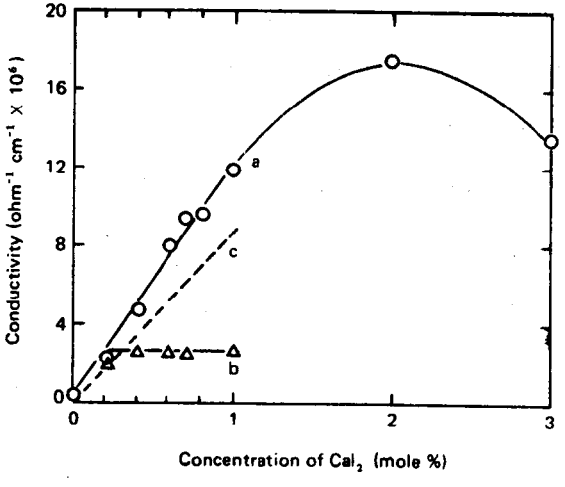

Figure 7. Conductivity of LiI as a function of CaI_2 concentration, 28°C. (a) Freshly annealed at 150°C for 30 min, (b) 500 hr after annealing, and (c) based on the calculated mobility of the V_{Li}'. Taken from Reference 29.

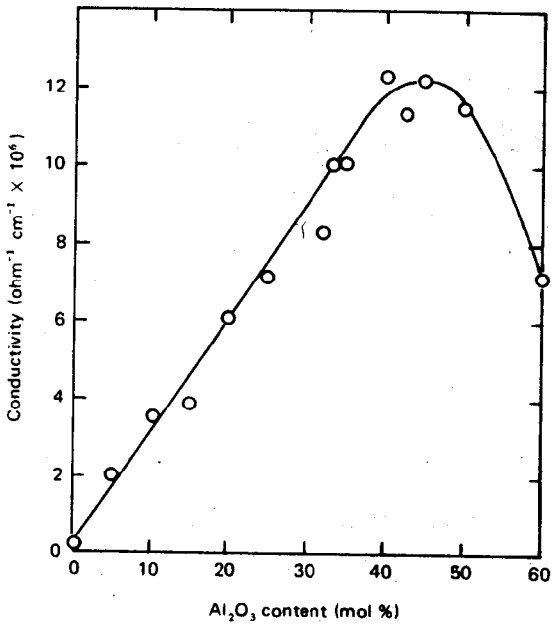

Figure 8. Conductivity of LiI as a function of Al_2O_3 content. Taken from Reference 25.

concentrations of small-particle-size Al_2O_3 for maximizing the effect as observed. The LiI(Al_2O_3) electrolyte exhibited negligible electronic conductivity and thus was a candidate for a long-life, high-specific-energy battery.

The simplest cell one can envisage using LiI as the electrolyte is Li–LiI–I_2,M, where M is some appropriate electronic conductor such as carbon. This cell has been shown to exhibit theoretical open-circuit potentials of nearly 3 V. Charge transfer complexes containing iodine such as poly-2-vinylpyridine·I_2 have also been used as cathode materials in the hopes of decreasing iodine vapor pressure. It was known that iodine vapor diffused through the LiI electrolyte, presumably along grain boundaries, to the Li anode and reacted chemically, a type of self-discharge. The charge transfer complexes operated satisfactorily at $<10\ \mu A/cm^2$ but at $50\ \mu A/cm^2$ the cell voltage dropped to 0.24 V after 100 hr.[31] Techniques to use iodine charge transfer complexes have advanced in recent years, and these cathode materials have been described in several patents. A comparison of lithium iodide solid state cells with conventional mercury cells is shown in Table 2.

Several other cathode materials have been investigated such as AgI, CuI, and PbI_2.[30] The cell reactions are the reduction of metal iodides, and the theoretical open-circuit potentials will be lower than with the iodine–iodide

Table 2
Comparison of Lithium–Iodine Cell with Mercury Cell[a]

Parameter	Mercury cell	Lithium–iodine cell
Electrolyte	NaOH (aq.)	LiI
Physical dimensions	15.8 mm diameter × 16.4 mm high	13.7 × 52.3 × 44.5 mm high
Weight, g	12.2	80
Chemical capacity, Ah	1.15	>4.14
Nominal voltage, V	1.38	2.8
Energy density, Wh/cm^3	0.57	0.37
Specific energy, Wh/g	0.130	0.145
Internal discharge rate, %/yr	4–7	<1
Calculated battery longevity in heart pacemaker, yr	6.9 to cell exhaustion	14.0 to replacement time (voltage = 1.8 V)

[a] Taken from Reference 32.

couple. In all cases the theoretical value was observed within experimental uncertainty as shown in Table 3. The most successful metal iodide cathode material to date is a mixture of 40 wt % PbI_2, 40 wt % PbS, and 20 wt % Pb described by Liang and Barnette.[33] A view of the solid electrolyte cell is shown in Figure 9 and typical discharge curves are shown in Figure 10. Test cells experience no capacity loss after storage periods up to two years at room temperature, or one year at 45 and 60°C, demonstrating that Li–LiI(Al_2O_3)–PbI_2,PbS,Pb batteries are stable and have a long shelf life. Volumetric energy density was estimated as 0.49 Wh/cm^3 (8 $Wh/in.^3$) at a power level of 150 $\mu W/in.^3$

6. Beta-Alumina Electrolyte Batteries

In the previous section it was pointed out that silver-ion-conducting electrolytes exhibit high conductivity but have low decomposition potentials

Table 3
Comparison of Open-Circuit Potentials of LiI Electrolyte Cells with Theoretical Values[a]

Cell	Open-circuit potential	
	Calculated	Observed
Li–LiI(Al_2O_3)–PbI_2,Pb	1.896	1.905 ± 0.010
Li–LiI(Al_2O_3)–CuI,Cu	2.075	2.080 ± 0.010
Li–LiI(Al_2O_3)–AgI,Ag	2.109	2.105 ± 0.010

[a] Taken from Reference 30.

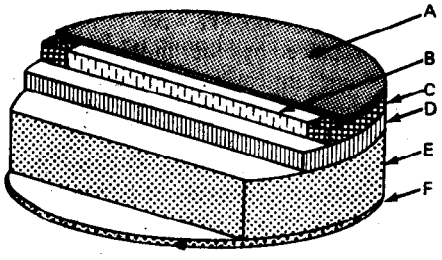

Figure 9. Sectioned view of Li-LiI(Al_2O_3)–PbI_2, PbS, Pb cell. (A) Anode current collector, (B) Li anode, (C) anode retaining ring, (D) LiI(Al_2O_3) solid electrolyte, (E) PbI_2,PbS, Pb cathode mixture, and (F) cathode current collector. Taken from Reference 33.

while the lithium-ion-conducting electrolytes exhibit high decomposition potentials but have low conductivities ($10^{-5}\ \Omega^{-1}\ cm^{-1}$ at best at 25°C). The search for solid electrolytes with intermediate properties has, to date, led to one group of promising materials, the beta-aluminas.

Beta-alumina is a general term that refers to a family of sodium aluminates with closely related structures and chemical properties. These ceramic materials exhibit compositions in the range $Na_2O{\cdot}5Al_2O_3$ to $Na_2O{\cdot}9Al_2O_3$. The two most important members of the family are the hexagonal form (designated β) and the rhombohedral form (designated β'') and are shown in Figure 3a. In addition, each member exhibits variable composition over a limited range. For example, the formula of β-alumina derived from the crystal structure is $Na_2O{\cdot}11Al_2O_3$ but always contains excess soda. The formula of β''-alumina is $Na_2O{\cdot}5Al_2O_3$ but is soda deficient and is normally stabilized by the addition of MgO and/or Li_2O. As shown in Figure 3a the β-aluminas contain spinel-like blocks consisting of aluminum and oxide ions separated by a loosely packed plane containing sodium and oxide ions. Because of the loose packing in this

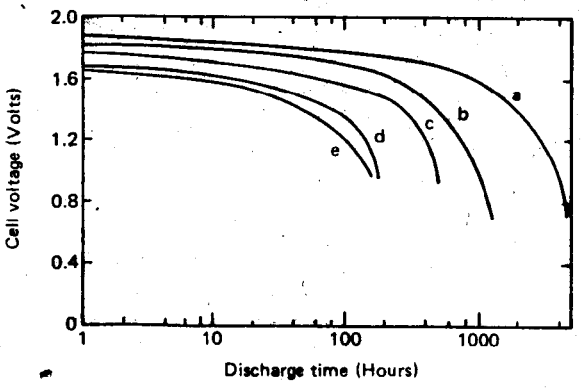

Figure 10. Discharge curves for Li-LiI(Al_2O_3)–PbI_2, PbS, Pb cells at 37°C under various constant currents. (a) 18 μA, (b) 36 μA, (c) 54 μA, (d) 90 μA, and (e) 108 μA. Taken from Reference 33.

plane, space is available for movement of the sodium ions leading to ionic conductivities $>0.03\ \Omega^{-1}\ cm^{-1}$ for single crystals at 25°C. The sodium ions can also be replaced by other mobile +1 ions using ion exchange techniques. Since the sodium ions can only move in two dimensions (i.e., along the conduction plane) the materials are highly anisotropic, and the crystals must be oriented properly for maximum conductivity.

For practical applications sintered polycrystalline compacts are generally used requiring a sintering of the ceramic materials to near theoretical density. The highest reported conductivities at 25°C for polycrystalline materials are $\sim 0.01\ \Omega^{-1}\ cm^{-1}$.[34] However, polycrystalline β''-alumina has been prepared with a conductivity of $0.4\ \Omega^{-1}\ cm^{-1}$ at 300°C (Reference 12) and would probably have a conductivity of $\sim 0.02\ \Omega^{-1}\ cm^{-1}$ at 25°C The major use for β-aluminas has been in high-temperature (300°C) secondary batteries using molten sodium as the anode material and molten sulfur (and polysulfides) as the cathode material (see Chapter 11). Therefore, much of the data concerning β-alumina are reported at 300°C and must be extrapolated to 25°C.

One of the major obstacles to the development of solid state batteries using β-alumina as an electrolyte is a satisfactory solid electrode–solid electrolyte contact. In the silver-based and lithium-based cells described earlier the powdered electrode and electrolyte materials can be pressed together in steel dies. However, β-alumina powder must be sintered at 1600–1800°C at ambient pressure or hot pressed at 1400°C, which rules out normal anode and cathode materials. Whittingham and Huggins[35] were able to use a tungsten bronze electrode which acted as a reversible sodium electrode for conductivity measurements but this material would have limited use as a battery electrode.

Ceramic-type electrode materials have been proposed by doping β-alumina with other metal ions. As early as 1968 Hever[36] described the use of β-alumina doped with iron and titanium as an electrode material in cells

Fe,Ti-doped β-alumina–β-alumina–Fe,Ti-doped β-alumina

Passage of current through the cell resulted in an increase in voltage, i.e., the cell acted as a capacitor. Hever envisaged its use as an electronic integrator or as a capacitor in filter circuits. Hever also conceived of using two different doped β-aluminas, one doped with an electron donor, the other with an electron acceptor to act as anolyte and catholyte in a secondary battery. This concept has been pursued in more detail by Kennedy and Sammells[13] and Dudley *et al.*[37]

The possibility of using solid sodium as an anode has also been studied but the solid–solid interface has not been entirely satisfactory. Because of the difficulties associated with solid–solid interfaces primary batteries using β-alumina electrolytes have normally employed liquid anolyte and catholyte regions. The typical anode is a sodium amalgam, while cathode materials have included aqueous or organic solutions of halogens, metal halides, oxygen, or water itself as the electron-accepting material. The role of β-alumina is to

Table 4
Summary of Cell Performance Characteristics of Low-Temperature Batteries Using β-Alumina[a]

Cell couple	Open-circuit voltage, V	Voltage at 0.1 mA/cm^2, V	Specific energy	
			Wh/kg theoretical	Wh/kg practical
Na-Hg-Br_2,H_2O	3.77	3.5	1026	330–440
Na-Hg-Br_2,propylene carbonate	3.34	3.1	910	330–440
Na-Hg-I_2,H_2O	3.25	3.0	579	220–330
Na-Hg-I_2, propylene carbonate	2.82	2.8	502	170–260
Na-Hg-O_2,$NaHCO_3$	2.90	2.8	1553	660
Na-Hg-H_2O,NaOH	1.85	1.7	991	440

[a] Taken from Reference 38.

prevent contact of sodium metal with water and to allow only passage of Na^+ ions from the anode to the cathode. The ambient temperature batteries have usually been pursued only as primary cells. Most of the results have appeared in patents although Will and Mitoff[38] summarized the properties of several systems as shown in Table 4. Note that open-circuit voltages of >3 V have been obtained with projected specific energies of several hundred Wh/kg for practical cells. Current densities of >0.1 mA/cm^2 can be drawn at ambient temperature.

The organic catholyte–β-alumina interface presents a new set of problems which have been studied by Farrington[39] and Voinov and Tannenberger.[40] They found that Na^+ transport across this interface may involve an adsorbed intermediate state and was influenced by the presence of H_2O or H_3O^+ in the β-alumina. Circumventing the physical problems associated with solid–solid interfaces has created a new set of chemical problems. In addition, the advantage of an all solid state battery requiring no seals has been lost. However, the characteristics given in Table 4 show that these systems have the potential to out-perform all present primary batteries for energy storage, and therefore they deserve serious consideration as new battery candidates.

Selected Reading

J. H. Crawford, Jr. and l. M. Slifkin, eds., *Point Defects in Solids*, Vol. 1, Plenum Press, New York and London (1972).

J. Hladik, ed., *Physics of Electrolytes*, Vols. 1 and 2, Academic Press, London and New York (1972).

J. T. Kummer, *Prog. Solid State Chem.* 7, 141 (1972).

C. C. Liang, *Appl. Solid State Sci.* **4**, 95 (1974).
A. B. Lidiard, in *Handbuch der Physik*, Vol. 20, S. Flugge, ed., Springer-Verlag, Berlin and New York (1957), pp. 246–349.
T. Takahashi, *J. Appl. Electrochem.* **3**, 79 (1973).
M. S. Whittingham, *Electrochim. Acta* **20**, 575 (1975).

References

1. J. Corish and P. W. M. Jacobs, *J. Phys. Chem. Solids* **33**, 1799 (1972).
2. J. Schoonman, *J. Solid State Chem.* **4**, 466 (1972).
3. K. Compaan and Y. Haven, *Trans. Faraday Soc.* **52**, 786 (1956); **54**, 1498 (1958).
4. M. S. Whittingham and R. A. Huggins, *J. Electrochem. Soc.* **118**, 1 (1971).
5. C. Wagner, *Proc. Int. Comm. Electrochem. Thermo. Kinetics (CITCE)* **7**, 361 (1957).
6. D. O. Raleigh, *Progr. Solid State Chem.* **3**, 83 (1967).
7. T. Takahashi and O. Yamamoto, *Electrochim. Acta* **11**, 911 (1966).
8. J. H. Kennedy and F. Chen, *J. Electrochem. Soc.* **116**, 207 (1969).
9. C. C. Liang, *Fast Ion Diffusion in Solids, Solid State Batteries and Devices*, W. van Gool, ed., North-Holland, Amsterdam (1973), pp. 19–31.
10. T. Takahashi and O. Yamamoto, *Electrochim. Acta* **11**, 779 (1966).
11. J. N. Mrgudich, *J. Electrochem. Soc.* **107**, 475 (1960).
12. S. A. Weiner, RANN Rept., Contract No. NSF-C805 (AER-73-07199), July 1975.
13. J. H. Kennedy and A. F. Sammells, *J. Electroqhem. Soc.* **121**, 1 (1974).
14. B. B. Owens, G. R. Argue, I. J. Groce, and L. D. Hermo, *J. Electrochem. Soc.* **116**, 312 (1969).
15. C. C. Liang, *J. Electrochem. Soc.* **118**, 894 (1971).
16. C. C. Liang, J. Epstein, and G. H. Boyle, *J. Electrochem. Soc.* **116**, 1452 (1969).
17. B. B. Owens and G. R. Argue, *J. Electrochem. Soc.* **117**, 898 (1970).
18. J. N. Bradley and P. D. Greene, *Trans. Faraday Soc.* **62**, 2069 (1969); **63**, 1023 (1967); **63**, 2516 (1967).
19. L. E. Topol, *Inorg. Chem.* **7**, 451 (1968).
20. O. Yamamoto and T. Takahashi, *Denki Kagaku* **34**, 833 (1966).
21. G. R. Argue, B. B. Owens, and I. J. Groce, *Proc. Ann. Power Sources Conf.* **22**, 103 (1968).
22. T. Takahashi and O. Yamamoto, *J. Electrochem. Soc.* **117**, 1 (1970).
23. G. Ervin III, U.S. Patent 3,701,685 (1972).
24. B. Scrosati, *J. Electrochem. Soc.* **120**, 78 (1973).
25. D. V. Louzos, W. G. Darland, and G. W. Mellors, *J. Electrochem. Soc.* **120**, 1151 (1973).
26. B. B. Owens, J. S. Sprouse, and D. L. Warburton, *Proc. Ann. Power Sources Conf.* **25**, 8 (1972).
27. T. Takahashi and O. Yamamoto, U.S. Patent 3,558,357 (1971).
28. L. I. Bodnaruk, A. V. Danilov, V. E. Kutlinkovich, and V. B. Aleskovskii, *Elektrokhimiya* **11**, 1325 (1975).
29. C. R. Schlaikjer and C. C. Liang, *J. Electrochem. Soc.* **118**, 1147 (1971).
30. C. C. Liang, *J. Electrochem. Soc.* **120**, 1289 (1973).
31. J. R. Moser, U.S. Patent 3,660,163 (1972).
32. M. Mosharrafa, *Biomed. Sci. Instrum.* **11**, 157 (1975).
33. C. C. Liang and L. H. Barnette, *J. Electrochem. Soc.* **123**, 453 (1976).
34. R. W. Powers and S. P. Mitoff, *J. Electrochem. Soc.* **122**, 226 (1975).
35. M. S. Whittingham and R. A. Huggins, *J. Chem. Phys.* **54**, 414 (1971).
36. K. O. Hever, *J. Electrochem. Soc.* **115**, 830 (1968).
37. G. J. Dudley, B. C. H. Steele, and A. T. Howe, *J. Solid State Chem.* **18**, 141 (1976).
38. F. G. Will and S. P. Mitoff, *J. Electrochem. Soc.* **122**, 457 (1975).
39. G. C. Farrington, *J. Electrochem. Soc.* **123**, 591 (1976).
40. M. Voinov and H. Tannenberger, *Electrochim. Acta* **19**, 959 (1974).

10

Secondary Batteries—Introduction

JAMES McBREEN

1. Classification, General Features, and Intercomparisons

1.1. Introduction

In the early texts on secondary batteries,[1,2] little consideration was given to intercomparison of various systems. These were essentially treatises on the lead–acid battery. This is understandable since the contributions of other secondary systems (e.g., the Edison and Jungner batteries) were then negligible. Since World War II, a number of alkaline electrolyte batteries have been developed and marketed; these have been described in detail.[3] In the past 20 years a host of new secondary battery systems have been investigated and, at present, research in this area is increasing. The impetus for this work is the great variety of new applications for small batteries in the consumer market, and growing interest in electric vehicles, and the possible application of large batteries for utility load leveling. Recently, batteries for electric vehicles[4,5] and utility load leveling[6] have been reviewed. No overall comparison has been made between the several secondary battery systems. The ideal battery using alkali metals and halogens of low atomic weight as the active materials, and meeting the requirements of all applications, has not materialized. As a result, many battery systems are being investigated. The likely outcome is a number of

JAMES McBREEN • Department of Energy and Environment, Brookhaven National Laboratory, Upton, New York 11973.

new secondary batteries, each occupying a particular niche in the marketplace because of its unique features. This section will discuss battery features in general, the general requirements of the various applications, the specific characteristics of various batteries, and the degrees to which these match possible applications. Where possible, intercomparisons will be given between various battery systems.

1.2. Battery Features

As with any other power generation equipment, desirable battery attributes are related to cost, performance, durability, safety, and environmental considerations.

Initial battery costs are determined both by materials cost and manufacturing costs. Manufacturing costs are determined by the simplicity of the manufacturing processes and are greatly influenced by the number of parts. Hence the desirability for high cell voltages, fast electrode kinetics, high electrolyte conductivities, and minimal volumetric differences between reactants and products. The three latter parameters generally permit designs with thicker electrodes and fewer cell elements.[7] Operating costs are influenced by cycle life, maintenance requirements, and energy efficiency of the charge–discharge cycle.

Important performance characteristics are:

(1) specific energy,
(2) specific power,
(3) compactness–energy and power per unit volume,
(4) charge retention on open circuit,
(5) nearly constant discharge voltage.

In general, high specific energies imply high cell voltages, low equivalent weights, and high utilization of the active materials. For most applications, high specific energies are only useful if the battery can be repetitively deep discharged, so as to remove a large fraction of its capacity, on each cycle. High specific power implies high cell voltages, rapid electrode kinetics, rapid mass transport, and low internal resistance. Ideally, high specific power should be associated with a large operating temperature range and good heat rejection characteristics.

Battery durability, unfortunately, is often the most elusive characteristic. Durability encompasses cycle life, calendar life, and resistance to environmental stresses. For many applications, the goal is long cycle life at deep depths of discharge with minimum maintenance. Long cycle life and calendar life imply reversible electrode reactions, low corrosion rates, and negligible rates of side reactions. Life is often limited by the cumulative effect of slight irreversibilities that occur from cycle to cycle. These often result in the slow degradation and decrease in performance of solid electrodes. Other durability factors

that have to be considered are resistance to electrochemical abuse (e.g., overcharge and cell reversal), ruggedness (resistance to shock and vibration), and degradation caused by fluctuations in operating temperature.

Safety and environmental considerations depend upon the application. It is generally desirable that batteries do not emit any corrosive or noxious fluids. Operation in different orientations without spillage is necessary for portable power applications, hence the desirability of completely sealed operation.

1.3. Battery Applications

About 75% of the present rechargeable battery market is still dominated by automotive SLI (starting, lighting, and ignition) batteries. The present, most rapidly growing market is for batteries for portable equipment. In the industrial sector, batteries are used for traction (e.g., forklift trucks) and emergency power applications such as emergency lighting and uninterruptible power systems. There is a sizable market for special purpose batteries for military and aerospace applications. Two possibly enormous markets are batteries for vehicle propulsion and utility load-leveling applications.

Each application has its own set of requirements. Table 1 lists, in order of importance, the critical battery characteristics for both the present consumer and industrial markets. In the noncivilian market, often many stringent requirements are of equal importance. However, cost is often no object. Battery characteristics for electric vehicles and load leveling are demanding, and many requirements have to be met while still maintaining low cost. The critical battery requirements for the present noncivilian markets and the emerging markets are also given in Table 1.

1.4. Characteristics and Classification of Secondary Batteries

The number of secondary batteries on the market and under development is understandable when the general characteristics, relative merits, present problems, and possible end uses of the various systems are considered. Even though those batteries will be discussed at length later, it is instructive to briefly consider these aspects and make intercomparisons between the various systems. Table 2 lists both currently available secondary batteries and those under development. Where appropriate, batteries are classified under their principal common feature. Table 3 lists the theoretical open-circuit voltages, the specific energies, operating temperature ranges, as well as the present performance and problems of the various batteries.

1.4.1. Lead–Acid Battery

Even though the lead–acid battery has a low specific energy, it still dominates more than 90% of the present market. The strong points are its

Table 1
Battery Requirements for Various Applications

Civilian consumer market			Industrial market		Noncivilian market		Emerging markets	
	Portable equipment							
Auto SLI	Electronic	Motor driven	Traction	Emergency power	Military	Aerospace	Electric vehicles	Load leveling
Cost	Sealed operation	Sealed operation	Cost	Calendar life	Specific energy	Specific energy	Cost	Cost
Specific power	Compactness	Specific power	Maintenance	Maintenance	Specific power	Specific power	Specific energy	Cycle life
Temperature range	Life	Compactness	Life	Cost	Compactness	Compactness	Specific power	Energy efficiency
Ruggedness	Cost	Life			Ruggedness	Sealed operation	Compactness	Temperature range
Life		Cost			Temperature range	Ruggedness	Ruggedness	Maintenance
					Life	Life	Cycle life	
							Temperature range	
							Energy efficiency	
							Maintenance	

Table 2
Classification of Secondary Batteries

Current battery technology

(a) Lead–acid battery
(b) Alkaline electrolyte batteries
Iron–nickel oxide
Cadmium–nickel oxide
Zinc–silver oxide
Cadmium–silver oxide

Emerging battery technology

Aqueous electrolyte batteries
(1) Zinc batteries
(a) Alkaline electrolyte batteries
Zinc–nickel oxide
Zinc–manganese dioxide
(b) Zinc–halogen batteries
Zinc–chlorine
Zinc–bromine
(2) Batteries with one gaseous reactant
(a) Metal–air (oxygen) batteries
Zinc–air (oxygen)
Iron–air (oxygen)
Cadmium–air (oxygen)
(b) Hydrogen–metal oxide batteries
Hydrogen–nickel oxide
Hydrogen–silver oxide
(3) Batteries with fluid reactants
(a) Hydrogen–oxygen
(b) Hydrogen–halogen batteries
Hydrogen–chlorine
Hydrogen–bromine
(c) Redox batteries
Titanium–iron
Chromium–iron

Nonaqueous electrolyte batteries
(1) Organic electrolyte batteries
(a) Lithium–bromine batteries
(b) Lithium–metal chalcogenide batteries
Lithium–titanium disulfide
Lithium–niobium diselenide
(2) High-temperature batteries
(a) Sodium batteries
Sodium–sulfur
Sodium chloroaluminate batteries
(b) Lithium batteries
Lithium–iron disulfide
Lithium–chlorine
Lithium charge storage batteries

low cost, simplicity of manufacture, high specific power, and wide operating temperature range.

1.4.2. Alkaline Electrolyte Batteries

Alkaline electrolyte secondary batteries now occupy the remainder of the market. In the U.S., prior to World War II, these were almost exclusively iron–nickel oxide batteries. They were used mostly for traction and lighting or trains because of their long life and resistance to electrochemical abuse. The latter factor is now of less importance because of recent advances in charging methods and equipment which prolong the life of lead–acid batteries. The

Table 3
Characteristics of Various Batteries

Battery type and system	Cell voltage, V	Theoretical specific energy, Wh/kg	Operating temperature, °C	Specific energy: 1-hr rate, Wh/kg	Specific energy: 5-hr rate, Wh/kg	Energy efficiency, % approx.	Cycle life, approx.	Calendar life, years
			Current battery technology					
$Pb-H_2SO_4-PbO_2$	2.1	184	−35–70	20–30	30–40	60	500	3–5
Cd-KOH-NiOOH	1.35	218	−40–65	30–40	40–50	75	>1000	5–15
$Cd-KOH-Ag_2O_2$	1.41, 1.15	269	−40–80	50–60	65–75	70	700	3–5
Fe-KOH-NiOOH	1.37	267	−40–80	30–35	35–45	50	>1000	>10
$Zn-KOH-Ag_2O_2$	1.86, 1.60	490	−40–55	100–110	85–95	70	500	3–5
			Emerging battery technology					
Ambient temperature batteries								
Zinc Batteries								
(a) Alkaline zinc batteries								
$Zn-KOH-NiOOH$	1.7	341	−40–65	50–60	65–75	75	300	3–5
$Zn-KOH-MnO_2$	1.55, 0.95	484	−40–65	50–60	50–60	75	200	3–5
(b) Zinc–halogen batteries								
$Zn-ZnCl_2-Cl_2$	2.1	826	15–60	60–80	75–90	55–65	100	N.A.[a]
$Zn-ZnCl_2-Cl_2\cdot 6H_2O$	2.1	460	15–60	60–80	75–90	55–65	100	N.A.
$Zn-ZnBr_2-Br_2$	1.8	428	0–50	50–60	65–75	75	300	>3
$Zn-ZnBr_2-(CH_3)_4NClO_4Br_6$	1.8	364	0–50	50–60	65–75	75	300	>3
Batteries with one gaseous reactant								
(a) Metal–air (oxygen) batteries								
$Zn-KOH-air\ (O_2)$	1.6	1054	25–65	100	110–170	<50	500	N.A.
$Fe-KOH-air\ (O_2)$	1.2	716	25–60	55–65	80–90	<30	>1000	>3
$Cd-KOH-air\ (O_2)$	1.18	432	0–80	60–70	80–90	<40	500	N.A.

(b) Hydrogen–metal oxide batteries								
H_2–KOH–NiOOH	1.36	393	−20–65	60–70	70–80	65	>1000	>3
H_2–KOH–Ag_2O_2	1.38, 1.12	532	−20–80	70–80	80–90	60	700	3
Batteries with fluid reactants								
H_2–KOH–O_2	1.23	3663	−20–180	—	—	50	500	>5
H_2–HCl–Cl_2	1.36	1000	0–100	75–90	75–90	80	—	—
H_2–HBr–Br_2	1.07	354	0–100	45–60	45–60	75	—	—
$TiCl_2$–$FeCl_3$	0.61	58	0–100	<25	<25	70	—	—
$CrCl_2$–$FeCl_3$	1.20	122	0–100	<30	<30	70	—	—
Lithium batteries								
Li–PC–TiS_2	2.15	484	0–70	50–60	110–120	60–75	—	>3
Li–Al–PC–TiS_2	1.85	339	0–70	40–50	80–90	60–75	100	>3
Li–PC–$NbSe_3$			0–70	40–50	80–90	60–75	150	>3
Li–PC–Br_2	4.05	1249		40–50	80–90	60–75	1000	>3
High-temperature batteries								
Li–LiCl-KCl–FeS_2	2.1, 1.6	1342	400–450	—	—	70	100	—
Li–LiCl-KCl–FeS	1.6	842	400–450	—	—	70	—	—
Li-Al–LiCl-KCl–FeS_2	1.8, 1.3	650	400–450	80–100	140–160	70	300	1
Li-Al–LiCl-KCl–FeS	1.3	447	400–450	—	—	—	120	—
Li_4Si–LiCl-KCl–FeS_2	2.05–1.26	944	400–450	—	—	—	—	—
Li_4Si–LiCl-KCl–FeS	1.55–1.26	637	400–450	—	—	—	—	—
Na–β-Al_2O_3–S	2.08–1.75	763	300–400	80–90	100	70	—	N.A.
Na–β-Al_2O_3–S	2.08–1.75	521	300–400	—	—	—	—	—
Na–β-Al_2O_3–$Na_2S_{5.2}$	2.08–1.75	308	300–400	—	—	—	—	—
Na–β-Al_2O_3–$NaAlCl_4$–M_xCl_y	2.7–3.2	792–1034	210	—	—	—	—	—
Li-Al–LiCl-KCl–C–$TeCl_4$	N.A.	N.A.	400	—	—	—	—	—
Li–LiCl-KCl-LiF–Cl_2	3.6	2275	450	150	200	75	700	0.1

[a] N.A. = not available.

durability of the system still makes it attractive for electric vehicles, and developments are under way to improve the specific energy of the system.[8] The low hydrogen overvoltage of the iron electrode reduces the charging efficiency and precludes sealed operation.

The other alkaline electrolyte batteries can be operated in either the sealed or vented mode. Materials costs are such that only the cadmium–nickel oxide battery has penetrated the consumer market, and has done so only in the smaller sizes where materials costs are less important. Sealed cadmium–nickel oxide cells now dominate the rechargeable portable power market. The attractive features of the system are long cycle life, ruggedness, and the ability of the sealed battery to accept continuous overcharge.

The zinc–silver oxide has the highest specific energy of any available system. Cost considerations limit its use almost exclusively to military and aerospace applications. Another drawback is limited cycle life. Cadmium–silver oxide batteries, used in aerospace applications requiring nonmagnetic components, are even more expensive.

1.4.3. Zinc Batteries

Until recently, most developmental effort on new aqueous electrolyte batteries has been focused on zinc batteries. Zinc is attractive as a negative electrode material because of its low cost, low equivalent weight, negative potential, high hydrogen overvoltage, and reversibility in many aqueous electrolytes. The major effort has been on the zinc–nickel oxide system. The incentives are development of a low-cost substitute for cadmium–nickel oxide batteries and a battery for vehicle propulsion. In the latter application, it more than doubles the vehicle range that can be obtained with lead–acid batteries of equivalent weight.[9] The battery can be sealed. Present limitations are related to problems with the zinc electrode. More recent efforts have been the development of other zinc systems with more plentiful, less costly positive electrode active materials such as manganese dioxide, chlorine, and bromine.

Progress on the zinc–manganese dioxide system has been hampered by irreversibilities that occur in the manganese dioxide electrode when it is deep discharged.[10,11]

Zinc–halogen batteries, if developed, have many characteristics that make them strong contenders for vehicle propulsion and load leveling. Since the reaction products are completely soluble, it should be possible to rejuvenate batteries by merely completely discharging them. If the current collectors remain inert, and no impurity buildup occurs in the electrolyte, it is theoretically possible to eliminate any irreversibilities that occur with cycling in this way, and indefinitely extend cycle life. Problems to be solved are the cycle life of the zinc electrode and self-discharge of the zinc–bromine system.

1.4.4. Metal–Air (Oxygen) Batteries

Several metal–air (oxygen) batteries were under development in the 1960s. The incentive was to capitalize on the advances in fuel cell electrodes and develop batteries of high specific energy. An attractive goal was the replacement of the expensive solid alkaline electrolyte positive electrodes with low-cost air cathodes which could be coupled with zinc or iron. Attempts to develop zinc–air batteries, with *in situ* charging, have been abandoned for a number of technical reasons.[12] A more promising approach in which the zinc is charged exterior to the primary power generation cell has also recently been abandoned.[13] Work still continues on iron–air batteries for vehicle propulsion. Metal–air systems suffer from low energy efficiencies due to the irreversibility of the oxygen electrode. In the case of iron–air batteries, this problem is exacerbated by the low charging efficiencies of the iron electrode. Heat management during discharge is a problem because of the compounding effects of oxygen electrode overvoltage and entropy effects.

1.4.5. Hydrogen–Metal Oxide Batteries

Hydrogen–metal oxide systems have recently rapidly reached an advanced state of development.[14] These batteries combine the durable alkaline electrolyte positive electrodes (nickel oxide and silver oxide) with fuel cell hydrogen electrodes. Attractive features are long cycle life and immunity from damage caused by cell reversal. Present concerns are the high negative electrode catalyst cost and the high pressure containers that are necessary.

1.4.6. Batteries with Fluid Reactants

For several reasons, batteries with fluid reactants are attractive for utility load leveling applications.[6] Fluid reactants avoid the cumulative degradation of structure, and morphology changes, that are often the life limiting factors in solid electrodes. Since the reactants can be stored outside the cell stack, it is possible to independently size systems for capacity and power. The electrolyte circulating systems that are used in these batteries simplify thermal management—a very important aspect in large battery systems.

Hydrogen–oxygen systems for load leveling offer a unique feature in that they can be designed to operate either as a passive storage device or an active peak-shaving generation. Energy is stored by charging the system, or power can be generated by feeding cracked fuel and air to the system. An attractive feature is the wide operating temperature range.[15] The biggest problem is hydrogen storage; however, a promising approach is the storage of hydrogen as a hydride.[16] Hydrogen–halogen batteries have higher energy efficiencies than hydrogen–oxygen systems, and storage of halogens is relatively simple.

Redox systems require ion exchange membranes to prevent cross-diffusion of the redox ions. So far, no totally satisfactory membrane has been

developed. Large volumes of electrolyte are required.[17] However, it has been suggested that this aspect be turned to an advantage by using redox systems for storing both electricity and heat from solar energy.[13]

1.4.7. Nonaqueous Electrolyte Batteries

Nonaqueous electrolytes permit the use of elements with low electronegativity (Li and Na) in rechargeable batteries. Both ambient temperature organic electrolyte batteries and high-temperature batteries with molten salt and solid electrolytes have been investigated.

Even though success has been attained in developing primary organic electrolyte lithium batteries, very few cases of long-term secondary operation have been demonstrated.[18] In the past, problems have been the irreversibility of the positive electrodes and morphological changes in the lithium electrode with cycling. Promising recent developments are the transition metal dichalcogenides as positive electrode active materials and the use of lithium–aluminum alloy electrodes.

High-temperature batteries offer the possibility of coupling high specific energy with high specific power and are attractive for vehicle propulsion. High-temperature operation poses many materials and corrosion problems. An elegant solution to the separation and containment of the active materials in high temperature sodium batteries is the use of sodium-ion-conductive β-alumina[19] and glasses.[20] Promising approaches to mitigate the materials problems are the use of lithium alloy negative electrodes, iron sulfide positive electrodes,[21] and redox positive electrodes in chloroaluminate melts.[22] Use of the latter permits operation of sodium solid electrolyte batteries at temperatures as low as 200°C, thereby mitigating the materials problems. Many of the approaches to solve these problems reduce the theoretical specific energy of the system. These specific energies are also given in Table 3.

1.5. Other Intercomparisons

Other important aspects of batteries are compactness, cycle life at various depths of discharge, and shelf life.

1.5.1. Compactness

Compactness is an important consideration for electric vehicles, portable power, aerospace, and military applications. Table 4 lists the densities of various batteries. When the specific energy and power are known, the energy and power per unit volume can easily be calculated.

The lead–acid battery has a uniquely high density. Other aqueous electrolyte batteries with solid electrodes have densities in the range 1.5–2.2 kg/liter. The density of metal–oxygen and hydrogen–metal oxide cells is

Table 4
Densities of Various Batteries

Battery	Density (kg/l)
$Pb-H_2SO_4-PbO_2$	2.3–3.3
Fe–KOH–NiOOH	~2.0
$Zn-KOH-Ag_2O_2$	1.5–2.0
$Cd-KOH-Ag_2O_2$	1.5–2.0
Zn–KOH–NiOOH	1.8–2.2
$Zn-ZnBr_2-Br_2$	~1.5
$Zn-ZnCl_2-Cl_2$	~1.5
$Zn-KOH-O_2$	~0.75
Zn–KOH–Air	1.0–1.3
Fe–KOH–Air	~1.0
$Cd-KOH-O_2$	~0.75
H_2–KOH–NiOOH	0.6–2.3
$H_2-KOH-Ag_2O_2$	0.5–2.0
$H_2-KOH-O_2$	0.3–0.6
Redox batteries	~1.25
Organic electrolyte batteries	~1.5
High-temperature batteries	~1.5

dependent on whether the design is optimized for minimum volume or minimum weight.[23] Metal–air batteries typically have densities of 1.0 kg/l.[13,24] If these batteries are to be competitive for electric vehicle use, then the specific energy would have to be at least three times that of lead–acid. Densities of nonaqueous electrolyte batteries are difficult to estimate at present. However, when provisions for thermal management are made, large systems will probably have densities of about 1.5 kg/l.

1.5.2. Cycle Life and Depth of Discharge

One feature of batteries with solid electrodes is that the cycle life is very dependent on the depth of discharge. Unfortunately, little data of this type are available. Figure 1 gives a plot of cycle life versus depth of discharge for a number of battery systems. In all cases, cycle life increases logarithmically with decreasing depth of discharge. This type of behavior is related to structural changes that are induced by the charge–discharge cycle. In cadmium batteries, it is due to recrystallization and migration of cadmium,[25] in zinc batteries to zinc electrode shape change,[26] and in lead–acid batteries to the development of a "corolloid" structure in the positive electrodes.[27] In all cases, the structural changes apparently are related to solid reactants and products with soluble intermediates in the charge–discharge reactions. Electrodes without soluble intermediates, such as nickel oxide, and electrodes with fluid reactants should not suffer such limitations, and their cycle life should not be dependent on depth of discharge.

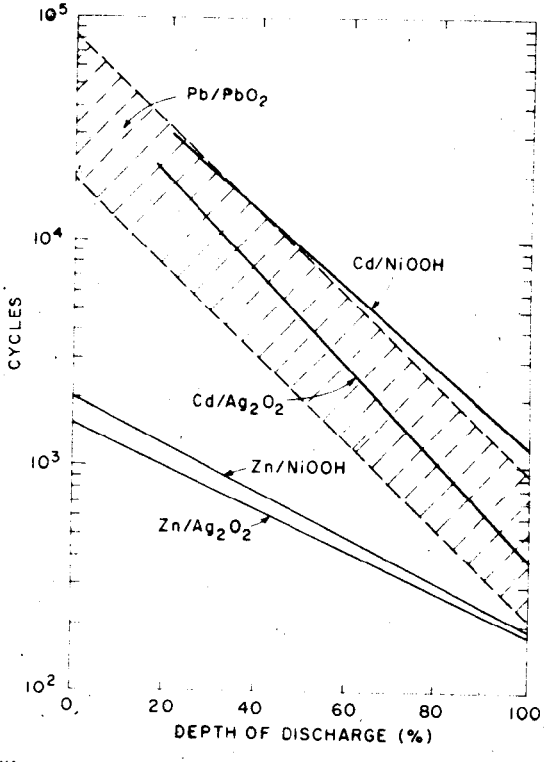

Figure 1. Cycle life vs. depth of discharge for various batteries. The lower part of the band for Pb-PbO$_2$ batteries is representative of thin-plate starting lighting and ignition (SLI) batteries; the upper part is representative of heavy-duty traction batteries.

When there is an exponential dependence of cycle life on depth of discharge, the ampere-hours throughout, during the life of a battery, are a maximum for a certain depth of discharge; these are given in Table 5.

2. New Ambient Temperature Batteries

2.1. The Zinc–Nickel Oxide Battery

The overall reaction of the zinc–nickel oxide battery is

$$2NiOOH + Zn + H_2O \rightleftarrows 2Ni(OH)_2 + ZnO$$

The open-circuit voltage is 1.7 V and the electrolyte is KOH, with concentrations in the range of 4–10 *M*. In its most elementary form, the cell uses the

Table 5
Depth of Discharge for Maximum Ampere-Hour Throughput during Life

Battery	Depth of discharge, %, for maximum Ah throughput
Lead–acid	
Cadmium–nickel oxide	25.1
Cadmium–silver oxide	20.4
Zinc–silver oxide	47.2
Zinc–nickel oxide	43.4

NiOOH electrode technology of the cadmium–nickel oxide battery and couples it with the Zn electrode and separator technology of the zinc–silver oxide battery to yield a vented zinc–nickel oxide cell. This results in a battery that is capable of being discharged at very high rates.[28,29] However, this simple combination of technologies results in a number of problems that do not arise, or are less intense, in either of the other two systems.

In vented zinc–nickel oxide cells, a number of operational problems can arise because of the disparity in charging efficiencies between the positive and negative electrodes. The NiOOH electrode is inefficient on charge; about 5–10% of current is used in evolving oxygen. Zinc deposition, on charge, is essentially 100% efficient if there is an adequate amount of reducible species (zinate and zinc oxide) present. However, if oxygen is vented from the cell, the reducible zinc species are depleted after a few cycles. This causes the Zn electrode overvoltage to increase at the end of the charge—the condition which favors zinc dendritic growth[30] and zinc penetration of the separator.[31]

Cellulosic separators are more rapidly oxidized in zinc–nickel oxide cells than in zinc–silver oxide cells. Separator oxidation is due to peroxyl ions that are generated at the positive electrode and produced at the Zn electrode edges by oxygen reduction. In zinc–silver oxide cells, the problem is less severe because silver and its compounds catalytically decompose peroxyl ions.

Work on the zinc–nickel oxide battery dates back to the turn of the century.[32] Most development efforts have been on compact cells (60–75 Wh/kg), of similar construction to zinc–silver oxide batteries. Research has focused on the difficulties arising from the differences in charging efficiencies between the positive and negative electrodes, separator oxidation, and the zinc electrodes. The problems of the zinc electrodes are shape change[26] and zinc penetration of the separator.

Two methods have been used to overcome interelectrode charge imbalance. One method is to incorporate stoichiometric excesses of zinc oxide in the zinc electrode and periodically carry out maintenance discharges by short

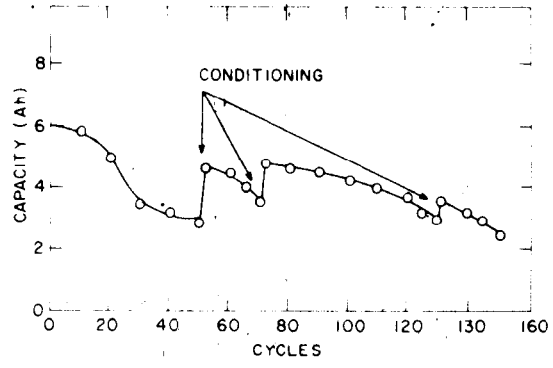

Figure 2. The effect of conditioning (draining to zero volts to regenerate ZnO) on the capacity of Zn–NiOOH cells.

circuiting the battery terminals at the end of a normal discharge.[33,34] When this is done, the zinc in the negative electrode is converted to zinc oxide, while hydrogen is evolved off the NiOOH electrode; in this way the zinc oxide reservoir in the Zn electrode is restored. Figure 2 shows the type of improvement that can be achieved in this way. A disadvantage of this procedure is that it is time consuming (10–20 hr) and usually entails water additions to replenish lost water.[34]

Interelectrode charge balance can also be achieved by sealing the cell and operating it on the oxygen cycle in a manner similar to sealed cadmium–nickel oxide cells. Successful sealed operation depends upon cell designs that enhance oxygen transport from the positive to negative electrode, and a proportioning of the cell active material in such a way that the evolution of hydrogen is avoided, and the kinetics of oxygen recombination on the negative electrode is enhanced.[35,36] The continuous film separators, which are necessary to prevent zinc penetration, militate against good oxygen transport. Hence it is often necessary to use oxygen recombination electrodes that are coupled with the zinc electrode.[37–39] Since the rate of hydrogen recombination on NiOOH electrodes is negligible,[39,40] little or no hydrogen evolution on the zinc electrode can be tolerated. Hydrogen evolution on the zinc electrode can be suppressed by amalgamation, elimination of impurities, and by providing an adequate reserve of zinc oxide in the negative electrode at all times.[39] Hydrogen evolution on the recombination electrodes can be avoided by using diode circuits[37] or by using electrodes with a high hydrogen overvoltage.[38,39] Recombination electrodes can be directly coupled to the zinc electrode after the cell has been charged once. Since a spongy zinc substrate will be present on the Zn electrodes, the charging potential will not exceed the nucleation overvoltage required to initiate zinc deposition on the recombination elec-

trode. Thus zinc deposition on directly coupled recombination electrodes does not present a problem.

Several oxidation-resistant substitutes for cellulosic separators have been used and are under development. One approach has been the use of acrylic-acid-grafted polyethylene separators.[41] Another approach has been the use of organic–inorganic composites. Inorganic materials that have been used are ceric oxyhydroxide,[42] zirconia,[43] and olivine.[44] Organic materials that have been used as binders are polytetrafluoroethylene and polyphenylene oxide.

The ultimate failure mode in compact high-energy cells is zinc electrode shape change. A number of engineering approaches have been used to circumvent the problems of the zinc electrode. These usually result in batteries with specific energies in the region of 40–50 Wh/kg. One approach has been to operate the zinc electrode with sufficient excess electrolyte to render the discharge products completely soluble.[45] Several methods have been used to prevent shorting by dendritic zinc. One approach has been to wrap the positive electrode with a fine nickel mesh containing a low hydrogen overvoltage catalyst such as nickel boride.[46] Zinc dendrites are consumed via the corrosion reaction upon hitting the screen. Another method is to vibrate the Zn electrode current collector so as to modify the hydrodynamic conditions at the electrode surface and generate smooth deposits.[47] An even more complex approach has been the use of revolving thin-apertured shutter separators.[48]

Attempts have been made to convert the Zn electrode to an electrode of the second kind using additives such as calcium hydroxide to suppress the zincate solubility.[49] Since stoichiometric amounts of calcium hydroxide have to be added, the specific energy is reduced to the vicinity of 40 Wh/kg.

The zinc–nickel oxide battery can be considered for vehicle propulsion if the cost of the NiOOH electrode is reduced.[4] About 60% of the total nickel content in conventional porous plaque electrodes serves as a current collector. The manufacturing process is slow and expensive. Several plastic bonded nonsintered electrodes have been developed.[34,38,50] These electrodes usually use graphite as the conductive diluent for the active material and can be made by simple continuous processes. The comparative performance of typical sintered and nonsintered electrodes in terms of volumetric and gravimetric capacity utilization as a function of discharge rate is shown in Figure 3.

Figure 4 gives plots of specific power versus specific energy for the various types of zinc–nickel oxide cells. Cycle life data are given in Table 6. Figure 5 shows performance versus temperature for compact aircraft-type cells. These data reflect the excellent kinetics of the system. However, so far, long life has only been achieved with great sacrifices of specific energy and power.

In zinc–nickel oxide cells, self-discharge occurs by a similar mechanism to that found in cadmium–nickel oxide cells. However, self-discharge should be less of a problem in zinc–nickel oxide cells because of the beneficial effect of zincate on the NiOOH electrode.[51,52]

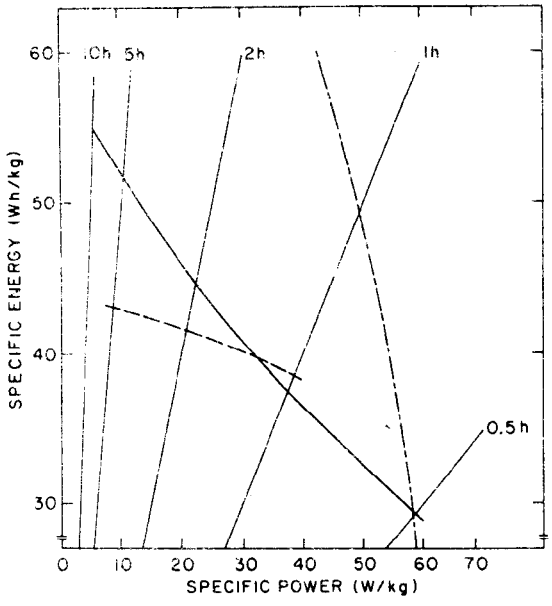

Figure 3. Specific power vs. specific energy for various Zn–NiOOH batteries. The solid line is for a battery with $Ca(OH)_2$ additives (Zn electrode of the second kind). The dashed line is for a zinc electrode of the first kind. The dots and dashes are the line for a compact thin-plate prismatic cell.

The Zinc–Manganese Dioxide Battery

The zinc–manganese dioxide system is attractive because of the low cost of the active materials and the excellent discharge kinetics of both electrodes. However, rechargeable zinc–manganese dioxide cells have been manufactured only in small sizes and in limited quantities.[10] Cells can be cycled for several

Table 6
Cycle Life of Various Types of Zn–NiOOH Cells

Cell type	Specific energy, Wh/kg, for 3-hr rate	Depth of discharge, %	Cycle life, cycles
Compact	65–75	100	150–300
Compact	65–75	60	~500
Compact	65–75	40	800–1000
Calcium zincate negatives	~40	100	300–500
Free electrolyte systems	~40	100	1000–2000

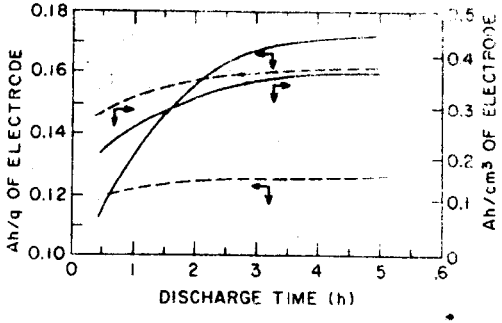

Figure 4. Performance of sintered (broken lines) and nonsintered plastic-bonded (solid lines) NiOOH electrodes at various discharge rates at 25°C.

hundred cycles if the depth of discharge remains below about 70% of the one-electron discharge capacity.[53] However, as little as one deep discharge to below 0.8 V can irreversibly damage the manganese dioxide electrode and drastically reduce the rechargeability of the cell.[54]

Several investigations have been carried out on the discharge of MnO_2 electrode in alkaline electrolytes since the 1950s.[55–64]

Since the late sixties, studies have been carried out on the recharge reaction and the problem of irreversibility. Some of this work has been done in pure KOH solutions.[11,54,65–67] Two investigators have reported work on zincate electrolytes.[68–70]

In all of these studies, there is general agreement that the first reduction of γ-MnO_2 involves the incorporation of protons into the MnO_2 lattice. This reaction is a homogenous solid state reaction and is reversible. There is also general agreement that if successive discharges are carried out below the composition $MnO_{1.5}$ that the electrode becomes irreversible. Irreversibility has been variously attributed to the formation of γ-MnO_2,[65] Mn_3O_4 films[54] and hydrohetaerolite.[69,70]

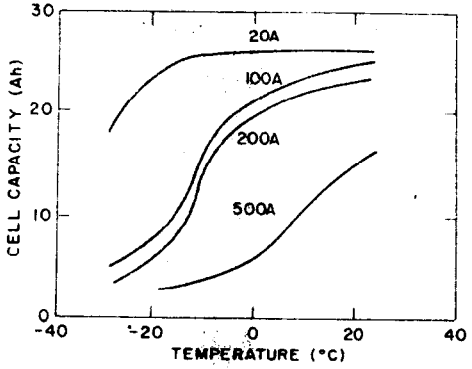

Figure 5. Performance of a 20-Ah Zn–NiOOH cell at various temperatures and discharge rates.

Much of the confusion that exists in the literature has been due to the complexity of manganese oxides (several oxidation states and crystallographic forms) and the amorphous nature of the reduction products.

Many of the above difficulties have been resolved by using low-scan-rate potentiodynamic techniques.[11,63,67,68] McBreen and Ruetschi have concluded that when an MnO_2 electrode is deeply discharged in KOH that the final reduction product is $Mn(OH)_2$. On charge, $Mn(OH)_2$, is first oxidized to a mixture of γ-Mn_2O_3, β-MnOOH, and γ-MnOOH. At more positive potentials, δ-MnO_2 is formed. Reduction of δ-MnO_2 yields Mn_3O_4 (hausmannite). Hausmannite cannot be electrochemically oxidized but can be partially reduced to $Mn(OH)_2$.[11,68] In zincate electrolyte hetaerolite is also formed. Neither hetaerolite nor Mn_3O_4 can be electrochemically oxidized. The resistivity of both of these compounds to electrochemical oxidation is not fully understood.

Commercially available zinc–manganese dioxide cells are very similar in construction to primary alkaline zinc–manganese dioxide cells.[10] Recently, it has been shown that considerable improvement in rechargeability can be obtained by using thin (~1-mm) manganese dioxide electrode structures.[53] Kordesch and Kozawa[53] estimate that this construction could yield cells with specific energies of 66 Wh/kg at the 1-hr rate.

The charging method also has a considerable influence on the cycle life of zinc–manganese dioxide cells. If cells are charged much above 1.7 V, soluble manganate (MnO_4^{2-}) can form. The recommended charging method is a voltage-limited taper current system with voltage limit set at 1.7 V per cell.

Oxygen evolution presents less problems in zinc–manganese dioxide cells than in zinc–nickel oxide cells so the system can easily be sealed. The shelf life is excellent. Capacity losses of as little as 1% per day have been found at 71°C.

2.3. The Zinc–Chlorine Battery

Even though the concept of a zinc–chlorine battery is old (Pearce, 1887; Reference 151), it was only recently that serious efforts have been made to develop a rechargeable battery.[71] Recent development efforts revolve around the concept of a battery with circulating electrolyte and the use of solid chlorine hydrate as the storage medium for chlorine. The zinc–chlorine couple is based on the electrochemical reaction between zinc and chlorine. Elemental zinc and chlorine are generated from an aqueous zinc chloride solution during battery charging, the zinc being retained on a substrate current collector while the chlorine is removed with the flowing electrolyte to a storage tank where the chlorine hydrate is frozen at a temperature between 0 and 10°C. The reaction is

$$Cl_2 + 6H_2O \underset{\text{discharge}}{\overset{\text{charge}}{\rightleftharpoons}} Cl_2 \cdot 6H_2O, \qquad \Delta H = 334.88 \text{ kJ/kg}$$

Chlorine hydrate is a bright yellow icelike solid that can be handled safely. The chlorine storage density is 0.5 kg/l. During discharge, the chlorine is regenerated by heat exchange between the cell stack and the chlorine hydrate reservoir and is transmitted to the cell stack in the circulating electrolyte. Hydrate storage permits battery operation at pressures within ±20 kPa of atmospheric. The chlorine solubility in the electrolyte is sufficiently high that either flow-by or flow-through chlorine electrodes can be used. The kinetics are such that no expensive electrocatalysts are required. A simplified schematic diagram of the zinc chlorine system is shown in Figure 6.

Cell stacks have been built using solid graphite sheet zinc electrode current collectors and porous graphite flow-through chlorine electrodes.[72,73] The use of precious-metal-coated titanium current collectors for both electrodes has also been reported.[74] Electrolyte concentrations are typically 20–30 wt % zinc chloride.

Zinc deposition and chlorine evolution are not the only electrochemical reactions occurring during charge. Zinc plating efficiencies between 99.73% and 99.95% and chlorine evolution efficiencies between 99.73% and 99.95% have been reported.[72,73] Hydrogen evolution occurs on the zinc electrode and the rate of evolution increases with decreasing pH and increasing temperature. Oxygen evolution occurs on the chlorine electrode when precious-metal-coated titanium current collectors are used. When carbonaceous materials are used the parasitic reaction is CO_2 evolution. Carbon dioxide evolution increases with increasing pH and increasing temperature. During the formation of chlorine hydrate it is possible to preferentially vent these gases without having chlorine escape.[72] More recently, the possibility of photolytically recombining hydrogen and chlorine has been considered.[73]

Successful cell operation depends upon avoiding the deposition of nodular or dendritic zinc. In the past, proprietary organic additives have been used to achieve compact smooth zinc deposits.[72,75] Low electrolyte pH and cationic impurities such as iron promote dendritic growth. One problem with organic additives is that they are oxidized at the chlorine electrode and generate hydrochloric acid. The pH reduction is a function of zinc chloride concentration. For example, a 25 wt % solution of zinc chloride containing 2.5 g/l

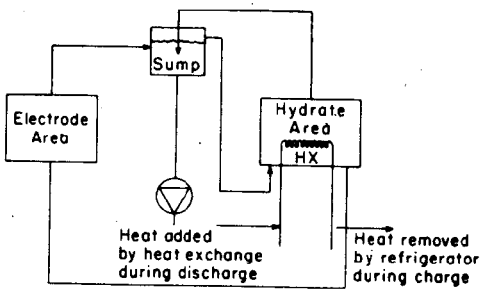

Figure 6. A schematic of a $Zn–Cl_2$ battery system.

hydrochloric acid will have a pH of 3.5 at 25°C. If the cell is charged so as to reduce the zinc chloride concentration to 15 wt % the pH becomes 1.3. A possible explanation of the variation of pH with zinc chloride concentration, in the presence of hydrochloric acid, is a reduction in the hydrogen ion activity by association with the complex $ZnCl_4(H_2O)_2^{2-}$ at concentrations above 10 wt %.[75] A reduction of electrolyte pH at the end of charge could result in both zinc dendritic growth and increased hydrogen evolution. However, this problem is not as serious as it might be because water removal from the electrolyte during hydrate formation helps maintain the zinc chloride concentration high even toward the end of charge.

The main parasitic reaction during battery operation is direct action between zinc metal and chlorine dissolved in the electrolyte to form zinc chloride. The rate of this reaction is a function of chlorine concentration, current density, temperature, and electrolyte flow rate, and probably occurs under diffusion-controlled conditions.[71] The rate is about 30% less during discharge than during charge. This is probably due to the high concentrations of zinc chloride adjacent to the metal surface. By proper control of the above parameters, coulombic efficiencies of about 70% can be achieved without using separators. The voltage efficiencies are in the vicinity of 90%, yielding an energy efficiency between 60% and 70%.

Specific energies of 66 Wh/kg (14% of theoretical) have been demonstrated, and it is likely that a specific energy of 88 Wh/kg at the 4-hr discharge rate will be achieved shortly.[73]

Very little data are available on cycle life. A cycle life of 100 deep cycles has been reported for a 100-kWh battery.[73] To achieve good cycle life, it is apparently necessary to prevent electrolyte contamination by organic materials and transition metal ions. In the work reported, so far, the electrolyte was periodically purified and the cells are periodically discharged completely to remove all the zinc from the current collector.

2.4. The Zinc–Bromine Battery

The concept of the zinc–bromine battery dates back to 1885.[76,77] Several efforts have been made to develop the battery since the early fifties.[78–89] A zinc–bromine cell can be constructed using two inert current collectors and an aqueous zinc bromide electrolyte. On charge the positive electrode reaction is

$$3Br^- \rightarrow Br_3^- + 2e$$

and the negative electrode reaction is

$$Zn^{2+} + 2e \rightarrow Zn$$

The overall cell reaction is

$$Zn^{2+} + 3Br^- \underset{\text{discharge}}{\overset{\text{charge}}{\rightleftharpoons}} Zn + Br_3^-, \qquad E^\circ = 1.828\ \text{V}$$

Most of the bromine in the cell is present as the complex tribromide and pentabromide ions

$$Br_2 + Br^- \rightleftarrows Br_3^-, \qquad K_1 = 16$$

$$2Br_2 + Br^- \rightleftarrows Br_5^-, \qquad K_2 = 40$$

In a cell such as this, the Br_3^- and the Br_5^- would rapidly diffuse to the negative electrode and react with the zinc. Even more rapid electromigration of these ions would occur on discharge. On charge, zinc dendrites would form on the zinc electrode.

In the past, work on the zinc–bromine system has focused on mitigating the self-discharge and suppression of zinc dendritic growth. Activated carbon and silica gel have been used to adsorb the bromine.[79–83] Blue and Leddy have described a scheme where the electrolyte is circulated and the bromine is stored by solvent extraction externally from the cell stack. Solvents such as bromobenzene or carbon tetrachloride could be used.[84] Organic bromine complexes have been used to lower the solubility of bromine in the electrolyte.[78,85–88] Tetraalkylammonium salts have been used as complexing agents. Tetrabutylammonium bromide can complex as many as ten atoms of bromine (Rallo and Silvestroni[152]). Other approaches have been the use of microporous separators[79] and gelled electrolytes[80] to decrease the rate of bromine diffusion. Even with these various schemes, the self-discharge remains high—about a 50% loss of capacity in 50 hr.[81,87] Will[89] has been able to extend the half-charge retention to 400 hr by using 0.3-mm-thick sulfonated polytetrafluoroethylene membranes.

Apart from dendritic zinc growth, other problems have been observed on the zinc electrode. These are poor adherence of the zinc deposits,[87] hydrogen evolution, and a thickening of the zinc deposit toward the bottom of the electrode. Hydrogen evolution is more severe at low pH. Apparently the pH can fall during cell operation by slow hydrolysis of bromine to yield hydrogen bromide.[81] The thickening of the zinc deposits toward the bottom of the electrode is caused by density gradients in the electrolyte. In one version of the cell, the electrolyte density increases from 1.20 to 1.68 during discharge.[87] Considerable headway has been made toward solving these problems of the zinc electrode by using circulating electrolytes, inorganic salt additives, semipermeable membranes, and by maintaining the charge current density below 50 mA/cm^2 and the zinc deposit thickness below 200 mAh/cm^2.[89] During cycling, there is a cumulative buildup of zinc on the negative electrode current collector even when discharges are carried out to 1.0 V. As a result, a maintenance cycle, wherein the cells are shorted, has to be carried out every few cycles.

Specific energies of 37.5 Wh/kg, at the 1-hr discharge rate, have been demonstrated in batteries,[81] and specific energies between 60 and 70 Wh/kg are projected.[89] Will has also demonstrated a cycle life of 2000 2.5-hr charge–discharge cycles and charge–discharge energy efficiencies of 75%.

2.5. The Zinc–Air Battery

A considerable amount of research and development work has been carried out on the zinc–air battery since the early sixties. The system is attractive because of its high specific energy (1068 Wh/kg based on $Zn + 1/2O_2 \rightarrow ZnO$). However, commercial development has been hampered by a number of fundamental problems.

All attempts to build a sample device by coupling a zinc electrode with a fuel cell oxygen electrode have resulted in cells with limited cycle life. To capitalize on the advantages of an air electrode, it is necessary to use thick zinc electrodes. This exacerbates the usual problems of the zinc electrode (dendrite formation, shape change, and densification). So far, no satisfactory long-lived, high-performance rechargeable air electrode has been developed. Other problems are carbonation of the electrolyte, water management, and thermal management.

Simple solutions such as the concept of mechanically replacing the zinc anodes on each cycle[90] and the use of ancillary charging electrodes[91,92] have not gained acceptance because of cost and reliability considerations.

The problems of water management and thermal management become apparent when one considers the thermodynamics and kinetics of the system. The theoretical open-circuit voltage at 25°C is 1.65 V and the thermoneutral voltage is 1.84 V. Because of the kinetic limitations of the air electrode, the cell-operating voltage on discharge is ~0.9 V. When charging with either direct use of the air electrode or with an auxiliary third electrode, the cell voltage is in the range 2.0–2.5 V. On discharge, a watt of heat is generated for every watt of electricity. This leads to water evaporation. Unlike hydrogen–oxygen fuel cells there is no water-generating reaction to compensate for this water loss.

Several schemes have been tried to overcome the problems of the zinc electrode. One method has been the use of rotating current collectors,[93] or rotating wipers[94] to produce compact adherent zinc deposits. Another method is the use of circulating electrolytes to modify the zinc morphology.[95] A major problem with all these methods is that the zinc morphology tends to change with cycling.[12,96] This problem has not been solved and as a result, these approaches have been abandoned.[12,96] In more recent approaches the idea of redepositing the zinc in the cell stack has been abandoned and, instead, the zinc powder is generated externally and the battery is operated in the fuel cell mode, with the zinc being fed as a slurry to the battery.[97–99] In one of these systems, the cells are in the form of tubes of constant cross section. The tube walls embody the air electrode, the separator, and the zinc current collector. The zinc "fuel" is fed through the tubes as a slurry in 12 *M* KOH with a silicate additive to stabilize the discharge products in solution.[100] The zinc can either be recharged externally or internally. A scheme for recharging the zinc in a separate set of tubular cells has recently been described.[100] A schematic view of the integrated generator charger unit is given in Figure 7. The fuel cell part of

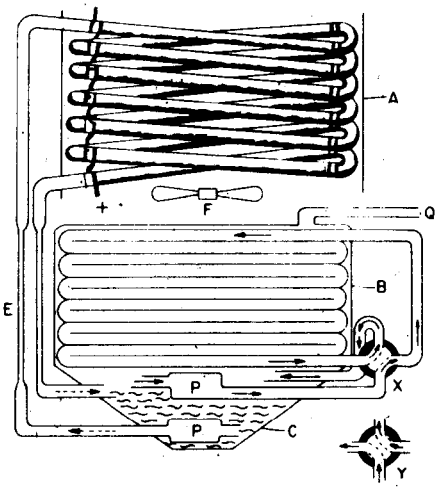

Figure 7. Schematic view of an integrated Zn–Air battery and charger system using slurry-type zinc electrodes.[100] A, Primary generator unit; B, reservoir with charge tubes; C, sump for zincate storage; E, electrolytic resistances (for minimizing leakage currents); F, fan; P, pumps; Q, suction pump; X, valve; inset Y indicates valve position during charge.

this unit has demonstrated the equivalent of 600 refueling cycles (1800 hr) in the laboratory before performance is affected by air electrode degradation. Specific energies of 110 Wh/kg have been obtained at the 3-hr discharge rate.[101] Even though the technical feasibility of the system has been demonstrated, the future of the system appears in doubt. The energy efficiency is inherently low (~40%) because of the irreversibility of the air electrode. The present emphasis on the efficiency of electrical systems and conservation of energy militate against the system.

2.6. The Iron–Air Battery

The iron–air cell couples the iron electrode of the Edison cell with an air electrode; the electrolyte is KOH. The iron–air battery is an attractive candidate for vehicle propulsion because of its high specific energy and low materials cost. Recent work includes improvements in the iron electrode,[102–104] the development of bifunctional air electrodes,[103,105] battery systems, and work on water management[24] and thermal management.[103]

The problems of the iron electrode are hydrogen evolution during charge, self-discharge on stand, passivation at high discharge rates and low temperatures, and stability of the discharge products at elevated temperatures and high carbonate concentrations in the electrolyte.

During discharge of the iron electrode, iron is first oxidized to $Fe(OH)_2$; at more positive potentials $Fe(OH)_2$ is oxidized to hydrated FeOOH.[106] In a battery, the first two-electron transfer is the only one of practical importance. The discharge products are voluminous and tend to cause pore plugging.

Considerable improvement in iron utilization can be achieved by increasing the electrode porosity and reducing electrode thickness.[103,104] Present practice is to fabricate sintered electrodes with 65% porosity as opposed to a porosity of 50% that was formerly used in iron–nickel oxide cells. This results in a 50% improvement in iron utilization at the 4-hr rate of discharge. Lithium hydroxide additions to the electrolyte considerably improve iron utilization. It is also important to exclude impurities such as aluminum and silicon.[103]

Hydrogen evolution decreases the charge efficiency of the iron electrode by as much as 20–50%. Charging efficiency can be improved by increasing electrode porosity, substituting copper for nickel current collectors, and by circulating the electrolyte so as to keep the battery temperature from rising during charge.[24,103]

Self-discharge occurs by a corrosion reaction involving hydrogen evolution. The addition of small amounts of sulfur compounds reduces the rate of self-discharge.[104]

Dissolution of the discharge products results in the formation of ferrites ($HFeO_2^-$) which can migrate to the air electrode, form $Fe(OH)_3$, and reduce the cell performance and life.[104] The problem is eliminated if CO_2 is scrubbed from the incoming air and the cell temperature is maintained below 60°C.

Several bifunctional air electrodes have been developed.[8,103,105] One approach has been to construct an electrode on which oxygen evolution occurs on a hydrophilic layer, in abuttal with the electrolyte, during charge and oxygen reduction occurs in a hydrophobic layer, in abuttal with the air plenum, during discharge.[105] Cycle lives of more than 1000 cycles have been reported for dual-layer nickel electrodes of this type.[103]

One approach to water management has been to fill the air plenum with water during charge. This water is separated from the cell electrolyte by the gas-filled hydrophobic layer of the air electrode. Water vapor will diffuse into the cell electrolyte because of the vapor pressure gradient between the water and the cell electrolyte. This ensures an even addition of water throughout the cell.[24] Another approach has been to circulate the electrolyte and make the water additions in the circulation loop. Electrolyte circulation has the additional advantage of simplifying thermal management.[103]

Figure 8 gives a plot of specific energy versus specific power for a 100-V battery and two projections for a battery based on cell data. Self-discharge rates at 25°C are about 1% per day.[24] The major drawback of the system is that the charge–discharge energy efficiency is very low (~35%), whereas most competing systems have energy efficiencies in the range of 80%.

2.7. The Hydrogen–Nickel Oxide Battery

The hydrogen–nickel oxide battery has undergone rapid development since the early seventies when early work on the system was reported.[107–109]

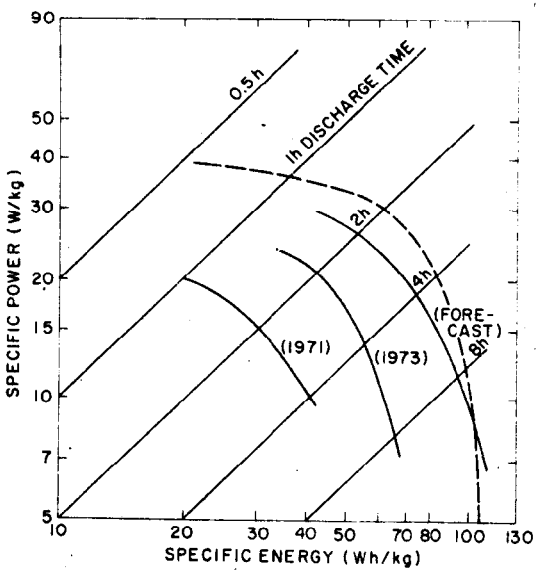

Figure 8. Specific power vs. specific energy for a Fe–air battery. Two curves are actual data obtained by Lindstrom in 1971 and 1973. The other solid line[103] and the broken line[24] are projected values based on cell data.

The system combines the positive electrode of the cadmium–nickel oxide battery with a hydrogen fuel cell electrode. The electrolyte is KOH.

The electrochemistry of the hydrogen–nickel oxide battery is rather interesting. The reaction at the nickel oxide electrode is

$$Ni(OH)_2 + OH^- \underset{\text{discharge}}{\overset{\text{charge}}{\rightleftharpoons}} NiOOH + H_2O + e$$

and at the hydrogen electrode

$$H_2O + e \underset{\text{discharge}}{\overset{\text{charge}}{\rightleftharpoons}} \tfrac{1}{2}H_2 + OH^-$$

The overall cell reaction is

$$N_2(OH)_2 \underset{\text{discharge}}{\overset{\text{charge}}{\rightleftharpoons}} NiOOH + \tfrac{1}{2}H_2$$

During cell overcharge, oxygen is evolved on the nickel oxide electrode:

$$4OH \rightarrow 2H_2O + O_2 + 4e$$

This oxygen is chemically and electrochemically reduced at the hydrogen electrode:

$$2H_2O + O_2 + 4e \rightarrow 4OH$$

$$\tfrac{1}{2}O_2 + H_2 \rightarrow H_2O$$

If the cell is reversed in the presence of excess hydrogen, then hydrogen will be evolved on the nickel oxide electrode and hydrogen oxidation will occur on the hydrogen electrode. The result is no net generation of hydrogen. No provisions have to be made to prevent hydrogen access to the nickel oxide electrode. The reaction between hydrogen and nickel oxide is extremely slow, probably because of the absence of dissociative adsorption on the oxide covered surface.

The open-circuit voltage for the hydrogen–nickel oxide cell is 1.36 V and the thermal–neutral voltage is 1.51 V. The average charging voltage at the 10-hr charge rate is 1.46 V and the average discharge voltage at the 1-hr discharge rate is 1.27 V.[109]

Typical cell construction for a hydrogen–nickel oxide cell is shown in Figure 9. Energy density and volume for this construction are dependent on whether the system is optimized for maximum energy or minimum volume. This dependence of specific energy on cell volume on the maximum operating cell pressure is shown in Figure 10. Another variant on this type of construction is to connect cells in series and enclose the battery in a common hydrogen container and have the battery hydrogen limited on discharge.[110] Several attempts have been made to reduce the operating pressure of the cell. One approach has been the use of reversible Ti_2NiH_x electrodes.[111] Another approach has been the chemical storage of hydrogen, external to the cell stack, as $LaNi_5H_x$.[112] The latter approach permits cell operation at pressure less than 600 kPa, reduces cell volume by 50%, and permits the construction of pris-

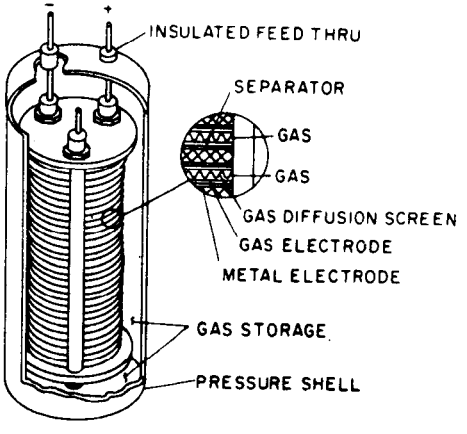

Figure 9. A schematic of a H_2–NiOOH cell with a cutaway of the pressure vessel. The inset shows the electrodes, the separator, and the hydrogen gas flow field.

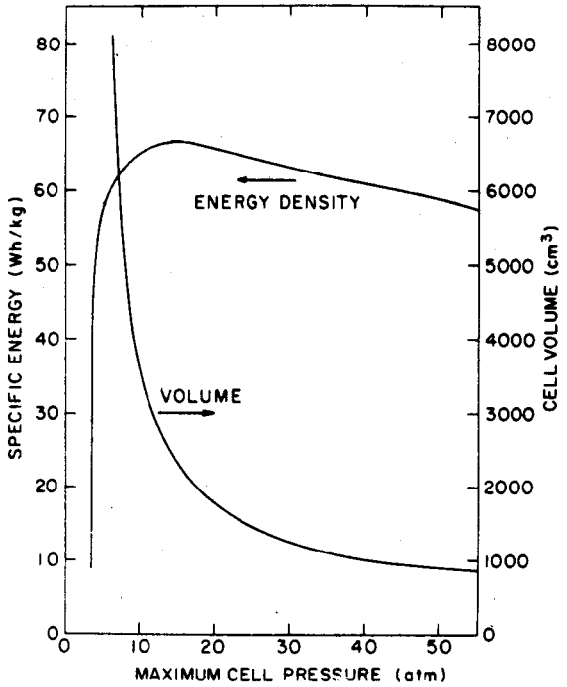

Figure 10. The dependence of the specific energy and cell volume of a H_2–NiOOH cell on the maximum operating pressure. Minimum pressure is assumed to be 3.4 atm or 20% of maximum pressure, whichever is higher. Calculations are for a 66 Wh cell 8.9 cm in diameter.

matic cells. Noble metal catalysts are used for the hydrogen electrode. This has limited system use to aerospace applications.

One salient feature of the hydrogen–nickel oxide system is its excellent durability. In excess of 1500 deep cycles have been demonstrated with substantially no change in performance.[113] A signal advantage of the system is its resistance to high rates of overcharge and cell reversal. The self-discharge rate is about 10% per day at 20°C.[114,115]

If catalyst cost could be reduced, this system would probably find wider applications. A concept for using hydrogen–nickel oxide cells for vehicle propulsion, in which the hydrogen is stored in high-strength tubes, has been proposed.[13]

2.8. The Hydrogen–Silver Oxide Battery

Development of the hydrogen–silver oxide battery has been concurrent with the hydrogen–nickel oxide development. The system combines the silver

oxide electrode of the zinc–silver oxide system with a hydrogen fuel cell electrode; the electrolyte is KOH. Cell operation is rather similar to that of the hydrogen–nickel oxide cell. The overall reaction is

$$Ag + H_2O \underset{\text{discharge}}{\overset{\text{charge}}{\rightleftharpoons}} AgO + H_2$$

Unlike the hydrogen–nickel oxide cell, water is generated on discharge. This causes a volume change in the electrolyte. The silver oxide electrodes and separators must have sufficient porosity to prevent expulsion of electrolyte from the cell stack during discharge.[115] The electrolyte concentration is typically 25 wt % KOH at the end of discharge and 35 wt % at the end of charge.

Cell construction is rather similar to that used in the hydrogen–nickel oxide battery. Identical hydrogen electrodes are used. The separator system is modified to accommodate the water generated on discharge and to prevent migration of soluble silver species to the hydrogen electrode.

Cells with specific energies of 75 Wh/kg have been constructed.[115] Cycle lives of 600 cycles have been achieved.[116] Cycle life is limited by silver migration through the separator; with better separator materials, even longer cycle life may be possible. The self-discharge rate at room temperatures is about 5% per day.[115]

2.9. The Hydrogen–Oxygen Battery

Work has been carried out on rechargeable hydrogen–oxygen batteries since the early sixties. Two general concepts have been tried. One is to use the same cells for electrolysis and discharge.[15,117,118] The other is to have separate cell stacks for both operations.[153] More recently, the system has been considered for utility load leveling.[119] The concept is to use a separate electrolyzer and fuel cell and have provisions for storing hydrogen and oxygen.

Two types of electrolyzers have been considered. One type uses an ion exchange membrane. The electrode materials are pressed on to each side of the membrane. During electrolysis, the electrodes are wetted with high-purity distilled water. Platinum black is used for the cathode, and the anode has a proprietary catalyst. Several types of ion exchange membranes have been used. More recent designs use perfluorinated sulfonic acid membranes.[120] Electrolyzers with alkaline electrolytes have also been developed. These electrolyzers use either nickel- or noble-metal-catalyzed electrodes and asbestos membranes.[15,121] More recently, the use of semiconducting oxides as oxygen electrodes, in electrolyzers of this type, has been reported.[122] A survey of various oxides suggested that $NiCO_2O_4$ is a promising material for oxygen electrodes. Electrolyzer currents of 1.6 A/cm^2 have been obtained.[123] System analysis indicates that the practical design point is in the range 0.15–0.35 A/cm^2.[124] At these current densities, both alkaline and ion exchange

membrane electrolyzers operate at voltages less than 1.7 V at operating temperatures in the range 40–80°C.[124,125] At present, there is no shortage of ideas for improving the efficiency of electrolyzers. Several methods such as the use of chemical, thermal, and photochemical assists have been proposed for improving electrolyzers.[126]

There has been considerable improvement in the lifetimes of electrolyzers and fuel cells. With present technology, electrolyzer and fuel cell stack lifetimes of greater than 20,000 hr can be expected. Electrolyzer efficiencies as high as 85% at 0.5 A/cm^2 have been reported.[127] Hydrogen–oxygen fuel cells have efficiencies in the vicinity of 60%. This yields an overall efficiency of 51%.

2.10. The Hydrogen–Halogen Battery

Both hydrogen–chlorine and hydrogen–bromine batteries have been considered recently for utility load-leveling applications.[128] The history of the hydrogen–chlorine cell dates back to the early twenties.[129,130] An investigation of the hydrogen–bromine battery was carried out in the early sixties.[131]

Table 7 lists the general characteristics of both hydrogen–chlorine and hydrogen–bromine cells. Both systems have high electric-to-electric efficiency. Present-day cells are based on the use of perfluorinated sulfonic acid membranes.[128] These are ideal for use in cells with gaseous reactants since large pressure differentials (up to 300 MPa) can be tolerated across the membrane. A schematic of a hydrogen–chlorine cell is shown in Figure 11. Provisions have to be made for reactant storage. Hydrogen can be stored either as a metal hydride (e.g., $FeTiH_x$) or as a compressed gas.

Until now, very little work has been done on hydrogen–halogen systems. Their high charge–discharge energy efficiencies and the fact that they can be independently sized for energy and power make them attractive for utility load-leveling applications.

2.11. The Redox Battery

A number of redox batteries have been considered for utility load-leveling applications. In these batteries, both reactants and products are completely

Table 7
Characteristics of Hydrogen–Chlorine and Hydrogen–Bromine Cells

Cell characteristic	H_2–Cl_2	H_2–Br_2
Open-circuit voltage	1.36 V	1.07 V
Thermoneutral voltage	1.74 V	1.26 V
Approximate charging voltage at 0.3 A/cm^2	1.51 V	1.22 V
Approximate discharge voltage at 0.3 A/cm^2	1.21 V	0.92 V
Approximate energy efficiency	80%	75%

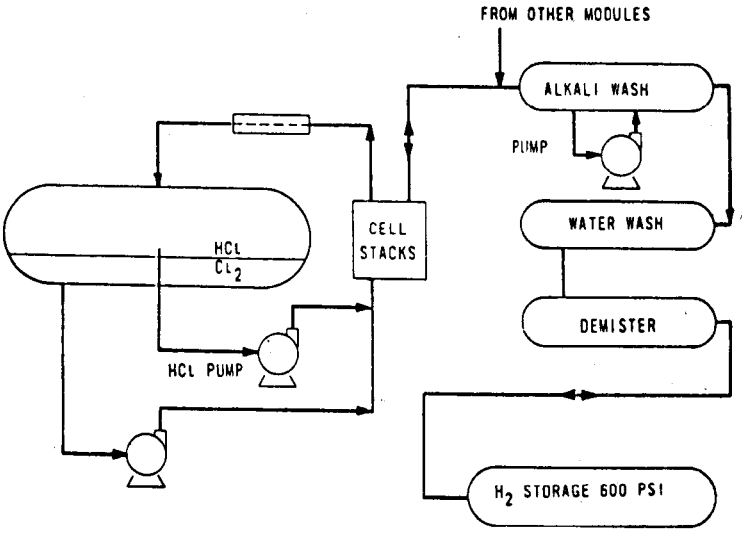

Figure 11. A schematic of a H_2–Cl_2 electrochemically regenerative energy storage system.

soluble in the electrolyte and are stored in tanks outside the cell. The requirements for these systems are as follows:

(1) The reactants and products should be sufficiently soluble in the electrolyte.
(2) The reversible potentials and kinetics of both electrodes should be such that no side reactions should occur charging and a sufficiently high voltage be maintained during discharge.
(3) The overall cell reaction should not cause large pH changes in the electrolyte.

Table 8 gives a listing of redox reactions that have been considered for redox batteries.[132] Since the electrode reactions are heterogenous phase reactions, the reversible potential changes with depth of discharge. An example is shown in Figure 12. Some of the reactions have low exchange currents. These can be improved by use of electrocatalysts. For instance, the Ti^{3+}/Fe^{2+} couple yields only 1.2 mA/cm^2 at a cell voltage of 0.52 V when graphite is used as the current collector[133]; however, when the anode current collector is platinized, currents of 50 mA/cm^2 can be achieved.[17]

Figure 13 shows a schematic drawing of a redox energy storage system.[132] An essential part of the system is an ion exchange membrane that is impermeable to the redox reactants and products. Cross-diffusion of these ions

Table 8
Exchange Currents and Reversible Potentials for Redox Reactions

Electrode reaction	Exchange current, A/cm^2	Reversible potential, V with respect to S.C.E.
$Cu(NH_3)_2^{+}$–$Cu(NH_3)_4$	2×10^{-2}	−0.3
Ti^{3+}–TiO^{2+} (6 *M* HCl)	10^{-3}	−0.1
Cr^{3+}–Cr^{3+} (1 *M* HCl)	10^{-4} to $>3 \times 10^{-3}$	−0.4
Sn^{2+}–Sn^{4+} (3.5 *M* HCl)	10^{-5} to $>3 \times 10^{-3}$	−0.1
Br^{-}–Br_3^{-} (NaBr)	3×10^{-3}	+0.8
Fe^{+2}–Fe^{+3} (1 *M* HCl)	10^{-2}	+0.5
Sb^{+3}–Sb^{+5} (3 *M* HCl)	10^{-4}	+0.6

represents a permanent loss of system capacity. Either a hydrogen ion transfer membrane or an anion transfer membrane can be used. When hydrogen ion transfer membranes are used, large changes in pH can occur on either side of the membrane. This could result in difficulties with solution stabilization. If chloride ion transport membranes are used, the pH remains constant and the chloride ion concentration changes on each side of the membrane. Anion membranes are more attractive since it is most likely they would have a better selectivity for preventing cross-diffusion of redox ions.

Inherently, redox systems should not present any materials or cycle life problems. Until now, development has been hampered by the lack of a sufficiently selective low resistivity anion exchange membrane. One drawback to these systems is their bulk. For instance, the Ti^{3+}/Fe^{2+} couple with solutions in the range 1–3 *M* yields specific energies in the range 7–20 Wh/kg and energy densities in the range 10–30 Wh/l.

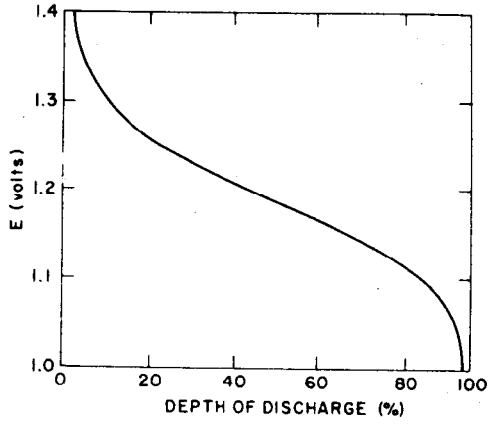

Figure 12. Open-circuit voltage vs. depth of discharge for a Cr^{2+}–Fe^{3+} redox system.

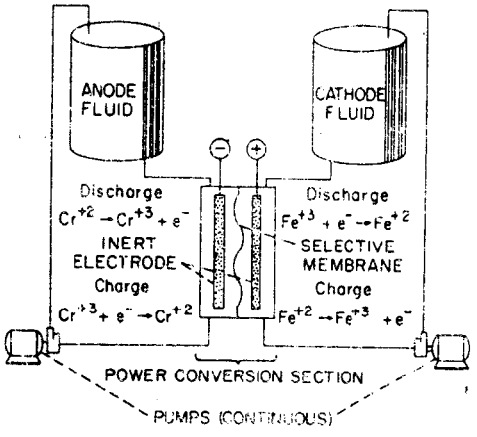

Figure 13. A schematic of a Cr^{2+}–Fe^{3+} redox system.

2.12. The Lithium–Organic Electrolyte Battery

Work on organic electrolyte–lithium batteries has progressed since the early sixties. This work has been extensively reviewed.[18,134–137] These batteries are based on the concept of using a lithium negative electrode, an organic electrolyte such as propylene carbonate with a positive electrode. Several positive electrode active materials such as bromine, metal fluorides, metal chlorides, sulfur dioxide, sulfonyl chloride, metal oxides, and carbon fluorides have been used. There has been rapid development of commercial lithium organic electrolyte primary batteries of high specific energy.

In the past, a number of problems have delayed the development of rechargeable systems. Cycling of metal fluorides is inhibited by the very low solubility ($\sim 10^{-5}$ M) of lithium fluoride in organic solvents. In the case of metal chlorides, many of them form complexes with excess halide and result in self-discharge of the cell. Some degree of success has been achieved with lithium–bromine cells with ultrafine porous polyethylene separators.[138] Cycle lives of 1000 cycles have been reported. However, diffusion and electromigration of bromides to the lithium electrode may present problems.

In recent years, the discovery that certain transition metal chalcogenides are electrochemically active in organic electrolytes with lithium salts[139] has led to a flurry of activity on rechargeable lithium organic electrolyte batteries. Most of the published work has dealt with TiS_2, TiS_3, and $NbSe_3$. The overall reaction for these electrode materials has recently been elucidated.[140,141] These materials undergo topochemical reactions with lithium during discharge in nonaqeuous cells to form compounds of the type Li_3MX_3. These compounds have a layered structure, and on discharge lithium moves into the lattice and the material expands. This movement of lithium in and out of the lattice is analogous to the proton movement in nickel oxide and γ-MnO_2 electrodes.

The reversibility of $NbSe_2$ and TiS_2 electrodes has been demonstrated. However, TiS_3 electrodes apparently undergo some irreversibility on cycling.[141] Cycle lives of 1000 deep cycles have been demonstrated for $NbSe_3$ electrodes at charge and discharge current densities of 1 mA/cm^2.[139] Lithium–titanium disulfide cells have been cycled at greater than 60% utilization for 250 cycles on a cycling regimen consisting of a charge of 2.5 mA/cm^2 followed by a deep discharge at 10 mA/cm^2.[142] These and other results[143,144] would indicate that the positive electrode is no longer the life-limiting factor in rechargeable lithium electrolyte batteries.

Other problems with organic electrolyte batteries are associated with the electrolyte and the lithium electrode. Propylene carbonate tends to decompose on cycling to yield propene and carbonate.[145] The reaction occurs on the positive electrode. In the case of electrodes with graphite conductive dilutents, the reaction mechanism involves alkali metal intercalation in the graphite. On other materials such as metals, the reaction occurs via direct electrochemical reduction.[146] The carbonate reacts to form lithium carbonate. This can isolate the lithium-active material and reduce the utilization of the lithium electrode. In propylene carbonate electrolytes, lithium tends to form dendritic nonadherent deposits with cycling.[147] Work is being carried out to solve these problems. One approach is to find a solvent-additive combination to circumvent the problem.[148,149] Another is to use a lithium–aluminum alloy in combination with a solvent.[150] For the first time since work started on lithium organic electrolyte batteries, the prospects for developing a rechargeable system look promising.

References

1. E. J. Wade, *Secondary Batteries*, Electrician Printing and Publishing Co., London (1902).
2. G. W. Vinal, *Storage Batteries*, John Wiley and Sons, New York (1924).
3. S. V. Falk and A. J. Salkind, *Alkaline Storage Batteries*, John Wiley and Sons, New York (1969).
4. J. McBreen and E. J. Cairns, *Ind. Res.* **17**(6), 57 (1975).
5. S. Gross, *Energy Convers.* **15**, 81 (1976).
6. J. R. Birk and F. R. Kalhammer, in Proceedings of the Symposium and Workshop on Advanced Battery Research and Design, Argonne National Laboratory, Argonne, Illinois, March 22–24, 1976, p. A-2.
7. J. Newman and W. Tiedeman, *AIChE J.* **21**, 25 (1975).
8. E. S. Buzzelli, in *Extended Abstracts*, Vol. 75-2, Electrochemical Society, Princeton, New Jersey (1975), Abstract No. 46, p. 115.
9. M-C. Yew and D. E. McCulloch, in Proceedings of the 11th IECEC Conference, 1976, paper No. 769060, pp. 363–368.
10. K. V. Kordesch, *Batteries*, Marcel Dekker, New York (1974), pp. 281–290.
11. J. McBreen, in *Power Sources 5*, D. H. Collins, ed., Academic Press, London (1975), pp. 525–538.
12. D. S. Adams, in *Power Sources 4*, D. H. Collins, ed., Oriel Press, Newcastle-Upon-Tyne (1973), pp. 347–360.

13. A. J. Appleby, in *Electrochemistry*, H. Bloom and F. Gutman, eds., Plenum Press, New York (1977), pp. 373–392.
14. F. Betz, J. Stockel, and A. Gaudet, in Proceedings of the 11th IECEC Conference, 1976, paper No. 769087, pp. 510–516.
15. E. Findl and M. Klein, in Proceedings of the 20th Annual Power Sources Conference, Atlantic City, New Jersey, 1966, pp. 49–52.
16. J. J. Reilly and R. H. Wiswall, *Inorg. Chem.* **13**, 218 (1974).
17. W. Vielstich, *Fuel Cells*, Wiley Interscience, New York (1965), p. 403.
18. G. Eichinger and J. O. Besenhard, *J. Electroanal. Chem.* **72**, 1 (1976).
19. J. T. Kummer and N. Weber, *SAE Trans.* paper No. 670179 (1967).
20. C. A. Levine, in Proceedings of the 10th IECEC Conference, 1975, paper No. 759095, pp. 621–626.
21. E. J. Cairns and J. S. Dunning, in Proceedings of the Symposium and Workshop on Advanced Battery Research and Design, Argonne National Laboratory, Argonne, Illinois, March 22–24, 1976, p. A-81.
22. J. Werth, J. Klein, and R. Wylie, in *Proceedings of the Symposium on Energy Storage*, 1975, J. B. Benkowitz and H. P. Silverman, eds., Electrochemical Society, Princeton, New Jersey (1975), pp. 198–205.
23. R. W. Easter, in Proceedings of the 9th IECEC Conference, 1974, paper No. 749126, pp. 888–895.
24. H. Cnobloch, D. Groppel, D. Kuhl, W. Nippe, and G. Siemsen, in *Power Sources 5*, D. H. Collins, ed., Academic Press, London (1975), pp. 261–282.
25. F. G. Will, in *Power Sources 4*, D. H. Collins, ed., Pergamon Press, Oxford (1970), pp. 149–165.
26. J. McBreen, *J. Electrochem. Soc.* **119**, 1620 (1972).
27. A. C. Simon and S. M. Caulder, in *Power Sources 5*, D. H. Collins, ed., Academic Press, London (1975), pp. 109–122.
28. M. Sulkes, in Proceedings of the 23rd Annual Power Sources Conference, Atlantic City, New Jersey, 1969, pp. 112–115.
29. W. S. Bishop, D. L. Call, J. K. Wilson, and R. A. Brown, in Proceedings of the 27th Power Sources Symposium, Atlantic City, New Jersey, 1976, pp. 97–99.
30. J. O'M. Bockris, Z. Nagy, and D. Drazic, *J. Electrochem. Soc.* **120**, 30 (1973).
31. J. McBreen and G. A. Dalin, in *Extended Abstracts*, Vol. 12, Electrochemical Society, New York (1967), abstract No. 36, p. 91.
32. T. Michalowski, Russian Patent, Group XI, No. SUD (April 28, 1901).
33. V. V. Romanov, *Zh. Priklad. Khim.* **35**, 1293 (1962).
34. D. P. Boden and E. Pearlman, in *Power Sources 4*, D. H. Collins, ed., Oriel Press, Newcastle-Upon-Tyne (1973), pp. 103–113.
35. H. Bode, K. Dehemelt, and H. Van Dohren, in Proceedings of the International Symposium on Batteries, Christchurch Hants., 1958, England, paper yy.
36. D. R. Turner, *Electrochem. Technol.* **2**, 313 (1964).
37. W. N. Carson, *Zinc–Silver Oxide Batteries*, A. Fleischer and J. J. Lander, eds., John Wiley and Sons, New York (1971), pp. 445–454.
38. A. Charkey, in *Power Sources 4*, D. H. Collins, ed., Oriel Press, Newcastle-Upon-Tyne (1973), pp. 103–113.
39. J. McBreen, in *Extended Abstracts*, Vol. 77-1, Electrochemical Society, Princeton, New Jersey, abstract No. 356, p. 909.
40. M. H. Gottlieb and T. H. Willis, *Electrochem. Technol.* **4**, 515 (1966).
41. V. D'Agostino, J. Lee, and G. Organ, in *Zinc–Silver Oxide Batteries*, A. Fleischer and J. J. Lander, eds., John Wiley and Sons, New York (1971), pp. 271–281.
42. A. Charkey, in Proceedings of the 11th IECEC Conference, paper No. 769076, pp. 452–456.

43. D. W. Shiebley, in *Extended Abstracts*, Vol. 76-2, Electrochemical Society, Princeton, New Jersey, Vol. 76-2, abstract No. 25, p. 64.
44. F. C. Arrance and A. G. Rosa, U.S. Patent 3,625,770 (December 7, 1971).
45. J. M. Fay and J. J. Drumm, *Railw. Eng.* **54**, 258, 280 (1933).
46. G. Benczur-Urmossy, K. Von Benda, and F. Hascka, in *Power Sources 5*, D. H. Collins, ed., Academic Press, London (1975), pp. 303–314.
47. O. von Krusenstierna, in Tenth International Power Sources Symposium, Brighton, England, 1975, paper No. 21.
48. L. R. McCoy, in Proceedings of the 10th IECEC Conference, paper No. 759169, 1975, pp. 1131–1133.
49. G. Krucera, H. Q. Plust, and C. Schneider, *SAE Trans.* paper No. 750147 (1975).
50. J. McBreen, U.S. Patent 4,000,005 (December 28, 1976).
51. B. Cupp, in Proceedings of the 13th Annual Power Sources Conference, Atlantic City, New Jersey, 1959, p. 75.
52. J. L. Weininger and J. G. Ruzzo, First Interim Technical Report, Contract No. F-33615-69-C-1312, Project No. 3145, General Electric Co., Schnectady, New York, 1969.
53. K. V. Kordesch and A. Kozawa, in Extended Abstracts of ISE Meeting, Brighton, England, 1974, p. 257.
54. D. Boden, C. J. Venuto, D. Wisler, and R. B. Wylie, *J. Electrochem. Soc.* **115**, 333 (1968).
55. W. S. Herbert, *J. Electrochem. Soc.* **99**, 190C (1952).
56. N. C. Cahoon and M. P. Kover, *J. Electrochem. Soc.* **106**, 745 (1959).
57. A. F. Daniel, J. J. Murphy, and J. M. Havendon, *Batteries*, D. H. Collins, ed., Macmillan, London (1963), pp. 157–169.
58. G. S. Bell and R. Huber, *J. Electrochem. Soc.* **111**, 1 (1964).
59. G. S. Bell and R. Huber, *Electrochim. Acta* **10**, 509 (1965).
60. A. Kozawa and J. F. Yeager, *J. Electrochem. Soc.* **112**, 959 (1965).
61. A. Kozawa and R. A. Powers, *J. Electrochem. Soc.* **113**, 870 (1966).
62. D. Boden, C. J. Venuto, D. Wisler, and R. B. Wylie, *J. Electrochem. Soc.* **114**, 415 (1967).
63. P. Ruetschi, R. Grovanoli, and P. Burki, in *Manganese Dioxide Symposium, Vol. 1, Cleveland*, A. Kozawa and R. J. Brodd, eds., I.C. Sample Office, Cleveland, pp. 12–30 (1975).
64. K. Micka, *Metalloberflaeche* **27**, 208 (1973).
65. H. Y. Kang and C. C. Liang, *J. Electrochem. Soc.* **115**, 6 (1968).
66. J. Ambrose and G W. D. Briggs, *Electrochim. Acta* **16**, 111 (1971).
67. J. McBreen, *Electrochim. Acta* **20**, 221 (1975).
68. J. McBreen, in *Manganese Dioxide Symposium, Vol. 1. Cleveland*, A. Kozawa and R. J. Brodd, eds., I.C. Sample Office, Cleveland, pp. 97–110 (1975).
69. K. Miyazaki, *J. Electroanal. Chem.* **21**, 414 (1969).
70. K. Miyazaki, in *Power Sources 3*, D. H. Collins, ed., Oriel Press, Newcastle-Upon-Tyne (1971), pp. 607–624.
71. P. C. Symons, *SAE Trans.* paper No. 730253 (1973).
72. P. C. Symons, paper presented at International Conference on Electrolytes for Power Sources, Society for Electrochemistry, Brighton, England, December 13–14, 1973.
73. P. C. Symons, presentation at 1st Annual ERDA Battery Contractors Coordination Meeting, Germantown, Maryland, January 27–28, 1977.
74. P. C. Symons, paper presented at Electric Vehicle Symposium, Washington, D.C., February 19–21, 1974.
75. A. F. Sammels, in *Proceedings of the Symposium on Energy Storage*, J. B. Berkowitze and H. P. Silverman, eds., Electrochemical Society, Princeton, New Jersey, pp. 121–129.
76. C. S. Bradley, U.S. Patent 312,802 (1885).
77. C. S. Bradley, U.S. Patent 409,448 (1889).
78. M. R. Bloch, U.S. Patent 2,566,114 (August 28, 1951).

79. S. Barnartt and D. A. Forejt, *J. Electrochem. Soc.* **111**, 1201 (1964).
80. R. Zito, U.S. Patent 3,285,781 (November 15, 1966).
81. R. Zito and D. L. Maricle, paper presented at Electric Vehicle Symposium, Atlantic City, New Jersey, 1971.
82. R. Zito, U.S. Patent 3,640,770 (February 8, 1972).
83. D. R. Riffe, U.S. Patent 3,328,202 (June 27, 1967).
84. R. D. Blue and J. J. Leddy, U.S. Patent 3,408,232 (October 29, 1968).
85. M. A. Walsh, U.S. Patent 3,816,177 (1974).
86. M. Walsh, B. Walsh, and D. Crouse, in Proceedings of the 10th IECEC Conference, 1975, paper No. 759171, pp. 1141–1142.
87. G. Clerici, M. deRossi, and M. Marchetto, in *Power Sources 5*, D. H. Collins, ed., Academic Press, London (1975), pp. 167–181.
88. J. E. Oxley, R. A. Putt, M. J. Montgomery, A. F. Sammels, and F. M. Walsh, in *Extended Abstracts*, Vol. 75-2, Electrochemical Society, Princeton, New Jersey (1976), abstract No. 63, p. 166.
89. F. G. Will, presentation 1st Annual ERDA Battery Contractors Coordination Committee, Germantown, Maryland, January 27–28, 1977.
90. R. R. Witherspoon, *SAE Trans.* paper No. 690204 (1969).
91. R. Salcedo-Gumucio, U.S. Patent 3,219,486 (November 23, 1965).
92. J. J. Postula and R. Thacker, *Energy Convers.* **10**, 45 (1969).
93. Z. Stachurski, J. O'M. Bockris, and G. A. Dalin, U.S. Patent 3,560,261 (February 2, 1971).
94. H. J. Hale, U.S. Patent 3,822,149 (July 2, 1974).
95. G. Caprioglio and A. Weinberg, in Proceedings of the 6th IECEC Conference, 1971, paper No. 719020, pp. 140–146.
96. R. Thacker, *Energy Convers.* **12**, 17 (1972).
97. H. Baba, *SAE Trans.* paper No. 710237 (1971).
98. A. J. Appleby, J. P. Pompon, and M. Jacquier, in Third International Electric Vehicle Symposium, Washington, D.C., 1974.
99. A. J. Appleby, J. P. Pompon, and M. Jacquier, in Proceedings of the 10th IECEC Conference, 1975, paper No. 759121, pp. 811–816.
100. A. J. Appleby, J. Jacquelin, and J. P. Pompon, *SAE Trans.*, paper No. 770381 (1977).
101. A. J. Appleby and J. P. Gabano, in Proceedings of the Symposium and Workshop on Advanced Battery Research and Design, Argonne National Laboratory, Argonne, Illinois, March 22–24, 1976, p. A-49.
102. E. R. Bowermann, in Proceedings of the 22nd Annual Power Sources Conference, Atlantic City, New Jersey, 1968, pp. 70–72.
103. O. Lundstrom, in *Power Sources 5*, D. H. Collins, ed., Academic Press, London (1975), pp. 283–301.
104. P. R. Vassie and A. C. C. Tseung, *Electrochim. Acta* **21**, 299 (1966).
105. H. Cnobloch, G. Siemsen, and F. Von Sturm, in *Power Sources 4*, D. H. Collins, ed., Oriel Press, Newcastle-Upon-Tyne (1973), pp. 311–325.
106. L. Ojefors, *J. Electrochem. Soc.* **123**, 1691 (1976).
107. B. Tsenter, A. I. Kloss, and V. M. Sergeev, British Patent 1,314,481 (April 26, 1973).
108. M. Klein, in Proceedings of the 7th IECEC Conference, 1972, paper No. 72018, pp. 79–85.
109. J. F. Stockel, G. Van Ommering, L. Swette, and L. Gaines, in Proceedings of the 7th IECEC Conference, 1972, paper No. 72019, pp. 87–94.
110. L. E. Miller, in Proceedings of the 26th Power Sources Symposium, Atlantic City, New Jersey, 1974, pp. 21–24.
111. M. A. Gutjahr, H. Buchner, K. D. Beccu, and H. Saufferer, in *Power Sources 4*, D. H. Collins, ed., Oriel Press, Newcastle-Upon-Tyne (1973), pp. 79–91.
112. M. W. Earl and J. D. Dunlop, in Proceedings of the 26th Power Sources Symposium, 1974, Atlantic City, New Jersey, 1974, pp. 24–27.

113. M. Klein and M. George, in Proceedings of the 26th Power Sources Symposium, Atlantic City, New Jersey, 1974, pp. 18–20.
114. S. Font and J. Goulard, in *Power Sources 5*, D. H. Collins, ed., Academic Press, London (1975), pp. 331–346.
115. M. Klein, in *Power Sources 5*, D. H. Collins, ed., Academic Press, London (1975), pp. 347–359.
116. J. Dunlop, J. Stockel, and G. Van Ommering, in *Power Sources 5*, D. H. Collins, ed., Academic Press, London (1975), pp. 315–329.
117. J. S. Bone, in Proceedings of the 14th Annual Power Sources Conference, Atlantic City, New Jersey, 1960, pp. 62–64.
118. M. Klein, in Proceedings of the Symposium on Battery Separators, Columbus Section, Electrochemical Society, February 18–19, 1970, p. 337.
119. J. M. Burger, P. Lewis, R. J. Tolen, F. J. Selzano, and J. M. King, in Proceedings of the 9th IECEC Conference, 1974, paper No. 749034, pp. 428–441.
120. A. F. Fickett, in Proceedings of the Symposium on Battery Separators, Columbus Section, Electrochemical Society, February 18–19, 1970, p. 354.
121. W. Vielstich, *Chemie-Ing. Techn.* **33**, 75 (1961).
122. A. C. C. Tseung and S. Jasem, *Electrochim. Acta* **22**, 31 (1977).
123. R. L. Costa and P. G. Grimes, *Chem. Eng. Prog.* **63**, 56 (1967).
124. W. C. Kincaide and C. F. Williams, in Proceedings of the Cornell International Symposium and Workshop on the Hydrogen Economy, August 20–22, 1973, pp. 170–193.
125. L. J. Nuttall, A. P. Fickett, and W. A. Titterington, in *Hydrogen Energy Part A*, T. N. Vezeroglu, ed., Plenum Press, New York (1975), pp. 441–455.
126. J. O'M. Bockris, in *Hydrogen Energy Part A*, T. N. Vezeroglu, ed., Plenum Press, New York (1975), pp. 371–403.
127. W. A. Titterington and J. F. Austin, in *Extended Abstracts*, Vol. 74-2, Electrochemical Society, Princeton, New Jersey (1974), abstract No. 233, p. 576.
128. S. Srinivasan, R. S. Yeo, and A. Beaufrere, presentation 1st Annual ERDA Battery Contractors, Coordination Committee, Germantown, Maryland, January 27–28, 1977.
129. F. Foerster, *Z. Elektrochem.* **29**, 64 (1923).
130. S. Yoshizawa, F. Hine, Z. Takehara, and Y. Kanaya, *J. Electrochem. Soc. (Japan)* **30**, E10 (1962).
131. W. Glass, Hydrogen–bromine fuel cell, Report on Contract No. AF 19(604)-8508, Project No. 6694, Task No. 669407, Ionics Inc., Cambridge, Massachusetts, 1964.
132. L. Thaller, presentation at 1st Annual ERDA Battery Contractors Coordination Meeting, Germantown, Maryland, January 27–28, 1977.
133. W. Kangro, and H. Pieper, *Electrochim. Acta* **7**, 435 (1962).
134. K. H. M. Braeuer and J. A. Harvey, Status report on organic electrolyte high energy density batteries, U.S. Government, No. AD-654813, 1967.
135. R. Jaminski, *Electrochem. Technol.* **6**, 28 (1968).
136. F. Conti and G. Pistoia, *J. Appl. Chem. Biotechnol.* **21**, 77 (1971).
137. T. O. Besenhard and G. Eichinger, *J. Electroanal. Chem.* **68**, 1 (1976).
138. J. L. Weininger and F. W. Secor, *J. Electrochem. Soc.* **121**, 315 (1974).
139. J. Broadhead, in *Power Sources 4*, D. H. Collins, ed., Oriel Press, Newcastle-Upon-Tyne (1973), pp. 469–482.
140. M. S. Whittingham, *J. Electrochem. Soc.* **123**, 315 (1976).
141. D. W. Murphy and F. A. Trumbore, *J. Electrochem. Soc.* **123**, 960 (1976).
142. L. H. Gaines, R. W. Francis, G. H. Newman, and B. M. L. Rao, in Proceedings of the 11th IECEC Conference, 1976, paper No. 769071, pp. 418–423.
143. G. L. Holleck, F. S. Shucker, and S. B. Brummer, in Proceedings of the 10th IECEC Conference, 1975, paper No. 759070, pp. 444–448.
144. G. L. Holleck, J. R. Driscoll, and F. S. Shucker, in Proceedings of the 27th Power Sources Symposium, Atlantic City, New Jersey 1976, pp. 80–82.

145. A. N. Dey and B. P. Sullivan, *J. Electrochem. Soc.* **117**, 222 (1970).
146. G. Eichinger, *J. Electroanal. Chem.* **74** 183 (1976).
147. R. Selim and P. Bro, *J. Electrochem. Soc* **121**, 1457 (1974).
148. R. D. Rauh and S. B. Brummer, *Electrochim. Acta* **22**, 75 (1977).
149. R. D. Rauh and S. B. Brummer, *Electrochim. Acta* **22**, 85 (1977).
150. B. M. L. Rao, R. W. Francis, and H. A. Christopher, in *Extended Abstracts*, Vol. 76-2, Electrochemical Society, Princeton, New Jersey (1976), abstract No. 68, p. 178.
151. J. E. Pearce, Letters Patent No. 356,261 (1887).
152. F. Rallo and P. Silvestroni, *J. Electrochem. Soc.* **119**, 1471 (1972).
153. W. H. Podolny, in Proceedings of the 14th Annual Power Sources Conference, Atlantic City, New Jersey, 1960, pp. 64–67.

11

Secondary Batteries—New Batteries: High Temperature

ELTON J. CAIRNS

1. Introduction

Since the mid-1960s there has been a growing research and development effort in the area of high-specific-energy, high-specific-power rechargeable batteries for use in electric vehicles, electric utility networks, and solar- and wind-powered electric generator systems. For a variety of reasons, including scientific, technological, and economic, high-temperature, nonaqueous systems have been found to be the most attractive candidates for the above relatively large-scale applications. Only the high-temperature cells offer the attractive combination of features sought for the cited applications: a specific energy above 100 Wh/kg, a specific power above 100 W/kg, a cycle life in excess of 500 cycles (at 100% depth of discharge), and a projected cost of less than $50† per kWh of energy storage capability.

Some perspective regarding the relative specific energies of various electrochemical cells can be gained by studying Figure 1, which shows the theoretical specific energy of various cells plotted against the equivalent weights of the reactants (or products). The theoretical specific energy is defined

† 1979 dollars.

ELTON J. CAIRNS • Head, Energy and Environment Division, Lawrence Berkeley Laboratory, University of California, Berkeley, California 94720.

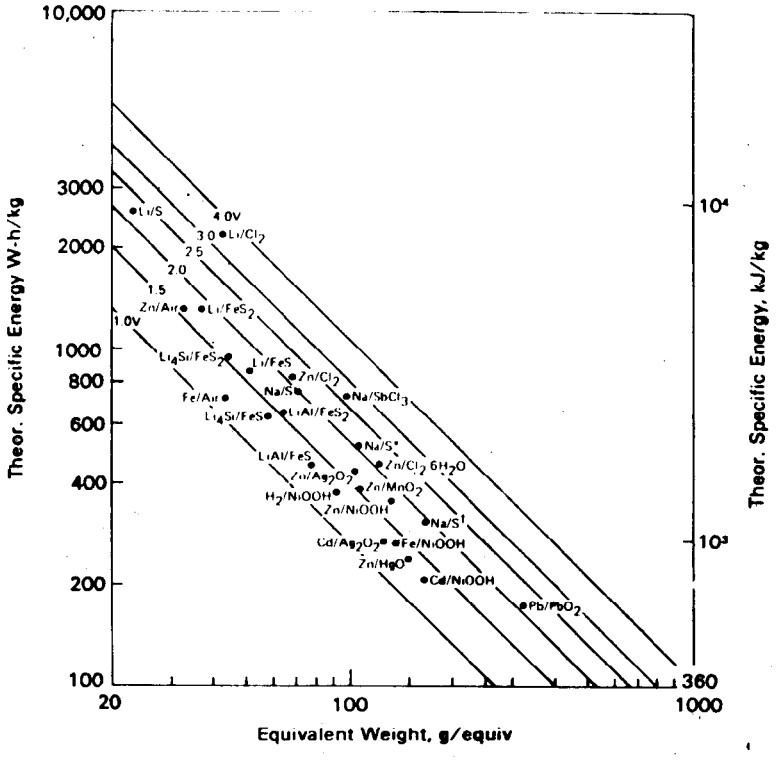

Figure 1. Theoretical specific energy (Wh/kg) for various electrochemical couples plotted against the sum of the molecular weights of the reactants times the number of moles of each involved in the balanced cell reaction. The straight lines are iso-emf lines. A good approximation to practical specific energies is obtained by multiplying the values in the figure by 0.2–0.25 for couples with solid reactants, and 0.15–0.2 if gaseous reactants are involved. Na/S* signifies $2Na + 5.2S \rightarrow Na_2S_{5.2}$, two-phase region; Na/S† signifies $Na_2S_1 + 2.2S \rightarrow Na_2S_{5.2}$, single-phase region.

as the Gibbs free energy change for the overall cell reaction, divided by the corresponding weights of the reactants:

$$\text{theoretical specific energy} = -\Delta G/\sum \nu_i M_i \qquad (1)$$

where ν_i is the number of moles of reactant i and M_i is the molecular weight of reactant i. It is evident from Figure 1 that the higher theoretical specific energy values correspond to cells with low-equivalent-weight reactants, and with large electronegativity differences between the reactants. The alkali metals are very attractive reactants for the negative electrodes, and the chalcogens and halogens (and some compounds containing them) are very attractive reactants

for the positive electrodes. Notice that most of the high-specific-energy couples involve reactants that are incompatible with aqueous electrolytes. Among the nonaqueous electrolytes, only those that are used at elevated temperatures have high conductivities ($>0.1\ \Omega^{-1}\ cm^{-1}$), consistent with specific power values above 100 W/kg. A summary of other desirable characteristics for cell reactants and electrolytes is given in Table 1.[1]

The electrolytes which are most useful in high-temperature cells are solid ionic conductors (either ceramics or glasses) or molten salts. These electrolytes must be chemically stable in contact with both the negative and positive electrode reactants, and must have a decomposition potential safely above the maximum operating voltage of the cell (unless a component of the electrolyte is a cell reaction product). The above considerations significantly narrow the field of choices, so that high-temperature cells with sodium electrodes now must use solid electrolytes (because sodium is soluble in its molten halides, yielding an electronically conductive electrolyte), and cells with lithium (and some other) electrodes now must use molten-salt electrolytes (because there are no solid lithium ion conductors sufficiently stable to lithium). Therefore there is a natural grouping of high-temperature cells which will be followed in the discussion below: sodium cells with solid electrolytes, and lithium (and calcium) cells with molten-salt electrolytes.

2. Cells with Solid Electrolytes

All of the high-temperature cells with solid electrolytes under current development contain molten sodium as the negative electrode, and rely upon sodium ion conduction in the electrolyte. The positive electrodes for these cells may be sulfur, a sulfide, or a halide. These cells operate at temperatures in the range 200–400°C.

Table 1
Desirable Characteristics of Systems for High-Performance Electrochemical Cells

Characteristic	Anode reactant	Cathode reactant	Electrolyte
Electronegativity	Low (~1)	High (>1.5)	—
Equivalent weight (g/g equiv.)	Low (<30)	Low (<30)	Low[a] (<30)
Conductivity ($\Omega^{-1}\ cm^{-1}$)	High ($>10^4$)	High ($>10^4$)	High (>1)
Electrochemical reaction rate (i_0, A/cm^2)	High ($>10^{-3}$)	High ($>10^{-3}$)	High ($>10^{-3}$)
Solubility in electrolyte (mol %)	Low (<0.1)	Low (<0.1)	—
Mass transport rate (equiv/sec cm^2)	High ($>10^{-4}$)	High ($>10^{-4}$)	High ($>10^{-4}$)

[a] A more important criterion for the electrolyte is low density.

2.1. The Sodium–Beta-Alumina–Sulfur Cell

The heart of the Na–β-Al_2O_3–S cell is the ceramic electrolyte, called beta-alumina.[2] Actually, the electrolyte is a sodium aluminate of the composition $Na_2O \cdot 11Al_2O_3$, consisting of hexagonal layers of spinel-like blocks containing aluminum and oxygen atoms, the layers being spaced apart by aluminum–oxygen bridges. The sodium ions are located in planes perpendicular to the C axis of the crystals, and are mobile in these planes. The conductivity is about 0.3 Ω^{-1} cm^{-1} at 300°C for single-crystal β-Al_2O_3, and 5–20 times lower for polycrystalline material. A related form of this material, β''-Al_2O_3, with a greater C-axis spacing, has a higher conductivity of 0.3 Ω^{-1} cm^{-1} for the polycrystalline form at 300°C. A typical composition for $\beta''Al_2O_3$ is $Na_2O \cdot 6Al_2O_3$ with up to 2 wt % MgO and/or Li_2O to stabilize the structure.

The beta-alumina electrolyte for Na–S cells is prepared (usually by pressing and sintering) in a tubular form, with a wall thickness of 1–2 mm. The original form of the cell, reported by Kummer and Weber,[3] is shown schematically in Figure 2, with sodium inside the electrolyte tube, and sulfur outside. The molten sodium, being an excellent electronic conductor, acts as its own current collector, and makes contact with the sodium container, which serves as the negative terminal of the cell. The sulfur and the polysulfides which form during discharge are poor electronic conductors, so a current collector network of graphite fibers (e.g., in the form of a felt matting) is used in the sulfur electrode, providing an electronically conductive pathway from the positive

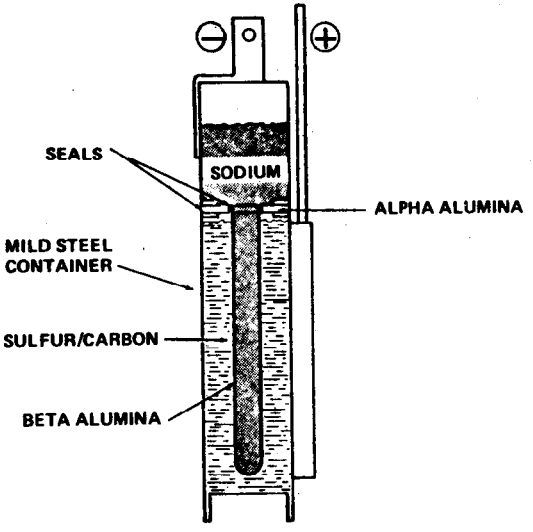

Figure 2. Cross section of a sodium–beta-alumina–sulfur cell, using the sodium-core design.

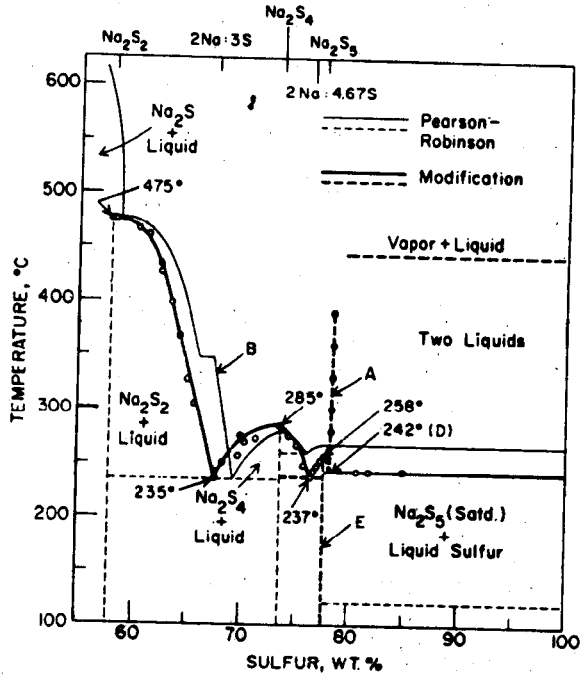

Figure 3. The sodium–sulfur phase diagram, after Gupta and Tischer.[4]

terminal through the metal cell case, to the sites of electrochemical reaction near or at the surface of the electrolyte.

The overall cell reaction is the conversion of sodium and sulfur to sodium sulfides at about 350°C:

$$2Na + xS \rightarrow Na_2S_x \qquad (2)$$

The phase diagram showing the coexistence of two immiscible sulfur-rich liquid phases is presented in Figure 3.[4] Starting with the cell in the fully charged state at 350°C, the positive electrode is essentially pure liquid sulfur, with a potential of 2.1–2.2 V vs. the Na electrode. As the cell is discharged, a sodium polysulfide is formed according to Eq. (2). When the amount of polysulfide formed exceeds the solubility limit in sulfur (a fraction of a percent), a separate polysulfide phase forms, having a composition (at 350°C) of $Na_2S_{5.2}$, comprised largely of Na_2S_5 and Na_2S_6. This phase has a high electrolytic conductivity. The amount of polysulfide phase increases at the expense of the sulfur phase as discharge continues. The reversible cell potential remains 2.07–2.08 V so long as the two phases coexist (see Figure 4).

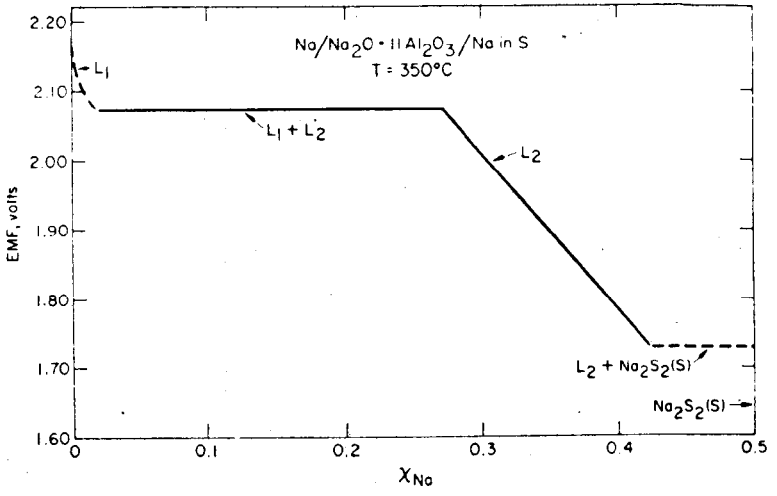

Figure 4. The reversible emf of the sodium-sulfur cell as a function of the sulfur electrode composition.[1]

When all of the sulfur is converted into polysulfide, the overall composition of the positive electrode is $Na_2S_{5.2}$. Further discharge is proposed by Ludwig[5] to take place as follows:

$$S_3 - S_2^- + e^- \rightarrow S_3 \cdots S_2^{2-} \quad (3)$$

$$S_3 \cdots S_2^{2-} + e^- \rightarrow S_3^{2-} + S_2^{2-} \quad (4)$$

$$2S_3^{2-} \rightarrow S_2^{2-} + S_4^{2-} \quad (5)$$

$$S_2^{2-} + 2S_5^{2-} \rightarrow 3S_4^{2-} \quad (6)$$

Reactions (3) and (4) are electrochemical, and are followed by chemical reactions (5) and (6), resulting in the conversion of the polysulfide phase to the overall composition Na_2S_4 (comprised of a mixture of Na_2S_2, Na_2S_4, and Na_2S_5). As discharge continues, a similar mechanism operates on Na_2S_4:

$$^-S_2 - S_2^- + e^- \rightarrow {}^{2-}S_2 \cdots S_2^- \quad (7)$$

$$^{2-}S_2 \cdots S_2^- + e^- \rightarrow 2S_2^{2-} \quad (8)$$

Na_2S_2 accumulates in the polysulfide melt until its solubility limit is reached, and solid Na_2S_2 precipitates at the electrolyte surface, preventing further reaction at a significant rate. The overall composition at this point is Na_2S_3 (at 350°C).

As the cell is recharged, the polysulfide phase is converted to sulfur, which tends to form insulating layers, wetting and coating the graphite current

collectors, preventing further reaction. This problem has resulted in a great deal of effort on improving the electronic conductivity of sulfur (by addition of such materials as C_6N_4), using specially shaped graphite felt current collectors,[6] and by tailoring the conductivity of the graphite current collector, in order to provide an optimized current distribution in the sulfur electrode, avoiding the blockage of the recharge process by insulating sulfur layers.

Most of the early Na–S cells were relatively small (tubes ~1 cm diameter × 10–15 cm long, <15 Ah), and many had glass housings and seals. The problems of corrosion and impurities were studied in terms of their influence on cell resistance and lifetime. High-purity sodium, free of potassium and other alkali metals, is needed to avoid cation exchange and cracking of the β-Al_2O_3. Impurities in the sulfur, such as Fe, Ni, etc., from corrosion of the steel cell case were found to cause problems with the sulfur electrode due to metal sulfide precipitation, blocking access of sulfur to the electrolyte. The corrosion of metal containers by sulfur remains a serious problem. Many coatings have been tested; chromium and molybdenum are among the best. Some borides are promising.

In spite of the various materials problems associated with the Na–β-Al_2O_3–S cell, the simplicity of the basic cell design and the low cost of the reactants have resulted in a wide-spread interest in this cell. Major efforts exist in the U.S., England, France, Germany, and Japan. In the last few years, progress has been good, and a number of approaches are being taken to the problems. Cells of significantly more than 100-Ah capacity (typically, 165 Ah) have been tested, having electrolyte tubes of up to 3 cm diameter and 45–60 cm long. A recent design of a 168-Ah cell used by General Electric is shown in Figure 5.[7] This cell has sodium inside of the electrolyte tube, as do the Ford and Brown Boveri cells. The cells of British Rail and Chloride Silent Power have sulfur inside the β''-Al_2O_3 tube, and sodium outside. This approach was taken to minimize the problem of corrosion by sulfur. Of course, the central current collector for the sulfur electrode must be corrosion resistant, but coatings are easier to apply to the outer surface of a current collector than to the inner surface of a cell case.

In all sodium–sulfur cells, the electrolyte tube is sealed to an alumina collar by a glass seal. This seal has been a cause of failure. Another difficult sealing problem for this cell is that of the metal cell container to the alumina collar. Various gasketed seals with bolts have been used, but these are too heavy and expensive. Recently, emphasis has been placed upon thermocompression-bonded seals, which appear to be more practical.

The internal resistance of the cells has a strong influence on the efficiency of operation, and the heat generation rate. In the interest of lowering the internal cell resistance to a value below 2 $\Omega\,cm^2$, a new sodium-ion electrolyte is being evaluated. This electrolyte, called NASICON, has the advantage of a high sodium ion mobility in all three crystallographic directions, rather than just two, as for β-Al_2O_3. The general formula for the family of NASICON

compositions is $Na_{1+x}Zr_2Si_xP_{3-x}O_{12}$. Resistivities in the range of 2–4 Ω cm have been reported at 300–350°C. Another problem with internal resistance in sodium–sulfur cells is due to the existence of a resistance associated with the sodium–β''-Al_2O_3 interface, which increases as cell cycling continues.[7] There is no general agreement on the precise source of this interfacial resistance, or means for eliminating it. The sulfur electrode, as one would expect, is a significant source of resistance. Various designs of graphite fiber current collectors have been investigated in attempts to reduce the cell internal resistance. Currently, the best values are about 2 Ω cm^2, and 1.2 Ω cm^2 may be achievable with present approaches (and electrolyte thicknesses near 1.5 mm).

Sodium–β-alumina–sulfur cells are typically operated at 350°C, a current density of 0.1 A/cm^2 or less, and have capacity densities of 0.2–0.4 Ah/cm^2, based on the surface area of the electrolyte. The resistance–area product for well-built cells is 2 Ω cm^2 at 350°C. The specific energy values achieved by the best-designed cells are near 150 Wh/kg, at about 40 W/kg. There is a great deal of variation in the reported lifetimes of individual cells, but the better ones operate for more than 200 deep cycles; some have achieved about 1500 deep cycles.

A few multi-kilowatt-hour sodium–sulfur batteries have been tested, but their lifetimes have been very short, owing to the variability of characteristics of the individual cells. The voltage–current curve for a 96-cell battery having a design capability of 10 kWh is shown in Figure 6.[8] The cells were arranged in

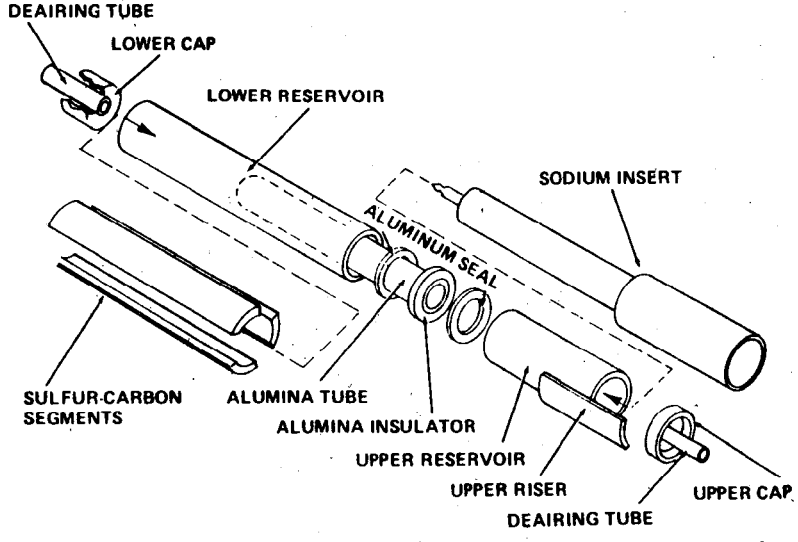

Figure 5. Exploded view of a 168-Ah sodium–sulfur cell of the sodium-core design.[7]

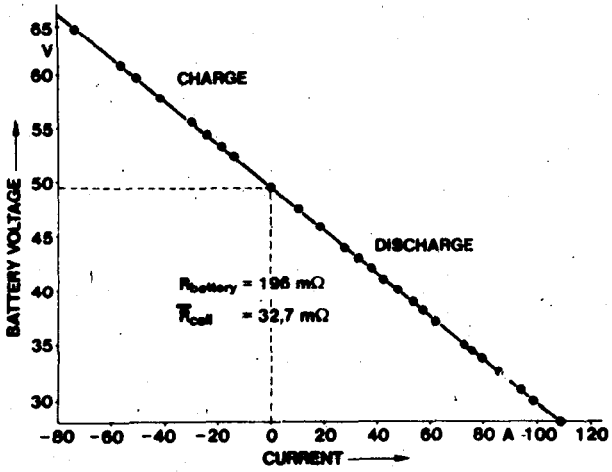

Figure 6. Voltage–current curve of a 96-cell, 10-kWh sodium–sulfur battery.[8] The cells were connected as four parallel strings of 24 cells each, with cross connections between strings every eight cells. Each cell was nominally 48 Ah. The battery yielded 177 Ah, with an energy efficiency of 61%.

four parallel strings, giving 50 V and 177 Ah. Currently, most of the sodium–sulfur battery programs are placing emphasis on semipilot production of cells having capacities of 100–200 Ah, the life-testing of these cells, and the preparation of batteries. The problems of thermal management and optimum interconnection of cells to form batteries are in the early stages of investigation. In the period 1980–1982, a number of demonstration batteries for electric vehicles will be constructed and tested.

Table 2 summarizes the present state of sodium–sulfur cell research and development. To put the status data into perspective, the best of the specific energy and specific power values are acceptable for energy storage and vehicle propulsion applications, as is the longest cycle life. The lifetime necessary for most applications is at least 3 years (26,000 hr), and the cost should be below $100/kWh.

2.2. The Sodium–Sodium-Glass–Sulfur Cell

This interesting cell operates according to the same principles as the sodium–β-alumina–sulfur cell. The β-alumina electrolyte, however, is replaced by a sodium-ion-conducting glass. This glass electrolyte has a much higher resistivity than β-alumina (10^4 Ω cm vs. 3–20 Ω cm at 300–350°C). It is necessary, therefore, to use a much thinner layer of electrolyte between the

electrodes, and to operate the cell at much lower current densities in order to have an acceptably small voltage loss due to the cell resistance. This is accomplished by using hollow fibers of glass electrolyte, 70 μm OD, and 50 μm ID, with a 10-μm wall thickness.

The design of the sodium–sodium glass–sulfur cell, using thousands of hollow glass fibers, is shown in Figure 7.[9] The fibers have one end sealed, and the other (open) end bonded to a glass tubesheet, providing communication between the insides of the fibers and the sodium reservoir. The sulfur is on the outside of the hollow fibers. Current collection in the sulfur electrode is provided by a carbon- or molybdenum-coated aluminum foil which is spirally wound among the glass fibers (a simple operation performed by rolling the fibers together with the Al foil before sealing into the tubesheet). Typically, the

Table 2
Summary of the Present State of Sodium–Sulfur Cell Research and Development

$Na–\beta\text{-}Al_2O_3–S$

$2Na + 3S \rightarrow Na_2S_3$

$\bar{E}$ = 2.0 V; 758 Wh/kg theoretical

Status	
Cell size	50–200 Ah
Specific energy	85–150 Wh/kg at 30–40 W/kg
Specific power	60–130 W/kg peak
Cycle life	200–1500
Lifetime	300–15,000 hr
Cost	>$1000/kWh
Recent Work	
Batteries, ~10 kWh	
C_6N_4 additive to S	
Ceramic (TiO_2) electronic conductors	
Shaped current collectors	
Tailored resistance current collectors	
Sulfur-core cells	
$Na_{1+x}Zr_2Si_xP_{3-x}O_{12}$	
Thermocompression-bonded seals	
Problems	
High $Na–\beta''\text{-}Al_2O_3$ interfacial resistance	
Corrosion of materials in contact with S	
High-cost seals	
High-cost electrolyte	
Thermal cycling causes failure	
Thermal control of batteries	
Cell mismatch in batteries	

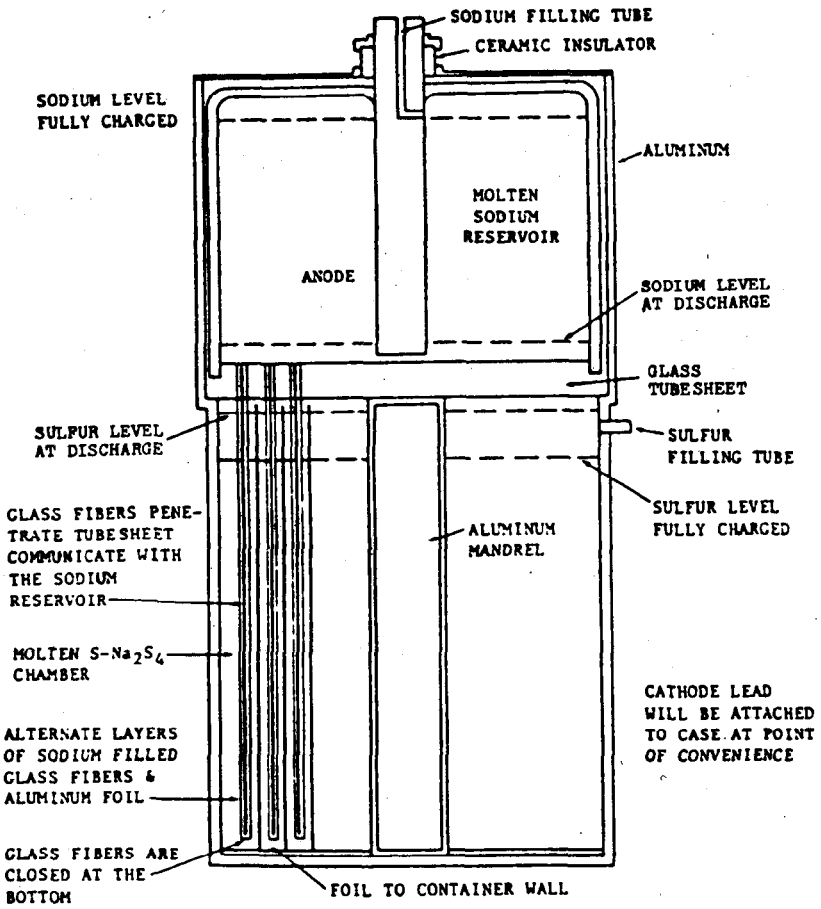
SODIUM FILLING TUBE
CERAMIC INSULATOR
SODIUM LEVEL FULLY CHARGED
ALUMINUM
MOLTEN SODIUM RESERVOIR
ANODE
SODIUM LEVEL AT DISCHARGE
GLASS TUBESHEET
SULFUR LEVEL AT DISCHARGE
SULFUR FILLING TUBE
SULFUR LEVEL FULLY CHARGED
GLASS FIBERS PENETRATE TUBESHEET COMMUNICATE WITH THE SODIUM RESERVOIR
ALUMINUM MANDREL
MOLTEN S-Na_2S_4 CHAMBER
CATHODE LEAD WILL BE ATTACHED TO CASE AT POINT OF CONVENIENCE
ALTERNATE LAYERS OF SODIUM FILLED GLASS FIBERS & ALUMINUM FOIL
GLASS FIBERS ARE CLOSED AT THE BOTTOM
FOIL TO CONTAINER WALL

Figure 7. Schematic cross section of the hollow glass fiber sodium–sulfur cell.[9]

distance between fibers is 200–500 μm, and the distance from a fiber to the Al current collector is 20 μm. Because of the very large total electrolyte area offered by the fibers, the operating current density is only 0.002 A/cm^2, yielding a low resistance loss (0.1 V), and a high efficiency (typically, 90% overall). This cell is designed to operate at 300°C between the composition limits Na_2S_{20} (charged) and $Na_2S_{3.5}$ (discharged), with a theoretical specific energy of 691 Wh/kg. A sulfur utilization of 90% (based on $Na_2S_{3.5}$) is achieved. As expected, the cell resistance rises rapidly toward the end of the charging process. Many small cells (0.5–6 Ah†) have been tested, and lifetimes

† The 6-Ah cells contain about 2000 fibers.

up to about 9000 hr, and 500 cycles have been achieved with stable performance. A small number of 40-Ah cells (with 13,000 fibers) have been tested also.

The current problems with the glass fiber cell include fracture of the fibers near the tubesheet, gradual sagging of the glass tubesheet, and undesirable interaction between the two glass compositions making up the fibers and the tubesheet. When a number of fibers fail, the exothermic reaction between sodium and sulfur can cause thermal runaway. This safety problem is currently receiving attention. Thermal control must be reasonably precise for these cells because the cell resistance (mostly glass fiber resistance) has a high temperature coefficient. Cooldown of cells after start-up is not permitted because of excessive fiber breakage.

Recent work with 40-Ah cells is encouraging, and development of these cells continues, with emphasis on increasing cell lifetime and improved safety. Table 3 presents a summary of the status of this cell.

Table 3
Summary of the Status of the Sodium–Sodium-Glass–Sulfur Cell

Na–Na-glass–S
$2Na + 3.5S \rightarrow Na_2S_{3.5}$
$\bar{E} = 2.0$ V; 691 Wh/kg

Status	
Cell sizes	0.5, 6, 40 Ah
Specific energy	n.a.
Specific power	n.a
Cycle life	500
Lifetime	9000 hr
Cost	>$1000/kWh
Recent work	
40 Ah Cells	
Mo coating on Al	
New glass for tubesheet	
Safety	
Problems	
Breakage of fibers near tubesheet	
Thermal runaway on failure	
Sagging of tubesheet	
Compatibility of fibers and tubesheet	
Impurities attack fibers	
High-temperature coefficient of resistance	
Thermal cycling	

2.3. The Sodium–Beta-Alumina–Antimony Trichloride Cell

This cell is a relative of the sodium–sulfur cells. It uses a molten salt mixture of $SbCl_3$ in $NaCl$–$AlCl_3$ in place of sulfur as the positive electrode reactant. The melting point of $NaCl$–$AlCl_3$ mixtures is low enough that cell operation can be carried out at 200°C. It was claimed by the investigators[10–12] that the lower operating temperature would permit polymeric materials to be used as insulators and seals; however, these were not satisfactorily developed and demonstrated.

The overall cell reaction is as follows:

$$3Na + SbCl_3 + 3AlCl_3 \rightarrow 3NaAlCl_4 + Sb \qquad (9)$$

With an average cell potential of 2.8 V, the theoretical specific energy is 328 Wh/kg.

Small cells, up to 6 Ah, were operated at current densities up to 7.5 mA/cm^2. These cells used graphite powder and molybdenum or tungsten as the current collector in the positive electrode. Cycle lives of about 100 have been demonstrated. Problems encountered in the work on this cell include difficulty of wetting of the β''-Al_2O_3 by sodium, inadequate seals, low current density, and degradation of the β''-Al_2O_3.

The status of this cell is shown in Table 4 where a projected specific energy of 90 Wh/kg is given. This value is low, compared to the values already demonstrated for the Na–S cell (150 Wh/kg).

2.4. The Sodium–Beta-Alumina–Sulfur Chloride Cell

The newest cell of the sodium–beta alumina family of cells uses SCl_4 in $NaCl$–$AlCl_3$ as the positive electrode reactant.[13] Again, a lower operating temperature is offered by the $NaCl$–$AlCl_3$ mixture: temperatures of 130–255°C have been used.

The overall cell reaction for reduction to S° is

$$4Na + SCl_3AlCl_4 + 3AlCl_3 \rightarrow S + 4NaAlCl_4 \qquad (10)$$

The cell voltage is impressively high: 4.2 V, yielding a theoretical specific energy for reaction (10) of 563 Wh/kg.

Some glass laboratory cells have been operated according to reaction (10), having a capacity of 4 Ah at 255°C.[13] These cells have used tungsten spiral current collectors, and were operated for at least 45 cycles before failure of the β''-Al_2O_3 electrolyte.

The status of the work on the Na–β''-Al_2O_3–SCl_4 in $NaCl$–$AlCl_3$ cell is shown in Table 5. The high cell voltage offers the possibility of high efficiency. If the S° can be reduced to S^{2-} by deeper discharge at a voltage above about 3 V, the specific energy in practical cells could be well above 100 Wh/kg.

Table 4
Summary of the Status of the Sodium–Beta-Alumina–Antimony Trichloride Cell

$Na–\beta''\text{-}Al_2O_3–SbCl_3$ in $AlCl_3$
$3Na + SbCl_3 + 3AlCl_3 \rightarrow 3NaAlCl_4 + Sb$
$\bar{E}$ = 2.8 V; 328 Wh/kg theoretical

Status	
Specific energy (projected)	90 Wh/kg at 12 W/kg
Specific power (projected)	30 W/kg
Cycle life	100 at 100% DOD[a]
Cost	Too early
Operating temperature	210°C
Recent work	
Tubular cells	6 Ah, 30 Ah
Improved electrode designs	
Problems	
Wetting of $\beta''\text{-}Al_2O_3$ by Na	
Current collectors (W or Mo)	
Seals	
Low current density (7.5 mA/cm^2)	
Degradation of $\beta''\text{-}Al_2O_3$	
Slow recharge (14 hr)	
Low specific energy	

[a] Depth of discharge.

3. Cells with Molten-Salt Electrolytes

All of the rechargeable cells with molten salt electrolytes currently under development make use of solid electrodes. These cells are an outgrowth of earlier work on cells with liquid electrodes and molten-salt electrolytes.[14–16] The forerunner of the present Li alloy–molten salt–FeS_x cells was the Li–LiCl-KCl–S cell,[15,16] which was very attractive because of its high theoretical specific energy (2600 Wh/kg) and attractive cell potential (~2.4 V). Significant problems with the solubility of polysulfides in the electrolyte, and the retention of liquid lithium in its current collector, caused attention to be focused upon immobilization of lithium in the form of a solid alloy (of relatively high lithium activity) and the insolubilization of sulfur and polysulfides by using transition metal sulfides (which have a very low solubility). These measures cause a significant decrease in the specific energy of the cell and a moderate decrease in voltage, but a great increase in cell lifetime.

In principle there are many lithium alloys that can be used as the negative electrode, but only a few of them have an acceptable combination of low weight

Table 5
Summary of the Status of the Sodium–Beta-Alumina–Sulfur Chloride Cell

$Na–Na_2O \cdot xAl_2O_3–SCl_3AlCl_4$ in $AlCl_3–NaCl$; $T = 250°C$

$4Na + SCl_3AlCl_4 + 3AlCl_3 \rightarrow 4NaCl \cdot AlCl_3 + S$

$E = 4.2$ V; 563 Wh/kg theoretical

Status: glass lab cells only (4 Ah)

Current density	20 mA/cm^2 at 3.5 V
Power density	150 mW/cm^2 max. at 2.5 V
Cycle life	45 at 100% DOD
Cost	Too early

Recent work
- Larger cells—4 Ah
- Less expensive current collectors

Problems
- Sodium wetting
- Vapor pressure
- Corrosion of metals and some electrolytes
- Electrolyte cracking
- Overcharge?

per electrochemical equivalent, low cost, ability to be recharged many times, high exchange current density, and high lithium diffusion coefficient. The alloys that have been investigated most are Li–Al[17,18] and Li–Si.[19,20] Some recent work has been performed with Ca–Si and other calcium alloys.[21,22]

The metal sulfides that have been investigated as positive electrodes include the iron sulfides, nickel sulfides, cobalt sulfides, copper sulfides, and molybdenum sulfide.[23] The ones receiving the most emphasis are FeS and FeS_2.

From the several negative and positive electrode materials indicated above, a long list of cells can be made; however, only two of these have been receiving a significant amount of research and development effort. These are LiAl–LiCl-KCl–FeS, Li_4Si–LiCl-KCl–FeS_2. Another system of interest is Ca_2Si–LiCl-NaCl-$CaCl_2$-$BaCl_2$–FeS_2.

3.1. The Lithium-Aluminum–Lithium Chloride-Potassium Chloride–Iron Monosulfide Cell

This electrochemical system is very stable in operation, with relatively few serious operating and materials problems. The overall cell reaction is

$$2LiAl + FeS \rightarrow Li_2S + Fe + 2Al \qquad (11)$$

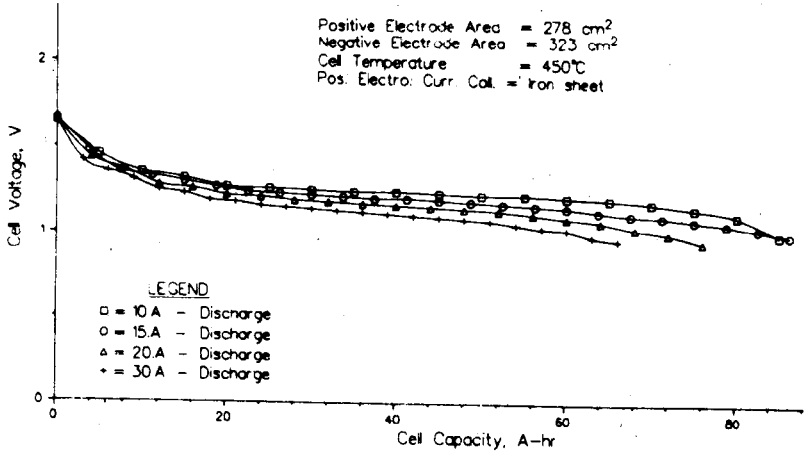

Figure 8. Voltage–capacity curve for a LiAl–FeS cell.[24]

This cell is usually operated at 450°C, and exhibits a single voltage plateau near 1.3 V, as shown in the constant current–discharge curves of Figure 8.[24] The overall reaction given above, and the single voltage plateau are, however, misleadingly simple. Detailed investigations of the phase transformations occurring during charge and discharge of the FeS electrode have led to the establishment of the phase diagram shown in Figure 9.[22]

The dashed line C–D in Figure 9 shows the path followed by the composition of the FeS electrode from the fully charged condition (point C) to the fully discharged condition (point D). Starting at point C, as lithium is added to the FeS electrode by electrochemical reaction, two new phases, Li_2FeS_2 and Fe, are formed:

$$2FeS + 2Li \rightarrow Li_2FeS_2 + Fe \qquad (12)$$

Additional discharge beyond the point where line C–D crosses the X–Fe line in Figure 9 results in a new phase, Li_2S, being formed:

$$Li_2FeS_2 + 2Li \rightarrow 2Li_2S + Fe \qquad (13)$$

Reactions (12) and (13) occur at essentially the same potential, near 1.6 V vs. reversible lithium, so the voltage vs. capacity curve for the discharge from point C to point D shows only one plateau.

Depending on the temperature of operation, and the composition of the LiCl–KCl electrolyte, another phase, called djerfischerite, may form, having the composition $LiK_6Fe_{24}S_{26}Cl$.[22] This material tends to reduce the rate at which the recharge reactions can be carried out, hence its formation is

undesirable. The extent of formation of $LiK_6Fe_{24}S_{26}Cl$ can be minimized by using an electrolyte that has more LiCl than the eutectic composition, and by operating at temperatures above 450°C.[25]

The negative electrode for the LiAl–FeS cell is the intermetallic compound LiAl, which has a potential 0.3 V positive with respect to a reversible pure lithium electrode. The phase diagram of Figure 10[26] shows that there is a broad composition range (from 10% to 45% Li in Al) over which there is a two-phase mixture ($\beta + \alpha$), yielding a single voltage plateau (0.3 V vs. reversible Li). This feature makes the Li–Al electrode attractive.

Lithium–iron monosulfide cells of various designs have been constructed and tested. A multiplate cell with two positive (FeS) and three negative (LiAl) electrodes is shown in Figure 11.[23] The electrodes for such cells may be prepared by various techniques, including cold or hot pressing of mixed powders of reactant and electrolyte (with or without a current collector powder such as graphite for the FeS added), or by using a conductive carbon cement (the so-called carbon-bonded structure). Various additives to the FeS electrode have been used to improve the utilization and current collection, including Cu_2S (about 6 at %). The current collectors are made of corrosion-resistant metals such as iron, iron alloys, stainless steels, etc. The electrolyte is soaked into a porous boron nitride mat, which may be a woven cloth or a felt. The boron nitride is not readily wetted by the LiCl–KCl electrolyte. Wettability is improved by the addition of $LiAlCl_4$ to the BN mat (~20 mg/cm^2).

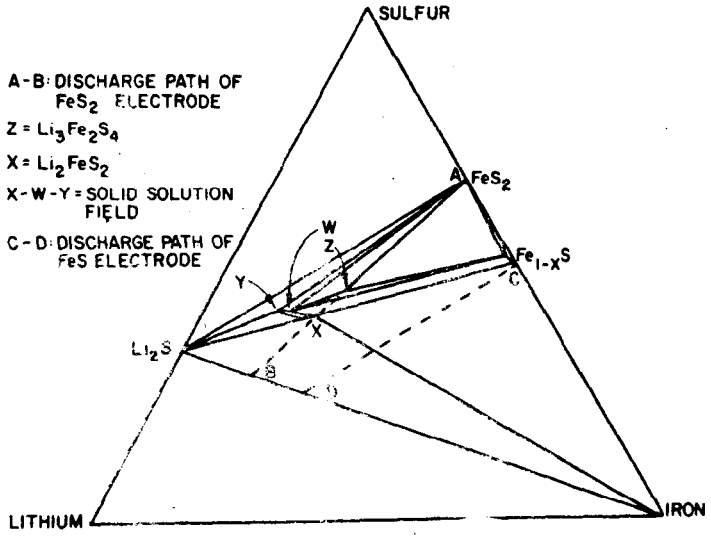

Figure 9. Isothermal section of the Li–Fe–S phase diagram at 450°C.[22]

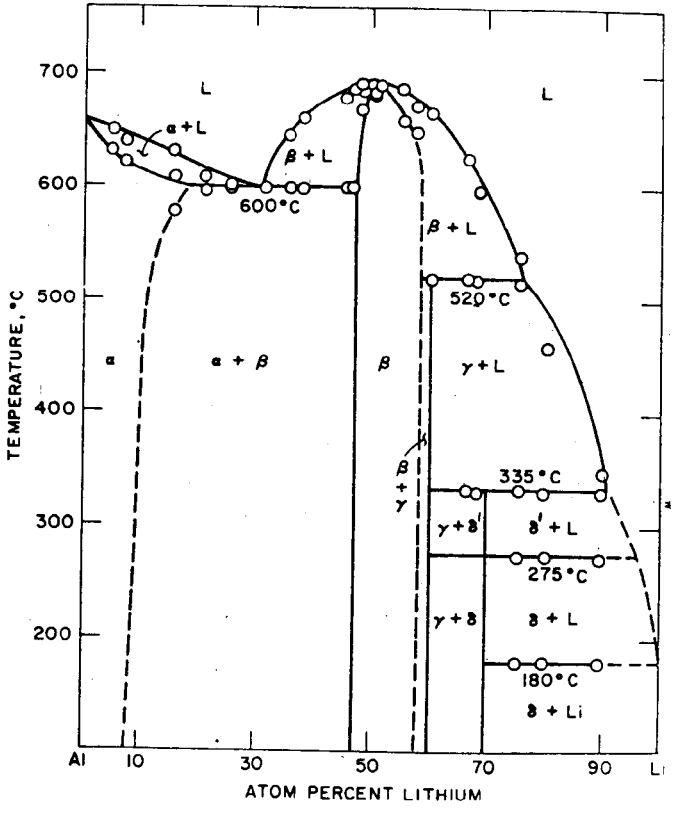

Figure 10. The lithium–aluminum phase diagram.[26] α = Al, β = LiAl, $\gamma = Li_3Al_2$, $\delta = \delta' = Li_9Al_4$.

Cells of the general multiplate type described above have been evaluated with regard to performance and lifetime. Figure 12[27] shows the specific energy vs. cycle number data of some 300-Ah cells designed for use in electric vehicles. Specific energies near 100 Wh/kg were achieved early in life (vs. 458 Wh/kg theoretical). Cycle lives of over 300 were achieved before 40% of the initial specific energy was lost.

Failure modes for these cells include shorting due to active material from the positive electrode extruding through openings in the structure, and touching the negative electrode. The gradual loss of capacity is to some degree associated with morphological changes in the Li–Al alloy (an agglomeration of the initially finely divided structure).

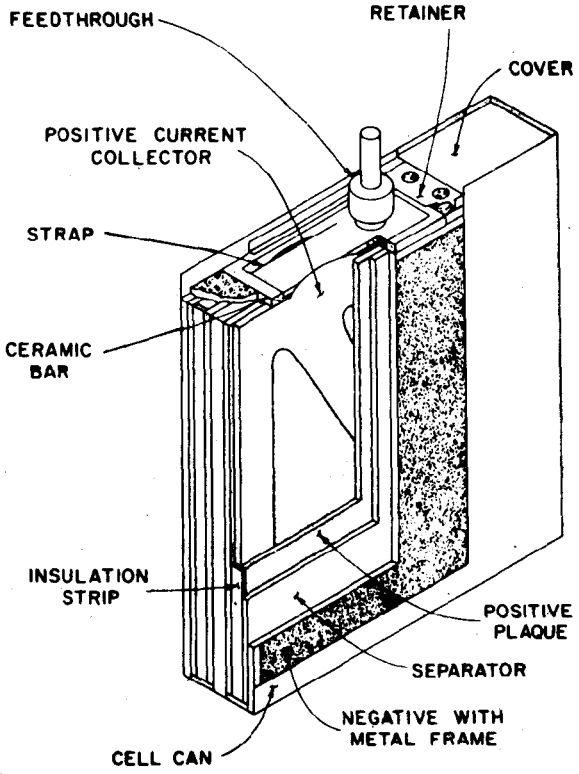

Figure 11. Multiplate LiAl–FeS cell design.[23]

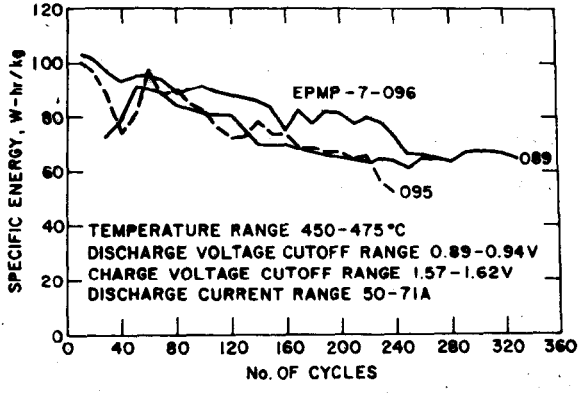

Figure 12. Specific energy vs. cycle number for 300-Ah LiAl–FeS cells.[27]

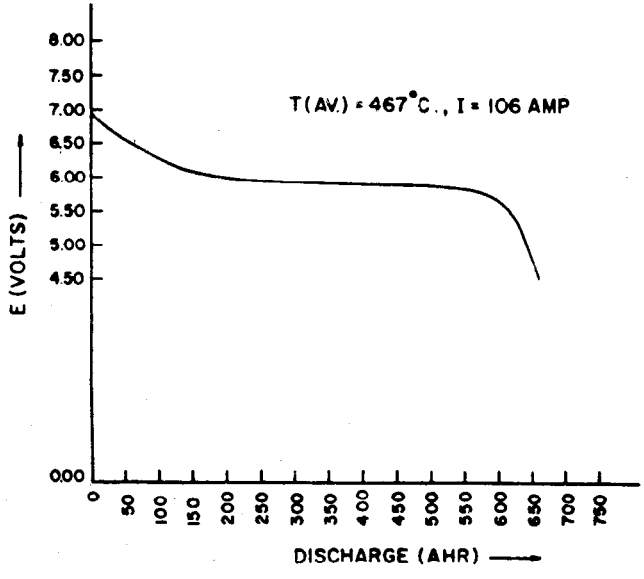

Figure 13. Voltage vs. capacity curve for a 10-cell LiAl–FeS battery, connected as two parallel strings, five cells each, with cross connections at each cell.[27]

Cells of the multiplate type (300 Ah) have been assembled into batteries, including a module for a forklift truck, and 20-kWh modules for electric van testing. Initial results for the 10-cell† forklift battery are shown in Figure 13.[27] The 20-kWh modules have had start-up problems; more will be tested. Experience with batteries and their thermal control is needed very much.

Table 6 summarizes the status of the LiAl–FeS cell. The current problems include a relatively low specific energy, internal cell shorting and high cost of BN separators. Sufficient promise has been shown by the results that industrial organizations are constructing pilot quantities of cells for testing and demonstration, under government sponsorship. This system may be the first to achieve commercial status among the rechargeable cells with molten salt electrolyte.

3.2. The Lithium-Silicon–Lithium Chloride-Potassium Chloride–Iron Disulfide Cell

This electrochemical cell is very closely related to the one described immediately above and operates at the same temperature (450°C). The main

† Two parallel strings of five ladder-connected cells.

Table 6
Summary of the Status of the Lithium-Aluminum–Lithium Chloride-Potassium Chloride–Iron Monosulfide Cell

LiAl–LiCl-KCl–FeS
$2LiAl + FeS \rightarrow Li_2S + Fe + 2Al$
$E = 1.33$ V; 458 Wh/kg theoretical

Status	
Cell size	320 Ah
Specific energy	50–90 Wh/kg at 30 W/kg
Specific power	60–100 W/kg, peak
Cycle life	300 at 100% DOD
Lifetime	~5000 + hr
Cost	>$1000/kWh
Recent work	
Multielectrode cells	
LiCl-rich electrolyte	
BN felt separators	
Batteries of 320-Ah cells	
Charging equipment	
Problems	
Low specific energy	
Low voltage per cell	
Cell shorting major failure made	
Electrolyte leakage	
Agglomeration of Li–Al with cycling	
High separator cost	
Leak-free feedthroughs	
Thermal control	

difference is that both the positive and the negative electrode reactants have significantly lower weights per electrochemical equivalent than those of the LiAl–FeS cell. The theoretical specific energy is 944 vs. 458 Wh/kg. The overall cell reaction is

$$Li_4Si + FeS_2 \rightarrow 2Li_2S + Fe + Si \qquad (14)$$

Reaction (14) actually takes place in stages, as indicated by the path A–Z–X–B in Figure 9. Starting at point A, representing the fully charged positive electrode, FeS_2 reacts with lithium as follows[27]:

$$2FeS_2 + 3Li \rightarrow Li_3Fe_2S_4, \quad E = 2.04 \text{ V} \qquad (15)$$

This is followed by a reaction involving only a few percent (~4.5%) of the total charge of reaction (14):

$$Li_3Fe_2S_4 + Li \rightarrow Fe_{1-x}S + W \text{ phase}, \qquad E = 1.9\ V \tag{16}$$

Reaction (16) is not balanced; its meaning is best seen by examination of Figure 9. W phase is a solid solution having the composition range shown in Figure 9. The next stage of reaction also involves only a small portion (~8.25%) of the charge associated with reaction (14):

$$Fe_{1-x}S + W + Li \rightarrow Li_2FeS_2, \qquad E = 1.9\text{–}1.64\ V \tag{17}$$

The final step is

$$2Li_2FeS_2 + 4Li \rightarrow 4Li_2S + 2Fe, \qquad E = 1.64\ V \tag{18}$$

Note that out of an overall eight-electron process for reactions (15)–(18), only one electron is associated with the sum of reactions (16) and (17). The reaction scheme above, proposed by Tomczuk and Martin,[27] is based upon extensive phase diagram work, voltage sweep experiments, and metallographic work on electrodes operated under well-controlled conditions, as well as electrodes from engineering cells.

The negative electrode, Li–Si, operates according to the phase diagram of Figure 14.[20] This electrode is operated between the extremes of silicon and Li_4Si. The phases encountered at 450°C are Si, Li_2Si, $Li_{21}Si_8$, $Li_{15}Si_4$, and $Li_{22}Si_5$, and the voltage plateaus (vs. reversible lithium) are given in Table 7.[20]

It is obvious that the combination of the FeS_2 electrode with two major plateaus and the Li–Si electrode with perhaps three major plateaus will yield a complex voltage vs. capacity curve for the complete cell, showing several plateaus.

A cross section of a typical lightweight development cell using Li_4Si and FeS_2 electrodes is shown in Figure 15.[23] This cell is in the form of a circular disk, with a central positive electrode, and two negative electrodes. The electrodes are separated by a BN cloth or felt. The electrodes may be prepared by various techniques, including pressing of powder mixtures into the desired

Table 7
Electromotive Force Values for the Li–Si Electrode at 725 K

Phases in Equilibrium	emf vs. Li
Si–Li_2Si	0.326
Li_2Si–$Li_{21}Si_8$	0.277
$Li_{21}Si_8$–$Li_{15}Si_4$	0.149
$Li_{15}Si_4$–$Li_{22}Si_5$	0.042
$Li_{22}Si_5$–Li (saturated with Si)	0.001

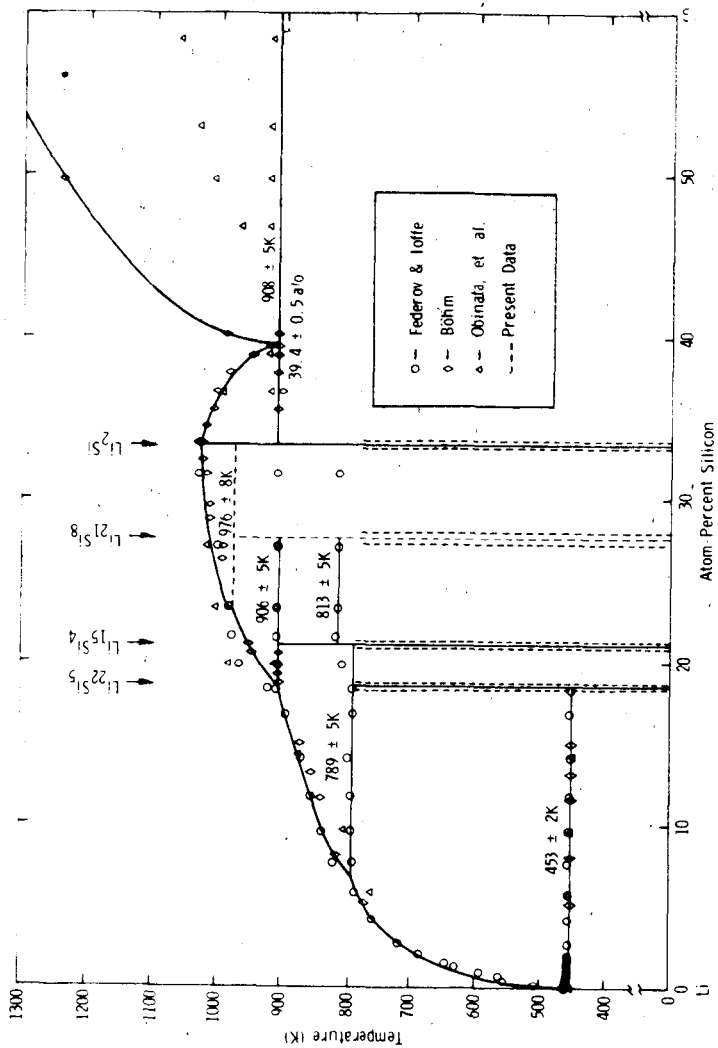

Figure 14. The lithium–silicon phase diagram.[20]

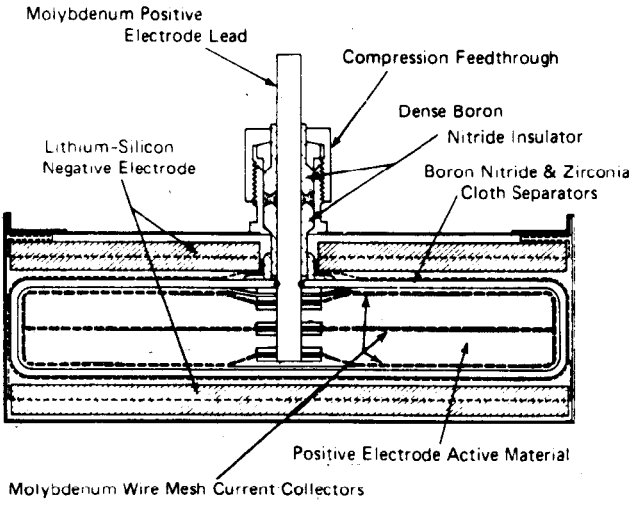

Figure 15. Cross section of a disk-shaped Li_4Si-FeS_2 cell, having about 70-Ah capacity.[28]

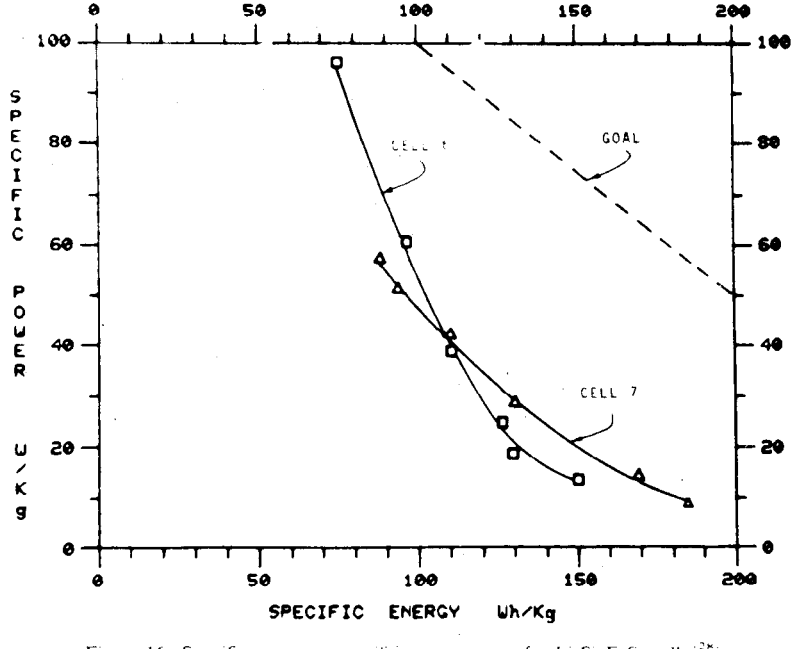

Figure 16. Specific power vs. specific energy curves for Li_4Si-FeS_2 cells.[28]

shapes. The specific energy vs. specific power curves for two cells of this type are shown in Figure 16.[23] Note that specific energies above 180 Wh/kg have been achieved at low specific power, and that specific powers up to about 100 W/kg have been demonstrated also. This is in contrast to the lower specific energy of the LiAl–FeS cell (~100 W/kg).

Life testing of Li_4Si–FeS_2 cells has shown that cycle lives of 700 cycles and lifetimes of over 15,000 hr can be achieved (see Figure 17). Even though good progress has been made in developing long-lived, high-specific-energy Li_4Si–FeS_2 cells, there are some significant problems requiring additional effort, as indicated in Table 8.

This cell has somewhat more severe materials problems than the LiAl–FeS cell, because the FeS_2 electrode presents a higher sulfur activity to the current collector, narrowing the selection of current collector materials. Currently, molybdenum is used in conjunction with graphite powder. There is some degree of concern about the formation of slightly soluble sulfur-containing species which can migrate gradually through the electrolyte toward the negative electrode. A full assessment of this problem has not been completed. In any event, the performance and lifetime data reported are encouraging.

The Li_4Si–FeS_2 cell is in an earlier stage of development than the Na–S or LiAl–FeS cells, but it is clear that the main problems have to do with materials, as is the case for those other cells. Electrochemical kinetics and transport processes are sufficiently rapid in all of these systems that rate processes,

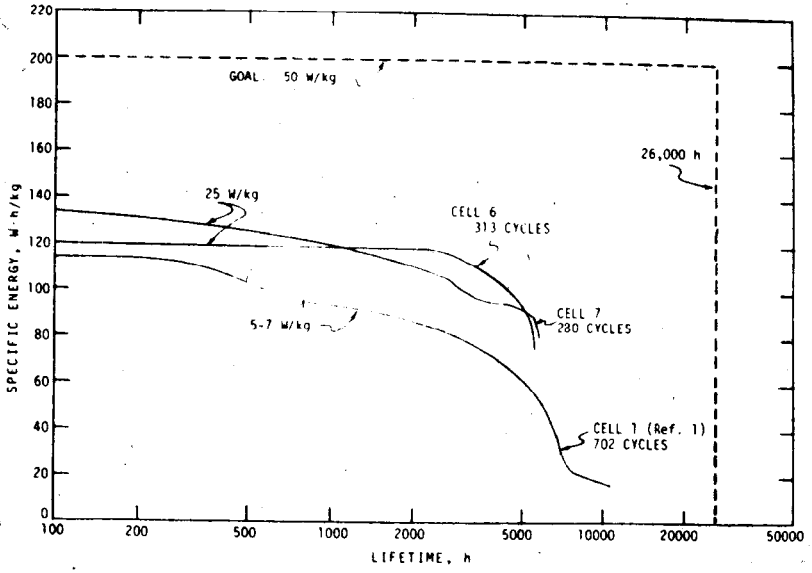

Figure 17. Specific energy vs. operating time curves for LiAl-FeS_2 and Li_4Si–FeS_2 cells.[28]

Table 8
Summary of the Status of the Lithium-Silicon–Lithium Chloride-Potassium Chloride–Iron Disulfide Cell

Li_4Si–LiCl-KCl–FeS_2
$Li_4Si + FeS_2 \rightarrow 2Li_2S + Fe + Si$
E = 1.8, 1.3 V; 944 Wh/kg theoretical

Status	
Cell size	70 Ah
Specific energy	120 Wh/kg at 30 W/kg 180 Wh/kg at 7.5 W/kg
Specific power	100 W/kg, peak
Cycle life	700 at 100% DOD
Lifetime	~15,000 hr
Cost	>$1000/kWh
Recent work	
Bipolar cells	
Li–Si electrodes	
BN felt separators	
70-Ah cells	
Problems	
Materials for FeS_2 current collector	
Leak-free feedthroughs	
High internal resistance	
Low-cost separators needed	
Thermal control	

properly taken into account in the designs, will not present formidable barriers to the development of cells with performance capabilities appropriate for such applications as vehicle propulsion and off-peak energy storage.

3.3. The Calcium-Silicon–Molten Halide–Iron Disulfide Cell

An interesting variant of the cell just described is obtained by replacing the lithium with calcium.[21,22] The negative electrode becomes a calcium–silicon alloy, which can be operated over the range Ca_2Si to at least $CaSi_2$. The electrolyte must contain calcium ions, of course, and the most effective electrolyte investigated is a mixture of 29% LiCl–20% NaCl–35% $CaCl_2$–16% $BaCl_2$, operating at 460°C.

Cells similar in structure to LiAl–FeS and Li_4Si–FeS_2 cells have been operated, but only at low current densities. A cell voltage vs. capacity curve for a 100 Ah cell is shown in Figure 18.[27] The voltage range over which this cell operates is similar to that for Li_4Si–FeS_2, and there is the possible advantage of being able to use the more abundant, lower-cost calcium instead of lithium.

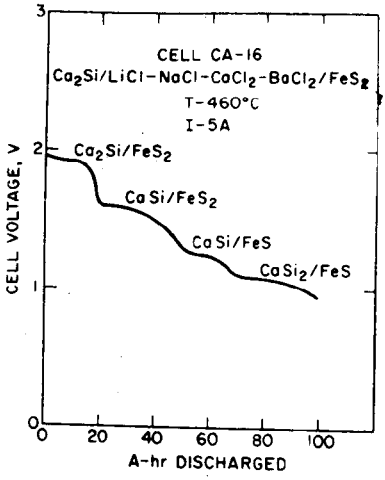

Figure 18. Voltage vs. capacity curve for a 100-Ah Ca_2Si–FeS_2 cell, operating at 460°C.[27]

The status of the work on this system is shown in Table 9. Note the low specific power and specific energy. These need improvement in order to make this system sufficiently interesting to work on extending the life to significantly longer values. Successful improvement in the cell performance and lifetime could yield a system of significant practical interest.

Table 9
Summary of the Status of the Calcium-Silicon–Molten Halide–Iron Disulfide Cell

Ca_2Si–LiCl-NaCl-$CaCl_2$-$BaCl_2$–FeS_2
$Ca_2Si + FeS_2 \rightarrow 2CaS + Fe + Si$
E = 2.0–1.2 V; ~750 Wh/kg theoretical

Status	
Specific energy	40 Wh/kg at 8 W/kg
Specific power	<10 W/kg
Cycle life	60
Cost	Too early
Recent work	
$BaCl_2$ added to electrolyte	
Larger cells—100 Ah	
Problems	
Low specific power	
Low current densities	

4. Conclusions

The discussion above, regarding various types of high-temperature cells in all stages of research and development, leads to the following conclusions:

1. Sodium–sulfur cells with ceramic electrolytes (β- and β''-Al_2O_3) are in the most advanced state of development. Several more multi-kilowatt-hour batteries will be developed and tested, both in Europe, and in the U.S., during the early 1980s. These batteries may find application in vehicle propulsion and stationary energy storage. Thermal cycling remains a problem.

2. Variants of the Na–S cell, such as the Na–SCl_3AlCl_4 cell may have advantages in certain applications where lower operating temperatures and higher cell voltages are important. This cell is still in the research stages.

3. Lithium alloy–iron sulfide cells are being improved in both lifetime and performance. Full-scale cells are being tested, and multi-kilowatt-hour batteries will be tested in the early 1980s. These systems appear to have the promise of being rugged and capable of thermal cycling.

4. The calcium-silicon–iron disulfide system may offer a lower-cost option to the lithium alloy–iron sulfide cells. This cell is in the early stages of research and development.

5. Overall, the pace-setting problems for high-temperature batteries are materials and materials-related problems. Major problem areas include sulfur- and sulfide-resistant current collectors, corrosion-resistant seals and feed-throughs, rugged solid electrolytes, including lithium ion conductors, and alkali-metal-resistant insulators.

The progress in the research and development of high-temperature rechargeable cells and batteries in the last decade has been remarkably good. There are at least a few systems from which to choose, and, at last, performances and cycle lives greater than those for many, if not all, high-performance ambient temperature systems are being realized. These systems have come a long way. Will they be made available commercially in the next decade? The probability is getting higher!

References

1. E. J. Cairns and R. K. Steunenberg, High-temperature batteries, in *Progress in High Temperature Physics and Chemistry*, Vol. 5, C. A. Rouse, ed., Pergamon, New York (1973), p. 63.
2. Y. Y. Yao and J. T. Kummer, *J. Inorg. Nucl. Chem.* **29**, 2453 (1967).
3. J. T. Kummer and N. Weber, A sodium–sulfur secondary battery, presented at SAE Automotive Engineering Congress, Detroit, Michigan, Preprint No. 670179, January 9–13, 1967.
4. N. K. Gupta and R. P. Tischer, *J. Electrochem. Soc.* **119**, 1033 (1972).
5. F. Ludwig, A review of the kinetics of the sulfur electrode in molten polysulfide, in Proceedings of the Symposium and Workshop on Advanced Battery Research and Design, Argonne National Laboratory Report No. ANL 76-8, March 1976.

6. R. W. Minck, The performance of shaped graphite electrodes in sodium sulfur cells, in Proceedings of the Symposium and Workshop on Advanced Battery Research and Design, Argonne National Laboratory Report No. ANL 76-8, March, 1976.
7. G.E. Review of the Advanced Battery Development Program for Electric Utility Application, May 16, 1979.
8. W. Fischer, H. B. Gels, F. Gross, K. Liemert, and H. Meinhold, Sodium/sulfur batteries for peak power generation, in *Proceedings of the 14th IECEC*, American Chemical Society, Washington, D.C. (1979), p. 710.
9. C. A. Levine, Progress in the development of the hollow fiber Na–S secondary cell, in *Proceedings of the 10th IECEC*, Institute of Electrical and Electronic Engineers, New York (1975), p. 621.
10. J. Werth, Alkali metal-metal chloride battery, U.S. Pat. 3,887,984 (April 15, 1975).
11. J. Werth, Sodium chloride battery development program for load leveling, Research Report 109-2-1 to Electric Power Research Insitute, June 1975.
12. J. Werth, Sodium chloroaluminate battery, in Proceedings of the Symposium and Workshop on Advanced Battery Research and Design, Argonne National Laboratory Report No. ANL 76-8, March 1976, p. B263.
13. G. Mamantov, Studies of high energy cathodes and anodes for molten salt batteries, Progress Report to U.S. Department of Energy, August 1978–July 1979.
14. E. J. Cairns and H. Shimotake, High-temperature batteries, *Science* **164**, 1347 (1969).
15. E. J. Cairns, J. P. Ackerman, P. D. Hunt, and B. S. Tani, The thermodynamics and electrochemistry of the lithium–sulfur cell by EMF and phase equilibration methods, presented at The Electrochemical Society Meeting, Cleveland, Ohio, Abstract No. 48, October 1971; see also Extended Abstracts, p. 118.
16. E. J. Cairns, H. Shimotake, E. C. Gay, M. L. Kyle, and R. K. Steunenberg, Lithium–sulfur secondary cells, presented at the International Society of Electrochemistry Meeting, Stockholm, Sweden, August 28–September 2, 1972.
17. E. S. Buzzelli, Aluminum anode electrical energy storage device, U.S. Patent No. 3,445,288, May 20, 1969.
18. N. P. Yao, L. A. Heredy, and R. C. Saunders, Secondary lithium/sulfur battery, presented at The Electrochemical Society Meeting, Atlantic City, New Jersey, October 1970.
19. S. Lai and L. McCoy, Lithium–silicon electrode, presented at The Electrochemical Society Meeting, Dallas, Texas, October 1975.
20. R. A. Sharma and R. N. Seefurth, Thermodynamic properties of the lithium–silicon system, *J. Electrochem. Soc.* **123**, 1763 (1976).
21. S. K. Preto and M. F. Roche, Electrochemistry of FeS_2, CoS_2 and NiS_2 electrodes in calcium cells, in *Extended Abstracts of The Electrochemical Society Meeting, Los Angeles, California*, The Electrochemical Society, Princeton, New Jersey, October 1979, Vol. 79-2 (1979), p. 391.
22. M. F. Roche, L. E. Ross, C. C. Sy, S. K. Preto, L. G. Bartholme, and P. F. Eshman, High-performance batteries for electric-vehicle propulsion and stationary energy storage, Progress Report for the Period October 1978–March 1979, in Argonne National Laboratory Report ANL 70-39, May 1979, pp. 94–106.
23. P. A. Nelson, D. L. Barney, R. K. Steunenberg, A. A. Chilenskas, E. C. Gay, J. E. Battles, F. Hornstra, W. E. Miller, M. F. Roche, H. Shimotake, R. Hudson, R. J. Rubischko, and S. Sudar, High performance batteries for electric-vehicle propulsion and stationary energy storage, Progress Report for the Period October 1977–September 1978, in Argonne National Laboratory Report ANL 78-94, November 1978.
24. H. Shimotake, W. J. Walsh, E. S. Carr, and L. G. Bartholme, Development of uncharged Li-Al/FeS, cells, in *Proceedings of the 11th IECEC*, Vol. 1, American Institute of Chemical Engineers, New York (1976), p. 473.
25. M. L. Saboungi, C. Bale, P. L. Lin, M. Blander, and A. Pelton, Calculations of phase equilibria for molten salt batteries and fuel cells from fundamental solution theories, in *Extended*

Abstracts of The Electrochemical Society Meeting, Los Angeles, California, October 1979, Vol. 79-2 (1979), Abstract No. 157, p. 405.

26. K. M. Myles, F. C. Mrazek, J. A. Smaga, and J. L. Settle, Materials development in the lithium–aluminum/iron sulfide battery program at Argonne National Laboratory, in Proceedings of the Symposium and Workshop on Advanced Battery Research and Design, March 22–24, 1976, Argonne National Laboratory Report ANL-76-8 (1976), p. B-69.
27. Argonne National Laboratory, Annual DOE Review of the Lithium/Metal Sulfide Battery Program, June 1979.
28. E. J. Zeitner and J. S. Dunning, High performance lithium/iron disulfide cells, in Proceedings of the 13th IECEC, Society of Automotive Engineers, Warrendale, Pennsylvania, 1978, p. 697.

12

Secondary Batteries—Lead–Acid Batteries

D. BERNDT

1. History

The lead–acid battery, which still represents the most important electrochemical system for energy storage, reached a rather high level of technical perfection by the end of the 19th century, when the production of lead–acid batteries was started in factories. Before that, in 1854 J. Sinsteden reported that lead electrodes immersed in diluted sulfuric acid could be used as a coulometer. The first accumulator in fact was developed by Planté in 1859, who applied the repeated charge–discharge procedure which is still used today to produce battery electrodes. The pasted plate which is most common today was patented concurrently by Faure and Volkmar in 1881.

2. General Theory

In principle the lead–acid battery consists of two electrodes immersed into a common electrolyte as shown in Figure 1. The characteristic feature of such a cell is the conversion of electron conduction into electrolytic conduction at the phase boundary electrode–electrolyte. This change in conductivity is

D. BERNDT • VARTA Batterie AG, Forschungs- und Entwicklungszentrum, D-6233 Kelkheim (Taunus), West Germany.

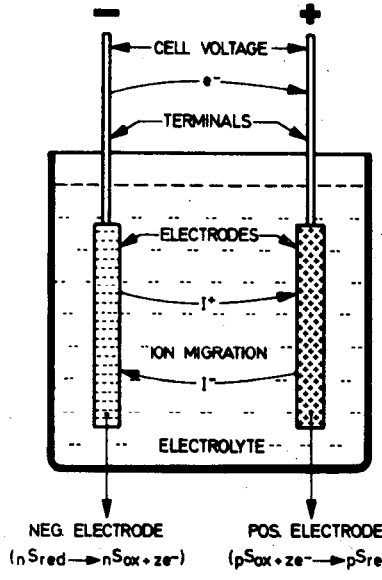

Figure 1. The galvanic cel.

established by the electrochemical reaction, i.e., a chemical reaction combined with the exchange of electric charge. As assumed, for example, in Figure 1, a reduced substance may be oxidized at the left-hand electrode. The electrons liberated in this reaction are consumed by the corresponding reduction reaction at the right-hand electrode. When the outer circuit is closed the electric current flows until one of the substances ${}_nS_{red}$ and ${}_pS_{ox}$ (or both of them) is exhausted.

The electrochemical reactions specify the most important parameters of the cell: the cell voltage determined by chemical affinity of the reacting substances and the capacity defined by the amount of electrode material which can be converted.

2.1. The Basic Electrochemical Reactions

For the lead–acid battery both reactions (shown schematically in Figure 1) are:

positive electrode: (reduction reaction) $$PbO_2 + 3H^+ + HSO_4^- + 2e \rightleftharpoons PbSO_4 + 2H_2O \quad (1a)$$

negative electrode: (oxidation reaction) $$Pb + HSO_4^- \rightleftharpoons PbSO_4 + H^+ + 2e^- \quad (1b)$$

overall reaction: $$Pb + PbO_2 + 2HSO_4^- + 2H^+ \rightleftharpoons 2PbSO_4 + 2H_2O \quad (1)$$

Read from the left to the right (top arrow) Eq. (1) represents the discharge reaction, i.e., lead dioxide is reduced to lead sulfate at the positive electrode, while metallic lead is oxidized at the negative electrode. Reversal of the current reverses Eq. (1) and recharges the cell.

To calculate the equilibrium cell voltage the change in free energy (ΔG) can be used, which is derived as the difference of the standard free energies of the substances involved in the reaction. For Eq. (1) this difference turns out to be

$$\Delta G = -372.5 \text{ kJ/mol} \tag{2}$$

and the standard equilibrium cell voltage (emf) is

$$E_0 = \frac{372.5}{2 \times 96{,}500} = 1.930 \text{ V} \tag{3}$$

On account of the concentration dependence of ΔG the equilibrium cell voltage changes with the concentration or activity of the reacting species except those present in solid state ($a = 1$) according to the Nernst equation:

$$E = E_0 + \frac{RT}{F} \ln \frac{a_{H^+} a_{HSO_4^-}}{a_{H_2O}} \tag{4}$$

E_0 represents the standard equilibrium cell voltage, a the activity (mol/liter).

2.1.1. Dependence of Cell Voltage on Acid Concentration

The dependence of cell voltage on acid concentration is shown in Figure 2. In battery practice the approximation $E = d + 0.84$ (d is density in g/cm^3) is often used. This dependence on acid concentration is a disadvantage of the

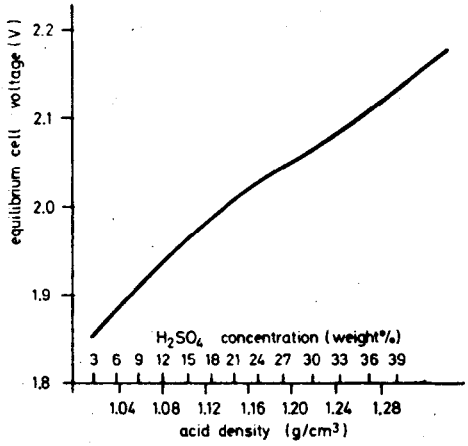

Figure 2. Equilibrium cell voltage of the lead–acid battery versus acid concentration and density (25°C). (For the meanings of the terms *density* and *specific gravity*, see Vinal (1955), pp. 120ff.)

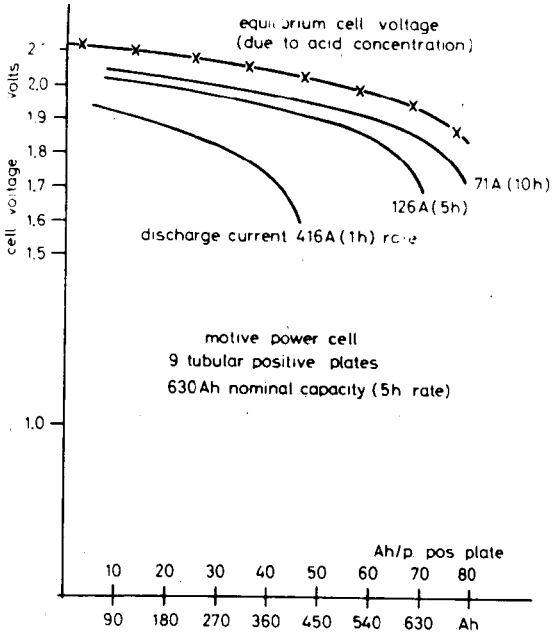

Figure 3. Discharge curves of a motive power battery at different discharge rates compared to the equilibrium cell voltage, which is changing with the state of charge due to decrease of acid concentration

lead–acid system because the H_2SO_4 consumption during discharge [Eq. (1)] causes a decrease of cell voltage, even though the load is extremely low. This can be seen in Figure 3, where the top curve shows the decrease of equilibrium cell voltage with discharge for a commercial motive power cell. To minimize this effect, stationary batteries are often provided with a large quantity of excess acid, which is not possible for motive power batteries because of the extra weight and volume.

2.1.2. The Heat of Reaction

The electrochemical reaction [Eq. (1)] is combined with heat exchange. The fundamental equation is

$$\Delta G = \Delta H - T\Delta S \tag{5}$$

where ΔG represents the already mentioned change in free reaction energy, while ΔH and ΔS are the changes in heat energy and entropy, respectively. $T\Delta S$ indicates the amount of heat absorbed or liberated by Eq. (1).

Since $\Delta H = -360.1$ kJ/mol, the heat of reaction comes to

$$T\Delta S = 12.4 \text{ kJ/mol} \qquad (T = 25°C) \tag{6}$$

or, referred to the free energy ΔG of the reaction

$$\frac{T\Delta S}{\Delta G} = -3.3\% \tag{7}$$

Thus about 3% of the energy produced by reaction (1) is converted into heat. The negative sign in Eq. (7) means that heat is absorbed, when the discharge takes place (ΔG negative), and that the same amount of heat is liberated during charge. On the whole this heat of reaction is rather small and always covered up by irreversible heat production, especially during discharge, when theoretically a cooling effect should be observed [cf. Eq. (13)].

2.1.3. The Power–Weight Ratio

The power–weight ratio of the lead–acid battery can be estimated starting with Eq. (1). The weights of the species involved amount to 642.4 g, while the converted electric energy [Eqs. (1a), (1b)] comes to $2 \times F = 53.61$ Ah. Using the equilibrium cell voltage 1.930 V [a hypothetical figure in this case, because E_0 in Eq. (3) is based on the assumption that the activities of the reacting species are 1 mol/liter, which of course is not true in pure H_2SO_4], the theoretical power–weight ratio is

$$\frac{(53.61)(1.930)}{0.6424} = 161 \text{ Wh/kg} \tag{8}$$

In practice only one quarter of this can be attained. To explain this great difference between theory and practice the proportionate weights of the different construction elements are compiled in Figure 4. The scale on the left shows the weights which are needed per kWh, while the reciprocal numbers (Wh/kg) are plotted on the right.

The bottom block in Figure 4 contains Eq. (1), which leads to the figure calculated in Eq. (8), which means that a weight of 6 kg would be able to store 1 kWh. However, pure H_2SO_4 is not an electrolyte; the acid has to be diluted to achieve adequate conductivity. Furthermore there must be some excess of acid to keep conductivity even when the battery becomes discharged completely. Therefore the pure electrochemical system provided with the correct acid requires 11.5 kg/kWh. Additional weight is caused by the fact that only a fraction of the active material can be utilized. At extremely low discharge rates mass utilization may be increased to about 70%, but at the usual rates (on the order of magnitude of hours), this figure decreases to about 35%, reducing the available power–weight ratio to nearly 50 Wh/kg. The limited mass utilization is comprehensible when it is kept in mind that chemical reactions occur at the

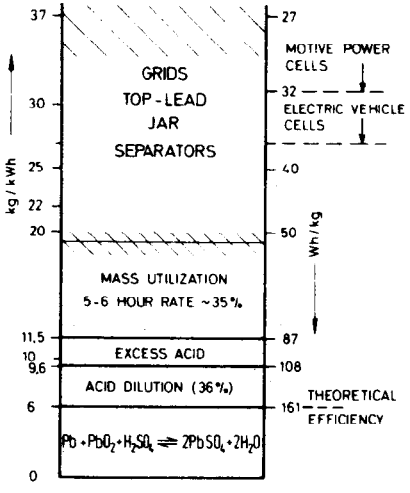

Figure 4. Weight contributions of the different construction elements (example: motive power cell).

electrode. During discharge, e.g., lead is dissolved at the negative electrode and lead sulfate precipitated, while at the positive electrode PbO_2 is reduced and dissolved Pb^{+2} ions give rise to lead sulfate precipitation. These reactions produce isolating layers on the active material which prevent further discharge. Furthermore dismantling of charged material by inhomogeneous attack will reduce the electric contact between parts of the active material and the grid, also restricting further discharge.

In addition to the facts discussed up to now, much extra weight is added by passive construction elements which are unavoidable in the actual lead–acid cell. So the grids supporting the active material and conducting the current usually contribute nearly as much weight as the active material itself does. But the acidic environment and corrosive potentials exclude the substitution by lightweight metals. The same is true for the so-called top lead, i.e., the conducting bars on top of the plates and terminals. Finally, the cell has to have a jar which (as well as the isolating separators between the plates) does increase the weight.

Therefore, in practice, even cells for electric vehicles, which are developed especially for low weight, deliver less than 40 Wh/kg and (as can be seen in Figure 4) little margin is left for further increase.

2.2. Discharge Performance

When current is drawn, the cell voltage is influenced by additional parameters. Limited rates of electrochemical or diffusion processes cause displacement of cell voltage, called overvoltage E_η; furthermore a voltage drop

due to the ohmic resistance R_i of the cell is also present. Thus when current flows the cell voltage is described by

$$E(i) = E_0 - E_\eta - i \cdot R_i \tag{9}$$

In practice it is difficult to distinguish overvoltage from ohmic voltage drop; therefore both terms in Eq. (9) usually are combined and called polarization (E_P); thus

$$E(i) = E_0 - E_P \tag{10}$$

The discharge curves in Figure 3 illustrate the influence of current on discharge performance. The capacity of a lead–acid cell is determined by a specified end-of-discharge voltage. The capacity, therefore, is not a constant value and the nominal capacity is valid only for a specified discharge rate (see, e.g., the 5-hr rate in Figure 3). Standardized rates have been set, e.g., 6- and 5-hr rates for motive power batteries, 8- and 10-hr rates for stationary batteries in the U.S.A. and Europe, respectively.

Both polarization and internal resistance change with temperature. Therefore discharge voltage and capacity also depend on temperature. The empirical equation for capacity is

$$\text{Corrected capacity (25°C)} = \frac{\text{actual capacity } (T°\text{C})}{1 + a(T - 25)} \tag{11}$$

The temperature coefficient a for different standards and cell types is between 0.0045 and 0.008 per °C.

The heat released during discharge is described:

$$W = -T\Delta S + i^2Rt + iE_\eta t = -T\Delta S + iE_P t \tag{12}$$

(t is time of discharge).

The heat of reaction was mentioned above [Eqs. (6) and (7)]. The second term in Eq. (12) usually exceeds $T\Delta S$ and the cell temperature is increased upon discharge as well as charge, e.g., the temperature rise for a motive power cell during a 5-hr discharge is on the order of 5–10°C, while an 8-hr charge raises the temperature of the cell by about 8–12°C, depending on the amount of heat carried away.

2.3. Charging Performance

Reversal of reaction (1) in principle describes the charging process. However, the following side reactions emerge during charge more and more until at the end of the charging process water decomposition consumes the current completely.

Oxygen evolution at the positive electrode:

$$H_2O \rightarrow H_2 + \tfrac{1}{2}O_2 \tag{13a}$$

Hydrogen evolution at the negative electrode:

$$2H^+ + 2e \rightarrow H_2 \qquad (13b)$$

Together,

$$H_2O \rightarrow \tfrac{1}{2}O_2 + 2H^+ + 2e \qquad (E_0 = 1.23\ V) \qquad (13)$$

As marked by the dotted areas in Figure 5 gas evolution is favored by the position of equilibrium potentials. However, the rates of both hydrogen and oxygen evolution are very slow at lead and lead oxide, respectively, and therefore gas evolution according to Eqs. (13a) and (13b) accompanied by simultaneous discharge [Eqs. (1a) and (1b)] is very slow during discharge or open circuit (self-discharge). During the charging process, however, especially when a constant current is impressed on the cell, the electrode potentials are raised, whereupon gas evolution becomes favored. Finally, when the rechargeable material is exhausted, Eq. (13) remains only.

As can be seen in Figure 5 the potential of the positive electrode increases from the very beginning of the charging process, which indicates that oxygen evolution accompanies the entire recharging process. The negative electrode, on the contrary, accepts charge during the first stage nearly completely until a sudden step in the charging curve signifies the beginning of hydrogen evolution.

In any case, the side reactions (13a) and (13b) reduce the efficiency of the accumulator and cause water loss [Eq. (13)]. In view of these facts it is important to know that the hydrogen overvoltage at the negative electrode can be reduced by many substances, which would cause an increase of gassing. Most effective are well-known catalysts like platinum or palladium, which therefore have to be carefully excluded from lead–acid cells. Well known is the

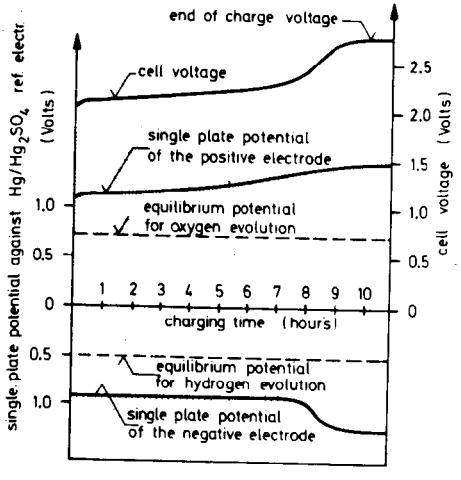

Figure 5. Single-plate potential and cell voltage during charge. Dotted areas: gas evolution favored by thermodynamics.

disadvantageous effect of antimony, which still is the preferred alloying element for battery grids, especially in motive power batteries submitted to extensive charge–discharge cycling. For low-maintenance batteries special alloys are selected which reduce or avoid antimony addition.

3. The Actual Appearance of Lead–Acid Batteries

Although lead–acid batteries always have the same design in principle, specific demands for different applications have resulted in a multitude of types. Within the scope of this chapter only a few examples can be described to gain a superficial insight.

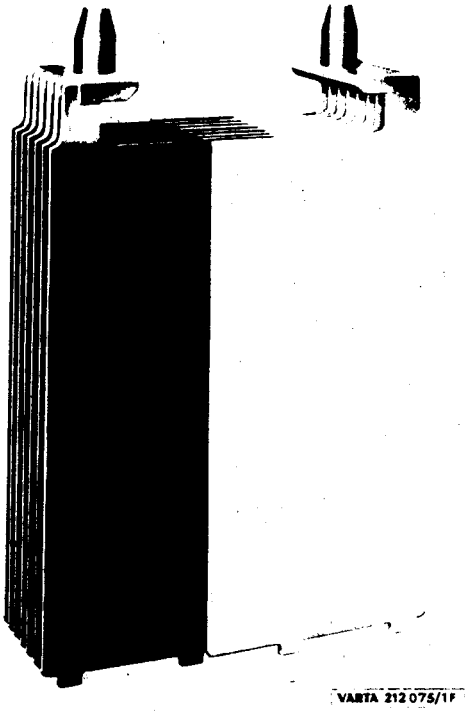

Figure 6. Plate assembly (without separators) with connecting bars and terminal posts (pasted grid plates).

3.1. Electrode Designs

All kinds of electrodes have been designed to gain a large surface area for the active material combined with high electric conductivity. The Planté-type plate consists of pure lead cast with fine lamellas to increase the geometric surface area. Lead dioxide as an active material is produced by electrochemical oxidation of a thin surface layer. The most common are pasted plates consisting of a grid (of lead or lead alloy) filled with a paste of porous active material (Pb; PbO_2). This grid can be recognized in Figure 6, which shows an assembly of positive and negative plates. The grid may be manufactured by casting, punching or expanding. For improvement of mechanical strength, alloys (e.g., Pb–Sb; Pb–Ca) are used. A section of a tubular plate (positives only) is shown in Figure 7. The grid in this case is represented by vertical rods (spines) surrounded by the active material. A tube of fabrics retains the active material, which therefore can be rather porous to provide high utilization. In most cells

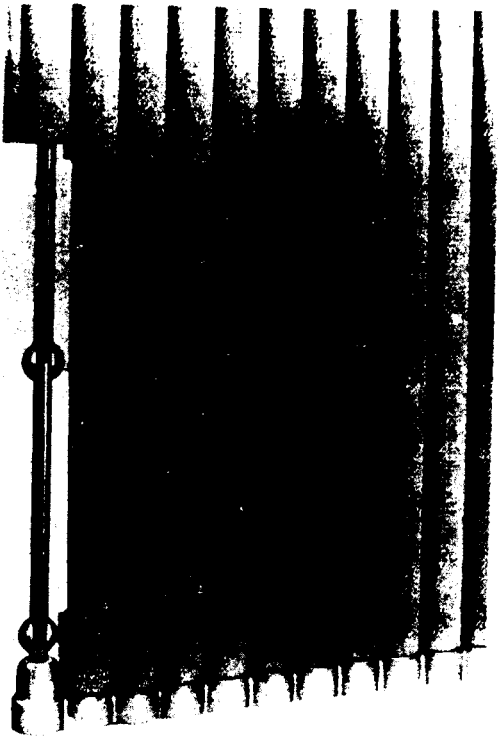

Figure 7. Cut of a tubular plate.

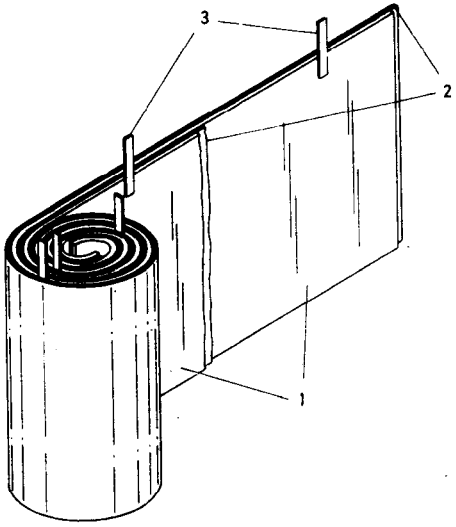

Figure 8. Wound-up electrode assembly. 1, Electrodes; 2, separators; 3, current connectors.

the plates are assembled as shown in Figure 6 (cf. Figures 9–11). Very thin electrodes may be wound up combined with the separators to form cylindric cells as shown in Figure 8.

3.2. Design of Cells and Batteries

In addition to the described electrodes, electrochemical passive parts are needed to form a complete cell. Porous sheets of plastics or rubber, the separators, are used to avoid short circuits between the narrowly spaced plates (even for tubular plates as can be seen in Figure 10).

The so-called "top lead" which mainly consists of lead bars connecting the plates and the terminal posts, can be seen in Figures 6, 9, and 11. Figure 9 represents a stationary battery, which may be used as a standby battery for telephone systems, power stations, or emergency lights to provide electric current in case the mains break down. These batteries usually are joined with the electric circuit in parallel connection, therefore nearly always a (very low) overcharge (2.15–2.25 V/cell) is impressed. As mentioned above, water consumption may be reduced by using grid alloys containing no or extremely small amounts of antimony.

The cut section of Figure 9 shows negative and positive grid and a separator in between them. In the foreground a specially formed plastic body keeps the distance to the wall and defines the pressure of the plate assembly. The jar in this case consists of very rigid (usually transparent) plastics, because these batteries are usually installed without any support.

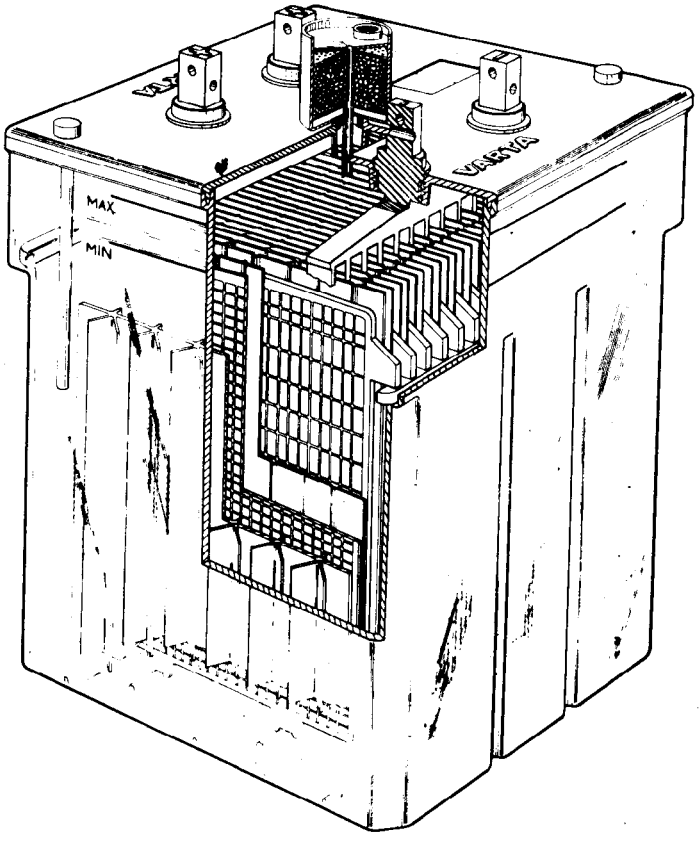

Figure 9. Stationary cell (1680-Ah nominal capacity).

Since the lifetime of stationary batteries is expected to be very high, the positive plates hang on special beams on the wall (Figure 9) to neutralize grid-growing effects.

The connecting bars and terminal posts can also be seen in Figure 9. To achieve sufficient high rate performance, two terminal posts are used in parallel.

A special vent furnished with a filling funnel protects the cell against fire hazards caused mainly by electrostatic discharges, e.g., when waiting personel touch parts of the battery and the hydrogen–oxygen mixture inside the cell ignites.

The motive power cell used for driving forklifts, electric tractors, and other vehicles is built much more compactly (Figure 10), because the stored energy

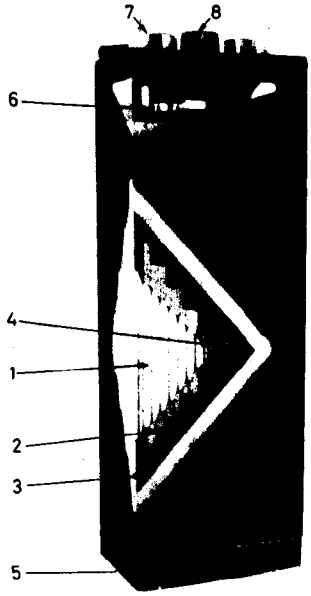

Figure 10. Motive power cell (tubular positive plates). 1, Positive plate; 2, separator; 3, part of negative plate; 4, part of negative grid; 5, plate support; 6, connecting bar; 7, terminal post; 8, vent plug (occasionally outfitted with a water refilling system).

per volume is the most important figure. The example shown in Figure 10 is equipped with tubular positive plates. Positive as well as negative plates rest on special supports at the bottom. The jar is usually made of polyolefin yielding rather low wall thickness. Mechanical support therefore is necessary, which is achieved by a tray made of steel or resin.

An automotive or SLI battery (starting, lighting, and ignition of motorcars) is shown in Figure 11. The construction principle of including the whole

Figure 11. SLI battery: six cells included in one jar (12V/36 Ah).

battery in one jar is applied for smaller types of stationary and motive power cells too. The very short connections between adjacent cells contribute to a very low internal resistance, which is needed for achieving the high cranking power for car engines (even at low temperatures). This starting requirement is the reason for using extremely thin plates and a very low distance between them. When the car is running, the battery is charged by the generator with constant voltage.

Selected Reading: *Studies on Lead–Acid Batteries*

C. Drotschmann, *Bleiakkumulatoren*, Verlag Chemie, Weinheim (1951).
G. W. Vinal, *Storage Batteries*, 4th ed., Wiley, New York (1955).
W. Garten, *Bleiakkumulatoren*, VDI-Verlag, Düsseldorf (1974).
H. Bode, *Lead Acid Batteries*, Wiley, New York (1977).
K. V. Kordesch, *Batteries*, Vol. 2, Marcel Dekker, New York (1977).
Journal of Power Sources 2, Special Issue: Lead Acid Batteries (comprehensive collection of data), D. H. Collins, ed., Elsevier Sequoia S.A., Lausanne (1977/1978).

13

Secondary Batteries—Nickel–Cadmium Battery

FERDINAND VON STURM

1. Introduction

In nickel–cadmium batteries, the energy is stored as the reaction enthalpy of the couple Cd and NiOOH. During current generation, i.e., during the discharging phase, the following overall chemical reaction takes place:

$$Cd \quad 2NiOOH + 2H_2O \rightarrow Cd(OH)_2 + 2Ni(OH)_2$$

In the idealized case, the total "free enthalpy of reaction" is released as electrical energy.

The given reaction can be reversed by passing electrical energy into the system. This occurs during the charging phase.

The active components of individual nickel–cadmium cells are outlined in Figure 1. The negative and the positive electrodes contain cadmium and nickel(III)-oxyhydroxide, respectively, as the active masses. The electrodes are interconnected over an aqueous, alkaline electrolyte.

Nickel–cadmium cells are classified as alkaline accumulators, which were developed considerably later than the lead–acid battery. The motive of the efforts of Edison and Jungner starting at about 1890 was the search for sturdy storage cells which would be suitable for electrical vehicles. Thus Edison

FERDINAND VON STURM • Sigri Elektrographit GmbH, D-8901 Meitingen, Federal Republic of Germany.

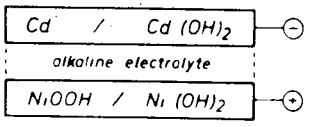

Figure 1. Set-up of the nickel-cadmium cell.

invented the Fe–Ni system, while Jungner came up with the Ni–Cd system. There were great hopes at that time that the electric motor could even compete with the internal combustion engine as a propulsion unit for motor vehicles.

Though the idea of electrical propulsion has been revived today and extensive developments have been made in several countries, the Ni–Cd system is not seriously discussed in this context. Availability and costs of materials rule out such a broad application.

However, the Ni–Cd system is invariably preferred where such qualities as mechanical rigidity, good low-temperature behavior, high-rate discharge, and simple handling are desired. A special impact was made by the sealed version, which was based on the initial work of Neumann[12] in Germany.

In this contribution, a treatment of thermodynamics and kinetics will be followed by a description of the preparation of materials and the construction of different types of electrodes and cells, as well as a discussion of their technical performance and application.

In the list of references, summarizing articles and monographs are mentioned first[1-11] and the original publications are cited subsequently.[12-33] The list represents a selection without appraisal and should facilitate access to the specific work.

2. Thermodynamics and Kinetics

The electrochemical process of a cell can be divided into partial reactions occurring at the cathode and the anode; together they lead to the net reaction. Standard potentials and standard enthalpies resulting from thermodynamic data or electrochemical measurements can be assigned to the net reaction and the partial reactions as well:

Cathodic partial reaction

$$2\beta\text{-Ni(OH)}_2 + 2\text{OH} \rightleftharpoons 2\beta\text{-NiOOH} + 2\text{H}_2\text{O} + 2e\ , \qquad E_0 = +0.490\ \text{V} \quad (1)$$

Anodic partial reaction

$$\text{Cd} + 2\text{OH} \rightleftharpoons \text{Cd(OH)}_2 + 2e\ , \qquad E_0 = -0.809\ \text{V} \quad (2)$$

Cell reaction

$$2\beta\text{-NiOOH} + Cd + 2H_2O \rightleftharpoons 2Ni(OH)_2 + Cd(OH)_2 \quad (3)$$

$$\Delta G_0 = \Delta H_0 - T\Delta S_0$$
$$= -276\ \text{kJ/mol} + (298\ \text{K})(0.093\ \text{kJ/mol K}) \quad (4)$$
$$= -248\ \text{kJ/mol}$$

Using the thermodynamic relation

$$E_0 = -\frac{\Delta G_0}{nF} \quad (5)$$

under standard conditions, i.e., at 25°C and an activity of 1 for all reactants participating in the reaction, an equilibrium voltage E_0 of 1.299 V is obtained:

$$E_0 = \frac{248\ \text{kJ/mol}}{2 \times 96{,}500\ \text{Asec/mol}} = 1.299\ \text{V}$$

In the following cell arrangement,

$$(-)\ Cd|Cd(OH)_2\|\text{electrolyte}\|Ni(OH)_2|\text{NiOOH}\ (+)$$

the sign of E_0 corresponds to that of the right electrode, i.e., the nickel electrode.

The influence of temperature can be derived from the thermodynamic relation

$$\left(\frac{d\Delta G}{dT}\right)_P = -nF\left(\frac{dE}{dT}\right)_P = -\Delta S$$

Since, ΔS is negative, the temperature coefficient of the cell voltage is also negative:

$$\left(\frac{dE}{dT}\right)_P = -0.5\ \text{mV/K}$$

The influence of the activities, a, for the substance i on the free enthalpy of reaction ΔG and the cell voltage E can be obtained from the equations

$$\Delta G = \Delta G_0 + RT\sum \nu_i \ln a_i$$

$$E = E_0 - \frac{RT}{nF}\sum \nu_i \ln a_i$$

Based on these data, the charge and energy contents can be derived as 162 Ah/kg [289 Ah/kg $Ni(OH)_2$ and 477 Ah/kg Cd] and 209 Wh/kg. The calculations are based on the idealized reactions of Eqs. (1)–(3).

However, these values are not attainable in practice for two reasons. First, Eqs. (1)–(3) are idealized models, and the calculated cell voltage E is valid only for the equilibrium state; as soon as current is drawn from the cell, the resulting

energy conversion will be accompanied by irreversible components which reduce the cell voltage and the efficiency. Second, the cell contains, in addition to the reactive partners, a number of materials such as solvents, electrolytes, separators, current collectors, and container materials which are equally necessary for its operation. Therefore more moderate values in the range 8–28 Ah/kg and 10–35 Wh/kg are achieved in practical cells and batteries. These values, however, can stand comparison with other storage systems (see, e.g., Section 4.5 of this chapter).

When the electrodes are loaded with current, a deviation from the thermodynamically calculated potential is observed due to the effect of electrolyte resistance and the polarization loss at the electrode–electrolyte interface. But even under zero current state the degree of oxidation of hydroxides, such as nickel hydroxide, is often undefined. During the precipitation of nickel hydroxide from nickel salt solutions, α-$Ni(OH)_2$ is initially formed which is unstable in potassium hydroxide. It contains a hexagonal layer lattice in which the individual nickel hydroxide layers are separated by intermediate layers occupied with water molecules. Thus, for each $Ni(OH)_2$, there are up to 0.55 water molecules which are firmly anchored in the crystal.[13]

Owing to water loss and aging, it is ultimately converted into the stable β-$Ni(OH)_2$ with a brucite structure. The anodic oxidation of this compound leads to β-NiOOH.[14–18] Besides the β-NiOOH mentioned in Eq. (1), at higher charging higher oxidized forms are obtained, e.g.,

$$[4NiO_2 \cdot 2NiOOH]\,[2H_2O \cdot 2OH^- \cdot 2K^+]$$

main layer — intermediate layer

with the nickel having an average oxidation number of 3.67. Compared with the data given in Eq. (1), the electrode potential of this material is shifted by more than 100 mV in the positive direction. Also, the inclusion of electrolyte in the lattice leads to volume displacements between electrolyte and active mass.

Oxygen exchange is not involved during the charging cycles but the redox reaction proceeds via the exchange of H^+ and e^-, as can be expressed for α- and β-nickel hydroxide in an idealized manner:

$$Ni(OH)_2 + H_2O \underset{+H^+ + e \text{ (discharge)}}{\overset{-H^+ - e \text{ (charge)}}{\rightleftharpoons}} Ni(OH)_2OH \rightleftharpoons NiOOH + H_2O$$

β-(II)-nickel hydroxide — β-(III)-nickel oxyhydroxide

$$[6Ni(OH)_2] \cdot [4H_2O] + 2KOH \underset{+10H^+ + 10e \text{ (discharge)}}{\overset{-10H^+ - 10e \text{ (charge)}}{\rightleftharpoons}} [4NiO_2 \cdot NiOOH][2H_2O, 2KOH] + 2H_2O$$

α-(II)-nickel hydroxide — γ-nickel oxyhydroxide

LiOH additives to the electrolyte allow a higher degree of oxidation of nickel hydroxide, probably by increasing the O_2 overvoltage at the material with occluded Li^+.[19,20] On the contrary, higher Li concentrations, lead to passivation by forming a phase having the crystal structure of $LiNiO_2$.[19,21,22]

Losses in the voltage efficiency of the Ni–Cd cell (Section 4.5) are essentially caused by the nickel hydroxide electrode; even at very low loadings, the charging voltage is around 100 mV higher than the discharging voltage.

The anodic oxidation of cadmium has been investigated preferably at flat electrodes. Before the passivation sets in Cd^{2+} ions in alkaline medium go into solution as hydroxyl complex, $[Cd(OH)_4]^{2-}$.[16,23,24] The first step will be the adsorption of an OH radical[24]:

$$Cd_s + OH^- \rightarrow Cd_s - OH_{ads} + e^-$$

β-$Cd(OH)_2$ is precipitated when the solution in the interfacial layer is supersaturated. There is also some evidence for γ-$Cd(OH)_2$ formation.

The soluble complex $[Cd(OH)_4]^{2-}$ is initially formed in porous electrodes during discharging. Progressive oxidation results in precipitation of the hydroxide and to an increasing blockade of the active surface area.[23,25] The concurrently occurring rise in polarization inside the porous system may eventually lead to a direct formation of $Cd(OH)_2$ and at a further stage to oxygen evolution.

The cathodic reaction during the charging process can be assumed to proceed over the solution phase:

$$[Cd(OH)_4]^{2-} + 2e^- \rightarrow Cd + 4OH^-$$

3. Materials, Electrodes, and Cells

3.1. Materials

3.1.1. Negative Active Mass

In vented cells, besides cadmium, Fe (25–40 wt %) or Ni (6–8 wt %) are frequently admixed to CdO or $Cd(OH)_2$ in order to counteract the recrystallization of Cd. Iron, however, favors H_2 evolution; thus it is of no use for sealed cells.

3.1.2. Positive Active Mass

Nickel(II) hydroxide is gained by precipitation from Ni-sulfate or Ni-nitrate solution with sodium hydroxide. Additives of cobalt nitrate to the solution enable one to stabilize the capacity at higher temperatures through formation of a mixed crystal. The antipolar mass, $Cd(OH)_2$ (~20%), is admixed before insertion into the sealed cells.

3.1.3. Electrolyte

Potassium hydroxide in the concentration range 3.8–7.2 mol/liter (corresponding to 18–31 wt % or a density of 1.17–1.30 g/cm^3) has prevailed exclusively as the electrolyte. The conductivity is at a maximum with a 27 wt % concentration at 25°C and amounts to 0.62 Ω^{-1} cm^{-1}. In cells with positive tubular and pocket electrodes, the addition of LiOH improves the cycle life, especially at elevated operating temperatures.

3.1.4. Passive Material

In sealed cells, polyamide and polypropylene are mostly used as the material for grids and textures to act as spacers, and in the form of nonwoven fabrics (fleeces) to act as an electrolyte matrix. The structure and housing materials consist of nickel or nickel-plated steel. Even cell containers made of polyamide have been used.

3.2. Electrode Types

A high specific interface between the active material and the electrolyte phase is desired to obtain a high current loading during charging and discharging. At the same time, care has to be taken to maintain good electronic contact with the current-collecting structure in the electrodes. A series of practical solutions has emerged from the efforts to match the structural specifications of electrodes. Tests with nickel foam as structural material and with organic binders[26] are under progress. All attempts are concentrated in realizing a long-life, high-load, low-cost nickel electrode.

3.2.1. Pressed Electrodes

Powdery active material is pressed into tablets or cylinders. A conducting material such as graphite can be admixed to improve the electrical contact. The pressed materials are often enclosed between nickel screens.

3.2.2. Tubular Electrodes

Edison used this sturdy type of electrode in which the active material is filled in tubes made of perforated, nickel-plated steel ribbons. The individual tubes have a diameter of 7–8 mm and are welded together to form larger electrode areas as shown in Figure 2. In the case of poorly conducting nickel hydroxide, nickel flakes are added that are galvanically produced and have a thickness of about 1 μm. The supporting structure is subjected to heavy mechanical stresses created by the great volume changes occurring during the exchange of charge. The stability can be ensured, however, by mounting steel rings around the tubes.

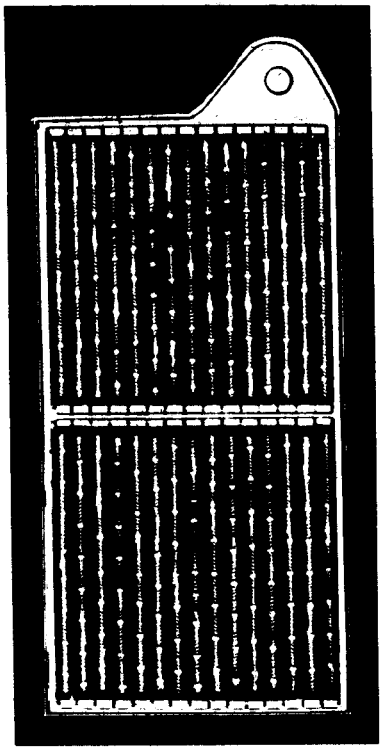

Figure 2. Tubular electrode filled with nickel hydroxide.

3.2.3. Pocket Electrodes

Electrodes as sturdy as the tubular type can also be prepared by incorporating the active mass in the hollow space between two perforated sheets. This type is found both on the cadmium side and on the nickel side. In this case, very coarse and open structures are adequate as spacers between the electrodes; the resistance in the electrolyte space is only slightly increased by them.

Stacks of nickel and cadmium electrodes of the pocket type are shown in Figure 3.

3.2.4. Sintered Electrodes

The shielding of active material by means of the encasing foil used in tubular and pocket electrodes proves to be particularly disadvantageous at a high current loading. This can be considerably improved by incorporating the

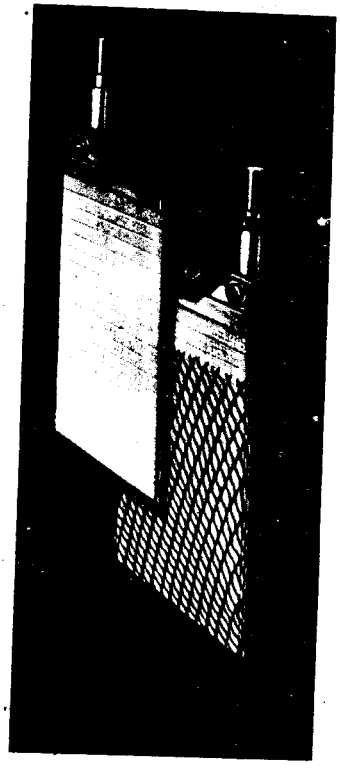

Figure 3. Stacks of pocket electrodes. (Left) Nickel hydroxide electrodes, (right) cadmium electrodes and separator net.

reactive materials in a sintered body of carbonyl nickel. The volume porosity is adjusted to approximately 80%. Thin supporting bodies can be stabilized by sintered, perforated metal ribbons.

In order to load the supporting body, it is soaked with nickel or cadmium nitrate solution, dried, and then immersed in potassium hydroxide solution to precipitate the hydroxide. The last stage of preparation can also be replaced by polarizing the electrodes cathodically[27,28]; owing to the diffusion limited mass transfer between the external electrolyte and the porous system, the pH value increases until the hydroxide is precipitated.

3.3. Cell Types

3.3.1. Vented Cells

In the past few years, development of Ni–Cd cells has been directed toward a large number of specific applications, leading to a correspondingly colorful palette of cell types.

Table 1
Capacity and Weight for Different Cell Types

Cell type	Electrode type	Capacity, Ah	Nominal discharge voltage, V	Cell weight, kg
Vented				
High-rate plastic container	Pocket	8.5 (nominal)	1.25	1.0
Low-rate steel container	Pocket	1090 (nominal)	1.25	54.0
High-rate nylon container	Sintered	80 (at 5-hr rate)	1.25	3.010
High-capacity nylon container	Sintered	230 (at 5-hr rate)	1.22	9.070
Sealed				
Button	Pocket	0.02 (at 10-hr rate)	1.22	0.0011
Cylindrical	Pocket	2.0 (at 10-hr rate)	1.22	0.170
Rectangular	Pocket	23 (at 10-hr rate)	1.22	1.390
Button	Sintered	0.04 (at 1-hr rate)	1.2	0.0035
		0.30 (at 1-hr rate)	1.2	0.018
Cylindrical	Sintered	1.8 (at 10-hr rate)	1.24	0.065
Rectangular	Sintered	15 (at 10-hr rate)	1.24	0.780

Table 1 denotes the Ah range in which cells of different types are available today.

The following types can be distinguished according to the constructive design:

Plate Cells. They are constructed on the lines of the lead–acid battery. Coarse plastic screens serve adequately as spacers where tubular and pocket electrodes are used. Thin sintered electrodes are separated by intermediate layers of nonwoven fabrics (fleeces).

Cylindrical Cells. These cells are formed from rod-shaped, pressed electrodes or coiled sintered electrodes as shown in Figure 4. This design is often selected for the sealed type which will be described in a special section.

Button Cells. Button cells are constructed from pressed or sintered electrodes as shown in Figure 5. They can be easily stacked to form a battery.

3.3.2. Sealed Cells

Attempts were made quite early to make secondary cells as maintenance free as primary cells. Thus T. A. Edison[29] had a patent granted which covered

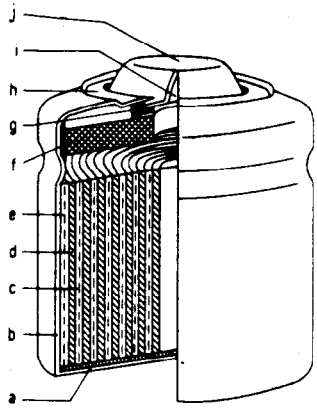

Figure 4. Cylindrical cell with coiled electrodes. (a) Bottom insulator, (b) case, (c) positive electrode, (d) separator, (e) negative electrode, (f) spacer ring, (g) gasket ring, (h) cell cap, (i) insulating disk; (j) pressure control (from Reference 5).

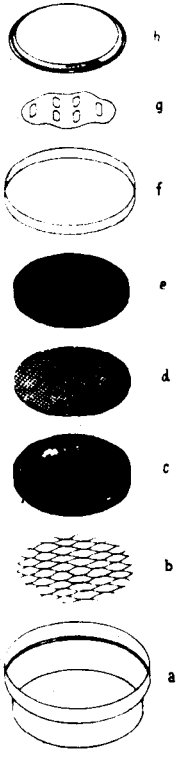

Figure 5. Exploded view of a button cell constructed for a capacity up to 3 Ah. (a) Can, (b) expanded metal spacer, (c) screen-wrapped positive electrode, (d) separator, (e) screen-wrapped negative electrode, (f) insulating and gasket ring, (g) contact spring, (h) cover (from Reference 5).

the catalytic combustion of gases that are liberated inside the cell upon charging.

The concealed objective behind the search over the decades was to develop a sealed accumulator that could be utilized in any position without spilling the aggressive electrolyte, without leakage of vapor and without any maintenance, especially the refilling of distilled water.

After the plate sintered from nickel powder had lead to a boom in production of the nickel–cadmium accumulator around 1940, a few years later a German research group had succeeded in sealing this system according to the initial patents of Dassler and co-workers[30,31] Peters,[32] and Neumann.[12]

The task imposed was to prevent the formation of an explosive gas mixture (oxyhydrogen gas) under all working conditions, because otherwise this gas would burst the sealed cell. This was achieved by an excess of the uncharged negative material $Cd(OH)_2$. During the charging process, oxygen will be evolved at the positive electrode before the negative material is completely reduced at the counterelectrode. If the electrolyte matrix is provided in such a manner that it not only contains the electrolyte-filled fine pores but also free coarse pores, oxygen can find its way through these pores to the cadmium electrode where it will be reduced; the oxygen transfer is indicated by the arrow in Figure 6. Thus under overloading there will be no net change in the chemical composition inside the cell: the oxygen evolved at the positive electrode will be consumed at the negative electrode.

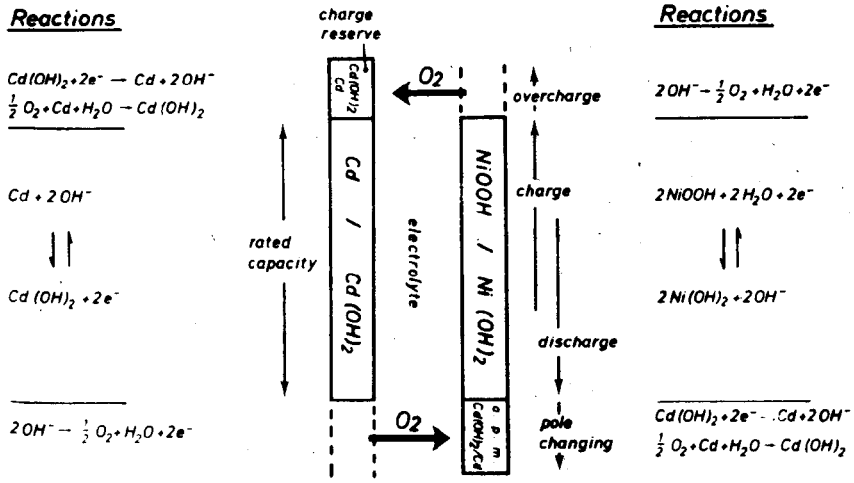

Figure 6. Reactions and oxygen flux in a sealed nickel–cadmium cell under normal and extreme conditions of operation.

The prevention of a pressure rise during overcharging is not the only concern. There is also a risk of excessive gas formation during deep discharge by pole changing. Owing to manufacturing deviations, not all cells have exactly the same storage capacity. In the cells connected in series, explosive oxyhydrogen gas can appear when the weakest cell undergoes a pole change after a total discharge of its capacity. Such an event will be accompanied by decomposition of the electrolyte. This difficulty was surmounted by introducing an "antipolar mass." In the types common today, $Cd(OH)_2$ is added to the nickel electrode to such an extent that unreduced $Cd(OH)_2$ still remains in the positive electrode even when cadmium in the negative electrode is completely oxidized. H_2 evolution is thus prevented. When the oxygen pressure exceeds a limiting value it can react again electrochemically at the Cd electrode, but this time at the cadmium of the antipolar mass.

The O_2 flow at overloading and at deep discharge with pole changing is schematically represented in Figure 6. The areas assigned to the electrodes depict their charge content

Several thousand cycles are possible at a 25% discharge, and still several hundred at a 75% discharge.

A cell which is maintenance free and independent of position is designed according to the button, cylindrical, or rectangular cell type as described in Table 1 and in Figure 7. In larger cells, electrodes with a sintered nickel skeleton in which the active mass is precipitated are prevailing more and more.

The capacities of sealed cells fabricated since 1953 range at present from 4 mAh up to about 50 Ah. The upper limit is given by the heat evolution during the O_2 reduction which leads to an additional pressure rise. Since the heat-radiating surface does not increase as rapidly as the capacity, which is almost proportional to the volume, the charging and discharging current must be brought into the correct relation to the electrode area and the capacity.

4. Technical Performance

4.1. Charge–Discharge Characteristic

The course of the cell voltage during charging and discharging is illustrated in Figure 8.

Charging can take place either at a constant current or at a constant or modified potential. The onset of H_2 and O_2 evolution is indicated by the jump in cell voltage from 1.4 to 1.7 V. Sealed cells with sintered plate electrodes can be fast charged within less than an hour.[11,33]

The usual discharging process lasts from 3 to 10 hr. Discharging should be terminated at 1.1–1.0 V. The working temperature in the cell should not exceed 45°C.

According to the thermodynamic treatment, the entropy of reaction for

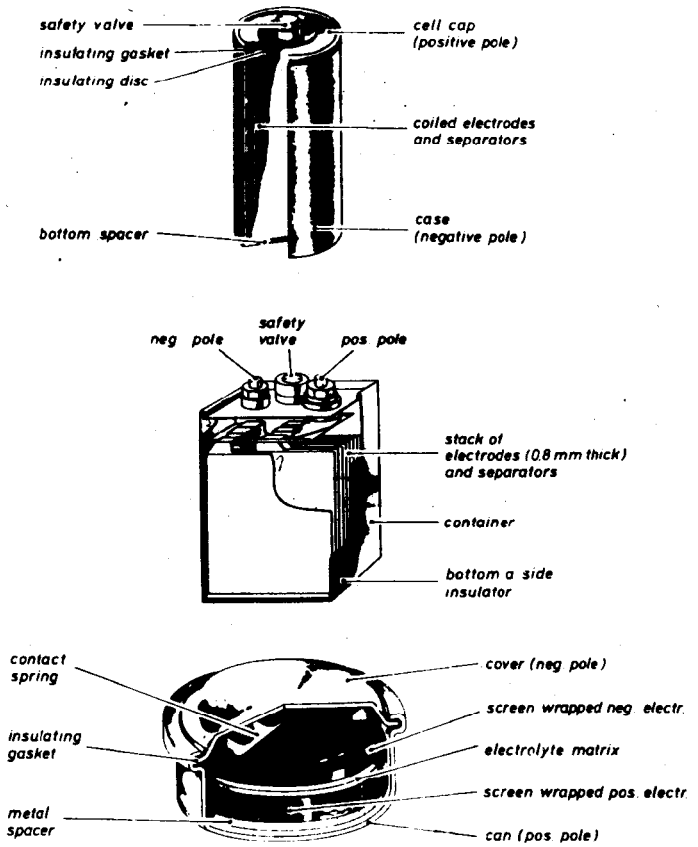

Figure 7. Cutaway views of sealed cells. (Top) Cylindrical cell with sintered electrodes, up to 7 Ah; (middle) rectangular cell with sintered electrodes, up to 50 Ah; (bottom) button cell, up to 1 Ah (from Reference 10).

the charging reaction is positive. The latent heat $T\Delta S$ is thus positive, i.e., heat will be absorbed from the surroundings during reversible isothermal charging:

$$T\Delta S = \sim +28 \text{ kJ/mol}$$

During reversible discharging, the same amount of heat will be set free.

These unavoidable heat conversions overlap with the heat losses that occur in practical operation with finite current to overcome the electrode polarization and the electrolyte and electrode resistances. The strong heating during the discharge is a limiting factor, especially for the sealed model.

The heat balance for a 100-Ah cell is given in Figure 9. The cell was charged with the 5-hr current for 7 hr and discharged for 5 hr. The heat evolved is integrated for the time intervals traced under the dashed line. It clearly shows that heat is absorbed from the surroundings during the first 5 hr of charging. The polarization losses become dominant only after this period.

The steep voltage rise during charging is absent in the sealed cell. The voltage stabilizes at about 1.5 V already, as shown in Figure 10. This is explained by the cathodic O_2 reduction at the cadmium electrode; this reaction occurs in sealed cells in place of the H_2 evolution with a higher voltage in vented cells. The formation of hydrogen takes place only at rapid charging and leads to an increased buildup of pressure in the sealed system. In order to eliminate risks which could arise due to improper handling, sealed cells, besides those of the button type, are provided with safety valves.

The energy that can be drawn from a cell is strongly dependent on the operating conditions. With a 10-hr current I_{10}, the maximum energy is drawn at a working temperature of about 30°C. The effective energy decreases strongly with decreasing temperature and with increasing discharge current. This can be explained by the diminution of the reaction and transport rates and by the increment in polarization The relations for a button cell are quantitatively represented in Figure 11. Fifty percent of the maximum energy value

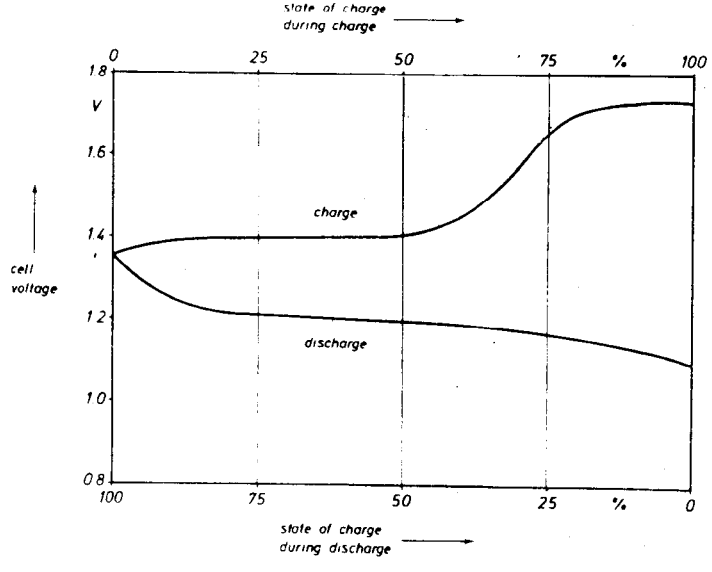

Figure 8. The course of cell voltage during charging and discharging of a nickel–cadmium cell with 5-hr current; charging time 7 hr.

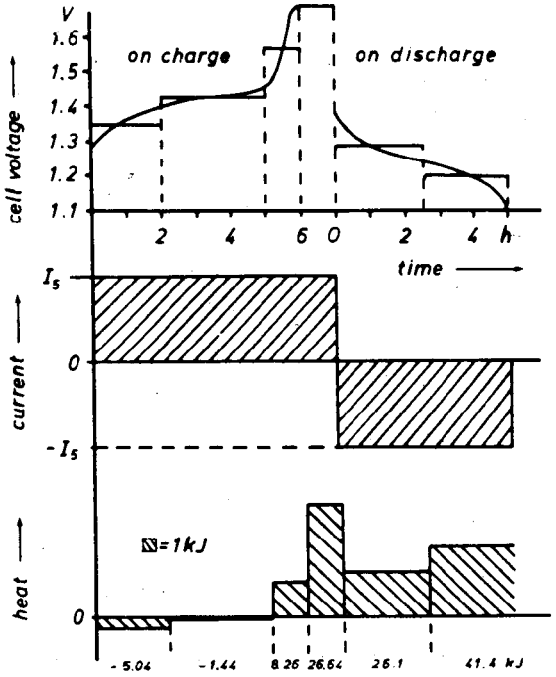

Figure 9. Heat balance of a nickel–cadmium cell during charging and discharging; TS cell, 100-Ah nominal capacity.

can still be derived at −20°C and I_{10}. The reason for the deterioration which sets in at higher temperatures lies in the declined degree of oxidation in nickel hydroxide.

The improved efficiency of cells equipped with sintered electrodes is exhibited by the set of dashed curves in Figure 11. The temperature range of discharge is extended in this case to −40°C.

4.2. Charge Retention

The Ni–Cd cells still possess 70–75% of their initial charge after a storage period of six months at room temperature. The loss is mainly due to O_2 depletion of higher oxidized nickel hydroxides by transition to NiOOH. The self-discharge of sealed cells is somewhat higher; when they contain sintered electrodes, the above-mentioned charge losses occur after one month.

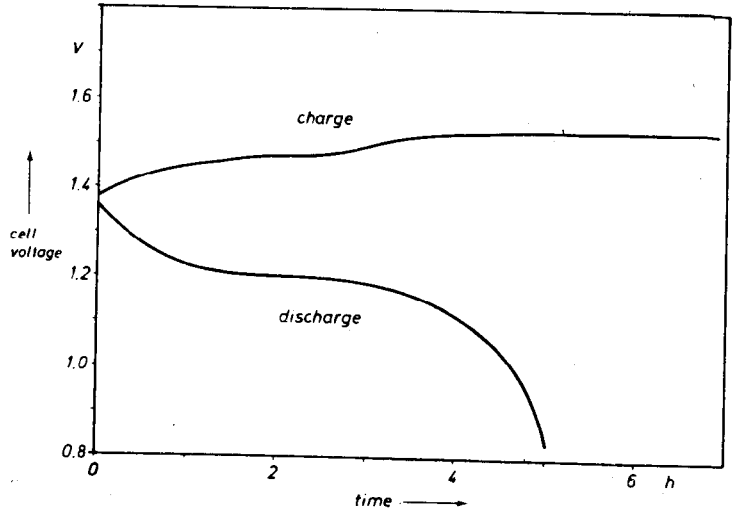

Figure 10. Characteristic of a sealed nickel–cadmium cell; charging and discharging with a 5-hr current.

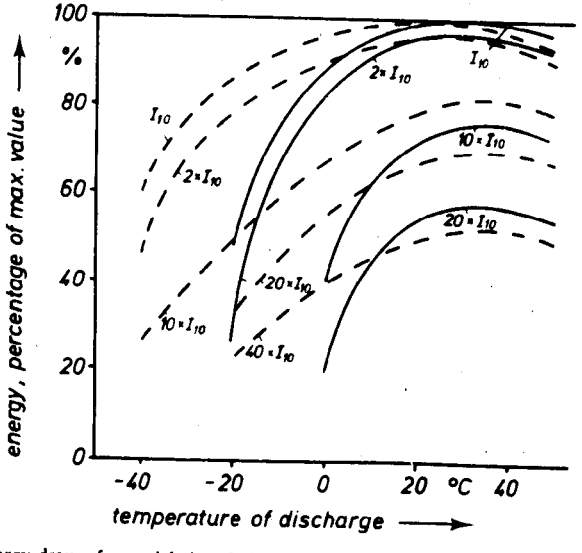

Figure 11. Energy drawn from nickel–cadmium cells as a function of discharging temperature. Solid curves, cells with presssed electrodes (DKZ cells); dashed curves, cells with sintered electrodes (RS cells) (Reference 11).

4.3. Cycle Life

Vented or sealed cells can withstand 2000 or even more deep discharge cycles with a charge exchange of more than 70% per cycle. Correspondingly, the total lifetime is several years, extending up to ten years. Cells with pocket electrodes can last well over 20 years; the lifetime of this electrode type, however, is distinctly shorter in the sealed version.

4.4. Maintenance

The Ah excess employed during charging brings about the decomposition of water. During the charging of a cell with a nominal capacity of 100 Ah, 14 g of water will be split electrolytically. An occasional water refilling, mostly after 20 cycles, is necessary. (The refilling should be done in the charged state since the electrolyte level under this condition is slightly higher due to the gas bubbles. Refilling in the discharged state can cause an electrolyte overflow during the subsequent charging.)

In spite of the effective caps, a gradual carbonatization of the alkaline solution is observed due to penetration of CO_2 from air, the consequence being a decrement of discharge voltage and effective capacity. A renewal of the electrolyte after three to five years is recommended. Pocket electrodes with graphite as a conducting additive lead to additional carbonatization by CO_2 of graphite oxidation. Their charging temperature should not exceed 35°C.

Although 60°C is tolerable up to a period of 24 hr, the temperature should be kept between 0 and 45°C during storage.

4.5. Energy Density and Efficiency

Practical energy densities of electrochemical cells are generally in the range 10–30% of the theoretical value calculated for the active materials. Thus the value for Ni–Cd cells is between 10 and 35 Wh/kg instead of the theoretical value of 209 Wh/kg. The energy densities of individual cells and batteries of different types are compared with those of Ni–Zn and Pb–acid systems in Figure 12.

The Ah efficiency η_{Ah} is the ratio of the ampere-hours output to the ampere-hours required to restore the initial state of charge:

$$\eta_{Ah} = \frac{\int_0^{t_d} I_d \, dt}{\int_0^{t_c} I_c \, dt}$$

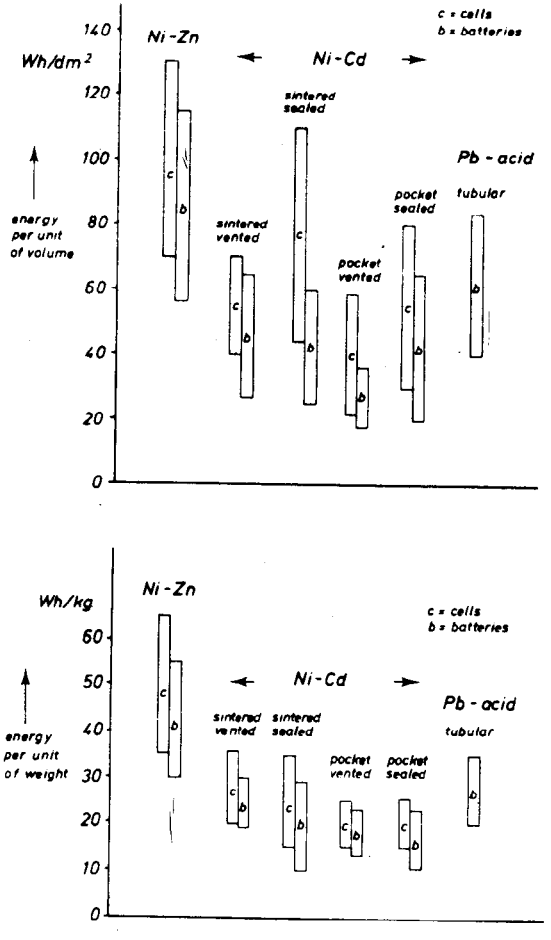

Figure 12. Energy per unit volume and per unit weight for different nickel–cadmium systems compared with Ni–Zn and Pb–acid cells. The data are based on nominal energy at room temperature (from References 2, 10, and 11).

I_d and I_c being the current, t_d and t_c the duration of discharge and charge, respectively. If I_d and I_c are constant, the formula simplifies to

$$\eta_{Ah} = \frac{I_d t_d}{I_c t_c}$$

The Ah efficiencies of individual cells are reported in Table 2. These values are calculated from the overloading factors recommended by the

Table 2
Ah and Wh Efficiencies of Various Systems[a,b]

System	Ah-efficiency, %	Wh efficiency, %
Ni–Zn (experimental cell)	~85	~70
Ni–Cd sintered, vented	71.5–83.5	62–75
Ni–Cd pocket, sealed	71.5–77	60–65
Ni–Cd pocket, vented	71.5	60
Ni–Cd sintered, sealed	67–71.5	60–65
Pb–acid tubular	83	68

[a] Room temperature; all data are referred to normal values of charge and discharge.
[b] From Reference 2.

manufacturers. The main part of the loss results from the simultaneous gas formation during the charging process.

The energy efficiency or Wh efficiency η_{Wh} is defined by the ratio of the watt-hours of output to the watt-hours of recharge

$$\eta_{Wh} = \frac{\int_0^{t_d} I_d E_d \, dt}{\int_0^{t_c} I_c E_c \, dt}$$

where E_d and E_c are the cell voltage during discharge and charge, respectively.

Experimentally measured Wh efficiencies are also included in Table 2 and are compared with the values of Ni–Zn and Pb–acid systems.

5. Application

In view of the variety of cell types with different dimensions that have been designed and developed, the practical application of Ni–Cd cells covers a wide range.[2,7,10,11] Thus they are used for stationary emergency power supplies. The sequential computer, for which relatively short current failures of only a few minutes have to be bridged, is a special case. The ability of sintered plaque cells with small internal resistance to produce the required high discharge current densities commend their choice in this case. These cells are thus also suitable to serve as batteries for starting emergency diesel-generating sets.

In comparison to other storage batteries, nickel–cadmium cells show excellent resistance to mechanical shocks, accelerations, and vibrations. These qualities have made them desirable for use in train lighting and for vehicle and rocket technology.

In view of their high specific energy content and cycle life, tubular batteries have prevailed as traction batteries for electrically driven vehicles, for instance,

electric boats, mine locomotives, electric carts for factories, trucks, and tractors.

The low maintenance and the independency of position of sealed nickel–cadmium accumulators have increasingly commended their use in past years as power sources in satellite technology and for portable equipments such as hand-held calculators, measuring instruments, radio receivers, hearing aids, electronic watches, cameras, security systems, tools, toys, and tape recorders. They can also be mounted rigidly in printed circuits and in solid state memories.

It is expected that the market for alkaline nickel–cadmium batteries will strongly expand in the future. At present the world turnover is estimated at about $150 million per year.

Acknowledgments

I sincerely thank many colleagues from the Battery Industry who supported this manuscript with their valuable suggestions and by offering recent data. Figures 9 and 11 were courteously provided by Dr. D. Berndt of VARTA Batterie AG, Kelkheim.

References

A. Monographs and Summarizing Papers

1. G. W. Vinal, *Storage Batteries*, 4th ed., John Wiley and Sons, New York (1955).
2. S. U. Falk and A. J. Salkind, *Alkaline Storage Batteries*, John Wiley and Sons, New York (1969).
3. F. v. Sturm, *Elektrochemische Stromerzeugung*, Verlag Chemie, Weinheim (1969).
4. J. O'M. Bockris and A. K. N. Reddy, *Modern Electrochemistry*, Plenum Press, New York (1970).
5. D. Berndt, Galvanische Elemente, Primär- und Sekundärelemente, in Ullmann's *Encyklopädie der technischen Chemie*, 4th ed., Vol. 12, Verlag Chemie, Weinheim (1976), pp. 73–111.
6. General Electric, *Nickel–Cadmium Battery, Application Engineering Handbook*, General Electric Co., Gainesville, Florida (1971); Supplement (1973).
7. G. A. Mueller, ed., *The Gould Battery Handbook*, Gould Inc., Mendota Heights, Minnesota (1973).
8. R. Kinzelbach, *Stahlakkumulatoren*, Varta Fachbuchreihe, Vol. 3, VDI Verlag, Düsseldorf (1974).
9. L. Martin, *Storage Batteries and Rechargeable Cell-Technology*, Noyes Data Corp., Park Ridge, New Jersey (1974).
10. E. Witte, *Blei- und Stahlakkumulatoren*, Varta Fachbuchreihe, Vol. 4, VDI Verlag, Düsseldorf (1977).
11. E. Buder, F. W. Busemann, B. Gnida, H. Hocke, H. A. Kiehne, G. Knaul, W. König, H. W. Köthe, W. Radszus, W. Tietze, and J. Woidt, *Gasdichte Nickel-Cadmium-Akkumulatoren*, VDI Verlag, Düsseldorf (1978).

B. Original Papers

12. G. Neumann, French Patent 1,004,176 (1947); German Patent 975,909 (1948).
13. W. Dennstedt and W. Löser, *Electrochem. Acta* **16**, 429 (1971).
14. O. Glemser and J. Einerhand, *Z. Elektrochem.* **54**, 302 (1950).
15. W. Feitknecht, H. R. Christen, and H. Studer, *Z. Anorg. Allg. Chem.* **283**, 88 (1956).
16. P. C. Milner and U. B. Thomas, in *Advances in Electrochemistry and Electrochemical Engineering*, C. W. Tobias, ed., Vol. 5, Interscience, New York (1967), pp. 1–86.
17. H. Bode, K. Dehmelt, and J. Witte, *Z. Anorg. Chem.* **366**, 1 (1969).
18. G. W. D. Briggs, in *Electrochemistry*, H. R. Thirsk, ed., Vol. 4, The Chemical Society, London (1974), p. 33.
19. N. Yu. Uflyand, S. V. Mendeleva, and S. A. Rosentsveig, *Sov. Electrochem.* **6**, 1268 (1970).
20. E. J. Rubin and R. Baboin, *J. Electrochem. Soc.* **118**, 428 (1971).
21. E. A. Kaminskaya, N. Yu. Uflyand, and S. A. Rosentsveig, *Sov. Electrochem.* **7**, 1776 (1971).
22. Yu. M. Gulyamov, M. D. Dolgushin, V. P. Morozov, and L. N. Sagoyan, *Sov. Electrochem.* **7**, 865 (1971).
23. R. D. Armstong, K. Edmondson, and G. D. West, in *Electrochemistry*, H. R. Thirsk, ed., Vol. 4, The Chemical Society, London (1974), pp. 18–32.
24. J. L. Weininger and M. W. Breiter, in *Power Sources*, D. H. Collins, ed., Vol. 1, Pergamon Press, Oxford (1967), pp. 269–285.
25. S. U. Falk, *J. Electrochem. Soc.* **107**, 661 (1960).
26. J. Jindra, J. Mrha, K. Micka, Z. Zábranský, B. Braunstein, J. Malik, and V. Kondelka, in *Power Sources*, D. H. Collins, ed., Vol. 6, Academic Press, London (1977), pp. 181–200.
27. L. Kandler, British Patent 917,291 (1963).
28. W. D. Wabner, L. Kandler, and W. Krienke, *Metall. Angew. Electrochem.* **26**, 68 (1972).
29. T. A. Edison, U.S. Patent 1,016,874.
30. A. E. Lange, E. Langguth, E. Breuning, and A. Dassler, German Patent 674,829 (1933).
31. A. Dassler, German Patent 899,216 (1951).
32. F. Peters, German Patent 949,576.
33. B. J. R. Hodge, R. Bonnaterre, and F. Putois, in *Power Sources*, D. H. Collins, ed., Vol. 5, Academic Press, London (1975), pp. 211–230.

14

Secondary Batteries—Silver–Zinc Battery

FERDINAND VON STURM

1. Introduction

Silver–zinc cells belong to the "noble" representatives of the group of alkaline secondary cells. The free enthalpy of reaction of the silver oxide–zinc couple is set free as electrical energy during discharging. The current generation is accompanied by the following chemical overall reaction:

$$Zn + Ag_2O + H_2O \rightarrow Zn(OH)_2 + 2Ag$$

In this expression the participation of higher silver oxide is neglected.

Like many electrochemical cells, this type has its roots in the past century. Volta had already experimented with silver-containing electrodes around 1800. A century later Jungner was so optimistic as to prophesize a bright future for the combination with cadmium. Also the combination with zinc led subsequently to patents.[9] A major breakthrough was brought about in the early 1940s by the work of H. André,[10,11] who introduced a separator such as cellophane into the electrolyte chamber to eliminate the migration of colloidal silver particles to the negative electrode and to avoid the electrical short circuits caused by zinc dendrites.

The set-up is outlined in Figure 1.

FERDINAND VON STURM • Sigri Elektrographit GmbH, D-8901 Meitingen, Federal Republic of Germany.

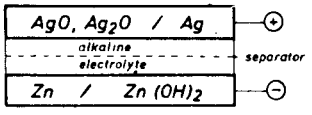

Figure 1. Set-up of a silver oxide–zinc cell.

After the pioneering works of Yardney International Corporation, with which H. André has been associated from 1948, a series of companies have become active as producers of primary as well as secondary cells of this type.

This cell can be denoted as "noble" because of its excellent properties such as high energy density, high discharge rate, and good charge retention. But this system is also distinguished by its high price, which is due to the use of expensive silver and to the unsatisfactory cycle life. Therefore the cell has succeeded in special applications where its volume and weight savings against other energy storage systems are readily appreciated.

Thermodynamics and kinetics of the cell reactions, design and construction of electrodes and cells, technical performance, and application will be described in the following. The list of references includes in addition to the survey articles and monographs,[1-8] some special publications[9-37] which should enable access to the original literature.

2. Thermodynamics and Kinetics

The expected cell voltage for the reversible case can be calculated from caloric data. The free enthalpy of reaction, ΔG_0, yields the effective energy under standard conditions:

$$\Delta G_0 = \Delta H_0 - T\Delta S_0$$

where ΔH_0 and ΔS_0 are the enthalpy and entropy of the reaction under standard conditions.

The derived value for the system considered here is

$$\Delta G_0 = -307.6 \text{ kJ/mol}$$

from which the cell voltage is evaluated according to

$$E_0 = -\frac{\Delta G_0}{nF} = 1.594 \text{ V}$$

In the following cell arrangement,

$$(-)\ \text{Zn}|\text{Zn(OH)}_2\|\text{electrolyte}\|\text{Ag}|\text{Ag}_2\text{O}\ (+)$$

the sign of E_0 corresponds to that of the right electrode, i.e., the silver electrode.

The occurrence taking place in the cell can be divided into anodic and cathodic partial reactions which can be characterized by the electrode potentials. The electrode potentials mentioned in the following set of reactions are referred to the normal hydrogen electrode as the reference electrode:

Anodic partial reaction

$$Zn + 2OH^- \rightleftharpoons \varepsilon\text{-}Zn(OH)_2 + 2e^-, \qquad E_0 = -1.249\ V \quad (1)$$

Cathodic partial reaction

$$2Ag + 2OH^- \rightleftharpoons Ag_2O + H_2O + 2e^-, \qquad E_0 = +0.345\ V \quad (2)$$

Cell reaction

$$Zn + Ag_2O + H_2O \rightleftharpoons \varepsilon\text{-}Zn(OH)_2 + 2Ag, \qquad E_0 = +1.594\ V \quad (3)$$

The concentration dependence of the quantities ΔG and E is given by the fundamental equations

$$\Delta G = \Delta G_0 + RT\Sigma\nu_i \ln a_i$$

$$E = E_0 - \frac{RT}{nF}\sum \nu_i \ln a_i$$

where ν_i and a_i are the mole number and the activity of the component i, respectively.

The temperature coefficient of the cell voltage E for reaction (3) is negative because ΔS is negative:

$$\Delta S = -66\ J/K\ mol$$

$$\left(\frac{dE}{dT}\right)_p = -\frac{1}{nF}\left(\frac{d\Delta G}{dT}\right)_p = \frac{\Delta S}{nF} = -0.34\ mV/K$$

This implies that with increasing temperature the cell voltage will be lowered by a value of 0.34 mV per degree.

Following the same procedure but starting with higher oxidized silver, a somewhat higher cell voltage is calculated for its preceding reduction reaction to monovalent silver:

Anodic partial reaction

$$Zn + 2OH \rightleftharpoons \varepsilon\text{-}Zn(OH)_2 + 2e^-, \qquad E_0 = -1.249\ V$$

Cathodic partial reaction

$$Ag_2O + 2OH^- \rightleftharpoons 2AgO + H_2O + 2e^-, \qquad E_0 = +0.607\ V$$

Cell reaction

$$Zn + 2AgO + H_2O \rightleftharpoons \varepsilon\text{-}Zn(OH)_2 + Ag_2O, \qquad E_0 = +1.856\ V$$

Table 1
Voltages of the Silver–Zinc Cells under Standard Conditions[a]

Phases	$Zn-Zn(OH)_2$ (amorphous)	$Zn-\varepsilon-Zn(OH)_2$	Zn-ZnO (inactive)
Ag_2O-Ag	1.566 V	1.594 V (− 0.337 mV/K)[b]	1.605 V (− 0.177 mV/K)
$AgO-Ag_2O$	1.828 V	1.856 V (− 0.116 mV/K)	1.867 V (+ 0.044 mV/K)

[a] Reference 12.
[b] The values in parentheses are the temperature coefficients of the cell voltage.

The treatment becomes more complicated since no uniform reaction product is formed at the zinc electrode as well. The stable ZnO is generally reached via unstable, amorphous $Zn(OH)_2$ and stable ε-$Zn(OH)_2$. It is precisely the ε-modification which forms the basis for the above calculations.

The cell voltages under standard conditions for all three forms of Zn^{2+} and for both stages of silver oxidation are summarized in Table 1.

In addition, the formation of soluble complexes and the undesired evolution of O_2 and H_2 cannot be prevented in practical operation. The voltage axis in Figure 2 provides a clear picture of the levels at which the different electrode reactions may occur thermodynamically.

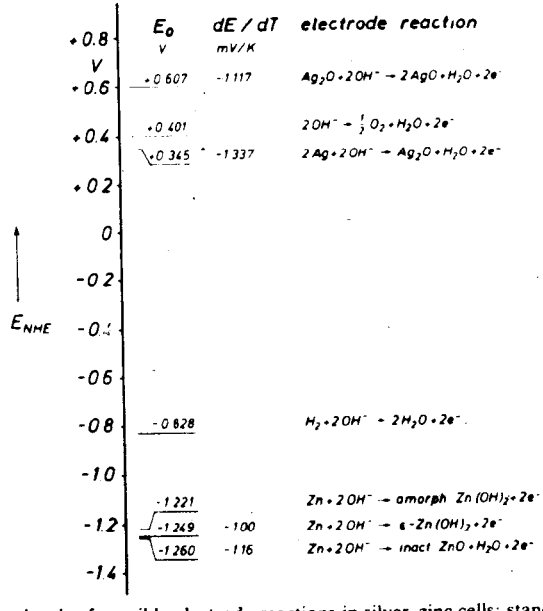

Figure 2. Voltage levels of possible electrode reactions in silver–zinc cells; standard conditions, pH 14.

Zinc exhibits a transition from active to passive behavior in the anodic part of the current–voltage curve.[13,14]

Several authors[15–19] have compared smooth and porous electrodes. There is an agreement that by a dissolution–precipitation mechanism a surface film will be formed whose ohmic resistance essentially determines the electrode polarization. The soluble species are OH^- complexes of Zn^{2+} ions, and the film consists of ZnO.

The cathodic deposition of zinc occurs in the form of dendrites. The enhancement of the zincate ion transport, e.g., by elevated temperature, by electrolyte pumping; by vibration of the electrode,[20] by lower viscosity of the solution or by higher zincate concentration, acts against the dendritic growth.[21,22] Additions to the electrolyte, for instance, Pb and Sn ions,[23–26] also effect dendrite growth in a similar manner.

The possibility of charging the silver electrode beyond the monovalent oxide Ag_2O to a formally bivalent oxide[27–29] is quite alluring at first sight. On one side the thermodynamically calculated cell voltage is increased from 1.594 to 1.856 V, and on the other the Ah capacity of the positive electrode is doubled.

The disadvantage, however, lies in the discharging which is associated with the two voltage levels. According to Wales and Burbank,[30] the potential drops when the starting material AgO is completely covered with Ag_2O. The length of the first discharging step is therefore essentially determined by the specific surface of the oxide. The exploitation of the upper voltage level is opposed by the much higher impedance during discharge of AgO as compared to Ag_2O, and by the intensified oxidative attack on the surroundings, especially the separator material.

The solubility of silver oxides[31] and also the formation of dendrites toward which the electrodes of silver and zinc have a tendency, demand effective separators. These separators should prevent the migration of silver ions to the counterelectrode and also avoid electronic short circuits caused by the ingrowth of fine metal crystals inside the electrolyte chamber. It is precisely to the separator development that special attention has to be devoted in the future, if the cycle life is to be improved.

3. Electrodes and Cells

3.1. Electrodes

3.1.1. Zinc Electrodes

Since solid zinc tends to passivate, it cannot be used as the active material. Therefore the starting material is either metallic zinc powder or zinc oxide which is reduced after being pressed to form an electrode.

Similarly to active zinc electrodes in other accumulator systems, mercury is added as HgO (a few percent) to the active mass. The formation of amalgam reduces—by increasing the hydrogen overvoltage—the hydrogen evolution, which is thermodynamically favored, as can be seen from Figure 2.

3.1.2. Silver Electrodes

Metallic silver powder can be shaped to form very sturdy electrodes by pressing and sintering with a supporting structure. The anodic oxidation to the active mass subsequently takes place inside the electrode.

An alternative is to start directly with chemically produced oxides and to press them into a supporting structure. The advantage of this method is that the complete conversion to the so-called bivalent oxide can be effectively utilized.

3.2. Cell Types

3.2.1. Cells with Plate Electrodes

In cell systems where high Ah capacities are required, plate-shaped electrodes with large areas are usually employed.

Membranes of radiation-grafted polyethylene of polyvinyl alcohol (poor in hydroxyl groups), parchment paper, cellophane, or microporous polypropylene and polyesters or, on an experimental basis, ion exchange membranes are in use as separators.

The separator materials are impaired in their elastic and semipermeable properties by the oxidative attack of AgO. Cells designed for high current discharge are equipped with larger electrode surfaces and low internal resistances. More rapid destruction of the separator must thus be accepted at present. In contrast, low rate cells can cope with higher internal resistances and attain a higher cycle life, as illustrated by the data in Table 2.

As in the button cells, the electrolyte used here is generally an aqueous potassium hydroxide solution of 30–45% concentration, saturated with zinc oxide.

Sodium hydroxide is employed when a long shelf life and an extremely low discharge rate are expected; it has less tendency to creep than potassium hydroxide. A slightly smaller conductivity has to be reckoned with in this case.

In a special version the so-called dry charged cell, the electrolyte is filled in the cell just before taking it into operation. This procedure is particularly advisable when high current loading is required. In dry state and protected from air, these cells can be stored up to 5 years without any significant loss in capacity.

Table 2
Characteristic Data of Silver–Zinc Cell Types

Type	Nominal current, A	Nominal voltage at 25°C, V	Current limit, A	Cycle number (for deep discharge)	Operating life, months	Internal resistance, Ω	Specific energy, Wh/dm^3	Specific energy, Wh/kg
Low rate	$C/10$	1.5	$5 \times C$	100–300	12–18	$0.20/C$	100–270	70–130
High rate	C	1.5	$20 \times C$	20–60	6–9	$0.03/C$	65–170	40–100

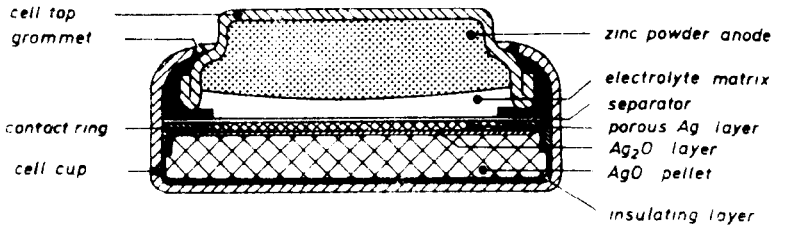

Figure 3. Design of a Ag–Zn button cell.[33]

3.2.2. Button Cells

Button cells have gained a place for the storage of smaller capacities in the range 30–175 mAh. Their design is analogous to the type described in the chapter on nickel–cadmium batteries in this volume (Chapter 13).

Within the past few years, a special version has been developed which makes use of the peculiarity of the silver oxide system very skillfully (Section 2 of this chapter and References 30 and 32). The starting substance, in fact, is AgO but the electrochemical reduction only attacks the Ag_2O, which forms a layer on the higher oxidized silver. The higher voltage step is thus renounced but an increased capacity at the positive electrode is gained.

As shown in Figure 3, the AgO stock is insulated from the metallic casing and remains in connection with the electrolyte-carrying separator only over the Ag_2O and porous Ag layers.

An increase in capacity of up to 35% is gained by this concept[34]; however, provision has to be made to allow the heat caused by the renounced voltage during discharging to be expelled from the system.

3.2.3. Sealed Cells

As in the sealed version of the Ni–Cd system (Chapter 13 of this volume) there is an excess of negative mass, the zinc oxide in this case. Thus only oxygen is evolved when the cell is overloaded. But because of the specific precautions in the electrolyte chamber of the Ag–Zn system, oxygen is transported to the counterelectrode only by diffusion through the electrolyte layer. Since loading is not needed and the voltage rises sharply at the end of charging (see Figure 4), the procedure is facilitated, at least in the case of single cells. In multicell arrangements the requirement of uniform capacities in the single cells must be fulfilled. Only limited quantities of the sealed version, especially with plate electrodes, have gained their application, mainly in space technology.

4. Technical Performance

4.1. Charge–Discharge Characteristic

Figure 4 illustrates the transition between the silver oxides of both valencies as voltage steps in the charging and discharging curves.

The cell voltage rises steeply towards the end of charging. This facilitates the control of charging. The cutoff voltage of charging should not exceed 2.0–2.1 V so as to prevent water loss by electrolysis.

A charging period of 10 hr is common, i.e., with a current

$$I_{\text{charging}} = C/10$$

but charging periods of only a few hours are possible.

The end of discharging is also indicated by a sharp voltage change. The current load should be interrupted when the cell voltage has dropped to 1 V. The allowable discharge currents are shown in Table 2. The discharging curves for high-rate cells are represented in Figure 5.

The effective capacity of the storage cell decreases with the decreasing temperature of operation. The manner in which the capacity and the mean discharging voltage depend on the discharging current and temperature may be seen from the empirically determined nomogram of Figure 6.

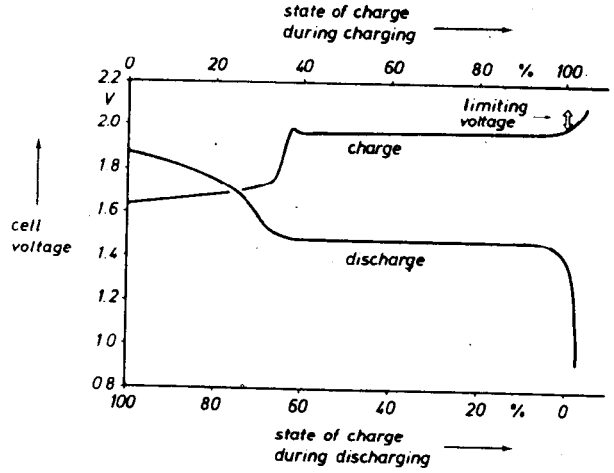

Figure 4. Cell voltage during charging and discharging as a function of the state of charge (percentage of the nominal Ah capacity).

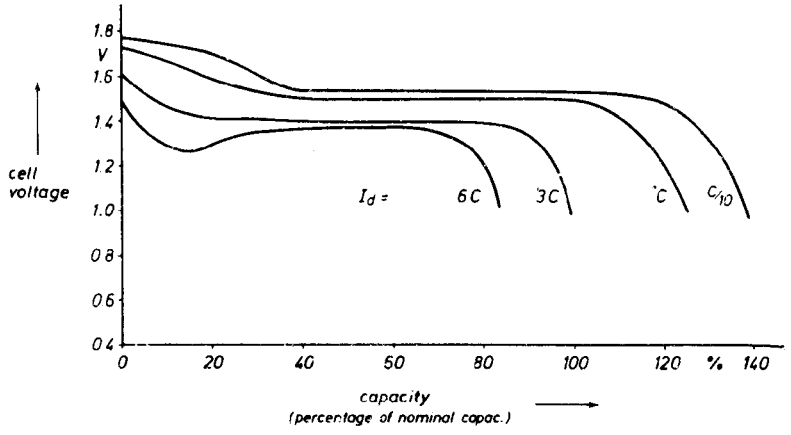

Figure 5. Discharge voltages of a high rate cell as a function of the withdrawn capacity (percentage of the nominal Ah capacity); discharge current as parameter.[35]

4.2. Charge Retention

Silver–zinc cells may possess 85% of their nominal capacity after three months charged stand at room temperature.

4.3. Cycle Life

Dendritic crystal growth at the electrodes and destruction of the separator lead to an unsatisfactory cycle life. Over 100 cycles can be attained with

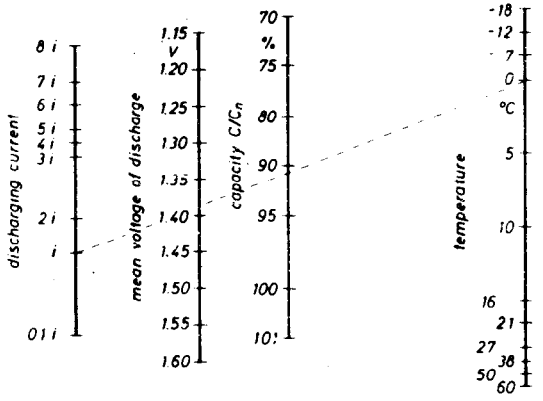

Figure 6. Nomogram for the evaluation of basis data of the silver–zinc cell; cell type HR, for 1-hr discharge current at 0°C; the diagonal line shows a mean discharge voltage of 1.39 V and an efficient capacity of 91%.[36]

low-rate cells as shown in Table 2. But a successful development to extend the cycle life will be decisive for widespread application.

Nevertheless, well over 2000 cycles have already been achieved with a battery of 22 cells, each having a capacity of 8 Ah, at a low depth of discharge of about 5%.[37]

4.4. Maintenance

The cells are compact in their construction and their electrolyte is almost immobile. Therefore they are very resistant to vibrations and shocks, as is proved by the tests conducted in the space programs. The cells can also be operated in any position.

4.5. Energy Density and Efficiency

The conspicuous feature of the Ag–Zn cell is its high energy density with respect to volume and with respect to weight. In this, it is far outstanding when compared with other conventional cell types. Figure 7 clearly illustrates these relations.

If the specified voltage limits are observed during cycling, the charge efficiency or ampere-hour efficiency, η_{Ah}, amounts approximately up to 0.9 and 0.95 (corresponding to a charging factor of 1.05):

$$\eta_{Ah} = \frac{\int_0^{t_d} I_d \, dt}{\int_0^{t_c} I_c \, dt} \sim 0.95$$

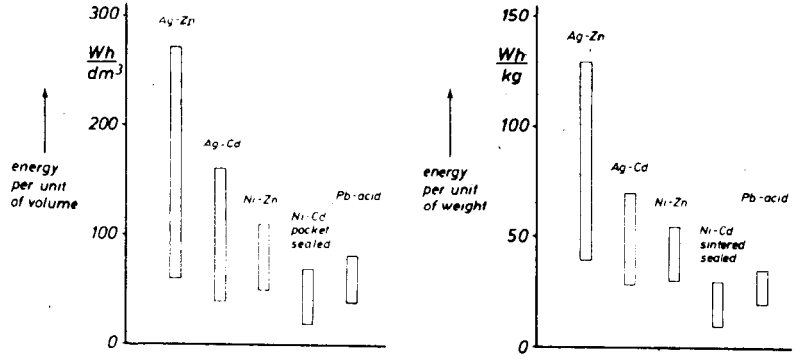

Figure 7. Energy per unit volume and per unit weight of the silver–zinc system; comparison with other electrochemical storage cells.[2]

I_d and I_c being the current, t_d and t_c the duration of discharge and charge, respectively.

The energy efficiency or watt-hour efficiency, η_{Wh}, is defined by the ratio of the watt-hours output to the watt-hours or recharge back to the initial state, by observing specified conditions of voltage limits, temperature, and current rate:

$$\eta_{Wh} = \frac{\int_0^{t_d} I_d E_d \, dt}{\int_0^{t_c} I_c E_c \, dt}$$

E_d and E_c being the cell voltage during discharge and charge, respectively.

Experimental values of 0.7–0.8 or even higher can be obtained.

5. Application

The energy density of the Ag–Zn battery is considerably higher than that of all other electrochemical storage systems on the market. This battery is thus suitable for all applications where compact design and low weight are required and where a lower cycle number and much higher costs are tolerable.

Thus the Ag–Zn cell has won a place in satellite technology and rocketry and is also used in supplying propulsion power to torpedos and submarines.

Its simple handling has further secured it a good share of the market in portable devices, for instance in transmitting and receiving systems, cameras, flashlights, powerful portable torches, electronic watches, hearing aids, and model construction.

Acknowledgments

I sincerely thank my colleagues from the Battery Industry who supported this manuscript with their valuable suggestions and by offering recent data. Figures 5 and 6 have been provided by the courtesy of Dr. E. Häusler of Silberkraft Leichtakkumulatoren GmbH, Duisburg, and Figure 3 by Dr. D. H. Spahrbier of VARTA Batterie AG, Kelkheim.

References

A. Monographs and Survey Articles

1. G. W. Vinal, *Storage Batteries*, 4th ed., John Wiley and Sons, New York (1955).
2. S. U. Falk and A. J. Salkind, *Alkaline Storage Batteries*, John Wiley and Sons, New York (1969).

3. F. von Sturm, *Elektrochemische Stromerzeugung*, Verlag Chemie, Weinheim (1969).
4. J. O'M. Bockris and A. K. N. Reddy, *Modern Electrochemistry*, Plenum, New York (1970).
5. A. Fleischer and J. J. Lander, eds., *Zinc–Silver Oxide Batteries*, John Wiley and Sons, New York (1971).
6. D. Berndt, Galvanische Elemente, Primär- und Sekundärelemente, in Ullmann's *Encyklopädie der technischen Chemie* 4th ed., Vol. 12, Verlag Chemie, Weinheim (1976), pp. 73–111.
7. L. Martin, *Storage Batteries and Rechargeable Cell-Technology*, Noyes Data Corp., Park Ridge, New Jersey (1974).
8. E. Witte, *Blei- und Stahlakkumulatoren*, Varta Fachbuchreihe, Vol. 4, VDI Verlag, Düsseldorf (1977).

B. Original Papers

9. W. Morrison, U.S. Patents 975,980, 975,981, 975,985, 976,092, 976,277–976,279 (1910).
10. H. André, *Bull. Soc. Franc. Electriciens* **1**(6), 132 (1941).
11. H. André, U.S. Patent 2,317,711 (1943); German Patent 962,347.
12. H. H. Bode, V. A. Oliapuram, D. Berndt, and P. Ness, in *Zinc–Silveroxide Batteries*, A. Fleischer and J. J. Lander, eds., John Wiley and Sons, New York (1971).
13. I. Sanghi and W. F. K. Wynne-Jones, *Proc. Indian Acad. Sci.* **47A**, 49 (1958).
14. I. Sanghi and M. Fleischmann, *Electrochim. Acta* **1**, 161 (1959).
15. M. W. Breiter, *Electrochim. Acta* **15**, 1297 (1970).
16. Z. Nagy and J. O'M. Bockris, *J. Electrochem. Soc.* **119**, 1129 (1972).
17. P. Ruetschi, in Power Sources, Vol. 4, D. H. Collins, ed., Oriel Press, Newcastle-upon-Tyne (1973), pp. 381–399.
18. R. N. Elsdale, N. A. Hampson, P. C. Jones, and A. N. Strachan, *J. Appl. Electrochem.* **1**, 213 (1971).
19. R. D. Armstrong and M. F. Bell, in *Electrochemistry*, Vol. 4, H. R. Thirsk, ed., The Chemical Society, London (1974), pp. 1–17.
20. O. von Krusenstierna, U.S. Patent 3,923,550 (1970); German Patent 2,150,005.
21. R. V. Bobker, *Zinc-in-alkali-batteries*, Society of Electrochemistry, University of Southampton, England (1973).
22. O. von Krusenstierna, in *Power Sources*, Vol. 6, D. H. Collins, ed., Academic Press, London (1977), pp. 303–317.
23. J. O'M. Bockris, J. W. Diggle, and A. Damjanovic, NASA Report, Contract No. NAS5-9591 March (1961).
24. R. Yu. Bek and N. T. Kudryavtsev, *Zh. Priklad. Khim.* **34**, 2020, 2613 (1961).
25. J. E. Oxley and C. W. Fleischmann, in Extended Abstracts, Battery Division, Vol. 10, The Electrochemical Society, Princeton, New Jersey (1965), pp. 3–5.
26. F. Mansfeld and S. Gilman, *J. Electrochem. Soc.* **117**, 588, 1154 (1970).
27. J. A. McMillan, *Acta Crystallogr.* **7**, 640 (1954); *J. Inorg. Nucl. Chem.* **13**, 28 (1960).
28. V. Scatturin, P. L. Bellon, and A. J. Salkind, *J. Electrochem. Soc.* **108**, 819 (1961).
29. V. N. Flerov, *Zh. Priklad. Khim.* **36**, 1980 (1963).
30. C. P. Wales and J. Burbank, *J. Electrochem. Soc.* **106**, 885 (1959).
31. R. F. Amlie and P. Ruetschi, *J. Electrochem. Soc.* **108**, 813 (1961).
32. T. P. Dirkse, *J. Electrochem. Soc.* **109**, 173 (1962).
33. H. M. Lippold and D. H. Spahrbier, *Prog. Batt. Solar Cells* **1**, 48 (1978).
34. VARTA Batterie AG, German Patent Appl. p. 2506399.4-45.
35. E. Häusler and K. Jeworreck, *Elektrotech. Z. Ausg. B* **27**, 99 (1975).
36. E. Häusler, *Elektrotech. Z. Ausg. B* **18**, 3 (1966).
37. G. Winzer, paper presented at DGLR-Symposium Wiss.-techn. Ergebn. d. AEROS-Progr., 1973.

15

Electrochemical Power for Transportation

ELTON J. CAIRNS and EARL H. HIETBRINK

1. Introduction

The use of electrochemical power in transportation vehicles is an old concept that has a good probability of again playing a significant role in the transportation industry. It is interesting to note that this is occurring almost a century after its initial success in the late 1800s and early 1900s. It is appropriate to include in this section some historical background of the rise and fall and subsequent rebirth of the electric vehicle, as well as a brief discussion of current transportation needs, and environmental and energy utilization issues that resulted in the renewed interest in applying electrochemical energy conversion technology to electric vehicle applications. Although energy utilization has become the most significant and important issue, the environmental issue will be discussed first in this section only because of its chronological occurrence.

The next part of the chapter is a review of passenger and commercial electric vehicle technology with emphasis on vehicle design, and demonstrated performance of vehicles with candidate power sources being developed. This is

ELTON J. CAIRNS • Head, Energy and Environment Division, Lawrence Berkeley Laboratory, University of California, Berkeley, California 94720. **EARL H. HIETBRINK** • Electrochemistry Department, General Motors Research Laboratories, GM Technical Center, Warren, Michigan 48090.

followed by a discussion of electrochemical power source requirements associated with future electric vehicles that can play a role in meeting modern transportation needs.

The last part of the chapter includes first a discussion of how to identify candidate electrochemical systems that might be of interest in meeting electric vehicle power source requirements. This is then followed by a review of the current technological status of these systems and a discussion of the most significant problems that must be resolved before each candidate system can be a viable power source.

1.1. Historical Background

Scientists, engineers, entrepreneurs, and hobbyists have been intrigued by the concept of battery-powered transportation vehicles for well over a century. As early as 1837, the first practical electric carriage was constructed by Robert Davidson of Aberdeen, Scotland.[1] The year 1888 is generally recognized as the beginning of the electric passenger car industry in the United States with the introduction of an electric car by Frederick M. Kimball of Boston, Massachusetts.[2] During the late 1880s and early 1900s, the electric vehicle was a serious contender, along with the steam engine vehicle and the internal combustion vehicle, in the technological race to replace the horse-drawn carriage as the dominant form of transportation. However, the electric vehicle technology could not keep pace with the rapid and exciting development of the combustion engine. Consequently, the combustion engine has played a dominant role in transportation and has also proved to be one of the most significant inventions of our time.

The annual production of electric vehicles in the United States reached a peak in 1916 when 10,000 electric vehicles were manufactured: 6000 passenger cars and 4000 commercial vehicles.[1] Since that time the manufacture of electric passenger vehicles has been discontinued, but the commercial electric vehicle industry continued to develop. By the late 1960s, there were on the order of 45,000 electric vehicles being used as milk wagons, post office trucks, and delivery vans in England and Europe.[3] In the United States there were approximately 65,000 lift trucks and perhaps 100,000 golf carts and an insignificant number of trucks and delivery vans.[4]

The downfall of the electric passenger vehicle was attributed primarily to (1) its inability to keep pace with the increasing speed of the internal combustion engine vehicles, (2) the high cost of electricity relative to gasoline, and (3) the unavailability of electricity in the rural areas. It is worth noting that the cost of electricity varied from 7 to 12 cents per kilowatt-hour and the cost of gasoline was 3.2 to 4.0 cents per liter.[5]

A resurgence of electric passenger vehicle activity began in the late 1950s and accelerated significantly in the early 1960s. This renewed interest was primarily motivated by a growing national concern over air pollution and

secondarily by an advancing *direct energy conversion* technology to meet the challenges of the Space Age. Simultaneous with the development of the fuel cell and advanced battery concepts for orbiting satellites and manned space vehicles, the environmentalists were advocating that the internal combustion engine be banned from our cities because it was the major contributor of pollutants to the atmosphere of our large metropolitan areas.

As the internal combustion engine was being developed to meet the environmental challenge of the 1960s, another motivating factor for increased electric vehicle activity began to emerge rapidly in the form of an ever-increasing demand for petroleum-based fuel and associated pressures, causing crude oil prices to increase.

By 1970 the stage was set for a petroleum fuel "crisis," and in the early 1970s the price of crude oil more than doubled and the supply of crude oil was demonstrated to be controlled by worldwide political pressures in addition to traditional supply–demand economics. Since the electric vehicle can readily utilize non-petroleum-based energy sources, such as coal and nuclear energy, the effect of the petroleum fuel "crisis" was a significant increase in electric vehicle development activities.

1.2. Modern Transportation Needs

A basic need to be met by any transportation system is to effectively transport people and goods from one point to another. Modern society has become dependent upon the predominant use of private automobiles and trucks to meet its transportation needs, not only effectively, but also very economically. This is particularly true in the United States where the automobile has had such a significant impact on individual life styles as well as on the total development of the country. History has shown that as any country becomes more affluent, there is an increasing pressure to develop improved transportation concepts that result in a greater degree of individual freedom and mobility. This has resulted in the relatively rapid development of the private automobile, of various sizes and styles, with a unique versatility and capability of meeting changing demands resulting from growth in population and the individual desires of a highly mobile society.

The relatively rapid growth in the population of automobiles and light trucks has also resulted in a variety of problems and issues that are of considerable concern to modern society. These include highway safety, air quality, traffic congestion, noise, and an increasing worldwide concern over the need to conserve petroleum resources. However, in spite of the problems that plague the private automobile, its use in meeting personal transportation needs is expected to continue to increase throughout the world. In order to satisfy the constraints associated with the issues mentioned above, there is expected to be increased emphasis on the development of specialty vehicles, including electric

vehicles, which would be effectively integrated into a total transportation system to meet future needs.[6] The use of the electric vehicle, in a small way, has already been initiated in the areas of personal transportation, public transportation, and delivery of goods and services. The trend is that these initiatives will continue with the greatest impact of the electric vehicle, over the near term, being made in the latter area.

1.2.1. Personal Transportation Characteristics

Statistics compiled and published by the Motor Vehicle Manufacturers Association of the United States, Inc.[7] show that private automobiles and trucks account for 90% of all personal travel in the United States. The distribution of this travel by purpose and related average trip length is presented in Table 1. The most significant information in Table 1 is the average trip length. Since the electric vehicle is limited in range between recharges, its scope of application to personal travel needs depends primarily on the trip length and the number of trips per day. (It is assumed that recharging will take place primarily during nighttime, off-peak hours.) Although the average trip length in Table 1 is relatively short, indicating that most personal travel could be accomplished with an electric vehicle, the randomness of travel in terms of the number and lengths of trips made on any given day must be taken into account. This has been done in an analysis referred to in Reference 8. The results of this work indicated that a vehicle range of 132 km would satisfy personal driving needs 95% of the days of the year based on total annual travel of about 16,295 km. Furthermore, if total annual travel continued to increase in the same manner that it did during the period 1963–1972, a range of about 160 km would satisfy the same needs until late in the 1990s.

Table 1
Personal Travel in the United States[a]

Purpose of travel	Percentage distribution		Average (one-way) trip length, km
	Trips	Travel	
Earning a living	36.7	42.1	16.3
Family business	31.3	19.5	9.0
Educational, civic, or religious	9.4	5.0	7.5
Social and recreational	22.6	33.4	21.0
All purposes	100.0	100.0	14.2

[a] From Reference 7. Original source: U.S. Federal Highway Administration, Nationwide Personal Study (1969).

1.2.2. Public Transportation Characteristics

The continuously increasing cost of owning and operating a private automobile results in an increased demand for effective public transportation vehicles, such as route buses and community vehicles. This area of transportation need has been primarily emphasized in Europe and, to some degree, in Japan. Although the desire for zero exhaust emissions and reduced noise in urban areas provides a strong incentive for the development of electric buses, other requirements, such as low cost, high daily use factor and, in some cases, long range, are difficult to satisfy. As a general rule, these vehicles are used for 8–16 hr and can travel up to 300 km per day.[9] Thus, in many cases, this area of need requires a vehicle designed for rapid battery exchange and the related use of battery exchange stations.

1.2.3. Delivery of Goods and Services Characteristics

Service and delivery vehicles are used for a wide range of applications in the urban and suburban areas throughout the world. These applications range from mail delivery and the distribution of goods to service vans which are used primarily by the utility industry. The desired vehicle characteristics are primarily low maintenance and low operating cost. In contrast to the privately owned automobile, the daily use of the delivery and service vehicle is quite well defined. Many of these vehicles are used as commercial fleets and are parked overnight near their point of daily use for normal recharging and servicing by experienced personnel. Although the range and payload requirements vary considerably for different applications, a majority of the needs can be met with a daily range of 60–120 km and a payload capability of 500 kg.[9,10]

1.3. Environmental and Energy Utilization Issues

An electric vehicle is normally thought of as a vehicle chassis that is powered by an electric motor which is driven by electrical power from a secondary battery. However, this simplified concept is not sufficient for a meaningful discussion of the environmental and energy utilization issues related to electric vehicles. Rather, the electric vehicle must be considered as a total system which includes the primary energy source, electric power generating plant, and the distribution network of electrical power, as shown in Figure 1. In comparison, the combustion engine vehicle must also be considered as a total system which includes the primary energy source, a chemical fuel processing plant, and a fuel distribution network, as shown in Figure 2. These two vehicle systems are very similar in many aspects but also have a very distinct and important difference. Both systems include a Carnot-limited energy conversion step which is the efficiency-limiting step in the total process and is also the step in the process where there is direct interaction with the air

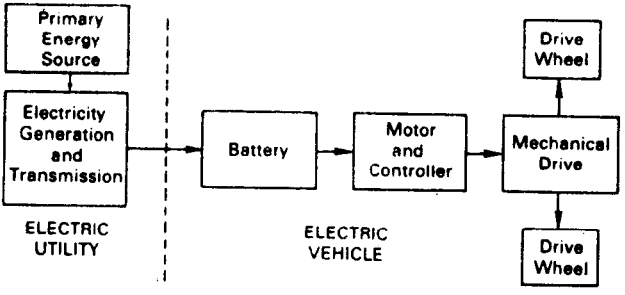

Figure 1. Electric vehicle schematic.

and/or water environment. In the case of the electric vehicle system, this conversion step is carried out in a relatively small number of large stationary equipment installations as contrasted to being carried out at the point of vehicle usage in millions of small, mobile combustion engines. Although this might appear to be a rather subtle difference, it is a particularly important aspect of the environmental issues related to electric vehicles.

1.3.1. The Environmental Issue

The *environmental crisis* of the 1960s provided the incentive for renewed interest in electric vehicles. The automobile became the "target" of some environmentalists who singled it out as being a dominant source of carbon monoxide, and a major contributor to photochemical smog by virtue of it being a major source of nitrogen oxide and hydrocarbon contaminants.[11] As a consequence, a great deal of vehicle emission legislation was enacted in the United States during this period to reduce and control the effect of vehicle emissions on atmospheric contaminant problems. The most significant legislation was the passage of the Clean Air Act of 1963 and its subsequent amendments in 1965 and 1970 which provided for the establishment and

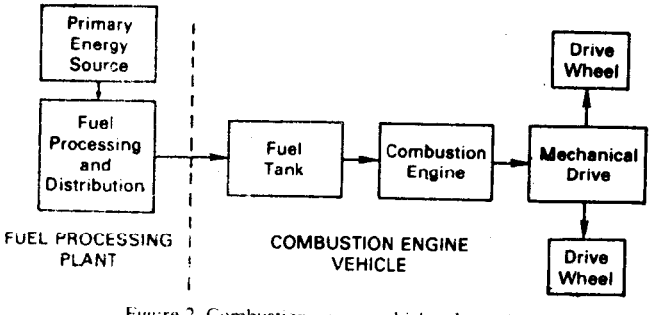

Figure 2. Combustion engine vehicle schematic.

enforcement of nationwide ambient air quality and related vehicle emission standards. The goal of the Clean Air Act Amendment of 1970 was to establish a 90% reduction and control of hydrocarbon (HC) and carbon monoxide (CO) emissions, based on 1970 levels, by January 1, 1975 and a similar 90% reduction in nitrogen oxides (NO_x) from 1971 levels, by January 1, 1976. The vehicle emission standards associated with these goals were determined administratively to be 2.1 g/km (3.4 g/mile) for CO, 0.26 g/km (0.41 g/mile) for HC, and 0.25 g/km (0.4 g/mile) for NO_x. However, subsequent action by the Environmental Protection Agency and the 1977 amendments to the Clean Air Act resulted in an extension of the time for meeting these goals and a relegation of the 0.25 g/km NO_x standard to a research goal. A summary of the emission standards that have been in effect since 1968 and the new schedule through 1981 are shown in Table 2.[12]

The impact of exhaust emission controls on the aggregate emissions from the automobile population is difficult to quantify. Heywood and Martin have examined several methodologies that have been used to make reasonable projections and have estimated the average vehicle urban emission rates (grams per vehicle mile) for the in-use urban vehicle population, as shown in Figure 3,[13] which can be used to calculate aggregate emission rates for any urban area for different assumptions of total vehicle miles traveled per year. These estimates indicate that by the mid-1980s the full impact of exhaust emission controls could begin to be realized, depending on the rate at which old, higher-polluting automobiles are retired from the in-use automobile population.

Within the framework of emission control regulation, the environmental issue associated with electric vehicles results in the following concerns: (1) the

Table 2
Federal Emission Standards

Year	Emission [g/km (g/mile)]		
	HC	CO	NO_x
Prior to 1961 (average level)	9.4 (15.0)	56.2 (90.0)	3.1 (5.0)
1968	3.9 (6.3)	31.9 (51.0)	—
1970	2.6 (4.1)	21.2 (34.0)	—
1972	1.9 (3.0)	17.5 (28.0)	—
1973	1.9 (3.0)	17.5 (28.0)	1.9 (3.1)
1974	1.9 (3.0)	17.5 (28.0)	1.9 (3.1)
1975	0.9 (1.5)	9.4 (15.0)	1.9 (3.1)
1977	0.9 (1.5)	9.4 (15.0)	1.2 (2.0)
1980	0.26 (0.41)	4.4 (7.0)	1.2 (2.0)
1981 and beyond	0.26 (0.41)	2.1 (3.4)	0.6 (1.0)

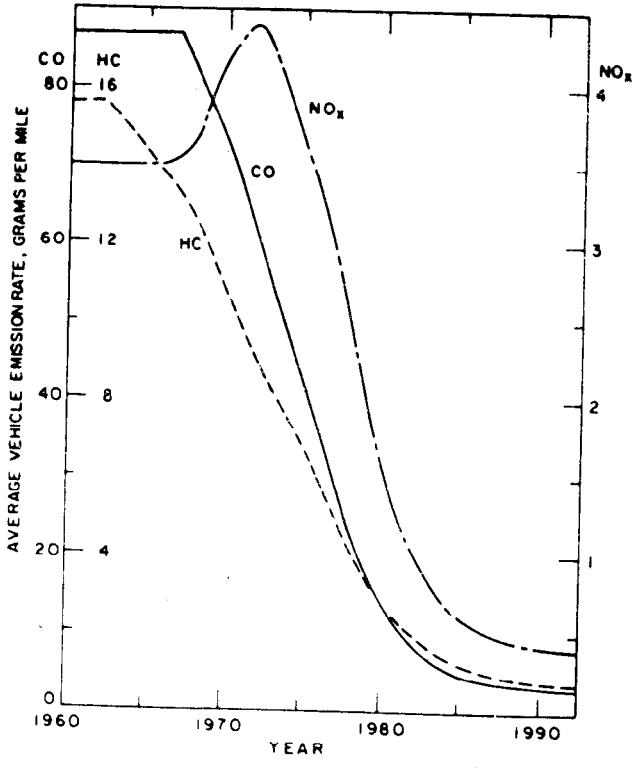

Figure 3. Average vehicle urban emission rates for HC, CO, and NO_x g/mile, base-line case.[13]

effect of changing the nature and location of the pollution from the primary automobile exhaust emissions (CO, HC, NO_x) to the primary emissions from the smokestacks of electric power generating stations (SO_2, particulates, NO_x), and (2) the control and maintenance of pollution abatement devices.

A significant issue related to the electric vehicle is the hazard of SO_2 and particulate emissions relative to CO and HC. There has recently been increased concern over the role that SO_2 plays in the production of sulfuric acid mist in the atmosphere. The rate of production of the acid increases with both increased humidity and SO_2 concentration.[14] The electric vehicle would contribute to this problem, although it is projected that the amount of electrical energy required by electric vehicles is a small fraction of total electrical demand.

The emissions related to an electric vehicle are released from smokestacks high above the ground rather than at ground level from combustion engine

vehicle exhausts. In general, this can mitigate the effect of a high concentration of contaminants, particularly CO, at ground level in highly congested areas. However, the position of the smokestack relative to the congested area and atmospheric conditions are key factors in this regard, and under unstable conditions the plume from the stack can touch down and, in fact, cause an increase in the concentration of emissions over a small area.[15]

Several models have been developed in order to analytically determine the atmospheric concentration of pollutants emitted from single sources either at ground level or from stacks.[16,17] A significant part of this effort has been spent on plume dispersion calculations, and the results have been rather widely used in the literature to imply a substantial advantage associated with the electric car in this regard.[18] However, the results can vary widely depending on the assumptions used. In addition, other considerations are quite often neglected, such as SO_2 interaction with vegetation, or more generally, the absorption or deposition of pollutants when the plume reaches the ground.

With regard to the control and maintenance of pollution abatement devices, it must be recognized that the use of fossil fuel in either power-generating plants or combustion engines, will require *effective* pollution abatement equipment in order to meet clean air standards. As a consequence, large amounts of capital are being invested in the development and application of pollution abatement technology. In this regard, the abatement equipment related to the electric vehicle is required on the power-generating plant and not on the vehicle itself. Thus this equipment is apportioned over the total electrical energy demand, rather than over just that relatively small fraction of the demand associated with the electric vehicle.

1.3.2. Energy Resource Considerations

A very important aspect of electric vehicle use is that it could have a favorable impact on achieving effective utilization of relatively abundant nonpetroleum primary energy sources. The projection of energy resource utilization for electric power generation shown in Figure 4[19] illustrates that by 1990, 82% of electrical energy in the United States will be generated from coal and nuclear energy in contrast to 7% from oil. Thus, on an aggregate basis, these sources are primarily providing the base load and oil is used during daily peak demand periods. Providing the electric vehicles are charged during off-peak hours, the result would be an increase in the use of coal and nuclear energy for transportation and a corresponding relief of the petroleum demand for transportation.

In this regard, the gasoline (spark-ignition) automobile can also use coal or nuclear energy as a primary source by using a synthetic fuel prepared from either or both sources. As an aid in evaluating the relative effectiveness of the two approaches, a first step is to consider the overall production efficiency of producing gasoline or a synthetic fuel and electricity from each of the primary

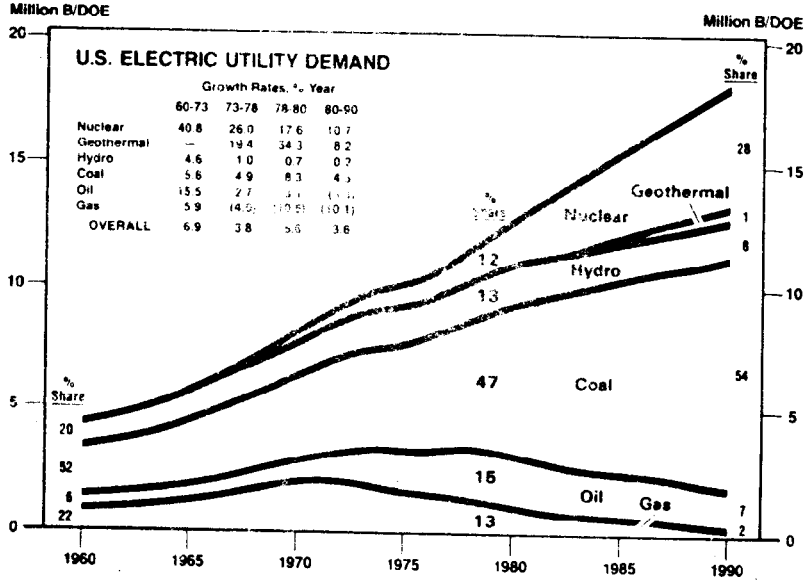

Figure 4. Projected energy resource utilization to 1990. Million B/DOE = million barrels/day oil equivalent.

energy sources introduced above. Efficiency values representative of present-day processes and operations associated with the use of petroleum and coal are shown in Figure 5.[120] In the case of nuclear fuel, shown in Figure 6, there is essentially no available experience to refer to with regard to the manufacture and distribution of a synthetic fuel. An efficiency of about 70% (probably a high value) was assumed for the preparation of a fuel such as hydrogen, ammonia, or methanol. This value is higher, in fact, than the present efficiency of producing hydrogen from water by electrolysis. It will probably be 10–15 years before synthetic fuel production can satisfy even a few percent of the demand for petroleum fuels.

Figures 5 and 6 indicate that, for all practical purposes, the efficiency associated with producing electricity (~30%) is essentially the same from all three energy sources. However, the production of a synthetic fuel from coal is significantly less efficient than the production of gasoline and this situation is even more pronounced in the case of nuclear fuel.

The next step is to consider the utilization of the fuel and electricity to accomplish the movement of people and goods safely in urban traffic. The detailed designs of SI (spark-ignition)-engine and electric automobiles to carry out a specific mission of moving a certain payload through a specific driving profile is beyond the scope of this work. As a step in the proper direction,

however, it is appropriate to state that for a given mission present-day electric urban automobiles are heavier than their SI-engine counterparts. In the case of current and near-term battery technology, such as lead–acid and zinc–nickel oxide batteries, the electric vehicle may be on the order of 50% heavier than the SI engine depending significantly on the desired range. The effect in terms of prime energy consumption would be to reduce the energy advantage of electric automobiles; however, the overall energy advantage, particularly for coal and nuclear energy utilization, would still be significant.

There is a limited amount of experimental data available for making a direct energy consumption comparison of electric and SI-engine automobiles of the same payload capability and performance, operating over the same driving cycle. This most meaningful comparison cannot be made with a high degree of confidence unless development and test activities are conducted for the purpose of obtaining directly comparable data. In an attempt to gain a reasonable perspective, a first-order comparison for a two-passenger commuter and a four-passenger sedan automobile is presented in Table 3. This table was constructed from the use of the overall production efficiency values

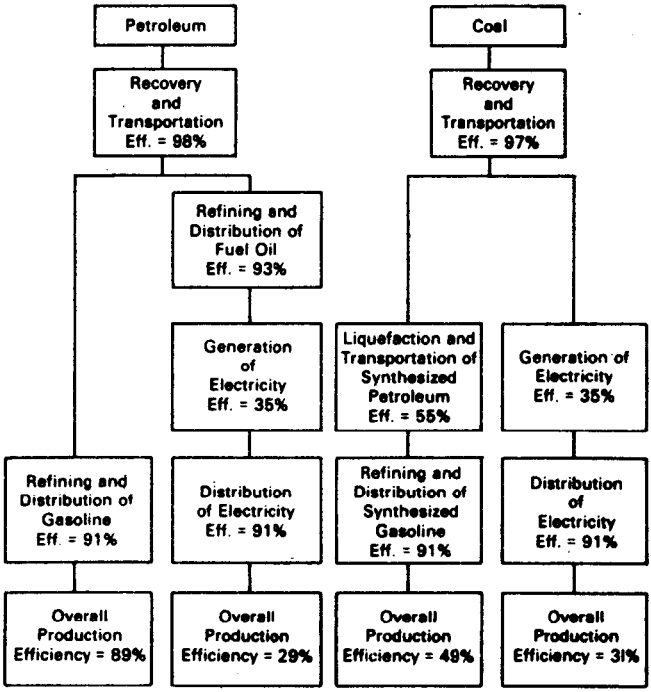
Petroleum
Recovery and Transportation Eff. = 98%
Refining and Distribution of Fuel Oil Eff. = 93%
Generation of Electricity Eff. = 35%
Refining and Distribution of Gasoline Eff. = 91%
Distribution of Electricity Eff. = 91%
Overall Production Efficiency = 89%
Overall Production Efficiency = 29%
Coal
Recovery and Transportation Eff. = 97%
Liquefaction and Transportation of Synthesized Petroleum Eff. = 55%
Generation of Electricity Eff. = 35%
Refining and Distribution of Synthesized Gasoline Eff. = 91%
Distribution of Electricity Eff. = 91%
Overall Production Efficiency = 49%
Overall Production Efficiency = 31%

Figure 5. Process efficiencies associated with the utilization of coal and petroleum.

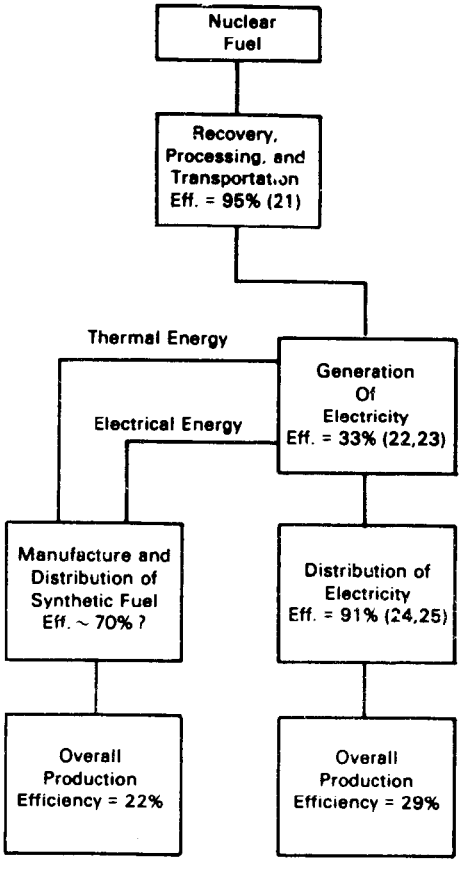
Nuclear Fuel
Recovery, Processing, and Transportation Eff. = 95% (21)
Thermal Energy
Electrical Energy
Generation Of Electricity Eff. = 33% (22,23)
Manufacture and Distribution of Synthetic Fuel Eff. ~ 70% ?
Distribution of Electricity Eff. = 91% (24,25)
Overall Production Efficiency = 22%
Overall Production Efficiency = 29%

Figure 6. Process efficiencies associated with the utilization of nuclear fuel.

for fuel and electricity from Figures 5 and 6, and from automobile design and energy utilization characteristics compatible with published results from analytical studies to compare the efficiency of energy utilization by electric and SI-engine-powered automobiles. Thus the prime source energy utilization values in Table 3 are obtained by dividing the fuel and electricity utilization values in Table 3 by the corresponding efficiency values for the production of fuel and electricity from Figures 5 and 6. Note that the automobile mass shown in Table 3 is associated with a two-passenger commuter automobile range of approximately 80 km and a four-passenger sedan automobile range of about 120 km. The results of Table 3 tend to confirm the energy advantage of the electric automobile with regard to the utilization of coal and nuclear energy; however, this is only significant with, at least, the near-term battery technology,

Table 3
Prime Source Energy Consumption

Automobile type	Automobile characteristics[a]		Energy used from prime source, kWh/km		
	Fuel or electricity utilization, kWh/km	Automobile mass, kg	Petroleum	Coal	Nuclear
Spark ignition					
Two-passenger commuter	0.49[b]	700	0.55	1.0	1.59
Four-passenger sedan	0.62[b]	1050	0.70	1.27	2.04
Lead–acid electric					
Two-passenger commuter	0.31	1500	1.07	1.0	1.07
Four-passenger sedan	0.51	2800	1.76	1.65	1.76
Zinc–nickel oxide electric					
Two-passenger commuter	0.22	1050	0.76	0.71	0.76
Four-passenger sedan	0.34	1650	1.17	1.1	1.17

[a] References 20, 24, and 26.
[b] A value of 0.35 and 0.45 was used for the commuter and sedan respectively in the nuclear case to reflect an increase in the thermal efficiency of the SI engine for these synthetic fuels relative to the other cases.[27]

such as zinc–nickel oxide. As the battery technology advances further, the electric automobile energy advantage will become greater.

One additional consideration associated with the use of electric vehicles to achieve effective utilization of nonpetroleum resources is the impact they would have on the electric power generation industry. This, of course, depends on several factors, such as (1) the energy consumption of the electric vehicle, (2) the growth rate of the electric vehicle population, (3) the electric vehicle battery charge mode, and (4) the growth in the electric-power-generating capacity.

The primary factors to be considered in determining the energy consumption are the vehicle mass, driving profile, accessory load, and component efficiencies. A summary of published energy consumption data is presented in Figure 7 in terms of kWh/km as a function of vehicle mass. The data points in the lower portion of Figure 7 represent the energy required from the battery power source to propel the vehicle over an urban driving profile. As a first approximation, these points lie reasonably close to a normalized value of 0.15 Wh/kg km of vehicle mass. The upper crosshatched banorepresents a reasonable range of the energy required from the power-generating utility. This range of values reflects variation in accessory equipment load, battery charge and discharge efficiency, and the vehicle driving profile.

With regard to the growth rate of the electric vehicle population, one author's projection of the impact of two different rates relative to a specific

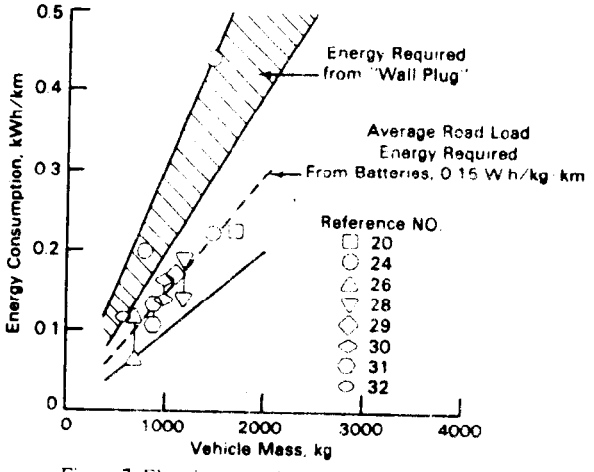

Figure 7. Electric automobile energy consumption.

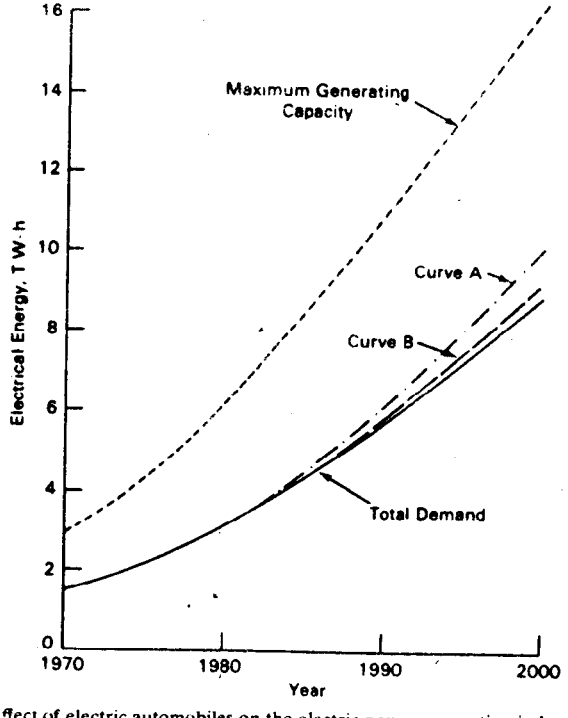

Figure 8. Effect of electric automobiles on the electric power generation industry.

projection of electric-power-generating capacity is shown in Figure 8.[24] Curve A represents a hypothetical worst case; conditioned with the assumptions that total electrification of all vehicles would take place by year 2000 and have an average energy consumption of 0.425 kWh/km, which represents a relatively heavy vehicle with current component efficiency technology. The impact of this condition was projected to be a 14% increase in total nonelectric vehicle nationwide demand by year 2000. Curve B represents a more probable growth rate where 40% of all vehicles would be electric by year 2000 and have an average energy consumption of 0.2 kWh/km, which represents a smaller vehicle with improved component efficiency technology. The impact of this condition is projected to be only a 2.5% increase in the total nonelectric vehicle nationwide demand by the year 2000.

An important consideration relative to the impact of the small increase in electrical demand projected for electric vehicles is how the electric vehicle batteries will be charged. If they are charged rapidly (<2 hr), then the relatively high power required could have an adverse impact on the power industry, particularly during periods of peak load. However, it is most probable that electric vehicles will be limited to a slower charge (4–10 hr) and that there will be economic incentives from the power industry to charge during the off-peak, nighttime hours. Under these conditions, the impact of electric vehicles on the power industry is considered to be a very favorable one.[33]

2. Electric Transportation Vehicles

A significant number of electric vehicles were built during the 1960s and 1970s. Most of these vehicles were demonstration or "test bed" vehicles which were primarily used to demonstrate technical feasibility of batteries and electric drive components and to obtain a first-order evaluation of vehicle acceleration, speed, and range capabilities. However, there has been some effort aimed specifically at the development of a marketable product which has resulted in a relatively small number of passenger, utility, and public transport vehicles being manufactured and marketed in recent years. The market for these vehicles has included the individual consumer as well as various industries and institutions interested in evaluating vehicle performance and overall feasibility for specific applications. It is not intended here to present a complete compilation of the various electric vehicles and their design and performance characteristics. Such a compilation can be found in References 34 and 35. Rather, the objective here is to emphasize specific automobiles and commercial vehicles that have had a significant effect on enhancing overall interest in electric vehicle development or are representative of recent developments in vehicle design, battery concepts, and drive train components for application to electric vehicles within the next few decades.

2.1. Automobiles

The electric automobile development efforts are primarily aimed at increasing overall performance to a point where personal transportation needs can be met. As a minimum, the electric automobile has to have a sufficient speed and acceleration capability to mix with other traffic on city streets and to have a sufficient range to meet daily driving needs. These performance characteristics are primarily affected by automobile design, type of battery, drive motor, controller, and mechanical drive components. The use of regenerative braking can also have a significant effect as indicated later in this section.

2.1.1. Design Considerations

A variety of design concepts have been demonstrated by the many experimental automobiles that have been constructed. The most significant factors that must be considered include the gross vehicle mass (GVM), battery mass, location of batteries for appropriate distribution of the GVM, front or rear wheel drive, passenger and cargo space requirements, aerodynamic drag, and other features important to the customer, such as styling, safety, and practicality.

The battery mass is the prime factor affecting the GVM. This in turn is directly related to the range requirement. Increasing the battery mass to enhance the range also results in an increase in the basic structure mass to support the battery mass. This has become known as the mass compounding factor. A uniformly accepted value has not been established as yet; however, a range of 30–50%[4] is common.[20] That is, for every 100 units increase in the battery mass, an additional 30–50 units increase in the structure mass should be added to the GVM. Modern electric automobile concepts result in a GVM ranging from about 750 kg for the two-passenger urban shopper shown in Figure 9 to about 1770 kg for the four-passenger sedan which is shown in Figure 18. It is also noted that the battery mass usually varies from 20% to 40% of GVM with a maximum 25–30% being the most desirable from a design and handling point of view.[26]

With regard to the location of batteries, a common design concept is one where the batteries are packaged under the floor of the passenger or cargo compartment, as illustrated by the GM Electrovette in Figure 10. This approach is normally used when the electric automobile is designed within the constraints of an existing gasoline engine automobile chassis which, in this case, is the standard Chevette. At the present time, there is a significant cost and convenience advantage to this approach in that the cost advantage of high-volume production components can be applied to the construction of a relatively small number of electric automobiles at this stage in their development.

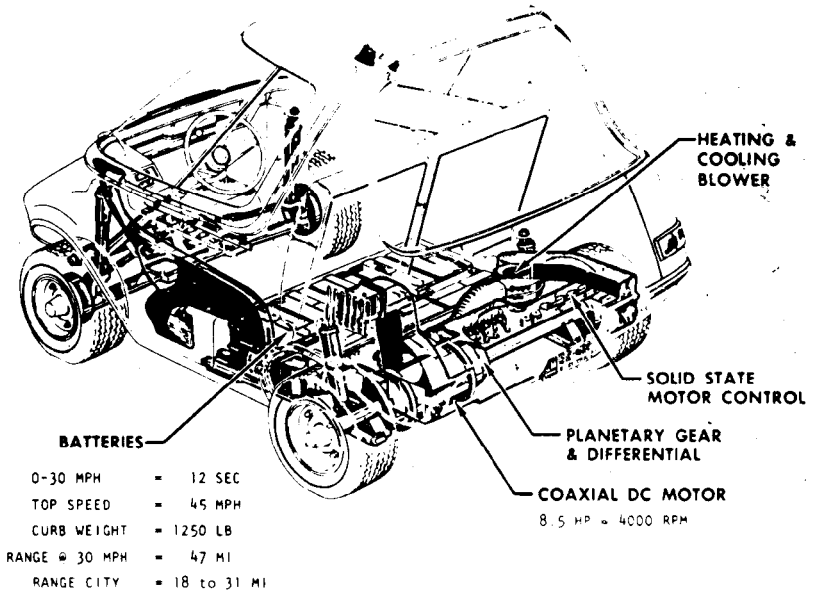
HEATING & COOLING BLOWER
SOLID STATE MOTOR CONTROL
PLANETARY GEAR & DIFFERENTIAL
COAXIAL DC MOTOR
8.5 HP @ 4000 RPM
BATTERIES
0-30 MPH = 12 SEC
TOP SPEED = 45 MPH
CURB WEIGHT = 1250 LB
RANGE @ 30 MPH = 47 MI
RANGE CITY = 18 to 31 MI

Figure 9. General Motors 512 electric car

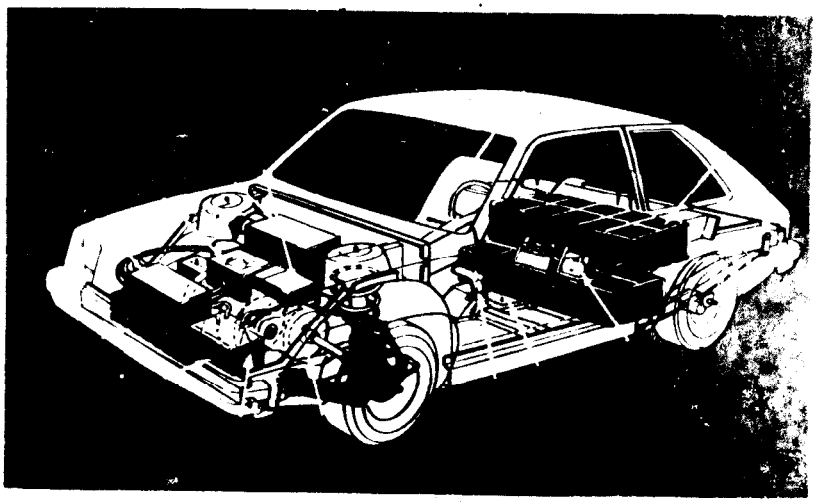

Figure 10. General Motors Electrovette

Another design concept has become known as the "backbone" structure where the batteries are packaged in a tunnel which also becomes the longitudinal axis of the chassis as demonstrated in Figures 11 and 12. This concept usually includes a mechanism to allow the batteries to be removed easily from either the front or the rear for replacement or service. Although both of these automobiles make use of the same chassis concept, they demonstrate considerable variation with regard to other design features.

The Runabout, described in Reference 36, features a front-wheel drive and a seating concept wherein the rear-seat occupants face rearward. It is primarily designed for manufacturability, marketability, and serviceability, but also includes good styling features with relatively low aerodynamic drag for improved range and performance. A fiberglass-reinforced polyester is used as the body surface and structure material. This has advantages of reduced weight, manufacturing flexibility, and relatively inexpensive tooling for initial, low-volume production.

The Endura, described in Reference 37, is designed with rear-wheel drive and has all four passenger seats facing the front. It is primarily designed to promote the feasibility of the electric automobile and to enhance their public acceptance. Thus such design features as safety, practicality, and aesthetics are strongly emphasized in addition to minimizing air drag through aerodynamic design for good performance.

Figure 11. Copper Electric Runabout.[36]

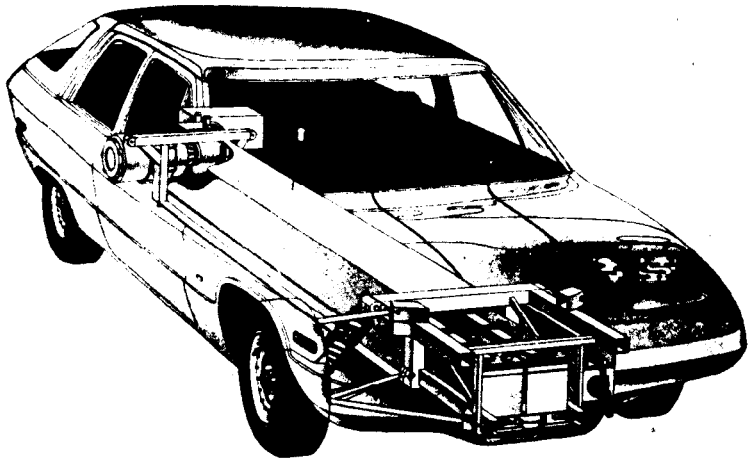

Figure 12. Globe-Union Endura.[37]

2.1.2. Battery Type

The lead–acid battery has been used most commonly for electric automobiles primarily because it is the only battery available at a reasonable cost on a production basis. However, in recent years a number of demonstration vehicles have been constructed and tested with power plants of alkaline batteries, such as zinc–nickel oxide, iron–nickel oxide, and metal–air (i.e., iron–air and zinc–air).

Figure 13 shows some initial work at General Motors Technical Center on electric automobile concepts, with the zinc–nickel oxide battery in mind.[38] Earlier GM work with the GM 512 car in Figure 9 verified the expected improvements in performance and range obtainable with this type of battery compared to the lead–acid battery.[26] More than a factor of 2 improvement in the range was demonstrated. Another zinc–nickel oxide battery-powered automobile is shown in Figure 14. The battery mass in this urban auto is only 17% of the GVM, which allows greater flexibility in component packaging.[39]

The iron–nickel oxide battery has been investigated for use in a variety of vehicles by the Westinghouse Corporation. Figure 15 shows this battery installed in the trunk compartment of a conventional automobile.[40] An off-vehicle heat exchanger and pump system was used with this battery pack to provide cooling and gas separation during recharge.

Metal–air batteries have been evaluated in experimental vehicles in Japan.[41] Owing to the low specific power capability of the metal–air systems, a hybrid power source is required wherein the metal–air battery provides the

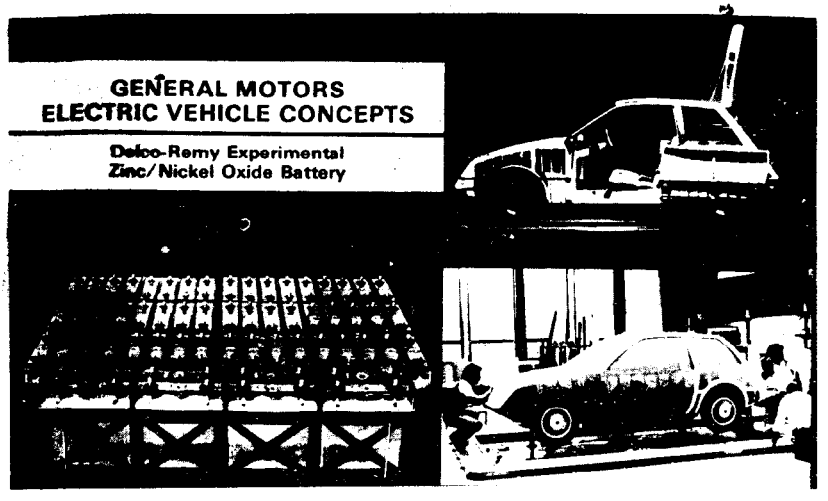

Figure 13. General Motors electric vehicle concepts.[38]

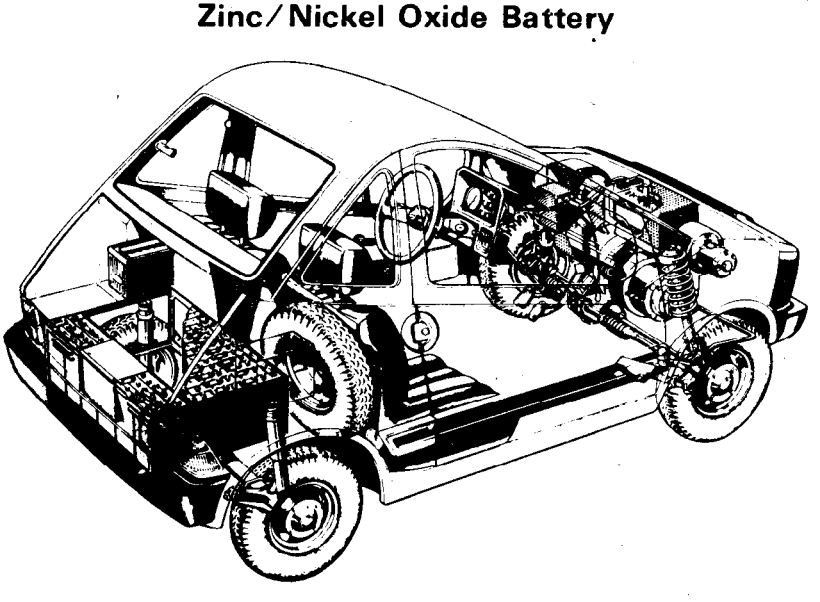

Figure 14. Fiat electric vehicle.[39]

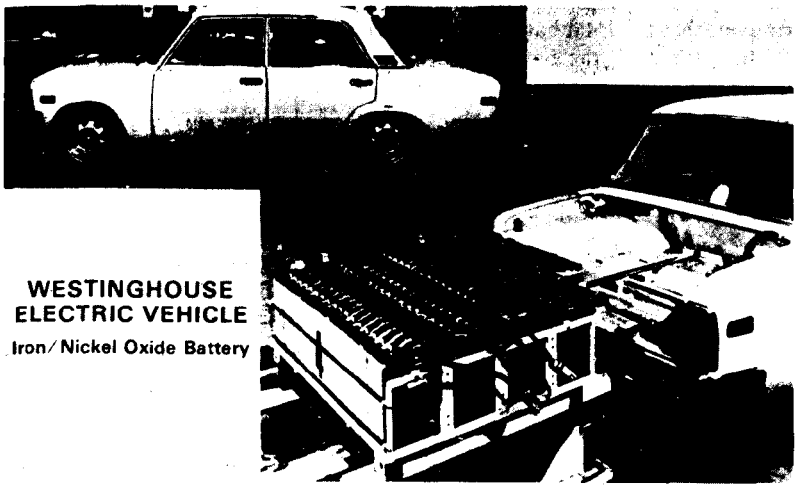

Figure 15. Westinghouse electric vehicle.[40]

energy for cruising, and a high power battery, such as lead–acid, provides power for acceleration. The installation of a hybrid system comprised of iron–air and lead–acid batteries in a lightweight electric passenger car is shown in Figure 16. Reported test results for this system indicate that a range of about

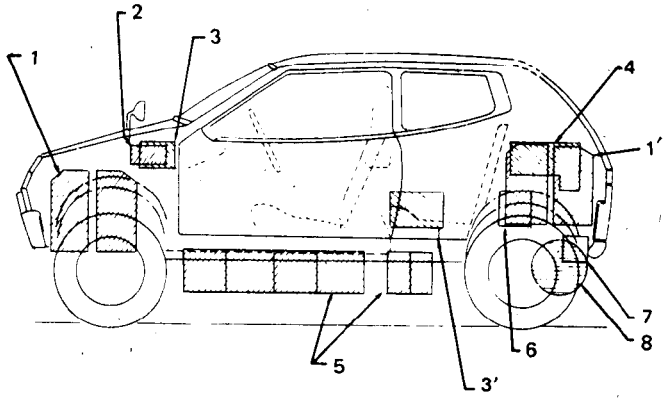

1	Iron-air storage batteries (4)	4	Controller
1′	Iron-air storage batteries (4)	5	Lead-acid storage battery
2	Battery charger	6	Power module
3	Contactor box (1)	7	Reactor
3′	Contactor box (2)	8	Electric motor

Figure 16. Toyota EV1H electric passenger car.[41]

260 km can be obtained at a constant speed of 48 km/hr.[41] It should be noted, however, that the total battery mass is about 37% of the GVM.

In addition to the battery concepts demonstrated here, there are other advanced concepts that are of interest for future electric vehicle applications. These are included in a detailed discussion of electrochemical power source technology in Section 5.

2.1.3. Overall Electric Drive System

The electric automobile drive system consists of an integrated design package including an electric motor and associated controller and related power-train components. Variations in drive systems result primarily from trade-offs between cost, efficiency, and driving comfort. Within this framework, five conventional motor and control concepts have been evaluated by Bader and Stephan, and the results are presented in Table 4.[42] The dc series-wound motor has been commonly used primarily because its torque-versus-speed characteristics are such that a transmission is not necessarily required. The use of a transmission in any electric drive system is usually based on the need to enhance the torque at low speeds for improved acceleration and hill-climbing capability. Thus the advantage of using a transmission becomes greater as the top speed and grade requirements increase.[43]

The function of the controller is to maintain the desired speed of the automobile under various road-load conditions by controlling the motor voltage. Advances in the field of power electronics have provided a more efficient means of doing this with so-called chopper circuits relative to using a variable series resistor or switching batteries into various parallel and series combinations. The chopper also provides smooth control over a wide range of

Table 4
Conventional Motors and Control Concepts for Electric Automobiles

Motor description	Control concept	Characteristics
Direct current series-wound	Variable resistor	Low cost Low efficiency
Direct current series-wound	Battery switching	Low cost Low driving comfort
Direct current series-wound	Electric chopper	Advanced efficiency High cost
Direct current shunt-wound	Separate electronic choppers in both armature and field circuits	High efficiency High cost
Direct current shunt-wound	Electronic chopper in field circuit and variable resistor in armature circuit	Low Cost Reduced efficiency and driving comfort

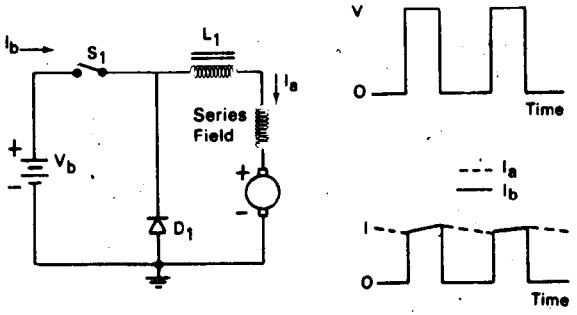

Figure 17. Armature chopper schematic and related waveforms.

motor speed. The most commonly used solid state controllers have utilized silicon-controlled rectifiers (SCRs) as the major element in the control circuit to switch the batteries in or out of the circuit to obtain pulsed dc with pulse width modulation. This approach is illustrated by the simplified schematic and the associated waveforms in Figure 17. The voltage applied to the motor can be varied continuously by controlling the conduction time of the switching SCR or transistor S_1. The inductor L_1 absorbs the difference between the motor voltage and the chopped voltage V, while diode D_1 provides a current path when S_1 is open. The current from the battery, I_b, is drawn in pulses as shown in Figure 17, which has the effect of increasing the I^2R loss in the battery, relative to an unchopped current, unless an additional filter is added between the battery and the controller.

With continuous improvements in power electronics, more consideration has been given to the trade-offs between a dc series-wound motor and the separately excited dc shunt-wound motor where the armature and the field currents are separately controlled. With this concept, the armature current is chopped only at low speeds to provide smooth acceleration and is not chopped at the higher speeds. Speed control is accomplished at the higher speeds by means of a chopper in the field circuit. This control concept is characterized by a relatively higher efficiency at cruise speed. In addition, it is easier to add regenerative braking capability, particularly in the field control range. This can be a significant advantage in that the effect of regenerative braking is reported to increase the range in urban electric automobiles by as much as 15%.[44] However, this advantage must be traded off against the increased cost to provide this capability.

With regard to future electric drive developments, there continues to be an interest in evaluating the potential advantages of ac drives as advances in microprocessors and other solid state technologies continue to develop.[45,46] Beyond that, there is some promise of reduced weight and additional increases in performance if development efforts now under way on the disk-type permanent magnet motor are successful.[47]

2.1.4. Demonstration of Modern Technology

The United States Department of Energy is funding a Near-Term Electric Vehicle Program with the general objective of showing that the electric vehicle concept is a promising near-term candidate for commercialization. In this regard, the four-passenger automobile concepts shown in Figures 18 and 19 have been designed to meet the performance objectives in Table 5, and performance testing began in late 1979.

In view of the objectives in Table 5, it is reasonable to conclude that these vehicles will demonstrate much of the latest technology in body and chassis design and drive train components that has been discussed in the previous paragraphs. Both of these vehicles include the "backbone"-type chassis structure, lightweight materials in the body and structure, and a lead–acid battery power source.

The GE/Chrysler vehicle demonstrates a significantly reduced aerodynamic drag as a result of extensive wind-tunnel testing. Regenerative braking is also incorporated in the separately excited, dc, shunt-wound propulsion motor which drives the front wheels.

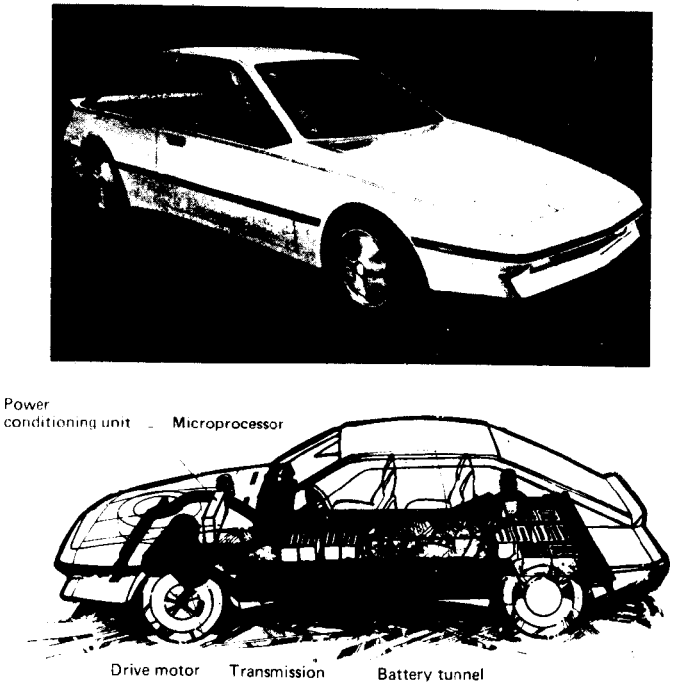

Figure 18. General Electric/Chrysler electric vehicle.

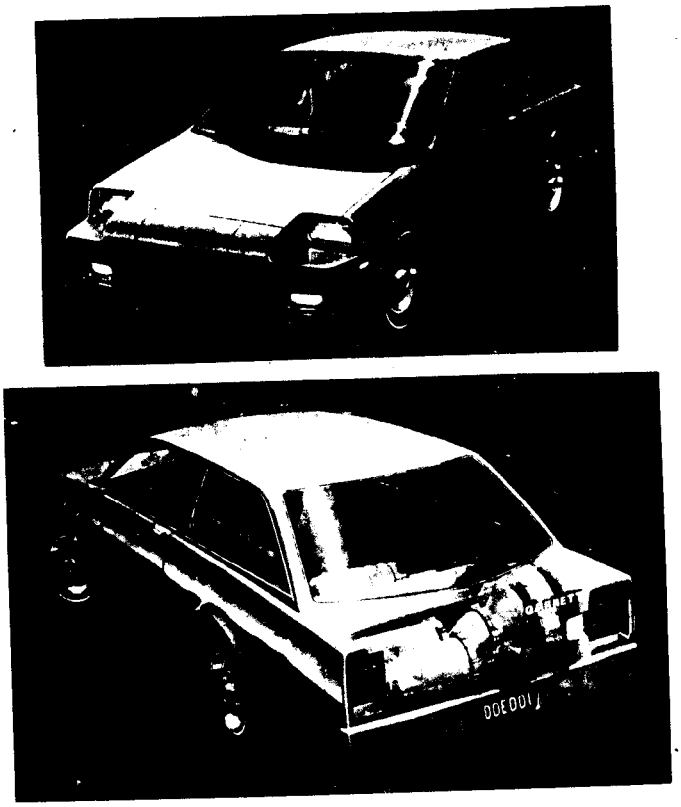

Figure 19. Garrett hybrid vehicle.

Table 5
Near-Term DOE Electric Vehicle Performance Objectives[a]

Minimum passenger capacity	Four adults
Maximum curb weight	Open
Minimum urban range, km	121
Maximum electric recharge energy in urban driving, kWh/km	0.32
Maximum recharge time, h	6
Safety features	Meet federal motor vehicle safety standards
Minimum ambient temperature range, °C	−29 to + 52
Minimum top speed, km/h	97
Maximum acceleration time, sec (0–48 km/h)	9
Maximum merging time, sec (40–89 km/h)	18

[a] Reference 48.

The Garrett vehicle demonstrates the use of a flywheel in the drive train to provide the peak power required for acceleration and to extend the effectiveness of regenerative braking to very low speeds. The flywheel is connected to the rear wheels through a continuously variable electromechanical transmission, and the main dc drive motor is a separately excited design developed specifically for this system.

2.1.5. Overall Performance Characteristics

At this relatively early stage in the development of the electric automobile, it is difficult to define state-of-the-art performance in terms of maximum cruise speed, acceleration capability, urban range, and energy consumption with any reasonable level of confidence. This situation exists primarily because of the following reasons: (1) Most of the electric automobiles reported in the literature are one-of-a-kind developmental vehicles representing differing levels of technology and design objectives, and (2) very little test data have been reported on these vehicles where the tests have been conducted in accordance with any standardized driving schedule, such as the SAE J227a schedules shown in Figure 20.

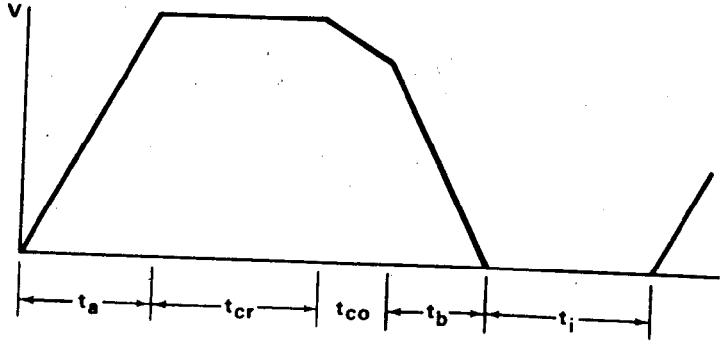

TEST PARAMETER	SAE J227a SCHEDULE			
	A	B	C	D
Maximum Speed V, km/h	16 ± 1.5	32 ± 1.5	48 ± 1.5	72 ± 1.5
Acceleration Time t_a, s	4 ± 1	19 ± 1	18 ± 2	28 ± 2
Cruise Time t_{cr}, s	0	19 ± 1	20 ± 1	50 ± 2
Coast Time t_{co}, s	2 ± 1	4 ± 1	8 ± 1	10 ± 1
Brake Time t_b, s	3 ± 1	5 ± 1	9 ± 1	9 ± 1
Idle Time t_i, s	30 ± 2	25 ± 2	25 ± 2	25 ± 2
Total Time, s	39 ± 2	72 ± 2	80 ± 2	122 ± 2

Figure 20. SAE J227a driving cycle schedules.[49]

The performance results presented in the following paragraphs are taken primarily from the results of two studies conducted for the United States Energy Research and Development Administration.[35,50] The results reported in Reference 35 are actual test results of selected automobiles to determine state-of-the-art performance. The results reported in Reference 50 are based on literature values that were, in most cases, then used as a basis for calculating specific performance characteristics using a computer simulation of electric vehicle performance.

The maximum cruising speed and the acceleration capability of an electric automobile are primarily determined by the drive train design and the specific power capability of the battery. The maximum cruising speed for the automobiles tested in Reference 35 varied primarily over a range of 60–80 km/hr for automobiles with a curb mass in the range of 500–1500 kg, respectively. With regard to acceleration capability, it was determined that about two-thirds of the automobiles tested were able to accelerate from 0 to 48 km/hr in from 7 to 13 sec.

The urban driving range (e.g., for the SAE J227a "C" schedule) that is typical of present-day electric automobiles is illustrated in Figure 21. These results demonstrate the effect of different ratios of battery mass to GVM from one automobile to another and also the effect of the specific energy of the battery power source. The specific energy bands define the urban range that can be expected from a power source when the specific energy of the power source is known for discharge conditions corresponding to urban driving requirements (see Figure 34, 30–35 W/kg). The width of the band allows for variation in road-load requirements from 0.13 to 0.17 Wh/kg km. The results of Figure 21 illustrate that with lead–acid battery technology and a battery fraction between 0.25 and 0.3, the maximum urban range that can be obtained with state-of-the-art technology is about 80 km.

The energy consumption results shown in Figure 22 are representative of the same electric automobiles that provided the data base for the urban range results in Figure 21. For most electric automobiles with a GVM in the range 750–1500 kg, the energy consumption from the "wall plug" is approximately 0.2–0.35 kWh/km. However, it was noted in Reference 35 that the limited data available from actual user experience with electric automobiles normally indicated about twice the energy consumption of the test results. This increase was speculated to be partly due to variations in road and climate conditions, driver's skill, and nonoptimum charging techniques and facilities.

2.2. Commercial Electric Vehicles

There is a relatively strong interest in the electric vehicle industry to develop vehicles for fleet operation. The types of vehicles that appear to be of greatest interest are (1) the utility vehicle, such as the postal service vehicle, (2) the delivery or service van, and (3) the passenger bus for public transport. The

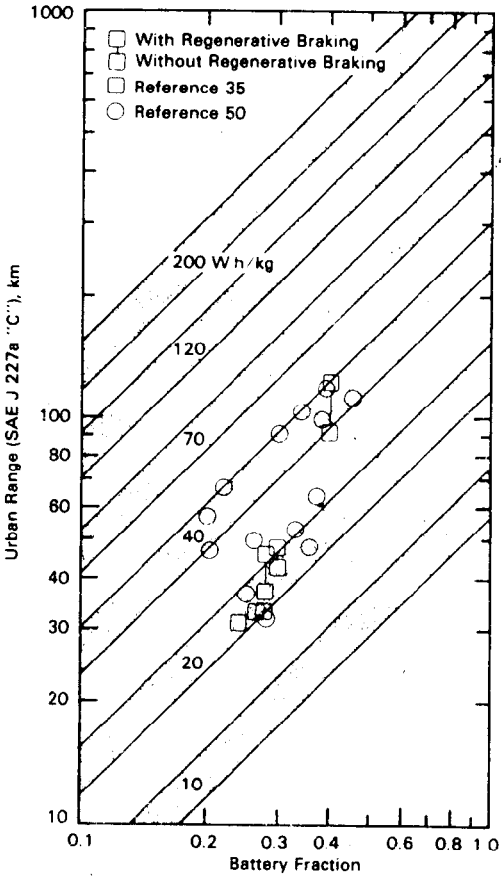

Figure 21. Typical urban range (SAE J227a "C") of present-day electric automobiles.

prime incentive for the development of electric commercial vehicles is to reduce the cost of owning and maintaining the vehicle fleet that is necessary to perform a desired service. The second incentive is that these vehicles operate primarily in urban areas where the eliminations of exhaust emission and the reduction of noise are desirable objectives.

The primary need to obtain a low total operating cost means that the design emphasis must be on high reliability for low maintenance, high efficiency for reduced energy costs, and sufficient performance and range capability to perform the desired service. For these reasons, the commercial vehicles do not necessarily represent the latest innovations in electric vehicle component technology as much as they represent the application of the most mature technology to the development of a marketable product. Thus most of these vehicles make use of an existing production-line body and structure, a dc series

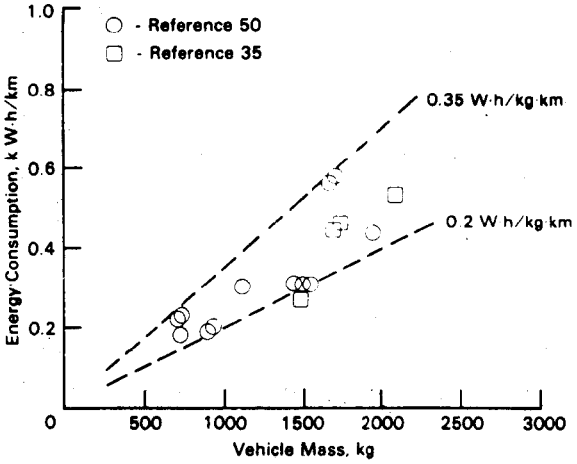

Figure 22. Typical energy consumption (SAE J227a "C") of present-day electric automobiles, measured at the wall plug.

or shunt-wound propulsion motor, a solid state chopper controller, limited regenerative braking, and a lead–acid power source.

2.2.1. Utility Vehicle

The relatively small utility vehicle which is used in the United States Postal Service represents the largest on-the-road electric vehicle fleet in the United States. This fleet includes 31 Harbilt and 352 AM General DJ-5E delivery vehicles operating primarily in Southern California. The AM General vehicle is shown in Figure 23, and its design and performance characteristics are listed in Table 6. The electric power train for this vehicle, consisting of batteries,

Table 6
AM General DJ-5E Design and Performance Characteristics

GVM, kg	1955
Payload, kg	306
Battery mass, kg	586
Cargo space, m^3	1.7
Acceleration time, sec (0–48 km/h)	20
Gradability	
Speed on 10% grade, km/h	22.4
Range, km	
Constant speed of 48 km/h	48
Postal cycle	40
Energy consumption, Wh/kg km	0.4–0.5

Figure 23. AM General DJ-5E postal service vehicle.[51]

controller, motor, and charger are supplied by Gould, Inc. It has been reported that this vehicle appears to be cost effective in this application and with continued success there could be a need in the United States Postal Service for about 5000 of these vehicles per year.[51]

2.2.2. Delivery and Service Van

The standard size electric delivery and service van is being developed by several groups in Europe and Japan as well as in the United States. The GVM of these vehicles is usually in the range 2600–3700 kg with a payload ranging from 500 to 1000 kg. The greatest interest for delivery applications is reported to be at the higher end of this range.[52]

The entry of General Motors Corporation Truck & Coach Division into this area is considered to be a significant indication that commercial electric vehicles can be developed into marketable products. The initial GMC vehicles being produced represent a conversion of a standard GMC van to electric propulsion and are aimed at satisfying the needs of limited-range service vehicles, such as telephone installation and repair trucks illustrated in Figure 24. The design and performance characteristics of this vehicle are listed in Table 7 and are quite typical of the overall developments in this field.

Energy economy data for the GMC van in actual service are not presently available. A very limited amount of data for delivery vans in actual service is reported in Reference 35 where energy economy at the "wall plug" is reported to be in the range 0.25–0.3 Wh/kg km.

Figure 24. GMC battery-powered commercial van.

The limited range obtained with lead–acid batteries significantly limits the scope of the electric delivery van applications. One approach to getting around this problem has been to design the vehicle to allow for a rapid exchange of the battery pack, as is illustrated by the Lucas Industries Limited (United Kingdom) conversion of the Bedford CF van shown in Figure 25.

Advanced battery technology is, of course, a more desirable approach to extending the range and broadening the scope of application of electric vans.

Table 7
GMC Design and Performance Characteristics[a]

GVM, kg	3682
Payload, kg	682
Battery mass, kg	1137
Lead–acid battery mounting	Single pack under vehicle
Safety	Full FMVSS compliance
Drive train	Direct current series motor with chain drive gear reduction and solid state continuous electronic speed control
Brakes	Vacuum assisted hydraulic with electrical regeneration
Acceleration time, sec (0–48 km/h)	12
Grade limit, %	20
Top speed, km/h	80
Range on SAE J227a "C," km	64

[a] From Reference 53.

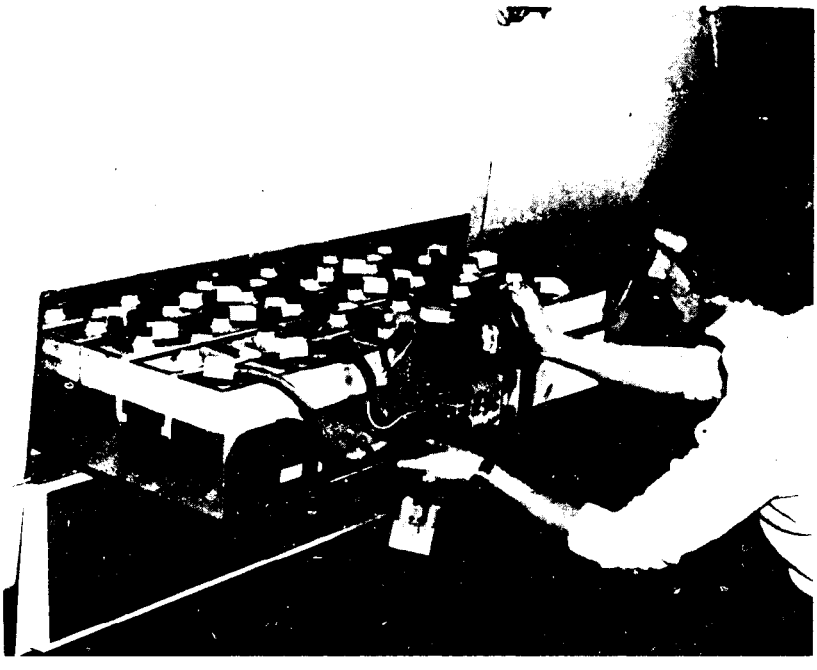

Figure 25. Bedford CF van and slide-in battery pack.[52]

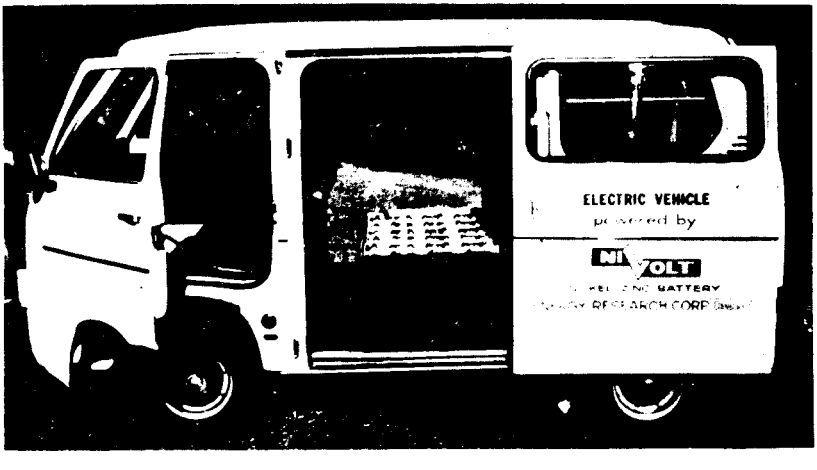

Figure 26. Zinc–nickel-oxide-powered van.[54]

The zinc–nickel oxide battery is a near-term candidate that would double the range of the electric van relative to lead–acid.[53] The van in Figure 26[54] illustrates the installation of zinc–nickel oxide batteries for demonstration purposes by Energy Research Corporation. Beyond this, the fuel cell and the high-temperature battery are potential long-term candidates. In this regard, it is noteworthy that the hydrogen–oxygen fuel cell powered van shown in Figure 27[55] was constructed and tested by General Motors in the late 1960s and that the sodium–sulfur battery powered van shown in Figure 28 was demonstrated by the Electricity Council Research Center in the United Kingdom in the early 1970s. The development status of these advanced concepts is discussed later in Section 5.

2.2.3. Passenger Buses

The major portion of the development of electric buses has taken place in Europe and Japan. The important operational requirements are high reliability, low operating cost and, in most cases, a high daily use factor with a relatively small amount of time available for battery charging and vehicle servicing. These requirements result in the use of proven components, maximum use of regenerative braking, and considerable innovation in battery charging techniques to reduce the amount of time the bus is out of service for battery recharge. The most noteworthy development efforts have taken place in West Germany where a fleet of 20 M.A.N. SL-E Elektrobuses have been running in a large-scale evaluation of overall performance under actual service conditions. The bus, shown in Figure 29,[56] demonstrates a unique battery containment and exchange concept wherein the batteries are contained in a trailer pulled behind the bus rather than being built into the bus chassis. Battery exchange is accomplished automatically during a five-minute rest period that the drivers are given between runs.

Overall performance data for the SL-E Elektrobus are reported in Reference 56. The bus has a GVM of 16,000 kg and half of the buses were built with separately excited dc motors and the other half with series-wound motors. The effect of regenerative braking was much more significant with the separately excited motor in that the energy required from the battery was about 16% less than for the series-wound motor. The overall average energy economy (from the "wall plug" for all of the buses in actual service was reported to be 2.35 kWh/km or about 0.15 Wh/kg km based on the 16,000-kg GVM.

3. Electrochemical Power Source Requirements

The characteristics of electrochemical power sources that are of primary concern in electric vehicle applications are peak specific power, average

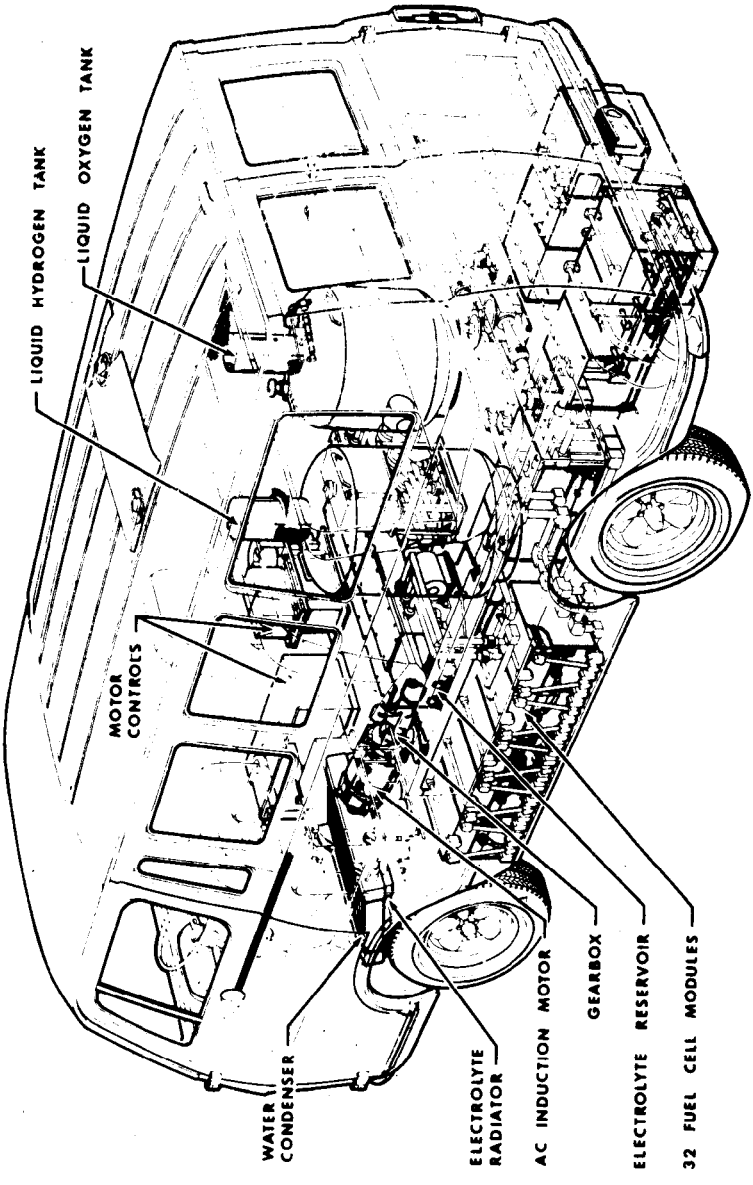

Figure 27. Cutaway view of General Motors Electrovan.[55]

Figure 28. Bedford van powered by a sodium–sulfur battery.[35] (Courtesy of Lewis Laboratories, NASA.)

specific energy, durability, and cost. The peak specific power must be interpreted to be a power level that can be sustained for at least 10–20 sec, and the average specific energy is the specific energy obtained by discharging at a specific power that represents an average of actual discharge conditions in a vehicle. This is typically a value of about 32 W/kg for an urban commuter type

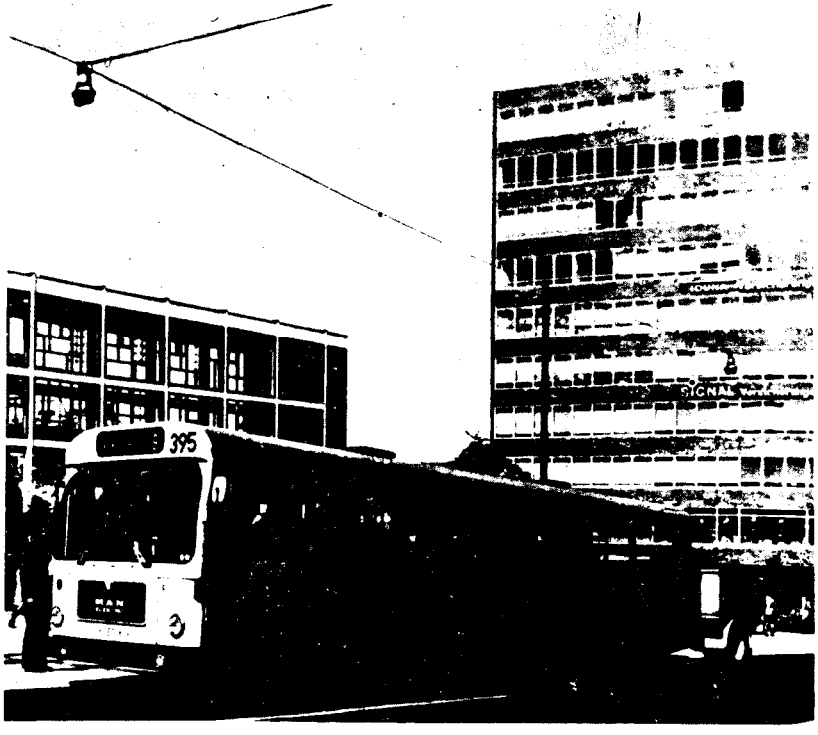

Figure 29. SL-E Elektrobus in route operation.[56] (Courtesy of Electric Vehicle News.)

of vehicle. In order to define specific power and energy requirements for the electrochemical power source, it is necessary to evaluate the power required to propel the vehicle. This can be done with sufficient accuracy for purposes of this discussion by the analytical treatment in the following paragraphs.

3.1. Vehicle Propulsion Power Calculations

The vehicle propulsion power requirement can be obtained from the product of vehicle velocity and the summation of the resistive forces for acceleration, aerodynamic drag, rolling resistance, and moving up a grade.

The force required for acceleration is represented by the relation

$$F_a = M_v \, dV/dt \tag{1}$$

where F_a is the acceleration force (newtons), M_v the vehicle mass (kilograms), V the vehicle velocity (m/sec), and t the time (seconds).

This relation applies only to linear acceleration, whereas some parts of the vehicle require rotational acceleration (such as the wheels, driveshaft, and motor). Tenniswood and Graetzel concluded that the force required for rotational acceleration is approximately 10% of that required for linear acceleration for the speed range 0–80 km/hr.[57] The total force required for both linear and rotational acceleration is then given by the relation

$$F_a = 1.1M_t\, dV/dt \tag{2}$$

The retarding effect of the aerodynamic drag force can be calculated from

$$F_d = \rho_A C_D A_f V^2/2 \tag{3}$$

where F_d is the aerodynamic drag force (newtons), ρ_A the air density (kg/m^3; 1.2255 kg/m^3 at 15°C and 760 torr), C_D is the air-drag coefficient (dimensionless), and A_f the frontal area of the vehicle (meters^2).

The coefficient of aerodynamic drag is determined by the design of the vehicle. Although the value can be on the order of 0.30 for highly streamlined cars, the average value for cars is closer to 0.5. The range of values for trucks is normally 0.5–0.7.

The resistive force due to the rolling resistance of the tires is typically approximated by the quadratic expression[58]

$$F_r = M_t gK(1 + 4.7 \times 10^{-3}V + 1.3 \times 10^{-4}V^2) \tag{4}$$

where F_r is the rolling resistance (newtons), g the gravitational constant (9.80665 m/s^2), and K the rolling resistance constant (dimensionless).

The rolling resistance constant, K, is primarily a function of the type of tire and the amount of inflation. The value of the constant varies over a range of about 0.008 for truck tires and radial ply automobile tires at high pressure to approximately 0.015 for normal automobile tires at low pressure. A typical value for an urban electric commuter automobile would be on the order of 0.012.

The resistive force associated with climbing a grade is defined as the downhill component of the force due to gravity and is expressed as

$$F_g = M_t g \sin\theta \tag{5}$$

where θ is the angle of the grade.

Where it is common to express the grade as a percent, then

$$\theta = \arctan(\%\ \text{grade}/100) \tag{6}$$

The power that must be provided to propel the vehicle can now be obtained by multiplying the sum of Eqs. (2)–(5) by the vehicle velocity. This results in the expression

$$P_p = V(F_a + F_r + F_g + F_d) \tag{7}$$

which is, by substituting Eqs. (2)–(5), the equation

$$P_p = M_v V[1.1\, dV/dt + gK(1 + 4.7 \times 10^{-3} V + 1.3 \times 10^{-4} V^2) + g \sin\theta] + \rho_A C_D A_f V^3/2 \quad (8)$$

where P_p is the propulsion power at the wheels (watts).

The propulsion power is a function of the vehicle design and also the manner in which the vehicle is driven. Thus to define P_p it is necessary to specify a driving profile, which defines the vehicle velocity as a function of time. Calculations of this type have been reported in the literature for different driving profiles using typical electric vehicle design parameters.[28,58]

Some of the pertinent results of those calculations are summarized in Table 8. The peak power and energy requirements shown in Table 8 will be referred to later in this section in the discussions of battery power and energy requirements.

In addition to the total propulsion power requirements shown in Table 8 for specific driving profiles, it is of interest to look at the contribution to the total power of each of the resistive forces in Eq. (7). Since the power required to accelerate the vehicle and to overcome rolling resistance and grade forces is proportional to the vehicle mass in each case, these contributions are plotted in Figure 30 as a function of vehicle speed. The power required for acceleration in Figure 30 is based on a simplifying assumption that dV/dt in Eqs. (2) and (8) is a linear function of vehicle velocity. That is,

$$dV/dt = C_a - 0.1V \quad (9)$$

where C_a is the initial acceleration (m/sec^2).

It can be illustrated that this is a reasonably good approximation of the actual acceleration characteristics of present-day combustion engine vehicles and that combustion engine compacts will typically fall in the range from

Table 8
Comparison of Driving Profile Power and Energy Requirements[a]

Driving profile	Maximum speed, km/h	Average speed, km/h	Number of stops, per km	Peak power[b] vehicle mass, W/kg	Energy[b]/vehicle mass × km, Wh/kg km
EPA urban	92	32	1.5	24.2	0.10
SAE J 1082 urban	48	25	2.5	25.0	0.09
SAE J 227 residential	48	33	0.7	13.3	0.08
SAE J 227 metropolitan	72	39	0.6	17.5	0.10

[a] From References 28 and 58.
[b] Requirements at the wheels of an automobile with a mass ranging from 1000 to 2000 kg.

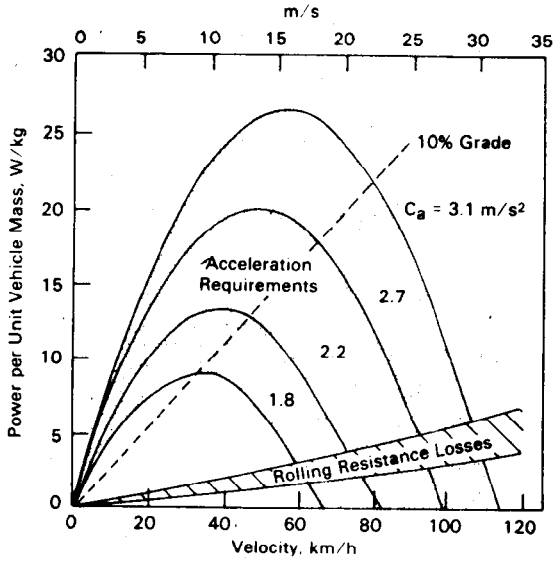

Figure 30. Power per unit vehicle mass required for acceleration and to overcome rolling resistance and grade forces.

C_a = 2.7 to C_a = 3.1 m/sec^2. The velocity versus time characteristics associated with the values of C_a plotted in Figure 30 are given in Table 9. It is noted that the values of C_a = 1.8 and C_a = 2.2 m/sec^2 are representative of the acceleration required for the SAE J 227a "C" and "D" driving schedules, respectively, which are shown in Figure 20. As mentioned above, the value of C_a = 2.7 m/sec^2 represents the minimum acceleration required for mixing with existing traffic on urban streets.

The power required to overcome the aerodynamic drag force is not a function of vehicle mass but is directly proportional to the frontal area of the

Table 9
Linear Acceleration Characteristics

Initial acceleration (C_a), m/sec^2	Time to reach 13.4 m/sec (48 km/h), sec	Velocity after 20 sec, m/sec (km/h)
1.8	14	15.6 (56
2.2	9	19.2 (69)
2.7	7	23.2 (83)
3.1	5.6	26.8 (96)

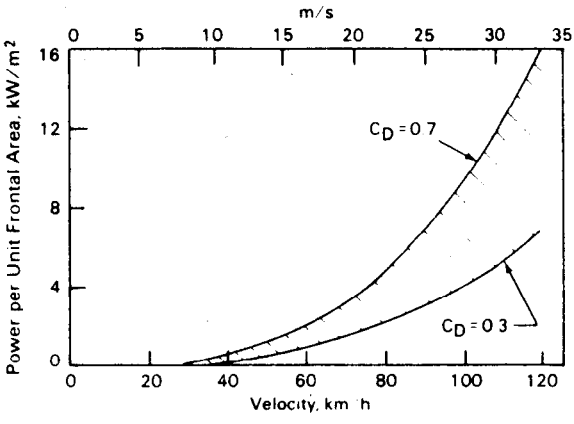

Figure 31. Power per unit frontal area to overcome aerodynamic drag.

vehicle. Thus this contribution to the total power is plotted in Figure 31 in terms of power per unit of frontal area as a function of vehicle velocity.

The results shown in Figures 30 and 31 are useful in that they can easily be applied to any vehicle, without the need of a large-scale computer, to approximate the maximum power required at the wheels of the vehicle as a function of aerodynamic drag coefficient, rolling resistance constant, and the initial value of linear acceleration.

3.2. Battery Power Requirements

The total power required from the power source includes the power delivered to the wheels for propulsion, defined by Eqs. (7) and (8) plus the losses resulting from electrical and mechanical inefficiencies in the power train and the power required to operate the accessory load. Thus the power delivered by the battery power source is

$$P_b = P_p/\eta_m\eta_e + P_{acc} \tag{10}$$

where P_b is the battery output power (watts), η_m the mechanical efficiency of the drive train, η_e the electrical efficiency of the drive train, and P_{acc} the accessory power required from the battery.

The accessory power includes the power required for heating and air conditioning, power steering, power brakes, lights, windshield wipers, etc. The most significant of these is the power that would be needed for air conditioning. It has been reported that a value of 1.3 kW would be a reasonable air conditioning power requirement for limited-range commuter electric vehicles.[59] Other authors[58] have reported a minimum accessory load without air

conditioning to be about 250 W and approximately 3000 W with air conditioning.

With regard to the inefficiencies of the drive train, the mechanical efficiency, η_m, is usually rather high and on the order of 93–95%. The electrical efficiency, η_e, of the motor and controller varies considerably with vehicle speed over a range of about 65% at low speeds to as high as 80% at high speeds. In view of this, an average value of 70% is a reasonable value for the product of $\eta_m\eta_e$ in Eq. (10).

A final consideration in determining the specific power requirement of the battery is the amount of vehicle mass that is allocated to the battery power source. This is normally expressed as a fraction of gross vehicle mass and ranges from about 0.2 to 0.4. A maximum value in the range 0.25–0.3 has been reported to be the most acceptable from the point of view of vehicle design and handling.[26]

A plot of battery specific power versus fraction of gross vehicle mass allocated to the battery power source for various acceleration characteristics is shown in Figure 32. The bold lines represent the peak power from Figures 30 and 31 at 0 grade, divided by the drive train efficiency of 70%. The broken lines are based on the peak power defined by specific driving profiles in Table 8. Since the increased aerodynamic drag of vans and light trucks is offset somewhat by a decrease in the rolling resistance constant relative to passenger

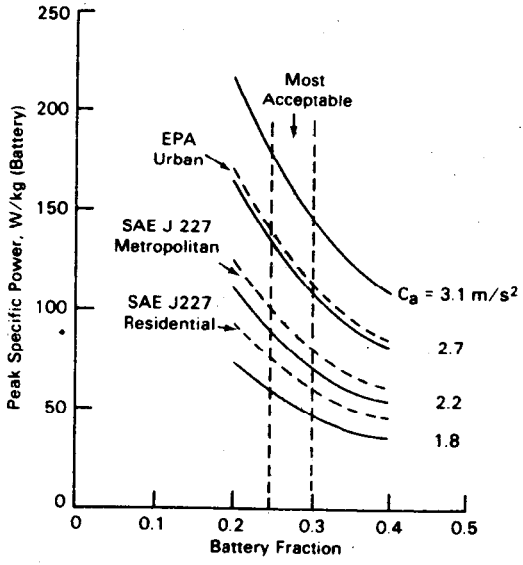

Figure 32. Battery peak specific power requirement for various acceleration characteristics vs. battery mass fraction.

vehicles, the curves of Figure 32 represent a reasonable approximation for these vehicles as well as for passenger vehicles. It can be seen from Figure 32 that in order to have a passenger vehicle with reasonable performance as defined by the EPA urban cycle or an initial linear acceleration of C_a = 2.7 m/sec^2, a battery specific power in the range 120–150 W/kg is necessary. In the case of delivery trucks, a reduced acceleration capability is acceptable in many applications; however, a mass fraction no greater than 0.25 is preferred to allow for a greater payload. In these applications, the lower curves in Figure 32 indicate that a battery specific power as low as 60–80 W/kg could be considered.

3.3. Battery Energy Requirements

The battery specific energy requirement is primarily defined by the range requirement of the vehicle. It is also important that this range be defined over a selected driving profile, in contrast to constant speed conditions, so that the efficiencies of the system and the effects of the driving schedule come into play and result in a more realistic measure of the energy required from the battery. A convenient approach to illustrating the relationships between vehicle range and battery specific energy is shown in Figure 21 of Section 2. In this plot, the range over urban driving conditions is plotted versus battery fraction for various values of battery specific energy. The specific energy lines are based on an energy requirement from the batteries of (0.15 ± 0.02) Wh/kg km, which is a typical value for various urban driving profiles as indicated by the energy requirements shown in Table 8. The band is used to allow for reasonable variation in vehicle design parameters and drive train efficiencies.

There appears to be reasonable agreement that a commuter passenger vehicle should have an urban range of at least 150 km.[8,26,38] From Figure 21, it is concluded that for a reasonable battery fraction in the range 0.25–0.3, a battery specific energy of at least 70 Wh/kg is required. With regard to many of the delivery and service vehicle applications, it has been indicated that a range in the order of 100–120 km would be quite adequate.[53] Thus for these applications a minimum specific energy of 60 Wh/kg could be of interest.

3.4. Durability and Cost Requirements

The subject of electrochemical power source requirements would not be complete without some consideration of the durability and cost requirements. The key factor here is operating cost in that the cost of the batteries is usually considered to be a cost item that is amortized over the number of kilometers driven before the batteries are replaced. This brings into focus the concept of durability in that the amortized battery cost is inversely related to durability or cycle life. This issue is further complicated by the fact that the battery cycle life

is a function of how the battery is used, which is discussed in more detail in the next section.

Owing to the lack of good information regarding the total operating costs of electric vehicles, it is rather meaningless to define objective requirements for durability and battery cost. However, the significant factors that come into play can be discussed, at least, in general terms.

It is reasonable to postulate that the operating cost of an electric vehicle would have to be competitive with the operating cost of a conventional combustion engine vehicle. The operating cost of an electric vehicle can be expressed as

$$C_{eo} = C_b + C_e + C_{me} + C_{ev} \tag{11}$$

where C_{eo} is the total electric vehicle operating cost ($/km), C_b the amortized battery cost ($/km), C_e the cost of electricity ($/km), C_{me} the amortized maintenance cost of electric power train ($/km), and C_{ev} the amortized electric vehicle (less batteries) ownership cost ($/km).

The related expression for a combustion engine vehicle could be

$$C_{co} = C_f + C_{mc} + C_{cv} \tag{12}$$

where C_{co} is the total combustion engine vehicle operating cost ($/km), C_f the cost of fuel ($/km), C_{mc} the amortized maintenance cost of combustion engine power train ($/km), and C_{cv} the amortized combustion engine vehicle ownership cost ($/km).

A comparison of Eqs. (11) and (12) leads to the following assumptions:

1. C_e will be less than C_f since the cost of electricity is not expected to increase as much as the cost of gasoline or synthetic fuels.
2. C_{me} will be less than C_{mc} primarily because of the relative simplicity of the power train and fewer parts.
3. C_{ev} will be less than C_{cv} since C_{ev} does not include battery cost, whereas C_{cv} includes the combustion engine cost. All other factors, such as insurance, body maintenance, tires, etc., should be similar.

The operating cost of the electric vehicle will be competitive if C_b is less than or, at most, equal to the savings realized by these assumptions. Thus

$$C_b \leq (C_f - C_e) + (C_{mc} - C_{me}) + (C_{cv} - C_{ev}) \tag{13}$$

Since C_b is directly proportional to the battery cost ($/kWh) and inversely proportional to durability (cycle life) as illustrated in the following section, the battery cost requirement can be expressed as

$$\text{battery cost (\$/kWh)} \leq K \times \text{durability}\,[C_{co} - (C_e + C_{me} + C_{ev})] \tag{14}$$

where K is the constant relating to the energy consumption of the electric vehicle and the depth-of-discharge of the battery power source, and durability is the number of charge–discharge cycles.

The expression above emphasizes the significance of the battery durability and the reliability of the electric power train with regard to battery cost. In general, the proponents of electric vehicles are optimistic that if the above assumptions prove to be reasonably valid and if the battery durability is on the order of 300–500 cycles at 80–100% depth-of-discharge, then the resulting battery cost requirement approaches a value that could be realized in production quantities.

4. Identification of Candidate Power Sources for Electric Vehicles

As discussed above, the success of an electric vehicle requires more than an electrochemical power source of acceptable performance; it must also have adequate durability and acceptable cost. It is not difficult to build a battery of acceptable performance *or* acceptable durability *or* acceptable cost. Even combinations of any two of these three requirements can be achieved. So far, it has been possible to achieve satisfactory battery performance *and* durability *and* cost in only a few electric vehicle applications. Currently, these applications are limited to a few specialized industrial, commercial, and recreational vehicles, such as forklift trucks, mining vehicles, personnel carriers, and golf carts. All of these vehicles have modest performance and range requirements, such that Pb–PbO_2 batteries have been acceptable.

4.1. Battery Performance

When the performance and range needs for electric automobiles are taken into consideration, it is clear from the previous sections of this chapter that a power source capable of providing more than 100 W/kg acceleration power, and more than 70 Wh/kg energy storage capability is necessary if a range of 150 km is to be achieved. As a first step, it is of interest to identify those candidate systems that show promise (or hope) of providing adequate performance and range for electric automobile use. Next, this list can be reviewed with materials cost and availability criteria in mind, yielding a group of candidate systems for further consideration.

In the first step of identifying those candidate electrochemical systems that might be of interest, it is useful to separate the candidate systems into two groups: batteries and fuel cells. This grouping is important because in batteries, at least one of the reactants is stored within each cell, and the *specific energy* of the system tends to be a performance-limiting factor. In fuel cells, neither reactant (fuel or oxygen from air) is stored in the cell, and the *specific power* of the system tends to be a performance-limiting factor. Most of the discussion to follow will be concerned with batteries, because they are much closer to being practical for electric automobiles than are fuel cells.

With regard to candidate couples for batteries, it is useful to consider the maximum amount of energy per unit mass of reactants that might be provided by a given electrochemical couple. This energy is called the theoretical specific energy, and is useful in focusing attention on the electrochemical couples that might provide batteries of high specific energy. Under ideal conditions (and at constant temperature and pressure), the maximum amount of electrical energy that might be obtained from an electrochemical reaction is the Gibbs free energy of reaction (ΔG), which can be calculated easily with the aid of thermodynamic tables. The minimum mass that might be associated with a cell is that of the reactants (or products), with no allowance for electrolyte or structural materials. Thus the maximum specific energy that theoretically might be available is

$$\text{theoretical specific energy} = \frac{-\Delta G}{\sum \gamma_r M_r} = \frac{nFE}{\sum \gamma_r M_r} \tag{15}$$

where n is the number of electrochemical equivalents involved in the cell reaction, F is Faraday's constant (96,487 C/equiv), E is the average emf of the cell reaction, M_r the molecular weight of cell reactant, γ_r the number of moles of cell reactant, and $\sum$ the summation over all cell reactants.

It is obvious from Eq. (15) that the theoretical specific energy is highest when the cell emf is high (or $-\Delta G$ is high), and the reactant equivalent weights are low.

A high cell emf is obtained from negative electrode reactants of low electronegativity (on the left-hand side of the periodic chart), and positive electrode reactants of high electronegativity (on the right-hand side of the periodic chart). Low equivalent weights correspond to the upper portion of the periodic chart. It follows, then, that the elements of interest for lightweight negative electrodes include H_2, Li, Na, Be, Mg, Ca, and several others. This list soon becomes modified, excluding some, such as Be, and adding others, such as Fe, Zn, Cd, and Pb, as a number of compromises are made among the many characteristics that must be considered. The elements that serve as candidates for positive electrodes include the chalcogens, such as O_2, S, Se, the halogens, such as F_2, Cl_2, Br_2, and compounds containing these elements, such as PbO_2, NiOOH, Ag_2O, MnO_2, FeS, FeS_2, $SbCl_3$, etc.

The list of couples that could be assembled from the above groups of reactants is impressively long. However, when practical chemical and electrochemical considerations are applied, such as compatibility with an electrolyte common to the positive and negative electrode reactants, the list becomes more manageable. Such a list is given in Table 10, showing the negative electrode reactant, electrolyte, and positive electrode reactant for each candidate couple. A number of reactants have been eliminated for reasons of cost (Ag, Cd, Hg), availability (Ag, Cd, Hg), health and environmental reasons (Cd, Hg, Se, F_2), and others.

Table 10
Candidate Cells for Electric Automobile Batteries

Ambient temperature cells	
Aqueous electrolytes	Nonaqueous electrolytes
$Pb-H_2SO_4-PbO_2$	$Li-LiClO_4-TiS_2$
$Zn-ZnCl_2-Cl_2$	
$Zn-ZnBr_2-Br_2$	
$Zn-KOH-NiOOH$	
$Zn-KOH-MnO_2$	
$Zn-KOH-Air$	
$Fe-KOH-NiOOH$	
$Fe-KOH-Air$	
$Al-KOH-Air$	

High temperature cells	
Molten-salt electrolytes	Solid electrolytes
$Li-LiCl-KCl-S$	$Na-\beta-Al_2O_3-S$
$LiAl-LiCl-KCl-FeS$	$Na-Na_{1+x}Zr_2Si_xP_{3-x}O_{12}-S$
$LiAl-LiCl-KCl-FeS_2$	$Na-Na-glass-S$
$Li_4Si-LiCl-KCl-FeS$	$Na-\beta-Al_2O_3-SbCl_3$ in $NaAlCl_4$
$Li_4Si-LiCl-KCl-FeS_2$	

To provide some perspective in comparing the candidate cells to one another, the theoretical specific energy values have been calculated for the couples of Table 10, and a number of others, using Eq. (15). The results are shown in Figure 33. Note the iso-emf lines. Other considerations being equal, it is advantageous to choose cells with a high emf, because resistive (and some other) losses tend to be a smaller fraction of the cell voltage for higher-emf cells. Also, a smaller number of cells in series connection is needed to provide a reasonable power system voltage (e.g., 100 V).

How does one use Figure 33 in assessing the specific energy that might be obtained from a cell of practical design and construction? A reliable set of guidelines is as follows: multiply the theoretical specific energy by 0.2–0.25 for cells with solid reactants, and by 0.15 for cells with an air electrode. These multipliers apply for systems developed to provide reasonable cycle life, at a minimum weight.

The results of the considerations above indicate that the specific energy values above 100 Wh/kg are expected to be obtainable mostly with high-temperature cells using alkali metal electrodes. In a number of situations, it may be appropriate to compromise the specific energy for the convenience of ambient temperature operation. This may be particularly appropriate for personal-use electric vehicles that are not operated every day.

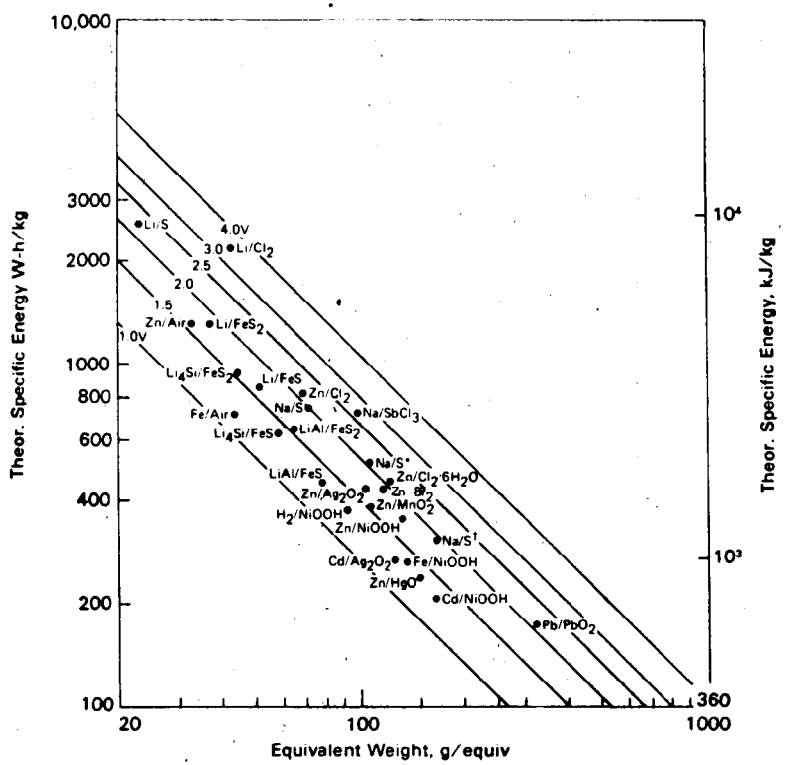

Figure 33. Theoretical specific energy of candidate cells for electric vehicle batteries. Na/S* signifies $2Na + 5.2S \rightarrow Na_2S_{5.2}$, two-phase region; Na/S+ signifies $Na_2S_3 + 2.2S \rightarrow Na_2S_{5.2}$, single-phase region.

The theoretical considerations above have allowed for the elimination of a number of cells from further evaluation, on the basis of specific energy, reactant cost, availability, and hazards. The next steps in comparing and selecting cells require experimental results, largely because the complex science of electrochemical cell design is not sufficiently advanced to allow accurate predictions of specific power, cycle life, and cost.

A simple but useful reflection of the relationship between the specific energy (Wh/kg) and the specific power (W/kg) of various batteries is shown in Figure 34. The lines curve toward lower specific energies at higher specific powers for a number of reasons, including higher voltage losses (resistive and other) at higher power levels and lower active material utilizations at higher power levels. Design improvements to make these curves more nearly vertical usually add weight, and cause the low specific power ends of the curves to shift to the left. The cell and battery design optimization process is a complex one,

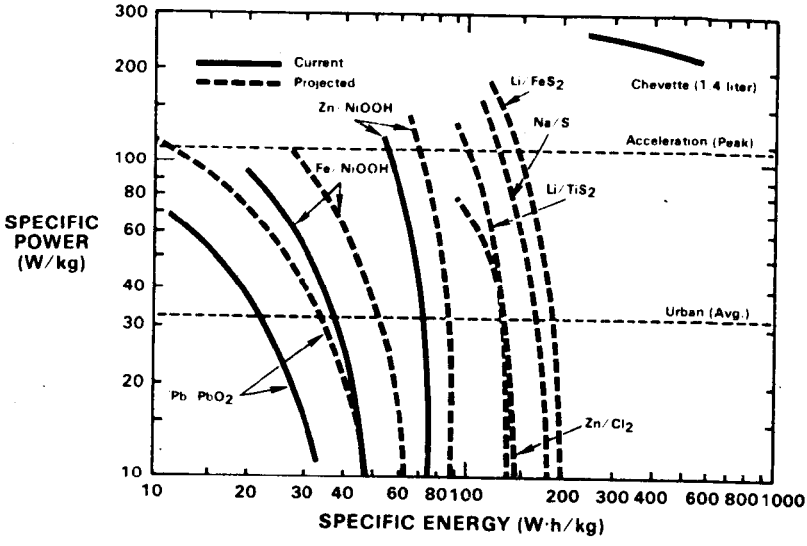

Figure 34. Specific power vs. specific energy for electric vehicle battery candidates.[150,70,76,90,85,128,129]

and requires a detailed knowledge of the motor and controller characteristics, and a map of the required vehicle performance.

The specific power required for reasonable acceleration is shown as 120 W/kg in Figure 34. All candidate batteries must have this capability for 10–20 sec for each major acceleration, over most of the capacity of the battery (0 to 75–80% depth of discharge) and over most of its range of operating temperatures. As discussed earlier in this chapter, the specific energy determines the range of the vehicle as shown in Figure 21. Use of the specific energy at 32 W/kg (average specific power) from Figure 34 in conjunction with Figure 21 allows the estimation of the urban range of an electric automobile with any of the candidate batteries. Obviously the curves of Figure 34 which lie to the right give longer ranges; all candidates for automobile propulsion must have curves that extend above 120 W/kg for good acceleration. The curves of Figure 34 allow the preliminary selection of batteries based on performance issues alone. Durability and cost of the batteries are also very important considerations.

4.2. Battery Durability

Battery durability (or cycle life) is most simply expressed in terms of the number of charge–discharge cycles to which the battery can be subjected

before a specified loss in energy delivery capability has occurred. As might be expected, the cycle life is a function of the conditions under which the battery is cycled. A partial list of variables (aside from design and construction parameters) influencing cycle life is given in Table 11. With this long list of important variables, it is not surprising that there is great scatter and uncertainty in the literature as to the values of cycle life under various conditions for even the most well-established cells (Pb–PbO_2 and Cd–NiOOH). There are very few data concerning the quantitative effect of the variables of Table 11 on the cycle life of any cells or batteries.

The most commonly reported cycle life data for cells and batteries correspond to operation at room temperature, at depths of discharge less than 50%, carried out at constant current corresponding to less than 10 W/kg with no mechanical movement, and some sort of maintenance. If any cell interconnections are used, they are almost always simple series connections of no more than a few cells. A few data are available for the cycle lives of cells

Table 11
Some Variables Affecting Battery Cycle Life

Temperature
Depth of discharge
Manner of discharge
1. Constant current
2. Constant power
3. Constant resistive load
4. Variable current (driving profile)
5. Variable power (driving profile)
6. Chopped current
Extent of charge (and overcharge)
Manner of charge
1. Constant current
2. Constant voltage
3. Current-limited constant voltage
4. Pulsed current
5. Charge, rest
Mechanical movement
1. Vibration
2. Shock
3. Tilting or rocking
4. Flow conditions
Cell interconnections
1. Series connections
2. Parallel connections
3. Ladder networks
Maintenance procedures
1. Water or electrolyte addition
2. Periodic special discharging or recharging
3. Periodic resting

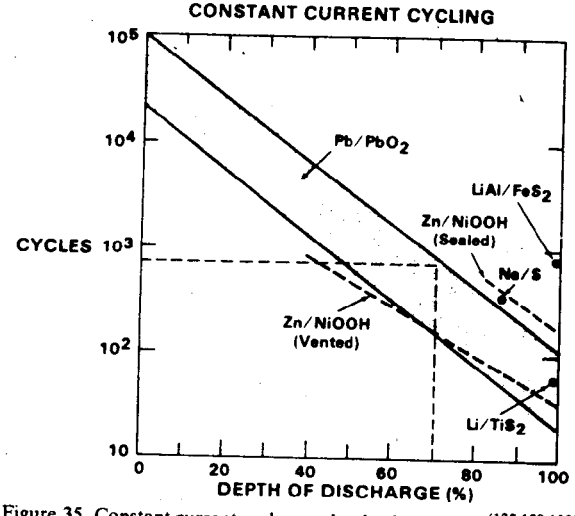

Figure 35. Constant current cycles vs. depth of discharge.[128,129,133]

currently under development, and a scattering of data for various designs of Pb–PbO_2 cells and batteries. These are summarized in Figure 35,[38] plotted as the logarithm of the cycle life vs. percent depth of discharge. For most of the data, the cycle life was reported as the number of cycles before failure to deliver the fraction of the design capacity indicated by the percent depth of discharge (DOD). In the case of 100% depth of discharge data, the reported cycle life usually represents the number of 100% DOD cycles to a given discharge cutoff voltage (e.g., 1.4 V per cell) executed before a loss of 20% or 25% of the design capacity is experienced.

At the present time, the exact shapes of the curves of Figure 35 are unclear because of the paucity of the data. If they are straight lines, then there is a depth of discharge for which the specific energy throughput is a maximum. The specific energy throughput is defined as follows:

$$\text{SET} \equiv n \times \text{SE} \times \text{DOD} \tag{16}$$

where SET is the specific energy throughput, the amount of energy passed through the cell or battery in its lifetime, per unit of battery mass (Wh/kg), n is the cycle life (the number of cycles before failure), SE is the specific energy (Wh/kg), and DOD is the depth of discharge (fraction of the total energy withdrawn from the cell or battery on each discharge).

If the relationships in Figure 35 are straight lines, then the following equation applies:

$$\log n = \log n_1 - b(1 - \text{DOD}) \tag{17}$$

Table 12
Values for DOD_m, n_m/n_1, and SET_m/SET_{n_1} for various slopes

$-b$	DOD_m	n_m/n_1	$SET_m/(SET_{n_1})$
3	0.1448	368	53.3
2	0.217	36.8	8.0
1	0.434	3.68	1.6

where n_1 is the cycle life at DOD = 1 and b is the slope. The maximum energy throughput then lies at the point

$$DOD_m = \frac{-1}{2.303b} \tag{18}$$

Values for DOD_m, n_m/n_1, and SET_m/SET_{n_1} are given in Table 12 for various slopes. In the case of an energy throughput which is independent of DOD, there is simply an inverse relationship between n and DOD:

$$n/n_1 = 1/DOD \tag{19}$$

A few data points exist which indicate that for some Pb–PbO_2 cells, a relationship applies that is intermediate between Eq. (17) (with $b = -2$) and Eq. (19). Limited data for other systems are consistent with Eq. (17) for DOD > 0.5, with $b \simeq -2$. The relationship between cycle life and depth of discharges remains an open issue, but an important one, because it may be feasible to increase significantly the energy throughput by operating at less than 100% DOD, as shown in the last column of the table above. This means that the distance that the electric automobile can be driven before replacing the battery may be increased very significantly by recharging the battery before it is completely discharged.

The battery durability issue currently represents one of the most important unknowns with regard to the economic viability of electric automobiles. It is essential that much more information be gathered about the effects of all of the variables of Table 11 on cell and battery life, especially temperature (and temperature gradients), depth of discharge, manner of discharge (driving profile), extent and manner of charge, mechanical movement (during discharge), cell interconnections, and maintenance. The equipment for such testing is expensive, and the time required is long. It is not surprising that these data are slow to appear.

4.3. Battery Cost

The cost of batteries suitable for use in electric automobiles is highly uncertain because none of the commercially available batteries has been

optimized for this application. At this time, it is only possible to bracket the costs of some types of batteries, and to set goals for others that are in earlier stages of development. As indicated above, the life of batteries is also very uncertain, causing the very important amortized cost of the battery to be in a highly unsatisfactory state of knowledge. A large amount of testing and field experience will be required before the amortized battery cost ($/km) will be known with reasonable confidence.

Something must be said about battery cost, in spite of the lack of information, because this subject is central to the viability of the electric automobile (and other electric road vehicles). As one point of reference, the present cost of Pb/PbO_2 traction batteries is about $100/kWh.[38] If this battery has a cycle life of 300 at 80% DOD, then the amortized cost (for the battery in a 1000 kg vehicle) is

$$\text{amortized cost (\$/km)} = \frac{\text{battery cost (\$/kWh)} \times 0.15 \text{ Wh/kg km} \times 1000 \text{ kg}}{n \times \text{DOD}}$$

$$= \frac{100 \times 0.15}{300 \times 0.8} = 0.0625 \text{ \$/km} \tag{20}$$

Note that the battery fraction does not enter this calculation, except as it may indirectly affect $n \times$ DOD. Therefore, to a good approximation, the amortized battery cost is insensitive to the battery fraction. (The range of the vehicle, however, is directly proportional to the battery fraction.) The amortized battery cost calculated above is significantly higher than present gasoline costs (it is equivalent to about $2.70/gal), hence battery amortization cost goals well below 0.06 $/km are advisable.

In the absence of firm cost information for electric vehicle batteries of various types, it is of some interest to review the cost goals for the battery development programs being funded by the Department of Energy (DOE).[38] These goals are set in terms of $/kWh. We have converted these into $/km, and $/battery for a 250-kg battery in a 1000-kg vehicle:

$$\text{\$/battery} = \text{\$/kWh} \times \text{kWh/kg} \times 250 \text{ kg} \tag{21}$$

The cost goal figures are summarized in Table 13.[38]

Most of the cost goals in Table 13 are reasonably close to 1¢/km for a 1000-kg vehicle, with a battery fraction of 0.25. This is certainly an ambitious goal, corresponding to $50/kWh or less, and a cycle life of about 1000. Ambitious as it is, this low cost may be a prerequisite to widespread use of electric automobiles. Considerably higher costs for batteries to be used in commercial vehicles (such as vans) or buses can be tolerated. It is likely that commercial electric vans will be in use in the U.S. with acceptable economics within the next few years.

Table 13
Battery Goals

Battery type	(Ref.)	State of the art	$/kWh	Cycle life	% DOD	Wh/kg at 32 W/kg	$/Battery[a]	$/km[b]
$Pb–PbO_2$	(124)	Now	~90	300	80	25	562	0.056
		Improved	50	800	80	40	500	0.012
		Advanced	40	1000	80	50	500	0.0075
Fe–NiOOH	(125)	Now	120	100+	100	50	1320	0.018–
		Advanced	60	1000+	100	60	900	0.0090–
Zn–NiOOH	(126)	Now	180	300	75	70	3150	0.12
		Improved	110	500	75	75	2062	0.044
		Advanced	55	1000	75	90	1238	0.011
$Zn–Cl_2$	(127)	Now	—	100	100	70	—	—
		Improved	75	500	100	130	2438	0.023
		Advanced	50	500	100	130	1625	0.015
$Li–TiS_2$	(128)	Now	—	50	100	40	—	—
		Advanced	50	500	80	130	1625	0.019
Na–S	(129)	Now	—	~300	80	80	—	—
		Advanced	35	1000	80	170	1488	0.0066
$Li–FeS_2$	(129)	Now	—	700	100	170	—	—
		Advanced	35	1000	100	200	1750	0.0053

[a] For a 250-kg electric automobile battery.

[b] $\$/km = \frac{\text{battery cost (\$/kWh)} \times 0.15\ \text{Wh/kg km} \times 1000\ \text{kg}}{\text{DOD} \times \text{cycle life}}$

The performance and cycle life goals were included with the cost goals in Table 13 to emphasize the point that it is necessary to meet simultaneously goals in all three areas before expecting to find acceptance in the marketplace. These goals for each of the batteries serve as a useful reference point against which to compare the status of the systems ("Now" in Table 13) to be discussed individually below.

4.4. Fuel Cells

The idea of using fuel cells as a high-efficiency source of pollution-free electrical power has been attractive for a very long time. The interest in fuel cells for vehicle propulsion relates to the ability to carry enough fuel to give the vehicle a range of hundreds of kilometers, but with greater efficiency than existing automobiles, and with the advantages of smooth, quiet, low-pollution, electrical propulsion. Unfortunately, there have been many scientific and engineering problems preventing the use of fuel cells in applications that could be served by any other means. Fuel cells were used in the space program because they alone possessed the combination of specific energy and specific power to meet the needs of the Gemini and Apollo missions. Continued

research and development efforts have made it possible to construct and operate a few fuel-cell-powered vehicles for demonstration purposes. These vehicles have included a farm tractor, golf carts, an army truck, and a full-performance van.[60] Also, hybrid systems of fuel cells (for range) plus batteries (for power) have been demonstrated, one in an electric car.[61]

The results of the above demonstrations have served to emphasize the problems that remain to be solved before fuel cell systems might be practical for some classes of electric vehicles. One of the major technical problems with regard to vehicle fuel cells is that of the fuel. The only fuel cells with performance capabilities within the range of acceptability for vehicle use must have hydrogen as the fuel, and the hydrogen must be free of carbon monoxide (at least in the 100-ppm range) and sulfur. This presents a significant problem with regard to on-board storage or preparation of hydrogen. Storage of hydrogen in tanks is bulky, heavy, and presents safety problems; storage as the hydride is also heavy,† and expensive. Preparation on board from carbonaceous fuels is bulky, complex, and slow to start up. The storage and/or preparation of hydrogen on the vehicle adds to the system weight and volume to the extent that the overall system specific power is low (<100 W/kg max.) and the power density is low (<100 W/l max.).

The lifetime of some fuel cells is probably more than adequate for vehicle propulsion, but the projected cost still is very high compared to a goal of $100/kW average, or about $25/kW peak. Cost reduction will result in large measure from system simplification. As progress in fuel cell system engineering is made, vehicle applications come closer to realization. In the meantime, battery-powered electric vehicles can be expected to find wider application.

5. Electrochemical Power Source Technology

5.1. Ambient Temperature Batteries

Inspection of Table 10 reveals that the ambient temperature batteries can be divided into groups according to the state of the reactants: solid, liquid, or gaseous. The batteries will be discussed in that order. Additional information on many of the batteries can be found in Chapters 10–14 of this volume.

The lead–acid cell ($Pb–H_2SO_4–PbO_2$) operates with the following overall reaction:

$$Pb + PbO_2 + 2H_2SO_4 \rightarrow 2PbSO_4 + 2H_2O \qquad (22)$$

which serves as the basis for the computation of the theoretical specific energy of 175 Wh/kg. This cell has proven to be the most widely used rechargeable

† Hydrogen storage as a metal hydride is interesting, but currently known alloys are expensive, and only store 1% or 2% hydrogen by weight. The kinetics of storage and release under vehicle operation conditions is problematical.

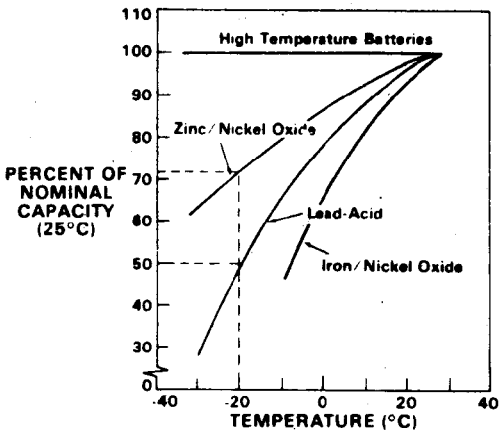

Figure 36. Constant current discharge corresponding to the average specific power for urban driving (32 W/kg).[130-132]

cell of all. It is relatively inexpensive and has met a wide variety of needs, in spite of its low specific energy (20–40 Wh/kg at 10 W/kg), and its loss of capacity at low temperatures (Figure 36).

The current interest in electric automobiles, and the government-sponsored electric vehicle demonstration program, have enhanced the incentive to optimize the design of the lead–acid battery for this application. The result is a design that is lighter weight than that for industrial traction batteries, but more robust than that for starting, lighting, and ignition (SLI) applications. The performance and cycle life of the electric vehicle (EV) battery represent a compromise between the above two types, resulting from weighing the conflicting requirements of high specific energy, high specific power, long cycle life at great depth of discharge, little or no maintenance, and low cost.

The cell design variables that are adjusted to meet the needs of a given application include the design of the current collectors,[62,63] the amount of active material in excess of that theoretically required, the thickness of the electrodes, the porosity and pore size distribution of the active material, the composition and amount of the electrolyte, the separator(s), the cell terminals, and the cell case. In addition to these variables, the design of a complete vehicle battery must take into account cell interconnections (series, parallel, ladder, etc.), and temperature control requirements.

As the development of the lead–acid cell for electric vehicles has progressed, a number of problems have been encountered. One of the common problems with rechargeable cells is the evolution of gases, especially during recharging. In the Pb–PbO_2 cell, both hydrogen and oxygen are evolved, resulting in a potential fire hazard and loss of water from the electrolyte. This problem can be ameliorated by removing antimony as an alloying agent from

the lead alloy current collector of the PbO_2 electrode and replacing it with calcium. A sufficiently low rate of gas evolution results such that a maintenance-free design is made practical. A vented battery case is used, allowing for the escape of the much smaller amounts of gases; however, water addition is unnecessary for the life of the battery.

The internal resistance of Pb–PbO_2 cells has been high enough that a significant loss of specific energy occurs at specific power levels needed for automobile propulsion. Some improvement has been made by the use of new polyvinyl chloride, and other polymeric separators of high porosity. Additional improvement is necessary because the internal resistance is still relatively high.

The present performance of Pb–PbO_2 batteries is such that electric vehicles having about 25% of their test mass as the battery can accelerate from 0 to 50 km/h in about 10 sec and demonstrate an urban driving range of 50–60 km. This may correspond to 100 km or more at a constant 50 km/h. Typical top-speed capabilities are 80–90 km/h. These values are consistent with the discussion of present electric vehicle performance information presented earlier in this chapter.

The cycle life of EV Pb–PbO_2 cells has been too low for electric automobile applications: generally 300 or fewer cycles at 80% DOD. This is one of the key areas requiring improvement. The issues that must be dealt with include the adhesion of the PbO_2 to the current collector, and the cohesion of the PbO_2 to itself. Corrosion of the positive electrode current collector is also a life-limiting factor.

The cost of Pb–PbO_2 EV batteries can probably be decreased to acceptable values near \$50/kWh for designs yielding more than 300 cycles at 80% DOD, and a specific energy of about 40 Wh/kg at 30 W/kg. Table 14 summarizes the situation for the Pb–PbO_2 battery, the standard against which the status of all other rechargeable cells is compared.

The iron–nickel oxide cell (Fe–KOH–NiOOH) may employ either of the following overall reactions, depending on the design:

$$3Fe + 8NiOOH + 4H_2O \rightarrow Fe_3O_4 + 8Ni(OH)_2 \quad (23)$$

$$Fe + 2NiOOH + 2H_2O \rightarrow Fe(OH)_2 + 2Ni(OH)_2 \quad (24)$$

Reaction (23) takes place in two stages, yielding two voltage plateaus, 1.37 V and 1.05 V, with a theoretical specific energy of 284 Wh/kg. If the cell is constructed to operate according to reaction (24), with only the 1.37-V plateau, then the theoretical specific energy is 267 Wh/kg.

The iron–nickel oxide cell has a long history; it is the famous Edison cell, used for the propulsion of electric cars developed by Henry Ford and Thomas Edison.[67] The rapid advances in gasoline engine performance prevented widespread use of electric automobiles, and the iron–nickel oxide cell found other applications. The classical constructions of this cell have involved heavy, bulky electrodes, resulting in low specific energies, in the same range as those

Table 14
Summary of the Status of the $Pb–H_2SO_4–PbO_2$ Battery System

$Pb–H_2SO_4–PbO_2$
$Pb + PbO_2 + 2H_2SO_4 \rightarrow 2PbSO_4 + 2H_2O$
E = 2.095 V; 175 Wh/kg theoretical

Status		*References*
Specific energy	22–40 Wh/kg at 10 W/kg	64
Specific power	50–100 W/kg at 10 Wh/kg	65
Cycle life	300 + at 10 W/kg, 60% DOD[a]	64, 65
Cost	$35–$50/kWh	65, 66
Recent work		
Replace Sb with Ca in positive current collector		64
Maintenance-free cells		64
Use $4PbO \cdot PbSO_4$ instead of $PbO + Pb_3O_4$ in positive		64
PVC separators		64
Problems		
Sealing of cells (gassing)		
Corrosion of positive current collector		
Cohesion and adhesion of PbO_2		
High internal resistance		
Heavy		

[a] Depth of discharge as percent of nominal (or rated) capacity.

for $Pb–PbO_2$, but at a higher cost. The cycle life has been excellent (1000–3000 cycles) and the cells have been rugged.[68]

In recent years, a number of laboratories have announced improvements in the weight and performance of both the iron electrode[69,70–72] and the nickel oxide electrode.[70–72] Some of the announcements include current collectors prepared from inexpensive steel wool, sintered to form a high-porosity plaque, into which is placed the electrochemically active material, Fe or $Ni(OH)_2$. The high specific area iron can be prepared by hydrogen reduction of an iron oxide; the $Ni(OH)_2$ can be precipitated in place by an electrochemical method from a nitrate solution, or can be prepared separately and then added to the porous current collector.

Cells prepared using the electrode technology described above have demonstrated specific energy values up to about 52 Wh/kg at 17 W/kg, and peak specific power values of 125 W/kg at 50% DOD. Cycle life data are still being gathered (presently in excess of 100 cycles, 100% DOD[72]), but projections based on the earlier electrode designs[70,71] are 1500 cycles at 80% DOD. The continuing problems that are inherent to the Fe–NiOOH cell include gas evolution during charge (H_2 and O_2) and on open circuit (H_2).

Significant efforts have been invested in the reduction of the hydrogen evolution rate at the iron electrode. Evidently, removal (or avoidance) of impurities in the iron significantly reduces, but does not eliminate hydrogen formation, both a source of inefficiency, and a safety issue. Accompanying hydrogen evolution during charge is the evolution of heat at a rate that makes electrolyte circulation to a heat removal system advisable[71,72] and complicates the system. One positive feature of the electrolyte circulation system is the opportunity to add make-up water to the electrolyte at a single point. The overall impact of the hydrogen evolution problem is to reduce the energy storage efficiency to 50–55%, compared to 70–80% for some other batteries. Another area requiring effort in the further development of the Fe–NiOOH system is the loss of energy storage capability at reduced temperatures. For example, a loss of about 40% of the capacity when the temperature is reduced from 25°C to 0°C.[72] Table 15 summarizes the status of the Fe–NiOOH system.

A significant amount of experience has been gained during the last several years on the use of Fe–NiOOH batteries in electric vehicles[70–72] (see Figure 15). The vehicle performance has been as expected based on the battery performance information presented above. Vehicle ranges of 80 km in urban driving are consistent with 50 Wh/kg. The durability projection of 1500 cycles is very attractive; the cost projections are in the range $350–500/kWh for pilot quantities; it is too early to speak with confidence about ultimate costs. Clearly, a factor of 7–10 reduction should be the goal.

Table 15
Summary of the Status of the Fe–KOH–NiOOH Battery System

Fe–KOH–NiOOH
$Fe + 2NiOOH + 2H_2O \rightarrow Fe(OH)_2 + 2Ni(OH)_2$
E = 1.37 V; 267 Wh/kg theoretical

		References
Status		
Specific energy	35–52 Wh/kg at 10 W/kg	70–73
Specific power	25–125 W/kg at 10 Wh/kg	72, 73
Cycle life	100 + at 10–25 W/kg, 80% DOD	72
Cost	~ $500/kWh	72
Recent Work		
Improved Fe and NiOOH electrodes with higher specific energy		74, 75
Problems		
H_2 evolution during recharge; cannot be sealed		73
Heat evolution		
Low efficiency, 50–55%		72, 73
Capacity loss at low temperature, 60% at 0°C		72, 73
High rate of self-discharge, with H_2 evolution; loss of 10% of charge in < 100 hr		72

The zinc–nickel oxide cell (Zn–KOH–NiOOH) is in some ways similar to the iron–nickel oxide cell, but offers a higher specific energy, and has different problems. The overall cell reaction

$$Zn + 2NiOOH + H_2O \rightarrow ZnO + 2Ni(OH)_2 \qquad (25)$$

corresponds to a theoretical specific energy of 373 Wh/kg and a cell voltage of 1.74 V. If this cell can be effectively produced in a compact configuration, then a very attractive specific energy of 90–95 Wh/kg may be achieved (23% of theoretical).

The zinc electrode has received a great deal of effort to improve its cycle life capabilities. It has suffered from a complex set of problems, which can be summarized in four categories[76]: dendrite formation, zinc redistribution (shape change), densification, and passivation. The relatively high solubility of zinc-containing species in the KOH electrolyte has been a major contributing factor to the difficulty in extending the cycle life because it contributes to all of the four problems above, except (possibly) for passivation.

The problem of dendrite formation has been reduced (but not totally eliminated) by the use of separators with extremely small pores (30–100 Å), such as cellophane, fibrous sausage casing, microporous polypropylene, and inorganic–organic composites. The rate of zinc redistribution has been reduced by the careful design of cells for uniform current distribution, the use of inorganic–organic separators, and proprietary additives to the zinc.

An important issue for EV batteries is that of maintenance. If the cells can be sealed, then no water or electrolyte addition should be required. It has been possible to reduce the amount of hydrogen evolution from the zinc electrode by the addition of 1% or 2% of metals with a high hydrogen overvoltage such as Hg or Pb,[77] so that sealed Zn–NiOOH cells can be operated successfully.[76,78] The oxygen formed at the NiOOH electrode during recharge can be recombined with zinc either by means of a porous oxygen reduction electrode (connected to the zinc electrode) or by direct reaction with the zinc electrode. Either of these options can be readily incorporated into the cell design, permitting sealed operation. Sealed cells have exhibited specific energies as high as 70–75 Wh/kg[76] in 125-Ah EV-sized cells.

As indicated in an earlier section of this chapter, several different electric vehicles, varying from small, two-passenger autos to vans have been evaluated with Zn–NiOOH batteries. Typically, these vehicles exhibit urban driving ranges of about twice that found for $Pb–PbO_2$ vehicles, or 110–120 km under urban driving conditions, and more at steady speeds below 80 km/hr.[54]

The status and current problems for the zinc–nickel oxide cell are summarized in Table 16. The establishment of pilot lines for the production of EV-sized cells and batteries is currently under way. Within the next year or two, there should be a reasonable amount of information on the performance of such cells and batteries, and perhaps some cycle life information as well. It

will be important to know if the energy throughput has a maximum at an intermediate depth of discharge.

The ambient temperature batteries using liquid reactants that may be candidates for use in certain types of electric vehicles are the zinc–halogen batteries: $Zn–ZnCl_2–Cl_2$ and $Zn–ZnBr_2–Br_2$. Both of these systems rely on the storage of the halogen external to the cells, and therefore require a flow system to supply the halogen reactant (dissolved in the electrolyte) to the electrodes.

The zinc–chlorine cell[83–85] operates according to the overall reaction

$$Zn + Cl_2 \cdot 6H_2O \rightarrow ZnCl_2 + 6H_2O \qquad (26)$$

The reversible potential is 2.12 V, and the theoretical specific energy is 461 Wh/kg when the chlorine is stored as the hexahydrate. In some cases, the octahydrate is used, corresponding to a theoretical specific energy of 401 Wh/kg. The use of solid, icelike chlorine hydrate as a storage medium increases the safety of the system, since the Cl_2 partial pressure is low. A refrigerator is required to form and store the hydrate (at about 9°C).[84,85] A schematic diagram of the system is shown in Figure 37.[84]

The electrodes are prepared from graphite: porous for the flow-through Cl_2 electrode, and solid for the Zn electrode. During charge, a dense zinc deposit is formed on the graphite substrate, with the aid of additives to the

Table 16
Summary of the Status of the Zinc–Nickel Oxide Battery System

Zn–KOH–NiOOH
$Zn + 2NiOOH + H_2O \rightarrow ZnO + 2Ni(OH)_2$
E = 1.74 V; 373 Wh/kg theoretical

Status		*References*
Specific energy	55–75 Wh/kg at 30 W/kg	76, 78, 79, 54, 77, 30, 80
Specific power	80–150 W/kg at 35 Wh/kg	76, 78, 79, 54, 77, 81
Cycle life	100–200 at 25–50 W/kg	30, 80, 82
	80% DOD	76, 78, 79, 54, 77
Cost	> $100/kWh	
Recent work		
Inorganic separators (e.g., K_2TiO_3, ZrO_2, others)		30, 80, 82
Sealed cells		78, 30, 80
Nonsintered electrodes		78, 30, 80
Problems		
Sealing of cells—O_2 evolution and recombination		
Shape change and densification of zinc electrode		
Separators		

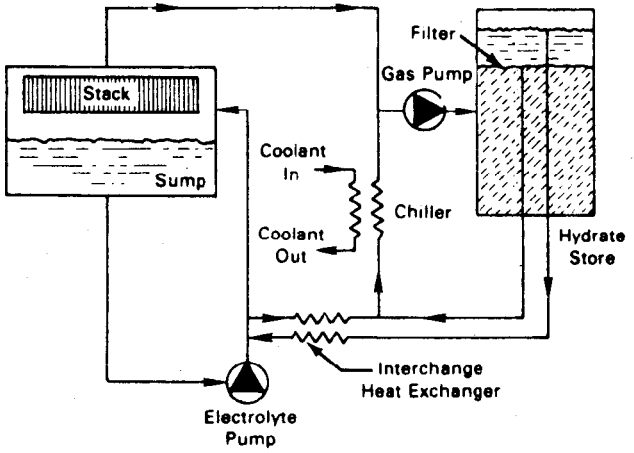

Figure 37. Flow schematic for an electric vehicle battery system.

electrolyte. Low-hydrogen-overvoltage impurities, including iron, must be absent, to avoid hydrogen formation. Chlorine gas is formed at the porous carbon electrode, is swept out of the cell, and pumped to the $Cl_2 \cdot 8H_2O$ formation area, held at a few degrees centigrade. During discharge, the processes are reversed, with Cl_2-saturated electrolyte being pumped through the porous graphite electrodes. No separators are used, and the flow patterns in combination with the electrochemical consumption of dissolved chlorine are arranged to minimize direct reaction of dissolved chlorine with zinc. After every few cycles, it is necessary to discharge all of the zinc in order to avoid dendritic zinc deposits on recharge.

A 1-kWh system has operated for over 1000 cycles, with some electrolyte maintenance. Other systems as large as 50 kWh, 40 kW have been constructed and operated at efficiencies in the range of 55%. These larger systems have demonstrated a specific energy of 71 Wh/kg† (at 18 W/kg) and 57 W/kg. Because of the many components and the plumbing required, the density of the system is low: only 1.17 kg/l (vs. a typical value of 2 kg/l for batteries with solid reactants).

An advantage of this system is the inexpensive reactants. Disadvantages include the inefficiencies associated with hydrogen formation, direct reaction of chlorine with the zinc, system complexity, corrosion problems of the acidic chlorine–chloride flowing electrolyte, and safety issues. The status of this system is summarized in Table 17.

It appears unlikely that Zn–Cl_2 systems will be used in automobiles, but they could find application in larger vehicles.

† About 17% of theoretical.

Table 17
Summary of the Status of the Zinc–Chlorine Battery System

$Zn–ZnCl_2–Cl_2$
$Zn + Cl_2 \cdot 6H_2O \rightarrow ZnCl_2 + 6H_2O$
$E = 2.12$ V; 461 Wh/kg theoretical

Status		*References*
Specific energy	71 Wh/kg at 18 W/kg	83, 84
Specific power	60 W/kg	83, 84
Cycle life	1000 + with maintenance	84
Cost	> $100/kWh	
Recent work		
Graphite for Cl_2 electrode		84
Additives for Zn deposition		85, 87, 88, 89
System components		90
Photocatalytic H_2 recombination		84, 84
50-kWh systems being tested		84
Problems		
Low efficiency (< 60%)		85
H_2 formation		
Bulky		
Complex		
Low specific power		
Need for Zn stripping		85
System component reliability		

Another liquid-reactant system similar in many ways to the $Zn–Cl_2$ battery is the $Zn–Br_2$ battery. The zinc electrode uses a graphite or titanium substrate, behaves very similarly to the zinc electrode in the $Zn–Cl_2$ cell, and has the same problems. The bromine electrode is made of catalyzed titanium or graphite, and serves to reduce Br_2 to Br^- on discharge. On recharge, the Br_2 can be stored as complex polybromide ions such as Br_3^- and Br_5^-, provided that they are prevented from contacting the zinc electrode (e.g., by use of a cation exchange membrane separating the electrodes[86]). Another alternative is to store the Br_2 as a tetra-alkyl ammonium complex, which has the properties of an oil which forms a separate phase and can be stored outside the cell.[91]

Individual, small cells (3.2 Wh) without the tetra-alkyl ammonium bromide complex have been operated with maintenance for 1800 cycles at efficiencies of 60–80% (no subtraction of the parasitic power required was made). Larger cells (32 Wh) have been cycled up to 600 times, with some shorting caused by zinc dendrites, and small systems of 1.2–2.5 kWh[91,92] have been operated with relatively low efficiencies of 40–65%. It is clear from the

experience with small systems that overall, there are many similarities to the $Zn–Cl_2$ system. There may be some advantages to the ambient temperature storage that is feasible with bromine.

The low density of the $Zn–Br_2$ system, caused by the circulating streams and external storage, make it unlikely that electric automobiles will be a practical application. Perhaps larger vehicles with more volume available for the power plant, and lower performance requirements, will be a future application. Current emphasis with the $Zn–Br_2$ system is for stationary energy storage. The status and problems are summarized in Table 18.

Cells with gaseous reactants are exemplified by the metal–air couples, which tend to have higher specific energies than those with liquid reactants because there is no need to carry along a supply of air. In the calculation of the theoretical specific energy, however, appropriate allowance should be made for the weight added to the system by the oxygen in the reaction products. The three metal–air systems that are under active investigation involve iron, zinc, or aluminum electrodes, which react in alkaline (KOH or NaOH) electrolyte

Table 18
Summary of the Status of the Zinc–Bromine Battery System

$Zn–ZnBr_2–Br_2$
$Zn + Br_2 \rightarrow ZnBr_2$
$E = 1.82$ V; 430 Wh/kg theoretical

		References
Status		
Specific energy	61 Wh/kg at 12 W/kg	92
Specific power	73 W/kg, peak	92
Cycle life	200 at 90–100% DOD (1800 for small cells)	91, 92
Cost	> $100/kWh	
Recent work		
Prototype battery of 2.5 kWh tested		92
Complexing of bromine		
Problems		
Complete discharge every few cycles is required		86, 91, 92
Zinc dendrites—uneven current distribution		
Flowing electrolyte—complex system		86, 91, 92
Low efficiency: 65% Wh		91, 92
High self-discharge rate: 50% in 50 h		92
Poor Zn adherence; Zn dendrites		92
Corrosion by bromide–bromine solutions		
Recharge of bromine electrode		86, 91, 92
Safety		
Low kWh/liter		

according to the following overall reactions, with the standard cell emf's and theoretical specific energies shown:

$$Fe + \tfrac{1}{2}O_2 + H_2O \rightarrow Fe(OH)_2 \quad 1.2\ V,\ 720\ Wh/kg$$

$$Zn + \tfrac{1}{2}O_2 \rightarrow ZnO \quad 1.6\ V,\ 1310\ Wh/kg$$

$$Al + \tfrac{3}{4}O_2 + \tfrac{3}{2}H_2O \rightarrow Al(OH)_3 \quad 2.7\ V,\ 2790\ Wh/kg$$

The metal–air cells represent the first group discussed in this chapter that is generally unable to operate at practical current densities at cell voltages within 0.1–0.2 V of the reversible value. A major portion of this voltage inefficiency is caused by the air electrode, and has been the subject of major efforts at improvement for many years. An air electrode capable of acting as an anode during recharge, and a cathode during discharge would be very useful in both the iron–air cell and the zinc–air cell, but operation during recharge tends to cause damage to the electrode structures and electrocatalysts, rendering them less active for oxygen reduction. Generally speaking, cycle lives for these bifunctional air electrodes at practical current densities ($> 0.05\ A/cm^2$) have been less than 100.† This difficulty has led to the attempted use of a third electrode for oxygen evolution during recharge. Third electrodes have proven to be impractical, and have added unreasonably to system complexity (and cost). Other approaches include metal anode replacement, removing the recharge requirement from the air electrode.

All of the metal–air systems are rather bulky and complex, making them unpromising for automobile applications. There is a possibility for use in vans, buses or industrial vehicles, if the fundamental problems of voltage efficiency and rechargeability can be solved.

The Fe–KOH–air system probably has reached the most advanced state of development of any of these three systems, in terms of electric vehicle propulsion, since it has been used in a demonstration industrial vehicle.[93] The iron electrode has the advantages pointed out in connection with the Fe–NiOOH cell: it is very rugged, has a long cycle life, and probably can be produced at an acceptable cost. The current inefficiency of the iron electrode is less of a disadvantage in the Fe–air cell, because no balancing of state of charge against the air electrode is required. The relatively low voltage of the iron–air cell is a disadvantage because it contributes to a low efficiency (about 45% now), and requires that more series-connected cells be used to meet a given voltage requirement (the operating voltage is 0.7–0.8 V per cell).

System-specific energies of 90 Wh/kg have been reported,[93] with cycle lives of about 200. The status of the iron–air system is summarized in Table 19. Work continues at a few laboratories in the U.S.A. and Europe.

† There have been occasional reports of 200 and 500 cycles, but firm supporting data for these reports have not been published.

Table 19
Summary of the Status of the Iron–Air Battery System

Fe–KOH–air
$Fe + \frac{1}{2}O_2 + H_2O \rightarrow Fe(OH)_2$
E = 1.2 V; 720 Wh/kg theoretical

Status		*References*
Specific energy	90 Wh/kg at 10 W/kg	93
Specific power	30 W/kg at 40 Wh/kg	93, 94
Cycle life	200 at ~ 20 W/kg	93, 94
Cost	> $100/kWh	93, 94
Recent work		
Improved Fe and air electrodes		93, 94
Systems of several kilowatts built for vehicles		93
Additives to reduce H_2 gassing		93
Problems		
Maintenance of water balance		93, 94
H_2 evolution during charge		
Self-discharge		93
Low specific power		
High internal resistance		
Low efficiency: < 45%		95

The zinc–air cell has received more attention than iron–air, probably because of its higher cell voltage and higher specific energy. The problems of the air electrode are the same as for other metal–air systems. The cycle lives of the zinc electrodes tend to be the same as for the bifunctional air electrodes. In some cases, the replacement of the zinc electrode has been practiced as a means of "mechanically" recharging the battery. The advantages of this are that the zinc electrode is not recharged *in situ*, and thus does not suffer from dendrite formation, shape change, etc. In addition, the air electrode is not required to operate as an anode, thus providing for a greatly extended life. Primary zinc–air batteries of this sort have included interesting design variations, such as a circulating zinc powder slurry electrode,[96,97] which can be replaced, or recharged electrically in a separate cell.[97]

Prototype zinc–KOH–air systems of several-kWh capability have been constructed and operated,[98] but no lifetime information has been made available. The status of the zinc–air battery is shown in Table 20.

The final metal–air system for consideration here is the Al–air system, which uses an aqueous alkaline or neutral electrolyte such as KOH, NaOH, or NaCl. The theoretical specific energy and the reversible potential are very high, as shown above. Because of the spontaneous reaction of aluminum with air and water, however, an oxide film is formed which causes very high overvoltages

Table 20
Summary of the Status of the Zinc–Air Battery System

	Zn–KOH–air $Zn + \frac{1}{2}O_2 \rightarrow ZnO$ E = 1.6 V; 1310 Wh/kg theoretical	
Status		*References*
Specific energy	70–90 Wh/kg at 20 W/kg	97
Specific power	80 W/kg, peak	97
Cycle life	< 100	99
Cost	> $100/kWh	
Recent work		
Improved circulating zinc electrodes		97
Improved air electrodes		97
Multicell batteries built (~ 3 kW)		100
Zinc recharge unit		97
Problems		
Complex system		
Rechargeable air electrodes		96, 100
Control of zinc in slurry		96
Wetting		
Carbonation		
Short Life		
Low efficiency: 35–40%		
Low Wh/liter		

(~ 1 V). Also, current inefficiency results from the direct chemical reaction of aluminum with water. Various measures have been taken to reduce these difficulties. The addition of 0.2% of Ga, In, or Tl reduces the anodic overvoltages of Al by 0.5–0.7 V in 2 *M* NaCl,[101] allowing current densities as high as 1 A/cm^2. In another approach, the 0.05 *M* $Na_2Sn(OH)_4$ has been used in 6 *M* NaOH, with proprietary Al alloys.[102] The reaction product is $Al(OH)_3$, which can be precipitated as crystals of $Al_2O_3 \cdot 3H_2O$ (hydrargillite). The plan[102] is to remove this precipitate from the battery and send it to an electrolytic plant for conversion to new aluminum anodes. Because of the high overvoltages, and the logistics, the efficiency and suitability of this system for vehicle use are not attractive. No cell stacks, batteries, or systems have been reported yet; the status is summarized in Table 21.

Last of the candidate ambient temperature batteries for vehicle propulsion to be discussed is the one with a nonaqueous electrolyte: Li–$LiClO_4$–dioxolane–TiS_2. This is one of the very few ambient temperature nonaqueous systems that claims to be rechargeable. In fact, a cycle life of 260 has been reported for a laboratory cell.[103] The overall reaction is

$$x\text{Li} + TiS_2 \rightarrow \text{Li}_x TiS_2 \qquad (27)$$

The lithium intercalates into the TiS_2 reversibly, yielding a positive electrode with a long cycle life and a low overvoltage at low, but probably acceptable, current densities (7.5 mA/cm^2). When x is 1.0, then the theoretical specific energy is 490 Wh/kg.

Because lithium is highly reactive, and readily reduces many materials forming lithium compounds, it is very difficult to obtain stable, inert, sufficiently pure nonaqueous solvents for use in lithium cells. Next, there must be adequate solubility of a stable lithium electrolyte. Lithium perchlorate has been used in dioxolane, but this combination is not stable with lithium and explosions have resulted. Research on safer electrolytes and solvents is progressing, but compromises on cycle life have been necessary, bringing the value down to 100 cycles.

In spite of the above difficulties, small cells (up to 20 Ah) have been constructed and tested. Utilizations of TiS_2 have been 55–82%, depending on the current density. A factor-of-10 excess lithium is used. The laboratory cell results have been used in design calculations for performance projections which indicate that large (400-Ah) cells might achieve 120 Wh/kg (24% of theoretical) at 30 W/kg. This system is still in the early stages of development, and should be watched with interest, especially to determine if the safety issues

Table 21
Summary of the Status of the Aluminum–Air Battery System

Al–NaOH–air

$Al + \frac{3}{4}O_2 + \frac{3}{2}H_2O \rightarrow Al(OH)_3$

E = 2.7 V; 2790 Wh/kg theoretical

Status (*Lab cells only*)

Current density	0.1 A/cm^2
Voltage	1.4 V typical
Cycle life	Not rechargeable
Cost	Too early

Recent work

Aluminum alloys of higher performance (In, Ga, Tl)
Electrolyte additives [e.g., $Na_2Sn(OH)_4$]
Removal of $Al(OH)_3$ as precipitate (hydrargillite)

Problems

Not electrically rechargeable
Control of precipitate formation
Low efficiency
Logistics
Air electrode
Low W/liter
Low performance at low temperatures

Table 22
Summary of the Status of the Lithium–Titanium Disulfide Battery System

$Li–LiClO_4–TiS_2$
$xLi + TiS_2 \rightarrow Li_xTiS_2$
E = 2.2 V (average); 490 Wh/kg theoretical for $x = 1$

Status		*References*
Specific energy	120 Wh/kg at 30 W/kg projected	103
Specific power	100 W/kg, peak projected	103
Cycle life	100–260 (lab cells)	
Cost	> $100/kWh	
Recent work		
New solvents—more stable		
New electrolytes—more stable		
Problems		
Safety		
Seals		
Low conductivity of electrolyte		
Low specific power		
Many parts per cell		
Lithium rechargeability		
Overcharge and overdischarge problems		
Manufacturability—water and air are contaminants		

can be adequately handled. Table 22 summarizes the information on the $Li–TiS_2$ cell. The potential advantages of this type of system include high specific energy for long vehicle range, completely sealed cells (therefore no maintenance), and ambient temperature operation.

5.2. High-Temperature Batteries

In contrast to ambient temperature batteries, most of which have aqueous electrolytes, high-temperature batteries have nonaqueous electrolytes, either molten salts or ionically conductive ceramics. This is the case because aqueous electrolytes have very high vapor pressures at the operating temperatures for high-temperature batteries (usually 300–500°C). Following the practice for ambient temperature batteries, systems with solid reactants will be discussed first, followed by those with liquid reactants.

A family of molten salt electrolyte systems that has evolved from early work on lithium–LiCl-KCl–sulfur cells[104] is that of lithium alloy–LiCl-KCl–metal sulfide cells. Several combinations of lithium alloy negative electrodes have been investigated; however, only two or three have received significant

development effort, especially for use in electric vehicles. The overall cell reactions, emf values, and theoretical specific energies are summarized below:

$$2LiAl + FeS \rightarrow Li_2S + Fe + 2Al \qquad 1.3\ V, 458\ Wh/kg$$

$$4LiAl + FeS_2 \rightarrow 2Li_2S + Fe + 4Al \qquad 1.75, 1.3\ V, 650\ Wh/kg$$

$$Li_4Si + FeS_2 \rightarrow 2Li_2S + Fe + Si \qquad 1.75, 1.3\ V, 944\ Wh/kg$$

All of the above cells make use of a molten salt electrolyte comprised of about 60 mol % LiCl–40 mol % KCl, which melts near 350°C. Typical operating temperatures are near 450°C. This temperature requires a high-performance insulation and thermal control system, in order to minimize thermal losses, especially during idle periods, and to maximize overall system efficiency.

These cells have demonstrated very long cycle lives[105,106] (~ 700 and more), with modest capacity losses[105,106] (~ 20%). The reactants are inexpensive, making these cells attractive from a potential-cost viewpoint.

One advantage of high-conductivity molten salts is the design flexibility they offer in meeting the high specific power required of electric vehicles. The electrodes can be thicker and of much higher capacity per unit area (e.g., 0.3 Ah/cm^2 vs. 0.03 Ah/cm^2) than those of ambient temperature cells. This means fewer electrodes are needed per unit energy and power, thus reducing manufacturing costs.

The electrodes can be prepared by simple powder mixing and pressing operations in a dry atmosphere. Compact cells[105,106] require small interelectrode distances and thin, corrosion-resistant, strong separators. Boron nitride cloth has been used as the separator in most of the work on these systems; however, it is extremely expensive (~ $5000/$m^2$). Recently, BN felts have been used with acceptable results, and much more acceptable cost projections (~ $25/$m^2$).

The need for isolation of lithium alloys from air and moisture makes necessary the use of hermetically sealed systems with electrical feedthroughs. Systems containing many cells of only two or three electrodes each would require too many expensive feedthroughs to be cost effective. Therefore recent efforts have included work on multielectrode cells[105,107] and bipolar batteries.[108] The development of Li_4Si as a successful, high-performance electrode has halved the weight of the negative electrode, compared to LiAl.[109]

The inconvenience of having a high-temperature battery in a vehicle must be offset by significant advantages such as the high specific energy available from the Li_4Si–FeS_2 cell,[106] the long cycle lives, and the potential for low cost. If these advantages are not preserved in the finally developed battery, then advanced ambient temperature systems will certainly continue to hold strong interest for automobile propulsion.

The continued development of Li-M–FeS_x cells for transportation applications will require careful attention to maximizing specific energy

Table 23
Summary of the Status of the LiAl–FeS Battery System

LiAl–LiCl-KCl–FeS
$2LiAl + FeS \rightarrow Li_2S + Fe + 2Al$
E = 1.33 V; 458 Wh/kg theoretical

		References
Status		
Specific energy	50–90 Wh/kg at 30 W/kg	105, 107
Specific power	60–100 W/kg, peak	105
Cycle life	300 at 100% DOD	105, 107
Lifetime	~ 5000 + h	107
Cost	> $100/kWh	
Recent work		
Multielectrode cells		105, 107
LiCl-rich electrolyte		107
BN felt separators		107
Batteries of 320-Ah cells		107
Charging equipment		107
Problems		
Low specific energy		
Low voltage per cell		
Cell shorting major failure mode		
Electrolyte leakage		
Agglomeration of Li–Al with cycling		
High separator cost		
Leak-free feedthroughs		
Thermal control		

(> 125 W/kg), cycle life (1000 cycles), calendar life (three years, minimum), and minimizing cost (< $100/kWh). The current problems include raising the specific energy of the LiAl–FeS cell, avoiding internal shorting, developing feedthroughs and improved corrosion-resistant current collectors for the FeS_2 and FeS electrodes, lower-cost separators, and thermal control systems for batteries (see Tables 23 and 24 for a summary). Even though much work remains to be done before these systems are ready for application, demonstration EV batteries are being constructed, and will be evaluated in vehicles during the next two years.

The only high-temperature cells with liquid reactants that now appear to be candidates for vehicle propulsion are two versions of the sodium–sulfur cell. The most vigorously developed version uses a beta-alumina ($Na_2O \cdot xAl_2O_3$, x = 5–11) ceramic electrolyte, and the other uses a Na_2O-containing glass electrolyte. Both cells rely on the same overall reaction,

$$2Na + 3S \rightarrow Na_2S_3 \qquad (28)$$

which has an average emf of 2.0 V, and a theoretical specific energy of 758 Wh/kg. The product, written as Na_2S_3 above, is not meant to represent a compound, but merely the overall composition of the sulfur electrode at the point defined as 100% DOD. This point is so defined because further discharge would cause the undesirable precipitation of solid Na_2S_2 from the liquid sulfur-rich positive electrode.

A very attractive feature of Na–S cells is their inherent simplicity, in addition to the idea that the electrodes, being liquid, should not change with cycling. If combinations of materials that are pure and stable in contact with one another are used, these cells should last a very long time. The basic materials of which the cell is made are mostly inexpensive: Na, S, Na_2CO_3, Al_2O_3, C. The electronic conductor for use with the sulfur electrode may be relatively costly (Cr-coated steel?). Most versions of this cell are tubular. The $Na_2O \cdot xAl_2O_3$ electrolyte is prepared in the shape of a closed-end tube, as shown in Figure 38. Cells with sodium inside the electrolyte tube and those with sodium outside of it have been evaluated. In the U.S.A., the sodium-inside design is predominant.

Cells of the beta-alumina type with capacities of up to about 170 Ah have been operated,[110–112] and a few multikilowatt-hour batteries have been

Table 24
Summary of the Status of the Li_4Si–FeS_2 Battery System

Li_4Si–LiCl-KCl–FeS_2
$Li_4Si + FeS_2 \rightarrow 2Li_2S + Fe + Si$
E = 1.8, 1.3 V; 944 Wh/kg theoretical

Status		*References*
Specific energy	120 Wh/kg at 30 W/kg	106
	180 Wh/kg at 7.5 W/kg	106
Specific power	100-W/kg peak	106
Cycle life	700 at 100% DOD	106
Lifetime	~ 15,000 h	
Cost	> $100/kWh	
Recent work		
Bipolar cells		108
Li–Si electrodes		106
BN felt separators		105, 107
70-Ah cells		
Problems		
Materials for FeS_2 current collector		
Leak-free feedthroughs		
High internal resistance		
Low-cost separators needed		
Thermal control		

demonstrated, one in an electric van, in England.[113] Other similar demonstrations are imminent. Table 25 indicates that the specific energy of single Na–S cells is in some cases above 100 Wh/kg, and the cycle life can be over 1000. The lifetime needs to be raised to at least 25,000 h. Recent efforts have been devoted to the several problem areas indicated, especially improving the capabilities of the sulfur electrode, the corrosion resistance of the container, and the seals. Major efforts are devoted to the preparation of the beta alumina and the cost reduction of the process.

The approach of using an electrolyte comprised of many thousands of hollow glass fibers (of high resistivity) has been showing increasing promise. The fibers are sealed into a common header, in contact with the sodium reservoir, as shown in Figure 39.[134] Cells of this design, having a nominal capacity of 6 Ah, have shown a durability of up to 400 cycles; some 40-Ah cells have been constructed and are under test. The current life-limiting problem is gradual sagging of the glass header, resulting in breakage of the glass fibers.

All of the sodium–sulfur cells have been of cylindrical design, causing the energy per unit volume to be lower than it otherwise might be. This may result in batteries that are very bulky for automotive use.

Sodium–sulfur cells are very sensitive to thermal cycling, and frequently fail upon freezing and reheating. This problem is one of the fundamental issues that is unresolved.

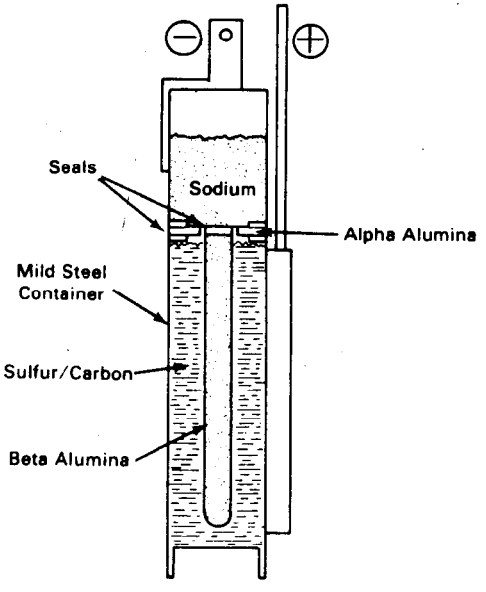

Figure 38. Sodium–sulfur cell.

Table 25
Summary of the Status of the Sodium–Sulfur Battery System

$Na–Na^+$ solid–S
$2Na + 3S \rightarrow Na_2S_3$
$\bar{E}$ = 2.0 V; 758 Wh/kg theoretical

		References
Status		
Specific energy	85–140 Wh/kg at 30 W/kg	111, 112, 114
Specific power	60–130 W/kg, peak	114, 115
Cycle life	200–1500	110, 111, 116
Lifetime	3000–15,000 hr	113, 116, 117
Cost	> $100/kWh	
Recent work		
Batteries ~ 10 kWh		
C_6N_4 additive to S		113, 116
Ceramic (TiO_2) electronic conductors		116
Shaped current collectors		
Tailored resistance current collectors		110
Sulfur-core cells		114
$Na_{3+x}Zr_2Si_xP_{3-x}O_{12}$		111
Thermocompression bonded seals		110
Problems		
Corrosion-resistant material for contact with S		
Low-cost seals		
Low-cost electrolyte		
Specific power is low		
Thermal cycling		

If progress on high-temperature batteries continues at the present pace, several major electric vehicle demonstrations will take place before 1985. If these are highly successful, some commercial applications may follow.

5.3. Fuel Cells

For many years, fuel cells† have been a hope for clean, efficient conversion of the chemical energy of a (conventional) fuel directly into the most useful form of energy: electricity. Hundred of millions of dollars have been invested in fuel cell research and development efforts around the world, but the practical fuel cell for commercial or consumer application still is in the future. The performance of fuel cell systems has steadily improved with time, to the point where it is marginally acceptable for a number of uses. The lifetime, and especially the cost, require a great deal of improvement.

† For a more complete discussion of fuel cells, see Chapter 2 of this volume.

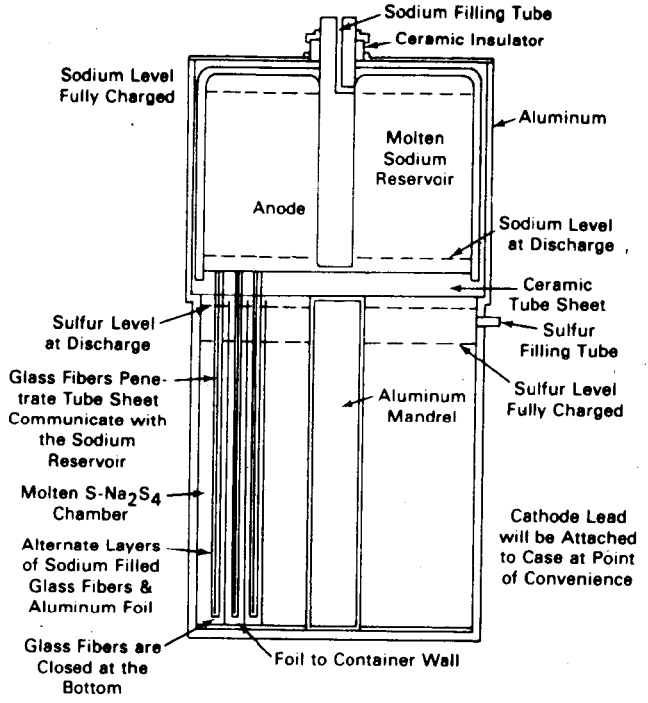
Sodium Filling Tube
Ceramic Insulator
Sodium Level Fully Charged
Aluminum
Molten Sodium Reservoir
Anode
Sodium Level at Discharge
Ceramic Tube Sheet
Sulfur Level at Discharge
Sulfur Filling Tube
Glass Fibers Penetrate Tube Sheet Communicate with the Sodium Reservoir
Aluminum Mandrel
Sulfur Level Fully Charged
Molten S-Na2S4 Chamber
Cathode Lead will be Attached to Case at Point of Convenience
Alternate Layers of Sodium Filled Glass Fibers & Aluminum Foil
Glass Fibers are Closed at the Bottom
Foil to Container Wall

Figure 39. The DOW sodium–sulfur hollow fiber cell.

By far, the greatest fraction of fuel cell development effort has been oriented toward stationary applications, where high specific power is not required, and higher (than acceptable for vehicle systems) cost is acceptable. From time to time, however, fuel cells are reevaluated for use in electric vehicles. A recent evaluation[118] of the applicability of present-day fuel cell technology to electric vehicles has indicated that the most appropriate system for development is a fuel cell–battery hybrid, arranged according to the diagram in Figure 40. The fuel cell is designed to meet the maximum cruising power requirements, and the battery is designed to provide additional power

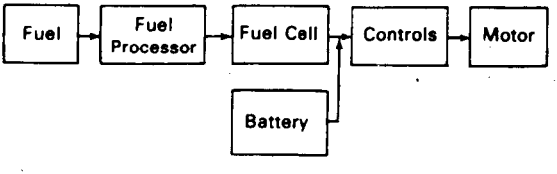

Figure 40. Proposed electric propulsion system diagram.

for acceleration. The battery also provides all power during the time required for fuel cell system startup (up to 15 min).

The fuel cell that is technologically the most advanced, and is closest to being manufactured in quantity, is the phosphoric acid electrolyte cell, with thin, porous PTFE-bonded gas diffusion electrodes comprised of platinoid electrocatalysts (≤ 1 mg/cm^2 total) supported on graphite, held against a thin, inert, absorbent matrix containing the electrolyte.[119-121] These cells operate best on hydrogen, or CO- and sulfur-free hydrogen-rich fuel streams. The optimum operating temperature is 150–200°C; sometimes pressurized operation (about 3 atm) is used to increase the current density.[119]

Recently, electrocatalyst loadings have been reduced below 1 mg/cm^2 (total of both electrodes), and methods for reducing the rate of surface area (therefore performance) loss have been sought. Single cells have reached lifetimes greater than 20,000 h.[119] Development efforts on stationary systems continue; little is being done toward vehicle propulsion. The status shown in Table 26 reflects the situation with regard to the H_3PO_4 electrolyte cell being developed for stationary applications. Before fuel cell or fuel cell–battery hybrid vehicle propulsion is appropriate (other than for demonstration purposes), it will be important to reduce the system volume (a power density of 100 W/liter is probably necessary), provide for rapid startup (< 5 min), improve system response to follow driving profiles, greatly reduce system complexity, and greatly reduce system cost.

6. Summary and Concluding Remarks

We have attempted, in only one chapter, to present an introduction to electrochemical power for transportation, with emphasis on such important items as the potential advantages of electric vehicles in shifting some of the transportation energy demand away from petroleum and toward other primary sources of energy, while retaining the individual freedom that accompanies the operation of one's own vehicle. In addition, it has been shown that gains in overall efficiency and effectiveness of primary energy use can be made if electric vehicles are used instead of conventional vehicles operating on synthetic fuels from coal or nuclear sources. Electric vehicles also offer opportunities for extremely low pollution.

The current situation for electric vehicles has been presented. Basically, only low-performance, short-range (< 80 km in urban traffic) vehicles are now in use or available; higher range and performance require better power sources. Several vehicles with next-generation batteries such as Fe–NiOOH and Zn–NiOOH have been demonstrated to have the expected higher performance and longer range. The cycle life and cost issues for these higher-performance batteries are still being addressed. Pilot lines are being constructed, and the cost and durability of electric vehicle batteries in pilot

Table 26
Summary of the Status of the Hydrogen–Air Battery System

$CH_3OH + H_2O \rightarrow CO_2 + 3H_2$ (reformer)
$H_2 + \frac{1}{2}O_2 \rightarrow H_2O$ (fuel cell)
$E = 1.23$ V; 6094 Wh/kg[a] theoretical

		References
Status		
Specific power	27–25 W/kg	118
Power density	12–35 W/liter	118
Efficiency	40%	
Lifetime	~4000–6000 h	118
Cost	>$100/kW	118
Recent work		
Lower electrocatalyst loadings		120, 122
Methods to reduce catalyst sintering rate		120, 123
Operation at elevated pressures		119
Scaleup for megawatt stationary systems		119
Compact reformers for hydrocarbons		
H_3PO_4 inventory control		122
Problems		
Low specific power and power density		
Slow system startup		
Slow system response		
System complexity		
System cost		
Corrosion of catalyst substrate		
Catalyst area loss		

[a] Based on methanol weight only; the oxygen is taken from the air and not carried; the water is assumed to be recovered from the exhaust.

production quantities will be assessed. Even advanced, high-temperature Na–S and Li-M–FeS_x batteries have been and are being tested in vehicles. Also fuel cell systems, both alone and as fuel cell–battery hybrids, have been evaluated in vehicles. The high-temperature batteries and fuel cell demonstrations were for technical feasibility only. The *system* performance, lifetime, and cost figures are still well outside of acceptable limits.

In reviewing the status of the individual candidate electrochemical power systems, it has become clear that meeting the performance, durability, and cost goals simultaneously represents a difficult but very important challenge. Each system reviewed has its own strong points and deficiencies. Several of the systems of intermediate specific energy seem to have fewer remaining problems than the very high specific energy systems and are therefore expected to find application in vehicles soon—within the next several years. Table 27 shows that such batteries as Fe–NiOOH and Zn–NiOOH have acceptable specific

Table 27
Candidate Power Sources for Electric Vehicles

System	Cell voltage	Theoretical, Wh/kg	Status						Remarks
			Wh/kg[a]	Wh/liter	W/kg[b]	Efficiency	Cycle[c] life	Range,[d] km	
$Pb-H_2SO_4-PbO_2$	2.1	175	20–40	45–90	80	70	300	35–65	Bench mark. Available now.
Fe–KOH–NiOOH	1.4	267	50	90	125	50–60	100 +[e]	85	Low efficiency, gassing.
Zn–KOH–NiOOH	1.7	373	75	140	150	75	200 +	125	Better cycle life needed.
$Zn-ZnCl_2-Cl_2$	2.1	461	70	~80	60		1000[f]	115	Complex, bulky, safety(?), maintenance.
$Zn-ZnBr_2-Br_2$	1.8	430	60	~60	75	65	200 +	100	Complex, bulky, safety(?)
Fe–KOH–air	1.2	720	90	~90	30	45	200	150	Low efficiency, bulky.
Zn–KOH–air	1.6	1310	70–90	70–90	80	35	MR[g]	115–150	Not rechargeable, bulky.
Al–NaOH–air	2.7	2790	N.A.[h]	N.A.	N.A.	~35	MR	—	Not rechargeable, low efficiency.
$Li-LiClO_4-TiS_2$	2.2	490	(120)[i]	(170)	(100)	~75	100 +	(200)	Safety(?) Cycle life(?)
LiAl–LiCl–KCl–FeS	1.3	458	50–90	75–130	60–100	~70	300 +	85–150	Thermal control needed.
$Li_4Si-LiCl-KCl-FeS_2$	1.8, 1.3	944	120	180	100	~75	700	200	Thermal control needed.
$Na-\beta-Al_2O_3-S$	2.0	758	85–140	100–165	60–130	~75	200–1500	140–235	Thermal control needed.
$H_2-H_3PO_4$–air	1.0	[j]	[j]	[j]	25–75	N.A.	40	400 +[k]	Complex, bulky, expensive.

[a] At 30 W/kg.
[b] Peak specific power, at least 15 sec.
[c] At least 80% DOD.
[d] 25% of vehicle test weight allocated to batteries. Urban driving profile, 0.15 kWh/km.
[e] Cycle lives of up to 1500 were demonstrated for earlier electrode designs.
[f] This cycle life for 1-kWh system with electrolyte maintenance.
[g] MR = mechanically rechargeable. The anodes are replaced periodically. Life data not available.
[h] N.A. = not applicable.
[i] Figures in parentheses are projections based on lab cells of low specific energy.
[j] Depends on amount of fuel carried—may be as high as ~ 6100, in principle.
[k] Typical range for fuel-carrying vehicle.

power and power density values. The Fe–NiOOH battery (in the prior version) has demonstrated long cycle life (~ 1500 cycles), and has been tested in several vehicles. Its main problems are low efficiency, hydrogen formation, and the requirement of electrolyte circulation during recharge. With cost reduction to below $100/kWh, it could find application in commercial vehicles with a range of about 85 km. The Zn–NiOOH battery offers an urban driving range well above 100 km, with a high energy per unit weight and volume. Improved cycle life (> 300 needed) is essential, as is a cost of < $100/kWh. The cycle life of the zinc electrode remains the most important problem.

The batteries with flowing reactants (Cl_2, Br_2, air) in Table 27 all have low efficiencies, low power per unit volume, and are complex relative to batteries with solid reactants, making them less attractive, other things being equal. They do, however, offer attractive specific energies. One of these systems may find application in commercial vehicles.

High-temperature batteries offer the highest performance and possibly the longest cycle life with the inconvenience of special thermal control requirements. These systems require several years of additional development and attention to materials and sealing issues.

Fuel cells remain elusive to the electric vehicle application. Their volume and complexity must be reduced, and the fuel (H_2) storage problem must be solved. Of course, all of this must be done concomitant with a greatly reduced cost (to < $100/kW average). Progress continues; fuel cells should not be eliminated from possible future use in electric vehicles. Perhaps 10 or 15 more years of development will be required before they can be used in specialized and commercial vehicles.

Overall, the prognosis is positive with regard to more extensive use of electric vehicles, and the development of electrochemical power plants which yield significantly higher performance and longer range than is possible with $Pb–PbO_2$ batteries. As this happens, more attention will be focused upon the electrochemical problems that remain to be solved, and the opportunities for significant contributions from electrochemists and electrochemical engineers.

References

1. Selected dates in history of electric vehicles, Edison Electric Institute Bulletin, Vol. 36, April 1968, p. 105.
2. J. H. Wherry, *Automobiles of the World*, Chilton, Philadelphia, Pennsylvania (1968), p. 713.
3. N. H. Tomblin, Electric vehicle development in the United Kingdom, in Proceedings of the First International Electric Vehicle Symposium, November 5–7, 1969, Phoenix, Arizona, p. 509.
4. A. A. Tullio, G. R. Fagan, and E. Hines, A progress report on electric vehicles, Edison Electric Institute Bulletin, Vol. 36, August 1968, p. 238.
5. Proceedings of the National Electric Automobile Symposium, sponsored by Santa Clara Valley Engineers' Council, San Jose State College, San Jose, California, February 24 and 25, 1967, p. 38.

6. H. J. Young, Electric vehicles: Economics and experience, SAE Publication 690115, Detroit, Michigan, January 13–17, 1969.
7. 1973/74 Automotive facts and figures, Motor Vehicle Manufacturers Association of the United States, Inc., Detroit, Michigan, 1974.
8. H. J. Schwartz, The computer simulation of automobile use patterns for defining battery requirements for electric cars, in Proceedings of the Fourth International Electric Vehicle Symposium, Düsseldorf, 1976.
9. T. Merkle and E. Zander, Basic requirements for the various items of equipment for supplying energy to electrically driven road vehicles from the point of view of the user, in Proceedings of the Fourth International Electric Vehicle Symposium, Düsseldorf, 1976.
10. M. C. Attendu and J. H. Beaudet, Electric delivery vans above the 45th parallel in North America, in Proceedings of the Fourth International Electric Vehicle Symposium, Düsseldorf, 1976.
11. The sources of air pollution and their control, U.S. Department of Health, Education, and Welfare, Public Health Service Publication No. 1548, U.S. Government Printing Office, Washington, D.C., December 1966.
12. Technology Assessment of Changes in the Future Use and Characteristics of the Automobile Transportation System, Vol. II, Congress of the United States, Office of Technology Assessment, Washington, D.C., February 1979, p. 150.
13. J. B. Heywood and M. K. Martin, Aggregate Emissions from the Automobile Population, SAE Publication 740536, Chicago, Illinois, June 17–21, 1974.
14. H. E. Hesketh, *Understanding and Controlling Air Pollution*, Ann Arbor Science Publishers, Ann Arbor, Michigan (1972).
15. A. Venkatram and J. Kurtz, Short-term dispersion from tall stocks, in Proceedings of the Ninth International Technical Meeting on Air Pollution Modeling and Its Application, No. 103, North Atlantic Treaty Organization, Toronto, Canada, August 28–31, 1978.
16. H. C. Perkins, *Air Pollution*, McGraw-Hill, New York (1974).
17. F. Pasquill, *Atmospheric Diffusion*, John Wiley & Sons, New York (1974).
18. J. T. Salihi, The electric car—fact and fancy, *IEEE Spectrum* **9**, 44–48 (June 1972).
19. U.S.A.'s Energy Outlook 1979–1990, Exxon Company, U.S.A., December 1978.
20. D. C. Sheridan, J. J. Bush, and W. R. Kuziak, Jr., A study of the energy utilization of gasoline and battery-electric powered special purpose vehicles, SAE Publication 760119, Detroit, Michigan, February 1976.
21. K. A. Hub, private communication to E. J. Cairns, December 11, 1973, based on an Argonne National Laboratory Report, Social cost study for alternate means of generating power for 1980 and 1990, March 1973.
22. M. S. Mashikian, Detroit Edison Co., private communication to E. H. Hietbrink, January 17, 1974.
23. Nuclear power 1973–2000, Office of Planning and Analysis, United States Atomic Energy Commission, U.S. Government Printing Office, Washington, D.C., WASH-1139(72), UC-80, December 1972.
24. J. T. Salihi, Energy requirements for electric cars and their impact on power generation and distribution systems, *IEEE Trans. Ind. Appl.* **1A9**(5), (September/October 1973).
25. D. P. Grimmer and K. Luszczynski, Lost power, *Environment* **14**(3), 14–56 (April 1972).
26. Ming-Chih Yew and D. E. McCullock, Small electric vehicle considerations in view of performance and energy usage, in *Eleventh Intersociety Energy Conversion Engineering Conference Proceedings*, Vol. 1, September 12–17, 1976, AIChE, New York (1976).
27. R. F. Stebar and F. B. Parks, Emission control with lean operation using hydrogen-supplemented fuel, SAE Publication 740187, Detroit, Michigan, February 1974.
28. A. W. Liles and G. P. Fetterman, Jr., Selection of driving cycles for electric vehicles of the 1990's, in *Eleventh Intersociety Energy Conversion Engineering Conference Proceedings*, Vol. 1, September 12–17, 1976, AIChE, New York (1976).

29. M. Klein, An analysis of electric vehicle mission, design, energy impact and cost, in *Eleventh Intersociety Energy Conversion Engineering Conference Proceedings*, Vol. 1, September 12–17, 1976, AIChE, New York (1976).
30. E. J. Cairns and J. McBreen, *Ind. Res.*, 56 (June 1975).
31. R. S. McKee, B. Borisoff, F. Lawn, and J. F. Norberg, Sundancer: A test bed electric vehicle, SAE Publication 720188, Detroit, Michigan, January 1972.
32. S. F. Powel III, N. Rosenburg, The advisability of regulating electric vehicles for energy conservation, transportation systems center, National Technology Information Service, Springfield, Virginia, Report No. DOT-TSC-OST-76-37, pp. 4–46.
33. E. Hines, M. S. Mashikian, and L. J. Van Tuyl, Effect of electric vehicles on the power industry, SAE Publication 690441, Chicago, Illinois, May 1969.
34. Recommended performance standards for electric vehicles, Arthur D. Little, Inc., SAN/1335-1, prepared for the Energy Research and Development Administration, final report on work performed under Contract No. EY-76-C-03-1335, C-79954, October 1977.
35. State-of-the-art assessment of electric and hybrid vehicles, HCP/M1011-01, UC-96, February 1978, prepared by National Aeronautics and Space Administration, Lewis Research Center, National Technical Information Service, U.S. Dept. of Congress, Springfield, Virginia, sponsored by U.S. Dept. of Energy under Interagency Agreement EC-77-A-31-1011.
36. D. K. Miner, M. A. Pocobello, and D. A. Armstrong, The copper electric Runabout, in Fifth International Electric Vehicle Symposium, Publication 784103(E), Philadelphia, Pennsylvania, October 1978.
37. J. R. Pierson, Road and range testing of high voltage lead-acid powered electric vehicles, in Fifth International Electric Vehicle Symposium Publication 783303(E), Philadelphia, Pennsylvania, October 1978.
38. J. L. Hartman, E. J. Cairns, and E. H. Hietbrink, Electric vehicles challenge battery technology, in Proceedings of the Fifth Energy Technology Conference, Washington, D.C., February 27, 1978.
39. Fiat electric vehicles, Electric Vehicle Brochure, Fiat Public Relations Dept., International Electric Vehicle Exposition and Conference, McCormick Place, Chicago, Illinois, April 1977.
40. J. T. Brown, Westinghouse E-180 nickel-iron oxide vehicle battery, brochure and data sheets, Westinghouse Research and Development Center, Pittsburgh, Pennsylvania, January 1978.
41. S. Matsumoto, The status of electric vehicles in Japan, The International Electric Vehicle Exposition and Conference, McCormick Place, Chicago, Illinois, April 26–29, 1977, paper No. 7748.
42. C. Badar and W. Stephan, Electric vehicles in Germany—present and future, SAE Publication 780087, Detroit, Michigan, February 27–March 3, 1978.
43. F. T. Thompson, Advanced electronic control systems for electric vehicles, in Proceedings of International Conference on Automotive Electronics and Electric Vehicles, September 20–22, 1976, Dearborn, Michigan, SAE Catalog No. P-68, IEEE Catalog No. 76CH1146-OVT.
44. D. K. Miner, Range improvement from regenerative braking on the copper electric Town Car, The International Electric Vehicle Exposition and Conference, McCormick Place, Chicago, Illinois, April 26–29, 1977, paper No. 7756.
45. A. M. Bueche, Advanced motor developments, in Proceedings of International Conference on Automotive Electronics and Electric Vehicles, September 20–22, 1976, Dearborn, Michigan, SAE Catalog No. P-68, IEEE Catalog No. 76CH1146-OVT.
46. D. Pohl and H. Ch. Skudelny, Induction motor drives for electric vehicles—an alternative to usual d.c. drives?, in The Fifth International Electric Vehicle Symposium Publication 782104(E), Philadelphia, Pennsylvania, October 2–5, 1978.

47. P. Campbell, The permanent magnet disc armature motor—an evaluation of its advantages compared with conventional electric vehicle drives, in The Fifth International Electric Vehicle Symposium Publication 782102(E), Philadelphia, Pennsylvania, October 2–5, 1978.
48. The second annual report to Congress for fiscal year 1978, Electric and Hybrid Vehicle Program, U.S. Dept. of Energy, DOE/CS-0068, January 1979, National Technical Information Service, U.S. Dept. of Commerce, Springfield, Virginia 22161.
49. Electric vehicle test procedure, SAE J227a, Society of Automotive Engineers, Inc., 1976.
50. J. Brennand, R. Curtis, H. Fox, and W. Hamilton, Electric and hybrid vehicle performance and design goal determination study, ERDA Contract No. EY-76-C-03-1215, General Research Corp., GRC Publication No. CR-1-734, SAN/1215-1, Santa Barbara, California, August 1977.
51. D. P. Crane and J. R. Bowman, United States Postal Service electric vehicle program, in Proceedings of the Fourth International Electric Vehicle Symposium, Düsseldorf, 1976.
52. G. G. Harding, High performance electric commercial vehicles for city use, SAE Publication 760073, Detroit, Michigan, February 1976.
53. P. O. Larsen, Commercial electric vehicle program at General Motors, presentation to Battery Council International, New Orleans, Louisiana, March 1979.
54. M. Klein, A. Charkey, H. Vaidyanathan, and S. Viswanathan, Performance characteristics of nickel-zinc electric vehicle battery, in 14th Intersociety Energy Conversion Engineering Conference, Boston, Massachusetts, August 1979.
55. C. Marks, E. A. Rishavy, and F. A. Wyczalek, Electrorian—a fuel cell powered vehicle, SAE Publication 670176, Detroit, Michigan, January 1967.
56. H. Hagen and R. Zelinka, The M.A.N. Elektrobus experience gained in large-scale tests, in Proceedings of the Fourth International Electric Vehicle Symposium, Düsseldorf, 1976.
57. D. M. Tenniswood and H. A. Graetzel, Minimum road load for electric cars, SAE Publication 670177, Detroit, Michigan, January 1967.
58. M. L. Kyle, H. Shimotake, R. K. Steunenberg, F. J. Martino, R. Rubischko, and E. J. Cairns, Lithium/sulfur batteries for electric vehicle propulsion, in 1971 Intersociety Energy Conversion Engineering Conference, Boston, Massachusetts, August 3–5, 1971.
59. L. E. Unnewehr, Electric vehicle systems study, in Proceedings of the Third International Electric Vehicle Symposium, Washington, D.C., February 1974.
60. E. J. Cairns and R. R. Witherspoon, Batteries, primary-fuel cells, Kirk/Othmer Encyclopedia of Chemical Technology, September 26, 1977.
61. K. V. Kordesch, *J. Electrochem. Soc.* **118**, 815 (1971).
62. N. E. Bagshaw, K. P. Bromelow, and J. Eaton, The effect of grid conductivity on the performance of tall lead–acid cells, in *Power Sources 6*, D. H. Collins, ed., Academic Press, New York (1977).
63. W. Tiedemann, J. Newman, and F. DeSua, Potential distribution in the lead–acid battery grid, *Power Sources 6*, D. H. Collins, ed., Academic Press, New York (1977).
64. A. C. Simon and S. M. Caulder, in Proceedings of the Symposium and Workshop on Advanced Battery Research and Design, Argonne National Laboratory, Argonne, Illinois, March 1976, ANL 76-8.
65. N. J. Maskalick, J. T. Brown and G. A. Monito, in *Proceedings of the 10th IECEC*, IEEE, New York (1975).
66. D. L. Douglas, Proceedings of the Symposium on Power Systems for Electric Vehicles, Columbia University, New York, April 1967.
67. T. A. Edison, German Patent 157,290 (1901); U.S. Patent 678,722 (1901).
68. S. U. Falk and A. J. Salkind, *Alkaline Storage Batteries*, sponsored by the Electrochemical Society, John Wiley & Sons, New York (1969).
69. *Power Source 5*, Research and development in non-mechanical electrical power sources, in Proceedings of the 9th International Symposium held at Brighton, September 1974, sponsored by the Joint Services Electrical Power Sources Committee, D. H. Collins, ed., 1975.

70. J. D. Birge, J. T. Brown, W. Feduska, C. C. Hardman, W. Pollack, R. Rosey, and J. Seidel, Performance characteristics of a new iron–nickel cell and battery for electric vehicles, *Power Sources 6*, D. H. Collins, ed., Academic Press, New York (1977).
71. R. E. Vaill and R. Rosey, Applications and developments of *W* iron–nickel battery systems, presented at MIDCON/77 Electrical and Electronics Exhibition, November 1977
72. R. Rosey, Westinghouse iron–nickel battery development, presented at the Joint ACS/CSJ Chemical Congress Honolulu, April 1979.
73. S. U. Falk and A. J. Salkind, *Alkaline Storage Batteries*, John Wiley & Sons, New York (1969).
74. E. Buzzelli, in Proceedings of the Electrochemical Society Meeting, Dallas, Texas, October 1975.
75. E. Buzzelli, private communication, 1976.
76. E. J. Cairns, Zinc/nickel oxide cells: Status and projections, *Extended Abstracts of the Electrochemical Society Meeting*, Atlanta, Georgia, October 1977, Vol. 77-2, The Electrochemical Society, Princeton, New Jersey (1978).
77. J. McBreen and E. J. Cairns, The zinc electrode, *Advances in Electrochemistry and Electrochemical Engineering*, Vol. 11, H. Gerischer and C. W. Tobias, eds., John Wiley & Sons, New York (1978).
78. E. J. Cairns, Zinc/nickel oxide cells, presented at International Society Electrochemical Meeting, Budapest, August 1978, *Extended Abstracts*, p. 1190.
79. O. Von Krusenstierna, High energy, long life-zinc battery for electric vehicles, in *Power Sources 6*, D. H. Collins, ed., Academic Press, New York (1977), p. 303.
80. A. Charkey, in *Proceedings of the 10th IECEC*, IEEE, New York (1975), p. 1126.
81. F. P. Kober and A. Charkey, *Power Sources 3*, D. H. Collins, ed., Oriel Press, Newcastle-upon-Tyne, England (1971).
82. R. G. Gunther, presented at the Electrochemical Society Meeting, Washington, D.C., May 1976, Abstract No. 2.
83. C. J. Warde, P. C. Symons, C. C. Whittlesey, and H. A. Catherino, 100 MWh zinc–chlorine peak-shaving battery plants, in *Proceedings of the 13th IECEC*, SAE, Warrendale, Pennsylvania (1978), p. 755.
84. C. H. Chi, P. Carr, and P. C. Symons, Modeling of zinc-chloride batteries for electric vehicles, in *Proceedings of the 14th IECEC*, American Chemical Society, Washington, D.C. (1979), p. 692.
85. P. C. Symons and M. J. Hammond, Evaluation of a 1 kWh zinc-chloride battery system, Energy Development Associates Report to EPRI, EM-249, September 1976.
86. F. G. Will, The zinc-bromine battery: Possible candidate for electric vehicles and load leveling, in Proceedings of the 12th IECEC, ANS, Hinsdale, Illinois, 1977, p. 250.
87. P. C. Symons, Preprint No. 730253, Society of Automotive Engineers, New York, 1973.
88. P. C. Symons and H. K. Bjorkman, Jr., presented at AIChE Meeting, Detroit, Michigan, June 1973.
89. P. C. Symons, presented at the Society for Electrochemistry Meeting, Brighton, England, December 1973.
90. P. C. Symons, in Proceedings of the 3rd International Electric Vehicle Symposium, Washington, D.C., February 1974.
91. R. A. Putt, A zinc-bromine battery for energy storage, in *Proceedings of the 14th IECEC*, American Chemical Society, Washington, D.C. (1979), p. 683.
92. G. Clerici, M. de Rossi, and M. Marchetto, Zn/Br_2 battery, in *Power Sources 5*, D. H. Collins, ed., Academic Press, New York (1975), p. 167.
93. O. Lindstrom, in *Power Sources 5*, D. H. Collins, ed., Academic Press, New York (1975).
94. H. Cnoblock, D. Groppel, D. Kükl, W. Nippe, and G. Siemsen, *Power Sources 5*, D. H. Collins, ed., Academic Press, New York (1975).
95. E. S. Buzzelli, C. T. Liu, and W. A. Bryant, Iron–air batteries for electric vehicles, in *Proceedings of the 13th IECEC*, SAE, Warrendale, Pennsylvania (1978), p. 745.

96. A. J. Appleby, J. P. Pompon, and M. Jacquier, *Proceedings of the 10th IECEC*, IEEE, New York (1975), p. 811.
97. A. J. Appleby, J. Jacquelin, and J. P. Pompon, SAE Publication No. 770381, February 1977.
98. N. P. Yao, in Proceedings of the Symposium and Workshop on Advanced Battery Research and Design, Report No. ANL-76-8, Argonne National Laboratory, Argonne, Illinois, March 1976.
99. A. J. Appleby and J. P. Gabano, Current status and prospects of the Zn–air and Na–S batteries in France, in Proceedings of the Symposium and Workshop on Advanced Battery Research and Design, Report No. ANL-76-8, Argonne National Laboratory, Illinois, March 1976.
100. H. Baba, SAE Transactions, Paper No. 710237, 1971.
101. A. R. Despic, D. M. Dracic, S. K. Zecevic, and T. D. Grozdic, Problems in the use of high-energy-density aluminum–air batteries for traction, in *Power Sources 6*, D. H. Collins, ed., Academic Press, New York (1977).
102. J. F. Cooper and E. L. Littauer, Mechanically rechargeable metal–air batteries for automotive propulsion, in *Proceedings of the 13th IECEC*, SAE, Warrendale, Pennsylvania (1978), p. 738.
103. L. H. Gaines, R. W. Francis, G. H. Newman, and B. M. L. Rao, Ambient temperature electric vehicle batteries based on lithium and titanium disulfide, in *Proceedings of the 11th IECEC*, AIChE, New York (1976).
104. E. J. Cairns and H. Shimotake, High-temperature batteries, *Science* **164**, 1347 (1969).
105. F. J. Martino, T. W. Olszanski, L. G. Bartholme, E. C. Gay, and H. Shimotake, Advances in the development of Li–Al/FeS cells for electric automobile batteries, in *Proceedings of the 14th IECEC*, American Chemical Society, Washington, D.C. (1978), p. 660.
106. E. J. Zeitner and J. S. Dunning, High performance lithium/iron disulfide cells, in *Proceedings of the 13th IECEC*, SAE, Warrendale, Pennsylvania (1978), p. 697.
107. Argonne National Laboratory, Proceedings of the Annual Department of Energy Review of the Lithium Metal Sulfide Battery Program, June 20–21, 1979.
108. T. G. Bradley, Bipolar lithium/iron disulfide cells, in *Proceedings of the 13th IECEC*, SAE, Warrendale, Pennsylvania (1978), p. 717.
109. E. J. Cairns and J. S. Dunning, High-temperature batteries, in Proceedings of the Symposium and Workshop on Advanced Battery Research and Design, Argonne National Laboratory Report ANL-76-8, March 1976, p. A-81.
110. General Electric, Review of the advanced battery development program for electric utility application, May 1979.
111. D. W. Bridges, R. W. Minck, and D. G. Paquette, Reproducibility and performance of large prototype Na/S cells, in *Proceedings of the 14th IECEC*, American Chemical Society, Washington, D.C. (1979), p. 703.
112. I. W. Jones, Recent advances in the development of sodium–sulfur batteries for load leveling and motive power applications, *Electrochim. Acta* **11**, 681 (1977).
113. R. M. Dell, J. L. Sudworth, and I. W. Jones, Sodium/sulfur battery development in the United Kingdom, in *Proceedings of the 11th IECEC*, AIChE, New York (1976), p. 503.
114. J. M. Bird, A. R. Tilley, and J. L. Sudworth, Sodium/sulfur cell designed for quantity production, in *Proceedings of the 13th IECEC*, SAE, Warrendale, Pennsylvania (1978), p. 685.
115. M. Mikkor, R. W. Minck, and L. E. Unnewehr, Pulse characteristics of sodium/sulfur cells for electric vehicle propulsion, in *Proceedings of the 13th IECEC*, SAE, Warrendale, Pennsylvania (1978), p. 662.
116. W. Fischer, H. B. Gels, F. Gross, K. Liemort, and H. Meinhold, Sodium/sulfur batteries for peak power generation, in *Proceedings of the 14th IECEC*, ACS, Washington, D.C. (1979), p. 710.
117. H. Y.-P. Hong, New lithium solid electrolyte, *Electrochemical Society Extended Abstracts*, Vol. 77-1, Electrochemical Society, Princeton, New Jersey (1977).

118. Los Alamos Scientific Laboratory, Proceedings of the Fuel Cell in Transportation Applications Workshop, Report No. LA-7270-C, July 1978.
119. W. H. Johnson, Phosphoric acid fuel cell technology improvement program, in Abstracts of the National Fuel Cell Seminar, Courtesy Associates, Washington, D.C., June 1979.
120. A. Kaufman, Phosphoric acid fuel cell stock development, in Abstracts of the National Fuel Cell Seminar, Courtesy Associates, Washington, D.C., June 1979.
121. H. C. Marv, L. G. Christner, S. G. Abens, and B. S. Baker, Phosphoric acid fuel cell stock and technology programs, in Abstracts of the National Fuel Cell Seminar, Courtesy Associates, Washington, D.C., June 1979.
122. P. R. Prokopius, M. Warshay, S. M. Simons, and R. B. King, Commercial phosphoric acid fuel cell system technology development, in *Proceedings of the 14th IECEC*, ACS, Washington, D.C. (1979), p. 538.
123. L. B. Welsh, R. W. Leyerle, and D. S. Scarlata, Stability of Kocite electrocatalysts in phosphoric acid cathodes, in Abstracts of the National Fuel Cell Seminar, Courtesy Associates, Washington, D.C., June 1979.
124. H. Shimotake, Lead–acid batteries, ANL Office for Electrochemical Project Management (OEPM), presented at the DOE/TEC Electric/Hybrid Vehicle Program Contractors' Coordination Meeting, Reston, Virginia, December 1977.
125. R. C. Elliott, Nickel/iron batteries, ANL Office for Electrochemical Project Management (OEPM), presented at the DOE/TEC Electric/Hybrid Vehicle Program Contractors' Coordination Meeting, Reston, Virginia, December 1977.
126. W. J. Walsh, Nickel/zinc batteries, ANL Office for Electrochemical Project Management (OEPM), presented at the DOE/TEC Electric/Hybrid Vehicle Program Contractors' Coordination Meeting, Reston, Virginia, December 1977.
127. Electric vehicle systems, FY1978, Environmental Development Plan, EDP/C-01(77), Energy Research & Development Administration, August 1977.
128. L. H. Gaines, private communication, Exxon Research and Engineering, January 1978.
129. E. J. Cairns and J. S. Dunning, High-temperature batteries, General Motors Research Laboratories, Warren, Michigan, GMR Publication 2065, January 1976.
130. J. F. Norberg, private communication, Automotive Division of ESB Incorporated, May 1974.
131. Zinc/nickel oxide brochure and data sheets, Energy Research Corporation, Third International Electric Vehicle Symposium and Exposition, Washington, D.C., February 1974.
132. Nickel–zinc secondary batteries, Eagle-Picher Industries, Inc., Joplin, Missouri, January 1975.
133. J. R. Kettler, Batteries for the hybrid heat engine/electric vehicle, in Proceedings of the Symposium on Batteries for Traction and Propulsion, Columbus Section of the Electrochemical Society, March 1972, p. 213.
134. C. A. Levine, Sodium–sulfur batteries, in *Proceedings of the 25th Power Sources Symposium*, May 1972, PSC Publications Committee, Red Bank, New Jersey (1972), pp. 75–77.

16

A Hydrogen Economy

J. O'M. BOCKRIS

1. History

The history of the "hydrogen economy" may be broken down into three parts. Firstly, there is the history of the founding of the Hydrogen Energy Society which took place in Miami, Florida, in 1974 under the chairmanship of Nejat Veziroglu. Earlier, a Hindenberg society was founded by William Escher. The beginning of the official society in Miami in 1974 has been followed by several international meetings, each attended by about 1000 persons.

However, the history of the concept of the hydrogen economy has seen two earlier beginnings. In modern times, it began with the invention of the phrase "the hydrogen economy" in the General Motors Technical Laboratory in 1969. This was succeeded by a note by Bockris in December, 1971,[1] where the concept of a hydrogen economy was set out as such: affluent economies would be fueled by hydrogen coming from the decomposition of water using atomic and solar sources.[2]

However, before the fully formed concept of Bockris, 1971, there had been isolated earlier mentions. Haldane[3] saw future supplies of hydrogen from wind energy underlying the economy. Lawaczeck, in the 1930s,[4] gave the first indication that the flow of energy as hydrogen through tubes might be cheaper than the flow of electricity through wires.

J. O'M. BOCKRIS • Department of Chemistry, Texas A & M University, College Station, Texas 77843.

In 1962 Bockris, in a memorandum to the Westinghouse Company,[5] proposed the concept of seaborne platforms utilizing photoelectrochemical conversions to obtain hydrogen from the sea. In 1965, Justi[6] envisioned desert-borne solar stations using hydrogen which would be piped to Europe. Other contributions to the concept of a hydrogen economy are described in the book *Energy: the Solar-Hydrogen Alternative*, by Bockris.[7]

In the late 1970s the concept of the hydrogen economy was present in the official energy policy of the United States, but as something that may be necessary "at a later date." It is not yet realized that hydrogen from coal would be the cheapest fuel with which to replace gasoline (cheaper indeed than gasoline), and the burning of this fuel would reduce the level of atmospheric pollution now caused by the burning of gasoline; furthermore the hydrogen that is bound to result from nuclear and solar sources could be used.

2. Hydrogen Economy and the Time Scale

It is not possible to envision the desirability of the hydrogen economy, and work thereon at this time, without an indication of the quantitive aspects of the time scale of the exhaustion of the present energy supplies. It is the very short duration of the time scale usually considered which obfuscates many of the present issues.

Firstly, there is a sinister character to resource availability–time curves (Figure 1). Nothing about exhaustion can be seen until a few years before the termination of the availability of the resource. Some few years before exhaustion becomes apparent by an actual diminution of supply there is increasing rise in prices.

High living standards and the plentiful availability of energy are equivalent. However, continuing to burn the same amount of oil will only result in the end of the nonrenewable resources before renewable machinery has been built. On the other hand, cutting back the supply of energy to stretch out supplies would be likely to give rise to social disorganization, for the voting populace considers on an extremely short-term scale at its own material comfort. The two-party system would always lead to reelection of the comfort-giving party. Resources would be likely to exhaust before the atomic and solar production centers have been built.

Thus long lead times are necessary to create a new basic energy supply. The decision to go into some new energy economy must be made at least a decade before significant contributions from that economy would be made. As the downturn time of the western world's supply of liquid and gaseous fossil fuels is less than a decade away, it may already be too late to begin the building of a new energy economy.

The major difficulty behind the building of this is that the cost is too great. To obtain the money, greatly increased taxation is necessary, but would be

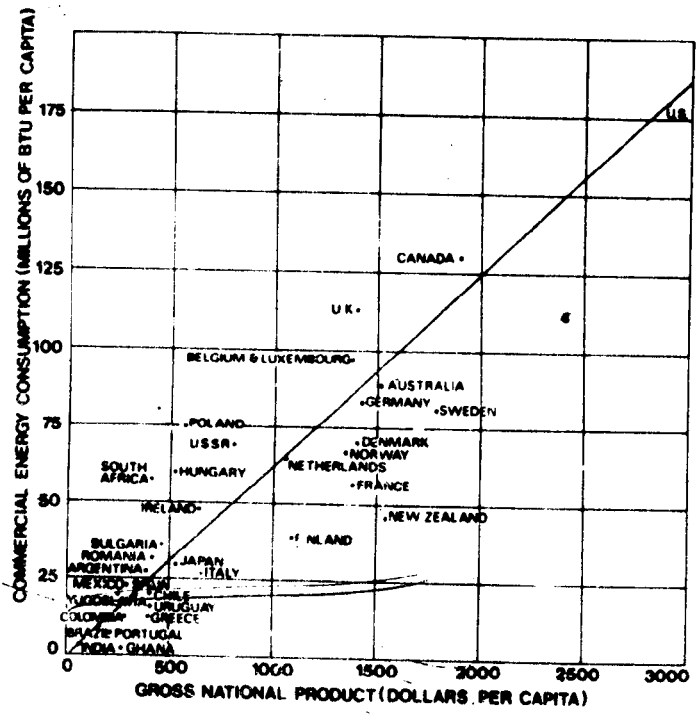

Figure 1. Rough correlation between per capita consumption of energy and gross national product is seen when the two are plotted together.

politically unacceptable. Alternatively, 15–20% inflation (the involuntary taxation) would be very unacceptable.

Another difficulty in changing the energy economy in the present social system is that political power originates with groups which have the major capital investments. These are groups which sell the exhausting fossil fuels. Thus the major change which must be made means a reduction in sales of organizations which sell oil, natural gas, and coal. Their cooperation is unlikely.

3. Three Possible Energy Futures during the Coming Century

There are three possibilities for the replacement of oil and natural gas, if the time scale viewed is less than 50 years (with respect to coal):

3.1. Coal

Gasoline can be replaced by liquid products from coal, and that is the option which will be the most advantageous one from the point of view of those who own the remaining resources, and who have, therefore, the major influence upon policy in the United States through members of the Congress.

Coal could be turned to the following products in order of increasing costs: (a) hydrogen, (b) synthetic natural gas, and (c) synthetic gasoline. Sunthetic gasoline, the most expensive, would leave the situation least perturbed, and be in the greatest interest of both the automotive and oil companies. This is the course which will, therefore, tend to be followed.

3.2. Nuclear Hydrogen

In this future, all energy would come from nuclear sources, which would then produce electricity for those purposes, i.e., to use hydrogen for purposes that are now supplied by natural gas and gasoline.

The difficulty of this future, which seemed in the early 1970s to be a suitable one, is that it involves the pollutional difficulties of breeder reactors, which do not seem easily surmounted (hijacking and waste disposal). Fission reactors use uranium supplies, which would not last much longer after the year 2000.

3.3. Coal–Nuclear Future

In this future, electricity will be supplied by nuclear sources and coal would supply synthetic oil and gasoline.

This is the kind of economy which would be favored by sources of capital investment which already own nuclear plants and the remaining oil and coal.

The first three energy schemes here discussed, though favorable from the point of view of capital already invested, are less favorable from the point of view of the public. The use of coal would introduce the Greenhouse effect. The use of breeder reactors would produce health hazards; and the use of the coal–nuclear situation would give rise to both CO_2 and health hazard problems.

4. A Solar–Hydrogen Economy

There is misunderstanding of this because it is not understood that solar energy can supply all needs, including those for transportation and industry. Thus solar energy is often thought to be "for less-developed countries" or "for rooftops, and for the supply of energy to houses." Solar energy in the United States is not less dense (energy per unit area) than oil, though the solar energy supply would be permanent. Its transfer to cities in the form of hydrogen is a proposition which has been analyzed from the economic point of view.[8] Some

of these analyses, the economic basis to a solar hydrogen economy, will be outlined in the present chapter.

5. The Necessity of Beginning the Development of a Hydrogen Economy Several Decades before the Ending of the Fossil Fuel Supply

The necessity of developing one of the new energy systems before the end of the reserves of fossil fuels is obvious. Hansen[9] has used the word "autophage" for the present tendency, which is to eat up the sources which we need to build the next energy system. The case that the next energy system should be hydrogen based needs economic arguments, as shall be seen below.†

During the 1980s and 1990s we shall be replacing the liquid and gaseous fossil fuels by three sources of energy. Coal will be used, atomic power will be used, and it will be increasingly realized that the massive collection of solar energy and its conversion of water to hydrogen is the least costly source of energy from the point of view of the population.

During this time, these three sources of energy will all be used: it would be uneconomic were they to be associated with a series of different fuels. In the classical view, atomic reactors produce electricity. Oil and petroleum would be produced from coal, and solar energy would be retained only in the production of rooftop energy. However, this fails to take into account the possibilities from the other sources, and the development of solar sources with their production of hydrogen from water splitting. On this basis it would be better to introduce hydrogen to avoid the proliferation of equipment.

6. The Relationship of Hydrogen to Coal

If decisions were optimized for the advantage of the consumer, coal would not be used as an energy source because of the damage caused by its products.

† In all economic arguments, it depends upon which kind of economics one takes. The economics stated in 99% of the literature is economics as seen from the viewpoint of the minority vendor, economics which considers the profits or losses of the vendors. It does not, for example, take into account the cost of pollution paid for in taxation by the consumer because of (earlier unrealized) pollution by the vendor's products.

There is another kind of economics, that to optimize the needs of the majority consumer. Thus, in the presentation made here, the energy system is regarded as optimal which optimizes the economic situation of the average citizen. This may or may not reach the same conclusion as that which optimizes the profit potential of the vendor.

Another consideration concerning economics is the *time* which is to be discussed. It cannot, of course, be applied to the present, but must be applied at a time when it would be relevant, namely, a time during which the liquid and gaseous fossil fuels fade from the scene—during the 1990s. (Anomalously, most discussions comparing energy prices take the present situation and hence always indicate the price superiority of fossil fuels.)

However, because of the influence of the minority vendors of coal, coal will be used at first as an energy source to replace oil. This would produce difficulties for the population, and for the world as a whole, because of the Greenhouse effect that would result from the burning of coal, in addition to the shorter time pollutional effects.

One way around this relates to the products made from coal, not expensive products like liquid gasoline, nor even of the medium-priced synthetic natural gas. Were *hydrogen* produced from the coal, the cheapest fuel which can be produced from coal, then the hydrogen could be piped to the user sites and coal gassification plants could be built on the shore. The carbon dioxide could then be piped into the deeper parts of the ocean, where there is enough water to take up the CO_2 load from the entire remaining fossil fuel supply.[10] Thus the production of hydrogen as an intermediate product from coal would make coal pollutionally more acceptable (though there are still difficulties with the sulfur).

As the solar and atomic reactors are built, the hydrogen from coal would then enter the mix to be produced from nuclear reactors and from the solar sources.

7. The Method of Obtaining Hydrogen on a Massive Scale

7.1. Hydrogen from Coal

It is easy to obtain hydrogen from coal. This is done by mixing powdered coal with steam at about 900°C (see Figure 2). The cost of the hydrogen has recently been estimated[11] as \$3.00 per MBTU. Gasoline at \$1.00 per gallon is equivalent to \$7.92 per MBTU.

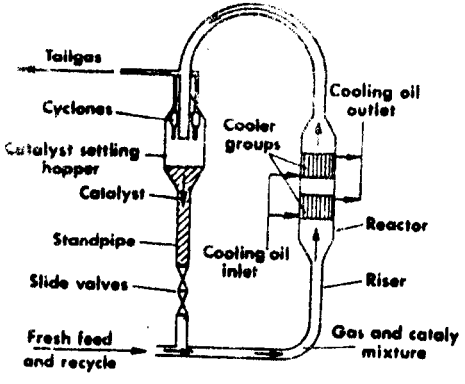

Figure 2. The synthol reactor of the South African plants.

7.2. Biomass

The production of hydrogen from biomass is more complex, not because of difficulty in the process, but because of the variety of methods available. Thus grass, wood, and trees could be burned anaerobically to produce hydrogen.

In a more sophisticated way, it would be possible to utilize solar light to convert blue-green algae, which contain the enzyme hydrogenase, to hydrogen in the decomposition of water. Such processes are not yet, however, well developed and give only 1% efficiency, together with doubtful lifetimes of operation.

7.3. Hydroelectric Plants and the Electrolysis of Water

Hydroelectric plants give the second cheapest source of hydrogen. Plants could be built from hydroelectric sources; these sources could supply enough hydrogen to take over a substantial amount of the automotive load. Numerous sources throughout the world have been neglected because they are far from the sources where the energy can be used if carried as electricity (where the cost increases greatly with distance). However, if it is carried in hydrogen form, the distance over which the energy from these hydroelectric sources can be used will be increased. Sources like Victoria Falls and the large hydroelectric source from Greenland could be applied to give hydrogen for automotive and other uses in faraway places.

7.4. Hydrogen from Wind Power

It is easy to show that there are places in the world where wind blows more than a yearly average of 20 km/hr. These are places where it is worthwhile building large wind generators, and these produce hydrogen at a cost of around $6–$9 per MBTU.

7.5. Hydrogen from the Kinetic Energy of Natural Streams of Water in the Earth

There are natural streams of water in the earth that flow at several km/hr; the placing of large rotors in these streams would give sufficient power to be a source of production of electrolysis of hydrogen from seaborne plants.

The Gulf Stream is the most well-known of these natural streams, but it is not the only one. Indeed, it seems likely that such sources exist all over the planet. They arise from the Coriolis forces generated by the earth's rotation. Such a stream runs between Victoria Island and Vancouver. The economics of the conversion of hydrogen from such sources is unknown.

8. The Manufacture of Hydrogen from Solar Energy

There are two paths here. One is the utilization of solar electricity from solar cell, or OTEC, sources, and then normal electrolysis, (see Figure 3). The other is utilization of solar light to energize electrochemical cells to furnish water and form hydrogen which can be transmitted or stored, depending upon the most practical method of the time. The use of doped silicon in an amorphous form connected with metal anodes would work with an efficiency competitive with the photovoltaic–electrolyzer situation.

9. Methods of Decomposing Water

There was a trend during the 1970s to carry out research on the thermal decomposition of water.[12] The decomposition of water considered is not the

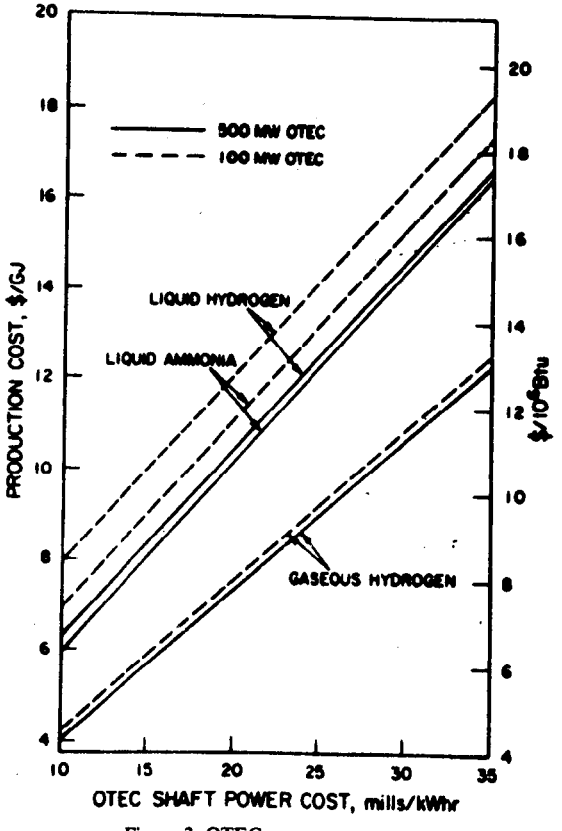

Figure 3. OTEC power costs.

direct thermal decomposition obtained by heating water to 3000°C (for there are no satisfactory refractories for containing the reaction at that temperature), but the cyclical decomposition at which much lower temperatures are practical. One brings into contact with water some substance which reacts with and produces hydrogen and another substance, and this substance (or other substances) are decomposed by reattaining the original substance and making oxygen. The reason why these reactions can be carried out at lower temperatures arises from the reduction in the overall $\Delta G°$ which can be attained in cyclical reactions by the careful balancing of the $T\Delta S$ terms. When the ΔS terms are positive, then the standard free energy can be brought in a more negative direction by using high temperatures. When the ΔS terms are negative, however, the reaction is carried out at lower temperatures.

In spite of the merit of this idea, the principal objective of it was to avoid the Carnot difficulty in the production of electricity; there is in fact a Carnot aspect of the matter. As the reactions work in cycles, there has to be a pumping action between the various pressures and temperatures of the cycles. This is the same type of cycle originally treated by Carnot.[13] Substantial amounts of work are used up in these changes of state of the reactants and products of the cyclical reactions and there is, in principle, no difference between the heat to electricity to hydrogen cycle and this one. It is claimed that higher temperatures can be used, and therefore the theoretical Carnot effect increased. This applies also to the production of electricity from heat.

There is, however, a negative aspect in the thermal decomposition suggestions. This is the cost of the plant involved. It is not likely that a plant will be built cheaply if it involves high-temperature equipment and has to guard itself against the corrosional activities of aqueous solutions at 800°C.[14] The likelihood, therefore, that the overall thermal decompositions of water by the cyclical method to hydrogen and oxygen will be more economical than the electrochemical methods is very small. Furthermore, the feasibility of the chemical method is small, for most of the cycles do not give, in practice, exclusively H_2 and O_2: there is a buildup of unwanted product.

10. Electrochemical Decomposition of Water

This has been dealt with particularly in Volume 2 and will only be outlined here in a summary fashion.

10.1. Classical Electrolyzers

Numerous large-scale electrolyzers exist throughout the world and work at about 2 V. The current density is around the order of 100 A/ft^2. These electrolyzers were built before the time in which energy became expensive, and little attention has been brought to minimizing the value of the applied potential of the electrodes.

10.2. Modern Electrolyzers

There are no large-scale electrolyzers at the present time which have been built on the basis of modern developments of electrode kinetics of the past few decades. The opportunities which exist here are large, but companies seem reluctant to develop them because of the unrealized state of the market (see Figure 4).

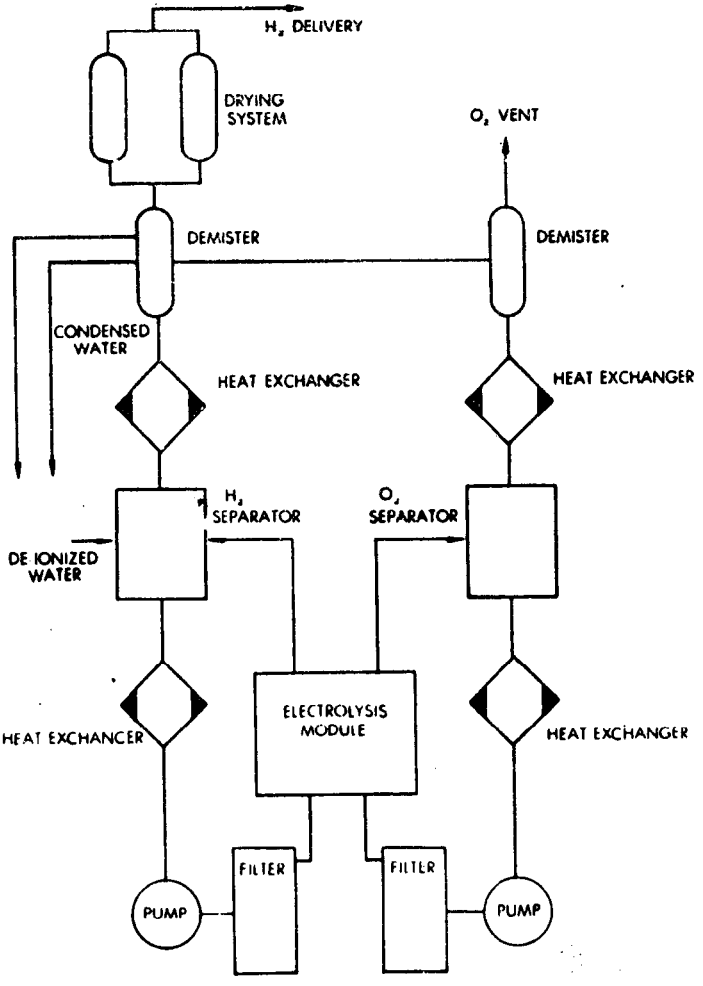

Figure 4. Block diagram of 1.25-tons/day capacity hydrogen plant. A 25% KOH solution is forced, through filters, into the electrolysis module, the gases thus produced are separated and freed from KOH vapors in the primary separators. The hydrogen is lead through the heat exchanger and finally collected by drying in a molecular sieve system.

10.3. Electrolysis of Thermal Systems

Were it possible to involve both electricity and heat in the splitting of water, there might be some financial gain. Again, it would be advantageous if the oxygen part of the production of hydrogen from water decomposition were avoided, for it is the evolution of oxygen which drives the total potential needed for the action of the cell, about 1.2 V. Hence some suggestions have been made that sulfuric acid can be decomposed by heat to form sulfur dioxide. The sulfur dioxide would then be used in the anodic reaction to form sulfuric acid back again. Against these concepts must be weighed the cost of a plant used for a two-stage process, and the fact that there are commonly losses.

11. Decomposition of Water by Light

Light can be used in two ways, first by the normal solar energy conversion means (photovoltaic, solar–thermal). However, the photoelectrochemical decomposition of water can be realized by having an amorphous silicon cathode working in conjunction with a metal anode (see Figure 5). If such a situation can reach more than 6%, it is likely that it will be utilized because it will mean only one plant, thus cutting costs.

12. Hydrogen at High Temperatures

The decomposition of water at high temperatures (1000–1500°C) is a viable process.[15] One utilizes a uranium–yttrium cathode and anode, and on these are placed a thin layer of U_3O_8–Y_2O_3, a conductor (see Figure 6). The

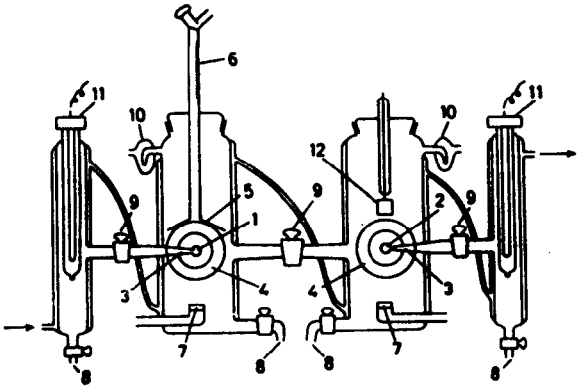

Figure 5. Schematic of a photoelectrochemical cell. 1, P-type CdTe electrode; 2, *n*-type TiO_2 electrode; 3, Luggin capillary; 4, window of quartz-optical flat; 5, gas collector; 6, gas burette; 7, frit; 8, drain; 9, stop cock; 10, gas outlet; 11, reference electrode; 12, Pt electrode.

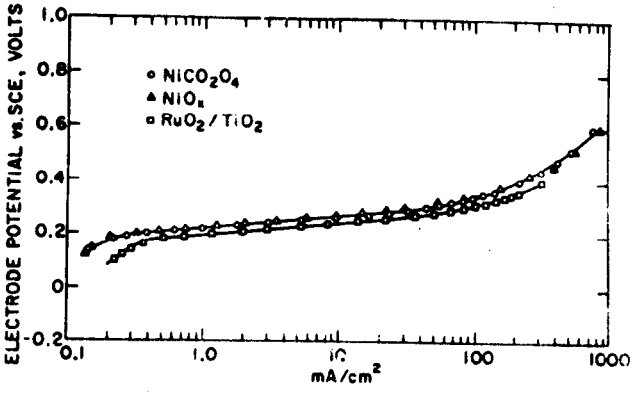

Figure 6. Tafel's slopes for the mixed oxide oxygen electrodes.

introduction of the uranium–yttria system is the key point, because the diffusion of oxygen and good electronic conductivity are foremost. Under these situations, and with thin zirconium electrodes, a decomposition of water can be made, and the temperatures are now so high that activation polarization is effectively zero. Furthermore, about 50% of the energy needed for the decomposition of water comes from the heat outside of the Carnot cycle, so the energy consumption is small.

One of the difficulties of this method would be the lifetime of the apparatus concerned. The thermal cycle method of decomposing water involves high temperatures; thus plant costs are great. In this case we have one plant apparatus, but the temperatures of operation are high. Can the apparatus be durable?

13. The Cost Aspect of the Production of Hydrogen

13.1. Time Scale

In a time of fluctuating prices, it is important to consider the price of hydrogen in the proper time scale. This can be confusing because we have several factors which are unique to the economic history of the period. First, there is inflation, which can be expected to increase each year by a factor of greater than 10%.

Second, there is the change brought about by the relative exhaustion of energy resources. Electrolytic hydrogen produced at the present time at a cost of about $9.00 per MBTU is not competitive with the cost of gasoline at $4.00 per MBTU; but, such comparisons are not valid—we are not expecting to

utilize hydrogen at this time. What will be the cost of gasoline in the year 2000 and what will be its availability?

13.2. Cost and Price

We are talking in all cases about costs. Prices are an entirely different matter which involve many aspects of markup caused by the application of various government regulations and, of course, profit margins.

13.3. Large- and Small-Scale Prices

There is a considerable difference in hydrogen prices based upon the scale of production. If one takes the price of hydrogen in a cylinder, it is an order of magnitude greater than the production of hydrogen on a larger scale, because of expenses of low-scale manufacturing, including the cost of pumping hydrogen into the cylinder.

13.4. The Cost of Electrochemical Processes in the Production of Hydrogen

The price of hydrogen in dollars per million BTUs is

$$2.29(e)(c) + C$$

where E is the volts needed to produce the hydrogen at a given rate, c is the cost of the hydrogen in cents per kilowatt-hour, and C is the cost of amortization of the plant, insurance, maintenance, etc., per MBTU.

A value of $1.00 per MBTU has been argued by Bockris,[8] based on some original observations of Gregory; and the value of E is as high as 2 and as low as 1.4. It seems reasonable to assume an E of 1.6 V for a date of about 1990 (using 1979 dollars). The current density assumed would be about 100 A/ft^2, and perhaps as high as 500 A/ft^2.

The main uncertainty is the value of c, the cost of 1 kWh of electricity. It is misleading to take this value as equal to the cost paid by a householder; there are clear reductions of scale. The ratio from the large-scale purchase of electricity to that charged to householders is around 1:2. However, there are other economies which can be brought into estimating the appropriate value of c. Electricity can be interrupted in the course of the production of hydrogen. From 6:00 a.m. to 9:00 p.m., no hydrogen need be produced; however, during the night hours (roughly 9:00 p.m. until 6:00 a.m.) the plant can produce hydrogen. In this way alternate economics on a higher scale can be determined such that the final cost of c is probably between one-third and one-half of the known cost.

Another method of economizing is to put the hydrogen or electrolysis plant next to the electricity-producing plant to eliminate the cost of transporting the electricity. The overall cost of the electricity can be one-third of the cost charged to household consumers. On this basis, we are considering hydrogen costs of around $8.00–$9.00 per MBTU (see Table 1). Of course, this involves the large-scale production of hydrogen with the above characteristics, new advanced electrolysis plants (presently unbuilt and only conceivable based on experimental results), and the use of temperatures near 100°C.

It is not feasible for hydrogen to be produced from electrochemical methods at the same costs as it can be obtained from coal, for basic reasons. In obtaining hydrogen from coal, no endothermic reaction has to be worked and no Carnot cycle has to be overcome. One utilizes the energy from coal to produce electricity through a Carnot cycle; electricity obtained in this manner will be two to three times more expensive than the energy in the original fuel.

Hydrogen will be obtained electrochemically, therefore, only from nuclear or solar plants. However, this is only true with respect to large-scale plants; in small plants the production of electricity and hydrogen from water may be cheaper: one cannot build a *small*-scale coal gassification plant economically.

Table 1
The First Law Costs of Hydrogen, 1979

Method	Cost	Remarks
Coal and steam, coal at $28/ton	$4.00	Considered D.O.E. estimate
Coal, electrolysis of suspension	$5.00	Assumed cost of massive, interruptable, electric power in large-scale blocks, used at site; 3¢/kWh
Advanced water electrolysis at 100°C	$12.00	Assumes laboratory results at 3¢/kWh
Electrolysis and steam at 1000°C	$11.00	Uncertain estimate
Electrolysis using depolarizers such as SO_2	$8.00	Calculations based on SO_2 at 100 mA/cm^2, but only possible if coal available as source of excess sulfur
Thermal decomposition of steam—cyclic chemical methods	$12.00	Assumes three cycles with energy cost $2.50/MBTU
Photovoltaic at 6¢/kWh and electrolysis at 1.6 V	$23.00	No remarks
OTEC and electrolysis at 1.6 V	$16.00	Lavi, private communication
Solar-Thermal at 1.6 V	$20.00	Smith, private communication
Photoelectrochemistry	$23.00?	Laboratory results only; electrode stability not established
Biomass	$5.00	Estimate is probably high, but what of space needed?

13.5. The Production of Hydrogen from Coal

The production of hydrogen from coal has already been mentioned above, and would cost on the order of $3.00 per MBTU at present costs.[8]

14. Applications of a Hydrogen Economy

14.1. Transmission

If one sends electricity through energy formed by electricity, there is no cost at zero distance; but, with increased distance, the *IR* drop through the wire causes a predictable loss of energy.[7]

If one uses the electricity to decompose water, than at zero distance one has lost no energy in the electrolysis, so the energy contained in hydrogen is too expensive. However, the cost of sending the hydrogen through a tube is small; after approximately 500 miles, the hydrogen is cheaper than electricity for this and greater distances. For example, at 1000 miles, the difference is substantial, even if one takes into account the reconversion of hydrogen to electricity (see Figure 7). Solar energy collected in Arizona, for instance, could be transported to New York state where it would be used as fuel for motor vehicles.

14.2. Transduction

Transduction of energy from hydrogen can be carried out by two methods: chemical and electrochemical. In the chemical engine, one utilizes hydrogen in

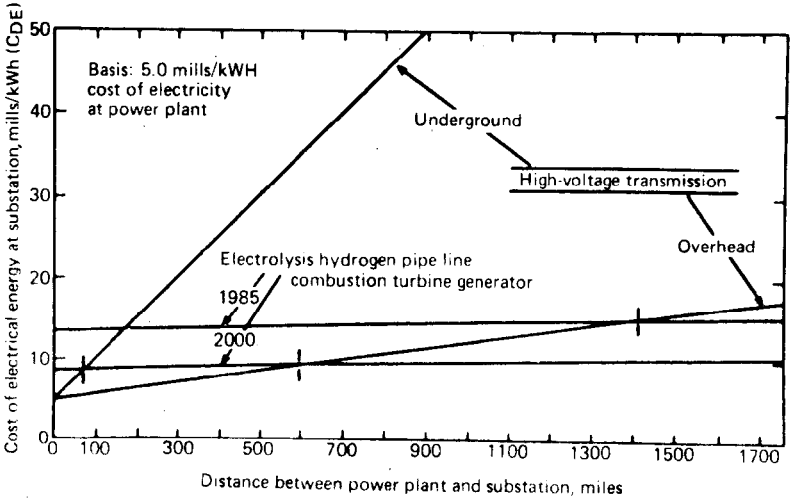

Figure 7. A liquid hydrogen container.

the same way as one would use natural gas or gasoline. Many hydrogen engines have been developed.[12] It is easy to convert a normal engine to a hydrogen engine by replacing the carburetor with a fuel-injection system at a stoichiometric ratio, and not a ratio above this as with gasoline.

For the obtaining of mechanical power, the transduction of hydrogen in internal combustion engines is acceptable. The efficiency of such transduction is low because the engine is a heat engine. However, to obtain electricity, it is better to go to the fuel cell—the electricity can be obtained at better than 60% efficiency, from hydrogen fuel (60% by heat engines).

It is also possible to consider the electrochemical engine: the fuel cell-electric motor combination.

15. Storage of Energy

There are substantial difficulties in the storage of hydrogen. Nevertheless, it could be an important storage medium. Three primary methods are listed below.

15.1. Reservoirs

The hydrogen may be stored in very large quantities in underground reservoirs, the natural reservoirs which, at present, contain natural gas. The disadvantage here is that the hydrogen contains only about one-third of the energy which natural gas contains per unit volume. It would have to be pumped at three times the rate. The pumping of hydrogen and its diffusion rate would be easier than that of natural gas. Negative features occur in the filling up of the natural gas fields with hydrogen. To obtain the pressure, some hydrogen has always to be kept in the field. Thus, in a sense, it is wasted.

15.2. Liquefaction

This seems the most suitable method, from the point of view of the consumer. However, the liquefaction would cost about $3.00 per MBTU at best. If one starts with the price of hydrogen at $3.00 per MBTU, it means an increase of 100% to liquify it. The technology of cryogenic storage has undergone increase because of the use of hydrogen as a fuel in space vehicles; however, such equipment is not available on a small scale (see Figure 8). Considerable services will be required to build it.

Losses from cryogenic containers are approximately 1% per day, not a serious loss.

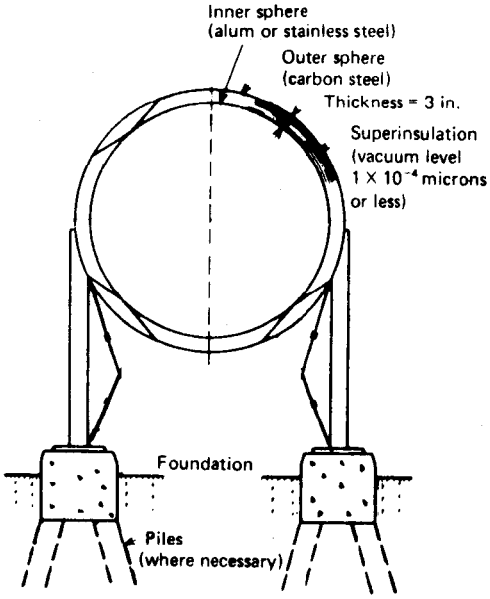

Figure 8. Comparison of cost of electrical energy at distribution substation for electrical transmission in hydrogen. $K = 0.0003$–0.0025 BTU/hr/ft^2 °F/in.

15.3. Alloys

These have not been sufficiently researched. One alloy which has recently been proposed is Fe–Ti, but this has disadvantages with respect to its weight. There are also difficulties with respect to repeated charging and discharging after about 100 times.[13]

There may be other alloys not yet discovered which contain hydrogen at more favorable weight conditions. Some such alloys have been found; these involve the rarer elements and are hence not economical; there is not sufficient information known relative to the theory of the storage of such systems.

16. Safety Aspects of Hydrogen as a Fuel

As with cost, safety matters are comparative and the more reasonable substances with which one must compare hydrogen are natural gas and gasoline. Chemical fuels cause explosions with air; so, all fuels must be dangerous.

Hydrogen is, no doubt, a dangerous fuel, and it is possibly somewhat more dangerous than gasoline or natural gas, as is commonly believed. The explosion limits have a larger range than those of methane and oxygen.

Difficulties with hydrogen are (1) the invisibility of its flame and (2) its rapid diffusion time through cracks.

There are some counteracting features which diminish the difficulty of hydrogen, in comparison with natural gas. The energy per unit volume is one-third that of natural gas. A hydrogen explosion would do less damage than a methane one. Again, in an accident in which the car's fuel tank is destroyed during impact the gasoline which leaks onto the ground has a heavy vapor and is likely to find a hot surface in the accident to explode. Conversely, liquid hydrogen spilled upon a roadway in an accident is likely to evaporate, rather than rolling along the ground seeking a hot surface.

The major difficulty seems to be that of image, and lack of understanding that difficulties in dealing with hydrogen are only of the same order of difficulty as those in dealing with any other chemical fuel.

16.1. Hydrogen in Transport and Housing

The use of hydrogen in transport involves two concepts: (1) hydrogen is used to drive the fuel cell, and (2) the fuel cell is used for long distance running at low power demands, such as charging a battery to provide the car with acceleration potential and starting energy. The other concept involves hydrogen in internal combustion.

The use of hydrogen in households has been developed by R. Billings in his house in Provo, Utah[8,13] (see Figure 9). Hydrogen is used in cooking and household heating, without the use of chimneys, because the only substance produced is water vapor. In lighting, in a more efficient way presently available, hydrogen would be used to induce phosphorescence and the emission of white light.[7]

16.2. Industry

There are as many applications as those which now use natural gas. Further, hydrogen can be used in large-scale reductions, e.g., with Al_2O_3, etc.[7]

16.3. Pollutional Aspects

The energy economy of the western world was undisturbed by pollutional considerations until the later 1960s when citizens began to complain about air pollution from cars, particularly smog. These pollutional aspects have been increased by the realization of the pollution from nuclear plants. The use of a hydrogen economy would eliminate such difficulties since the only product is water. Water need not even be vented as steam, but condensed to liquid water to be recycled back into the system, or used as drinking water.

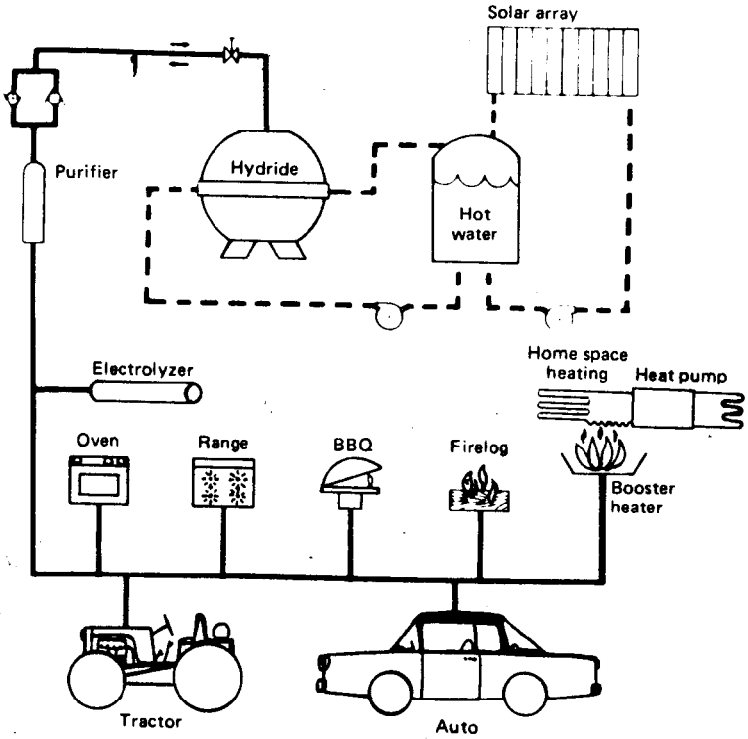

Figure 9. The plan at Billings' place.

17. The Hydrogen Economy as the Cheapest Economy

It is usual to choose that system which seems to be the cheapest. It depends, however, upon the subject's viewpoint chosen at the time scale of the comparison. Nuclear sources could give energy relatively inexpensively (if one only looks at the cost of one unit of energy). However, if after some decades, a percentage of the population dies from cancer, the cause of deaths being caused by the absorption of radiations from atomic energy sources some years earlier, the cost of the deaths must be taken into account in determining the cost of the energy.

First law economics is the cost of a unit of fuel burned at 100% efficiency. Second law economics refers to the cost of carrying out one unit of action using the fuel concerned, such as driving a car 1 km. Fuels differ considerably in the ratio of first to second law efficiencies. Hydrogen drives an automobile in a suburban driving cycle about 1.5 times more efficiently than does gasoline.[11]

This ratio differs with the driving cycle, speed, and includes other considerations as well.

If one is comparing the cost of fuels, it is simple to take such ratios into account (see Figure 10). One should take into account the second law efficiency of hydrogen versus gasoline for many applications and then weigh the applications with regards to the total amount of use. This is an exercise yet to be done. If one takes the urban driving cycle, the factor of 1.5 is in favor of hydrogen.

Another factor which must be brought into cost considerations is the pollutional aspect. Fossil fuels damage the population by causing illness (e.g., emphysema[23]); they also increase the dirt in cities.[9]

It is not an honest price to neglect taxes which are being spent by the Environmental Pollutional Agency to attempt to right the damage done by the sellers of fossil fuel. The majority is thereby unconsciously increasing the profit of the minority. Were a crop-spraying company who has sent its products to a farmer to have incapacitated the surrounding countryside, the farmer would not have to pay for the damage; the producer of the damaging goods would be liable.

Thus the true comparison of the fuel costs would take into account the second law and the cost of the environmental pollution and health damage prorated to one unit of fuel.

There are difficulties in estimating these latter costs, and much work has to be done on the matter. At present, wrong comparisons are being made: first law costs *at this time* are being compared, and pollutional damage is being neglected.

The hydrogen economy becomes easily the cheapest economy (to the majority consumer) when these facts are taken into account. The use of another

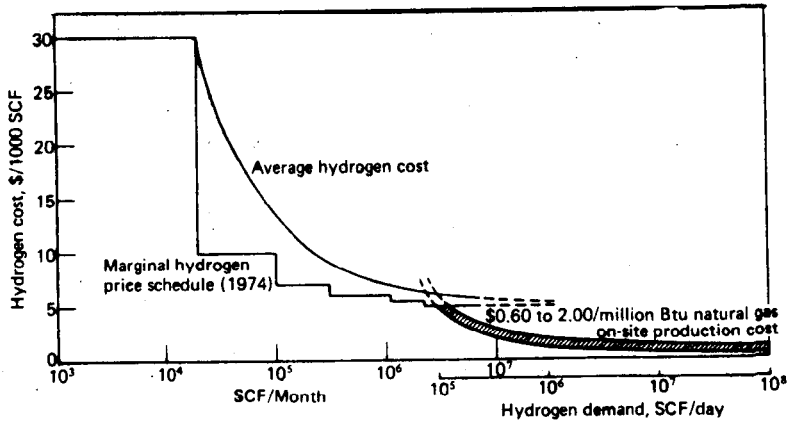

Figure 10. Dependence of price of hydrogen on amount produced.

system (e.g., the sale of synthetic gasoline) benefits the minority vendor much better.

18. Electrochemical Technology from Hydrogen Economy

The availability of hydrogen as a fuel would give correlated effects in the use of electrochemical processes as fuel cells in transportation.

18.1. Transportation

The first hydrogen-driven cars would be internal combustion, because an expectation of the performance of "the old gasoline type of car" will be present with respect to acceleration. Should the public begin to feel that such a type of rapid and noisy acceleration is not necessary, it may be that they will settle for the battery–fuel cell combination in hydrogen-driven cars, for the fuel cell conversion would give a cheaper per-km cost.

18.2. Industry

There have been many chemical processes in industry which could be run on hydrogen, the processes which are now run by means of heating and with natural gas.

Electrochemical processes of oxidation–reduction, and those involving large amounts of oxygen, could also be facilitated.

These matters are pointed out in specialist's articles on the hydrogen economy and particularly in the *International Journal of Hydrogen Energy*.

References

1. J. O'M. Bockris, *Environment* **12**, 51 (1971).
2. J. O'M. Bockris and J. Appleby, *Environment This Month*, 29 (July 1972).
3. J. B. S. Haldane, in a lecture, Daedalus or science of the future, at Cambridge, 4 February 1923.
4. F. Lawaczeck (1930), quoted by E. W. Justi in ref. 6; also in private communication, 6 May 1974.
5. J. O'M. Bockris, Westinghouse Co., Pittsburgh, Pennsylvania, 1962.
6. E. W. Justi, *Leitungsmechanisms and Energieunwandlung in Festrorpen*, Vandehoeck and Ruprecht, Gottingen (1965).
7. J. O'M. Bockris, *Energy: The Solar Hydrogen Alternative*, Halstead, New York (1976).
8. J. O'M. Bockris, *Energy Options: The Solar Hydrogen System*, Halstead, New York (1980).
9. R. Hansen, private communication, February 1978.
10. Friedrich Niehaus, International Institute for Applied Systems Analysis, 2361, Laxenburg, Austria.

11. *Chem. Eng. News*, 7 (June 25, 1979).
12. A. S. Mann and C. Marchetti, paper presented at Hydrogen Economy Miami Energy (THEME) Conference, March 1974.
13. L. B. McGown and J. O'M. Bockris, *How to Obtain Abundant Clean Energy*, Plenum Press, New York (1980).

Index

Acceleration characteristics, of electric vehicles, 459
Activation overvoltage, in Galvanic cells, 141
Aging phenomena, in fuel cells, 64
Air–iron battery, 325
Alkali-metal–high temperature systems, 161
Alkire, and dynamic response of porous electrodes, 87
Alloys, for storing hydrogen, 521
Aluminum–air battery system, for electric cars, 487
Aluminum Company of America, 9
American Cyanimide and liquid cathode cells, 263
André
  and the invention of silver–zinc cells, 407
  and the Yardney International Corporation, 408
Anode delay phenomena and lithium cells, 273
Anodes
  in primary cells, 199
  Pourbaix diagrams, 135
Appleby, and phosphoric acid fuel cells, 100
Applications
  of a hydrogen economy, 519
  of primary batteries, tabulated, 194
  of silver cells, 418
  of silver–zinc batteries, 418
Argue, and silver-containing cells, 293
Aschenbach, and the first dry cell, 220
Auborn and Marincic, and sulfonyl chloride cells, 273
Automobiles
  electric, their characteristics, 436
  needed electrical power plant, 180

β-aluminas
  Beevers–Ross sites, 287
  electrolyte batteries, 298
  their structure, 286
Bacon, and dual-porosity nickel electrode 170
Basic principles of primary batteries, 193
Battery
  applications, secondary, 305
  cycle life, 469
  durability, 468
  energy requirements, 461
  features, secondary, 304
  goals, for electric cars, 473
  performance, suitable for electric cars?, 464
  power requirements, of electric vehicles, 460
  systems 1930–1977, improvements portrayed, 178
Batteries
  at ambient temperatures, 475
  for cars, costs of, 471
  characteristics of, 308
  containing lithium iodide, 294
  economics, 182
  future ones, tabulated, 159
  high temperature–low temperature, 144

Batteries (*cont.*)
industrial–economic aspects, 179
summary and outlook, 179
their densities, 312
for transportation, 421
up to 2 MW, 180
using lithium, 247
with silver-ion conductivity, 290
Baur and Tobler, the second cycle of fuel cell research, 169
Bedford van
electric battery, 452
running on sodium–sulfur, 455
Beer, his patent on titanium nitrites, 26
Beneficiation of ores, electrochemical mechanisms, 23
Berndt, and ionic species, 137
Besenhard, and review of lithium batteries, 248
Besenhard and Schollhorn, and discharge of molybdic oxide cathodes, 263
Bevan, Badwal, and Bockris, and uranium oxide for use in steam electrolysis, 28
Billings
and use of hydrogen in households, 522
and work in hydrogen production from coat, 522
place, diagramed, 523
Biofuel cells, e.g., for heart pacers, 20
Biomass, 511
Biomedical applications, 15
Biomedical sciences, and electrochemistry, 16
Birk, and the zinc–chlorine cell, 164
Bischoff and Justi, and a cycle in fuel cell research, 169
Blomgren, and reduction mechanism of $SOCl_2$, 266
Blomgren and Kronenberg, liquid cathodes, 263
Blood plasmas, and potential–time relations, 20
Bobbin cells, 272
Bockris
and cost of production of hydrogen, 517
and first statement of hydrogen economy, 505
and 1975 book *Energy: The Solar-Hydrogen Economy*, 524
and work on lead-ion addition with respect to dendrite, 411
his work on rotating current collectors, 324
Bockris and Cahan, theory of porous electrodes, 72
Bockris, Devanathan, and Muller, and the model for the double layer, 143
Bockris and Drazic
explanation of sensitivity in terms of electrons per square centimeter, 139
and origin of current–potential curves, 140
Bockris and Pound, mechanism with uranium oxide, 28
Bockris and Reddy
and double layer structure, 139
use of terms *ionics* and *electrodics*, 126
Bockris and Srinivasan
and electrocatalysis, 142
their book on fuel cells, 110
theory of porous electrodes, 72
Bockris and Tunulli theory, compared with that of Mitchell, for metabolic functions, 17
Bodnaruk, and thin-film galvanic cells, 294
Borderline phenomena, and electrochemistry, 34
Borucka, and molten carbonate fuel cells, 102
Bottin cell, 299
of silver–zinc, diagramed, 414
Bradley and Green, and conductivity of solid electrolytes, 292
Breiter, and electrocatalysis, 142
Bro, and use of SO_2 for lithium cells, 265
Brodd, and primary batteries, 165
Broers, his super battery, 174
Bromate–zinc cell, 321
Broussely, and efficiency of lithium cells, 255
Burshtein, and theory of porous electrodes, 80
Butler–Volmer, their equation, 140
Button cells, development of, 259

Cairns, work in organizing research on high-temperature cells, 368
Calcium-containing cells, summarized, 367
Calcium-silicon–molten halide–iron disulfide cells, 366
Capacity
as applied to electrochemical systems, 147
as function of temperature, 153
of organic compounds in batteries, 167
for various cells, containing nickel, 392
Capital costs, and electricity costs, of fuel-cell power plants, 102

Carbon dioxide
its evolution in zinc cells, 321
reduction of, a promising field, 28
variation with time, 2
Carbon–lithium fluoride cells, 252
Carbon monoxide, its effect upon fuel-cell performance, 57
Car
characteristics for, 180
hydrogen–air batteries for, 181
Catalyst
for fuel cells, 62
supported, 80
Catalytic activity, for oxygen reduction mechanisms, 60
Cathode
cells
liquid, 263
with lithium, 248
performance, in oxygen reduction reactions, 59
Cathodes, in primary batteries, properties of, 203
Cell
configuration, in fuel cells, 115
designs, of Leclanché cells, 223
discharge characteristics, for Ruben cell, 238
operation, successful for zinc, 321
performance, using β-alumina, summary, 300
structure
for mercurial cathode dry cells, 233
in Ruben cell, 244
types, containing nickel, 392
voltage
and acid concentration, for lead–acid battery, 373
as a function of state of charge, for nickel cells, 399
Cells
and batteries, containing lead, 381
candidate, for electric cars, 466
with molten electrolytes, 354
Centering
effects in fuel cells, 65
of supported metal crystallites, 63
Characteristics
for discharged lithium cells, 253
for energy storage systems, 180
for goods and service delivery, 424
of redox batteries, tabulated, 331
of secondary batteries, 305
Characteristics (*cont.*)
of various batteries, 308
of zinc batteries, 310
Charge–discharge characteristics, 397
Charge retention
for nickel cells, 399
for silver cells, 416
Charging performance, for lead–acid battery, 377
Chemical reactions, in Leclanché systems, 209
Chemical storage, 126
Chemistry, and electrochemistry, 3
Chevette, as electric car, 438
Chlorine
evolution, and zinc cells, 321
gas, and electric cars, 481
Chlorine–zinc battery, 320
Chloro-aluminate melts, 312
Choppers, schematic, 443
Chromium–ferric-iron redox system, 334
Classification
of fuel cell electrodes, 172
of secondary batteries, 305
Coal
as an energy source, 508
and hydrogen, relation of, 509
as primary energy source, in vehicular efficiencies, 108
as a source of hydrogen, 7, 510
source of hydrogen, production costs, 519
Collins, his treatise on the lead–acid battery, –155
Compressed air storage, 124
Conditioning, effect on batteries, 316
Conduction mechanism
determination of, 282
of solid electrolytes, 280
Conductivity
of lithium iodide, 296, 297
of silver bromide, 288
of silver-ion-conducting solid electrolytes, 291
of solutions used with lithium cells, 265
Configuration, the "jelly roll" with lithium, 267
Conservation, electrochemical, 13
Copper electric Runabout, 438
Copper oxide–lithium cells, 254
Corolloid structures in positive electrodes, 314
Corrosion, and high-temperature batteries, 476

Cost
of hydrogen, scaling factor, 517
minimal, of hydrogen from coal, 510
related to price, for hydrogen, 517
of sodium-sulfur cell, 349
Costs
of batteries for cars, 471
calculated for electric car batteries, 472
for producing hydrogen, 516
Crystallites, growth of, 64
Current
cycling, 470
density, and efficiency in fuel cells, 50
distribution, according to simple pore model, 74
Current–potential relationships, 139
Current–voltage curves for manganese dioxide batteries, 209
Cycle life, 314
and depth of discharge, 313
for nickel cells, 400
for zinc cells, 319, 322

Dalin, his work on rotating current collectors, 324
Damjanovic, and work on lead additions affecting dendrites, 411
Dassler, and sealing of cells containing nickel, 395
Davidson, his 1837 electric carriage, 421
Davtyan, and fuel cell research, 169
Decomposition
of metals, 30
of water by light, 514
Dendrites, of zinc, 317
Dendritic growth
and silver cells, 416
in zinc cells, 323
Densities, of various batteries, 312
Depth of discharge, 315
and cycle life, 313
Determination of conduction mechanism, 282
Dey
and lithium batteries, 248
and SEM studies of lithium surface, 248
and two-electron reduction of SO_2, 267
Difficulties in present society, 9
Diffusion
electrodes, porous, 64
potential theory, evidence against, 17
Discharge
characteristics, of acetylene black galvanic cells, 293
curves
as a function of time in primary cells, 227
with lithium-manganese dioxide, 257
with solid electrolytes, 294
data on liquid cathode cells, 267
performance, lead-acid battery, 376
times, for zinc cells, 319
DOE electric vehicle objectives, 445
Doping
effects, and conductivity, 284
by iron, 300
techniques, and conduction mechanism, 283
Driving profile, for energy requirements, in electric vehicles, 458
Dual porosity model, 76
Dudley, and secondary batteries, 300
Durability, in electric batteries for cars, 463

Economics
of batteries, 182
of fuel cells, 182
of hydrogen economy, 523
Edison
and electric cars, 467
his early work on fuel cells, 168
and the nickel–iron battery, 156
Edison and Jungner, and secondary batteries, 303
Efficiency
of fuel cells, 49
silver cells, 417
some fuel cell reactions, 146
Efficiencies
associated with the utilization of nuclear fuel, 432
of direct energy conversion devices, 40
in nickel cells, 402
in utilization of coal and petroleum, 431
Eichinger and Fritz, and cupric sulfide used with lithium cells, 261
Eisenberg, and effect of hydrodynamics, 143
Electric batteries, for cars, conclusions on, 496
Electric cars, 435
and battery goals, 473
the candidate cells, 465

Electric cars (*cont.*)
and electric power generation industry, 434
and the environmental issue, 425, 426
and fuel cells, 473
and high temperature batteries, 475
historical background, 421
and modern transport, 423
Electric drive system, 442
Electric motors for cars, tabulated, 442
Electric power generation industry, and electric cars, 434
Electric propulsion, diagramed, 494
Electric transportation, vehicles, 435
Electric utilities
and fuel cells, 42
their demand, 430
Electric utility, load curve, 180
Electric van by General Motors, 454
Electric vehicle
battery system, diagramed, 481
objectives, 445
power calculations, 456
Electric vehicles
candidate power systems, 496
commercial, 447
Electrocatalysis
and fuel cells, 56
future of, 26
major role in fuel cells, 55
Electrobus, in operation, 456
Electrochemical activity, and concentration of Teflon, 80
Electrochemical conservation, 13
Electrochemical conversion, 13, 126
Electrochemical destruction, of tumors, 19
Electrochemical energy conversion
and electrochemical principles, 43
its dependence on electrocatalysis, 56
and primary energy sources, 42
Electrochemical energy storage
limits of, 174
research objectives, 182
Electrochemical house, 12
Electrochemical industry
by-product types, 10
economics of, 9
and present society, 10
Electrochemical mechanisms, 23
Electrochemical methods, and material conversion, 27
Electrochemical power source technology, 474
Electrochemical power sources, requirements for electric cars, 453
Electrochemical processes, in production of hydrogen, 517
Electrochemical production of hydrogen, 12
Electrochemical properties of solutions used with lithium cells, 265
Electrochemical reactions, in lead–acid battery, 372
Electrochemical recycling, 13
Electrochemical storage, 126
how it works, 145
Electrochemical transportation, 12
Electrochemical treatment, of liver cells, 20
Electrochemistry
for the alkaline MnO_2 system, 220
for a better world, 30
in biomedical sciences, 16
of cleaner environments, 29
and the life sciences, 33
in the life systems, 31
and light conversion, a new field, 14
nature of, 3
and other sciences, 3
of water splitting, 513
as a young science, 183
Electrochemists, and the periodic table, 183
Electrode
kinetics, and fuel cells, 50
potential, for manganese dioxide system, 134
potentials, in alkaline–zinc cells, 222
reactions, kinetic aspects, 196
Electrodeposition of materials, from high-temperature melts, 22
Electrodes
hydrophilic and hydrophobic, characteristics, 66
porous, 64
for silver–zinc cells, 411
Electrodesign, for lead–acid battery, 380
Electrodialysis, and future of electrochemistry, 29
Electrolysis
of thermal systems, 514
of water, and production of hydrogen, 511
Electrolyte
batteries, 290
for nickel cells, 290
and primary batteries, 202
for the sodium–sulfur cell, 347

Electrolyzers, classical, 513
Electron transfer at hemoproteins, 18
Electronic conductivity, in solids, 287
Electro-organic chemistry, 29
Electro-organic oxidation, 61
Electro-oxidation of methanol, 62
Electropolymerization, 28
Elliot and Turner, their graphs for production of fossil fuels, 10
Ellipsometry and electrochemistry, 5
Emission
  from fuel cells, and other modes of generation, 93
  rates, for vehicles, 428
  standards, federal, 427
Energy
  concept, and fuel cells, 97
  consumption
    and electric vehicles, 447
    prime sourve, 433
  conversion
    electrochemical, 13
    principles, 39
  convertors, from galvanic cells, 145
  densities, for rechargeable batteries, 156
  density
    of lithium–copper oxide cells, 255
    and nickel cells, 401
    for silver cells, 417
  industries, and electrochemistry, 30
  for lithium batteries, 253
  media of, 7
  metabolism, and Szent-Gyorgyi, 21
  output of a cell, 129
  per head, and income per head, 506
  storage
    electrochemical, 123
    technology of, 124
  storage systems
    characteristics for, 181
    modern, 179
  stored by hydrogen, 520
  versus power, 109
Environmental and energy utilization, 425
Environmental impact, of fuel cells, 92
Environmental Pollution Agency, and battery requirements, 461
Environmental regulation, in fuel cells, 115
Ervin, and silver cells, 294
Euler, and galvanic fuel cells, 168
Exchange currents in reversible potential, with redox reactions, 333
Falk and Salkind, reviews of the literature, 156
Faraday, his laws, 191
Farrington, and problems in β-alumina, 300
Fauré, and the early contributions to the lead–acid cell, 149
Fiat, their electric car, 441
Fickett, and phosphoric acid fuel cell program, 184
First Law costs of hydrogen, 1979, 518
Fleischmann, and fluidized bed reactor, 22
Flooded and nonflooded porous electrodes, 84
Flooding, in porous electrodes, 79
Flotation, mechanism of, 24
Flywheel
  energy storage, 125
  performance, in electric cars, 446
  used in Garrett vehicle, 446
Ford and Edison, and electric cars, 476
Ford Company, and sodium–sulfur cell, 344
Free-energy–metal-bond relationship, in electrochemistry, 25
Frumkin, pioneering the trend away from Nernst, 127
Fuel, and oxygen utilization, 114
Fuel cell
  power plants, their costs, 102
  research, a third period, 169
  systems, classification of, 171
Fuel cells
  classification, 41
  differences compared, 99
  and economics, 182
  for electric and gas utilities, 90
  and electric cars, 473, 493
  and electrochemistry, 34
  and electrode kinetics, 50
  and electrolyte thickness, 115
  and environmental impact, 92
  and fuel cells, 113
  historical background, 39
  ideal kinetic parameters, 54
  integrated with coal gasifier and steam bottoming cycle, 104
  and power, 50
  and power plant efficiency, 94
  as power plants, 113
  for space application, 106
  systems, uses of, 88
  their comparison with other methods of energy conversion, 40

Fuel cells (*cont.*)
their efficiencies, 92
their flexibility, 90
thermodynamic aspects, 44
thermodynamic data, 46
and transportation, 31
for transportation, 106
use in utility industries, 90
uses of, 89
and various kinds of overpotential, 50
and waste heat recovery, 112
Fuel processes, and fuel, 97
Future possibilities, for lithium cells, 274

Gabino, and lithium cells, 261
Galvanic cells
as energy convertors, 145
theory of, 126
General Electric, their electric car, 443
General Motors
design characteristics for electric cars, 451
electric van, 453
and electric vehicle concepts, 440
electrode plating and storage batteries, 9
electrovan, 437
post office van, 450
German research groups, and sealing of cells, 395
Gibbs free energy, of primary batteries, 195
Gileadi, and importance of electroadsorption of fuels, 143
Gilman, and sulfuryl chloride cells, 273
Giner, his theory of flooding, 79
Glass-fiber–sodium–sulfur cell, 352
Gordon, and fused organic salts, 28
Graphite, and oxygen reduction, 79
Greenland, as possible hydroelectric source, 511
Gregory, and cost of production of hydrogen, 517
Grens and Tobias, and dynamic response of porous electrodes, 87
Gupta and Tischer, and sulfur cell, 345

Haldane, and early mention of hydrogen from wind energy, 505
Halogen–hydrogen battery, 330
Halogen–oxygen systems, 311
Hansen, and the "autophage," 509
Harber and Brunner, their contribution to fuel cells, 168
Harris, and discovery that lithium is stable with cyclic esters, 247
Haver, and doping of β-alumina, 300
Healing, 21
Heart, artificial, electrochemical, 20
Heat
balance, for nickel cells, 399
changes, reversible, 50
generation, in fuel cells, 54
of reaction, for lead–acid battery, 374
Heise and Cahoon, and primary batteries, 165
Heller, and liquid cathode cells, 263
Herbert and Ulam, and lithium cells, 261
High-temperature batteries, for electric cars, 475, 488
High-temperature cells, conclusions, 368
High-temperature electrolytes, 28
High temperature, and secondary batteries, 341
Hodgkin and Katz, their theory on membrane potentials, 15
Homogeneous models, for porous electrodes, 70
Honeywell Corporation, and lithium cells, 260
House, electrochemical, 12
Huber, and heterogeneous phases, 133
Hunger, and reduction of fluorocarbons, 254
Hydrocarbon conversion, for fuel cells, 178
Hydrogen
car produced by electrochemical means, 12
from coal, 7, 508, 510
economy
applications of, 519
and cheapest economy, 523
and electrochemical plants, 524
first described by Boekris, 505
the necessity to begin early, 508
and time scale, 506
and environmental impact, 522
evolution, in zinc cells, 323
at high temperatures, 515
and its costs, 516
from kinetic energy of natural streams of of water in earth, 511
from nuclear power, 508
price as function of amount produced, 524

Hydrogen (*cont.*)
produced by electrochemical processes, 517
solar economy, 508
from solar energy, 512
and transmission, 519
in transport and housing, 522
from wind power, 511
Hydrogen-air batteries, for cars, 181
Hydrogen-air battery system, conclusions on, 496
Hydrogen-air-phosphoric-acid cell, 45
Hydrogen-chlorine, schematic, 332
Hydrogen-halogen batteries, 311, 330
Hydrogen-metal oxide batteries, characteristics, 311
Hydrogen-nickel oxide battery, 326
Hydrogen-oxygen battery, 330
Hydrogen-oxygen reaction, 56
Hydrogen-silver oxide battery, 328
Hydrophobic electrodes, and fuel cell electrodes, 77
Hydropumped storage technology, 124

Ibl, and effect of hydrodynamics, 143
Ikeda, and low drains on lithium cells, 256
Improvements, for lead-acid cell, 153
Indirect fuel cells, 174
Industrial processes, and electrochemistry of, 33
Industry
and hydrogen economy, 524
and large-scale use of hydrogen, 522
Inman and Williams, and recovery of metals from waste materials, 22
Interface effects, in solid electrolyte cells, 289
Internal resistance
its function of time in Ruben cells, 241
for Ruben cell, 240
in the sodium-sulfur cell, 347
Ion-doping, 300
Ion-exchange membrane batteries, 176
Ion transport, through membranes, 17
Iron, in monosulfide cell, 355
Iron-air battery, 325
its performance, schematic, 327
Iron-air system, its status, for electric cars, 486
Iron-nickel battery, for electric cars, 478
Iron-nickel oxide battery, and Westinghouse Corporation, 438
Issues, of environment, and electric cars, 425

Jacques, his famous article on fuel cells, in Harpers Magazine, 168
Japan
and development of metal-air battery, 439
and production of lithium cells, 252
Jarrett, hybrid vehicle, 444
Jasinski, review of lithium, 248
Jungner, and the nickel-cadmium battery, 156
Justi, and Raney-nickel electrodes, 170

Kalhammer, and fuel-cell-electrolyzer combination, 178
Kennedy and Samuels, and β-alumina, 300
Kilroy and Dalak, and violent reaction in lithium cells, 275
Kinetic aspects, of electrode reactions, 196
Kinetics
the determining factor in corrosion, 133
of lithium-cadmium cells, 387
Kistyakovsky, his definition of electrochemistry, 3
Knapp, and molybdic oxide cells, 262
Knobloch, his better iron electrode, 159
Kobayashi, and zinc chloride cells, 215
Kordesch
and economics of fuel cells, 112
and importance of Tafel slopes, 143
and tremendous difference use of fuel cells would mean, 148
Kordesch and Kozawa, and manganese dioxide batteries, 320
Kordesch and Marko, and instrumentation for technical batteries, 142
Kozawa
and mechanisms in discharged reactions, 133
and polarization of manganese dioxide, 209
Kuhn, and red-mud threat to the Mediterranean, 24
Kummer and Webber, their famous contribution to battery technology, 344
Kunz, and megawatt electrochemical plants, 184

Latimer, and thermodynamic publications, 127

Lavacazek, first indication of cheap flow of hydrogen through tubes, 505
Lead-acid battery, 305, 371
appearance, 379
and charging performance, 377
and electric cars, 478
mechanism of, 372
and power-weight ratio, 376
reactions, 139
and Ruetschi, 136
and wound-up electrode, 381
Lead-acid cell, 148
construction, details, 151
cut-through diagram, 153
highlights in its early work, 149
improvements planned, 153
Lead-acid cells
discharge process at, 151
mode of failure, 153
Leclanché batteries, technical changes, 209
Leclanché cell, and zinc chloride cell, compared, 215
Leclanché cells, new areas of study, 215
Leclanché system, portrayed, 205
Lehmann, and lithium cells, 254
Levich, and effect of hydrodynamics, 142
Liang
and conductivity of doped lithium iodide, 296
and discharge efficiency, 289
and silver iodide, 290
Liang and Barnett, and lithium cell conductivity, 298
Light conversion, electrochemical, 14
Lindstrom, and schematic of performance, 327
Liquefaction, of hydrogen, 520
Liquid cathodes, 263
Lithium
and anodic protection, 273
batteries, 247
and energy densities, 253
nonaqueous, 166
cells
and discharge characteristics, 253
and Eagle Pitcher, 252
with liquid cathodes, 263
and safety considerations, 274
their construction, 268
electrode and cell construction, 250
electrolyte solution considerations, 248
iodide
doped, 296
Lithium (*cont.*)
iodide (*cont.*)
electrolyte batteries, 294
in mercury cell, 298
in primary batteries, 201
specific systems, 251
and spiral wound cells, 271
Lithium-aluminum
alloys, 335
phase diagram, 358
Lithium-aluminum-iron-sulfite system, for electric cars, 490
Lithium-aluminum-lithium chloride-potassium chloride-iron monosulfide cell, 355, 361
Lithium-carbon fluoride cells, 252
Lithium-copper oxide cells, 254
Lithium-cuprous sulfide cells, 261
Lithium-manganese dioxide
cells, 256
and discharge curves, diagramed, 257
Lithium-molybdic oxide cells, 262
Lithium-organic electrolyte battery, 334
Lithium-silicide-iron sulfite, battery system, 491
Lithium-silicon-lithium chloride-potassium chloride-iron disulfide cell, 360
Lithium-silicon phase diagram, 363
Lithium-sulfonyl chloride cells, 272
Lithium-sulfur dioxide cells, 267, 269
Lithium-vanadium dioxide cells, 260
Livingston Electric Corporation, and lithium cells, 260
Load curve, for electric utility, 180
Ludwig, and reactions in the sulfur cell, 346

Maintenance
and nickel cells, 404
of silver cells, 417
Mallory, and lithium cell characteristics, 258
Mallory Corporation, and lithium cells, 260
Manganese dioxide
as a battery material, 216
system, and electrode potential, 134
Manganese dioxide-zinc cells, secondary, 227
Map of the Balkans, 110
Maricle and Mohns, and lithium dithionite, 266
Martin and Sawyer, and SO_2 for lithium cells, 266
Material components of fuel systems, 67
Material conservation, 27

Matsuda, and lithium–cupric oxide cells, 255
Mattson, and material conversion, 27
Maximum power, for fuel cells, 53
McBreen and Ruetschi, and manganese dioxide batteries, 320
McLaughlin and Eisenberg, and antibiotic mechanisms, 18
Media, of energy, 7
Medical engineering
  and glucose, driven pacemakers, 22
  and heart pacers, 22
Membrane potentials, 15
Membranes, and metabolic processes, 17
Mercurial cathode dry cells, 233
Mercury voltage reference cell, 240
Metabolic processes, and membranes, 17
Metal–air batteries, characteristics, 311
Metal–air systems, 159
  and electric cars, 485
Metal–gas systems, 161
Metal oxide cathodes, 131
Metal oxide–hydrogen systems, 161
Methanol
  as an electroactive organic fuel, 62
  electro-oxidation of, 62
Military, their use of fuel cells, 89
Mineral processing
  contributions of Wark, 23
  summarizing its electrochemical nature, 24
  and work in the Australian CSIRO
Miniature cells, diagrams of , 225
Mitchell, his theory for membranes, and the Nobel prize, 17
Models of porous electrodes, 78
Modern electrolyzers, 514
Molten carbonate fuel cells, 102
Molten carbonates, and steam bottoming cycles, 108
Molten salts, as electrolytes in cells, 354
Monosulfide cell, with iron, 355
Morehouse, his classical investigations of cells with organic electrolytes, 166

Naray-Szabo, and fuel cell research, 169
Neumann, and nickel cells, 395
Neurophysiology, retrograde Nernstian character of its theory, 21
Nicholson and Carlisle, and electrolysis of water, 191
Nickel cells
  applications of, 403
Nickel cells (*cont.*)
  and centered electrodes, 391
  and charge retention, 399
  and cycle life, 400
  and energy density, 401
  and maintenance, 401, 404
  and pocket electrodes, 390
  their capacity, 394
Nickel–cadmium battery, and Jungner, 156
Nickel–cadmium cells
  and materials, 389
  overcharge, 158
Nickel–cobalt oxide, as catalyst, 61
Nickel–hydrogen battery, schematic, 328
Nickel–iron battery
  Edison's invention, 156
  for electric cars, 478
Nickel oxide–hydrogen battery, 326
Nickel oxide–hydrogen cell construction, 161
Nickel oxide–zinc batteries, 314
Nickel–zinc cell, 157
Nonaqueous cells, 168
Nonaqueous electrolyte batteries, 312
Nonaqueous lithium batteries, 166
Nuclear hydrogen, as energy source, 508

Ohmic conditions, and transient response, 87
Ohmic polarization, and fuel cell theory, 73
Open-circuit voltage, for chromium–iron redox systems, 333
Operating flexibility, of fuel cells, 90
Organic electrolytes, cells with, 165
Ostvelt, his early work on fuel cells, 168
OTEC, as a source of energy for decomposition of hydrogen, 513
Output of primary cells, as a function of current density, 204
Overall efficiency, and fuel cells, 93
Overpotential–current density relationship, according to Bockris and Cahan, 75
Owens and Argue, and conductivity of solid electrolytes, 292
Oxidant type, and fuel cells, 114
Oxygen
  electrodes, in alkaline medium, 61
  evolution, and manganese dioxide batteries, 320
  exchange, in nickel–cadmium cells, 388
  reduction reaction, in fuel cells, 58
Oxygen–hydrogen battery, 330
Oxygen–oxygen bond, in fuel cells, 59

Parameters, and overall efficiency, 110
Parasitic reactions, 321
Passenger buses, electric, 453
Passive electrode types, for nickel cells, 390
Pathogens, and electrochemical deactivation, 19
Peled, and anodic protection, of lithium, 273
Performance data, for primary cells, 226
Periodic table, and electrochemists, 183
Peters, and nickel cells, 395
Peuckert, and current discharge time in batteries, 197
Phase diagrams
  involving sulfur cells, 357
  for lithium–aluminum, 358
Phosphoric acid
  cell, 45
  fuel cells, 100
Photoelectrochemical cell, 515
Photoelectrochemistry, 515
Physical characteristics
  of alkaline MnO_2–zinc cells, 228
  of primary cells, 227
Physical properties, for solutions suitable for lithium cells, 264
Pilla, and therapeutic effects of magnetic fields, 21
Pilla and Bassett, and oscillating magnetic fields, 21
Planté, and the lead-acid cell, 148, 371
Platinum bronzes, and spillover theory, 26
Pocket electrodes, for nickel cells, 390, 392
Polarization, in the Leclanché cell, 213
Pollution
  lack thereof with hydrogen, 522
  and reduction of by use of electric cars, 181
Polysulfide phase, 345
Polytetrafluoroethylene, as a binder, 65
Porous electrodes
  and centering effects, 65
  models of, 78
  their description, 69
  theory of, 72, 73, 85
  transient techniques, 85
Porous gas diffusion electrodes, 64
Porous matrix, structural details of internal, for fuel cells, 66
Positive active mass, with nickel cells, 389
Postal service vehicles, 449
Potential
  as a function of time, for lead-acid battery, 378
  of the oxygen electrode, 130
Pourbaix diagrams, their difficulties, 133
Power
  anode and cathode structures, 237
  and current density, in fuel cells, 50
  density, and useful life, 111
  and energy, compared, 148
  sources, those chosen for electric cars, 463
  systems, for electric vehicles, tabulated, 497
  versus energy, 109
Power plant
  characteristics, and fuel cells, 93
  efficiency, and fuel cells, 94
Power-weight ratio, for lead-acid battery, 375
Present society, difficulties of, 9
Price, related to cost, for hydrogen, 517
Primary batteries, 164, 165, 191, 279
  and the Leclanché cell, 192
  basic principles, 193
  classification, 200
  properties, 199
  zinc, 219
Primary cells
  in batteries, classification, 198
  physical characteristics, 227
  practical output of, 205
  properties of, 203
Prime source energy consumption, 433
Properties of primary batteries, 199
Propylene carbonate, and electrolyte for batteries, 335
Proton transfer, in the homogeneous phase, 221
Pshenichinikov's model, for porous electrodes, 77
Raleigh, and amalgamation processes, 289
Rangarajan, and dynamic response of porous electrodes, 87
Reactions
  and lead-acid battery, 139
  in the sulfur cell, 347
Rechargeable
  batteries, conventional technology, 148
  cells, 173
  reactions
    and exchange currents, 333
    and reversible potential, 333

Rechargeable (*cont.*)
system, involving chromium and iron, schematic, 334
systems, 311
Rejection, and electrochemical considerations, 19
Research objectives, for electrochemical energy storage, 182
Reservoirs, for storing hydrogen, 520
Response, of porous electrodes, 88
Reversible emf of sodium–sulfur cell, 346
Reversible potential and redox reactions, 333
Robinson and Stokes, and Debye theory, 135
Rolls and Silvestroni, and tetrabutylammonium bromide, in zinc cells, 323
Rosenberg and Van Camp, and electrochemical destruction of tumors, 19
Rotating current collectors, 324
Ruben cells, 234
internal resistance, 240
Ruch, and the aluminum cell, 161
Ruckenstein–Pulvermacher, model for centering, 63
Ruetschi, and structural data for manganese dioxide, 222

Safety aspects, of hydrogen, 521
Safety considerations, and lithium cells, 274
Salmon and Kramer, and the nickel-iron battery, 156
Sanstede
and electrocatalysis, 142
and organic materials in electrolytes, 166
Sanyo Electric Company
and lithium–manganese dioxide systems, 256
performance of their button cell, 256
Sawyer, and electrochemical aspects of thrombosis, 19
Scanning electron micrographs, of manganese dioxide, 217
Scharf, an early patent on fuel cells, 169
Schematic
of hydrogen–nickel battery, 328
of zinc–chlorine cell, 321
Schottky defects
in lithium batteries, 294
in sodium chloride, 281
Schwarz, and electric cars, 158
Sealed cells involving silver–zinc, 414
Secondary batteries, 303
classification, 305, 307
high-temperature, 341
nickel–cadmium, 385
Secondary cell, diagramed, 382
Shah, and instability in lithium cells, 275
Shedlovsky, his description of bioelectrochemistry, 15
Silver bromide, conductivity of, 288
Silver cells, 412
and charge retention, 416
and dendritic growth, 416
and efficiency, 417
and energy density, 417
and maintenance, 417
Silver electrodes, 412
Silver oxide–hydrogen battery, 328
Silver–zinc batteries, applications, 418
Silver–zinc Bottin cell, diagramed, 414
Silver–zinc cells
and André, 407
characteristic data tabulated, 413
and performance, 415
and voltage cells, 410
their electrodes, 411
thermodynamics and kinetics, 408
Sinsteden, 1854, and the lead–acid battery, 371
Sodium–air batteries, 161
Sodium–β-alumina–antinomytrichloride cell, 353
Sodium–β-alumina–sulfur cell, 344
diagramed, 344
Sodium–sodium-glass–sulfur cell, 352
Sodium–sulfur batteries, multikilowatt hour, 348
Sodium–sulfur battery system, 493
Sodium–sulfur cell, 162, 492
and cost, 349
exploded view, 348
and internal resistance, 347
summarized in table, 350
their formation, 347
Sodium–sulfur systems, 161
Solar energy, and earth's high insolation areas, 8
Solar-hydrogen economy, 508
Solid electrolytes
conduction mechanism, 280
containing silver ions, 291
and discharge curves, 294
and the specific energy batteries, 343

Solid state batteries, 168
Solids, their electronic conductivity, 287
Solvents, for lithium, 249
South Africa, leading country in gasification of coal, 511
Specific energy
of batteries, tabulated, 309
of candidate cells, for electric vehicles, 467
density, 342
and batteries, 342
of hydrogen–nickel cell, as function of pressure, 329
of lithium–sulfur dioxide cells, 270
theoretical, for electric batteries used in cars, 465
and time, with lithium cells, 365
versus cycle number, 359
of zinc cells, 322
Specific power
and specific energy, 468
and specific energy, in lithium cells, 364
and use of battery, 461
Spillover theory, for platinum bronzes, 26
Spinell-like blocks, 299
Srinivasen, and electrochemical aspects of thrombosis, 19
Stachurski, his work on rotating current collectors, 324
Stainless steel, as container in lithium cells, 257
Standard potential, as a function of temperature, 48
Standard potentials, tabulated, 128, 129
Statistical models, for porous electrodes, 70
Status
for lead-acid batteries, for electric cars, 476
of calcium–silicon–molten-halide–calcium-sulfite cells, 367
Steady state, and electrochemical world, 5
Steam bottoming, and fuel cells, 105
Stoner, and anticoagulant properties, 19
Storage, of energy, in the form of hydrogen, 520
Structure, of β-aluminas, 286
Surface area, of supported catalysts, 80
Szent-Gyorgyi, and energy metabolism, 21

Tafel behavior, and porous electrodes, 80
Tafel equation, for smooth and porous electrodes, 143
Tafel lines, in oxygen reduction, 59
Tafel slopes, for mixed oxide oxygen electrodes, 516
Tafel's law, 139
and batteries, 139
Takahashi and Yamamoto, and patents of the silver cells, 294
Technology, electrochemical, and hydrogen economy, 524
Temperature
and pressure coefficiencies, of reversible electrodes, 45
and standard potential, 48
Tenniswood and Graetzel, and forced rotation in electric vehicle propulsion, 457
Thermal energy assistance, 125
Thermochemical storage, 126
Thermodynamic aspects, of fuel cells, 44
Thermodynamics
of nickel–cadmium cells, 386
of silver–zinc cells, 409
Tiedemann, and lithium cells, 254
Time scale, and the hydrogen economy, 506
Tobias, and effect of hydrodynamics, 142
Toyota, their electric car, 441
Traction, and secondary cells usable for, 33
Transduction, of hydrogen, 519
Transient response, and ohmic conditions, 87
Transient techniques, for porous electrodes, 85
Transmission and hydrogen, 519
Transportation
and batteries, 421
and electrochemistry, 30
and fuel cells, 89
and hydrogen economy, 524
by means of electrochemistry, 12
personal, needed characteristics, 424
Trasatti, and literature reviews concerning electrocatalysis, 143
Tseung, and intermediates of electrode reactions, 184
Tumors, electrochemical destruction of, 19
Twenty-first century
electrochemistry in, 1
and steady state, 5

Union Carbide, Leclanché cell, 224–225
Uranium oxide–yttrium oxide, 28
Urban range, for electric vehicles, 448
Utilities, their use of fuel cells, 89
Utility vehicles, electric, 449

Utilization, degree of, for porous electrodes, 83

Vanadium dioxide and lithium cells, 260
Vehicle applications, tabulated for batteries, 306
Vehicular efficiencies, with coal as primary energy source, 108
Velocity, as a function of platinum content, in hydrogen evolution, 26
Vetter, and his kinetic treatment of electrode processes, 126
Victoria Falls, as a possible hydroelectric source, 511
Voinov and Tannenberger, work on β-alumina, 300
Volkswagen, and electric cars, 181
Volta, the first to have a primary battery, 191
Voltage–capacity curve, with lithium–aluminum cell, 356
Voltage degradation, in fuel cells, 115
Voltage levels, in silver–zinc cell, 410

Walkeley, and the reactions in an alkaline zinc cell, 220
Waste heat recovery, in fuel cells, 95, 112
Water, decomposition of, 512
Weight contribution, for a different construction of elements, and lead–acid battery, 376
Wenglowski, and economics of electrochemical industry, 9
West Germany, and fleet of electric buses, 453
Westinghouse Corporation, and iron–nickel battery, 438
Will, and half-charge for tension, in zinc cells, 323
Will and Mitoff, and patents involving β-alumina, 301
Windpower, source of hydrogen, 511
Worrell and Nagelberg, electrochemistry of transition metals, 168
Wuttke, and patent literature on lithium cells, 261

Yal and Birk, and the lithium systems, 162
Yamamoto and Takahashi, and systems containing silver, 292
Yardney Electric
  and lithium cells, 252
  and silver–zinc cells, 408
Yeager, and use of Auger studies on electrodes, 184

Zamboni, and first use of lead dioxide, 191
Zaromb, and the aluminum cell, 161
Zinc–air batteries, 324
  for electric cars, 486
  schematic, 325
Zinc batteries, characteristics, 310
Zinc–bromine cell, 164, 321
  in status for electric cars, 483
Zinc cells, in hydrogen evolution, 323
Zinc–chlorine battery, 320
  system, and status, 482
Zinc–chlorine cell, schematic, 321
Zinc–chlorine hydrate systems, 163
Zinc–chlorine system for electric cars, 480
Zinc deposition, with respect to batteries, 321
Zinc electrode, and electric cars, 479
Zinc–manganese dioxide, 318
Zinc–mercuric dioxysulfate cell, 243
Zinc–mercurous oxide reference cells with temperature, 242
Zinc–nickel oxide batteries, 314
  for electric cars, 480
  at General Motors, 440

内部交流

F 186/158

电化学大全 第3卷
(英2 -4/2367 - 3)

C—00450

[General Information]
书名=10457904
SS号=10457904